NASA CR-159487
PWA-5594-49

NASA

(NASA-CR-159487) ENERGY EFFICIENT ENGINE FLIGHT PROPULSION SYSTEM PRELIMINARY ANALYSIS AND DESIGN REPORT Progress Report, Mar. 1978 - Feb. 1979 (Pratt and Whitney Aircraft Group) 480 p HC A21/MF A01 G3/07

N79-30189

Unclas 31873

ENERGY EFFICIENT ENGINE
FLIGHT PROPULSION SYSTEM
PRELIMINARY ANALYSIS AND DESIGN REPORT

Prepared
by

Energy Efficient Engine Project Engineering
Engine Technology Engineering
Engine Design Engineering

UNITED TECHNOLOGIES CORPORATION
Pratt & Whitney Aircraft Group
Commercial Products Division

Prepared for
NATIONAL AERONAUTICS AND SPACE ADMINISTRATION
NASA-Lewis Research Center
Contract NAS3-20646

FOREWORD

The Energy Efficient Engine-Component Development and Integration Project is being conducted under parallel National Aeronautics and Space Administration (NASA) contracts to Pratt & Whitney Aircraft Group and General Electric. The overall project is under the direction of Mr. Neal T. Saunders. Mr. John W. Schaefer is the NASA Assistant Project Manager for the Pratt & Whitney Aircraft Group effort under NASA Contract NAS3-20646, and Mr. Edward T. Meleason is the NASA Project Engineer responsible for the portion of the project described in this report. Mr. William B. Gardner is Manager of the Energy Efficient Engine Project at Pratt & Whitney Aircraft Group.

This report describes the preliminary analysis and design of the flight propulsion system conducted during 1978. A wide contingent of Pratt & Whitney Aircraft engineering personnel were involved in conducting the analysis and design tasks, and in preparing this report.

Pratt & Whitney Aircraft was assisted in aircraft installation studies reported herein by Boeing Commerical Airplane Company, Douglas Aircraft Company, and Lockheed - California Company. Airframe manufacturer personnel responsible for this work were Mr. Paul Johnson (Boeing), Mr. Ron Kawai (Douglas), and Mr. Robert Tullis (Lockheed).

TABLE OF CONTENTS

TABLE OF CONTENTS (Cont'd)

TABLE OF CONTENTS (Cont'd)

TABLE OF CONTENTS (Cont'd)

TABLE OF CONTENTS (Cont'd)

TABLE OF CONTENTS (Cont'd)

TABLE OF CONTENTS (Cont'd)

TABLE OF CONTENTS (Cont'd)

TABLE OF CONTENTS (Cont'd)

LIST OF ILLUSTRATIONS

LIST OF ILLUSTRATIONS (Cont'd)

LIST OF ILLUSTRATIONS (Cont'd)

LIST OF ILLUSTRATIONS (Cont'd)

LIST OF ILLUSTRATIONS (Cont'd)

LIST OF ILLUSTRATIONS (Cont'd)

LIST OF ILLUSTRATIONS (Cont'd)

LIST OF ILLUSTRATIONS (Cont'd)

LIST OF ILLUSTRATIONS (Cont'd)

LIST OF ILLUSTRATIONS (Cont'd)

LIST OF ILLUSTRATIONS (Cont'd)

LIST OF TABLES

LIST OF TABLES

LIST OF TABLES

LIST OF TABLES

LIST OF TABLES

1.0 SUMMARY

The National Aeronautics and Space Administration is sponsoring an Energy Efficient Engine Project to develop and demonstrate an advanced technology base for a new generation of fuel-conservative engines in future commercial transport aircraft.

This report summarizes the preliminary analysis and design of a Flight Propulsion System established by Pratt & Whitney Aircraft under the Energy Efficient Engine project. All aspects of the Flight Propulsion System preliminary analysis and design are covered, including component design, internal subsystem design, nacelle design, and aircraft integration. Inputs from Boeing, Douglas, and Lockheed, who participated as subcontractors, are also included as part of the nacelle design and aircraft integration results.

The purpose of the effort described in this report was to evaluate and confirm the feasibility of the Flight Propulsion System (FPS) design, and to define the performance potential of the design against the overall goals established by NASA. The Flight Propulsion System design will be used as the configurational baseline for subsequent component development and integration activities during the remainder of the program. The Flight Propulsion System definition will be revised periodically during the project duration and will be completely updated at the conclusion of the experimental program in 1983.

The design goals for the Energy Efficient Engine Flight Propulsion System are listed below:

1. 12% minimum cruise TSFC reduction*
2. 5% minimum Direct Operating Cost reduction*
3. 50% less performance deterioration*
4. Meet FAR Part 36 (1978) noise rules
5. Meet EPA proposed 1981 exhaust emission standards

*relative to JT9D-7A reference engine

These multiple goals assure attractive economics and improved environmental quality, in addition to performance improvement.

The preliminary analysis and design efforts show that the Pratt & Whitney Aircraft Flight Propulsion System design is feasible, and capable of meeting all design goals, except for the EPA-proposed 1981 NO_x standard.

The Flight Propulsion System preliminary design includes all systems required for normal commercial aircraft operation, and these systems are designed to be easily inspectable, removable, and maintainable. Cruise TSFC, estimated to be 14.9 percent lower than that of the JT9D-7A reference engine, surpasses the NASA design goal. A direct

operating cost reduction of 8.2 percent is estimated, based on averaging the calculations done for Boeing, Douglas, Lockheed, and Pratt & Whitney Aircraft study aircraft on design and typical stage length flights. The direct operating cost reduction reflects the reduced fuel costs attendent with performance improvement.

Design features aimed at better matching of rotor and stator deflections in order to avoid rubbing during normal operation have resulted in an estimated performance deterioration rate one-half that of the JT9D-7A engine, which, meets the NASA goal. Noise calculations for a fully-treated, mixed exhaust nacelle indicate the potential of meeting the 1978 noise rules in future domestic and international aircraft. EPA parameter estimates fall below proposed 1981 carbon monoxide and unburned hydrocarbon levels and meet the design goals. But despite the use of staged combustion and low NO_x fuel injection, NO_x estimates exceed the 1981 regulations by over 50 percent. The SAE smoke number estimate is equal to the design goal level of 20.

2.0 INTRODUCTION

The objective of the National Aeronautics and Space Administration's Aircraft Energy Efficiency (ACEE) Program is to improve the efficiency of future commercial aircraft, and thereby realize substantial savings in domestic fuel use. One of the elements of the technology plan for implementing this program is the Energy Efficient Engine project.

The Energy Efficient Engine Project is to develop and demonstrate the technology for achieving higher thermodynamic and propulsive efficiencies in future commercial turbofan engines. It is estimated that these improvements will result in 10 to 15 percent lower specific fuel consumption, as compared to that of the most-efficient current engines.

The current Energy Efficient Engine Component Development and Integration Program is the second of two contractual efforts. This effort is based on an engine concept previously defined under the Preliminary Design and Integration Studies (Contract NAS3-20628), the initial Energy Efficient Engine Project contract effort as reported in Reference 1. The engine is a twin-spool, direct drive, mixed flow exhaust configuration utilizing an integrated engine-nacelle structure. A short, stiff high rotor and a single-stage high-pressure turbine are among the major features provided for performance retention and/or major reductions in maintenance and direct operating costs. Improved active clearance control in the high-pressure compressor and turbines, advanced single crystal materials in turbine blades and vanes, and shroudless fan blades are among the many performance improvement features.

Under the current contractual effort, the program has progressed from the Preliminary Design and Integration Studies to completion of a preliminary design of the flight propulsion system. Design feasibility has been established sufficiently to allow Pratt & Whitney Aircraft to proceed with the experimental technology development phase of the program.

To meet the objectives of the program, four technical tasks were established by NASA and jointly developed with the Pratt & Whitney Aircraft project team:

Task 1 - Flight Propulsion System Analysis, Design and Integration
Task 2 - Component Analysis, Design and Development
Task 3 - Core Engine Design, Fabrication and Test
Task 4 - Integrated Core/Low Spool Design, Fabrication and Test

Under Task 1, the preliminary design of the Flight Propulsion System (FPS) is initially defined and updated at intervals throughout the program. The analytical evaluations to provide flight and economic performance characteristics of future commercial aircraft using Energy Efficient Engine Propulsion Systems are conducted in Task I with the assistance of airframe manufacturers.

Task 2 consists of the design, fabrication, and testing of experimental component hardware, and a Supporting Technology effort directed toward evaluating many of the individual Energy Efficient Engine concepts before, or concurrent with, the component experimental hardware design activity.

Task 3 includes the design, fabrication, and test of a core engine utilizing the core components designed in Task 2. Two core engine altitude chamber tests are planned starting in mid-1982 in conjunction with this task.

Task 4 is the design, fabrication, and test of an Integrated Core/Low Spool (IC/LS). The core from Task 3 will be mated with low spool components designed in Task 2 and tested to determine overall system performance, mechanical integrity, noise, and emissions. This testing is scheduled to commence in the second quarter of 1983.

Portions of Task 1 and 2 noted above encompass the work required to establish feasibility of the Energy Efficient Engine Flight Propulsion System Design. Preliminary design efforts on the FPS and its components were completed during the first year of the contract effort.

This report describes the preliminary design and results of analysis for the FPS and its subsystems. The design effort has included a preliminary definition of the engine, major components, internal subsystems, and nacelle. Various analytical representations were used to verify aerodynamic and structural design concepts and to predict performance. Specific design goals and requirements, reflecting the anticipated late 1980's or early 1990's energy efficient commercial conventional takeoff and landing (CTOL) aircraft propulsion system technology requirements, were specified by NASA as guidelines to the engine definition.

Section 3.0 is an overview of the FPS preliminary design summarizing the major component subsystem design features, overall system design goals, and design requirements. Section 4.0 is a detailed discussion of the individual component and subsystem preliminary analyses and design. Section 5.0 presents the results of performance, economic, and environmental evaluations on the flight propulsion system. Summary conclusions are presented in Section 6.0.

3.0 OVERVIEW OF DESIGN

Task 1 of the Pratt & Whitney Aircraft Group Component Development and Integration Program is devoted to the preliminary design, evaluation, and updates of an Energy Efficient Engine Flight Propulsion System (FPS). A flight engine preliminary design is necessary to 1) identify the areas of new technology required to establish the technology base, 2) evaluate the configuration's operating economics, and 3) serve as a benchmark by which component and overall system performance may be measured and tracked throughout the program.

As Tasks 2, 3, and 4 progress, overall FPS performance is tracked under Task 1 to reflect results from these program elements with periodic updates of the FPS status to coincide with completion of major groups of program elements. The final update, which follows completion of Task 4, will incorporate all of the program analytical and test results into an updated Flight Propulsion System design.

The flight propulsion system, described in Section 3.1, is designed to satisfy the goals discussed in Section 3.2. The performance and design of the propulsion system are consistent with standard commercial aircraft engine practice and with applicable FAA and EPA regulations, as discussed in Section 3.3.

There is no intention on the part of NASA to carry this Flight Propulsion System preliminary design through into prototype, development, or production programs. This program is intended solely to provide a focus for the technology needed by an engine manufacturer to initiate design and development of an energy efficient commercial engine with only the usual and normal business risk.

3.1 FLIGHT PROPULSION SYSTEM DESCRIPTION

3.1.1 General Description

The flight propulsion system preliminary design (STF505M-7) cross-sectional drawing is shown on Figure 1. A larger fold-out cross-section is also included at the end of the report for detailed reference. The cross section shows the large fan blades and wasp-waisted engine core gaspath, the two-frame rotor support system, and the acoustically-treated, single-nozzle long-duct nacelle, with fan-only thrust reversing.

Inlet air is channeled to the long-chord, shroudless fan blades by the inlet duct and spinner. Sixty-seven percent of the fan discharge air is ducted around the outside of the close-coupled flow splitter. The remainder is further supercharged by a four-stage low-pressure compressor which also forces the air inward within a curved flowpath. The smaller diameter, 10-stage high-pressure compressor increases the

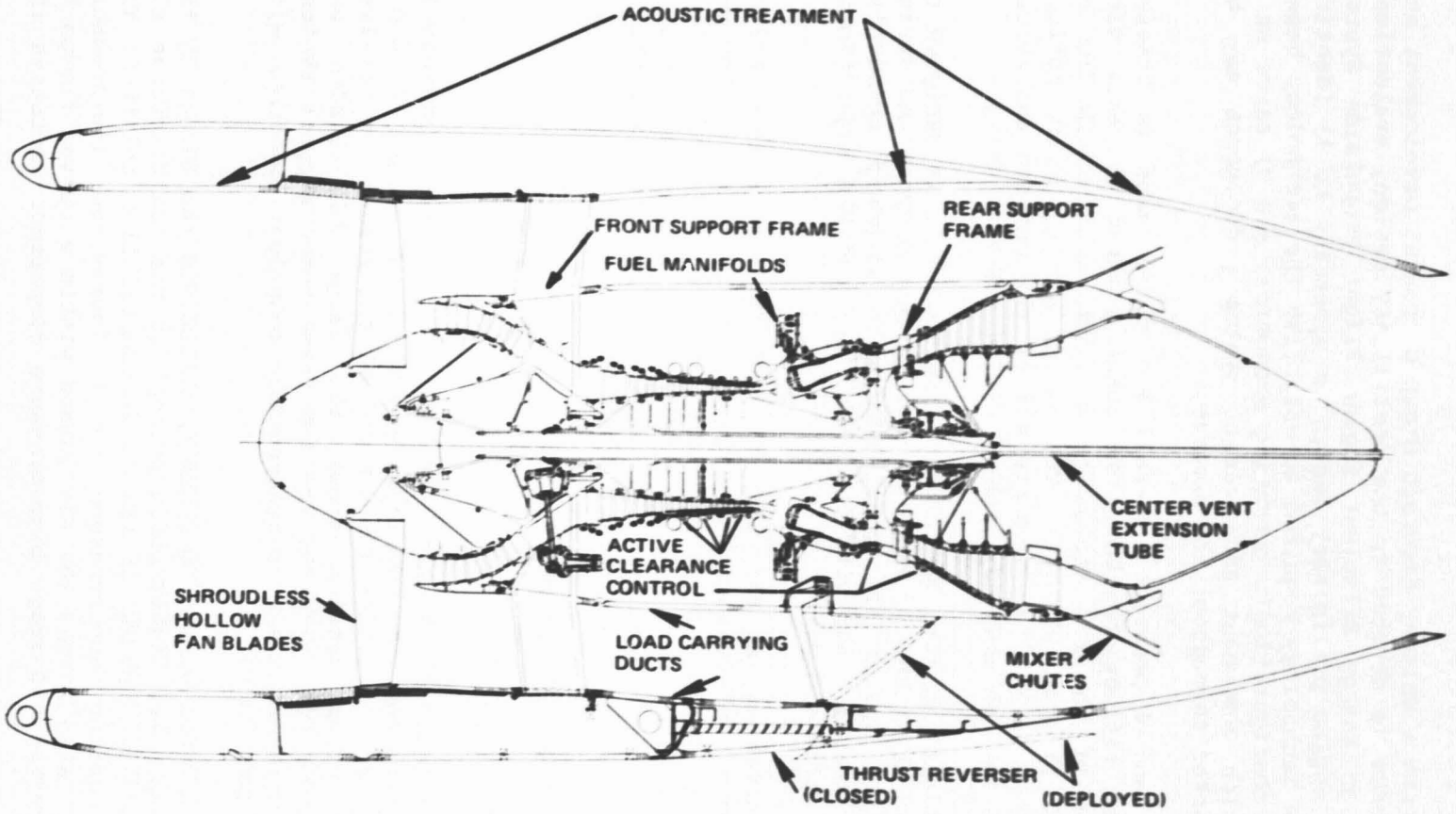

Figure 1 Energy Efficient Engine (STF 505M-7). Cross-Section Showing Major Features

pressure, providing a design overall pressure ratio of 38.6:1. Compressor exit flow is turned radially outward 14 degrees through the exit guide vanes and curved wall pre-diffuser to direct the air into the combustion zones. The outwardly canted combustor, which has two independent fuel supply manifold systems and combustion zones for low emissions, feeds hot gases (up to 1435°C or 2615°F) directly into a one-stage, 4.0 pressure ratio air-cooled high-pressure turbine which drives the high-pressure compressor. The discharge gases are decelerated and turned slightly outward to be further expanded through an uncooled four-stage low-pressure turbine which drives the fan and low-pressure compressor. The core exhaust and the fan duct air are mixed by means of chutes positioned around a large diameter central tailplug and then discharged through a common-flow, 1.02 area ratio convergent-divergent exhaust nozzle.

Gaspath aerodynamics have been advanced by means of novel airfoil shapes and in-flight airfoil-to-case gap control. In the fan and compressor, airfoils are specifically tailored to individual Mach number and loading requirements to control diffusion rates through the rows and to minimize both profile and endwall region aerodynamic losses. Thermally actuated active clearance control on the rear section of the compressor (four external air impingement tubes) and on the turbines (internal case systems) match rotor and case diameters during cruise operation without inducing rubs during takeoff and climb maneuvers. The low and high spools counter-rotate, permitting lightly-cambered low-pressure turbine inlet vanes for higher turbine efficiency.

Only two major support frames and main shaft bearing compartments are used to support both of the rotor systems compared with three or four support assemblies in current high bypass ratio turbofan engines. The assemblies, located between the compressors and between the turbines, house the five mainshaft bearings and the lube oil feed and scavenge systems. The two rotors are supported independently thus avoiding potentially troublesome intershaft bearings. The two support, five bearing concept was implemented with a simple mechanical design configuration requiring only six compartment seals and four labyrinth buffer-air seals. Compartment ventilation is provided by a low fire hazard, center vent breather system utilizing cool low-pressure compressor exit air which is discharged into the shafts and extension tube and exhausted through the tailplug.

The nacelle is designed to share flight loads, serve as an aerodynamic shell around the engine, provide access to the engine, absorb noise, and provide for thrust reverse. The engine structural design evolved from the load sharing concept, in which engine and flight-induced loads are divided between integrated nacelle and engine structures to minimize case ovalization and "back-bone" bending. Engine thrust induced back-bone bending has been eliminated by directing the thrust at the engine horizontal center line through thrust links attached

directly from the front support frame to the pylon. Load-carrying fan ducts are designed to transmit much of the inlet gust moment and other cowl loads around the engine cases to the mounts.

3.1.2 Overall Cycle Characteristics

The flight propulsion system has a 6.5 fan bypass ratio, a 38.6 overall pressure ratio, a 1225°C (2240°F) turbine rotor inlet temperature, and a design fan airflow size of 707 kg/sec (1560 lb/sec) at the 10,668 m (35,000 ft) Mach 0.8 design point. The fan has a pressure ratio of 1.74 through the duct section of the blades and exit guide vanes. The fan root section/low-pressure compressor ratio is 2.76 with an inlet corrected airflow of 94 kg/sec (208 lb/sec). The high-pressure compressor pressure ratio is 14:1 from the intermediate case inlet through the exit guide vanes. Combustor design pressure drop through the pre-diffuser, dump section, and two combustion zones is 5.5 percent. The high-pressure turbine is a one-stage 4.0:1 pressure ratio design; the low-pressure turbine design pressure ratio is 5.6:1. The core stream total pressure loss is 3.0 percent through the turbine intermediate and discharge cases, the mixer, and the tailpipe. Fan air total pressure loss in the ducts, mixer, and tailpipe is 1.1 percent. The principal component performance levels at the altitude aerodynamic design point are shown in Table 1.

The cycle characteristics were optimized and selected during studies (Reference 1) which considered medium- and long-range conventional takeoff and landing (CTOL) commercial aircraft expected around 1990 and emphasized cruise fuel economy and low operating costs. These aircraft designs will be subjected to more stringent noise and exhaust emissions environmental regulations which influenced both the cycle selection and engine design.

The overall objective was to substantially reduce cruise thrust specific fuel consumption (TSFC). Overall pressure ratio was selected at as high a level as possible when considering thrust growth capability, nitrogen oxide (NO_x) generation, and design practicality. Turbine inlet temperature selection was based on minimizing the TSFC while allowing uncooled low-pressure turbine airfoils for cost savings. The fan cycle parameters were selected to minimize direct operating cost. The mixer was chosen to reduce both fuel consumption and direct operating cost. These overall cycle characteristics were used in establishing the current engine preliminary design configuration.

3.1.3 Thrust Size

The Energy Efficient Engine is sized in the 178,000 N (40,000 lb) takeoff thrust class to provide flexibility for producing derivative model thrust capability over a thrust range from 133,000 to 222,000 N (30,000 to 50,000 lb) and thereby encompass the wide range in future aircraft requirements being forecast by the airframe manufacturers. The fan was sized to a corrected airflow size of 707 kg/sec (1560 lb/sec),

which produces an uninstalled takeoff thrust of 182,900 N (41,100 lb). The installation sketch of the flight propulsion system is shown with overall dimensions superimposed in Figure 2.

Substantial thrust flexibility is available relative to the base engine size by utilizing a common core size in conjunction with modified low-spool components to configure derivative engines. Thrust capability can be increased 25 percent by uprating turbine rotor inlet temperature and cooling air to maintain the same metal temperature levels, and by increasing the fan pressure ratio and bypass ratio with a given core size. Thrust size reduction can be accomplished by engine turbine temperature and compressor derating, and/or by fan scale-down. However, TSFC effects must be carefully considered in choosing the path for thrust flexibility. The Energy Efficient Engine core can be matched to various low-pressure spool components to provide derivative configurations with takeoff thrust capabilities from 133,000 to 222,000 N (30,000 to 50,000 lb) without compromising the NASA TSFC goal.

3.1.4 Fan and Compressor Section

A one-stage fan, with hollow titanium blades for light weight, and a 14-stage compression system, are designed to produce the required overall pressure ratio of 38.6:1. The compressor intermediate case section includes a major structural frame which supports the fan rotor, the low-pressure compressor rotor, and the front end of the high-pressure spool rotor.

Twenty-four shroudless, hollow fan blades have been designed to produce a tip section pressure ratio of 1.74 at a corrected tip wheel speed of 460 m/sec (1500 ft/sec). The overall diameter of the blade and disk assembly is 220 cm (86.7 in). To reduce weight and cost, the blades have a low hub-to-tip radius ratio (0.34) and a high inlet specific flow, 210 kg/sec/m^2 (43 lb/sec/ft^2). Blade chord is tapered approximately linearly from 27.8 cm (10.9 in) at the root to 36.1 cm (14.2 in) at the tip. Blade airfoil sections are contoured throughout the passage length in order to diffuse the air through compression waves and oblique shocks rather than through higher-loss normal shocks that can occur with more conventional airfoils.

In deciding internal geometry, various degrees of hollowness and several internal stiffening rib patterns were examined to maximize blade natural frequency and to provide acceptable flutter and vibration operational margins. The internal geometry which evolved during this design effort, two-thirds hollow for lightness with three radial stiffening ribs, is shown in Figure 3. The blades are mounted in dovetail disk broach slots in the one-piece disk and hub assembly.

The fan case design is a wrought aluminum structure wrapped on the outside with KEVLAR® synthetic fiber material for blade containment. The inner wall of the case is lined with acoustical treatment which is

TABLE 1

COMPONENT PERFORMANCE LEVELS

Fan Efficiency	87.3% Duct Section 90.2% Root Section
Low-Pressure Compressor Efficiency	89.9%
High-Pressure Compressor Efficiency	88.2% Adiabatic 91.7% Polytropic
Combustor Efficiency	99.95%
High-Pressure Turbine Efficiency	88.2%
Low-Pressure Turbine Efficiency	91.5%
Mixer Efficiency	85%
Nozzle Velocity Coefficient	99.6%

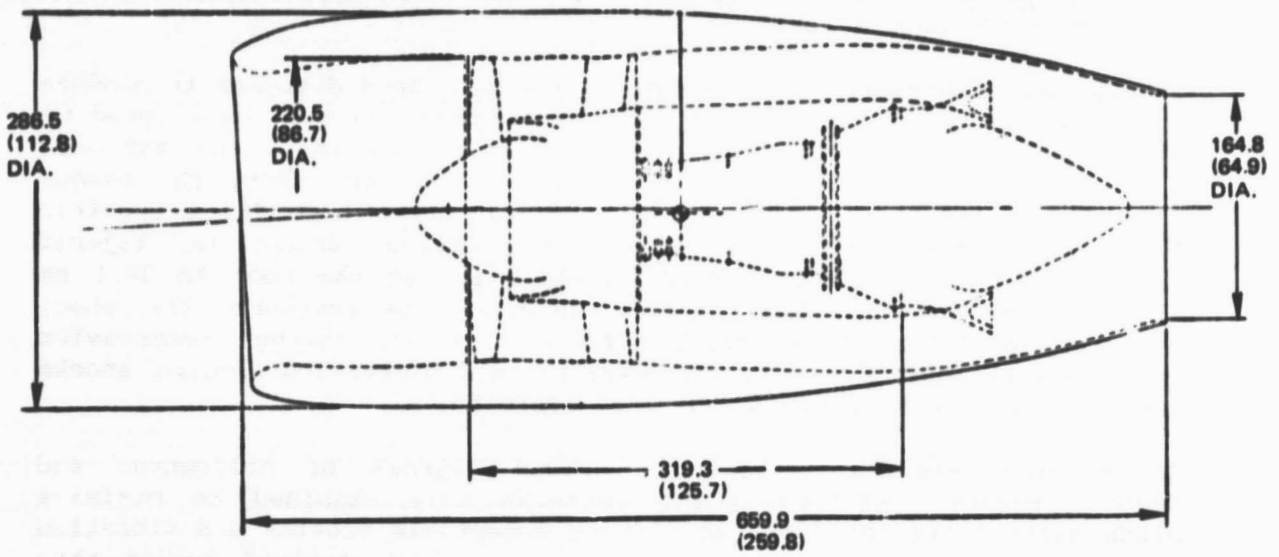

Figure 2 Energy Efficient Engine Installation Drawing With Overall Dimensions

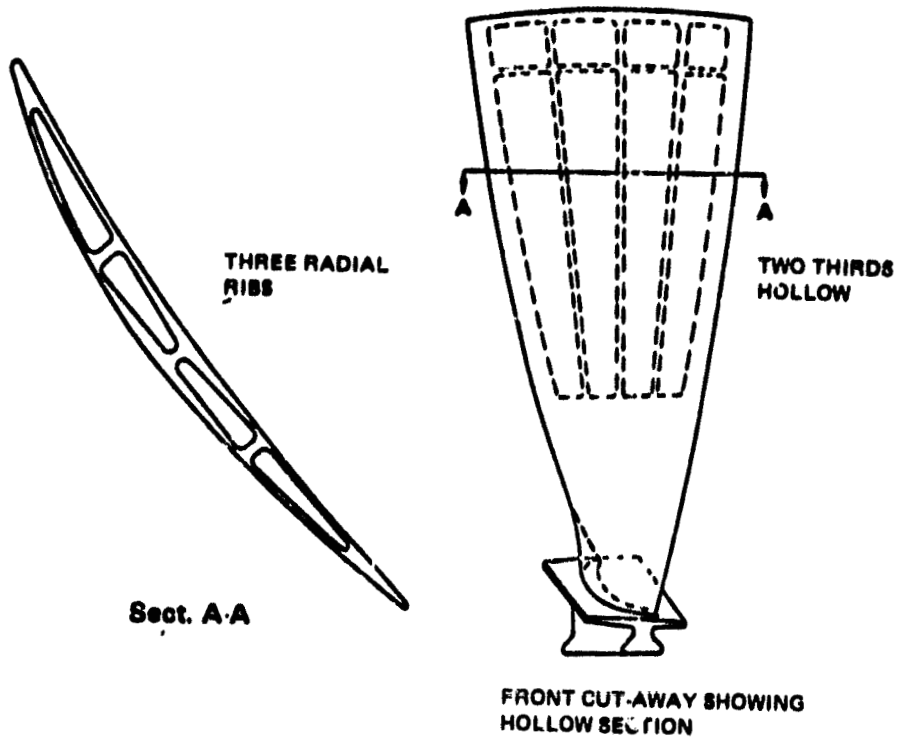

Figure 3 Fan Blade Internal Configuration With Partial Hollowness

frequency-matched to fan noise. The case is machined over the blades to receive an abradable rubstrip which is trenched directly over the rotor. This design concept, which has proven to be beneficial in higher hub-to-tip radius configurations such as compressors, should also benefit the low hub-to-tip radius ratio fan.

The four-stage low-pressure compressor is designed for a 1.77 pressure ratio at an inlet corrected flow of 64.9 kg/sec (142.7 lb/sec). Airfoils are canted rearward to remain perpendicular to the curved flowpath.

An electron-beam-welded low-pressure compressor drum rotor assembly has very small inner cavities beneath the inner stator vane platforms to minimize windage losses. Knife-edges on the rotor are used to seal the cavities and limit air recirculation. As in the fan, abradable rubstrips are installed in trenches over the blades to improve performance.

A low-pressure compressor exit-to-fan duct bleed system is included in the design for surge protection.

The 10-stage high-pressure compressor has a design pressure ratio of 14:1 at 403 m/sec (1323 ft/sec) tip speed and an inlet corrected airflow of 40.0 kg/sec (88.1 lb/sec). Airfoils in the constant mean diameter flowpath are tailored to local Mach numbers to maximize the efficiency potential of the compressor i.e., multiple circular-arc airfoils in the front end transonic flowfield, shockless contoured airfoils in the mid-section high subsonic Mach number region, and NACA 400 series airfoils in the lower Mach number rear stages. The front four stages have variable stagger stator vanes to provide for off-design stage-to-stage rematch. The exit guide vanes are canted outward five degrees to initiate turning into the combustor pre-diffuser. Smooth, erosion resistant coatings are applied on the blades and stator vanes to produce a smoother surface and to reduce erosion induced long-term performance deterioration.

The rotor assembly consists of two sub-assemblies with only one bolt circle where the rotor material is changed from titanium to a higher strength nickel base alloy. Integral knife-edge seals on the rotor run in mini-cavities beneath the stator vanes to minimize related parasitic performance losses.

The compressor case in between the compressor intermediate case and extended combustor diffuser case, is designed in two sections. The front case section over the variable stator vanes includes bosses to provide vane trunnion support and is axially split into two halves to allow for interlacing of the stator vane and blade rows. The rear case section is designed as a one-piece outer shell (for roundness control) that is slipped over previously stacked stator vanes, outer shroud

segments, and insulation before bolt-up to the front case. Two manifolds are positioned on the case to provide customer service bleed, start bleed, and turbine coolant.

Variable stator vane actuation unison-rings surround the front case. Four circumferential air impingement tubes are placed near stator vane outer support rings along the rear of the compressor to maximize the seal movement when fan air is impinged on the case during cruise operation.

The intermediate compressor case consists of 11 titanium structural struts that extend through the core and fan duct flowpaths and are welded to stand-ups on an inner ring and to the casing between the two flowpaths. The beam ends are mechanically attached to the outer aluminum ring with high shear rivets. Twenty-two non-structural, simply supported fan exit guide vanes are located in the duct section between the structural beams. The overall assembly is designed to carry mainshaft thrust bearing loads, the low-pressure and high-pressure compressor case loads, front mount link loads, fan duct loads, gas and pressure loads, cowl moment load, and blade loss induced unbalance loads.

3.1.5 Combustor

The combustor design evolved from the Experimental Clean Combustor Program (ECCP) where both high- and low-power emissions were reduced by incorporating two combustion zones, each individually optimized to have specific low-emission characteristics. The combustor section design consists of a low-loss, curved-wall prediffuser and dump section, a two-zone annular combustor, and a unique high temperature liner. The diffuser case supports the liner and fuel supply system and incorporates struts to transfer the large pressure loads on the inner case across the gaspath.

The diffuser section consists of a strutless, curved-wall prediffuser with 24 thin aerodynamic support struts located downstream of the pre-diffuser dump plane. To align the compressor flow approximately along the burner centerline, 14 degrees of outward turning is obtained by providing five degrees of turning in the compressor exit guide vanes and nine degrees in the prediffuser. The prediffuser has a length-to-inlet annulus height ratio of 3.5 and an area ratio of 1.5, ensuring flow stability.

The pilot combustion zone is a bulkhead design with 24 single-pipe aerating nozzle fuel injectors. The main zone is a carburetor tube design consisting of 48 individual fuel injectors with air supplied through concentric radial inflow swirlers. The fuel and air mixture flows into the combustor through the carbureting tubes. The pilot zone, providing the bulk of the heat input at low power, is optimized for low carbon monoxide and unburned hydrocarbon generation. The main zone is optimized to minimize high power NO_x and smoke emissions.

The combustor liners are designed as double-walled panels of turbine nickel-base alloy (B-1900). The liners are fabricated from cast segments supported by a cooler Hastelloy X structural framework. An advanced counter-parallel FINWALL® (CPFW) cooling system, as shown in Figure 4, is utilized in the design to reduce cooling requirements and allow additional air needed for emissions and exit temperature profile control.

The diffuser/combustor case is designed to carry the high pressure loads. The outer case includes 24 openings and boss regions for mounting the clustered fuel nozzle assemblies consisting of one pilot zone nozzle and two main zone nozzles. A dual fuel manifold and transfer valve system supplies fuel independently to the two combustion zones. A bleed manifold is also included on the outer case to supply pre-diffuser discharge air for low power customer bleed and for turbine active clearance control during takeoff and climb-out.

3.1.6 Turbines

The turbine section consists of an air-cooled single-stage high-pressure turbine and an uncooled four-stage low-pressure turbine. An intermediate case section, which serves as a flowpath transition between turbines, contains the rear rotor support frame. A turbine exhaust case assembly de-swirls the discharge flow and carries various loads at the rear of the section.

The high-pressure turbine is designed for high efficiency with high rim speed and a large flowpath annulus area. Vanes and blades are two-piece designs made of coated, single crystal nickel alloys. The turbine disk, according to plan, will be made from an advanced powder metallurgy material. The case assembly includes a ceramic outer air seal and internal active clearance control system.

Twenty-four long-chord vanes with S-shaped outer platform cross-sections are designed with double internal ribs, showerhead cooling of the leading edges, and full-pedestal trailing edge coolant discharge. Film cooling of the pressure wall and forward suction surface of the airfoils is augmented with internal impingement cooling throughout the airfoils. The coolant air is supplied to the inside of the vanes through both the inner and the outer platforms.

Considerable attention was paid to reducing vane region leakage in the design details. The vanes are individually restrained at both ends to allow the use of low-leak, full-ring, flexible metal seals at the attachments. Chordal cuts on the vane attachments eliminate a leakage path around the vane buttresses as the vanes tilt from differential inner and outer diameter axial thermal growth. Improved feather seals are used between vane platforms. Vane support rails are to be machined at assembly to avoid steps and attendant leakage paths. Finally, the overall design concept is one of minimizing the number of gaps through the vane section which can produce air leaks.

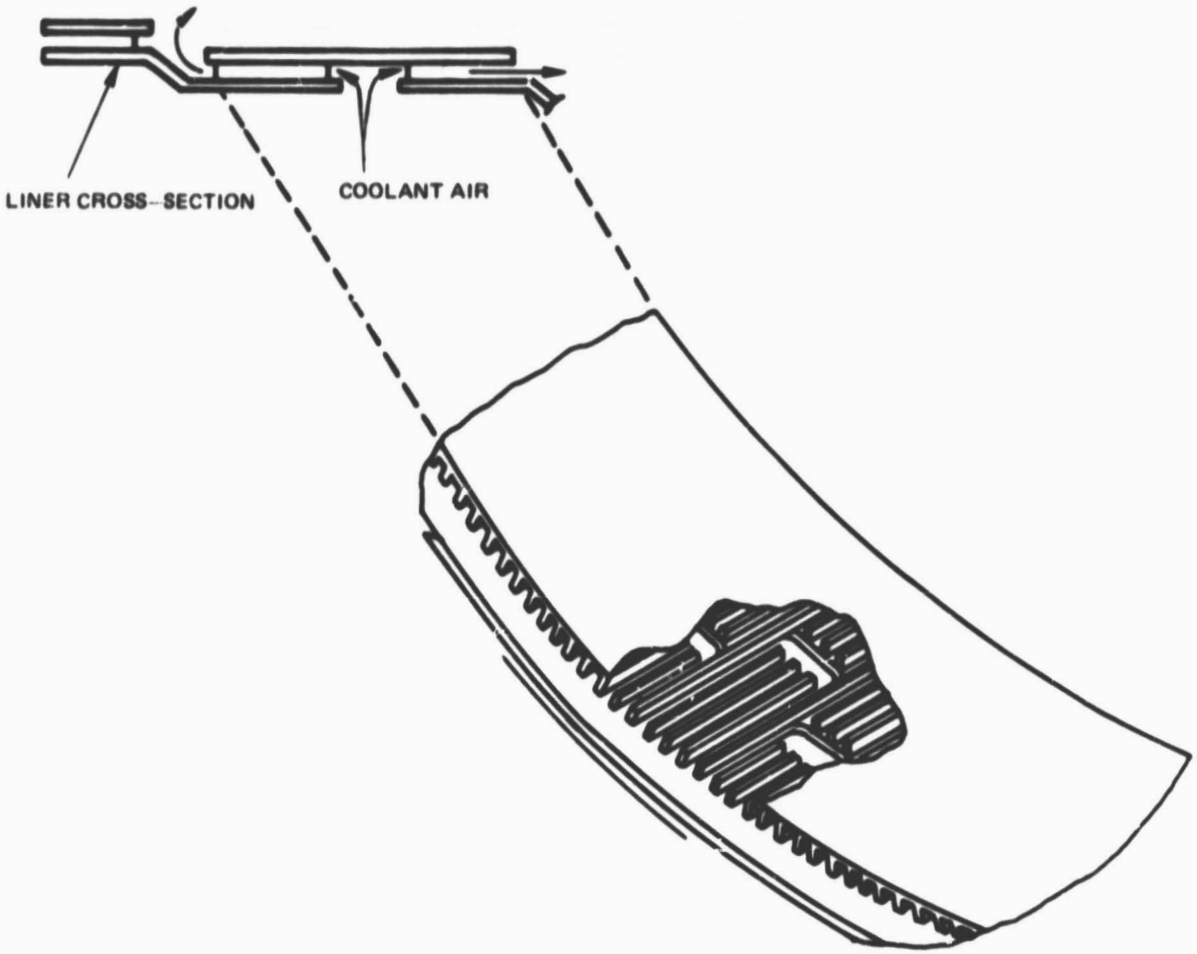

Figure 4 Double-Walled Combustor Liner With Advanced Counter-Parallel FINWALL® Cooling System

Fifty-four blades accelerate flow from a relative Mach number of approximately 0.23 at the inlet to over 1.2 at the trailing edge, and thereby produce the high work output required to drive the high-pressure compressor rotor. The blade leading edge is twisted 42 degrees from the root to tip. The trailing edge angle is within $\pm$ one degree of being constant at all radii.

Because of the maximum rim speed of 530 m/sec (1730 ft/sec) with this design, special attention was paid to blade construction and internal cooling path geometry. The selected blade configuration, shown in Figure 5, is cast in two halves and bonded at the leading and trailing edge sections and along the ribs of the multipass internal cooling system. Front cavity air cools the leading edge section internally and is ejected through showerhead holes along the leading edge of the airfoil. Additional cooling air flows into the second cavity and traverses the length of the blade twice before exiting through a pedestal array in the trailing edge region. Internal trip strips are used to promote turbulance for increased heat transfer effectiveness. An abrasive tip cap is bonded to the blade halves to wear into the abradable ceramic outer air seal when rubs occur. Blade centrifugal loads are distributed over four teeth in the "firtree" attachment design.

The high speed disk assembly includes full-ring sideplates, which are attached to the disk with low windage bolts and nuts to seal off the disk broach regions. High windage protrusions are either avoided or shielded along the entire disk surface. Cooling air is supplied to the blade root through supply holes angled outward through the disk.

Case assembly design features include a ceramic outer air seal and internal active clearance control. Thirty-four zirconium oxide graded ceramic seal segments are retained by front and rear full ring supports. An active clearance control manifold between the two rings is supplied by either combustor pre-diffuser air (during takeoff) or mid-compressor air (during cruise) which is then impinged on the outer air seal support rings to control their temperature and degree of thermal stretch. Separate cooling air is routed around the manifold to impingement cool the backing plates of the outer air seals. The case is designed for the high pressure loads, the 593°C (1100°F) temperature environment, and the cyclic loads imposed on the case flanges and outer air seal support ring case hooks.

The four-stage low-pressure turbine counter-rotates relative to the high-pressure turbine. Uncooled vanes and blades are designed for low through-flow velocities in a large annulus area flowpath. The rotor stack is supported by front and rear hubs. The case system includes internal active clearance control for tighter blade tip clearances during cruise.

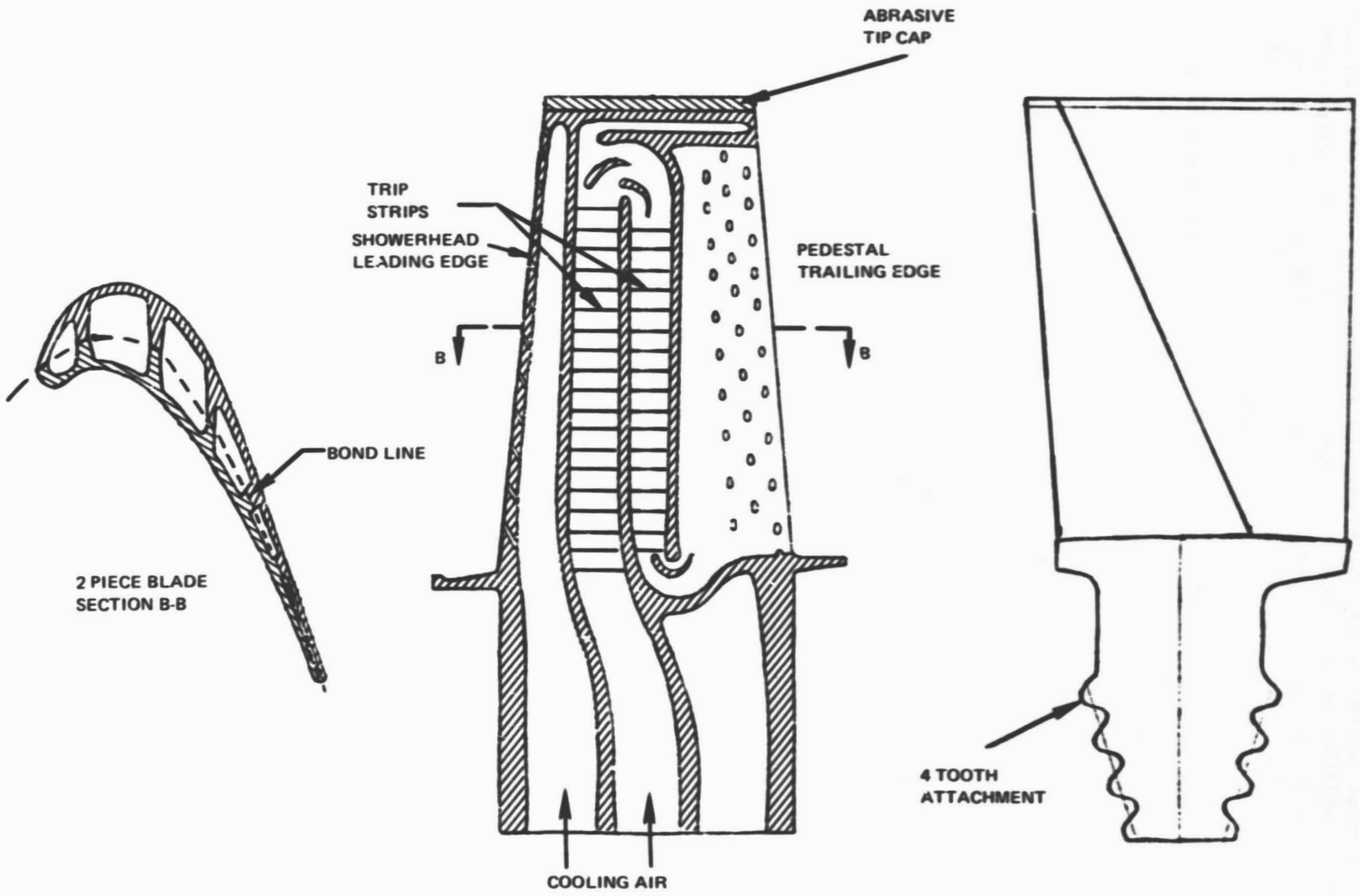

Figure 5 High-Pressure Turbine Blade Configuration Showing Two-Piece Fabrication and Cooling System

The low-pressure turbine first-stage vanes are of a high temperature single crystal nickel alloy to eliminate the need for airfoil cooling air. The remainder of the vane rows are of a conventional low-pressure turbine cast nickel base alloy (INCONEL®713C). The first-stage vanes are cambered only 13 degrees in contrast to the 100 degrees required for turning with co-rotation of the two rotors.

The low-pressure turbine blades operate at relative Mach numbers up to 0.76. Conventional tip shroud dampers with two knife-edge seals are included on all stages. The inner blade platforms are extended beneath the adjacent vane platforms to form flow guides which channel the flow more uniformly for increased efficiency. The first-stage blades are of directionally solidified nickel alloy for strength at higher temperatures. The next two rows are of INCONEL 713C. The last row is of an advanced, high-creep-strength titanium-aluminide material, with one-half the density of INCONEL 713C, for light weight.

The single backbone bolted rotor construction consists of high strength, powder metallurgy nickel alloy disks separated by three INCOLOY®901 wrought nickel alloy spacers. A front knife-edge seal appendage is bolted to the front disk to seal off the inner cavity. Two INCOLOY 901 hubs bonded to the front and rear disks provide axial stiffening of the rotor and form a plenum for disk and spacer cooling air. The front hub is designed to be splined onto the end of the rotor shaft for engine assembly.

The spacer and disk arrangement controls leakage. Full ring, wide channel seals were selected for the three spacers. Radial appendages at the rear of the spacers are designed as thermal shields which separate inner cavity air from hub plenum coolant air used to more precisely control disk rim region temperatures.

The outer turbine case, in addition to being a one-piece pressure vessel, is designed to support the vanes and outer air seals, support the turbine exhaust case, provide active clearance control, and provide blade containment. Cooling air bled from the compressor is passed between double case walls to cool the outer cavity region structure and control the diameter of the segmented outer air seals. The air is exhausted into various places along the main flowpath, as shown on Figure 6. A different source of compressor air is used for takeoff than for cruise to provide the correct cooling effect as dictated by individual clearance requirements.

The turbine intermediate case structure supports the rear of the high-pressure rotor and low-pressure turbine, carries service lines across the flowpath, and serves as the rear engine mount structure to carry vertical, torsional, and side loads through links connected to the pylon structure. The inner box, the 14 equally spaced support struts, and the outer polygonal case design, are all of INCONEL 718 cast nickel base alloy. The struts are cooled with air bled from the

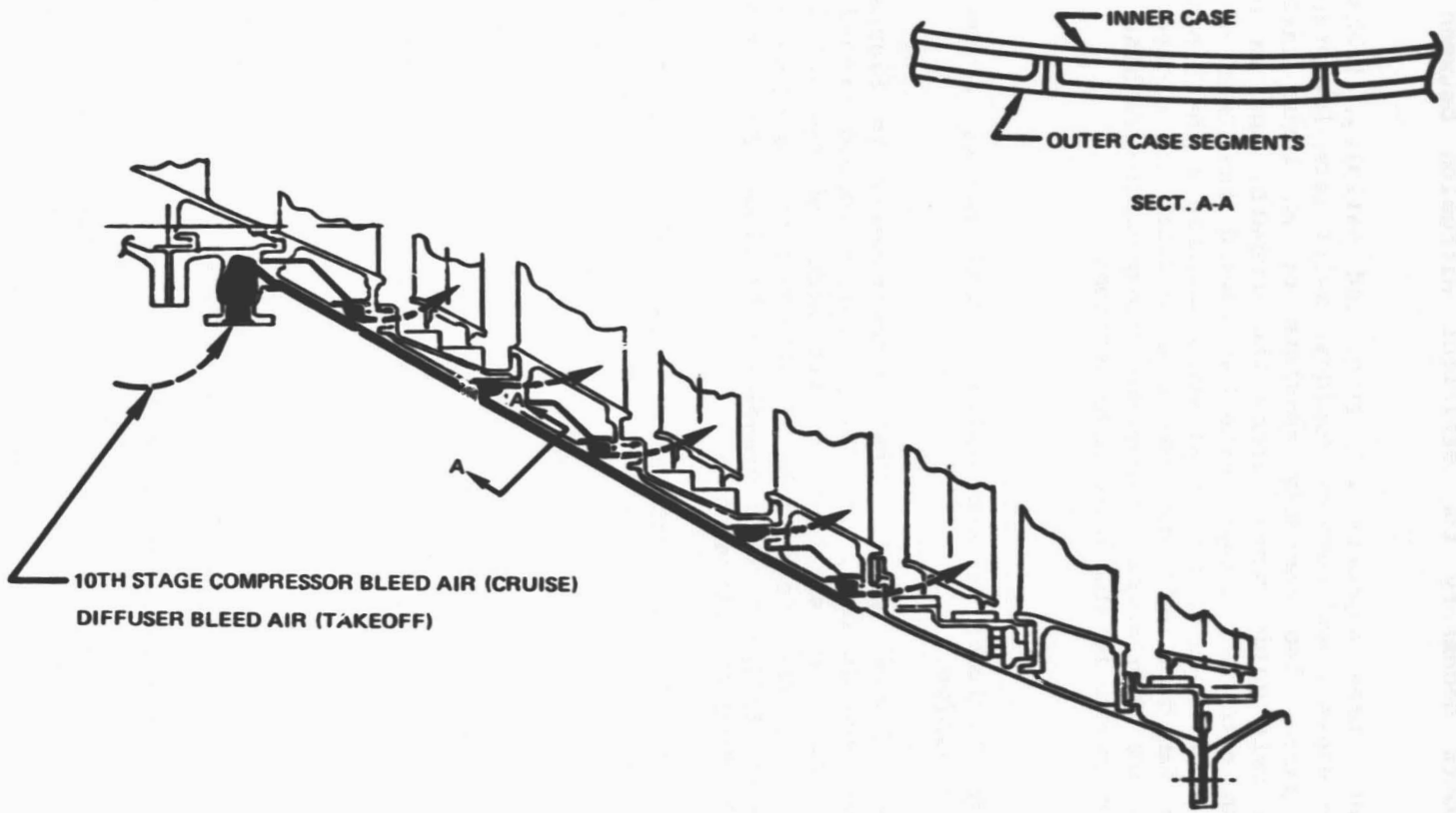

Figure 6 Low-Pressure Turbine Active Clearance Control System Utilizing Double Walled Case Construction

J20127-5
R780412

high-pressure compressor and piped to the turbine section. Uncooled, single-crystal alloy strut fairings and transistion ducting provide the aerodynamic contours necessary for efficient diffusion between the turbines.

The turbine exhaust case supports the mixer and tailplug, transfers cowl loads to the engine, and removes residual swirl from low-pressure turbine exhaust gases. The assembly consists of an inner tailplug support ring, 24 exit guide vanes across the gaspath, and an outer circular ring. An external flange, situated toward the rear of the case, supports a load transfer ring that seats against a "hat" section ring on the inner fan duct wall when the nacelle doors are closed. The transferred loads are then carried along the low-pressure turbine case to the mount links in the intermediate case section.

3.1.7 Mixer

The mixer section includes a convoluted forced mixer, a central tailplug, and the tailpipe.

The titanium alloy forced mixer, shown isometrically in Figure 7, consists of twelve convolutions, or lobes, equally spaced around the circumference. Cut-outs, or scallops, on the sides of the lobes are used to enhance mixing. Each inner lobe is attached to a support strut which connects to the tailplug. Free-standing outer lobes have external titanium shrouds to damp out vibration.

The tailplug is made of high temperature nickel alloy in the front section and of lighter titanium in the cooler rear section, aft of the mixer. The plug is acoustically treated over a half of its length with turbine tone-matched porous plate brazed to a honeycomb substructure.

The acoustically treated tailpipe is designed to a length-to-diameter ratio of only 0.5, which is about 30 percent shorter than in current technology mixed-flow exhaust systems. The short mixing length, in combination with the high mixing efficiency goal of 85 percent, represents a major aerodynamic design challenge.

3.1.8 Nacelle

The nacelle system consists of an inlet section, fan case cowling, a D-shaped duct mid-section, and the exhaust system, as shown in Figure 8.

The inlet section is bolted directly to the fan case front flange to eliminate flowpath steps or gaps near the fan front face. The inlet is designed for a maximum throat Mach number of 0.77. The inlet length is sufficient to allow internal acoustic treatment over a length equal to one-half the fan face diameter. The inlet is drooped three degrees from the engine centerline to account for in-flight aircraft angle-of-attack. The inlet is constructed of an aluminum lip, aluminum honeycomb

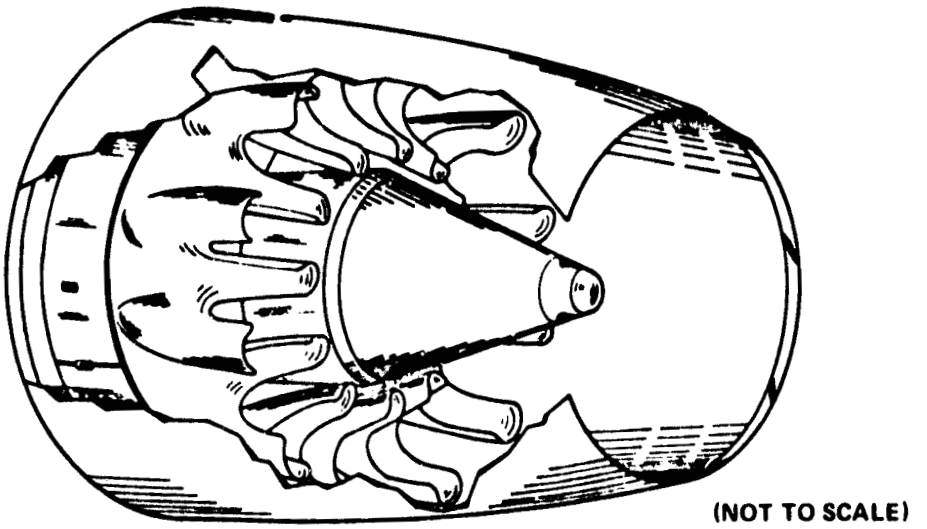

Figure 7 Isometric Drawing of Energy Efficient Engine Mixer

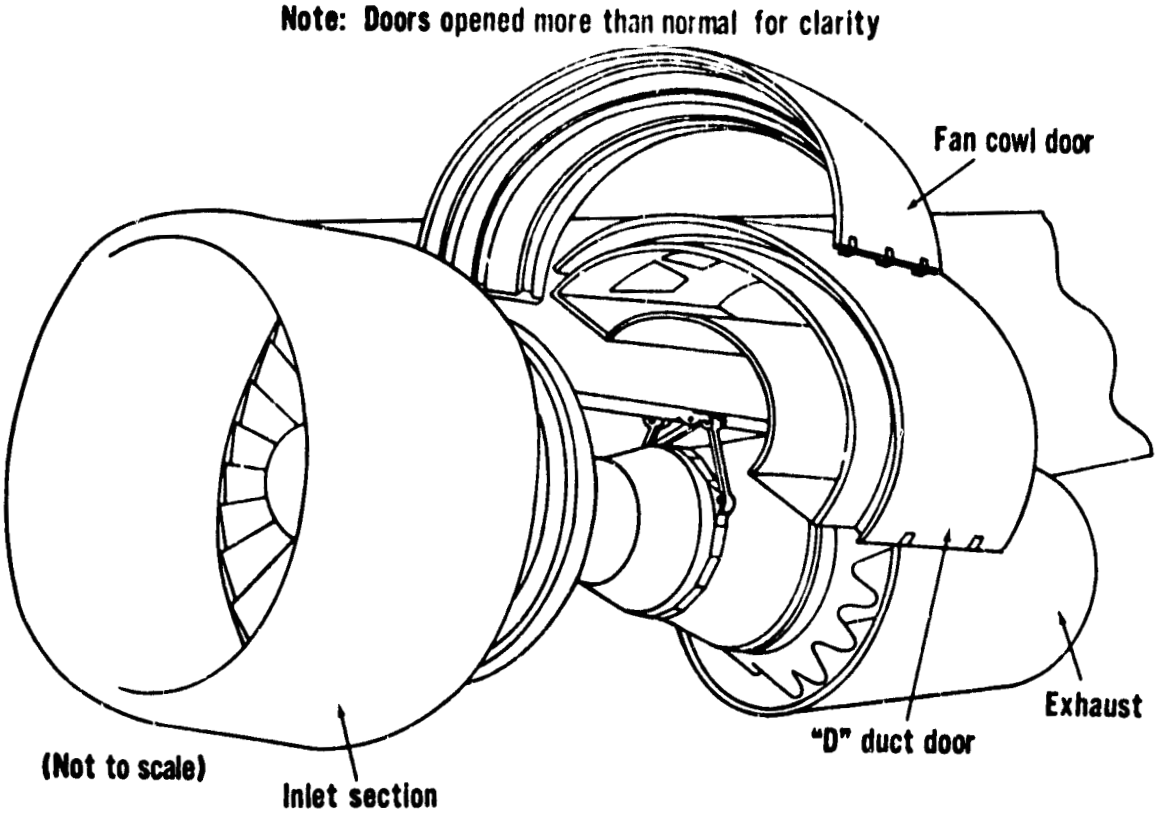

Figure 8 Pylon Mounted Nacelle Schematic Showing Open Doors

and graphite/KEVLAR fabric outer skin, and fan tone matched acoustic lining followed by deeper "buzzsaw" treatment on the inside surface. The design includes inlet lip anti-icing provisions.

The fan cowling section consists of two doors which are hinged from the pylon and latched at three locations along the bottom of the nacelle. These doors provide access to the electronic fuel control, the thrust reverser air motors, the air lines, the jack-shaft drive units, and the oil tank. As in the inlet, aluminum honeycomb with graphite/KEVLAR fabric skin is used in the doors for weight saving purposes.

The mid-section of the nacelle is made up of two large D-shaped semi-circular structural doors, each consisting of inner and outer duct walls and outer skins tied together with webs at the top and bottom of the engine. Contained within the two sections are the carbon/epoxy reverser cascades, duct blocker doors, and translating cascade covers which remain with the doors as they are opened and closed. The doors provide full access to the rear of the fan and lower service lines, the core mounted full duty gearbox and accessories, the compressor, the combustor, and the turbines.

Cammed upper hinges transfer the weight of the doors from the engine to the pylon as the doors are opened. In the closed position the doors are structurally isolated from the pylon to avoid redundant, indeterminate load paths. The doors are latched together across a web section at the bottom to engage structural V-shaped groove connectors between the door and compressor intermediate case; the doors then provide an unbroken load path needed for cowl load sharing. A hat-shaped section ring is attached to the extreme rear of the inner duct walls to transfer the cowl loads to the load transfer ring attached to the turbine exhaust case, through the low-pressure turbine case, and to the rear mount links.

To eliminate leakage, the exhaust system was designed as a one-piece unit. The system is suspended on rollers which run in a track in the aft pylon. It is axially restrained by V-shaped grooves which mate with the D-shaped duct doors. The exhaust system is translated rearward to expose the mixer and tailplug.

To remove the engine, the fan cowl doors are opened first followed by the D-shaped duct doors. The exhaust case can then be translated aft to allow the engine and inlet to be lowered vertically from the nacelle.

3.1.9 Advanced Material Applications

Advanced metal alloys are used in the rotor systems and support structures to withstand the high rotation speeds, high pressure, and high temperatures encountered in the engine. A brief summary of five key advanced materials and their associated benefits is presented below.

An advanced, heat treatable, high strength, nickel base alloy utilizing powder metallurgy (MERL 80) is used in the high-pressure turbine, the rear high-pressure compressor disks, and the other rotating, hot parts because of its high strength-to-density ratio and superior tensile and low cycle fatigue capabilities. An advanced, high-strength titanium material (MERL 130) is used in compressor disks operating below 480°C (900°F).

Titanium-aluminide (MERL 101), a high creep strength wrought alloy, is used in the lightly stressed last turbine blade row, turbine exhaust case, and mixer support struts, to reduce engine weight.

Cast, heat treatable nickel base alloys with no grain boundaries (MERL 200/220) are used in the high-pressure turbine airfoils, the turbine intermediate case fairings, and low-pressure turbine inlet vanes to reduce cooling air requirements. This material increases the allowable metal temperature by up to 95°C (175°F) over presently used alloys.

All of the above materials are expected to be available for use in the flight propulsion system by the late 1980's. The Energy Efficient Engine experimental hardware is expected to use currently available, substitute materials that provide adequate life for testing the hardware and which are functionally representative of the ultimate flight engine design.

3.1.10 Clearance Control

The principal clearance control design objective of the Energy Efficient Engine is to achieve very tight cruise running clearances while precluding rubs of rotating parts on adjacent stationary structures during engine operation normally encountered in commercial service. The preliminary design contains many features, including straddle mounting of the high spool rotor, optimal three bearing support of the low spool rotor, location mounts, structural integration of the nacelle and engine, and active clearance control, all directed towards meeting the tight clearance objective. Adjacent rotor and case materials have also been carefully selected for thermal response compatibility.

Straddle-mounting of the short, stiff, high-spool rotor, by locating the two mainshaft bearings just fore and aft of the front and rear stages, is intended to eliminate large overhung masses that can create large radial rotor deflections during flight maneuvers. The centralization of the masses between and near the support structure causes the cases and the rotors to deflect in more similar fashions under normally encountered flight loads.

Straddle-mounting of the low spool rotor components would require four bearings, and two additional bearing compartments. The design choice of three bearings in the two compartments utilizing the same support

structure as the high rotor bearings evolved from examination of the various possibilities and their effects on clearances. The fan and low-pressure compressor are overhung from two widely-spaced bearings to provide a firm wheel base. The low-pressure compressor is centered between the bearings to further control rotor deflections. The rear bearing is positioned beneath the two shorter front low-pressure turbine stages where clearances have a more significant effect on efficiency than with the longer rear stages.

Mount links are positioned to transmit loads directly to the pylon structure. Thrust links are attached to the compressor intermediate case at the horizontal centerline of the engine to be in line with the engine produced thrust. Two rear mount links, which carry vertical loads, are connected to the turbine intermediate case 25 degrees above the horizontal centerline to minimize the ovalization tendencies in the turbine case (see Figure 9).

The nacelle's major load sharing function is to transmit inlet cowl moments and other aerodynamic loads through the fan ducts to the turbine exhaust case and out to the pylon strut through the rear mount links. Since the inlet is bolted directly to the fan case, inlet loads are divided between the fan ducts and the engine cases. The larger diameter, stiffer fan ducts are designed to carry up to 80 percent of the total load to substantially reduce engine deflections in the fan region.

The active clearance control system, shown schematically in Figure 10, is used to control clearance in the rear of the high-pressure compressor, in the high-pressure turbine, and in the front two stages of the low-pressure turbine. The active clearance control uses external fan air impingement tubes on the compressor and a dual manifold compressor air feed system to supply the turbines with different cooling air between takeoff and cruise. Electrically actuated, solenoid air valves are used to control air flow. The fan air valve, a simple two position device, is opened in response to an electronic control signal that indicates altitudes above 6720 m (22,000 ft) cruise operation. The valve is designed to be loaded in the closed position so that the compressor case remains uncooled in the event of a system malfunction. A three-way valve is used to route cooling air from either of the two manifolds feeding the turbines. In the event of system malfunction, the valve is designed to feed hotter takeoff manifold air continuously to the turbine throughout the mission. Cruise performance benefits of active clearance control are temporarily lost but rubs during takeoff and climb-out are avoided.

Analysis of the preliminary design, using an analyical model that accounted for all clearance control features, resulted in takeoff and cruise clearances that were satisfactory, except for the last two low-pressure turbine stages which exceed the blade tip clearance goal by 0.112 cm (0.044 in). Rear stage outer airseal modifications will be examined during detailed design to achieve the required tighter running clearances.

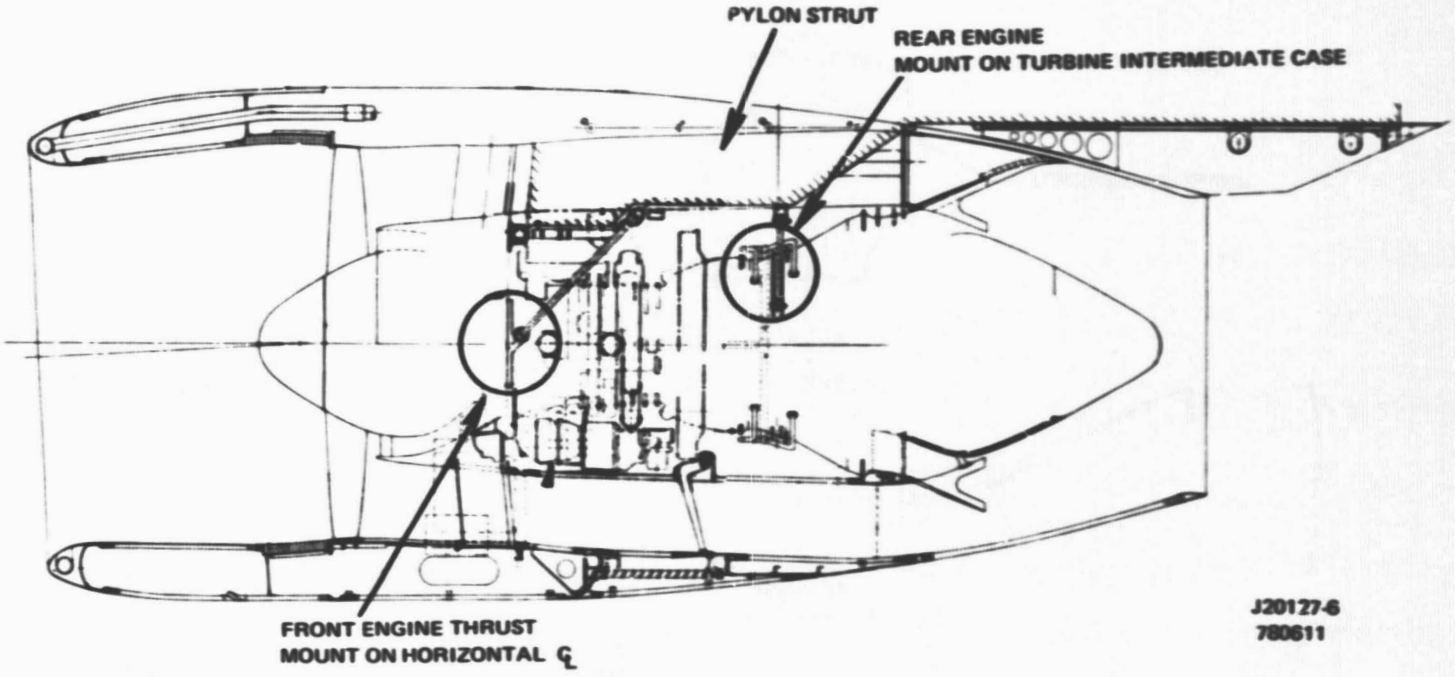

Figure 9 Engine Mount System Cross-Section Illustrating Locations and Links

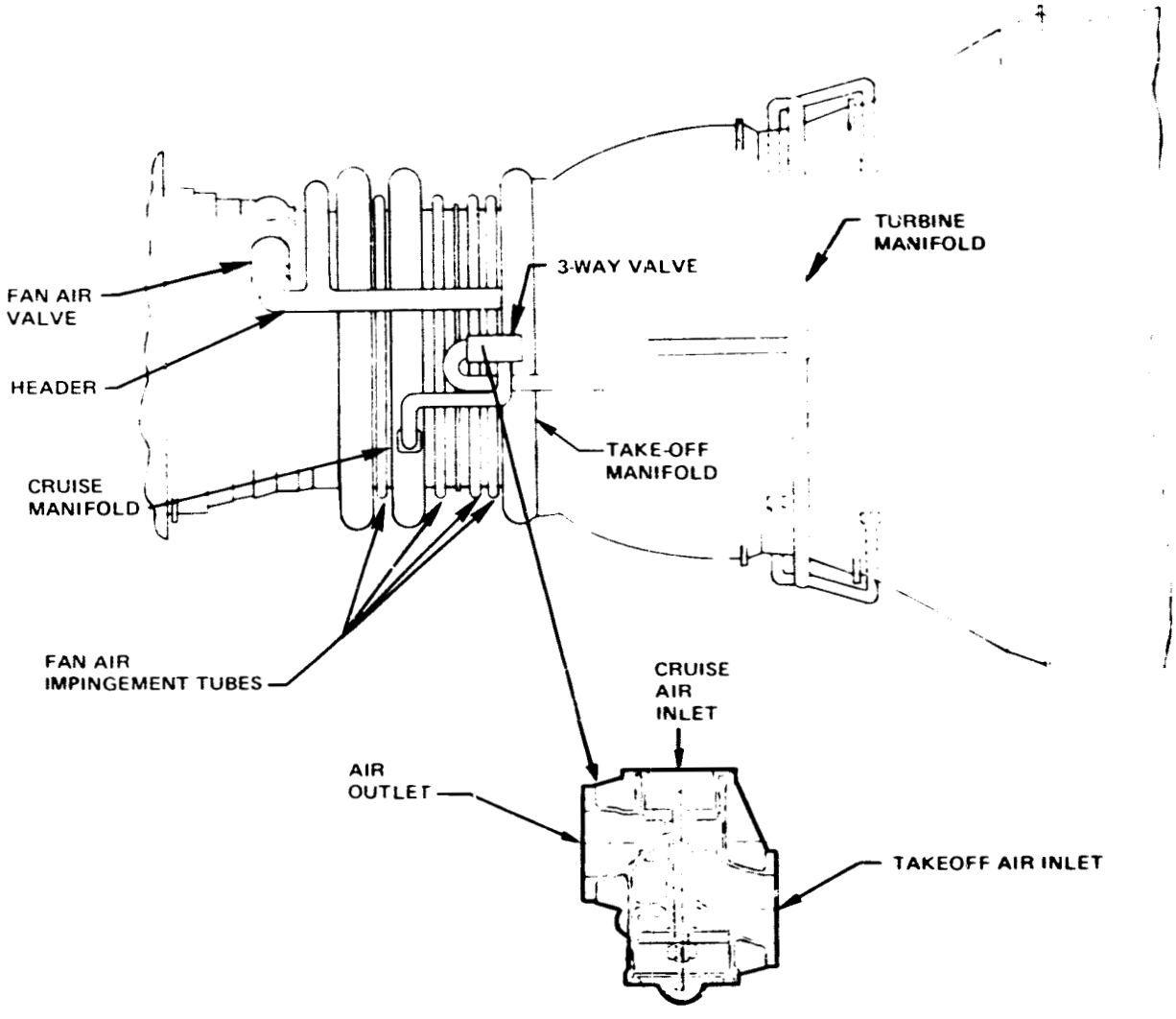

Figure 10 Active Clearance Control System Schematic Illustrating External Tubes and Valves

3.1.11 Performance Retention Features

A major design objective is to minimize in-service performance deterioration from clearance increases caused by internal engine rubs and from gaspath parts erosion. These two deterioration modes are believed to be the principal causes for current in-service degradation.

Many of the design features to control clearances are expected to reduce performance deterioration from clearance increases. For example, the stiff rotors and cases and load sharing nacelle will reduce deflections and rubs under severe maneuver loads. With the use of abradable rub strips over abrasive blade tips, interactions between the tips and seals result only in a local region of clearance increase and the blade tip diameter and clearance over a large percentage of the circumference remains unchanged. Therefore, the preferential wear characteristics of the abradable seal system minimizes clearance deterioration during severe airplane maneuvers, case ovalization, and other operational conditions which may cause blade-to-seal interaction.

Performance retention of compressor airfoils is also addressed in the engine design with increased durability airfoil shapes and erosion resistant coatings. Thicker leading edges are used in the high-pressure compressor for their increased tolerance to foreign objects. The use of erosion resistant coatings on the compressor blades can result in more durable, smoother airfoils. A double-edged benefit, first a higher Reynolds number (smoothness) for increased efficiency, and second, reduced wear of the airfoils by erosive particles, can be realized with these coatings. For the Energy Efficient Engine compressors, several coatings are being considered, including plasma applied coatings, laser glazing, and spray-on coatings, to achieve the desired hardness and durability for erosion resistance.

Performance analysis of the engine indicates a long-time (1000 cycles) TSFC deterioration rate, approximately one-half that of the JT9D (see Section 3.2.3 for additional discussion).

3.1.12 Rotor Vibration Control

High strain energy rotor vibrational modes are well above redline rotor RPM's with the stiff, lightweight rotors. Lower energy high spool rotor vibration modes were forced below idle RPM with the incorporation of a front support spring and a rear support oil film damper.

An analytical model of the engine, based on a system of masses, springs, and dampers, was used to analyze dynamic behavior of the rotors. Exercise of this model to rotor inbalance response identified the need to reduce the spring rate of the front high-spool rotor support frame in order to drive low energy bounce and pitch vibration modes below idle RPM. A mechanical spring arrangement, shown in Figure 11, is inserted between the front bearing outer race and compressor intermediate case to provide the needed structural "softening".

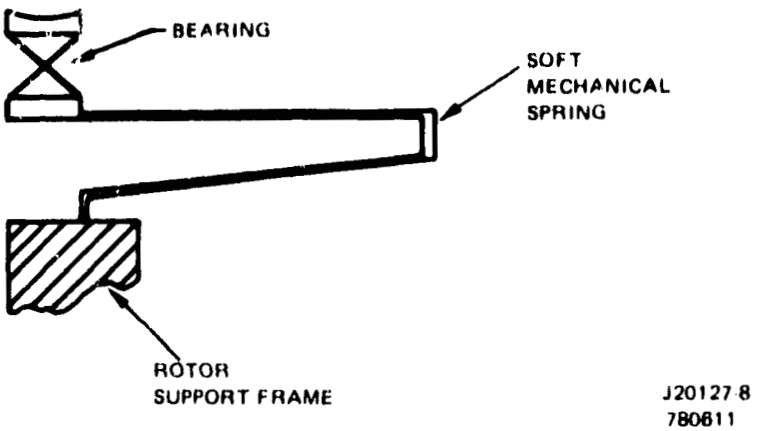

Figure 11 Schematic of High Rotor Front Support Spring Used to "Soften" Front Support

An oil film viscous damper is included under the outer race of the high spool rear bearing to limit rotor whirl deflection to acceptable levels. With the addition of the mechanical spring and oil film damper, the engine has both acceptable rotor deflections and acceptable bearing loads.

3.1.13 Mainshaft Bearings and Seals

Five mainshaft bearings and six main seals are contained within the two bearing compartments, as shown on Figure 12. Lube oil is fed to the compartments in oil lines which pass through the intermediate case struts. A conventional oil scavenge system to the gearbox and oil tank is used. A fuel/oil heat exchanger provides sufficient oil cooling without requiring an auxiliary air/oil cooler. Compartment buffer/breather air is bled-off the inner flowpath wall aft of the compressor intermediate case struts, leaked past the seals into the compartments, and discharged through rotating de-oilers into the low spool shaft and out of a center vent tube in the tailplug. A tube between the third high-pressure compressor stage disk bore and the high-pressure turbine disk hub provides an annular passage from the bleed port to the rear bearing compartment.

The low rotor support bearings are state-of-the-art designs. The two high rotor support bearings (No. 3 and No. 4) represent advancements in the state-of-the-art in terms of DN (race diameter times RPM) with design maximums of 2.3×10^6 mm x RPM. The high DN levels are required to provide a large inner shaft cavity to internally accommodate a low speed shaft having adequate critical speed margin and acceptable spline stresses.

The compartment sealing, breathing, and venting system design was selected over an all carbon seal, gearbox breather system on the basis of cost, weight, and operating safety. The selected system, which utilizes labyrinth, knife-edge seals at four locations and two dry-face carbon seals at the forward and aft locations, includes a center vent breather system for its improved seal pressure margin in preventing oil weepage past the seals at idle and windmilling engine operation. The risk of internal compartment oil fires is reduced through the use of cool low-pressure compressor discharge air in the buffer/breather system instead of the normally used hotter mid high-pressure compressor air.

3.1.14 Secondary Flow System

The secondary flow system channels the airbleed used for component cooling, bearing compartment breathing, service bleeds, active clearance control and rotor thrust balance. Three highlight features of the Energy Efficient Engine system are the high-pressure turbine blade cooling supply system, a mid-engine seal used to provide high spool thrust balance, and a flow separator between the high-pressure turbine disk and intermediate case. (See Figure 13).

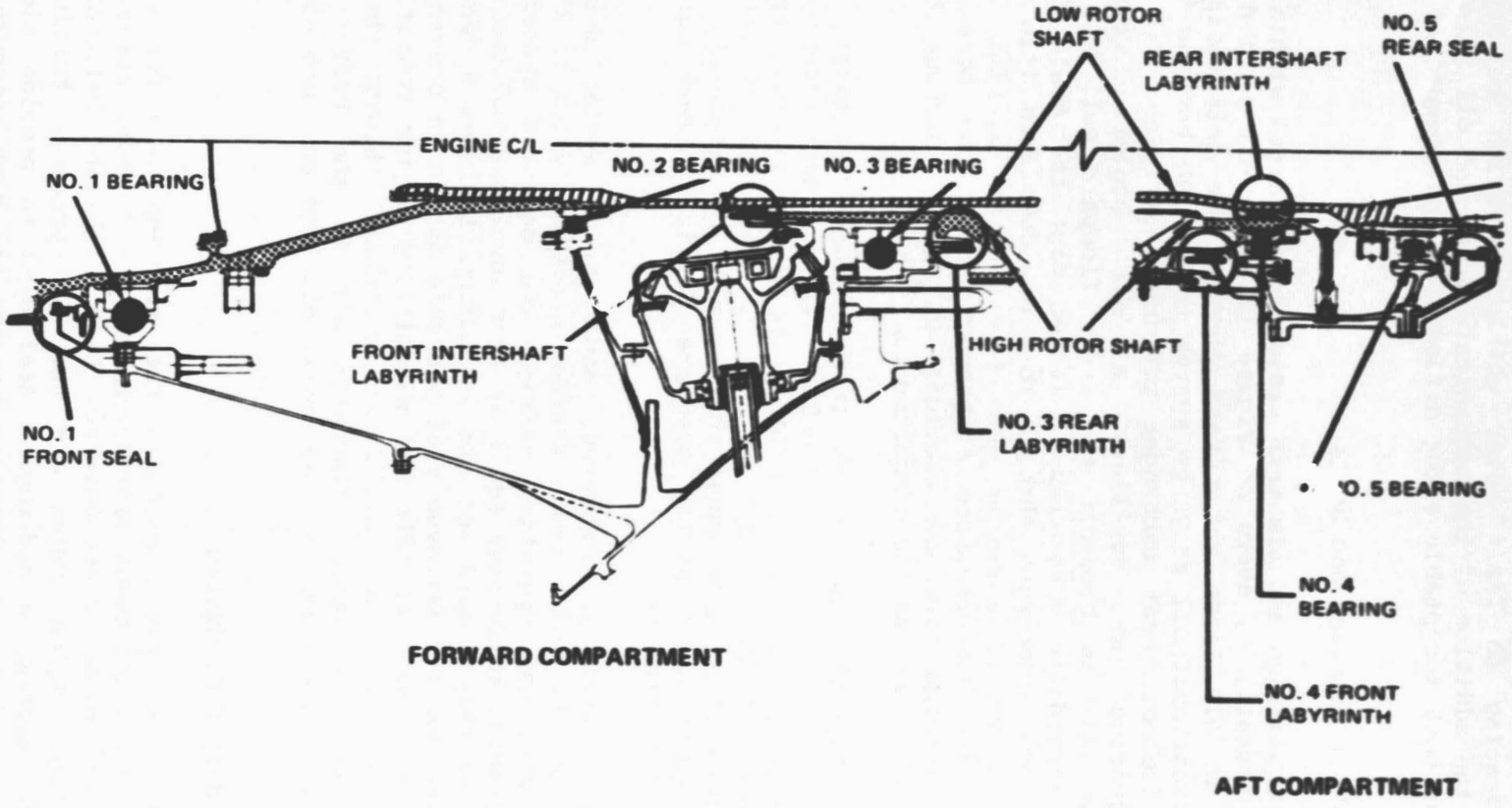

Figure 12 Mainshaft Bearings and Seals Illustrating Forward and Aft Compartment Arrangements

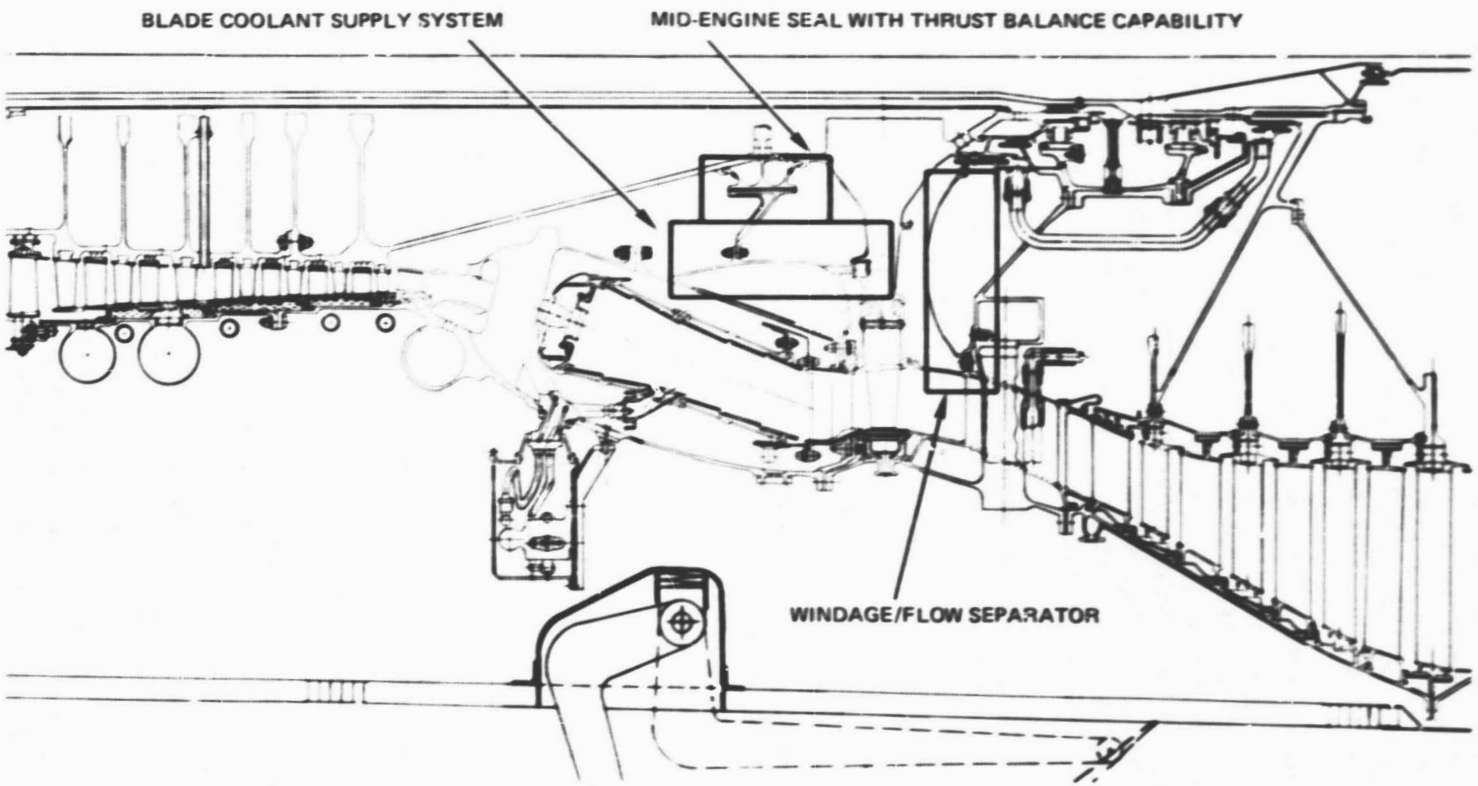

Figure 13 Three Secondary Flow System Features

"Tangential on-board injection" (TOBI) nozzles are used to preswirl the high-pressure turbine blade cooling air up to wheel speed at the inlets to the disk feed holes. The energy required, and the resulting increase in cooling air temperature to circumferentially accelerate the air, is thereby eliminated. The supply pressure in the inner cavity in front of the turbine disk is balanced with the gaspath to eliminate the need for a large seal outboard of the TOBI nozzles.

Pressure differential across the mid-engine seal is used to control the thrust bearing load that exists when all the axial pressure forces are considered along the rotor system. By shifting the seal radially to change the projected area, the pressure force can be altered to adjust the resultant high rotor thrust bearing load. The present seal location limits the No.3 ball bearing thrust load to 31,100 N (7,000 lb) which is well within acceptable limits. Low-rotor ball bearing loads are sufficiently low to preclude the need for thrust load adjustment.

A diaphram-type flow separator is attached to the turbine intermediate case to isolate disk cooling air from the low-pressure turbine coolant. The disk region air is lowered in pressure by two knife-edge seals in order to control the leakage rate into the gaspath through the seal aft of the blade. The higher pressure air aft of the separator is leaked back into the gaspath downstream, where the pressure level is higher because of intermediate case section diffusion. The separator is also useful in controlling the inner air cavity volume behind the high-pressure turbine disk to reduce disk windage to a minimum.

3.1.15 Electronic Fuel Control

The flight engine control system is based on a single-channel full authority digital control, vibration isolation mounted on the fan case and air cooled. The control provides isochronous governing on low spool rotor speed with governing on high spool rotor speed at idle. Fuel flow management is by closed loop control of variable delivery pumps with solid state flowmeter feedback. Additional control functions are compressor stator vane actuation, control of valves for compressor and turbine clearance control, thrust reverse, and start and inter-compressor bleeds. Electronics implementation will be with large and very large scale integrated design chips. A number of the control inputs and outputs are defined as digital with optical signal transmission. Examples of optical inputs are: data link with aircraft, power lever input, compressor stator vane stagger angle, thrust reverser position, low rotor speed, turbine blade temperature, and turbine blade clearance. Control outputs will be digital, with modulated outputs effected by saturated high frequency drivers, pulse width modulated through Gallium Arsenide switches into dual solenoids or a torque motor. Discrete outputs will be low level electrical signals to remote Gallium Arsenide switches mounted on solenoids. The system concept and defined technologies were chosen to fulfill the requirements of an advanced commercial engine while minimizing control system cost and weight.

3.2 DESIGN GOALS AND CAPABILITIES

Studies conducted prior to the Energy Efficient Engine program identified promising, advanced, turbofan engine cycles and associated conceptual designs for use in advanced commercial subsonic aircraft. Engine capabilities were sufficiently established to allow generation of specific design goals for fuel consumption, operating economics, and environmental factors of noise and emissions. These design goals, while being reasonable, require the implementation of many technological advancements.

3.2.1 Fuel Consumption

The fuel consumption goal is to reduce installed cruise TSFC by at least 12 percent, relative to that of the JT9D-7A engine. The cruise condition is defined as Mach 0.8 and 10,668 m (35,000 ft) on a standard day at a maximum cruise power setting without customer bleed or power extraction.

Current performance predictions for the flight propulsion system indicate a 14.9 percent installed cruise TSFC reduction relative to the JT9D-7A, as shown on Figure 14. Projected improvements in the components account for approximately two-thirds of the TSFC reduction. The other one-third is provided by the 50 percent higher pressure ratio Energy Efficient Engine cycle, and by exhaust mixing. On the basis of these predictions, the ultimate flight propulsion system is assessed at having a greater than 99 percent probability of surpassing the 12 percent design goal.

3.2.2 Direct Operating Cost

The economic goal is at least a five percent reduction in direct operating cost (DOC) to the airlines. The DOC reduction is based on the performance of advanced aircraft equipped with the Energy Efficient Engine compared with the performance of the same aircraft, resized to provide the same operational capability, equipped with appropriately scaled JT9D-7A engines.

DOC predictions, incorporating economic ground rules universally applied to seven study aircraft, are shown in Figure 15. These trends encompass a Boeing 3,700 km (2,000 Naut. Mi.) range domestic twinjet, Douglas/Lockheed/Pratt & Whitney Aircraft 5,560 km (3,000 Naut. Mi.) range domestic trijets, a Douglas 10,190 km (5,500 Naut. Mi.) intercontinental range trijet, a Pratt & Whitney Aircraft 10,190 km (5,500 Naut. Mi.) intercontinental quadjet, and a Lockheed 12,040 km (6,500 Naut. Mi.) intercontinental quadjet. All airplanes show a design mission DOC reduction greater than the goal of five percent; all surpass the goal on typical missions except for the shortest range Boeing turbojet. Average DOC reductions are 8.6 percent on design missions and 7.7 percent on typical missions.

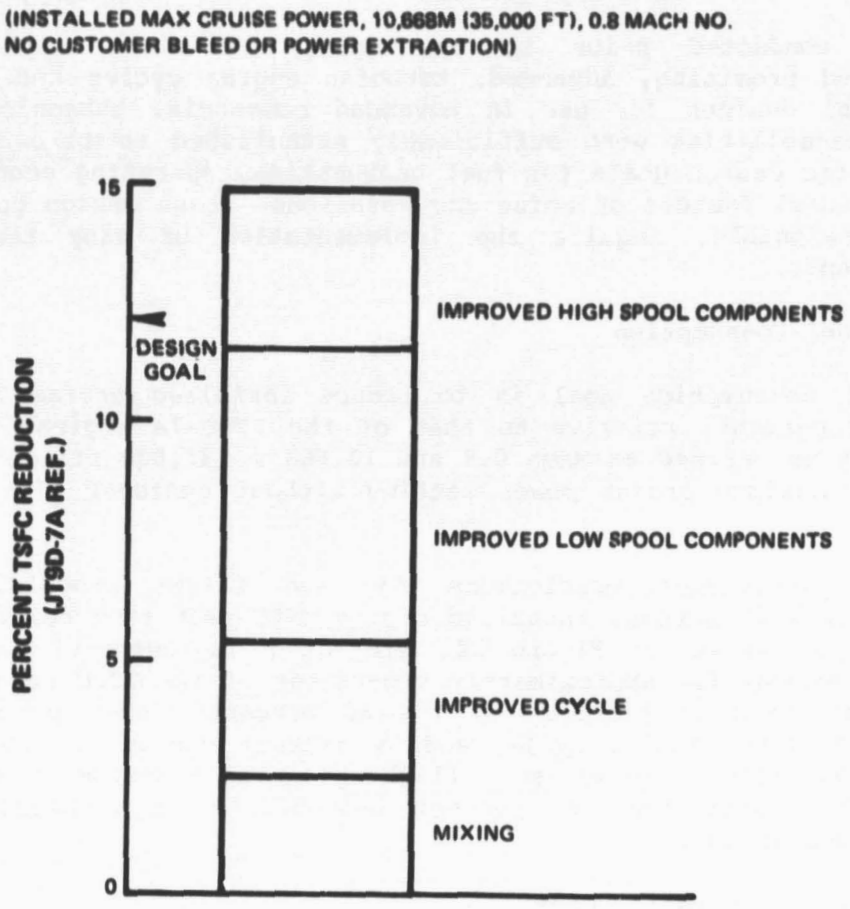

Figure 14 Major Technology Contributors to Achieve TSFC Design Goal

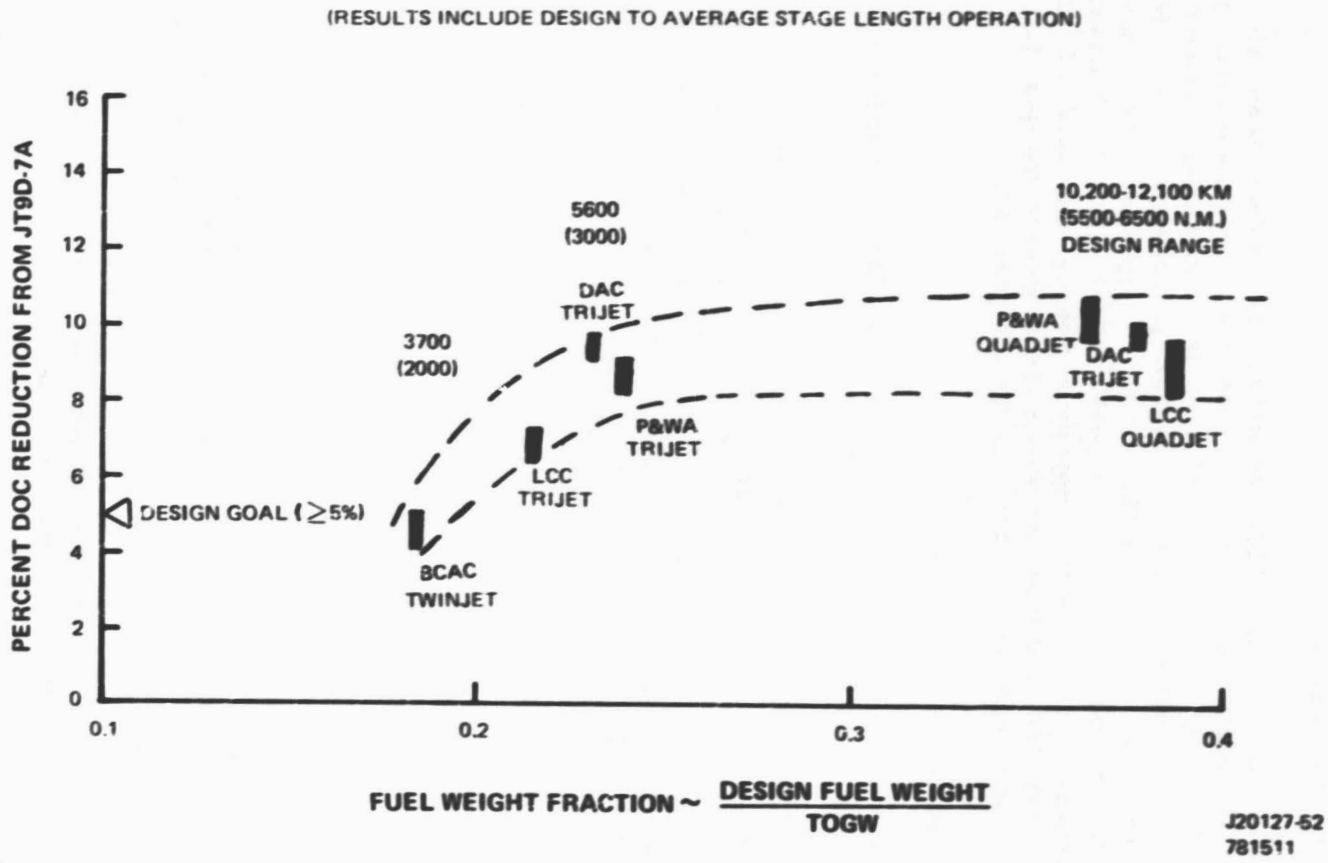

Figure 15 Direct Operating Cost Reduction Potential in Study Aircraft

The DOC reductions are principally a result of fuel burned reductions of 13 to 18 percent reflecting the TSFC reduction. Fuel prices of 10.5¢/l (40¢/gal) for the domestic aircraft and 11.9¢/l (45¢/gal) for the intercontinental range aircraft were assumed in converting the fuel burned data to fuel cost.

Using an average of the study results, a greater than 85 percent probability of surpassing the five percent DOC reduction goal is predicted. As fuel weight fraction is increased (longer range capability), fuel costs become a greater percentage of the DOC. For example, with the Boeing shorter range airplane, fuel costs are comparable to the cost of a three-member crew. In the longest range Lockheed aircraft, fuel costs represent nearly one-half of the DOC. The band of results includes missions from design ranges to average stage lengths and load factors from 55 to 100 percent.

3.2.3 Performance Deterioration

The performance deterioration goal is a TSFC deterioration rate reduction to one-half that of the JT9D-7A engine.

Operational JT9D engine condition monitoring, conducted under the NASA Engine Component Improvement Program, has indicated deterioration of performance early in-service. Approximately one-half of the 1000 cycle TSFC deterioration is believed to occur within the first 100 flight cycles. Major modes of early deterioration include increased running clearances from rubs, and turbine second vane distortion with attendant increased leakage. Over the longer term, at 1000 cycles, erosion of airfoils and rub strips, combined with additional tip clearance and turbine vane distortion, cause an additional performance loss.

Rotor-frame analysis of the Energy Efficient Engine indicates that the early deterioration is essentially eliminated with advanced design concepts, and that the JT9D-7 engine deterioration rate from 100 to 1000 cycles can be matched despite the higher pressure ratio cycle and smaller compressor blades that (1), increase sensitivity to tip clearances and airfoil surface roughness, and (2), increase the concentration of erosive particles in the gaspath (Figure 16). Therefore, the initial 14.9 percent Energy Efficient Engine TSFC advantage, which is based on a comparison of newly installed engines, should rapidly increase to over 16 percent for the major period of in-service operation.

To achieve this lower deterioration rate, four specific anti-deterioration objectives must be met:

1. Avoid rubs early in-service under "normal" gravitational, gyroscopic, cowl, and thrust loads

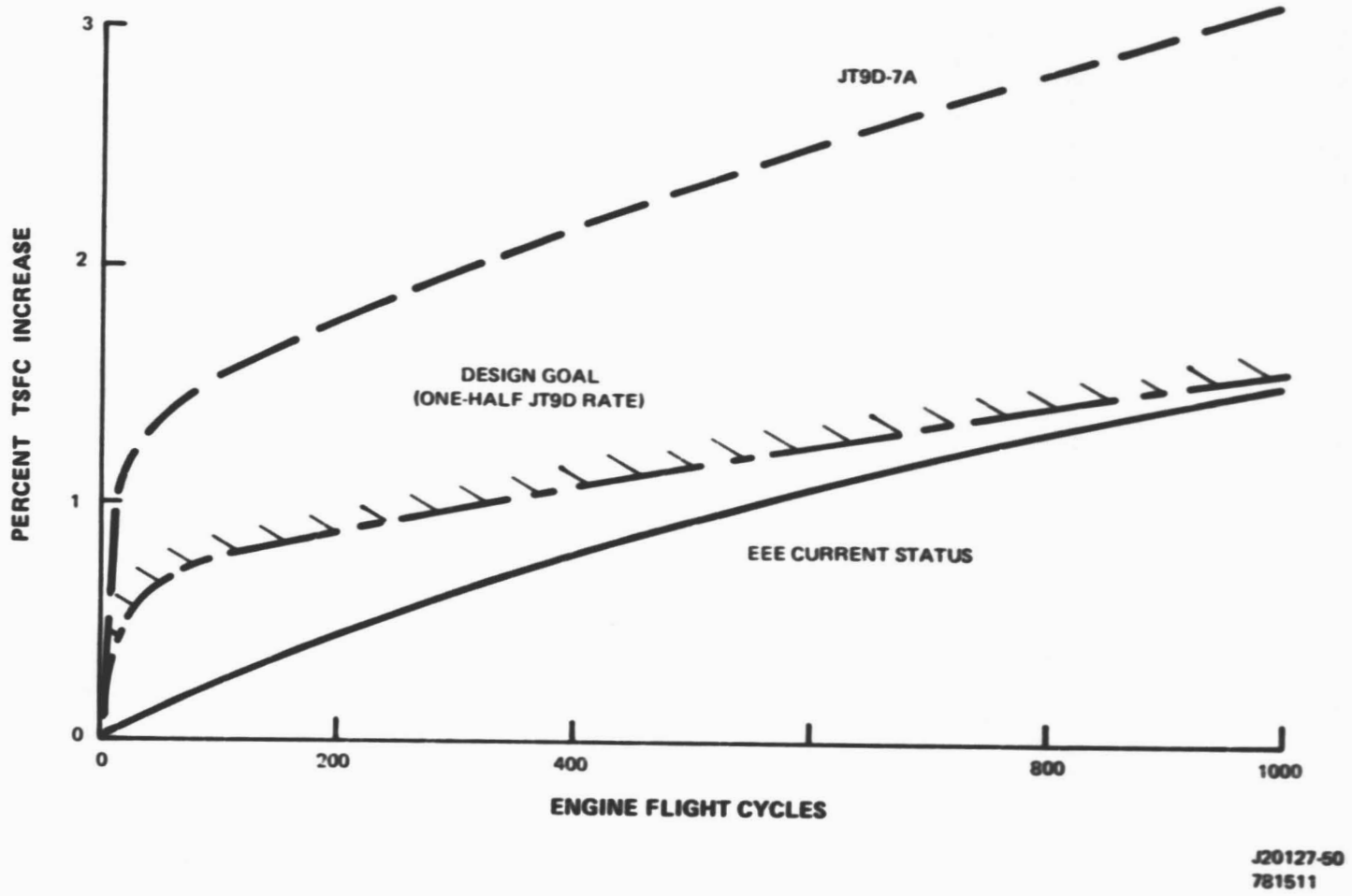

Figure 16 Thrust Specific Fuel Consumption Deterioration vs Design Goal

2. Provide sufficient structural stiffness to reduce by one-half, the radial clearance increases from rubs under "severe" flight loads

3. Assure prejudicial wear of rub strips instead of blade tips when rubs occur

4. Keep compressor airfoils smooth

The specific anti-deterioration design concepts and their relationship with these objectives are listed in Table 2.

When fully developed, these design concepts show promise for reversing the trend of increasing in-service performance deterioration evident with succeeding generations of jet engines.

3.2.4 Noise

The noise goal for the flight propulsion system is FAR - Part 36 (1978 rules) with provisions for engine thrust growth corresponding to future engine applications.

Current noise predictions for study aircraft systems of Boeing, Douglas, Lockheed, and Pratt & Whitney Aircraft are summarized, together with the limits at the three FAR noise measurement points in Figure 17.

Fan noise is the dominant propulsion noise constituent, despite the wide fan blading-to-exit guide vane spacing, fully lined inlet walls, and long, acoustically treated fan exhaust duct. The Energy Efficient Engine is predicted to meet FAR-Part 36 (1978) noise limits in six of the seven study aircraft. In the Boeing twinjet, the takeoff limit is exceeded by approximately 0.5 dB, while the approach and sideline limits are met. The noise levels of the trijet and quadjet airplanes are an average of 2 dB or more below the limits. These noise margins are retained with thrust growth assuming a constant thrust loading, i.e., takeoff gross weight increases at the same rate as thrust. Refined matching of the acoustic configuration of the flight propulsion system to each airplane, and/or further optimization of the airplanes for minimum noise, could further reduce noise levels.

The noise assessments, when considered with trades, provide a greater than 80 percent probability of meeting the 1978 rules. This level of confidence in meeting the noise rules is sufficiently high to generally enable the manufacturer to initiate a development program.

TABLE 2

ANTI-DETERIORATION DESIGN CONCEPTS AND OBJECTIVES

Design Concepts	Anti-Deterioration Objectives (See Text)			
	1	2	3	4
Short, Stiff Rotors	X	X		
Minimum "Wobble" Bearing Locations	X	X		
Cowl Load Sharing	X	X		
Centerline Thrust Links	X			
Turbine Intermediate Case Rear Mount	X	X		
Improved Thermal Matching	X			
Abradable Rub Strips			X	
Abrasive Blade Tips			X	
Smooth, Erosion Resistant Airfoil Coatings				X

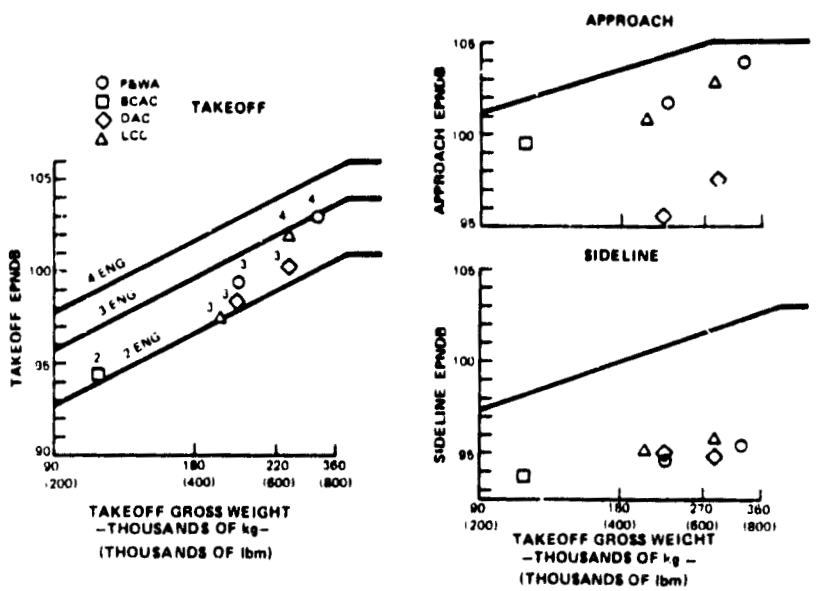

Figure 17 Predicted Noise Levels Vs. FAR Part 36-1978 Design Goal

3.2.5 Emissions

The gaseous emissions goals defined by the EPA standards for engines newly certified after 1 January 1981 are:

CO - 3.0 lb per klb thrust-hr per cycle

UHC - 0.4 lb per klb thrust-hr per cycle

NO_x - 3.0 lb per klb thrust-hr per cycle

The allowable SAE Smoke Number is 20, as determined by the procedure set forth in Reference 2. The cycle for the emissions goal values is summarized in Table 3.

EPA parameter estimates were made using emissions indices (EI's) (pounds of pollutant per pound of fuel). The EI's were obtained from correlations of the test results of the Experimental Clean Combustor Program (ECCP) two-stage combustor. These tests correlated the EI with operating pressure, temperature, and fuel-to-air ratio for the three pollutants at each of the five operating modes. Margins for development and engine-to-engine variations were superimposed on these estimates. The EI's and individual mode engine performance levels were then combined with the time-in-mode information to arrive at the final EPA parameter estimates.

EPA parameter estimates for the gaseous emissions, as summarized in Table 4, fall below CO and HC 1981 regulations and, therefore, meet the design goals. NO_x estimates exceed the 1981 regulation, based on full use of NO_x reduction combustor features known at Pratt & Whitney Aircraft. The current SAE smoke number estimate equals the design goal level.

Smoke estimates are based on correlations of SAE smoke number versus pressure and fuel-to-air ratio, assuming the presence of carburetor tubes in the main zone to reduce both NO_x and smoke.

Even with all of the emissions reduction features included in the combustor design, the design goals for gaseous emissions are not fully met. Although the probability of meeting the CO and HC 1981 goal levels are currently assessed at over 99 percent, the achievement of the NO_x goal is currently assessed at less than 10 percent. Advanced NO_x-reducing combustor technology from other programs will be assessed on a continual basis for possible incorporation into the Energy Efficient Engine design to further reduce NO_x toward the goal levels.

TABLE 3

CYCLE USED IN GASEOUS EMISSIONS ESTIMATES

Operating Mode	Power Setting % Fn T/O	Time (min)
Taxi out	7(ground idle)	19.0
Takeoff	100	0.7
Climb	85	2.2
Approach	30	4.0
Taxi in	7(ground idle)	7.0

TABLE 4

ENERGY EFFICIENT ENGINE EMISSIONS

EPA Parameter	Current Status(1)	Design Goals (EPA Proposed 1981 Regulations)
CO	1.7	3.0
THC	0.2	0.4
NO_x	4.6	3.0
SAE Smoke Number	20	20

(1) Gaseous emissions estimates include margins for combustor development and production tolerances of 34 percent for CO, 47 percent for THC, and 22 percent for NO_x.

3.3 DESIGN REQUIREMENTS

The design of the propulsion system is consistent with standard commercial aircraft engine practice, and with applicable FAA and EPA regulations.

3.3.1 General Description

The propulsion system includes all systems required for normal commercial aircraft operation (nacelle, control, aircraft engine accessories, etc.) and these systems are designed to be easily inspectible, removable, and maintainable. The following design requirements were used in establishing the propulsion system and sub-systems designs. Where available, these requirements include inputs from the airframe companies and airlines.

3.3.2 Operational Envelope

The propulsion system is capable of operating at any point within the commercial aircraft flight envelope shown in Figure 8. The engine is capable of starting with starter assist throughout the region defined (altitude relight envelope).

3.3.3 Mission and Parts Lives

The propulsion system is designed for both an international and a domestic mission as defined in Table 5. These missions are used for all low cycle fatigue predictions, which include the effects of all stress variations from engine start-up through shutdown. The structural design is capable of the most limiting condition of these missions.

The design life for all engine parts is to standard commercial design practice.

3.3.4 Flight Maneuver Loads

The flight propulsion system has been designed for flight maneuver loads consistent with Pratt & Whitney Aircraft standard design practice. This procedure considers three categories of maneuver loads (normal, limit, and ultimate) which are applied to various aspects of the design as appropriate.

Normal operating loads are combinations of loads that may be expected to occur on an average of once per flight. A limit load is the maximum operational load that a structure may encounter during engine life. An ultimate load is the maximum load the structure can withstand without failing, although local permanent deformation and distress may occur.

3.3.5 Engine Attitudes

The propulsion system is capable of operating at the flight attitudes and time periods consistent with Pratt & Whitney Aircraft standard

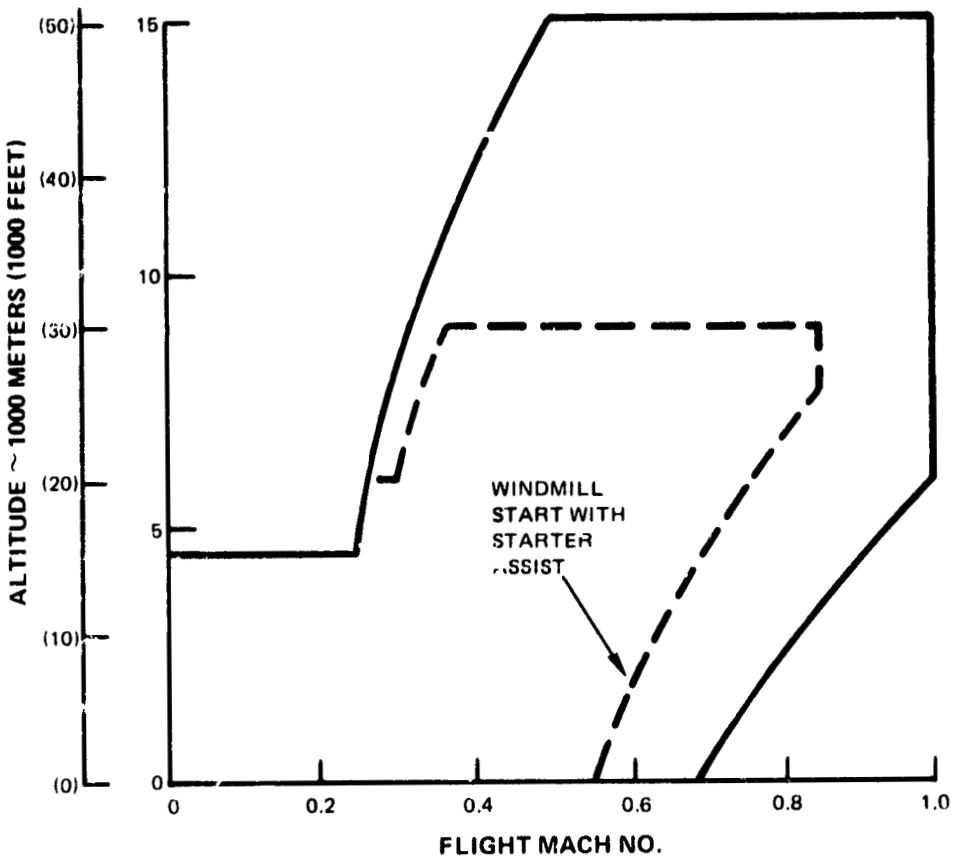

Figure 18 Flight Propulsion System Operating and Relight Envelopes

TABLE 5

FLIGHT PROPULSION SYSTEM DESIGN REQUIREMENTS
NORMAL COMMERCIAL OPERATION

Flight Missions Specified in Traditional Engineering Units
(Design life = 30,000 hours or 20,000 missions)

		Domestic (700 nm)		International (2000 nm)	
Segment	Power Setting	Altitude/ Speed (ft/Mach No.)	Time (min)	Altitude/ Speed (ft/Mach No.)	Time (min)
Start and Idle-Taxi	Gr. idle	0/0	7.5	0.0	7.5
Takeoff	T.O.	0-1500/0-.39	2.0	0-1500/0-0.39	2.0
Climb	M. Cl.	1500-35,000/0.39-0.80	17.4	1500-39,000/0.39/0.80	21.0
Cruise	0.85-0.82 M. Cr.	35,000/0.80	56.6	39,000/0.80	224.0
Descent	Fl. idle	35,000-1500/0.80-0.39	20.4	39,000-1500/0.80-0.39	24.0
Approach/Landing	0.30 T.O.-Fl.idle	1500-0/0.39-0.17	2.0	1500-0/0.39-0.17	2.1
Reverse	M. rev.	0/0.15	0.2	0/0.15	0.2
Idle-Taxi	Gr. idle	0/0	7.5	0/0	7.5
			113.7		288.3

design practice. To avoid oil coking c[illegible]kage, bearing compartments are configured so that seals are not subm[illegible]ged in oil for excessive time periods during extreme flight attitudes.

3.3.6 Customer Airbleed and Power Extraction

The propulsion system is designed to provide a nominal mid-compressor customer bleed with altitude as shown in Figure 19, and a customer power extraction of 107 kilowatts (144 horsepower). These customer requirements were based on an average of airframe company estimated requirements.

3.3.7 Anti-Icing

The propulsion system operates satisfactorily with no serious degradation in thrust resulting from propulsion system icing under conditions specified in FAR Part 33. All parts subject to anti-icing are designed without compromising the structural integrity should a valve failure occur.

3.3.8 Fire Safety

The propulsion system is designed in accordance with Pratt & Whitney Aircraft fire safety design practice and with the appropriate FAA regulations. These include requirements regarding the prevention of ignition, fire containment, fire detection, and fire extinction. All hydraulic plumbing is fireproofed and designed in accordance with FAR safety requirements.

3.3.9 Fuels

The design assumes the use of Jet A fuel. The impact of using broad-specification fuels on the propulsion system design will be determined later in the program when combustor tests will be conducted with both types of fuel.

3.3.10 Fuel and Oil Leakage

There is no external leakage of fuel or oil from any part of the propulsion system. Provisions are made for draining the engine of fuel after each false start, and for preventing excess fuel from entering the combustion areas after shutdown. In addition, drains are installed where required to collect oil that may leak past the seals. All such collected fuel or oil will be stored in ecology tanks.

3.3.11 Dumping

The propulsion system is designed so that no fuels or lubricants are dumped during normal operations.

3.3.12 Thrust Reverse

The propulsion system incorporates a thrust reverser system capable of providing reverse thrust of at least 35 percent of the static takeoff forward thrust. The reverser is designed to direct the exhaust airflow to avoid impingement on the airframe structure and ingestion into the engine inlet. In addition, the reverser is designed to be fail safe and capable of maintaining position should a failure occur.

3.3.13 Thrust Growth

The propulsion system is designed to provide thrust growth capability without requiring major design changes to the high spool or compromising the other program goals. Thrust growth is obtained by increasing turbine temperature, increasing fan airflow and pressure ratio, and by adding a low pressure compressor supercharging stage. Moderate thrust growth up to 15 percent increase is obtainable within existing nacelle lines; up to 25 percent thrust increase is obtainable with a new nacelle. Cooling airflow requirements to obtain the described thrust growth are not included in the initial propulsion system design.

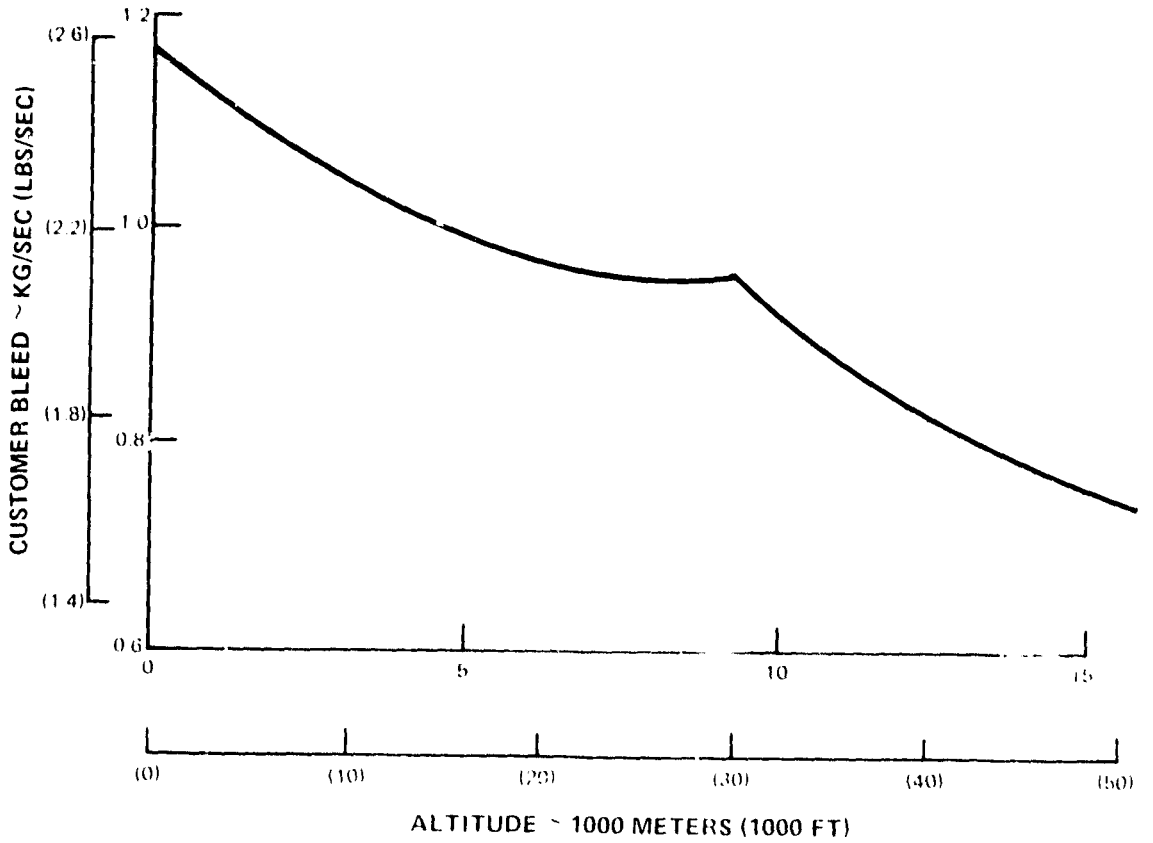

Figure 19 Customer Airbleed Schedule Assumed for Design

4.0 COMPONENT AND SUBSYSTEM PRELIMINARY DESIGN AND ANALYSIS

This section describes the status of the preliminary designs and results of analyses on the engine components and subsystems. Individual component preliminary designs were integrated with the nacelle preliminary design as part of this effort. The low pressure spool was further optimized based on the design goals and was combined with the high pressure spool preliminary design developed under the earlier study reported in Reference 1. Other subsystems, including the active clearance control system, main bearing compartments and lubrication system, secondary airflow system, and the flight engine nacelle were analyzed and defined in this effort. Boeing, Douglas, and Lockheed, as subcontractors to Pratt & Whitney Aircraft, assisted in the nacelle preliminary design definition.

For proper understanding of the following text, it should be noted that component stages are numbered consecutively from the front to the rear of the compressor and turbine systems, respectively. As a result, the fan is stage number 1 of the compression system, and the last stage of the high-pressure compressor is stage number 15. Similarly, the high-pressure turbine is stage number 1 of the turbine system, and the low-pressure turbine exit stage is stage number 5.

4.1 FAN

4.1.1 Design Requirements

The fan aerodynamic design requirements have been established by the engine cycle definitions at design and off-design conditions. Two important off-design flight conditions in terms of efficient operation are maximum climb and maximum cruise at 10,668 m (35,000 ft). As a result, the aerodynamic design point for the fan was located between these two points. Fan aerodynamic requirements for high altitude, efficient operation at these particular points are presented in Table 6. Fan efficiency goals at these flight conditions are tabulated as well. The predicted fan map, showing these major points and the takeoff operating point, is shown in Figure 20. Also shown is a typical fan operating line.

Structural and mechanical design requirements were established on the basis of commercial acceptability. Experience indicated that the fan blades be designed for 30,000 missions life. All other fan module rotating and static parts were designed to life requirements of 30,000 hours or 20,000 missions.

4.1.2 Design Background

JT9D, JT3D, and JT8D fans currently in service have either one or two part span shrouds between blades to restrain them from vibrating. Experience with research stages has demonstrated that a part span shroud can reduce fan efficiency by as much as 1 to 1.5 percent.

TABLE 6

FAN DESIGN REQUIREMENTS
(Mach 0.8 - 10,668 m (35,000 ft)

Aerodynamic Parameters	Max Climb	Max Cruise	Aerodynamic Design Point
Pressure Ratio - Duct Section	1.79	1.71	1.74
- ID Section	1.59	1.55	1.56
Inlet Corrected Flow, kg/sec	719	698	707
(lb/sec)	1585	1541	1560
Bypass Ratio	6.38	6.59	6.5
Surge Margin, %	15	15	15
Adiabatic Stage Efficiency Goals			
Duct Section	0.871	0.873	0.873
ID Section	0.901	0.904	0.902
Life Requirements			
Low Cycle Fatigue Life			
Blade	30,000 mission		
Other	20,000 missions or 30,000 hours		

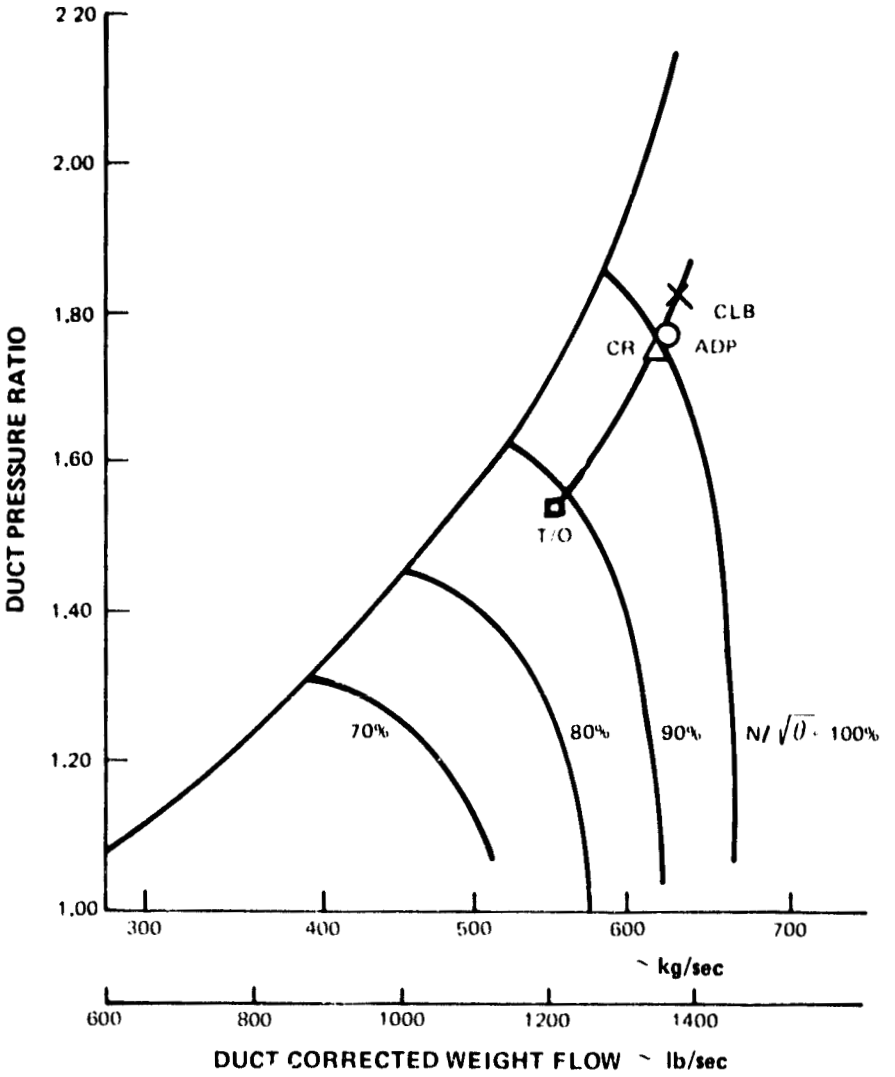

Figure 20 Predicted Fan Operating Map. Data shows aerodynamic design, cruise/climb and takeoff points.

A large amount of performance data on shrouded and unshrouded fans of varying designs has been generated and correlated into a design system which predicts losses as a function of shroud shape, location, and the aerodynamic flow field. A similar system was recently independently developed as described in Reference 3. Both of these systems show that shroudless fans have a significant efficiency benefit over even the best shrouded configurations.

Although Pratt & Whitney Aircraft has, at present, no production experience with shroudless fans, structural design techniques such as NASTRAN for hollow blades, and sophisticated flutter and resonance analyses are currently being used for the structural design task.

In addition, Pratt & Whitney Aircraft has substantiated flutter-free operation of low aspect ratio, shroudless graphite epoxy and advanced titanium spar-boron aluminum shell fans.

4.1.3 General Configuration Description

4.1.3.1 Major Subassemblies

A cross-section of the fan, indicating the basic design features, is shown in Figure 21. The rotor assembly consists of a composite spinner mounted on a titanium disk and 24 shroudless, hollow titanium blades with an average span-to-root chord aspect ratio of 2.5 and a leading edge hub-to-tip radius ratio of 0.34. Disk stiffness required to support blade centrifugal loads uniformly along the disk/blade attachment contact angle was the determining factor in sizing the disk. The resulting disk burst margin is more than adequate, at 60 percent. A positioning spring between the bottom of the blade attachment and the disk broach prevents galling when the rotor windmills. The outer sections of the blades, for approximately 2/3 of their length, are hollow. At 2.5 aspect ratio, this approach permits the elimination of the part-span shrouds while keeping blade resonant frequencies above two excitations per revolution (2E) outside of the engine operating range. The blade is designed to encounter 2E resonance low in the operating speed range where it can be safely penetrated. Specially contoured blades are employed instead of standardized airfoil shapes to minimize losses by tailoring pressure and suction surfaces to reduce shock losses and locally control the diffusion rate.

An abradable rubstrip with a circumferential trench is used in the fan case over the blade tips. Acoustically matched casing treatment is used between the blade trailing edges and the fan exit guide vane leading edges to absorb fan noise. Additionally, the fan exit guide vanes are located 3.5 blade tip axial chords downstream of the rotor and canted rearward to reduce the noise generated by the interaction of blade wakes and the fan exit guide vanes. Varying thicknesses of KEVLAR material are used around the fan case to provide blade containment while allowing the case to be fabricated from aluminum to reduce overall weight.

The 33 fan exit guide vanes are included in an integral fan exit/intermediate case assembly discussed in Section 4.3. Aerodynamically, the fan exit guide vanes are designed to eliminate a non-symmetrical back pressure resulting from the engine upper support pylon and bottom fan duct bifurcation, which introduce significant blockage at the top and bottom of the flowpath annulus. This design is accomplished by fairing the fan exit guide vanes directly in front of the pylon and lower bifurcation and by varying the airfoil shapes of the fan exit vanes located at different circumferential positions relative to the pylon and bifurcation to properly guide the fan duct flow around these obstructions. Eleven different designs result. Specially contoured airfoil designs are utilized for the fan exit guide vanes as well as for the fan blades. The core exit stators, behind the fan, will be designed with controlled diffusion airfoils to increase core efficiency.

4.1.3.2 Efficiency Improvement Features

There are three major features incorporated into the fan design which contribute to the increased efficiency potential: shroud elimination, contoured airfoils, and tip trenches.

The major efficiency increment results from the removal of the part span shrouds, based on analysis projecting from background information discussed under Paragraph 4.1.2.1 of this section.

A second efficiency increment results from specially contouring fan airfoil shapes. Previously, fan blades have been designed from standard sections such as multiple-circular-arc airfoils. These sections were not necessarily optimum, so the design contouring method is being used to select airfoil shapes that produce the lowest loss flow field between the blades. Figure 22 illustrates the principle by showing the suction surface pressure distribution near the tip section for two blades designed in the NASA 1800 ft/sec fan program (NAS3-18020 and NAS3-20591). The standard precompression blade shape produces rapid accelerations and decelerations which result in strong, high loss shocks in the non-viscous part of the flow field. Increased viscous losses occur along the blade surface as a result of strong shock and boundary layer interactions and increased boundary layer growth in the adverse pressure gradient regions. The superiority of the specially contoured blade results from selecting an airfoil shape which gives a more even pressure distribution.

Finally, the use of a tip trench over the rotor tips increases fan efficiency by reducing tip clearance losses.

4.1.3.3 Principal Aerodynamic Design Parameters

The major fan aerodynamic design parameters are shown in Table 7. The fan tip speed was determined from low spool optimization studies. This

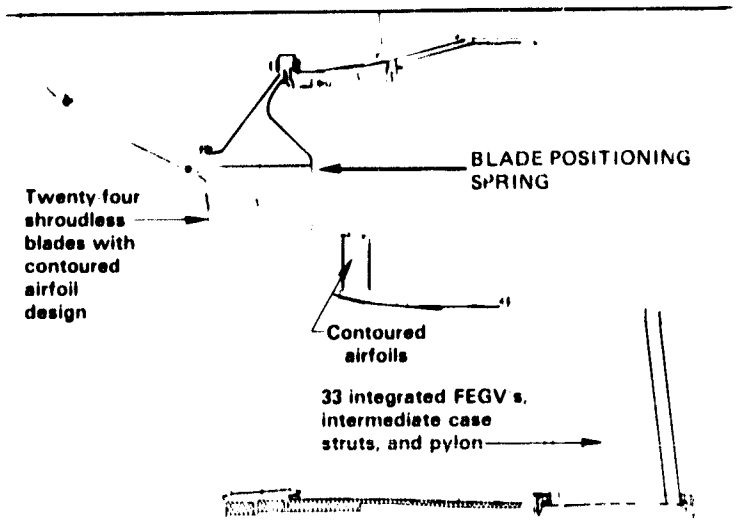

Figure 21 Fan Preliminary Design. Cross-section includes identification of major features

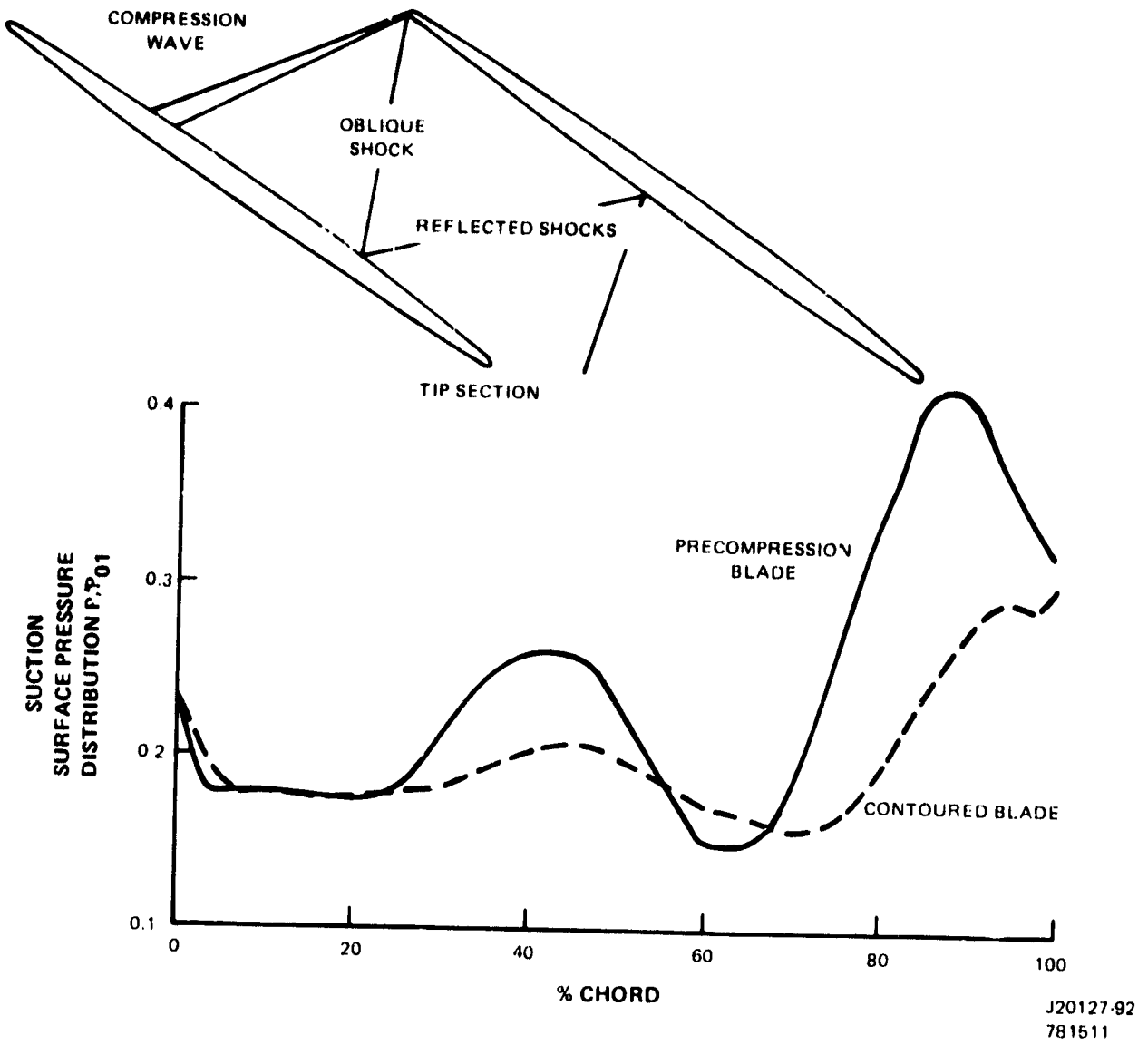

Figure 22 Comparison of Standard and Contoured Fan Blade Suction Surface Pressure Distributions. Contoured blade provides a more even pressure distribution.

TABLE 7

FAN AERODYNAMIC DESIGN PARAMETERS
AERODYNAMIC DESIGN POINT

Number of Stages	1
Pressure Ratio - Duct	1.74
Corrected Flow, kg/sec	707
lb/sec	1560
Bypass Ratio	6.51
Surge Margin, %	15
Corrected Tip Speed, m/sec	457
ft/sec	1500
Inlet Specific Weight Flow, $kg/sec/m^2$	210
$lb/sec/ft^2$	43
Inlet Hub-Tip Radius Ratio	0.34
Blade Aspect Ratio $\frac{\text{(Avg Length)}}{\text{(Root Chord)}}$	2.5
Number of Shrouds	0
Number of Blades	24
Number of Duct Exit Guide Vanes	33

optimization was accomplished by considering performance, weight, and cost changes in the fan, low-pressure compressor, and the low-pressure turbine with speed variation.

The aspect ratio and number of blades represent major changes from current practice. A typical production blade has an aspect ratio of 4.6 compared to 2.5 for the Energy Efficient Engine fan. The use of low aspect ratio can result in a major reduction in the number of fan blades. The JT9D has 46 blades compared to only 24 blades for the Energy Efficient Engine fan.

Other key aerodynamic design parameters, such as inlet specific flow and hub-tip radius ratio, were selected from fan design optimization studies.

4.1.3.4 Technology Development Requirements

4.1.3.4.1 Higher Efficiency Airfoils

The projected efficiency increase of the fan blade represents technology that is not fully developed. For instance, about one percent fan efficiency increase is attributed to the improved aerodynamic performance of the specially contoured airfoils. The ability to design through the blade row in a mixed supersonic and subsonic flow field was only recently developed to experimental design status. The first substantiating data from a fan designed with this tool will be generated in the test of the NASA 1800 ft/sec (NAS3-20541) fan. The system is also being employed in the design of an advanced commercial engine fan, and these data will also become available in 1979. Laser velocimetry data are planned for the NASA 1800 ft/sec fan, which will permit improved calibration of predicted and test blade pressure distributions.

The elimination of a part span shroud accounts for approximately a 0.7 percent efficiency gain relative to an equal technology shrouded design. This gain has been fairly well substantiated and is considered low risk. However, many structural questions on shroudless fans have been raised. An Energy Efficient Engine hollow fan structural program has already been initiated to address these questions. Under this program, specimens made by candidate fabrication methods will be tested. As blade design and fabrication techniques are identified, structural testing will be conducted. These tests will include stress surveys, untwist measurements, and foreign object damage (FOD) evaluation. Other tests to determine low and high cycle fatigue lives of the blades will also be conducted. Additionally, a solid titanium scaled fan stage will be run in the program to obtain structural and aerodynamic data on a scaled representation of the Energy Efficient Engine fan. This fan will be subjected to flight type distortions to determine its resonant stress characteristics. This program will also determine if back pressure distortion generated in the exit guide vanes by the

pylon blockage is significant, will identify any resonant stresses that may be introduced as a result of this distortion. The exit guide vanes will be adjusted to minimize this distortion.

The tip trenches are estimated to produce an efficiency gain of 0.2 percent. A program utilizing a low speed 1.52 m (5 ft) diameter rig is planned for 1979 to more fully understand the tip flow phenomenon in the presence of trenches.

4.1.3.4.2 Blade Fabrication

Several fabrication methods for the Energy Efficient Engine shroudless, hollow fan blade were considered during the preliminary design and analysis effort. These methods included:

1. Superplastic Forming/Diffusion Bonding (SPF/DB) by a Rockwell International process.

2. Conventional forging with numerical controlled machining of the hollow section and diffusion bonding a cover on the hollow section.

3. Isothermally forging, to size, a blade half with intergral hollow cavity, and diffusion bonding on a cover.

4. Laminating and diffusion bonding an entire blade from titanium sheet.

5. Laminating the hollow section from titanium sheet and diffusion bonding it to a forged blade root.

Evaluation of these various methods resulted in the selection of the approach utilizing lamination and diffusion bonding of the entire blade from titanium sheet. Both the conventional and isothermally forged methods were found to be too costly to produce in the blade size required. At first glance, the SPF/DB process appeared attractive; however, upon further evaluation, it was discovered that this process does not yield a hollow blade internal structure that can accommodate the high centrifugal stresses associated with fan rotation at engine operating speeds.

Both the fully-laminated and laminated blade/forged root methods were judged to be suitable for fabricating the hollow blade. The laminated blade forged root method had the potential for improving experimental blade delivery time, but there is a degree of uncertainty about the integrity of the bond joint between the forged root and the laminated blade section. The fully-laminated approach was selected because it eliminates the potential bond joint problem, and is more suitable to an automated production process, which in turn, could reduce considerably the cost of blades manufactured in quantity.

4.1.4 Supporting Analyses

4.1.4.1 Efficiency Prediction

The fan is aerodynamically designed using a streamline analysis computer program to produce high efficiency over the operating range. The fan duct efficiency prediction at the aerodynamic design point is 87.3 percent. The corresponding fan root efficiency is 90.2 percent. A breakdown of the predicted duct section efficiency is presented in Table 8. The efficiency predicted for the design with the current state-of-the-art fan design system is 85.9 percent. Incorporation of the advanced technology features discussed in Section 4.1.3.4.1 results in the efficiency increments shown in Table 8. The specially contoured airfoils are expected to increase the efficiency on the order of one percent because of the improved intrablade flow field. The use of pylon-matched, contoured airfoil shapes in the duct exit guide vanes is expected to contribute an additional 0.2 percent to the fan efficiency. The tip trench over the rotor is predicted to provide another 0.2 percent efficiency increment by reducing tip clearance losses. Adding the efficiency increments offered by the advanced technology features results in the goal 87.3 percent efficiency.

4.1.4.2 Stability Audit

Surge margin requirements for the fan were established by a stability audit taken at the major operating points in the flight envelope. For each of these points, the surge margin reduction resulting from surge line and operating line shifts caused by destabilizing factors was examined to determine how much initial surge margin was required. The destabilizing factors include such events as engine and control deterioration, inlet distortion, production tolerances, and power transients. The results of the fan stability audit are shown in Table 9 for the sea level static takeoff point. This audit revealed that the design fan surge margin of 15 percent is sufficient to assure ample surge margin during takeoff, climb, cruise, idle, and reverse (Table 10).

4.1.4.3 Fan Blade Analysis

4.1.4.3.1 Diameter Selection

During the preliminary design phase, a diameter sensitivity trade study was conducted to optimize the fan configuration. This study resulted in a change of the major fan design parameters as shown in Table 11. This diameter change was independent of a 5 percent tip diameter increase that occurred as a result of the 10 percent thrust size increase since the start of the program.

The base fan had a 472 m/sec (1550 ft/sec) tip speed and an inlet specific weight flow of 202 kg/sec/m^2 (41.5 lbs/sec/ft^2). The trade

TABLE 8

FAN ADIABATIC EFFICIENCY PREDICTION
(DUCT SECTION)
AERODYNAMIC DESIGN POINT

Base:	
Current Design System with Shroudless Fan Blade	85.9%
Technology Benefits:	
Specially Contoured Airfoils	1.0%
Specially Contoured Exit Guide Vanes	0.2%
Rotor Tip Trench	0.2%
Status:	87.3%

TABLE 9

FAN STABILITY AUDIT RESULTS
AT TAKEOFF

Surge Line Degradation	Fixed Quantity (%)	Random Quantity (%)
Engine Deterioration	2.3	±1.2
Distortion	3.0	0
Engine Production Tolerance	0	±1.0
Operating Line Degradation		
Engine Production Tolerance	0	±0.5
Control Production Tolerance	0	0
Engine Deterioration	0.5	±0.5
Control Deterioration	0	0
Power Transients	0	0
Sum of Fixed	5.8	
Sum of Random (RSS)		±1.7
Required Surge Margin	7.5	
Available Surge Margin	16.2	

TABLE 10

FAN STABILITY AUDIT RESULTS
AT MAJOR OPERATING POINTS

Flight Condition	% Flow	Surge Margin (%) Required	Available
Aerodynamic Design Point(1)	100	4.5	15.0
Idle (SLS)	29.7	1.9	7.4
Takeoff	89.7	7.5	16.2
Reverse	88.9	9.5	16.7

(1)Representative of maximum climb and cruise operation

TABLE 11

FAN DIAMETER TRADE STUDY RESULTS LEADING TO
SELECTION OF REDUCED DIAMETER

	Base Fan	Reduced Diameter Fan
Diameter, cm	Base	-7
, (in)	Base	(-2.9)
Hub-Tip Ratio	0.38	0.34
Specific Flow, kg/sec/m^2	202	210
, (lb/sec/ft^2)	(41.5)	(43)
Low Rotor Speed, RPM	Base	Base
Tip Speed, m/sec	472	457
, (ft/sec)	(1550)	(1500)
Adiabatic Efficiency-Duct/ I.D., %	Base	+0.1/+0.7
LPC Configuration	Base	Base
Engine Weight, kg	Base	-13.6
, (lbs)	(Base)	(-30)
Engine Length, cm	Base	+2.54
, (in)	(Base)	+1.0
Cost, Dollars	Base	-20,000
TSFC, Percent	Base	-0.3

study, which exercised inlet hub-tip ratio and specific weight flow, held low rotor speed constant to avoid changes in the low pressure turbine and low pressure compressor. An increase in specific weight flow to 210 kg/sec/m^2 (43.0 lbs/sec/ft^2) concurrent with a reduction in inlet hub tip ratio from 0.38 to 0.34, was identified as a fan performance improvement. The reduced diameter fan featured a 2.1 percent increase in duct efficiency, primarily resulting from the reduction in blade tip Mach number associated with the reduction in tip speed from 472 to 457 m/sec (1550 to 1500 ft/sec). The shorter, more efficient blades translate into an engine weight reduction of 13.6 kg (30 lbs), and a reduction in installed thrust specific fuel consumption of 0.3 percent.

4.1.4.3.2 Airfoil Geometry Selection

The fan blade configuration selected for the Energy Efficient Engine program is an all titanium, shroudless, 2.5 aspect ratio design with a hollow airfoil section and a solid root section with integral platforms and a dovetail attachment. The solid portion is approximately 1/3 of the blade length, including the root and part of the airfoil, with the hollow section comprising the remaining 2/3. Figure 23 shows the basic configuration with three internal radial ribs and one chordwise rib. The structural analysis employed to arrive at this configuration considered bird strike, steady state stress, low cycle fatigue, resonance, and flutter.

Generally, structural design criteria were examined with the aid of a NASTRAN finite element analytical model of the blade. Plate elements were used to describe the skin, internal ribs, and solid inner portion.

The bird strike design criteria were met by controlling the material thickness distribution. NASTRAN was used to define blade leading edge depth and tip section wall thickness that maintained the stress parameter below experienced levels. This analysis resulted in the selection of a 2.54 cm (1 in.) leading edge insert depth and a 0.115 cm (0.045 in.) skin thickness.

A combination of NASTRAN and beam analyses was used to determine the stress distribution throughout the blade and focus on stresses at key internal and external locations. Consideration was given to tensile and bending stresses caused by centrifugal loads, bending moments, and untwist torque based on achieving an acceptable low cycle fatigue blade life. Blade internal stress estimates recognized the reduced low cycle fatigue strength associated with a surface lacking the compressive residual stresses associated with normal machining practices, while the blade external estimates allowed for compressive stresses from shot or glass bead peening during manufacture. Key internal stress concerns were eliminated with the incorporation of the solid inner portion, and the proper establishment of the hollow-to-solid juncture point, and the wall thickness at that location. These analyses showed the present 2.5

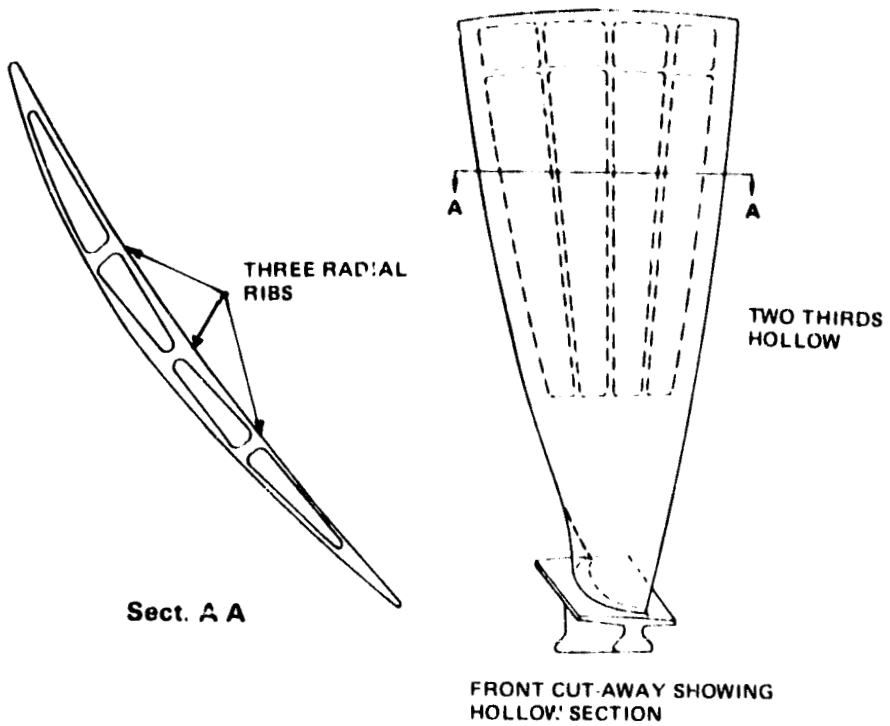

Figure 23 Fan Blade Internal Configuration. Cut-away shows two-thirds hollow blade internal configuration, including three radial rib locations.

aspect ratio, 24-blade design to successfully meet all imposed stress and low cycle fatigue criteria.

Initial NASTRAN resonance analysis on a 2.7 aspect ratio blade showed the basic two thirds hollow, one third solid blade, that met bird ingestion and stress criteria, to have the first vibratory mode (bending) for 2 excitations per revolution properly positioned low in the operating range just above idle. However, frequency margins relative to the second mode (bending) and third mode (torsion) for three and four excitations per revolution, respectively, were found to be inadequate. A number of blade modifications were analyzed in an attempt to achieve adequate margins. These included changing the rib configurations, tailoring of root chord and camber, increasing the chord at the solid-to-hollow interface, moving the radial location of the interface, and redistribution mass. The more complex rib schemes, incorporating both diagonal and radial orientations to control torsion and bending, respectively, did not appreciably affect the blade vibration characteristics. The selected configuration resulting from these perturbations has the predicted vibration characteristics shown in Figure 24 using a NASTRAN model. As shown, the second bending and first torsion intersections now occur above redline speed.

NASTRAN was also used to define coupled bending and torsional modes of vibration and natural frequencies so that flutter stability analyses could be conducted. Both supersonic unstalled and stall flutter were investigated. Concepts considered which are known to increase natural frequencies were:

1. Utilization of PWA 1202 (8-1-1) titanium
2. Reduction in tip chord
3. Increase in midspan thickness-to-chord ratio
4. Addition of an internal chordwise rib 7.6 cm (3 in.) inboard of the tip
5. A disk rim broached on a conical surface
6. A two tooth attachment
7. A reduction in aspect ratio from 2.7 to 2.5 aspect ratio

Results showed that the current blade configuration will be stable in all modes.

4.1.4.3.3 Attachment Region Geometry Selection

Structural analyses of the blade root attachment area were done concurrently with blade geometry evolution because of the interrelationships

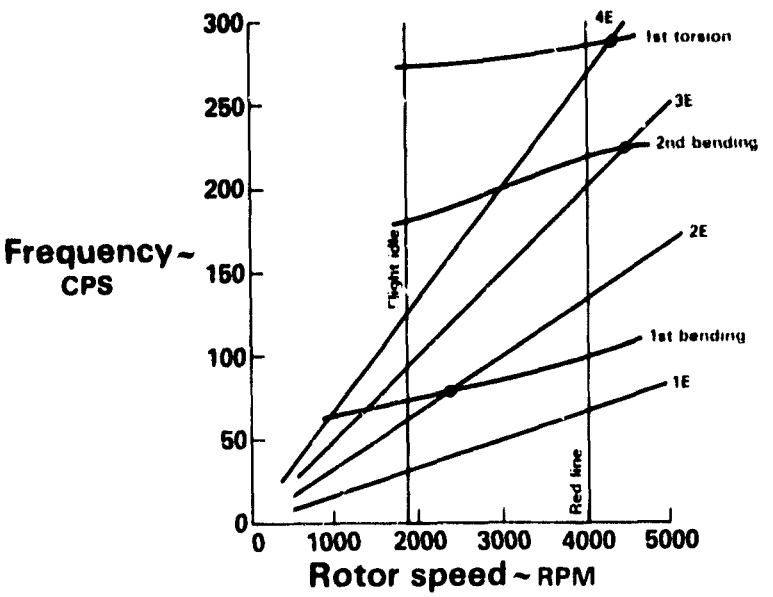

Figure 24 Predicted Fan Vibration Characteristics. First-bending occurs low in operating speed range; second bending and first torsion intersect above redline speed.

involved. Simplified computer modeling techniques were used to evaluate stresses. In addition, because of the lack of positive blade positioning (during startup, shutdown or windmilling) without shrouds, the effect of these conditions on attachment wear was assessed.

Evaluations were made of several attachment variations including the conical versus straight rim broach, separate versus integral and split versus pinned jointed platforms, and contoured versus standard root neck. Because of its simplicity (reduced risk) combined with acceptable attachment bearing, bending, and shear stresses, the conventional straight dovetail with an integral platform was selected. The dovetail neck width was sized to assure lower stress levels in the attachment than in the airfoil root section to minimize potential liberation damage. Because of the selection of a straight rim broach, a conventional tang type blade lock used in conjunction with a retaining ring was found to be acceptable for securing the blades to the disk.

Several schemes were explored to reduce side-to-side rocking of the shroudless blades during their aerodynamically unloaded rotation when windmilling. The aim was to minimize galling of the attachment. A ready solution was found that positions a spring steel insert between the bottom of the blade attachment and the disk broach.

4.1.4.4 Disk/Hub/Spinner Definition

To complete the preliminary design of the fan rotor configuration, the disk, hub, and nose cone spinner were defined.

General shell analyses were used to evaluate disk bore, rim, and hub stresses versus low cycle fatigue life and burst design criteria. Initially, both a solid disk and a lighter weight hollow disk were evaluated. The solid disk was selected for continued design effort when the hollow configuration was found to have higher cost and higher concentrated attachment stress combined with a more difficult load path.

The solid disk was sized by blade attachment region stiffness requirements. With this configuration, shell analysis showed disk lug and average tangential stresses to be within design criteria limits. In addition, a disk burst margin of 60% was calculated.

The fiberglass nose cone spinner was configured by scaling the JT9D design. In order to facilitate fan maintenance by reducing the number of fasteners involved with blade changes, the spinner was designed to fasten directly to the fan retainer ring to form a module.

4.1.4.5 Case Analysis

Fan case structural analyses consisted of stress and blade containment evaluations.

4.1.4.5.1 Stress Prediction

General shell analysis was used to estimate case stresses and define its configuration. For reduced weight, case construction was selected to be aluminum wrapped with KEVLAR. An aluminum thickness of 0.381 cm (0.15 in.) was found to be structurally adequate, with low predicted stresses. Steady state pressure loads resulted in only 20.6 x 10^6 N/m^2 (3000 psi) stress. Transient maneuver load stresses were even lower.

Case natural frequencies were analyzed and tuned relative to blade passing frequency to meet the criteria governing the occurrence of vibratory stresses in the engine operating range. Circumferential ring location and thickness variations provided the tuning requirements. A natural frequency of 2270 Hz, providing 24 percent margin relative to blade passing frequency, was estimated for the case's integral rub-strip-seal ring.

4.1.4.5.2 Containment Definition

Three areas requiring blade containment capability were assessed: forward, in-plane, and aft. KEVLAR, a high tensile strength capacity fabric, is wrapped over all three areas to provide containment because it has the unique flexibility capability to deflect and absorb the energy from liberated blade segments in tension, (circumferentially in the hoop) where it is stronger, rather than in shear (radially across the hoop). In-plane, the KEVLAR is wrapped over the aluminum fan case. Forward and aft of this area the wrapping is over structural honeycomb.

A punch load analysis was conducted to determine the KEVLAR wrap thickness requirements. Inputs to the analysis included case definition and liberated particle size, trajectory, and energy. Results showed KEVLAR thickness requirements to vary from a maximum of 2.92 cm (1.15 in) in the in-plane area, to a minimum of 1.14 cm (0.45 in) in the aft containment area.

4.1.5 Design Summary

The results of the fan preliminary design fan are shown in Table 12. Resonance and flutter design requirements have been met.

The preliminary aerodynamic design of the blade has been completed and analysis of the preliminary airfoil sections has confirmed that the aerodynamic design goals can be attained.

4.2 LOW-PRESSURE COMPRESSOR

4.2.1 Design Requirements

The low-pressure compressor aerodynamic design requirements were also established by the engine cycle definitions at design and off-design

TABLE 12

FAN PRELIMINARY DESIGN SUMMARY
AERODYNAMIC DESIGN POINT

Pressure Ratio - Duct		1.74
Inlet Corrected Flow, kg/sec		707
, lb/sec		1560
Surge Margin, %		15
Bypass Ratio		6.51
Low Cycle Fatigue Life, Missions		
Blade	30,000	
Disk	20,000	
	(30,000 Hrs.)	

conditions. Because of concern for efficient operation, the two important flight conditions were again considered to be maximum cruise and maximum climb at 10,668m (35,000 ft). Therefore, the low-pressure compressor aerodynamic design point was located between these two flight conditions. Table 13 shows the design requirements for the low-pressure compressor at this aerodynamic design point. The low-pressure compressor efficiency goal is also tabulated. The predicted low-pressure compressor map is shown in Figure 25. Superimposed on this map are these major operating points, the takeoff operating point, and a typical operating line.

Low-pressure compressor structural and mechanical design requirements were defined considering commercial acceptability. This experience led to a design life requirement of 20,000 missions or 30,000 hours for all low-pressure compressor component parts, as shown in Table 13.

4.2.2 Design Background

The low-pressure compressor configuration resembles the four stage JT9D-70 compressor that is currently in production. The airfoils are canted from the radial direction to remain perpendicular to the flowpath. This design technique, also used in the JT9D, has a proven aerodynamic benefit at the root of the low-pressure compressor airfoils. The result is improved efficiency and higher loading capability.

4.2.3 General Configuration Description

4.2.3.1 Major Subassemblies

The low-pressure compressor is composed of four stages with an average blade aspect ratio of 2.4 and an average gap-chord ratio of 0.9. Leading edge hub-to-tip radius ratios at the inlet and exit are 0.82 and 0.84, respectively.

The general low-pressure compressor configuration is shown in Figure 26. The electron beam welded titanium drum rotor assembly is attached to the low rotor shaft through a single support hub. The rotor system includes canted titanium blades with axial dovetail attachments and rotor rim knife edge seals to minimize inner cavity volumes. Disks are sized for adequate burst margin and life.

The compressor stator assembly, sectional case, and inlet splitter are fabricated from aluminum. The low-pressure compressor case includes circumferentially trenched abradable rub strips over the blade tips to provide the radial clearances needed to prevent rubbing under transient engine conditions, while minimizing the efficiency penalty associated with increased tip clearance. The inner stator shrouds also have abradable rubstrips under the rotor knife-edge seals. Rub strip material in both I.D. and O.D. locations is highly abradable silicone rubber, which is used in current engine service.

TABLE 13

LOW-PRESSURE COMPRESSOR DESIGN REQUIREMENTS
AERODYNAMIC DESIGN POINT

Pressure Ratio	1.77
Inlet Corrected Flow kg/sec (lbs/sec)	64.7 (142.7)
Surge Margin - %	20
Adiabatic Efficiency Goal	0.899
Life Requirements (LCF)	20,000 missions or 30,000 hours

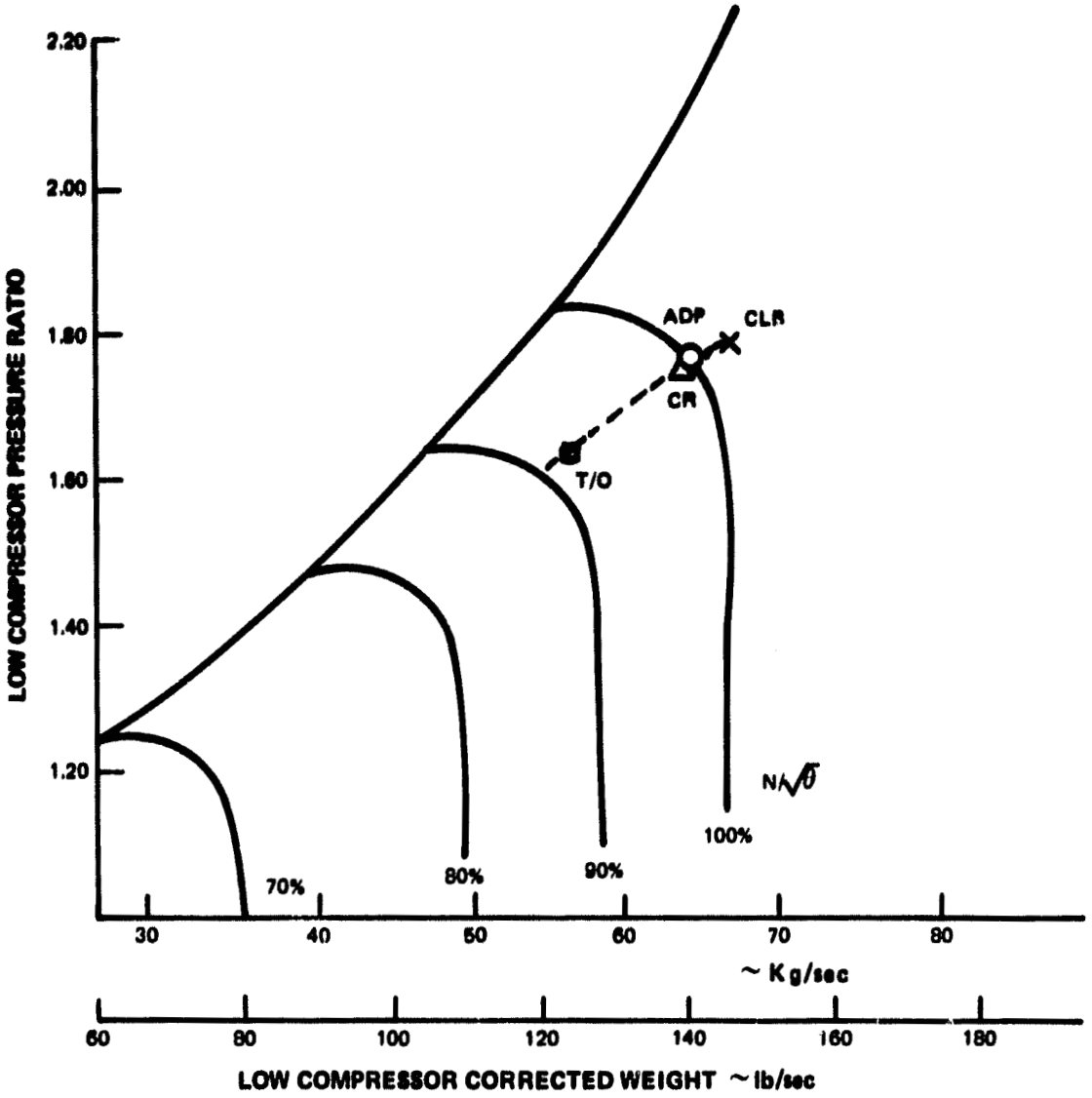

Figure 25 Predicted Low Pressure Compressor Operating Map. Callouts identify predicted aerodynamic design, cruise/climb, and takeoff points.

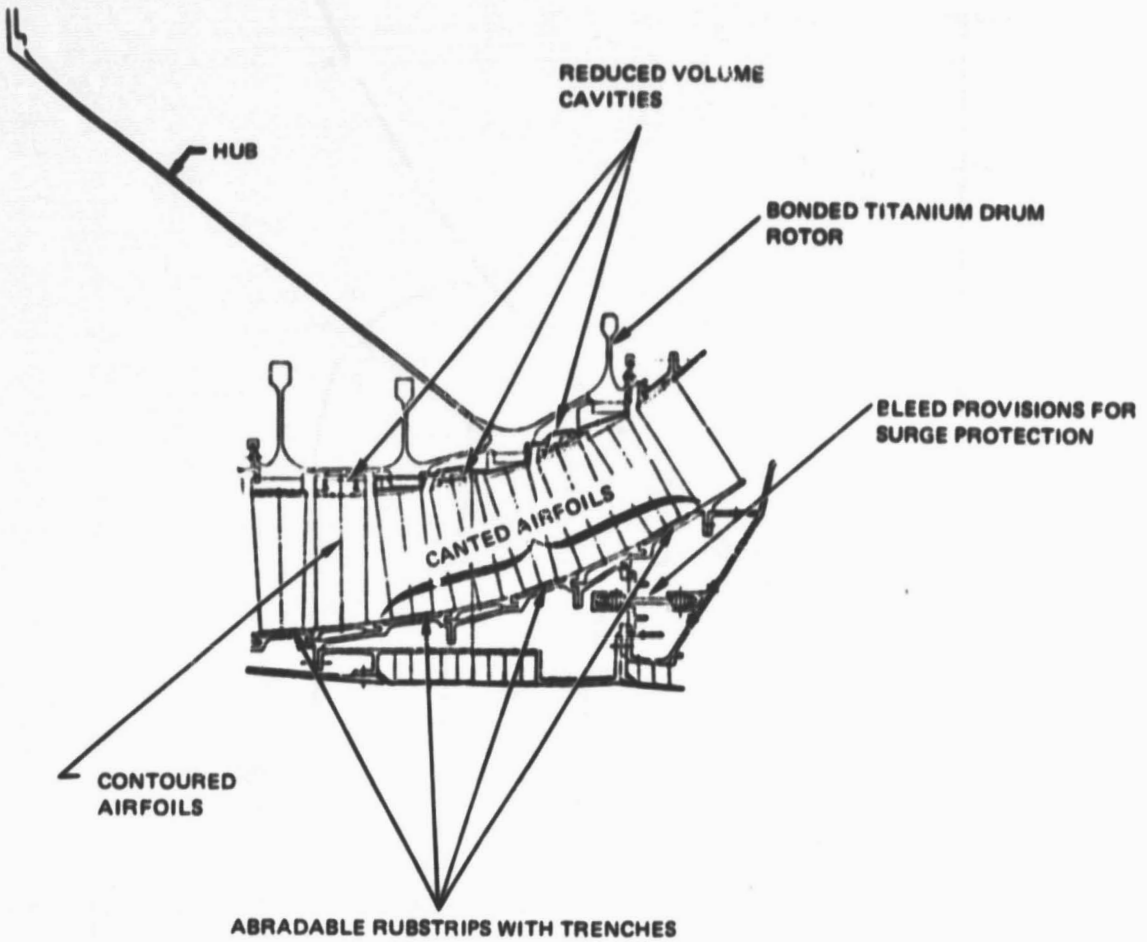

Figure 26 Low-Pressure Compressor Preliminary Design. Cross-section view provides identification of components.

The stator vanes are constructed of AMS 4135 aluminum with forged feet at the outer wall.

The vane inner platforms are also aluminum. Vane damping is accomplished with rubber filler material.

Compressor surge protection and reverse thrust stability are provided by a low-pressure compressor exit bleed. Circumferential holes aft of the fifth stage stator provide the required airflow to a fully modulated annular bleed ring. This ring translates forward via a linkage system to allow bleed air to exit from the compressor. For convenience, bleed air is discharged into the fan duct upstream of the fan exit vanes.

4.2.3.2 Efficiency Improvement Features

The low-pressure compressor design incorporates several aerodynamic features to increase efficiency. The largest efficiency benefit is expected from the low axial through-flow velocity of the increased annulus flowpath. Further efficiency improvements are gained through the incorporation of tip trenches over the rotor tips.

Inner cavity volumes are minimized to reduce end wall losses caused by pumping action from within the root cavities. The small cavity designs also lower the windage potential.

The airfoils will have thick, specially-contoured leading-edges which offer a broad incidence range capability and have superior erosion resistance.

4.2.3.3 Surge Bleed System

The low-pressure compressor design incorporates a modulated bleed capable of extracting up to 15 percent of the exit air from the flowpath and discharging it into the fan duct. This bleed is utilized during reverse to avoid surge in the low- and high-pressure compressors.

4.2.3.4 Principal Aerodynamic Design Parameters

The principal aerodynamic design parameters of the low-pressure compressor are presented in Table 14. The design has a low axial velocity-to-wheel speed ratio and low inlet specific weight flow compared with current P&WA designs. In addition, the blading gap-to-chord ratio is higher for improved efficiency. Higher than normal tip speed is used to offset the unloading effects of the large gap-to-chord ratios and produce the required pressure ratio in four stages.

4.2.3.5 Technology Development Requirements

Several of the advanced technology features incorporated into the low-pressure compressor design require further technology development.

C-2

TABLE 14

LOW-PRESSURE COMPRESSOR AERODYNAMIC DESIGN PARAMETERS
AERODYNAMIC DESIGN POINT

Number of Stages	4
Pressure Ratio	1.77
Corrected Inlet Flow, kg/sec (lbm/sec)	64.7 (142.7)
Inlet Corrected Tip Speed, m/sec (ft/sec)	24.3 (797)
Inlet Specific Flow, kg/sec/m^2 (lbm/sec/ft^2)	16.1 (35.6)
Hub-Tip Radius Ratio - Inlet	0.82
- Exit	0.84
Average Airfoil Aspect Ratio	2.4
Average Gap-Chord Ratio	0.9
Average Axial Velocity-to-Wheel Speed Ratio	0.7
Number of Airfoils	779

Tip trenches have been demonstrated at P&WA in a three-stage research compressor. Several geometries were examined to determine the aerodynamic effects. Some limited full-scale multistage compressor trench data is also available. The full effect of trench geometry on the complex three dimensional flow within a compressor has yet to be established. Programs are planned to supply additional design data. The most immediate will be a high speed, three-stage compressor test at NASA Lewis, which will be run with and without tip trenches. A JT8D engine high-pressure compressor will also be tested with trenches under the NASA ECI program (NAS3-20630).

The reduced cavity design approach has also been tested in a P&WA three-stage research compressor. These mini-cavities have also been utilized in a multistage compressor tested under Navy sponsorship (N00140-73-C-0803).

Specially contoured (low loss) leading-edge airfoils have been tested, primarily in cascades. Rotating compressor test verification remains to be accomplished.

4.2.4 Supporting Analyses

4.2.4.1 Efficiency Prediction

The low-pressure compressor is aerodynamically designed using a streamline analysis computer program. This analysis led to an adiabatic efficiency prediction of 89.9% at the aerodynamic design point. A breakdown of the predicted efficiency is presented in Table 15. This prediction consists of an 89.4 percent value estimated with the current state-of-the-art design system, plus an additional 0.5 point increase attributed to rotor tip trenches. The current design system accounts for the efficiency benefits of the specially contoured airfoil leading edges and the improved cavity design discussed in Section 4.2.3.2.

4.2.4.2 Stability Audit

A stability audit was used to establish minimum low-pressure compressor surge margin requirements. The audit examined surge margin impacts of surge and operating lines shifts caused by destabilizing factors. Table 16 shows the evaluation results at takeoff. Takeoff operation is indicated to be surge free. Table 17 shows a summary of the results of similar analyses conducted at other potentially critical flight conditions. This stability audit substantiated that the design surge margin of 20 percent is sufficient to avoid surge over the flight envelope, providing an exit bleed to the fan duct is used during thrust reverse and low power operation.

TABLE 15

LOW-PRESSURE COMPRESSOR ADIABATIC EFFICIENCY PREDICTION
AT DYNAMIC DESIGN POINT

Base:	
Design System Including- Low-Loss Leading Edges Improved Cavity Design	89.4%
Technology Benefit:	
Rotor Tip Trenches	0.5%
Status:	89.9%

4.2.4.3 Blade Attachment Analysis

The low-pressure compressor flowpath was defined within the initial portion of the gaspath transition from the fan hub section to the high-pressure compressor inlet. With this configuration, the aerodynamic analysis indicated a significant performance benefit with the airfoils canted such that their leading edges are essentially normal to the airflow. Past experience with canted airfoil orientation in the JT9D engine indicated that a more difficult blade attachment design definition is involved because a bending moment is associated with the centrifugally imposed restoring force.

Attachment structural analyses were done primarily for the last stage blade, since it has the largest degree of cant. Traditional computer programs were used to estimate tensile, shear, bending, bearing, and combined stresses. The initial attachment definition was refined, as required, until all stress criteria were met. Blade centrifugal force data used in these analyses were obtained from the compressor aerodynamic design system.

Both tangential and axial dovetail attachments were considered for the blades. The axial broach design was calculated to have lower stresses (longer life) and to reduce the axial disk width requirement (lower weight). As a result, the axial configuration was selected and refined. A forward extension was added to the blade root to help counter-balance the canted blade. Computer techniques were used to select a broach geometry that met the geometric requirements, and a pin type blade retainer was defined to complete the preliminary design of the attachment. Figure 27 shows the resultant design.

4.2.4.4 Blade Vibration Analysis

Front and last stage blade frequency calculations were made to establish initial airfoil shape feasibility. Coupled blade and disk frequency analysis on the front rotor stage indicated it to be free of all critical resonances throughout the operating range. Similar analysis in the last rotor stage indicated the need to redistribute the spanwise thickness-to-chord ratio as shown in Figure 28 to obtain adequate vibration margins. These modifications will be included in subsequent design work.

Evaluation of the flutter stability of the front and rear stages indicated that both will operate well within the safe experience range for bending and torsional flutter.

4.2.4.5 Vane Inner Shroud Analysis

A study was conducted to establish and evaluate trades for several low-pressure compressor vane inner shroud configurations. Primary concerns in this analysis were cavity size, sealing, and cost. Small

TABLE 16

LOW-PRESSURE COMPRESSOR STABILITY AUDIT RESULTS AT MAJOR OPERATING POINTS

Flight Condition	% Flow	Surge Margin (%) Required	Available
Aerodynamic Design Point(1)	100	11.3	20
Idle (SLS)	17.2	2.7	9.4
Takeoff	85.5	11.2	21.3
Reverse	90	26.7	26.7*

*With 7.5% Exit Bleed To Fan Duct

(1) Representative of maximum climb and cruise operation.

TABLE 17

LOW-PRESSURE COMPRESSOR STABILITY AUDIT RESULTS AT TAKEOFF

Surge Line Degradation	Fixed Quantity (%)	Random Quantity (%)
Engine Deterioration	1.0	± 0.5
Distortion	2.0	0
Engine Production Tolerance	0	± 1.0
Operating Line Degradation		
Engine Power Transients	4	0
Control Production Tolerance	0	± 1.1
Control Deterioration	0	± 0.6
Engine Deterioration	2.0	± 1.1
Engine Production Tolerance	0	± 1.0
Sum of Fixed	9.0	
Sum of Random (RSS)		± 2.2
Required Surge Margin	11.2	
Available Surge Margin	21.3	

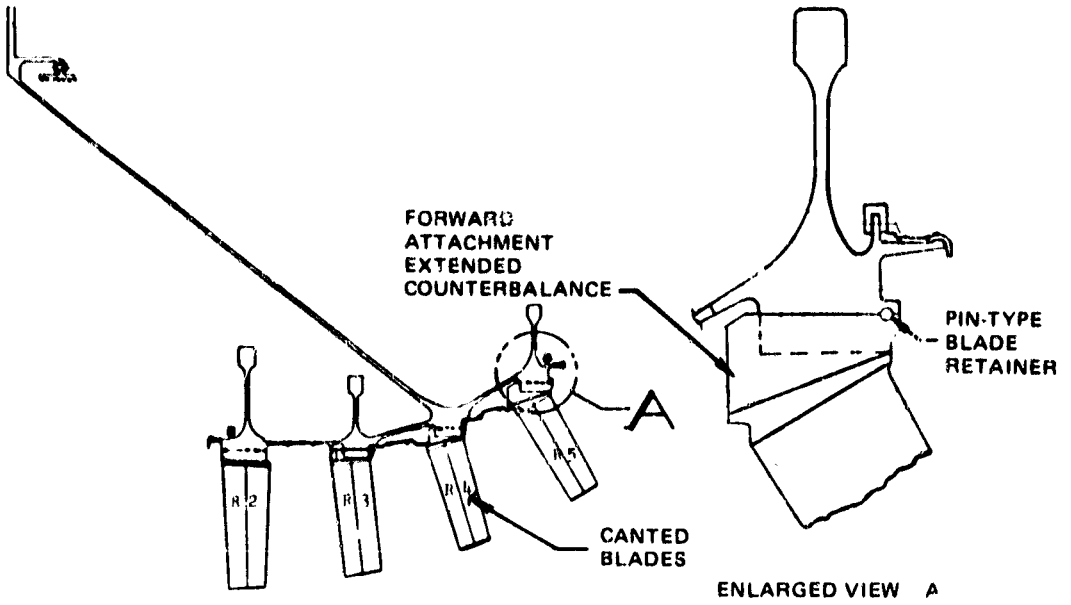

Figure 27 Canted Blade Axial Dovetail Attachment. Enlarged cross-section view shows centrifugally induced bending moment

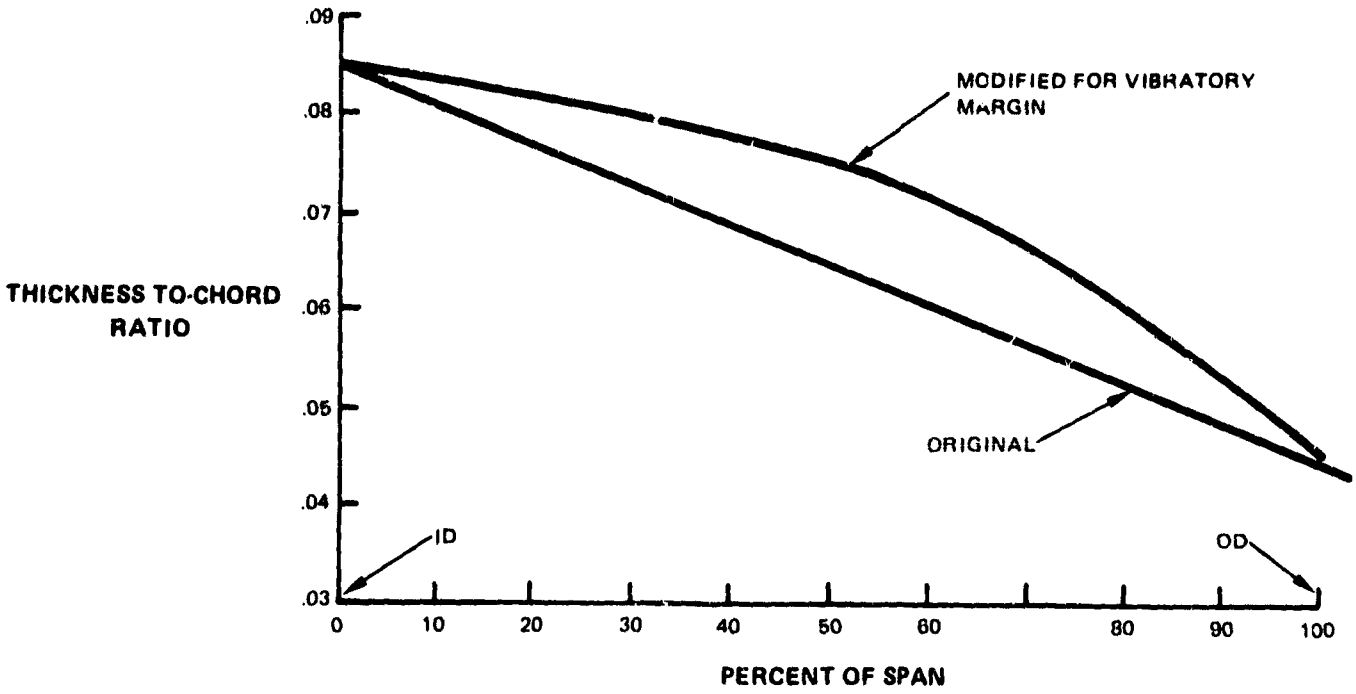

Figure 28 Last Stage Low-Pressure Compressor Thickness Redistribution. Details show redesign necessary to achieve adequate vibration margin.

cavities and good sealing were sought to achieve the desired stability and performance in the intermediate case and high-pressure compressor. A relatively simple design was also a goal to meet cost objectives.

Several basic configurations (and variations) were considered in the study.

These included

1. Platformless vanes individually potted with rubber to a slotted aluminum shroud

2. A full-platform with vanes collectively potted to the shroud with injected rubber

3. Seals/shrouds riveted/brazed to the vanes

All of these concepts utilize a rubber seal that is molded to the inner surface of the shroud. Knife edges on the drum rotor complete the sealing.

Aerodynamic analyses of the cavity size effects for each of these concepts were based on rig test results. All concepts were similar to production engine configurations, making cost estimating relatively straightforward. Results indicated that the first two inner shroud approaches were more expensive than the third. They also had smaller cavity size and, therefore, better performance. Even though the third concept traded most favorably on cost effectiveness, it was rejected because of stability concerns with the large cavity volume. Although estimated to be more expensive than the second option, the first concept was selected, pending a more detailed design, because of the substantial successful operating experience with it in production engines. The selected concept is shown in Figure 29.

4.2.5 Design Summary

Table 18 summarizes current design results for the low-pressure compressor. The preliminary design satisfies all of the aerodynamic, mechanical, and structural requirements discussed in Section 4.2.1.

4.3 COMPRESSOR INTERMEDIATE CASE

4.3.1 Design Requirements

The compressor intermediate case assembly performs many functions in support of other engine parts and components, and as such has a very important effect on the overall engine cost, weight, and performance. The basic aerodynamic requirement of the compressor intermediate case

TABLE 18

LOW-PRESSURE COMPRESSOR PRELIMINARY DESIGN SUMMARY
AERODYNAMIC DESIGN POINT

Pressure Ratio	1.77
Corrected Inlet Flow kg/sec (lb/sec)	64.7 (142.7)
Surge Margin, %	20
Adiabatic Efficiency, %	89.9
Low Cycle Fatigue Life, missions	20,000
hours	30,000

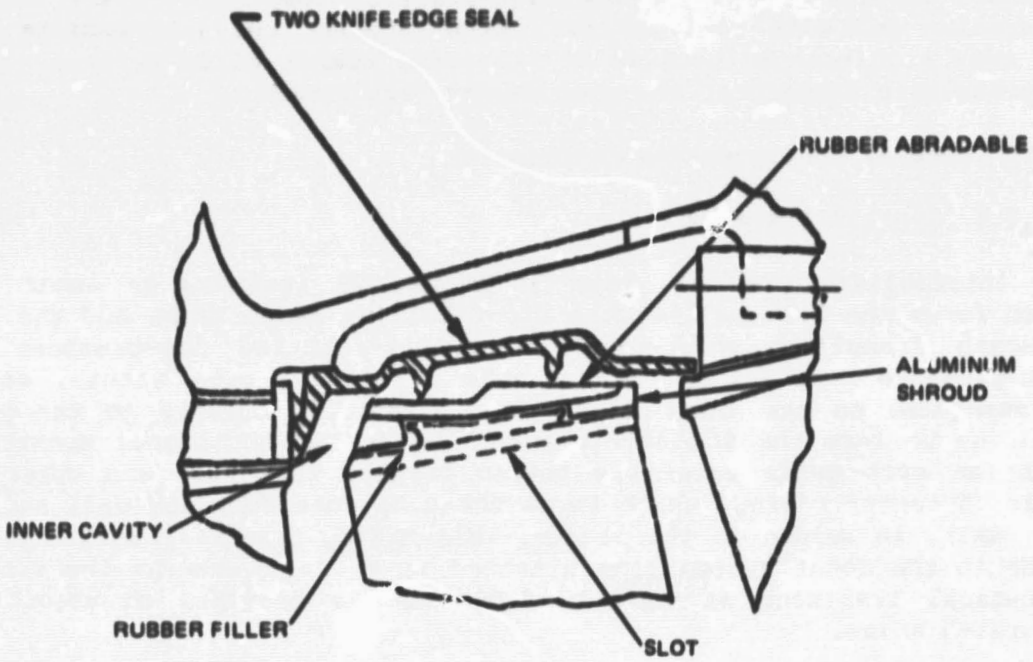

Material: AMS 6304 Steel

Alternates Considered

1. Integral K.E. Rotor Seal
2. Bolted in K.E. Ring

Figure 29 Cross-Section of Low-Pressure Compressor Inner Seal. Configuration is chosen based on proven performance advantages of minimal cavity volume.

is to duct air from the low-pressure compressor exit to the high-pressure compressor exit to the high-pressure compressor inlet without separation and with minimum loss. Structurally, the intermediate case has many requirements because of its large number of interfaces. Table 19 presents a summary of the case design requirements.

4.3.2 General Configuration Description

4.3.2.1 Overall Assembly

The intermediate case as shown in Figure 30 includes an inner ring which forms the O.D. wall of the front bearing compartment and the I.D. flowpath transition wall between counter-rotating low-pressure and high-pressure compressors. Eleven main structural core struts, welded to standoffs on the inner ring, extend radially outward to the outer fan case to form the fan exit struts. Twenty two additional nonstructural fan exit guide vanes are bolted between the inner and outer fan walls. A center casing, which forms the O.D. core flowpath wall and fan I.D. wall, is welded to the struts. This casing transfers engine torque loads to the mount system ring attached to the backside of the struts. Acoustical treatment at the fan I.D. wall is provided to absorb fan generated noise.

The accessory drive system (see Figure 31) includes a drive gear, supported from the core inner ring, which transfers power from the high-pressure compressor rotor to the accessory drive shaft within the bottom strut. The shaft then transfers the torque to an angled gearbox located behind the center casing. The gears are sized by starting torque. The shaft diameter is sized to accept required torque loads and to avoid critical speeds.

4.3.2.2 Major Subassemblies

4.3.2.2.1 Structural Struts

The 11 structural struts act as beams which change in cross-section from the core flowpath I.D. to the fan case O.D. (see Figure 32). Core section cross-sections are axial and symmetrical, uncambered airfoils. The fan portion of the struts double as turning fan exit guide vanes. The core and fan sections are connected by a transitional beam section within the center casing. The struts are made of 6Al-4V titanium and are hollow to reduce weight and to provide passages for the towershaft and oil lines. The thicker top strut forms the front end of the pylon. Adjacent struts are aerodynamically matched to the pylon airflow blockage. Pads at the transition portion of the struts receive mount ring bolts to transfer engine loads to the mount system. The leading edge of the struts is slanted perpendicularly forward to the flowpath to provide a direct loadpath from the No. 1 bearing support through the struts to the mount to minimize rotor deflections.

TABLE 19

COMPRESSOR INTERMEDIATE CASE DESIGN REQUIREMENTS

Aerodynamic

1. Form stable, low-loss flowpath transition between compressors

Structural/Mechanical

1. Support the fan case
2. Provide a portion of the fan flowpath and "V" grooves for clamping of nacelle "D" ducts
3. Carry nacelle loads (load sharing assumed)
4. Support fan exit vanes
5. Support low-pressure compressor static structure and bleed system
6. Support fan and high-pressure compressor rotors
7. Provide front mount locations
8. Support accessory drive shaft and gears

Life

1. Greater than overall engine

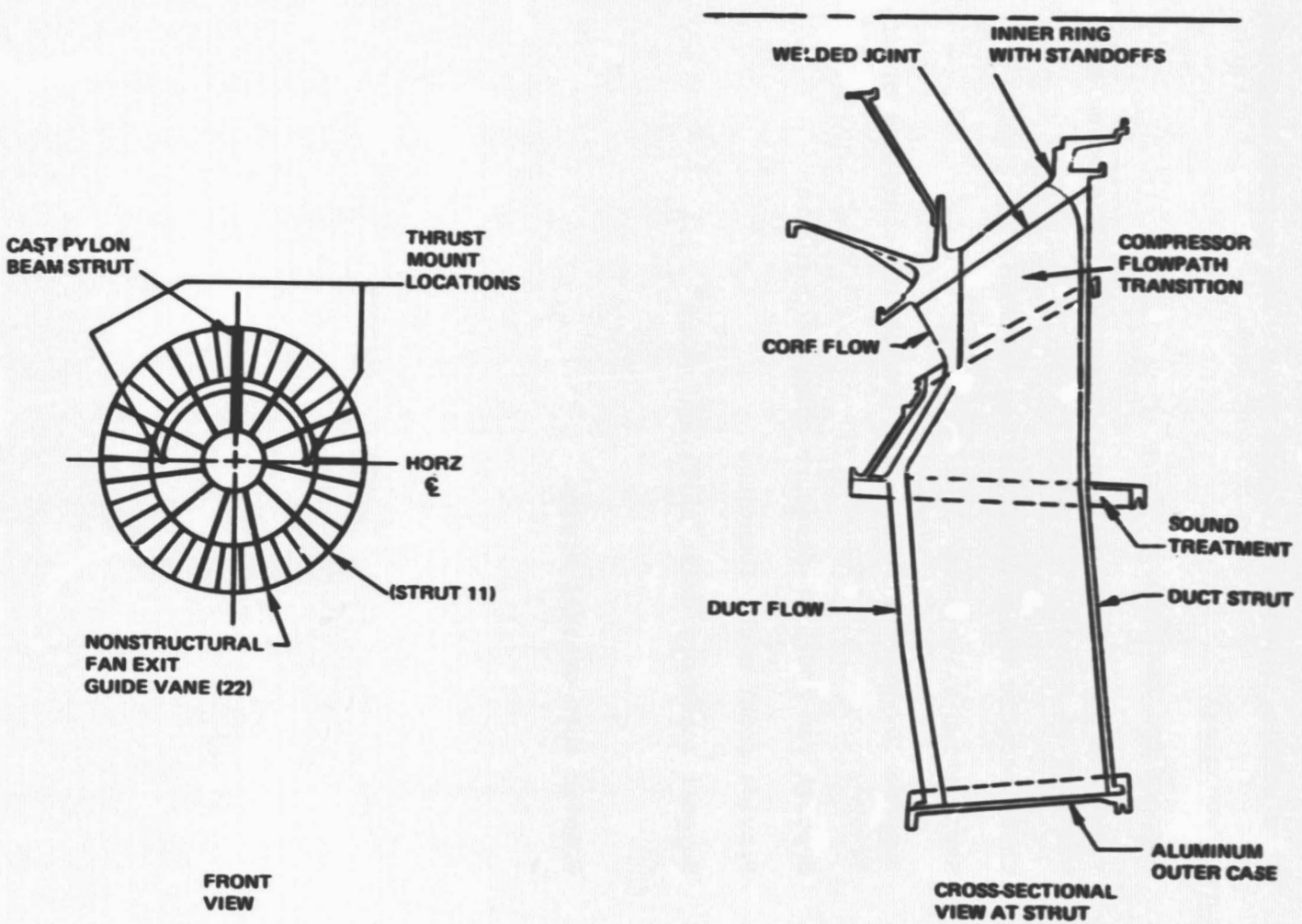

Figure 30 Compressor Intermediate Case. Callouts define major features of the 11 struts, 22 vane configuration.

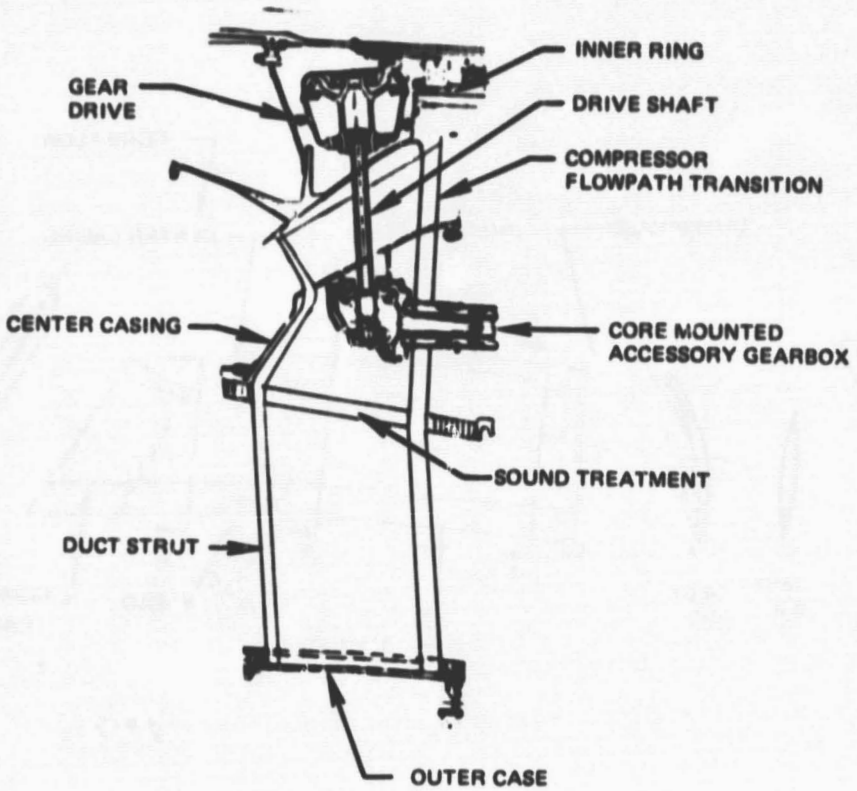

Figure 31 Compressor Intermediate Case Bottom Strut. Cross-section view shows accessory drive design.

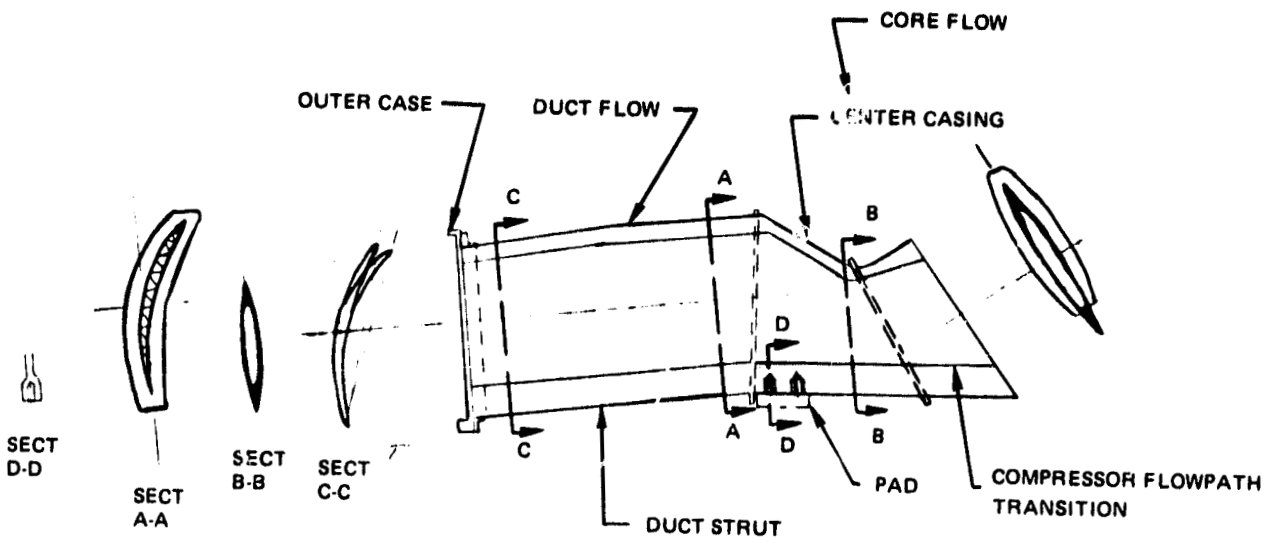

Figure 32 Compressor Intermediate Case Strut. Spanwise cross-sections show variations from uncambered, symmetrical root sections to cambered outer sections.

4.3.2.2.2 Non-Structural Fan Exit Guide Vanes

The 22 non-structural fan exit vanes are located in groups of two between the 11 structural vanes. The aerodynamics of these vanes are also tailored for pylon matching. The vanes (see Figure 33) are hollow with 0.038 cm (0.015 in.) thick skin and stiffeners. These vanes are fabricated from 6Al-4V titanium to save weight. Composites were also considered but were rejected since higher projected costs traded unfavorably with a small 0.14 kg per vane (0.3 lb) weight savings. The vanes are mounted in collars filled with rubber for damping to ensure that no loads are transferred into them. The collars are bolted to the I.D. and O.D. duct walls for vane retention.

4.3.2.2.3 Transition Duct Flowpath

The compressor intermediate case transition duct flowpath is shown in Figure 34. Diffusion rates were controlled by adjusting wall curvature and utilizing strut blockage. The peak curvature and blockage effects occur on the inner diameter wall just forward of the trailing edges of the struts where local diffusion reaches a maximum. The assumed flowpath blockage effects are shown in Figure 35 to illustrate the influence of blockage on diffusion rate.

4.3.2.3 Technology Development Requirements

Both the structural struts and non-structural fan exit vanes are planned to be manufactured by a process currently under development. This process consists of diffusion bonding followed by superplastic forming to a finished shape. The process allows use of complex vane structures, provides smooth, accurate aerodynamic shapes and lends itself well to the complex spanwise transitions of the struts. Various standoffs and support collars will also be diffusion bonded in one operation, resulting in considerable savings in cost compared to conventional manufacturing techniques.

4.3.3 Supporting Analysis

4.3.3.1 Structural Arrangement Selection

Existing Pratt & Whitney Aircraft commercial engines have a separate fan exit vane row located upstream of the intermediate case struts. This separation can lead to extra cost and weight compared with the selected integrated vane and strut design. Integrated vane designs proposed in the past, however, have had high cost and weight due to complex center box structures between the fan and core flowpaths. Therefore this area of the structure was carefully examined to obtain a simpler design approach. The number of structural fan exit vanes carrying loads into the inner case was studied and optimized leading to the simpler ring-beam-ring construction. A low cost steel design was also studied on a cost/weight trade basis, but lightweight titanium

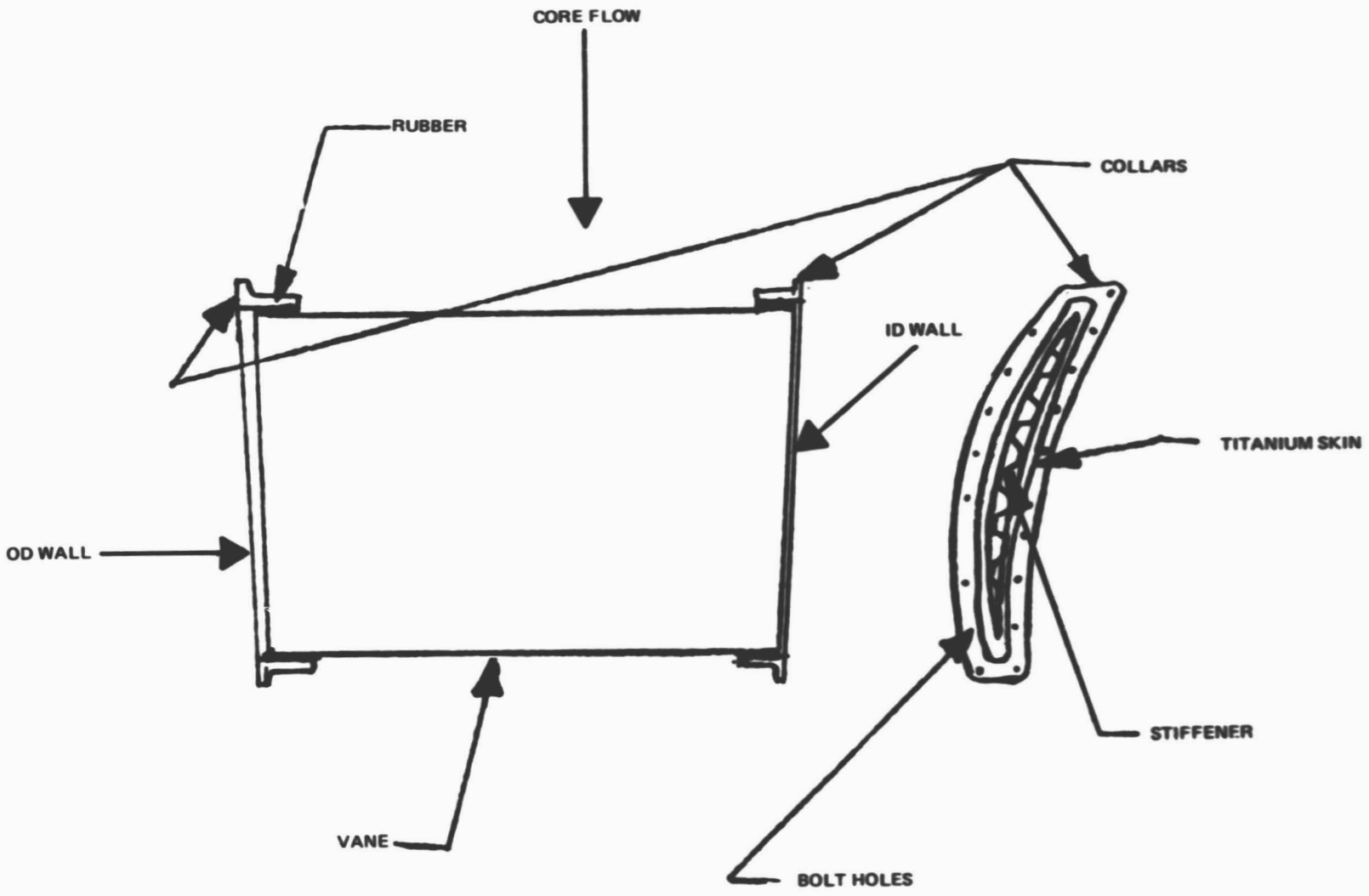

Figure 33 Compressor Intermediate Case. Cross-section shows non-structural fan exit vanes construction.

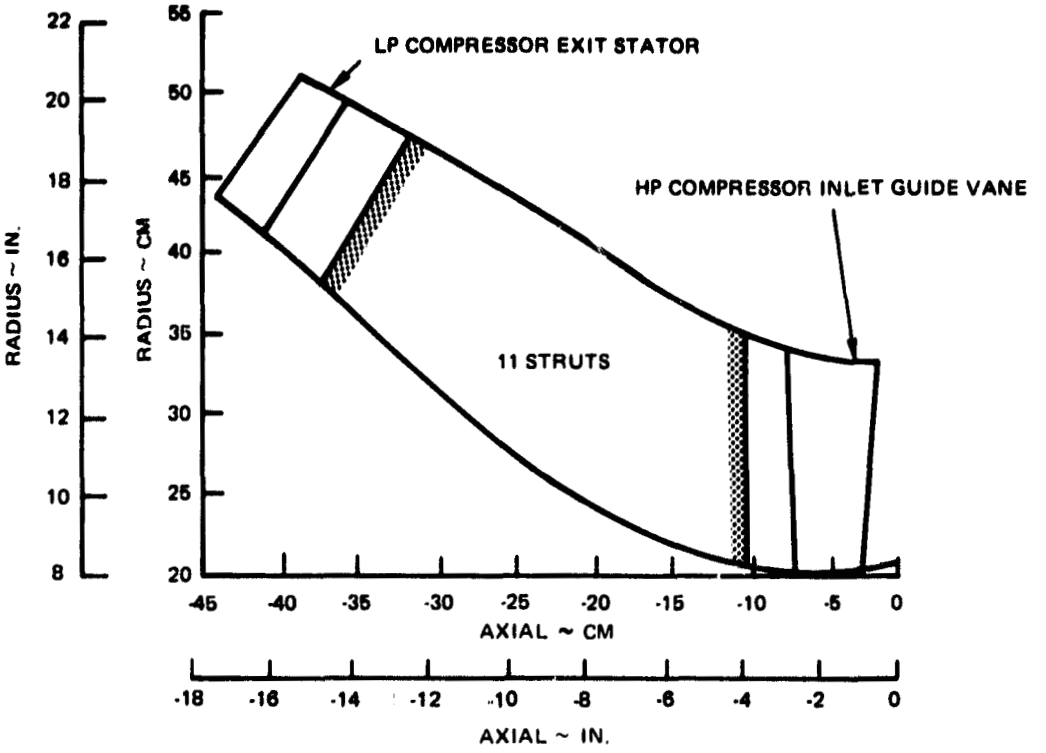

Figure 34 Compressor Intermediate Case. Transition Duct flowpath indicates radial transition between low and high-pressure compressors.

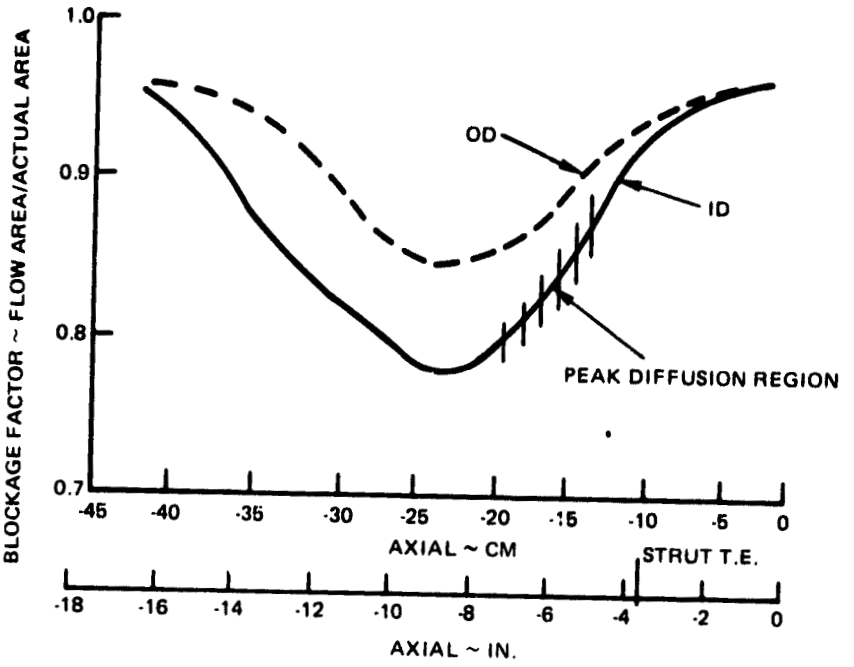

Figure 35 Compressor Intermediate Case. Data indicates inner flowpath blockage distribution and peak diffusion region.

provided a better DOC trade. All other intermediate case designs studied during the preliminary analysis and design phase were found to be significantly more expensive and/or heavier than the selected design.

4.3.3.2 Inner Flowpath Diffusion Rate Prediction

A streamline analysis was conducted on the intermediate case inner flowpath to assess peak diffusion rates on the case walls. This diffusion is caused by the blockage distribution of the intermediate case struts and the curvature of the intermediate case walls. The peak diffusion rate calculated for the case is approximately one-half that of an intermediate case which has successfully performed during repeated testing.

The maximum endwall loading of .20 $P_s/(P_o - P_s)$ for the Energy Efficient Engine design (see Figure 36) is considered to be conservative and within P&WA experience for diffusing passages.

4.3.3.3 Load Analysis

The compressor intermediate case transfers the loads from the high rotor thrust bearing, high-pressure compressor case, low-pressure compressor case, fan outer duct, fan exit guide vane gas loads, center casing pressure, and fan rotor thrust to the mount system. Moments caused from fan blade loss and nacelle maneuver loads are also transferred through the case to the mounts. An estimate of these loads at sea level takeoff was made to quantify the loading requirements and assure adequate case structural stiffness. The approximate loads are shown in Figure 37.

The cummulative loads used to calculate deflections and stress levels were:

1. mount system - 19,350 N (43,000 lb)
2. nacelle moment - 2,820,000 cm-N (250,000 in-lb)
3. blade liberation moment - 85,600,000 cm-N (7,590,000 in-lb).

4.3.3.4 Stress and Deflection Estimates

The compressor intermediate case has relatively low stresses because it is designed to be stiff to limit rotor deflections. The case deflection

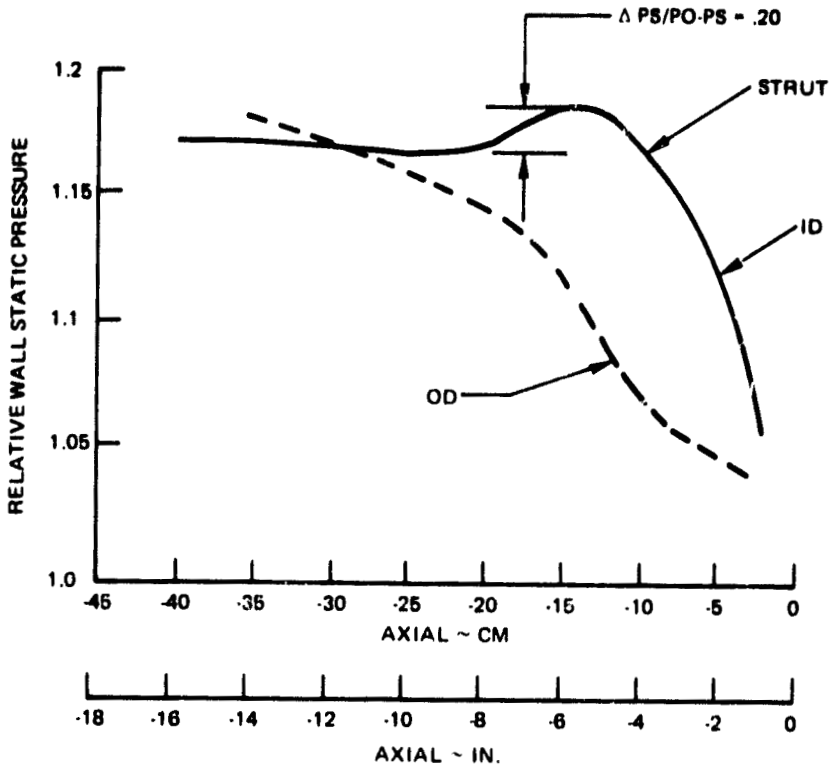

Figure 36 Compressor Intermediate Case. Inner flowpath wall static pressure distributions are within P&WA experience.

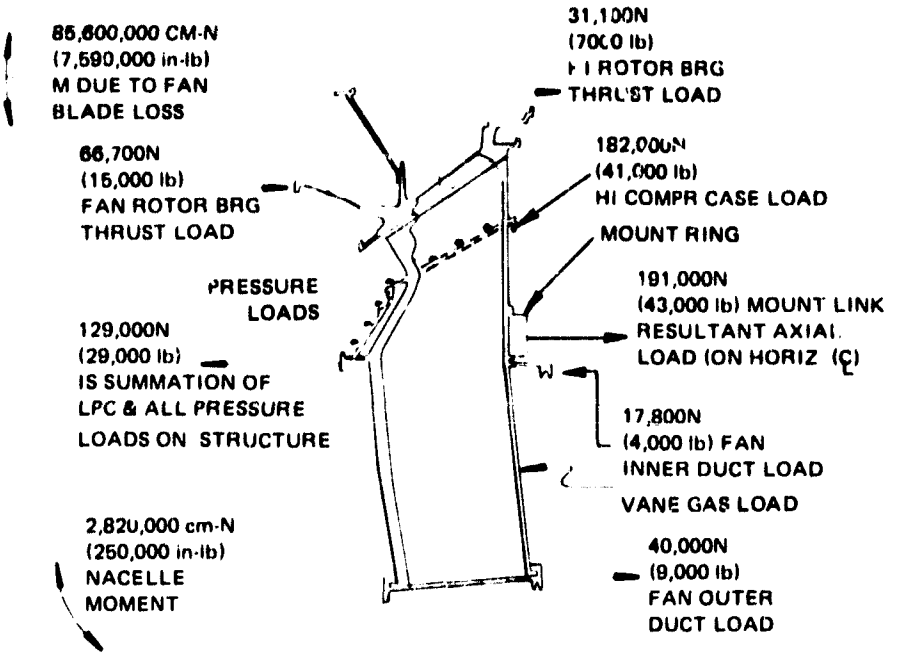

Figure 37 Compressor Intermediate Case. Data includes estimates of structural loading used in stress analysis.

caused from nacelle loads results in only a 0.13 cm (0.050 in) maximum fan blade tip clearance reduction. Preliminary analysis indicates that the maximum beam bending stress is 30 kN/cm^2 (43 ksi). The nonstructural fan exit guide vane bending stress is 21 kN/cm^2 (30 ksi) from tangential gas loads. The No. 1 bearing support cone maximum bending stress caused by fan blade liberation is 38 kN/cm^2 (55 ksi). Results are summarized in Table 20. The preliminary analysis indicates that the stiffness requirements are satisfied with this design.

4.3.4 Design Summary

The ring-beam-ring construction concept, having shown basic feasibility, will be carried into detail design. The preliminary design meets all of the imposed design requirements. Design deflections will be further refined with additional thermal analysis, stress analysis, and fabrication studies to establish final case geometry.

4.4 HIGH PRESSURE COMPRESSOR

4.4.1 Design Requirements

The high-pressure compressor aerodynamic design requirements were also established by the engine cycle definitions at design and off-design conditions. The two key flight conditions were again considered to be maximum cruise and maximum climb at 10,668m (35,000 ft), and the high-pressure compressor aerodynamic design point was located between them. Design requirements at these conditions are summarized by Table 21. The high-pressure compressor efficiency goal is also presented. The takeoff operating condition, major points, and a typical operating line, are shown on the predicted high-pressure compressor map, Figure 38.

Commercial acceptability again dictated high-pressure compressor structural and mechanical design requirements. Based on experience, a design life of 20,000 missions or 30,000 hours was selected for all high-pressure compressor component parts, as shown in Table 21.

4.4.2 Design Background

4.4.2.1 Advanced Multistage Axial Compressor (AMAC)

The high-compressor compressor is technologically evolved from the NASA Advanced Multistage Axial Compressor (AMAC) program, NAS3-19445. The objective of that program was to reduce the number of stages required to provide an 18:1 pressure ratio by increasing wheel speed and blade loading. Forty-nine high-pressure compressors were evaluated in AMAC, and because of the prodigious number of variables involved, a regression analysis was employed during the program.

TABLE 20

COMPRESSOR INTERMEDIATE CASE STRESS AND DEFLECTION SUMMARY (SLTO)

1. Structure is designed to limit fan rotor deflections; therefore majority of stresses are low.

2. Stresses:
   - o Strut bending @ fan duct I.D. - 7.6 kN/cm^2 (11 ksi) - Tangential; 4.8 kN/cm^2 (7 ksi) - Axial
   - o Strut bending @ core duct O.D. - 6.9 kN/cm^2 (10 ksi) - Tangential; 30 kN/cm^2 (43 ksi) - Axial
   - o Fan exit guide vanes - 21 kN/cm^2 (30 ksi) from tangential gas load
   - o No. 1 bearing support cone - 38 kN/cm^2 (55 ksi) due to fan blade loss

3. Deflection limits
   - o Imposed nacelle loads result in 0.13 cm (0.050 in.) maximum reduction in fan blade tip clearance.

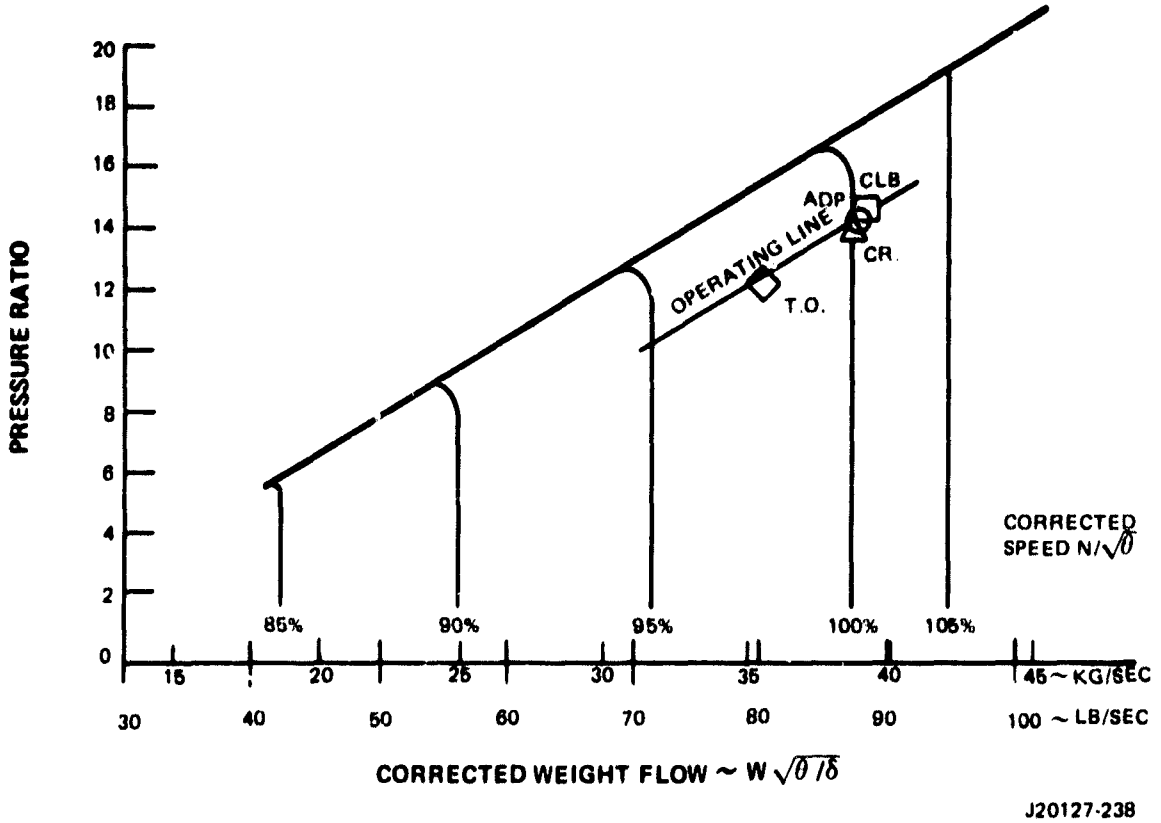

Figure 38 Predicted High-Pressure Compressor Operating Map. Data shows aerodynamic design, 10,668 m (35,000 ft) Mach No. 0.8 cruise/climb, and takeoff points.

TABLE 21

HIGH-PRESSURE COMPRESSOR DESIGN REQUIREMENTS
(Mach 0.8 - 10,668 m (35,000 ft)

Aerodynamic Parameters	Max Climb	Max Cruise	Aerodynamic Design Point
Pressure Ratio	14.2	13.85	14.0
Inlet Corrected Flow			
kg/sec	39.6	38.7	40.0
(lb/sec)	(88.7)	(87.5)	(88.1)
Surge Margin	25%	25%	25%
Adiabatic Efficiency Goal			
Efficiency	0.880	0.803	0.882
Life Requirements			
Low Cycle Fatigue Life	20,000 missions or 30,000 hours		

Table 22 summarizes the major aspects of the AMAC program, outlining the figures of merit employed and the parametric design variables investigated. This program identified several features that were incorporated into the Energy Efficient Engine compressor design. Some of the trends identified are presented in Table 23.

4.4.2.2 Energy Efficient Engine Preliminary Design and Integration Studies (NAS3-20628)

The preliminary design and integration studies conducted under NASA contract NAS3-20628, expanded from the AMAC study to the consideration of high-pressure compressors with 18:1 and 14:1 pressure ratios. Parameters explored on a meanline basis were similar for both pressure ratio levels.

A second phase of the contract was devoted to the preliminary aerodynamic design of the selected high-pressure compressor airfoils. The streamline analysis computer program was utilized to establish the spanwise velocity triangles throughout the high-pressure compressor. This phase included loading and surge studies. The preliminary airfoils were selected, utilizing cascade design decks. Preliminary flutter and resonance studies were conducted to ensure structural integrity. Because of these considerations, airfoil changes were also made. The resultant high-pressure compressor definition, reported in Reference 1, became the starting-point for the current preliminary design.

4.4.3 General Configuration Description

4.4.3.1 Major Subassemblies

The Energy Efficient Engine high-pressure compressor has ten stages. Its inlet diameter is 71.6 cm (28.2 in.) and the exit is 56.9cm (22.4 in.). The first four stages have variable geometry stators. The front case is axially split, and the rear case is not. Active clearance control is incorporated only in the rear stages. Inlet and exit hub-to tip leading edge radius ratios are 0.63 and 0.922, respectively. An average aspect ratio of 1.56 results in a total of only 1352 airfoils, including 32 inlet guide vanes.

The high-pressure compressor cross-section and flowpath design features are shown in Figure 39. Major subassemblies and features shown include the drum rotor, inner flowpath seals, front case and variable stators, rear case and fixed stators, active clearance control (ACC) system on the rear case, and bleed systems. The rotor assembly is comprised of separate front and rear drum sections bolted together. Seven stages are included in the forward drum with three stages in the rear drum. The front two stages have axial blade slots, and the remainder have circumferential slots. The circumferential slots are sealed by a unique ladder seal to prevent leakage around the blade platform (see Figure 40). The seal is held tightly against the underside of the platform by

TABLE 22

MAJOR ASPECTS OF AMAC DESIGN STUDY

1. Define Optimum 18:1 Pressure Ratio Compressor
   - Advanced Technology Transport Engine STF477
   - Engine OPR 45:1
   - 6 to 12 HPC Stages

2. Figures of Merit
   - HPC Efficiency
   - Fuel Burned
   - DOC
   - ROI

3. Matrix of HPC Configurations Evaluated by Regression Analysis to Select Optimum HPC

4. Parametric Variables

Rotor Speed	-	Reaction
Flowpath Geometry	-	Blade Aspect Ratio
Inlet Specific Flow	-	Solidity
Inlet Hub-Tip Ratio	-	Number of Stages
Exit Mach Number		

TABLE 23

TRENDS IDENTIFIED IN THE AMAC STUDY FOR MAXIMIZING HIGH-PRESSURE COMPRESSOR EFFICIENCY AND MINIMIZING DOC

- Low Aspect Ratio
- Low Hub-Tip Ratio
- High Tip Speed
- Increased Gap-to-Chord
- Reduced Number of Stages

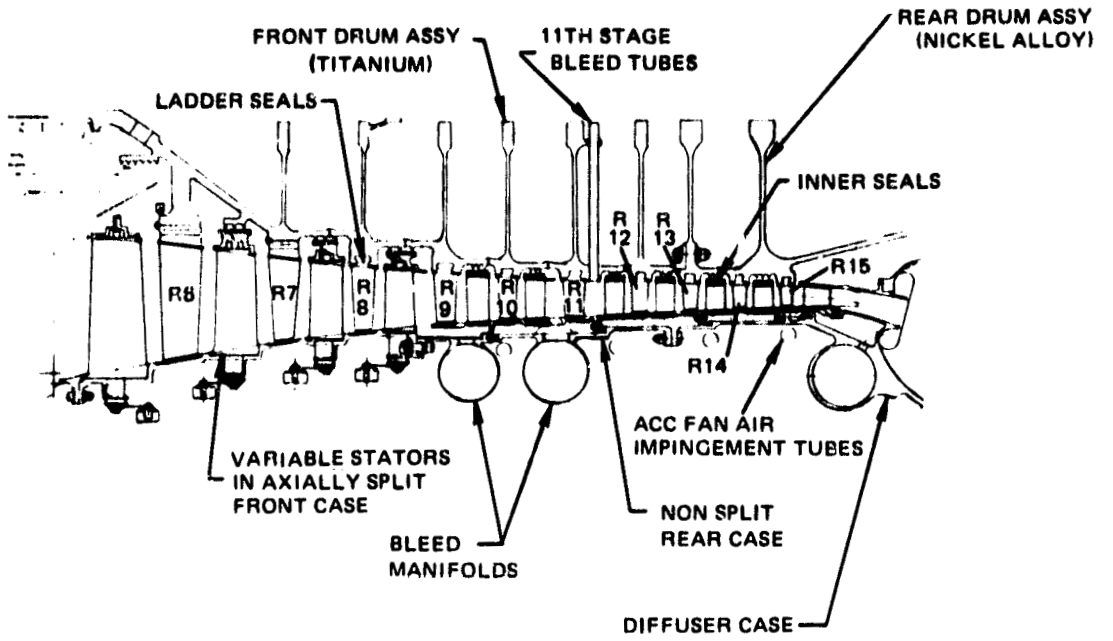

Figure 39 High-Pressure Compressor. Cross-section shows main design features.

centrifugal force; disk rim grooves hold the seal firmly in the axial direction.

Rotor assembly cavities to accommodate stator inner shrouds are small in volume and sealed to improve efficiency. These seals consist of three knife edges, as an integral part of the drum rotor, which run on seal lands supported by the stator vanes. The knife edges are abrasively coated to minimize wear, while abradable seal lands for the static parts are made from rubber for stages 6 through 8, and nichrome polyester for stages 9 through 15.

Variable geometry stator mechanisms used in the first four stages are of a proven P&WA design. The front case and stator inner shroud ring are axially split for assembly over the drum rotor. Stator material selection was governed by fire avoidance criteria. Stators 6, 7, and 8 and the stator inner shrouds are stainless steel, whereas the highpressure compressor IGV, which is subjected only to low stresses, is aluminum, (AMS 4132). Rotor blade tip rubstrips include a steel insert under abradable rubber to prevent the blade from rubbing the titanium case. A circumferential trench is included in the rubstrip to improve performance.

The rear case, shown in Figure 41 is a full-hoop configuration. This configuration reduces cost and weight, provides a continuous pressure vessel and load path, reduces leakage, and eliminates ovalization, all of which allow tighter blade tip running clearances. A titanium case is used with the titanium drum rotor portion, and a nickel alloy diffuser case extension is used with the nickel rear drum rotor to provide thermal expansion matching for tip clearance control. Assembly is accomplished by sliding the case over segmented stator assemblies to engage stator retaining hooks and provide sealing. Strip stock airfoils with brazed inner and outer shrouds are used to form the stator assembly. Both the inner and outer stator shrouds are segmented to permit the ACC system to set the tip clearances. Slots and clearances provide for thermal movement of the segments, while slot positioning and feather seals minimize leakage. Nichrome-polyester is used in the rear case for the abradable rub strip over the blade tips. Trenches are also employed in these rub strips to improve performance.

An external ACC tube system impinges fan air directly on the rear high pressure compressor case to control tip clearances at cruise.

The rear case and stator assembly was designed to accommodate the ACC system. Vanes are brazed into segmented shroud subassemblies that provide the circumferential gap needed to permit case thermal movement that occurs with the impingement of fan air. The ends of the segments are attached to the outer case by means of hooks. Insulation is provided between the shrouds and the outer case to isolate the case from the gas path temperatures, thereby reducing the fan air needed to effect a given clearance change. The details of the rear case assembly, showing ACC and bleed manifolds, are shown in Figure 41.

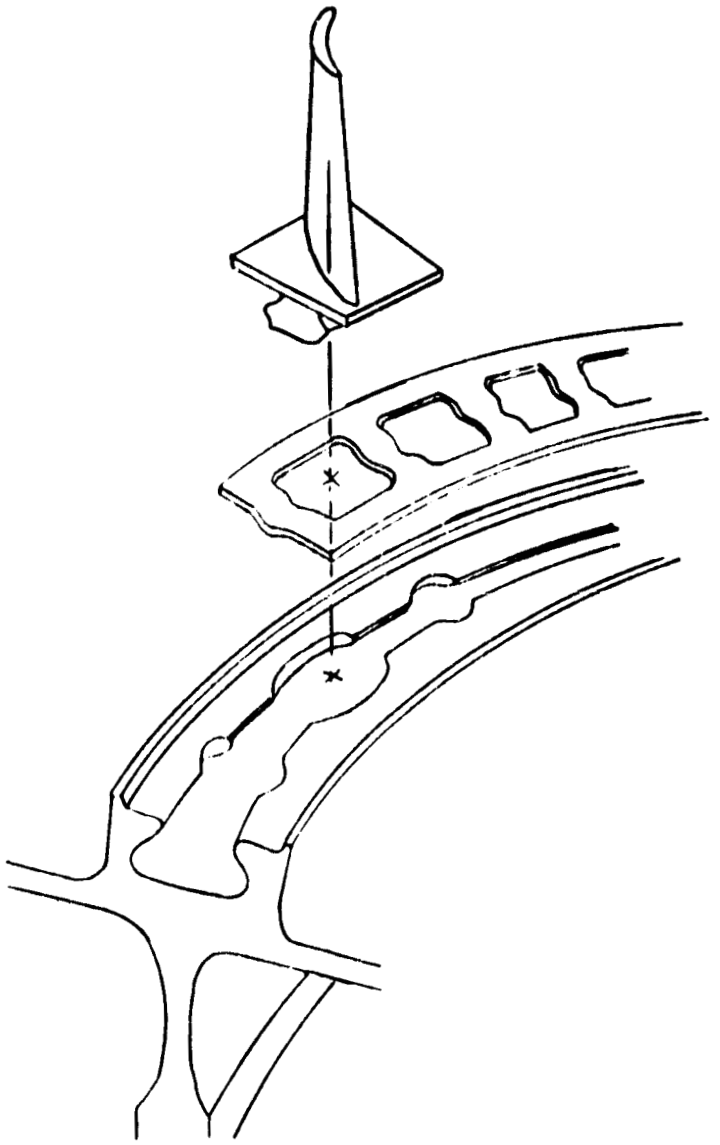

Figure 40 High-Pressure Compressor. Ladder seals prevent compressor blade platform leakage.

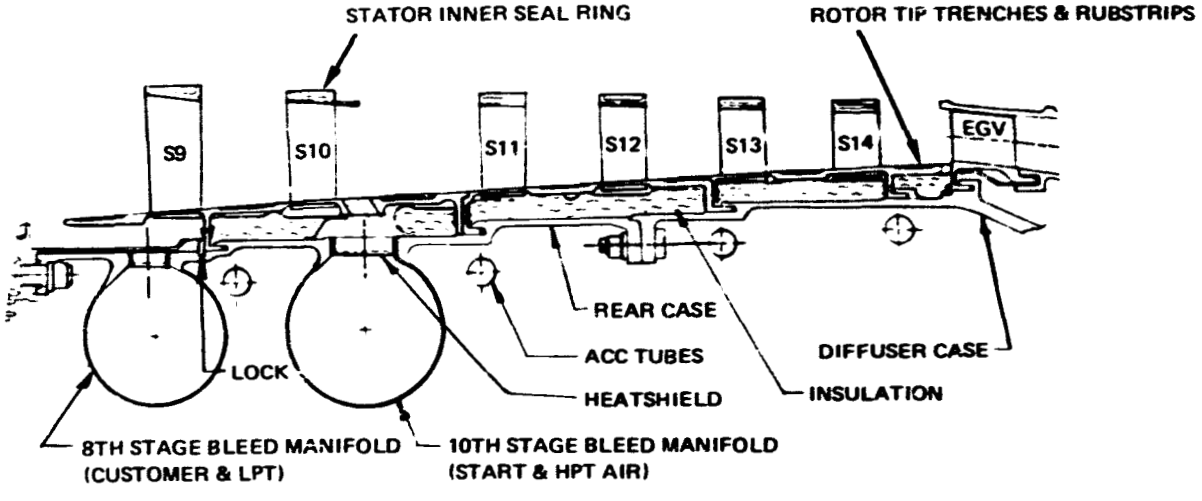

Figure 41 High-Pressure Compressor. Rear case assembly incorporates active clearance control features.

J20127-235
783011

Bleed air is extracted at the 8th stator row trailing edge outer diameter, 10th stator row trailing edge outer diameter, and 11th rotor row trailing edge inner diameter. Manifolds are used to collect the 8th and 10th stage bleed air while the 11th stage bleed air is extracted by means of solid body rotation tubes. These tubes prevent the heat rise and pressure loss that would occur in a free vortex system.

4.4.3.2 Efficiency Improvement Features

High loading and high relative Mach numbers are employed in the front stages of the high-pressure compressor. The airfoils used in these stages - multiple circular arcs - have been developed to minimize losses at supersonic velocities. The effectiveness of the multiple circular-arc airfoil has been demonstrated during fan research programs.

The efficiency of the middle sections of the high-pressure compressor is improved through the employment of controlled diffusion and low loss leading edge airfoils. The controlled diffusion airfoil is a specially designed configuration made practical during the past few years by new computational techniques. Heretofore, only NACA standard series airfoils could be employed.

Aerodynamic losses have been found to decrease with reductions in airfoil surface roughness. Coatings and improved manufacturing processes are to be used to reduce the roughness of blade surfaces from about 60 microns to 30 microns.

The rear stages of the high-pressure compressor employ active clearance control. This advanced concept provides the single largest increase in high-pressure compressor efficiency. Active clearance control reduces leakage by minimizing blade tip running clearance requirements. The size of the stator cavities is also being reduced to minimize endwall losses.

4.4.3.3 Titanium Fire Preventive Features

Titanium is not used beyond the inlet guide vane leading edge plane for the stators or beyond the seventh rotor trailing edge plane for the blades. Steel or nickel alloy inserts and liners are used in the titanium cases over the blade tips and in the bleed manifolds to prevent titanium fires.

4.4.3.4 Principal Aerodynamic Design Parameters

The principal aerodynamic design parameters are listed in Table 24. The pressure ratio of 14:1 in ten stages and the use of only four variable-geometry stages is an aggressive design step. The tip speed is moderate, reflecting the need both to minimize the number of stages and to achieve high efficiency. The inlet flow per unit area and the average gap chord ratio are at the high extreme of Pratt & Whitney Aircraft

experience. The average aspect ratio of 1.56 is set low to minimize both the size of the compressor and the number of blades. Surge loading levels for the high-pressure compressor are high and represent aggressive design increases.

The exit Mach number of 0.28 is typical of current commercial engine experience. The average axial-velocity-to-wheel-speed ratio of 0.55 is low, and was chosen to achieve optimim efficiency. The surge margin for the preliminary design is 25 percent.

4.4.3.5 Technology Development Requirements

The major advanced aerodynamic concepts incorporated in the high-pressure compressor design to increase efficiency potential are presented in Table 25. A discussion of each feature and its status is presented in the following sections.

4.4.3.5.1 Contoured Airfoil

The multiple circular arc (MCA) airfoil is one example of specially contoured airfoils to be used in the high Mach number front stages of compressors. MCA airfoils feature straight leading edges at the suction surface to minimize supersonic acceleration prior to the normal shock. This results in a lower shock inlet Mach number, which reduces the pressure loss across the shock. Viscous losses are also reduced because of less shock-induced endwall boundary layer separation.

Pratt & Whitney Aircraft is currently engaged in a NASA Front Stage Program (NAS3-20809) to further demonstrate MCA airfoil potential in compressors. The Front Stage Program is investigating the application of MCA airfoils in the rotor of a 428 m/sec (1450 ft/sec) tip speed compressor stage that develops a pressure ratio of about 1.8:1. This stage, operating at a somewhat lower speed, would have velocity triangles closely resembling the first stage of the compressor designed for the Energy Efficient Engine. The design of the stage has been completed, and it is scheduled for testing in 1979.

The advantages of MCA airfoils have also been demonstrated in a NASA sponsored program (NASA CR-72298) in which two stator designs were run behind the same rotor. The first design had conventional double circular-arc (DCA) airfoils, while the other had MCA airfoils. At Mach numbers of 0.9 and greater, the MCA airfoils had substantially lower loss coefficients. The data presented in Figure 42 compares the minimum loss coefficients for both designs at the optimum incidence angle.

Recently, it has also become practical to calculate compressible flow through a cascade, including viscous effects. Pressure distribution on the suction surface of an airfoil can now be tailored to avoid strong shock waves, reducing both inviscid shock losses and viscous losses in the cascade passages. As a result, passage shock strength is reduced,

TABLE 24

HIGH-PRESSURE COMPRESSOR DESIGN PARAMETERS
AERODYNAMIC DESIGN POINT

Number of Stages	10
Pressure Ratio	14
Adiabatic Efficiency, per cent	88.2
Polytropic Efficiency, per cent	91.7
Surge Margin, per cent	25
Inlet Corrected Flow, kg/sec (lb/sec)	40.0 (88.1)
Inlet Corrected Tip Speed, m/sec (ft/sec)	404 (1323)
Inlet Specific Weight Flow, kg/sec/m^2 (lbs/sec/ft^2)	186 (38)
Hub/Tip Radius Ratio - Inlet Exit	0.63 0.922
Exit Mach Number (without blockage)	0.28
Average Airfoil Aspect Ratio	1.56
Average Gap-Chord Ratio	0.93
Average Axial Velocity/Wheel Speed Ratio	0.55
Number of Variable Stator Vanes	4
Number of Airfoils (incl. IGV's)	1352
Number of IGV's	32
Flowpath Type	Const. Mean Dia.

TABLE 25

HIGH-PRESSURE COMPRESSOR ADVANCED TECHNOLOGY CONCEPTS

Contoured Airfoils
Rotor Tip Trenches
Reduced Rotor Tip Clearances
Reduced Roughness Airfoils
Low Loss Leading Edge Airfoils
High Loadings
Improved Inner Flowpath Cavity Design

diffusion is nearly uniform, and shock-induced boundary layer separation is minimized, to create a "shockless" airfoil. The technique was originally suggested and perfected for isolated airfoils by R. Whitcomb of NASA Langley in the 1960's .

A program has been proposed to NAVAIR which would experimentally verify a deviation system for these airfoils. A follow-on to the NASA Front Stage Program (NAS3-20809) has been proposed which would replace the stator in the original program with a controlled diffusion stator. This program would be very important since it would provide data in a full-stage environment.

4.4.3.5.2 Tighter Running Clearances

That high losses in compressor efficiency are associated with ordinary blade-tip clearance requirements of rotors is well documented. Figure 43, which correlates a reduction in compressor efficiency with the ratio of tip clearance to blade height, indicates about a two percentage point drop in polytropic efficiency for each percent age point increase in the normalized clearance. Mechanical design innovation and effective use of ACC are needed to further reduce clearances from current designs.

In concert with reduced clearances, the use of tip trenches appears to offer an effective means for improving efficiency.

4.4.3.5.3 Increased Blade Loading

High stage loading in the Energy Efficient Engine high-pressure compressor, the primary means of reducing the number of stages, was limited to levels consistent with high efficiency. The relationship of loading level and loss utilized in selecting these loading levels is illustrated in Figure 44.

The upper curve, which denotes loss parameter as a function of diffusion factor, was taken from Reference 4. This curve can be transformed into the lower curve by cross plotting loss against gap-to-chord ratio which increases with the diffusion factor. As the gap is increased, cascade loss (Zp) decreases, reaches a minimum, and then increases. For high performance it is advantageous to set blade and stator loading levels at the point of minimum loss. This increased loading, low loss concept has also been incorporated into the NASA Front Stage Program, NAS3-20809, discussed earlier. For additional test verification, this philosophy is also included in the Energy Efficient Engine compressor design.

4.4.3.5.4 More Durable, Smoother Airfoils

Experience with in-service production engines has shown that the leading edges of compressor airfoils erode away steadily to cause a

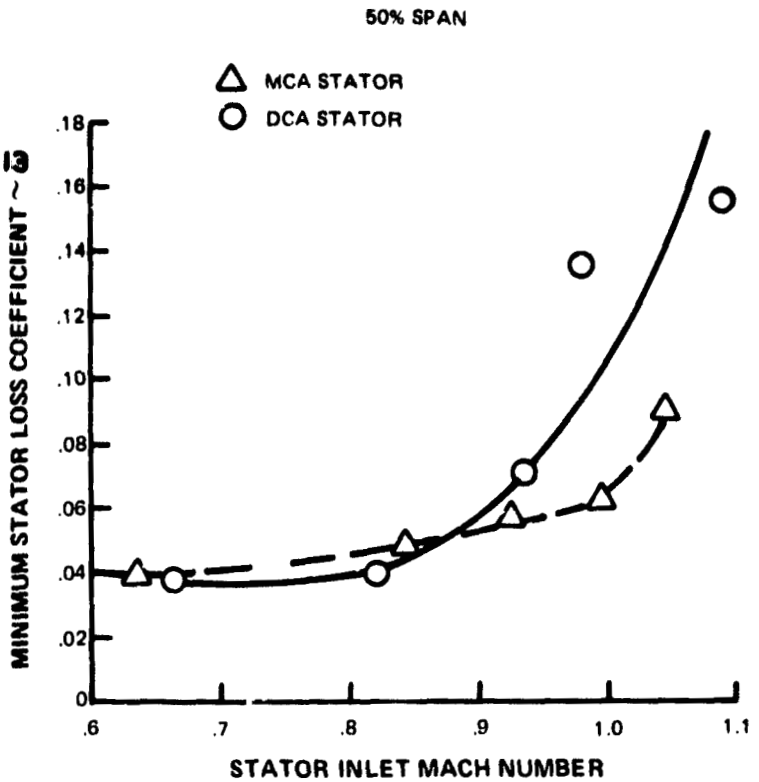

Figure 42 High-Pressure Compressor Advanced Technology. Data shows high Mach number loss comparison of MCA and DCA compressor airfoils.

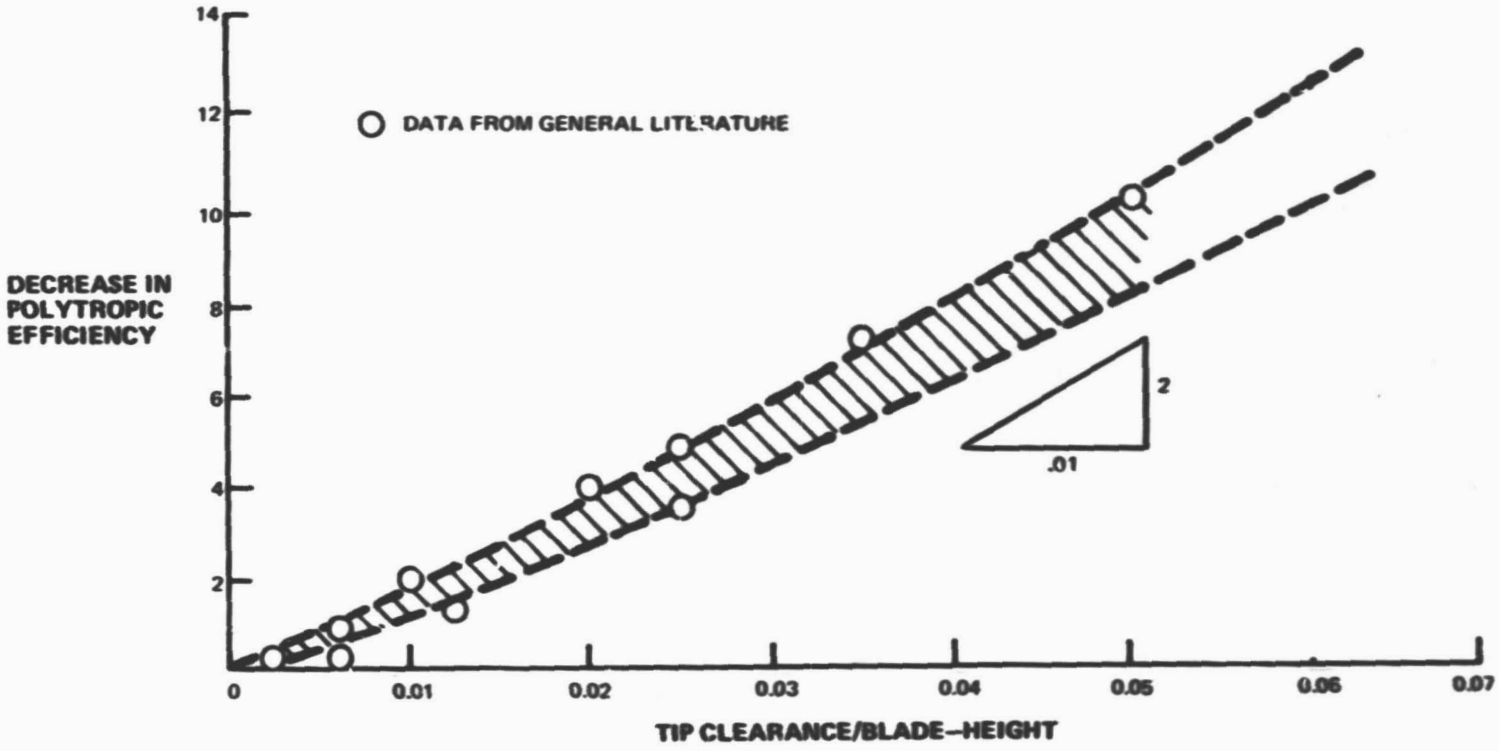

Figure 43 High-Pressure Compressor. Efficiency versus tip clearance correlation plus test data illustrate importance of tight clearances.

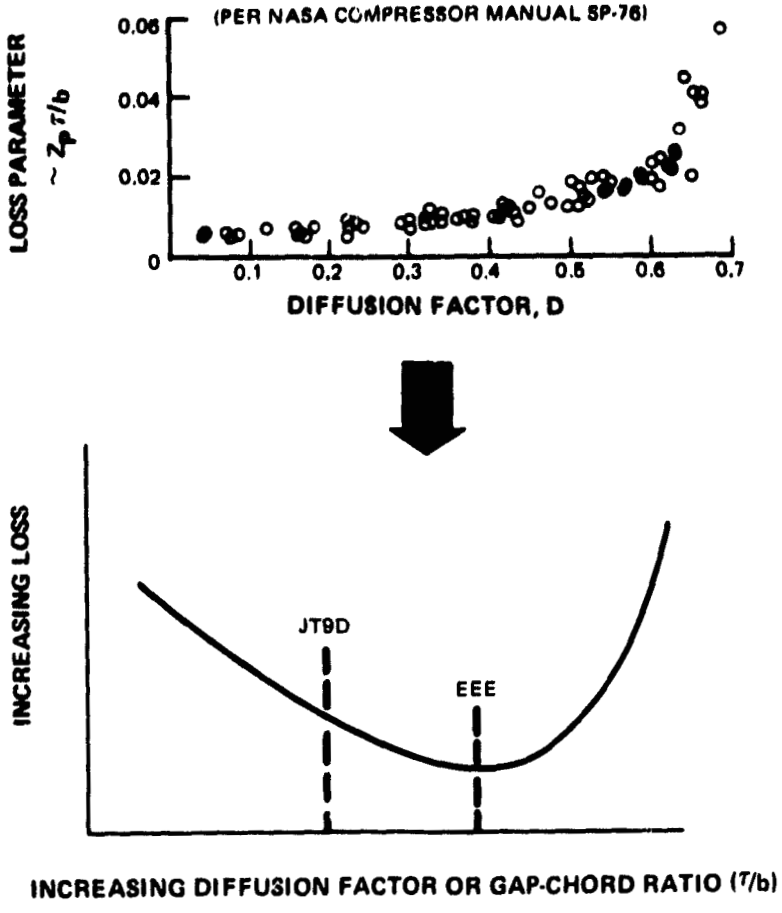

Figure 44 Cascade Loss with Loading. Optimal blade loading minimizes compressor airfoil losses.

gradual loss in compressor performances. The controlled diffusion design technology now permits design of airfoils with increased leading edge radii at no penalty in performance. Cascade tests have confirmed this observation. The Energy Efficient Engine high-pressure-compressor will include thicker leading edge blading to verify the performance potential of the more durable airfoils in a multi-stage test environment.

The performance of airfoils is highly sensitive to airfoil surface roughness, as shown by Figure 45. This correlation shows that a significant loss reduction can be attained by minimizing surface roughness at Reynolds numbers representative of those for the Energy Efficient Engine high-pressure compressor.

Advanced coatings and machining techniques are believed capable of reducing airfoil roughness to 30 microns. These techniques will be utilized in the high-pressure compressor to establish the feasibility and benefits of the smoother airfoils. Prior to the Energy Efficient Engine Program demonstrations, the improvement attainable through reduced roughness will be evaluated in the JT8D Engine Performance Improvement Program (NAS3-20630).

4.4.3.5.5 Improved Inner Cavity Design

Recent low speed research compressor tests at Pratt & Whitney Aircraft have evaluated the relationship of stator root cavity size and shape to efficiency potential. Additionally, Pratt & Whitney Aircraft research stage test trends have shown a significant efficiency improvement by minimizing the cavity windage sources and sealing the inner cavity to reduce air recirculation. The Energy Efficient Engine highpressure compressor is designed with very small inner cavities with knife-edge seals to benefit from this technology.

4.4.4 Supporting Analyses

4.4.4.1 Efficiency Prediction

The high-pressure compressor is aerodynamically designed using a streamline analysis computer program. This analysis resulted in an aerodynamic design point efficiency prediction of 88.2 percent. A breakdown of the efficiency projection for the high-pressure compressor is shown in Table 26. The prediction consists of factors accounted for by the current state-of-the-art compressor design system, with projected incremental increases attainable with the incorporation of the advanced technology items discussed in the previous section. As shown in the table, the current design system predicts a base efficiency of 86.2. The advanced technology features are estimated to present a performance potential of 2 percent. Airfoil surface smoothness improvements were estimated to increase efficiency by 0.8 percentage points. A similar improvement was projected with the use of

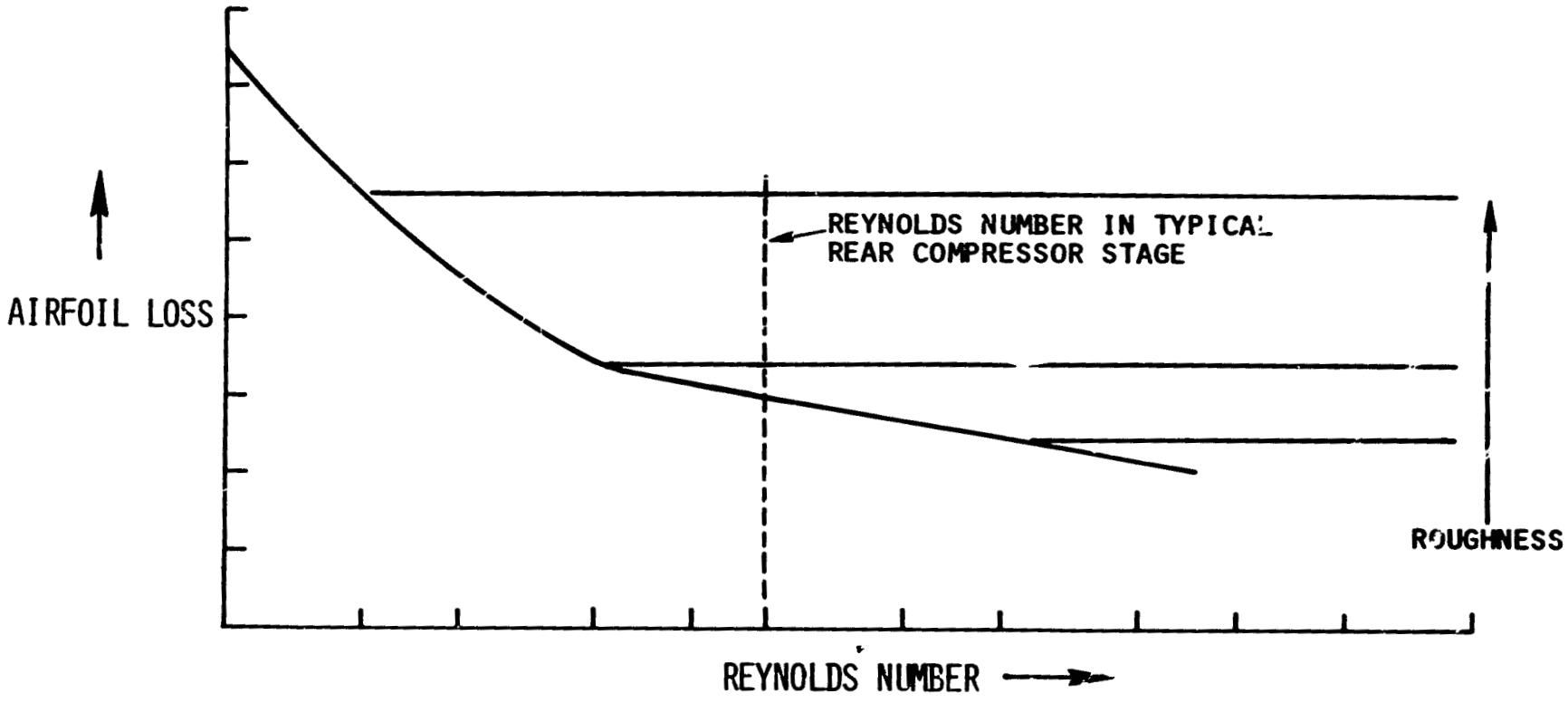

Figure 45 Airfoil Loss with Reynolds Number and Surface Roughness. Loss can be reduced by minimizing roughness.

tip trenches to reduce the adverse effects of tip clearance. Finally, the use of controlled diffusion airfoils was predicted to increase efficiency by 0.4 percentage points.

4.4.4.2 Stability Audit

A stability audit was conducted at the major points in the flight envelope to establish high-pressure compressor surge margin requirements. For each of these points, the surge margin reduction resulting from surge line or operating line degradation was examined to determine the validity of the design surge margin requirement. The destabilizing factors for the high-pressure compressor include variable vane tracking errors, engine deterioration, inlet pressure or temperature distortion, control production tolerance and deterioration, and engine production tolerance. The stability audit made at takeoff is shown in Table 27. Results show takeoff operation to be surge-free. Similar audit results are listed in Table 28 for the other potentially critical flight conditions. The overall audit shows that the high-pressure compressor surge margin requirement at the aerodynamic design point of 25 percent is adequate to assure ample surge margin at all major operating conditions without stability bleeds.

4.4.4.3 Drum Rotor Analysis

A single-wall drum rotor construction was selected over a conventional bolted-up rotor stack to reduce weight and to provide the high stiffness needed for proper clearance control.

A summary of selected materials and calculated stresses in the high pressure compressor rotor system is shown in Figure 46.

4.4.4.4 Airfoil Analysis

4.4.4.4.1 Series Selection

The selection of airfoils is based on the Mach number environment in which they operate and the incidence range requirement of the particular airfoil row. The front high-pressure compressor stages operate at high Mach numbers and require MCA airfoils. The mid-compressor stages operate at high transonic Mach numbers and are candidates for controlled diffusion airfoils. The rear stages operate at low Mach numbers, but over a wide range of incidence angles. As a result, NACA 400 series airfoils are being considered for the five rear stages. Final selection will be made during the detail high-pressure compressor design.

4.4.4.4.2. Stage Loading Distribution Selection

The high-pressure compressor aerodynamic loading distributions were predicated on a loading correlation through the upper limits of P&WA

TABLE 26

HIGH-PRESSURE COMPRESSOR EFFICIENCY PREDICTION

EFFICIENCY

1.	Design System Including: MCA Airfoils Low Loss Leading Edges Reduced Cavity Volumes High Stage Loadings Active Clearance Control Intermediate Case Losses	86.2%
2.	Technology Benefits	
	Smoother Airfoils	+0.8
	Tip Trenches	+0.8
	Controlled Diffusion Airfoils	+0.4
3.	Status	88.2%

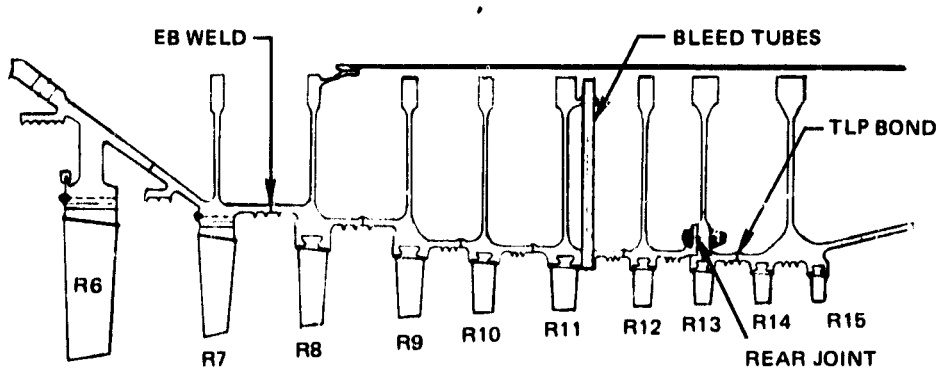

MATERIALS

DISKS	R6-7	AMS 4928 (Ti)
	R8-12	MERL 130 (Ti)
	R13-14	MERL 80 (N_1)
BLADES	R6-7	PWA 1202 (Ti)
	R8-15	PWA 1003 (N_1)
BLEED TUBE		STEEL

ALL STRESSES ARE WITHIN ALLOWABLES

TYPICAL STRESSES ARE

DISK	R8	71,000	PSI	HOOP AVG.
	R13	98,000	PSI	HOOP AVG.
BLADE ATTACH	R8	33,200	PSI	BEARING
	R13	45,800	PSI	BEARING
BLADE A/F ROOT	R8	16,800	PSI	TENSILE
	R13	13,500	PSI	TENSILE

- LCF LIVES ARE OVER 20,000 CYCLES IN ALL AREAS

Figure 46 High-Pressure Compressor Rotor. Summary of materials and stresses to meet life requirements.

TABLE 27

HIGH-PRESSURE COMPRESSOR STABILITY AUDIT RESULTS AT TAKEOFF

Surge Line Degradation	Fixed Quantity (%)	Randon Quantity (%)
Reynolds Number	-1.0	0
Steady State Vane Tracking Error	0	±0.9
Engine Deterioration	2.0	±1.0
Distortion	1.0	0
Engine Production Tolerance	0	±1.9
Operating Line Degradation		
Engine Power Transients	7.0	0
Control Production Tolerance	0	±1.0
Control Deterioration	0	±0.7
Engine Deterioration	0	±1.2
Engine Production Tolerance	0	±0.7
Sum of Fixed	9.0	
Sum of Random (RSS)		±3.0
Required Surge Margin	12	
Available Surge Margin	21.4	

TABLE 28

HIGH-PRESSURE COMPRESSOR STABILITY AUDIT RESULTS AT MAJOR OPERATING POINTS

Flight Condition	% Flow	Surge Margin (%) Required	Available
Aerodynamic Design Point[1]	100	13.4	25
Idle (SLS)	37.8	18.6	23
Takeoff	95.7	12	21.4
Reverse	91.0	15.0	20.5

(1) Representative of maximum cruise and climb operation

experience. To achieve this high overall design level of surge loading ($\Delta P_s/P_s$-P_s), the loadings were balanced throughout the compressor. Figure 47 indicates the balanced axial loading distribution of rotors and stators at mid-span. Loading levels are also shown to be reasonably well balanced between the rotors and stators at the root and tip.

The blade loading is based on the diffusion factor of the airfoil. Figure 48 indicates that diffusion factor, D-factor loading is reasonably balanced between rotors and stators, and that gross spanwise loadings are also balanced. Some root-to-tip balancing in the stators will be accomplished during the detail design. Generally, higher levels of back end stator loadings are a result of the axial reaction distribution.

4.4.4.4.3 Stage Aerodynamic Definition

The geometries of the high-pressure compressor airfoil sections were selected to produce the design velocity triangles. The cascade design system was employed to reflect geometry for blade rows utilizing standard NACA airfoil sections. Non-standard sections, such as MCA and controlled diffusion airfoils, were designed with the aid of computer programs.

Figure 49 and Figure 50 present the axial distribution of some of the more important aerodynamic design parameters.

The stage inlet α_3 represents the swirl distribution through the compressor (an angle of $\alpha_3 = 90^o$ indicates axial flow). At the inlet guide vane leading edge, the airflow is axial. Swirl is introduced at the high-pressure compressor inlet by the inlet guide vanes to reduce rotor Mach numbers and is gradually reduced through the compressor to provide axial flow at the discharge.

Axial velocity distribution is made essentially linear as a compromise between efficiency and compressor length and weight.

Gap-to-chord ratios are unbalanced in the preliminary design because the stator gap-to-chord ratios were reduced to maintain stator cambers within current experience. This unbalance will be adjusted during the final design.

The axial aspect ratio distribution is linear except for rows where chord was adjusted in order to satisfy structural requirements. The basic shape and level of the aspect ratio distribution was dictated by vibration limits.

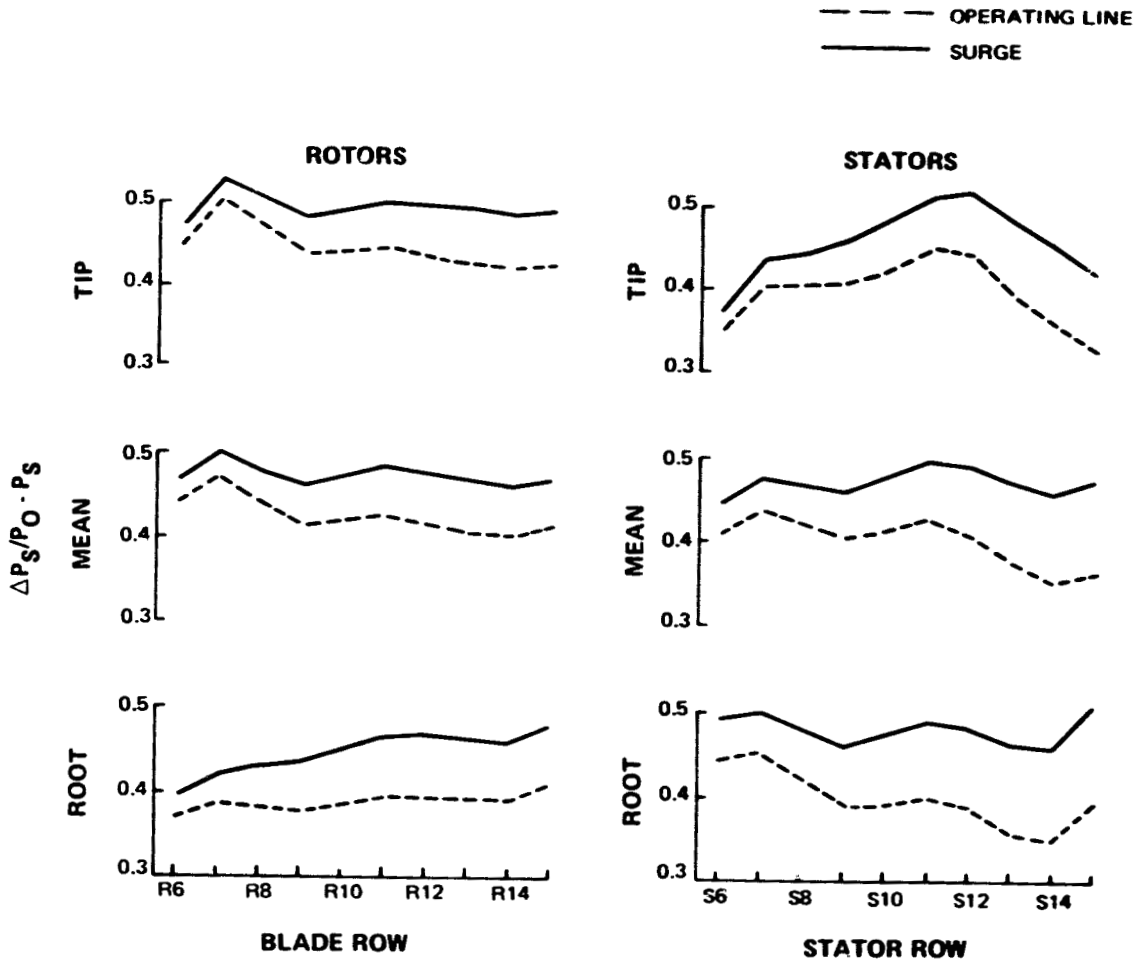

Figure 47 High-Pressure Compressor. Endwall loading (P_s/P_o-P_s) stage distribution illustrates generally well-balanced loading levels.

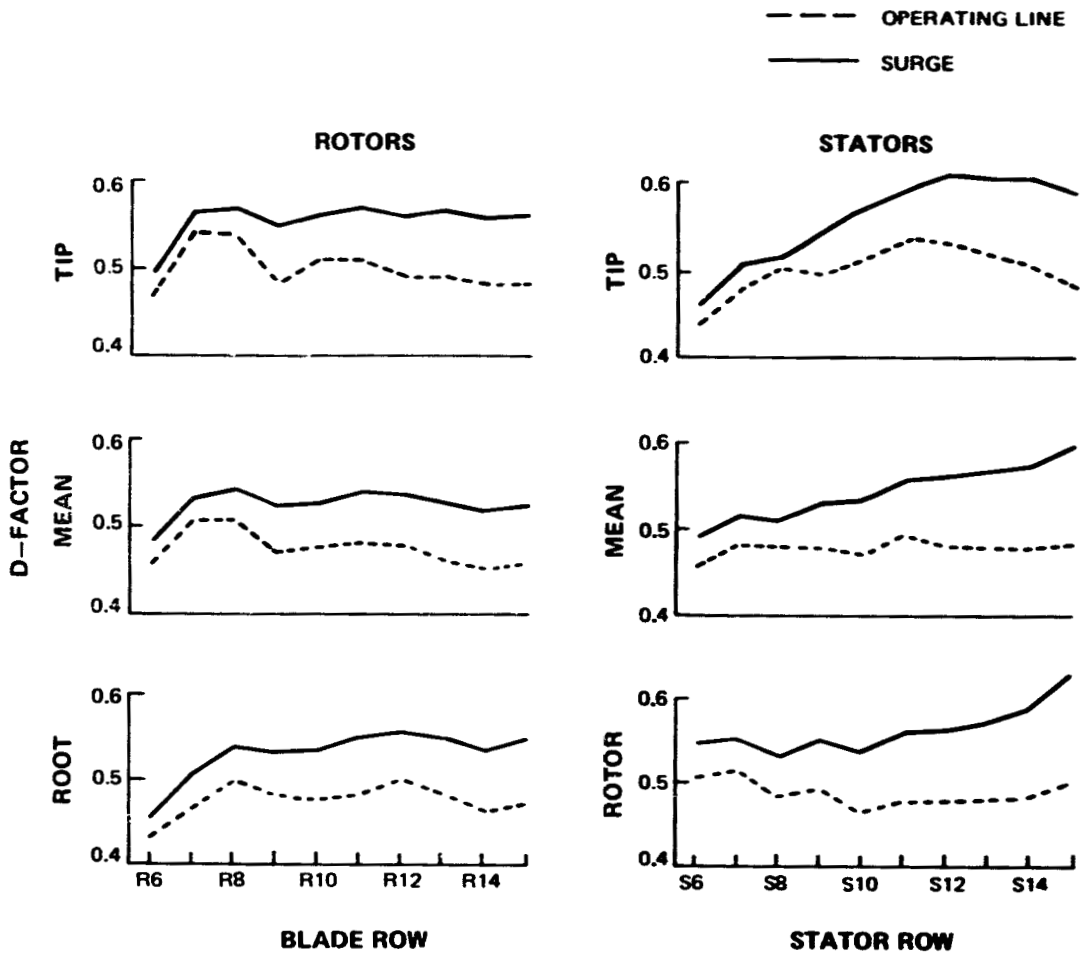

Figure 48 High-Pressure Compressor. Airfoil loading (D-factor) stage distribution illustrates acceptable preliminary loading levels.

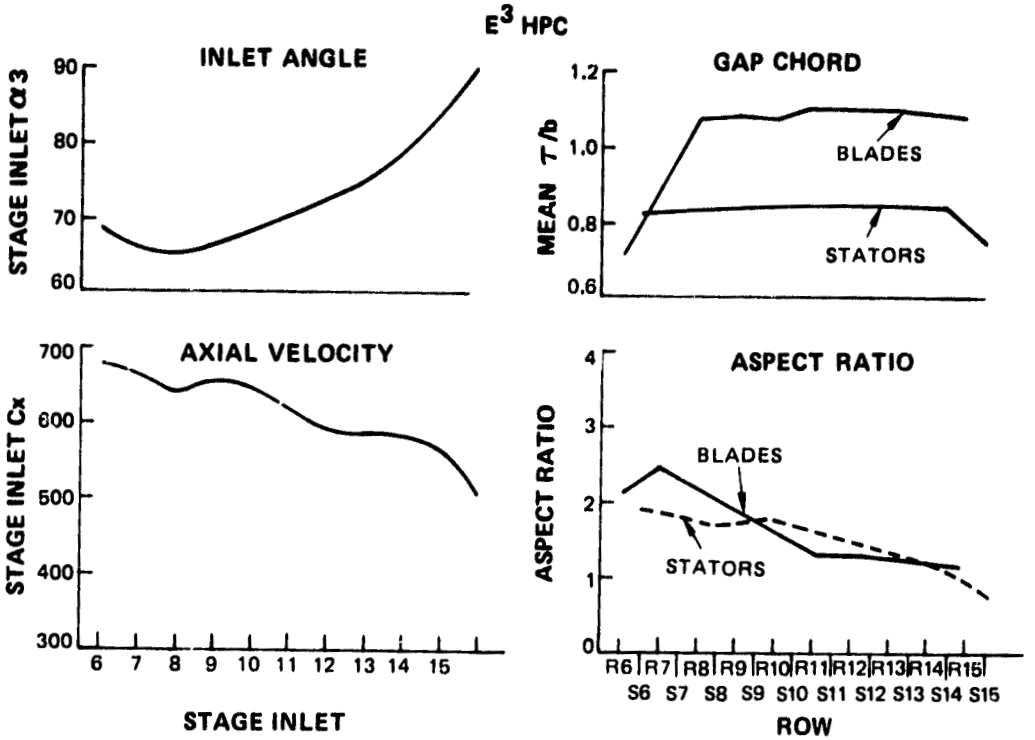

Figure 49 High-Pressure Compressor. Mid-span geometry parameters show axial distribution of important parameters.

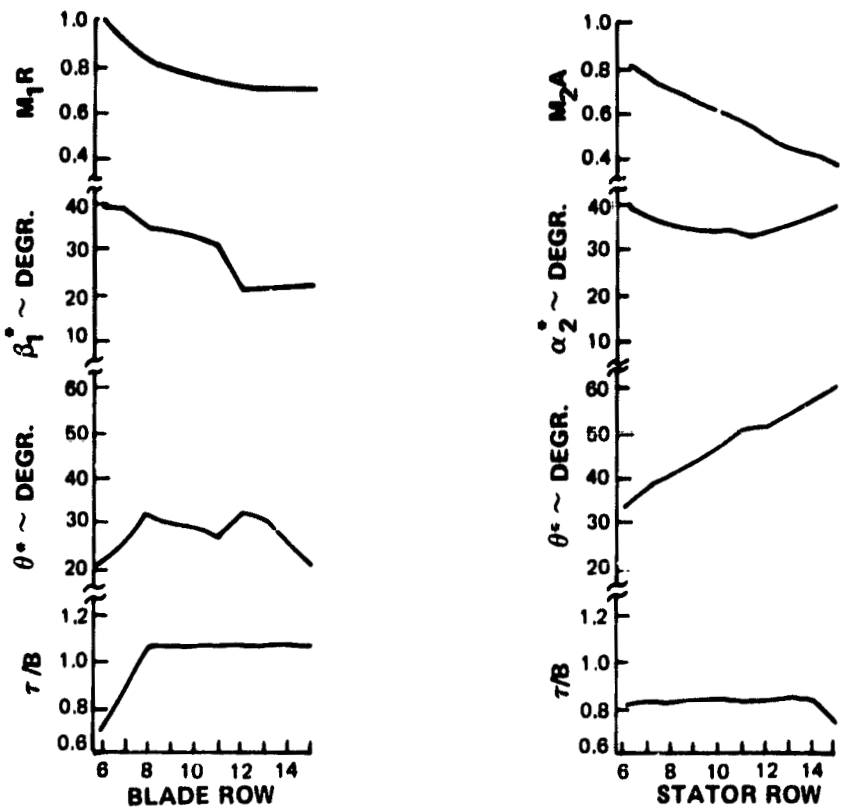

Figure 50 High-Pressure Compressor. Principal aerodynamic design parameters by stage illustrate near linear axial velocity and aspect ratio variations.

4.4.4.4.4 Blade and Vane Flutter Predictions

Blades and stators were examined for flutter using a prediction system which relates the frequency required to avoid both torsional and bending flutter with stage pressure level. The airfoils selected as a result of the aerodynamic design are examined to assure adequate flutter margin. Stage 14 and 15 blades required an 18 percent increase in root thickness to obtain adequate bending flutter stability. Stator 12 required a 15 percent increase in thickness to meet torsional flutter margin requirements. All of the other rows met the design limits. The required airfoil recontouring will be accomplished during detail design.

4.4.4.4.5 Stage Resonance Prediction

The rotor blades are subjected to the largest wakes from the intermediate case struts. As a result, the major modes of vibration were examined to assure that strong resonant stresses do not occur within the engine operating range. Figures 51 and 52 show the predicted resonance diagrams for the coupled blades and disk. The rotor 6 resonance diagram indicates adequate frequency margins for all modes. Rotor 7 results show adequate margins for modes 1 through 4. However, the tip mode relative to 42E (the number of stage 7 stators) is between minimum cruise and redline high spool speeds. During detail design, the number of stage 7 stators will be tailored to increase this frequency and eliminate any tip mode problem.

4.4.4.5 Inner Gaspath Seal Selection

Several inner seal designs were considered for the high-pressure compressor, as shown by Figure 53. The knife-edge configuration was selected from this study because it provides both good sealing and minimum cavity size. The wide channel inner seal design, shown early in the design process, was rejected when research testing indicated that its high effectiveness as a gaspath seal would be negated by high air heatup power losses. Because, with their large estimated running clearances, a performance loss would be incurred, the cantilever and flowguide schemes were eliminated.

4.4.4.6 Analysis of Rear Case Equipped With Active Clearance Control

The selected ACC system for the high-pressure compressor impinges air directly on the rear rotor case to reduce tip clearance at the cruise condition. This air is then ducted overboard. Figure 54 schematically shows this system. The ACC selection and evaluation and the structural analysis of the rear high-pressure compressor case incorporating the selected ACC system are discussed in the following sections.

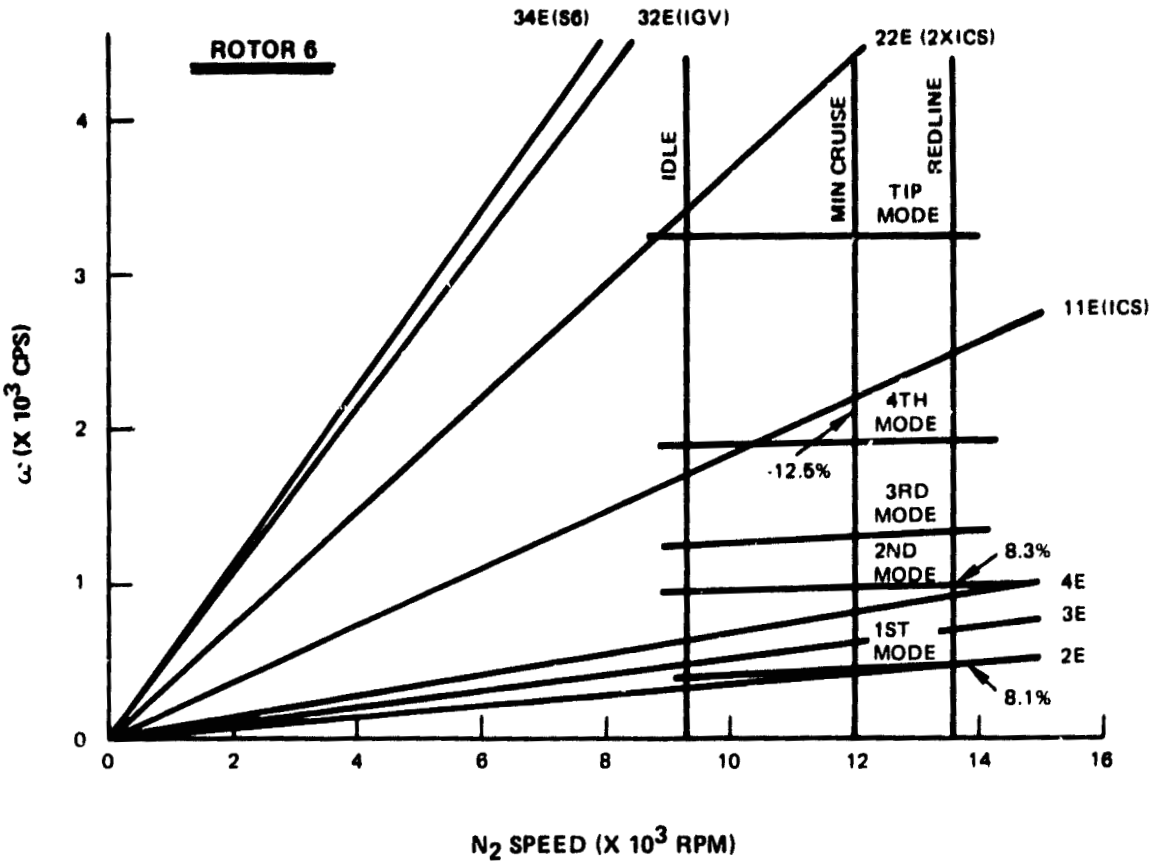

Figure 51 Sixth-Stage Compressor Blade/Disk Resonance Diagram. Data illustrates frequency margins.

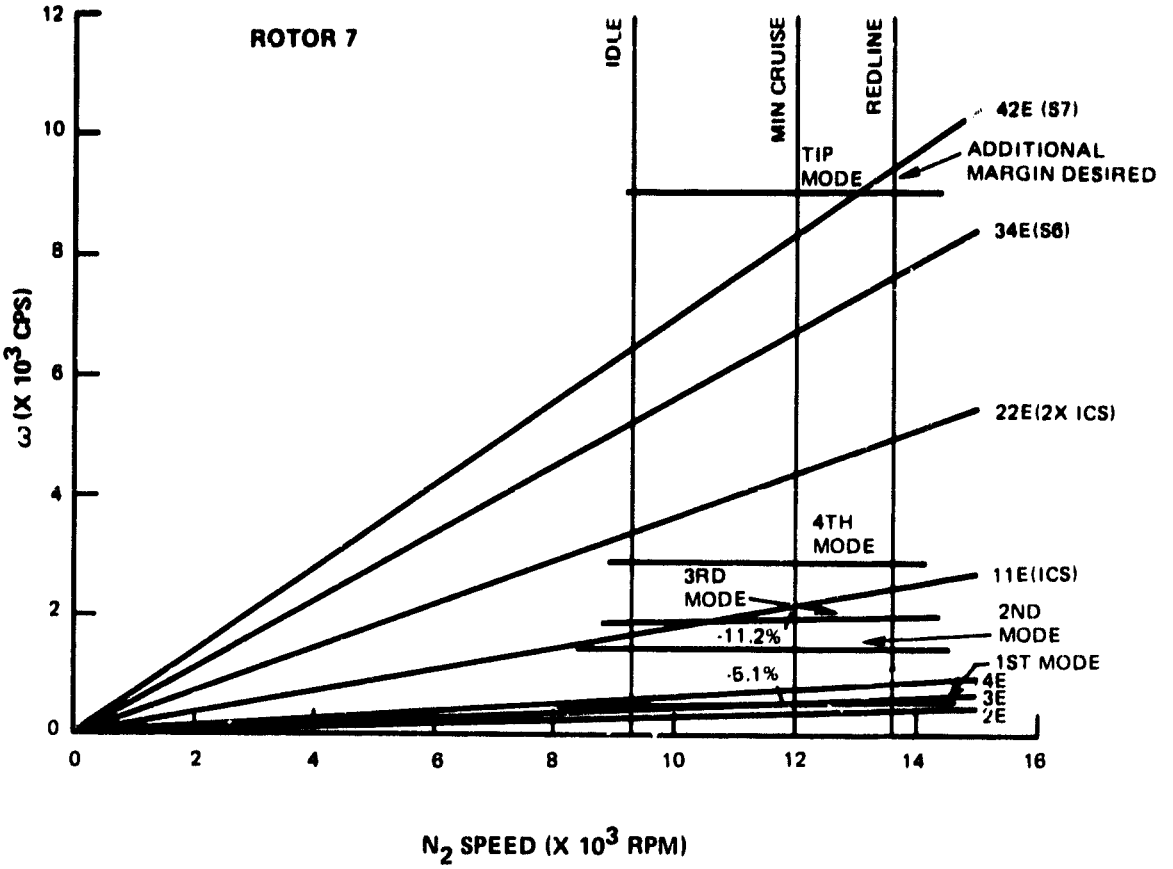

Figure 52 Seventh-Stage Compressor Blade/Disk Resonance Diagram. Data illustrates frequency margins.

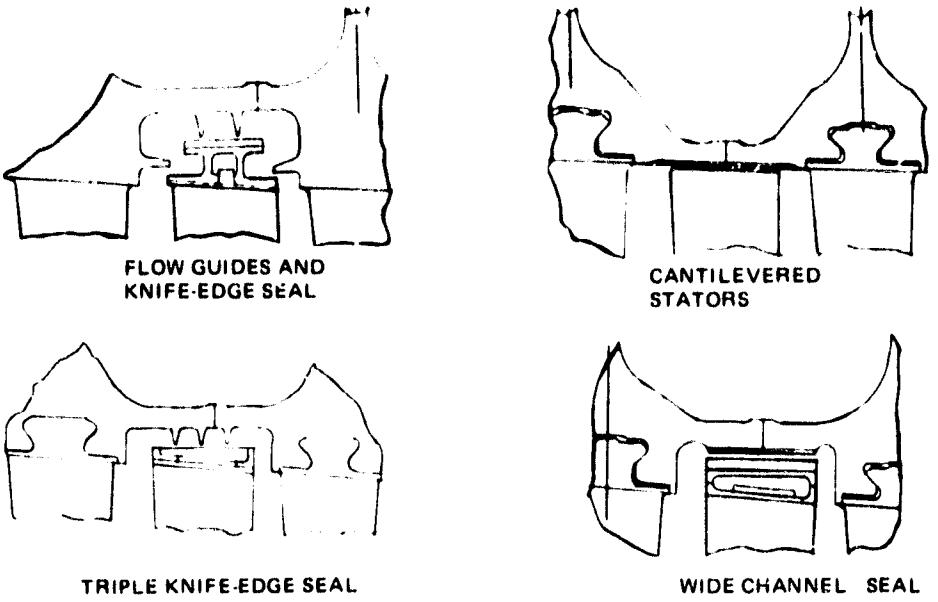

Figure 53 High-Pressure Compressor. Candidate inner seal configuration concepts studied.

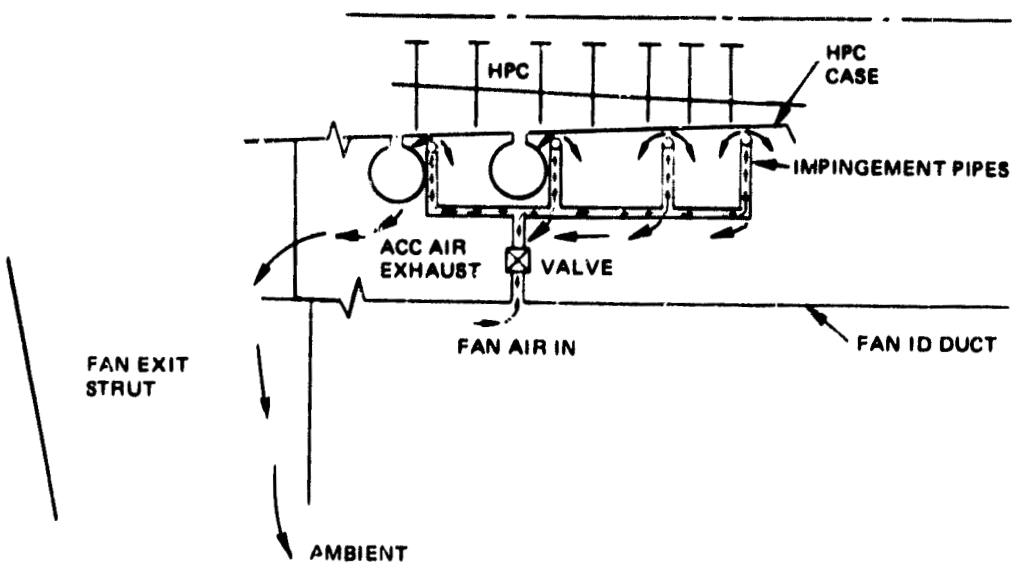

Figure 54 High-Pressure Compressor. Schematic of selected external active clearance control system showing fan air circuit.

4.4.4.6.1 Active Clearance Control System Evaluation and Selection

For the high-pressure compressor, the alternative to the selected external ACC system was an internal system. The internal system, shown schematically in Figure 55, was originally considered attractive because air for compressor ACC was also used for turbine ACC. This approach minimized the TSFC penalty for using this air.

In the selection process performance, cost, weight and mechanical complexity were used as criteria. Resulting DOC comparisons slightly favored the external system. However, mechanical complexity and the associated high probability of incurring cost, weight, and performance penalties in executing the internal system mechanical design, shown in Figure 56, were the leading factors in the selection of the external system. The case construction with internal ACC has numerous flanges that require sealing, coaxial case walls with large temperature gradients, and an internal case that is exposed to very hot compressor discharge air over its entire length. As a result, problems identified with the internal system include increased leakage airflow and low cycle fatigue (LCF) at the flanges, potentially high stresses in the coaxial cases caused by thermal gradients, inability to adjust ACC case movement by stage to experimentally tune clearances, and an extremely complex structure which would be very difficult to analyze. The reasons for rejecting the internal system are summarized in Table 29.

4.4.4.6.2 Stress Predictions

Because the stator case assembly must be flexible enough to move with the outer case clearance control and stiff enough to carry vane loads without distorting or being over-stressed, a preliminary NASTRAN finite element analysis was made of the assembly. The results of this analysis showed that the external ACC case configuration satisfies all the clearance control and stress requirements. No stress or deflection limitations were discovered and case excursions resulting from the application of ACC were shown to move the stator outer shroud uniformly. Stress estimates at critical case locations are summarized in Figure 57.

During the detail design, the rear high-pressure compressor case will be further optimized to reduce weight while retaining acceptable stresses.

4.4.5 Design Summary

The current design status of the high-pressure compressor aerodynamic design is shown in Table 30. The preliminary design satisfies all of the aerodynamic, mechanical, and structural requirements discussed in Section 4.3.1.

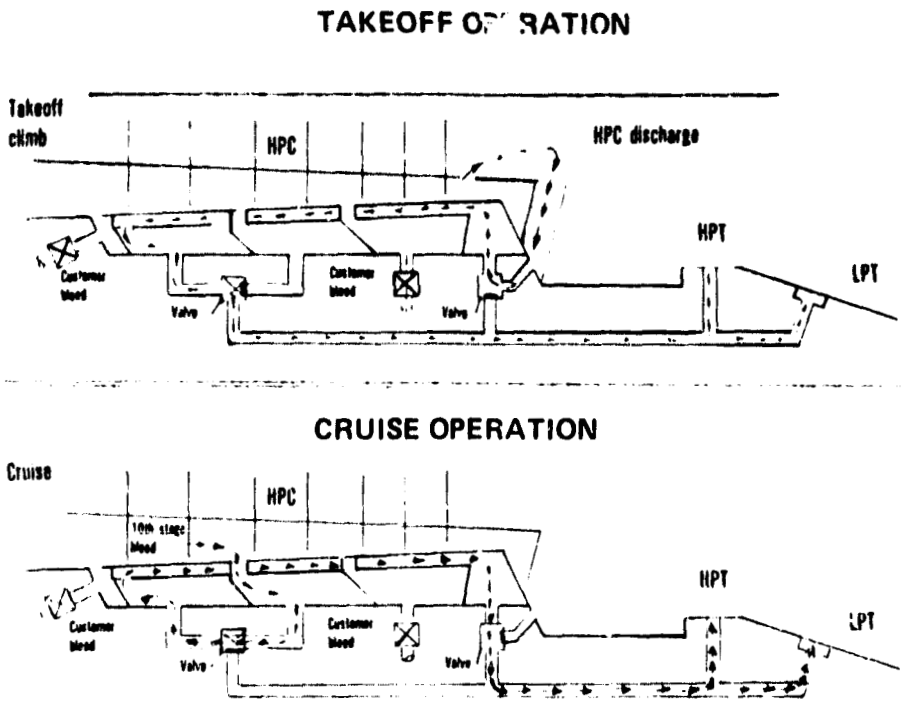

Figure 55 High-Pressure Compressor. Originally proposed internal active clearance control system as integrated with turbine ACC to minimize TSFC.

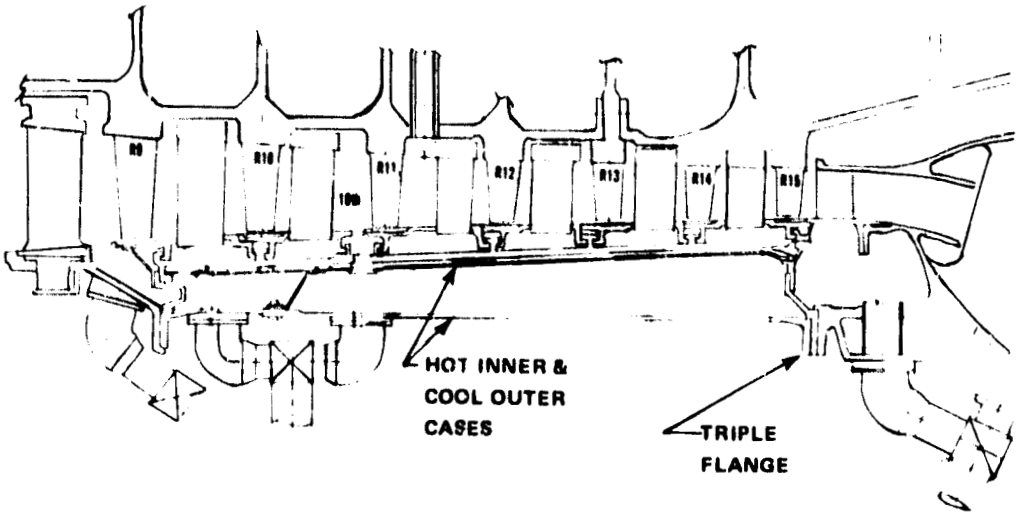

Figure 56 High-Pressure Compressor. Internal compressor active clearance control system mechanical arrangement showing complexity representing major elimination factor.

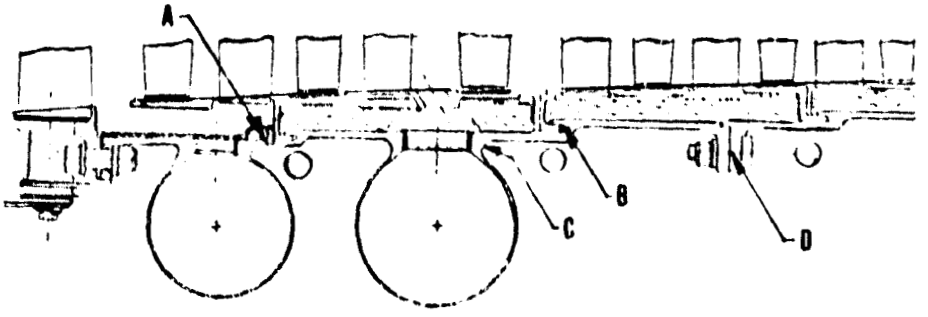

All stresses are within allowables

	Max stress contributor	MAXIMUM STRESS
A	Shear load	8 N/cm^2 (12 KSI)
B	Gas/thermal loads	.7 N/cm^2 (1 KSI)
C	Thermal	17 N/cm^2 (25KSI)
D	Thermal (mat incompatibility) blade loss	39 N/cm^2 (57 KSI)

Figure 57 High-Pressure Compressor. Rear case stress analysis indicates maximum stresses within allowables.

TABLE 29

HIGH-PRESSURE COMPRESSOR PROBLEMS WITH INTERNAL ACTIVE CLEARANCE CONTROL SYSTEM RESULTING IN SELECTION OF EXTERNAL SYSTEM

Increased leakage-potential at bolted joints.

Walls of multi-wall case must move together with ACC - high stresses, LCF problems at flanges, increased ACC flow required.

All nickel base case required - causes thermal pinch in forward stages, loss of tip clearance.

Very difficult to adjust ACC movement stage to stage and to tune experimentally.

High weight and cost.

Extremely difficult to analyze complex structure.

TABLE 30

HIGH-PRESSURE COMPRESSOR PRELIMINARY DESIGN SUMMARY
AERODYNAMIC DESIGN POINT

Pressure Ratio	14
Inlet Corrected Flow, kg/sec (lb/sec)	39.9 (88.1)
Surge Margin, %	25
Adiabatic Efficiency, %	88.2
Inlet Corrected Tip Speed, m/sec (ft/sec)	404 (1323)
Low Cycle Fatigue Life, Missions	
Blade	20,000 (or 30,000 hr)
Disk	20,000 (or 30,000 hr)

4.5 COMBUSTOR

4.5.1 Design Requirements

The combustor aerodynamic, thermodynamic, and structural design requirements were established by the engine cycle definitions at design and off-design conditions. A number of key operating conditions were involved depending on performance, durability, emissions, and operational design considerations.

General combustor design requirements are summarized in Table 31.

Performance considerations resulted in requirements being established at the 10,668m (35,000 ft) aerodynamic design point which is located between maximum cruise and maximum climb. Combustor efficiency and pressure loss, were set here, as was exit temperature profile.

Liner durability requirements were established based on life analysis over the airplane mission. Average life-to-first-repair was selected as the criterion.

Emissions requirements established were those of the proposed 1981 Environmental Protection Agency (EPA) regulations. Carbon monoxide (CO), hydrocarbon (HC), oxides of nitrogen (NOx), and smoke requirements were included.

Operational requirements established consisted of lighting, acceleration, and safety considerations.

4.5.2 Design Background

4.5.2.1 Background Technology Sources

The NASA Experimental Clean Combustor Program (ECCP) two-stage Vorbix combustor forms the basis for the Energy Efficient Engine combustor design. Detailed investigation with the two-stage Vorbix combustor included JT9D-7 engine test substantiation of the ability to meet the 1979 EPA gaseous emissions regulations. Two-stage Vorbix engine emissions data were also obtained in a annular burner technology program conducted by P&WA under IR&D funding which paralleled the NASA ECCP. Additional technology utilized in the combustor design was obtained from Pratt & Whitney Aircraft IR&D programs conducted with short carburetor tube combustors and with two-stage JT8D can-annular combustors.

Aerodynamic design data for the prediffuser and combustor front end flow fields have been internally generated in a diffuser/combustor interaction computer program in which parameters for optimizing the location of the combustor front end relative to the diffuser dump plane were determined. Curved wall prediffuser design data were also obtained in P&WA liner cooling scheme IR&D tests.

TABLE 31

COMBUSTOR DESIGN REQUIREMENTS

Aerothermodynamic Parameters

Efficiency %	99.95
Overall Pressure Loss, %	5.5
Maximum Temperature Pattern Factor	0.37
OD Skewed Radial Temperature Exit Profile (Peak-to-Average), ^{o}C (^{o}F)	139 (250)

Life Requirement

Low Cycle Fatigue Life, missions	4900

Emissions Requirements

CO, EPA Parameter	3.0
HC, EPA Parameter	0.4
NO_x, EPA Parameter	3.0
Smoke Number (SAE)	20

Operational Requirements

- o Commercially acceptable altitude relight capability
- o Commercially acceptable sea level starting capability
- o Commercially acceptable idle-to-takeoff acceleration time
- o Main and pilot zones lit at approach to minimize aborted landing acceleration time
- o No autoignition of fuel external to combustor.

4.5.2.2 Relationship to NASA Experimental Clean Combustor

Figure 58 is a cross section of the two-stage Vorbix combustor which was JT9D engine tested in the Experimental Clean Combustor Program. It consists of a pilot zone with 30 pressure atomizing fuel injectors located upstream of a main zone into which fuel is injected through 60 pressure atomizing fuel injectors. In the main zone of the Vorbix combustor, large quantities of air enter through swirlers in both the inner and outer liners downstream of the fuel injector plane. Rapid mixing of swirling air and fuel takes place to produce fuel-lean burning, conducive to reduced emissions of oxides of nitrogen (NO_x). The pilot zone is designed to minimize the emissions of carbon monoxide (CO) and hydrocarbons (HC) at idle operation. Only the pilot zone is fueled at idle conditions. At power settings above idle, both the main and pilot zones are fueled with the percentage of fuel entering the main zone increasing with engine power. Very low NO_x emissions were demonstrated in this combustor with approximately 75 percent of the total fuel being burned in the main zone at maximum power conditions.

Although the ECCP Vorbix combustor demonstrated the potential for meeting the CO, HC and NO_x emissions regulations applicable to T2 class engines, such as the JT9D-7, smoke exceeded the goal by approximately 50 percent. Carbon deposits were noted on the liner downstream of the main zone injectors, which is indicative of poor fuel penetration. Carbon was also observed on the faces of the main zone fuel injectors which were located flush with the combustor liner and, therefore, exposed to high radiation and high convection heat transfer loads from the combustion gases. In addition, thermal distress of the liner occurred in the converging throat section between the pilot zone and the main zone because of the high velocities and attendant high heat transfer coefficients in this area.

The Energy Efficient Engine combustor design was intended to be an evolutionary extension of the ECCP Vorbix combustor simplified to a durable, commercially acceptable, low gaseous emissions design which also met the EPA smoke regulation.

4.5.3 General Configuration Description

The combustor section, shown schematically in Figure 59, includes a curved-wall prediffuser which turns the flow outward to more nearly align the flow with the combustor centerline and to reduce pressure losses associated with flow turning around the front end of the combustor. An outward flowpath cant of five degrees in the compressor exit guide vanes initiates the turning. The recommended prediffuser has an overall area ratio of 1.5, with a length-to-inlet height ratio of 3.5, and accomplishes in itself, nine degrees of turning relative to the engine centerline.

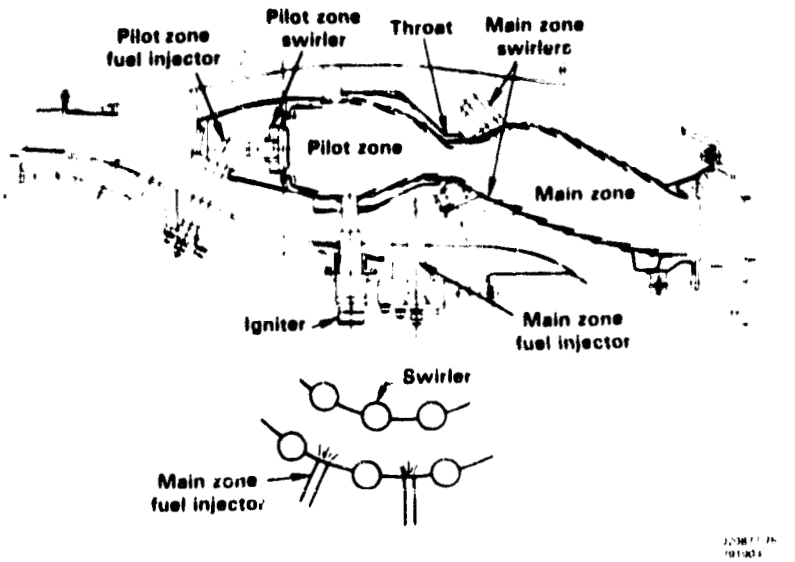

Figure 58 Two-Stage Vorbix Combustor. Test results from the JT9D engine were used for the Energy Efficient Engine combustor design.

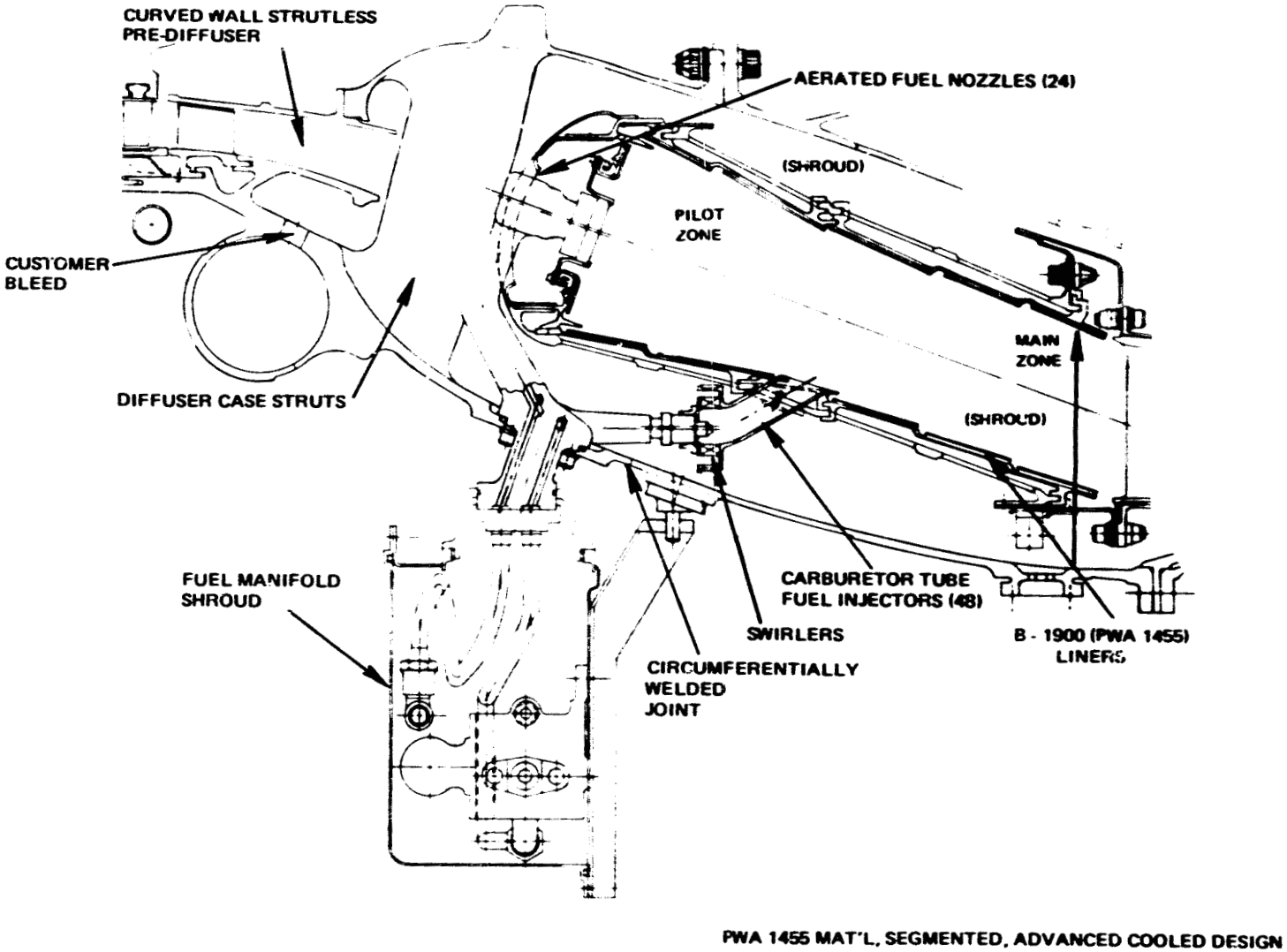

Figure 59 Energy Efficient Engine Diffuser-Combustor. Cross-section view shows major design features.

The prediffuser does not contain struts; however, 24 diffuser case struts are located downstream of the prediffuser dump plane to transfer inner case loads to the outer case. These struts are thin and aerodynamic in cross-section to minimize wakes which could propagate through the combustor to create hot section distress.

The combustor includes pilot and main burning zones patterned after the ECCP two-stage design to control emissions. The pilot zone is designed to minimize emissions of CO and HC at idle while providing acceptable sea level and altitude starting and stability characteristics with 24 aerating nozzles to prepare the fuel. At higher powers, the majority of the fuel is injected in the main zone, which is designed to minimize NO_x and smoke emissions. The pilot zone provides hot gases to ignite the main zone fuel supplied through 48 carburetor tubes in which fuel and air are premixed to create the lean burning zone mixture needed for low smoke and NO_x. Carburetor tubes and fuel nozzles are configured to permit outer liner removal without disassembling the fuel system. The two-stages are designed to a maximum temperature rise of 865°C (1560°F) within a 30.2 cm (11.9 in) overall combustion length.

The recommended combustor liner design is a segmented, counterparallel FINWALL (CPFW) configuration cast from PWA 1455 turbine airfoil alloy. The liner assembly is formed by arranging 24 segments circumferentially in both the pilot and main zones. A total of 96 segments are required to assemble the complete combustor. Hooks on the back of each segment mate with circumferential rails on the structural framework to position the segments. The combustor life goal can be achieved with segments constructed of either PWA 1455 or oxide dispersion strengthened (ODS) alloy. However, PWA 1455 is recommended because there is more practical experience associated with its use.

External to the diffuser case, fuel supply tubes and manifolds are completely shrouded to contain potential fuel leaks which could ignite and cause fire damage to the engine.

The diffuser case is constructed of cast hot isostatic pressed INCO 718 material which has 80 percent of wrought material strength. The case centerbody includes integrally cast struts and bosses for installing fuel nozzles mount pins, and igniters. Case skirts of wrought INCO 718 are circumferentially welded to the centerbody to form the complete case contour. Longitudinally welded joints, where cracks characteristically start in current combustor cases, are avoided. The prediffuser is assembled by bolting a machined inner contoured wall to the diffuser case. The cast outer duct wall is integrally cast with the case centerbody and is machined after heat treatment. Machining both the inner and outer gaspath walls of the prediffuser section provides close dimensional tolerance control of the flowpath through the critical prediffuser section.

4.5.3.1 Major Sub-Assemblies

Clustered fuel assemblies are used to minimize the number of case penetrations and mounting bosses (see Figure 60). One aerated, low pressure drop pilot nozzle is combined with two pressure-atomized main zone fuel nozzles on each assembly. Nozzle supports are heat-shielded in order to minimize the potential for fuel coking.

The main zone carburetor tube design, shown in Figure 61, features a radial inflow swirler located concentrically with the zone fuel nozzle. Air is swirled radially inward around the fuel nozzle. The strong centrifugal field created by the swirler centrifuges fuel to the walls of the carburetor tube. A certain amount of fuel remains in the center core of the carburetor tube and premixes with the air. Fuel atomization occurs at the carburetor tube exit lip where the fuel film is sheared and fine drops of fuel are distributed into the combustion zone.

The carburetor tube is attached to the liner by support straps located on the shell adjacent to the radial inflow swirler. A liner port, into which the carburetor tube is inserted, provides purge airflow around the tube to prevent aspiration of fuel into the shroud region outside of the combustor liner. The downstream end of the carburetor tube is left unconstrained to allow differential thermal growth of the hot liner and the cooler carburetor tube.

Figure 62 indicates some of the mechanical design features of the combustor front end. Twenty-four Hastelloy X nozzle guides, which are free to move normally to the combustor centerline, are installed in a cast Hastelloy X bulkhead. The guides permit thermal growth of the liner relative to the fuel injectors and facilitate installation of the fuel nozzles. Heatshields are provided around each nozzle guide to direct film cooling air radially outward along the bulkhead. A toroidal hood is attached to the bulkhead to provide a plenum to capture compressor discharge air for cooling and injection through air ports in the bulkhead. The hood has 24 cutouts to accommodate the pilot zone fuel nozzles.

Segmented counter parallel FINWALL (CPFW) liner panels constructed of PWA 1455 turbine airfoil alloy were selected because this combination provides a combustor liner design which meets the program life goal. Segmenting the liner hoops improves life by reducing liner stresses. The CPFW concept is an advanced cooling scheme which utilizes a combination of convective and film cooling to cool the liner. In this concept, (See Figure 63) cooling air enters the cool side of the liner through slots and is fed into axially oriented channels in the liner. A portion of this air flows forward (counter to the direction hot gas flow), turns 180 degrees upon exiting the forward end of the channel, and film cools the hot gas side of the liner. The remaining portion flows aft and convectively cools the liner. This predicted method of cooling has the potential to reduce the maximum liner wall temperature

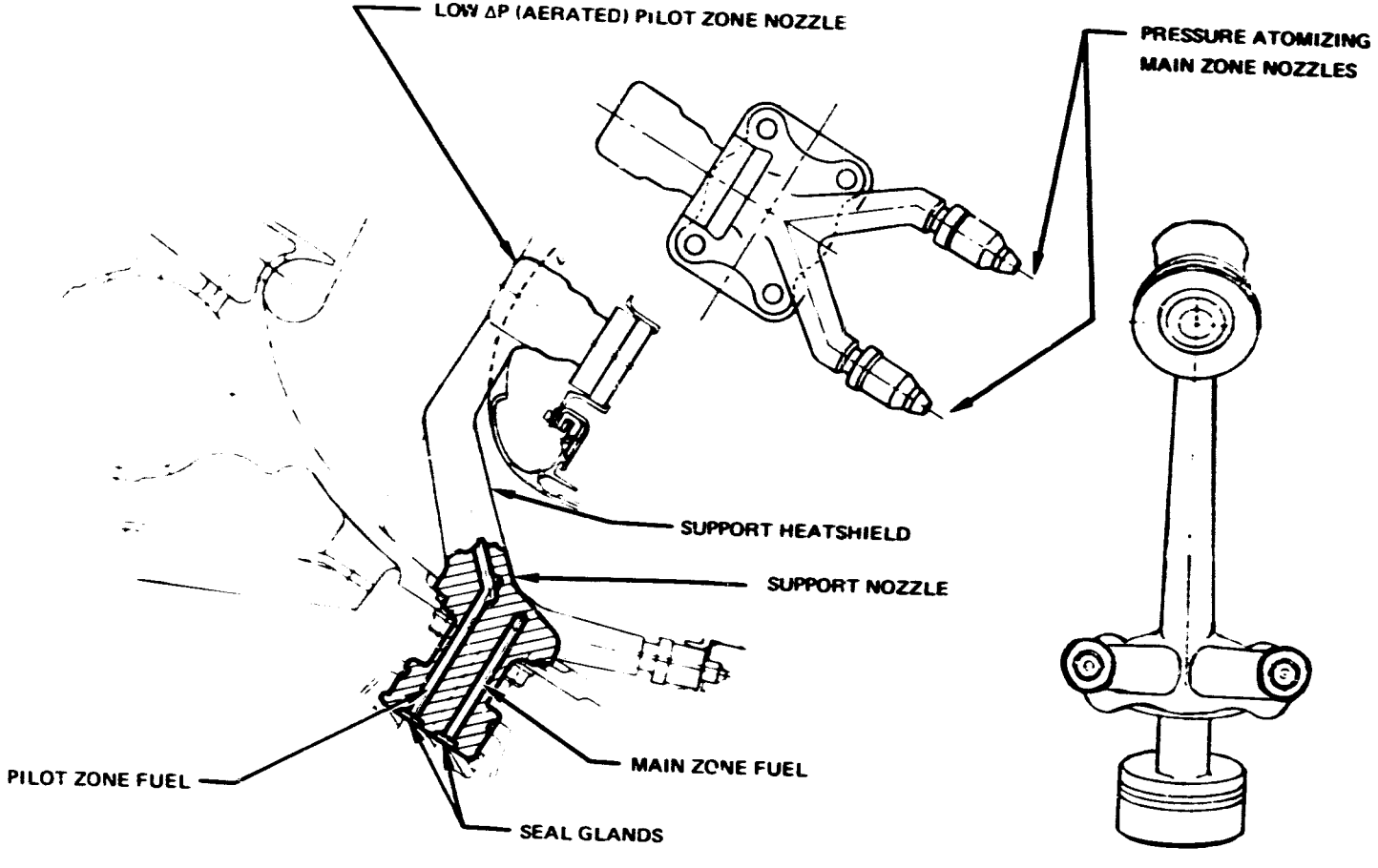

Figure 60 Multiple Views of Clustered Fuel Nozzles. Design permits minimal combustor case penetrations.

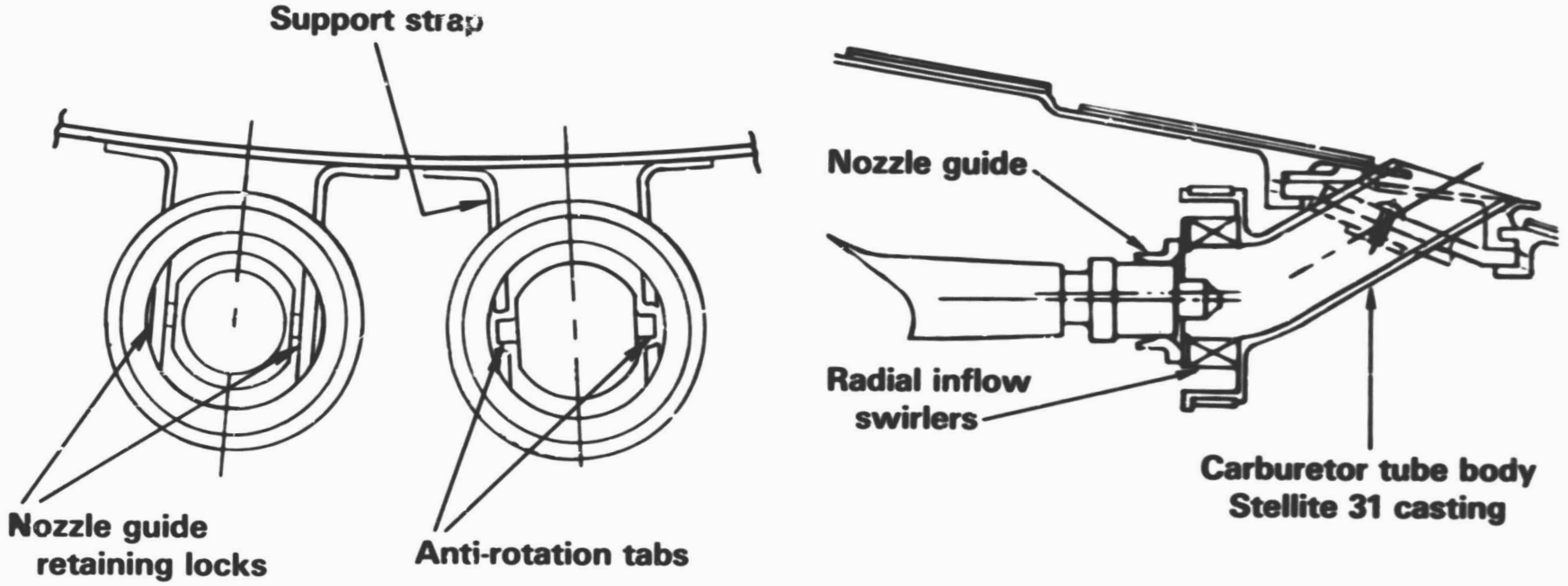

Figure 61 Main Zone Carburetor Tube. Part designed with air swirlers for low NO_x and smoke.

J20945-16
792603

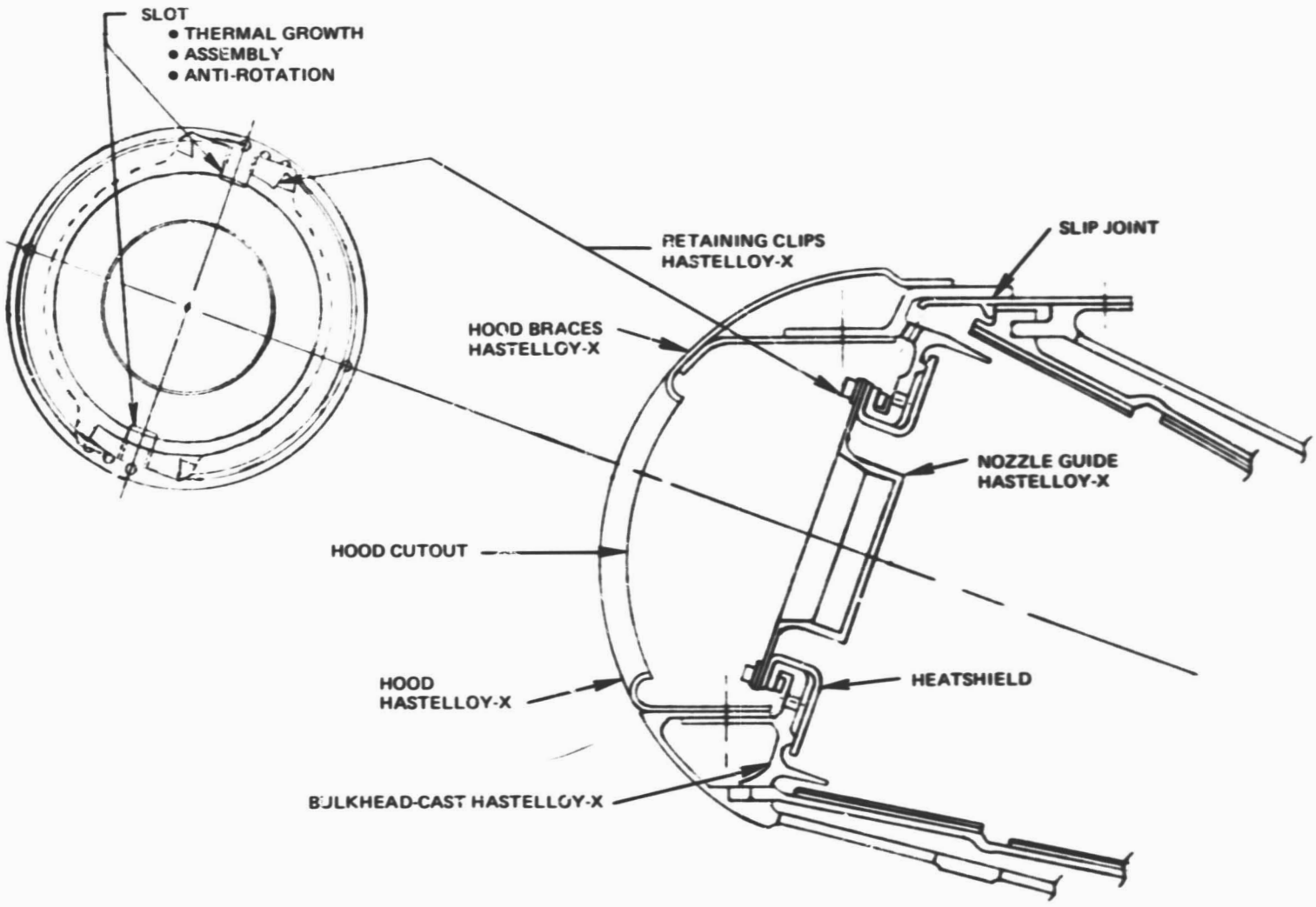

Figure 62 Combustor Front End. Cross section includes definition of design features and material.

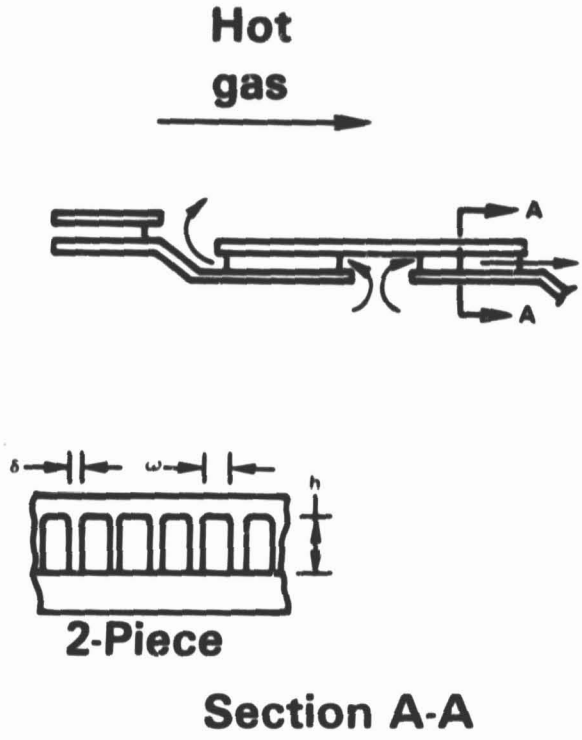

Figure 63 Combustor Liner Design. Segmented counter-parallel liner panels are made from PWA 1455 turbine airfoil alloy.

approximately 167°C (300°F) relative to the wall temperature achieveable through the use of louver or impingement cooling at the design limit of 35 percent combustor air available for cooling. This reduction in wall temperature translates directly into improved liner life.

4.5.3.2 Principal Aerothermodynamic Design Parameters

4.5.3.2.1 Comparison of Pilot Zone Parameters

Pilot zone heat release rate in the Energy Efficient Engine combustor is 6.1 x 10^6 BTU/ft^3 hr atm, which is approximately one-half that of the Experimental Clean Combustor Program (ECCP) Vorbix combustor. The lower heat release rate is accomplished by increasing the combustor volume per unit of airflow which promotes longer residence time for more complete burning and allows better recirculation of gases to improve stability and provide better lighting characteristics both at sea level and altitude relight. This change relative to the ECCP is intended to reduce emissions to meet the more stringent CO and HC regulations applicable to the Energy Efficient Engine and to address the relight deficiency observed in rig testing of the ECCP combustor. The overall length of the pilot zone in the Energy Efficient Engine, however, is shorter by approximately 3.3 cm (1.3 in.). The dome height is approximately the same in both pilot zones, and the nozzle spacing is approximately the same when non-dimensionalized by the respective dome height. Aerated fuel nozzles were selected for the Energy Efficient Engine instead of the ECCP pressure atomized nozzles to improve the fuel spray atomization characteristics at idle where the fuel pressure drop is only 3.1 N/cm^2 (5 psi).

4.5.3.2.2 Comparison of Main Zone Parameters

The main zone is 7.6 cm (3 in.) shorter than the main zone of the Experimental Clean Combustor Program Vorbix combustor. Approximately 2.5 cm (1 in.) of this difference is attributable to residence time which has been reduced from 5 milliseconds in the Experimental Clean Combustor Program Vorbix combustor to 4.5 milliseconds in the Energy Efficient Engine design. The remainder of the difference in length is attributable to thrust size differences.

The number of fuel nozzles has been reduced from 60 to 48. A major difference is in the fuel nozzle concepts. The Energy Efficient Engine combustor includes a carburetor tube injector in which fuel and air are mixed external to the main combustion zone. The ECCP Vorbix combustor utilized pressure atomized fuel nozzles which injected fuel directly into the combustor. Air swirlers were situated between each nozzle to achieve good mixing and provides lean fuel-air mixtures intended to control NO_x emissions and smoke. The carburetor tube has been selected for its greater potential to provide more uniform fuel penetration over the entire combustor operating range to alleviate

carbon build-up on the liner and poor fuel penetration at off-design conditions which was noted during the Vorbix combustor testing. In addition, extrapolation of rig test data indicates that the smoke requirement at Energy Efficient Engine engine operating conditions can be met with carburetor tube fuel injection.

4.5.3.3 Technology Development Requirements

A number of features included in the Energy Efficient Engine combustor design require additional substantiation prior to detailed combustor design. Additional technology development is necessary to verify the curved-wall prediffuser design and to substantiate the fuel injection system and liner construction. The required technology related to the curved-wall prediffuser and the two-stage combustor performance and emissions characteristics will be generated in programs within the Energy Efficient Engine program. The technology required to evolve a durable combustor liner of segmented construction with advanced cooling techniques will be addressed in the sector rig portion of the supporting technology program.

4.5.3.3.1 Prediffuser

A supporting technology program is being conducted to demonstrate the maximum turning angle and diffusion rate which can be included in a curved wall prediffuser while providing separation-free operation over a wide range of simulated engine operating conditions. The program will also verify the ability to meet the combustor section pressure loss goal. Tests of a full scale, full-annular plexiglass rig, which simulates the contours of the engine prediffuser and combustor section, are being conducted to determine the sensitivity of the prediffuser to variations in inlet total pressure profile, inlet turbulence, swirl angle, amount of turning accomplished in the prediffuser, length of the prediffuser, and the rate of diffusion in the prediffuser. In addition, the location of the combustor hood relative to the prediffuser dump plane will be established. The final tests to be conducted with the rig will be with a complete simulation of prediffuser, combustor and fuel injectors to determine the shroud flow characteristics and the overall combustor section pressure loss.

4.5.3.3.2 Two-Stage Combustor

This technology program will be conducted to determine the impact of the reduced number of fuel injectors and the shorter combustion zones on emissions, performance, and durability. The program will include the development of carburetor tube characteristics for the main zone fuel injectors. The effects of tube convergence, turning angle, swirl strength, and fuel nozzle pressure drop on aerodynamics and fuel preparation will be empirically investigated in a series of plastic model rigs allowing air and fuel flow visualization.The impact of changing the number and type of pilot and main zone fuel injectors and

main zone length on performance and emissions levels will be investigated in a series of sector test rigs. When a promising configuration has been identified in high pressure sector rig tests, and again at the end of the sector rig tests when the final configuration has been selected, altitude and sea level starting characteristics will be demonstrated.

4.5.3.3.3 Combustor Liner

The technology for the combustor liner design will be generated in the Sector Rig part of the combustor Supporting Technology program. Analytical and design support for the liner will be provided by the Detailed Analysis and Design portion of the combustor component effort. The Sector Rig program will involve fabrication of advanced cooling design liner segments, testing of the segments at full engine operating conditions and post-test analysis of the test data. A series of tests are planned to select the fuel injection configuration, the air introduction schedule and liner dilution hole configuration best suited for this advanced cooling configuration liner.

4.5.4 Supporting Analyses

4.5.4.1 Emissions Reduction Feature Selection

The pilot zone and main zone fuel injection systems were selected primarily on the basis of being feasible designs that could reduce gaseous and smoke emissions.

4.5.4.1.1 Pilot Zone Aerating Fuel Nozzles Selection

The originally proposed Energy Efficient Engine combustor employed 24 pressure-atomized pilot zone nozzles which were similar to those in the ECCP combustor.

During ECCP testing, starting characteristics of the Vorbix combustor were found to be inadequate because of the poor fuel atomization caused by the low available pressure drop across the pilot zone nozzles. Fuel flow was increased by approximately 60 percent relative to the JT9D-7 production combustor to accomplish start-up. Sector burning with only 10 of the 30 pilot zone nozzles flowing fuel at the starting conditions was attempted to improve the atomization characteristics but this adversely affected circumferential flame propagation. The net result was no significant improvement in starting characteristics.

Analysis of the Energy Efficient Engine fuel flows and operating conditions verified the need for good pilot zone fuel atomization with a low fuel pressure drop.

Aerating-type fuel injectors of the type shown schematically in Figure 64 have shown good fuel atomization at low pressure drops. This fuel

injector relies primarily on the shearing action between low velocity fuel and two surrounding high velocity air streams to generate small fuel droplets. The internal and external air streams co-rotationally swirl to distribute the fuel in the front end of the combustor and to establish a recirculation zone required for combustion stability. The Energy Efficient Engine design will be similar to the one shown in the figure with geometric details evolved through development efforts by fuel nozzle vendors.

4.5.4.1.2 Estimates of Starting and Relight Characteristics

The fuel atomization characteristics of the pilot zone aerated nozzle at the sea level and altitude 10,668 m (35,000 ft) starting/relight conditions were estimated using the nozzle droplet size correlation generated by Lefebvre and Rizkalla (Equation 1). Typical values are 52 microns at sea level starting and 77 microns at altitude relight conditions.

Equation 1

$$SMD = \left[1.25 \left(\frac{\sigma f \rho f}{D}\right) \frac{1/2\ (1 + W_f/W)_a}{\rho a\ Va}\right] + \left[0.73 \left(\frac{\mu f^2}{\sigma f \rho a}\right)^{.425} \frac{(1 + W_f/W_a)}{D^{.575}}\right]$$

where:

SMD	=	Sauter mean diameter (microns)
σ	=	surface tension - dynes/cm.
ρ	=	density - GR/cm^3
D	=	Diameter - cm
W	=	Mass flow rate - GM/sec
V	=	Velocity - m/sec
μ	=	Absolute viscosity - centipoise
f	=	Fuel
a	=	Air

While meeting the droplet size noted does not completely ensure adequate starting and relight characteristics, it establishes initial feasibility. Additional parameters which can ultimately influence the starting characteristics are fuel spray distribution and igniter locations.

Air velocities were assumed consistent with current experience with aerated fuel injectors. The SMD's calculated for sea level and altitude starting conditions are consistent with current practice utilizing pressure atomizing nozzles.

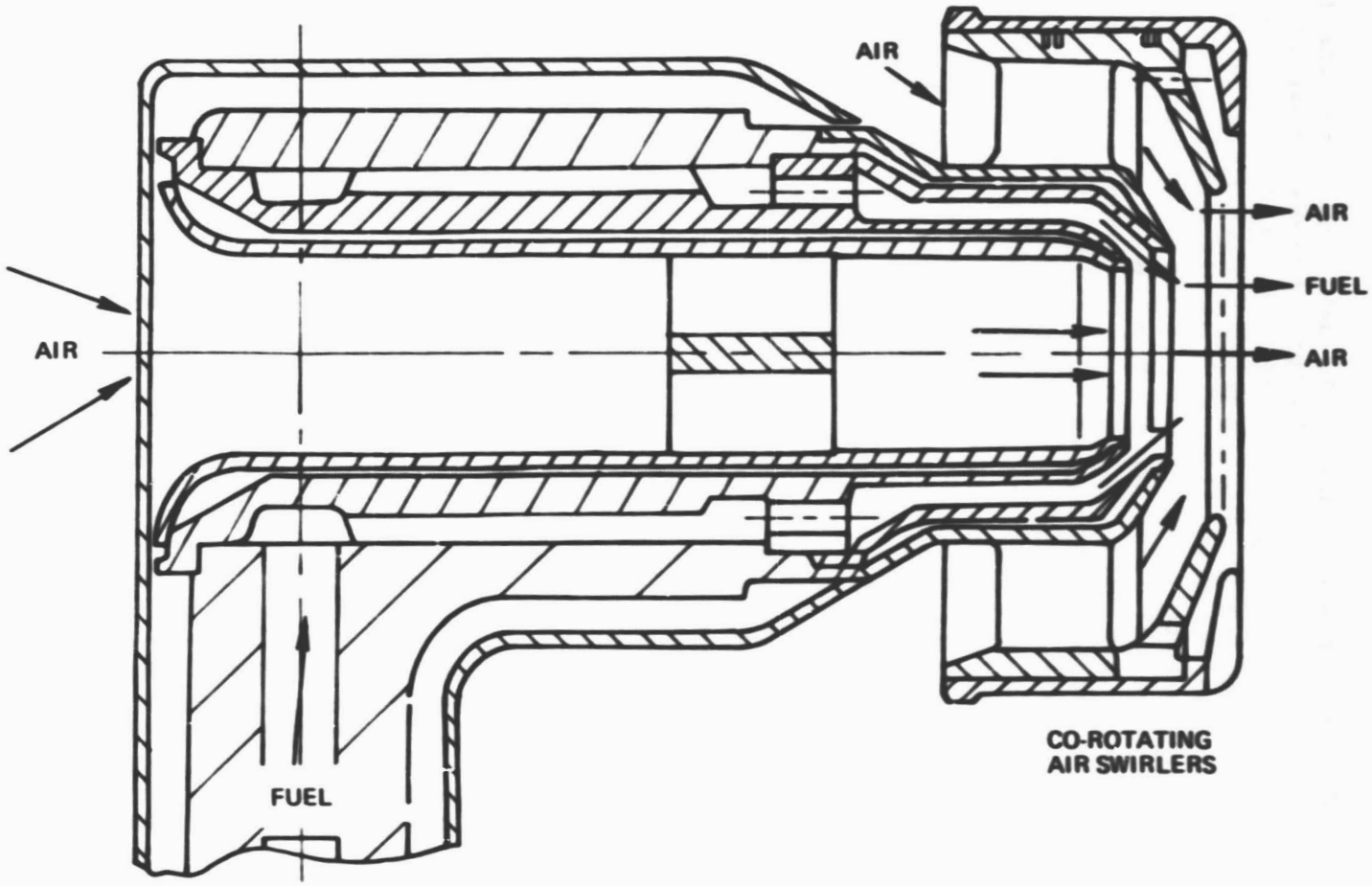

Figure 64 Aerating-Type Fuel Injector. The low-pressure design has good pilot zone fuel atomization with a low fuel pressure drop.

4.5.4.1.3 Main Zone Carburetor Tube Fuel Injectors Selection

The original design intent was to model the main zone after the ECCP Vorbix combustor. Figure 65 is a schematic representation of the translation of the Vorbix design in to the Energy Efficient Engine application, maintaining similar main zone stoichiometry while adding the capability to remove the outer liner without disassembling the fuel supply system. This required large liner sleeves to accommodate the fuel injectors. A large amount of shroud blockage is created by the sleeves and swirlers, (See view "A", Figure 65) which increases the shroud pressure loss and make proper supply of coolant to the aft liner section extremely difficult. The fuel injector sleeves partially shielded the swirlers which could adversely affect the swirler aerodyamics.

The Vorbix combustor exhibited high smoke emissions, indicating need for more air in the vicinity of the fuel injectors to eliminate rich burning zones which contribute to high smoke. Providing this air would further increase shroud blockage. Because of the cooling and combustion air requirements at the more severe Energy Efficient Engine operating conditions, the amount of air characteristically reserved for dilution and control of exit temperature profiles was judged to be inadequate with this design approach.

Therefore, the current design has been reconfigured as shown schematically in Figure 66. A carburetor tube main zone fuel injector system, in which outer liner swirler air is introduced through radial inflow swirlers concentric with the fuel injectors, premixes fuel and air to eliminate fuel rich pockets, reduces the combined swirlers and fuel injectors blockage area (view "A" of Figure 66), and convects the fuel into the burning zone with swirling air to increase fuel penetration. Since the momentum flux of the carburetor tube fuel-air mixture relative to the main zone combustion gas momentum flux remains relatively constant over the entire range of engine operating conditions, the fuel penetration distance will also remain relatively constant and carbon deposition on the combustor walls will be alleviated. The level of dilution air flow is increased to an acceptable 8.1 percent of combustor air flow from the unacceptable 2.6 percent estimated with the Vorbix approach.

The NO_x emission reduction potential of the carburetor tube is predicted to be the same as that demonstrated by the Vorbix combustor, based on a comparison of carburetor tube rig data with extrapolated ECCP data.

Carburetor tube rig test data also indicate that the smoke requirement can be met in the Energy Efficient Engine cycle with the carburetor tube injector. The Vorbix combustor smoke emissions would be over twice as great as the Energy Efficient Engine requirement.

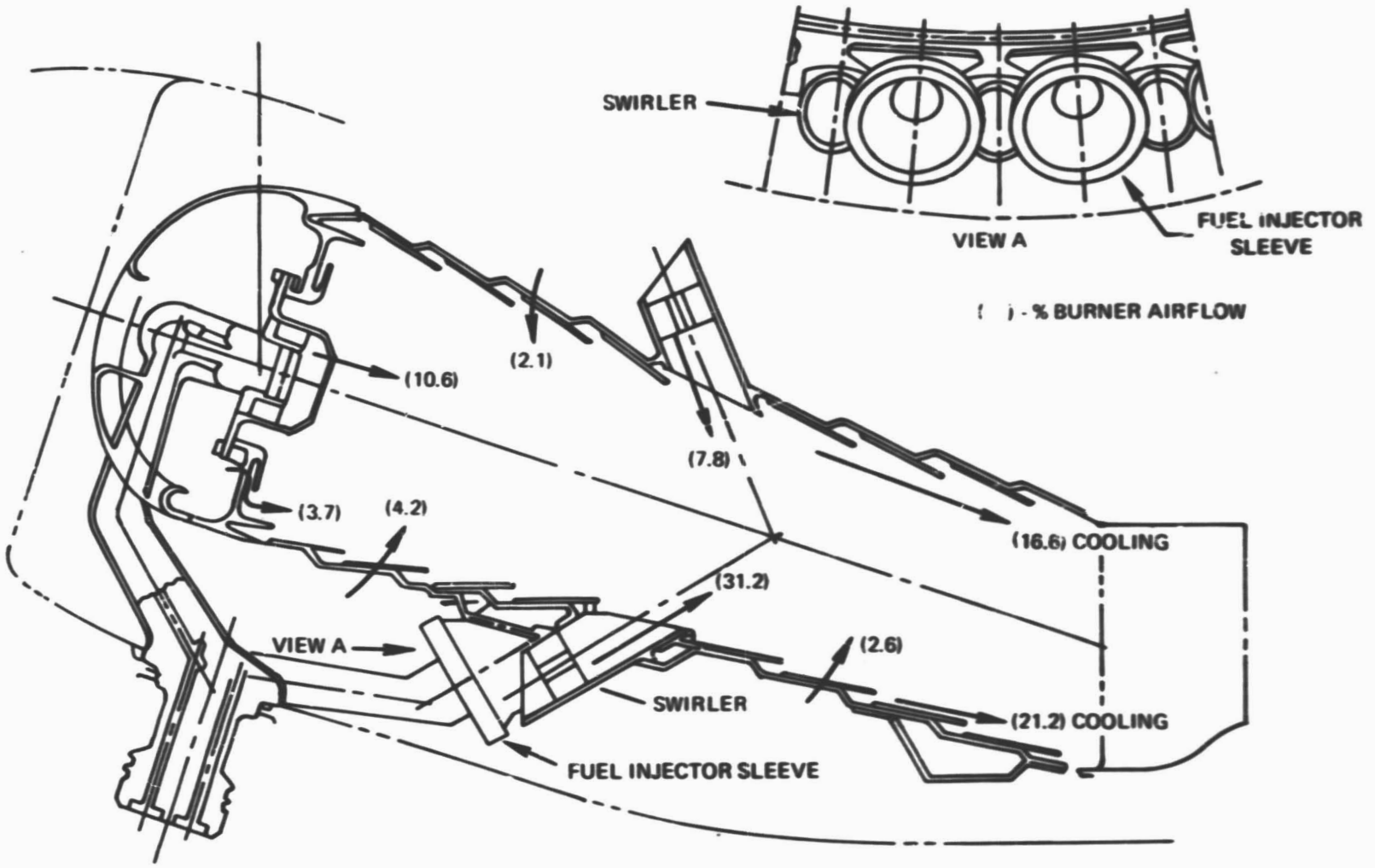

Figure 65 Originally Proposed Combustor Based on ECCP Vorbix Design. Substantial aft shroud blockage was created by swirlers and fuel injector ports.

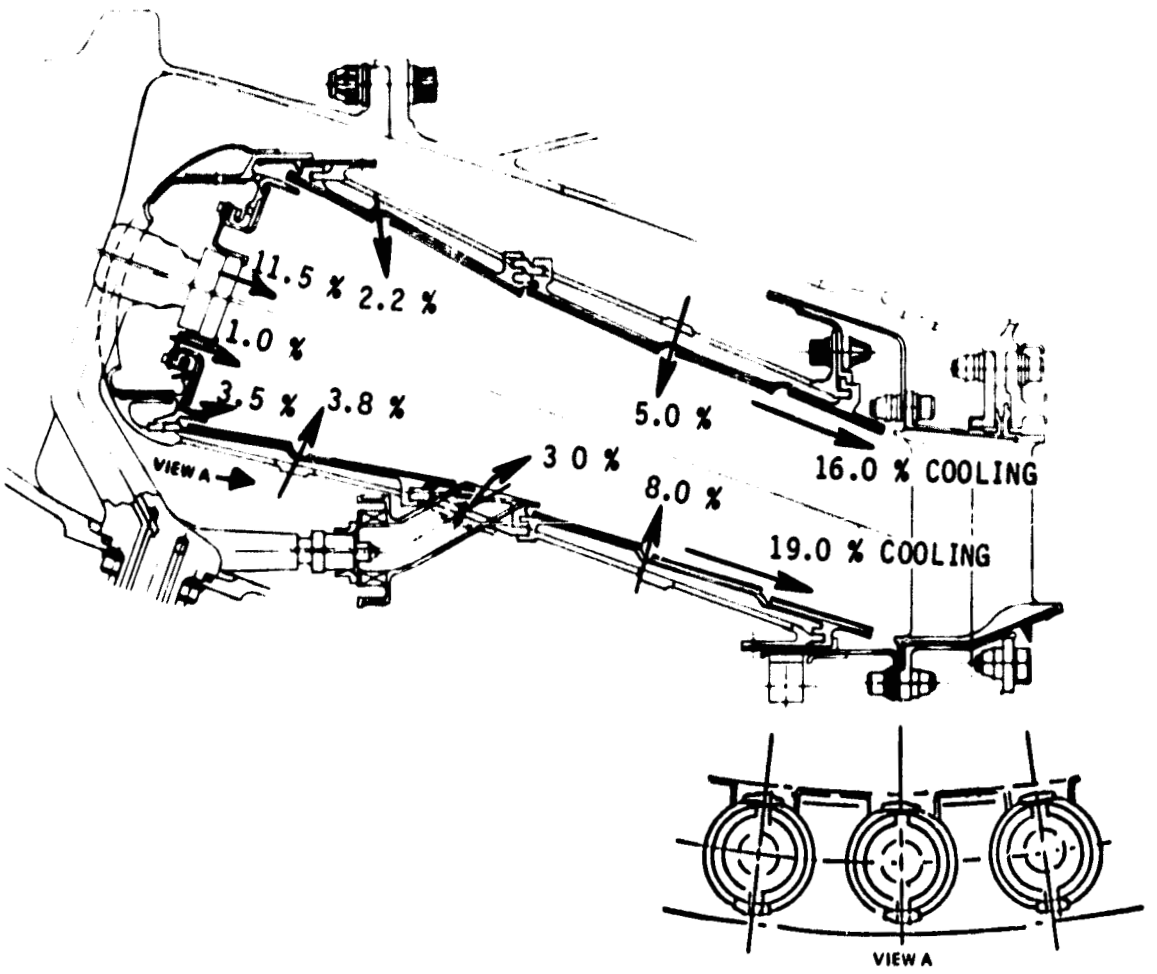

Figure 66 Present Combustor Design Configuration. Cross-section shows low shroud blockage.

An important safety consideration in the design of a carburetor tube is the prevention of autoignition of the fuel-air mixture external to the combustion zone. Design parameters were therefore set for the carburetor tubes which provided residence times and mixture axial velocities to preclude autoignition and flame flashback into the carburetor tubes. The carburetor tube diameter of approximately 1.5 cm (0.6 in.) provides a residence time of approximately 1 millisecond for the fuel-air mixture in the carburetor tube. This is well below the predicted residence time for autoignition at the sea level takeoff conditions as predicted by both Spadaccini (Reference 5) and Marek (Reference 6) and shown in Figure 67. This work assumes perfectly pre mixed, pre-vaporized conditions. The average axial velocity of the fuel-air mixture in the carburetor tube is approximately 183 m/sec (600 ft/sec). This is substantially higher than the turbulent flame flashback velocity of approximately 61 m/sec (200 ft/sec) at a representative carburetor tube equivalence ratio of 0.8. The design is believed to have adequate autoignition and flashback margins.

4.5.4.2 Fuel Supply and Staging Control System Preliminary Design

Each fuel injector support is designed to be connected to pilot and main zone manifolds by jumper tubes as shown in Figure 68. Jumper tube pairs are housed within a toroidal shroud to confine potential fuel leaks. The pilot and main zone fuel manifolds as well as the transfer valves are all housed in the same shroud to confine potential fuel leaks.

The pilot jumper tubes connect the pilot manifold directly to the pilot fuel passage in the fuel injector support. The main fuel manifold supplies fuel to the eight main fuel transfer valves. The main jumper tubes connect the valves to the secondary passage of the fuel injector support. The transfer valves stage the main zone fuel flow and fuel flow is initiated to the main zone. Eight transfer valves are used, each supplying six main zone fuel nozzles through these jumper tubes.

To prevent possible carbon buildup due to residual fuel in hot main zone fuel injectors when operating with only the pilot zone fueled, a purge system is included to inject a small amount of nitrogen or air downstream of the main zone manifold to carry the residual fuel into the main zone.

4.5.4.3 Prediffuser Configuration Selection

A trade study was initially conducted to establish the general configuration. The first configurations considered, which incorporate load carrying compressor exit guide vanes upstream of the prediffuser, were either structurally inadequate or could not meet aerodynamic design requirements. An arrangement which positioned the struts in the prediffuser section resulted in unacceptable weight and specific fuel consumption penalties because of the necessity to lengthen the curved wall prediffuser for adequate flow stability.

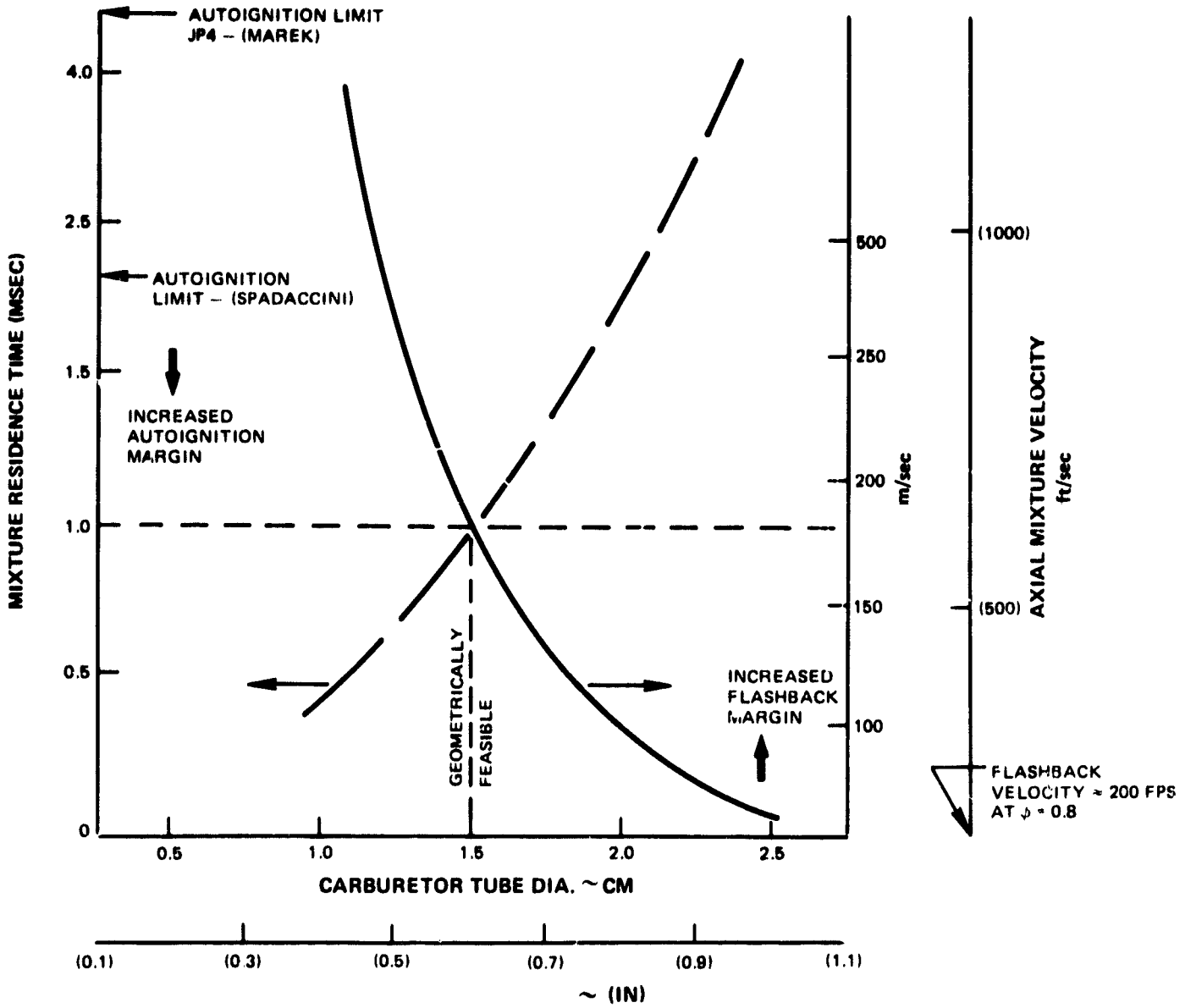

Figure 67 Estimated Autoignition Characteristics of Carburetor Tube Design. Data indicates increased autoignition and flashback margins.

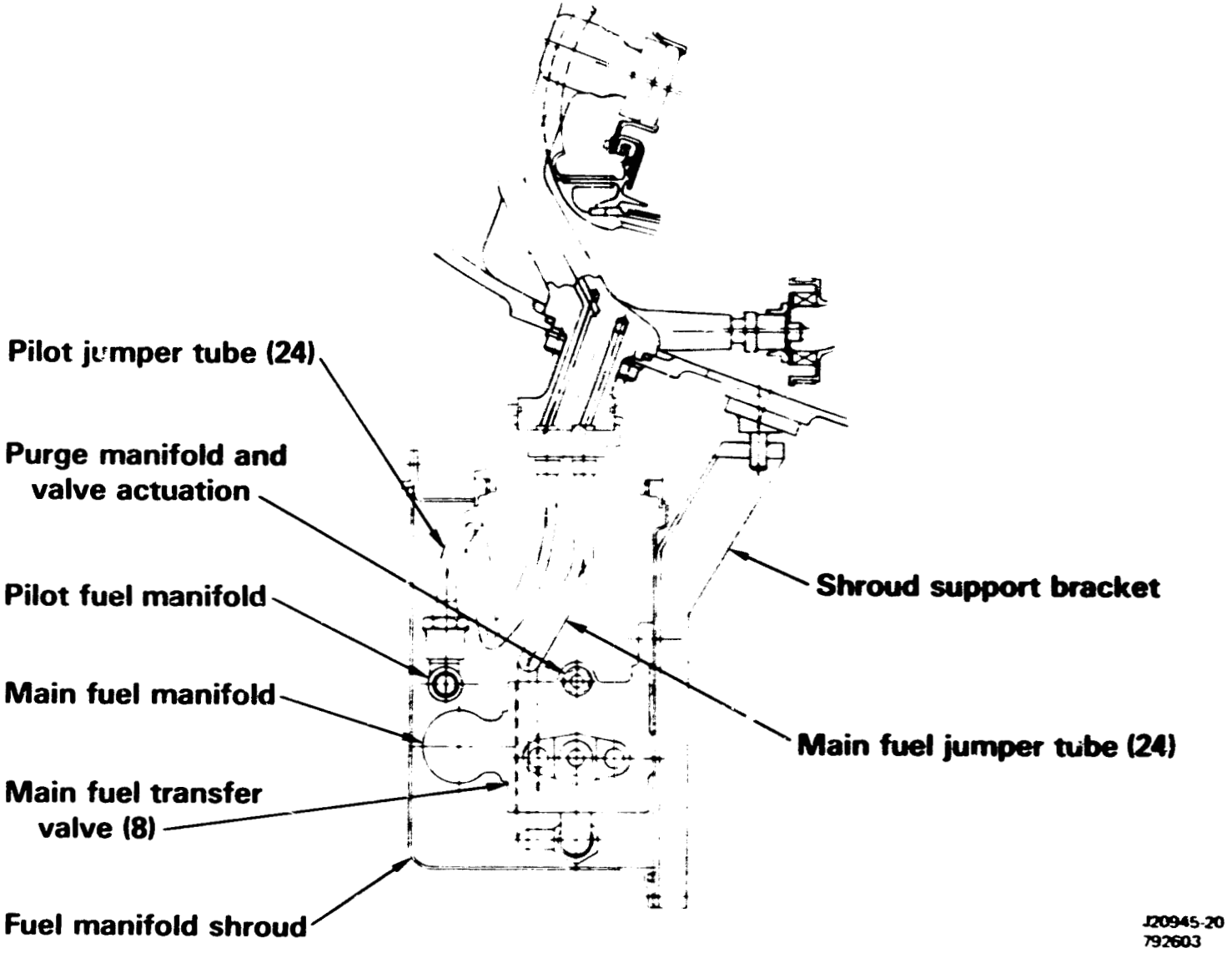

Figure 68 Fuel Supply System Manifold/Valve/Shroud Design. Cross section illustrates dual feed arrangement.

The configuration which was selected has a clean strutless prediffuser section with the structural struts located downstream of the dump plane of the prediffuser. This configuration results in the lowest pressure loss and the lowest overall cost and weight. The design incorporates 24 solid struts with maximum thicknesses of 0.89 cm (0.350 in.). The trailing edge of the struts are truncated to relieve stress concentrations at the junction between the struts and the diffuser case.

The original prediffuser design approach was to incorporate the strutless curved wall prediffuser which turned the compressor discharge flow outward and directed it along the centerline of the outward canted combustor. Figure 69 compares the initial design parameter to current experience and also to the design for optimum overall pressure recovery. The initial design was felt to be an aggressive curved-wall prediffuser configuration which had the potential of meeting the design criteria for separation-free operation.

An analytical prediffuser design study was conducted using an axisymmetric viscid flow model. The analytical model was initially substantiated with curved wall prediffuser data obtained through P&WA IR&D programs. The analytical model was then used to evaluate several prediffuser geometries which differed in prediffuser length, area ratio, rate of diffusion, or amount of prediffuser turning.

Having established the analytical model as a representative tool for conducting the prediffuser design study, a trade study was initiated, using the inlet total pressure profile of Figure 70. A displacement thickness of one percent of duct annular height was assumed for both the hub and tip walls corresponding to boundary layer thicknesses of approximately 8 percent on each wall.

Early analytical results indicated that the amount of prediffuser turning was excessive. Another study was undertaken to determine if pre-turning could be incorporated in the high-pressure compressor.

A range of outward turning in the compressor exit guide vanes, ranging from zero to 8 degrees was investigated. The benefit to the prediffuser of initiating outward turning in the exit guide vanes is indicated on Figure 71. The reduction in static pressure on the O.D. wall downstream of the compressor exit guide vanes is less when turning is initiated in the exit guide vane assembly, which reduces the subsequent rate of diffusion in the prediffuser section and minimizes the tendency for boundary layer separation.

Initiation of outward turning in the exit guide vanes also improves the performance of the exit guide vane section, as shown in Figure 72. This is due to the reduced spanwise pressure gradient in the exit guide vanes and significantly lower pressure rise near the inner wall. Both factors result in a more desirable boundary layer and free stream total pressure profile leaving the exit guide vanes. Further investigation of

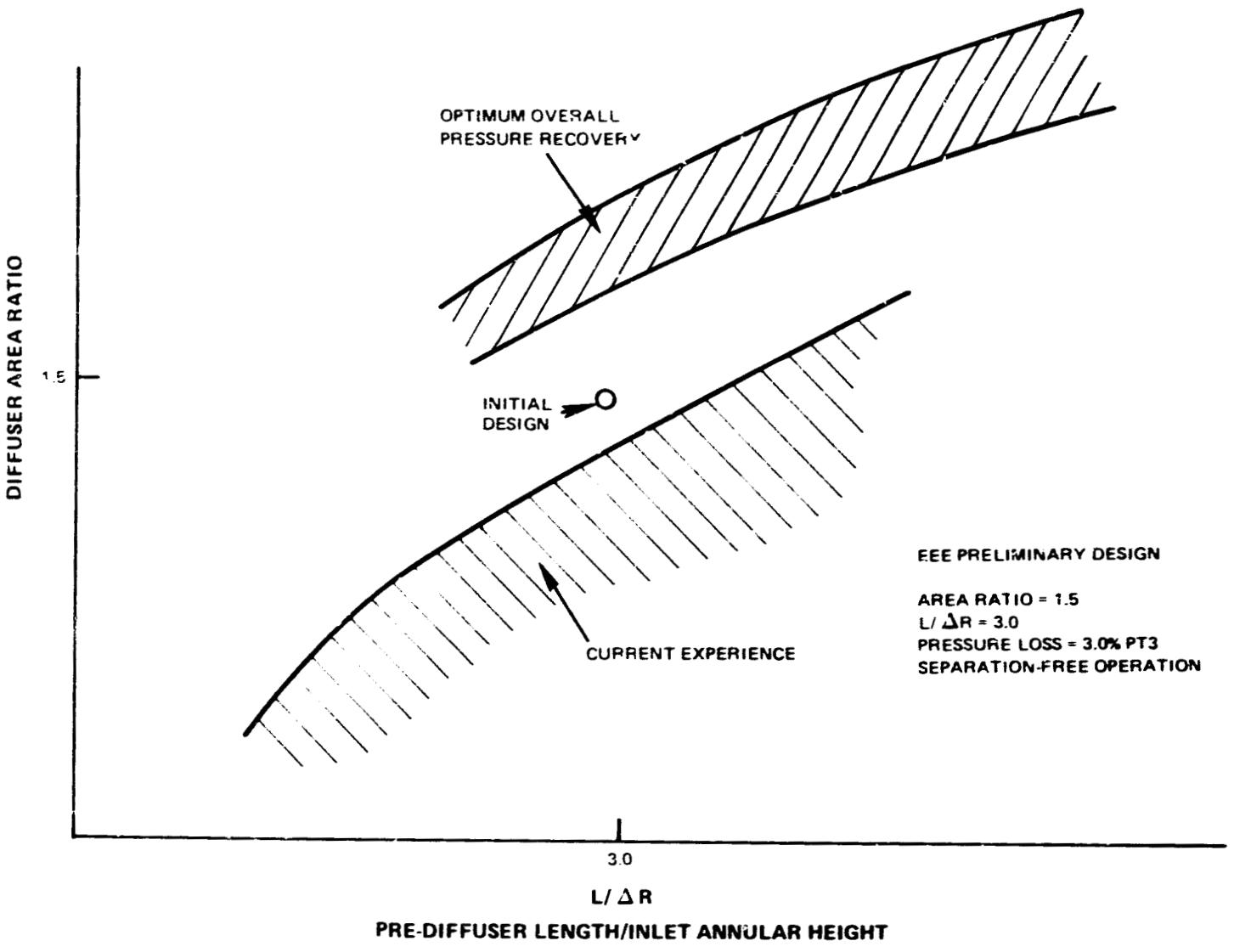

Figure 69 Initial Combustor Prediffuser Geometry. Comparison made between less aggressive current experience envelope and theoretical potential.

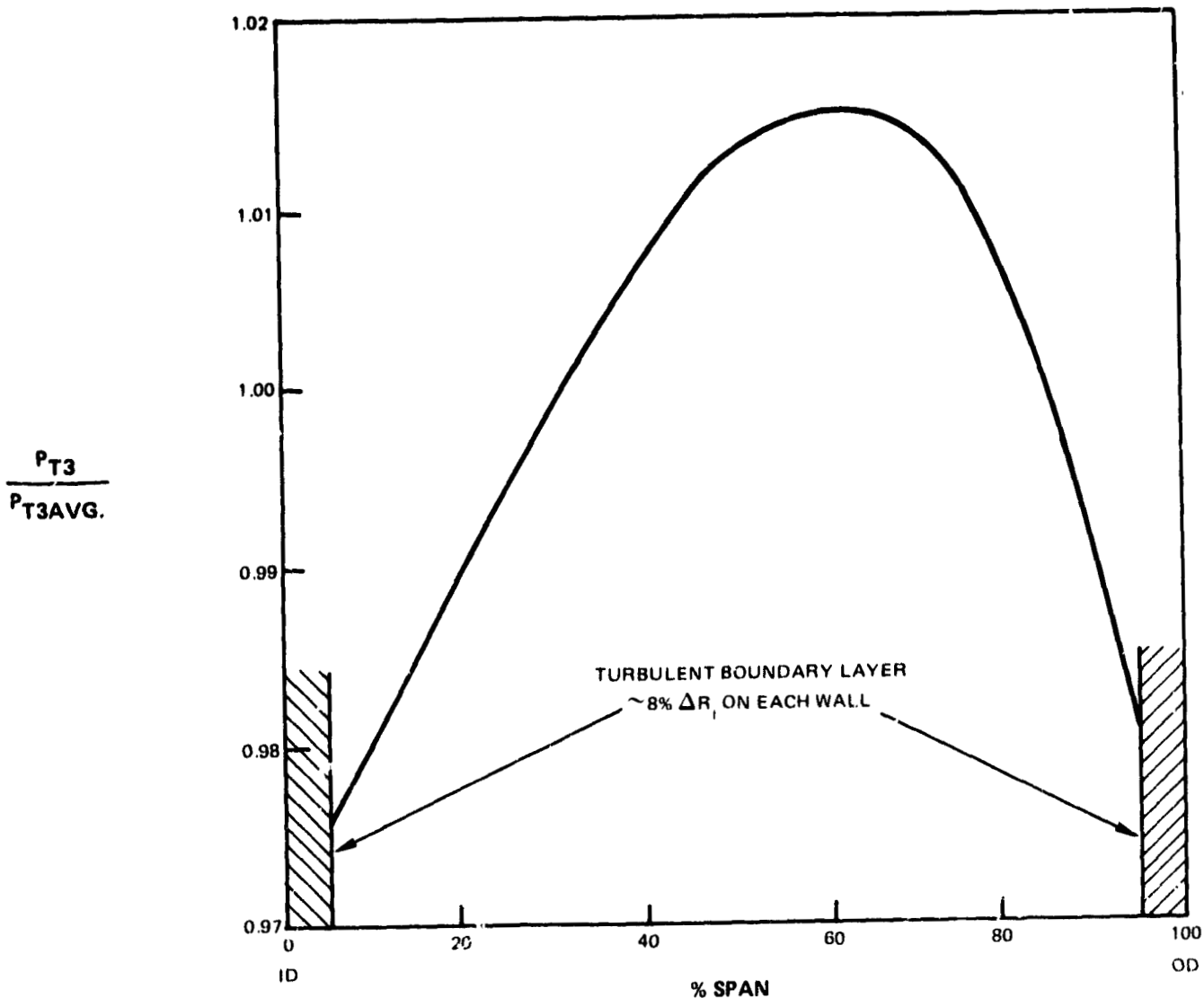

Figure 70 Inlet Pressure. Profile shows assumption used in prediffuser design studies.

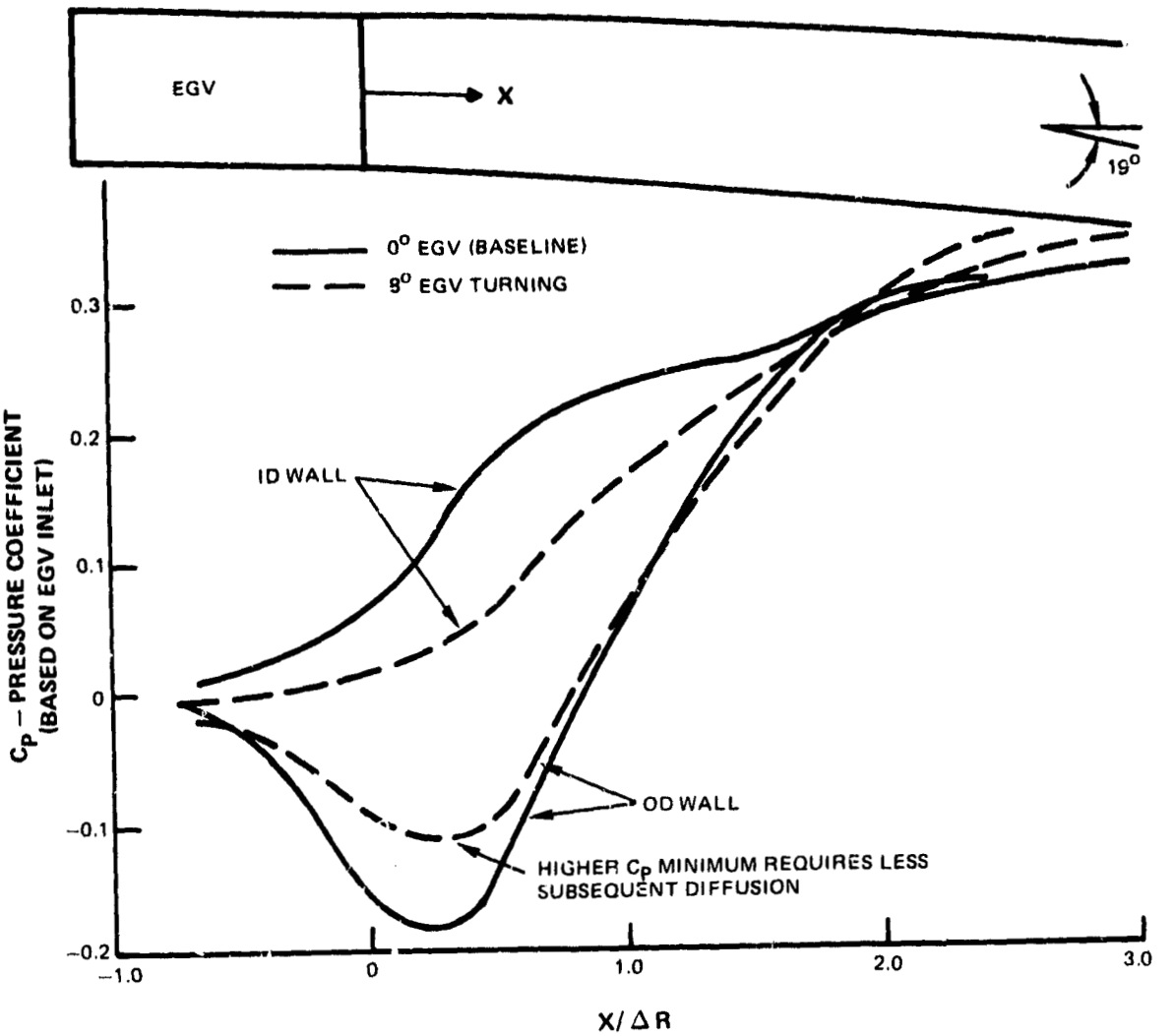

Figure 71 Analytical Predictions of Preturned Diffuser Air. Data indicates need for less prediffuser diffusion with compressor EGV cant angle of eight degrees.

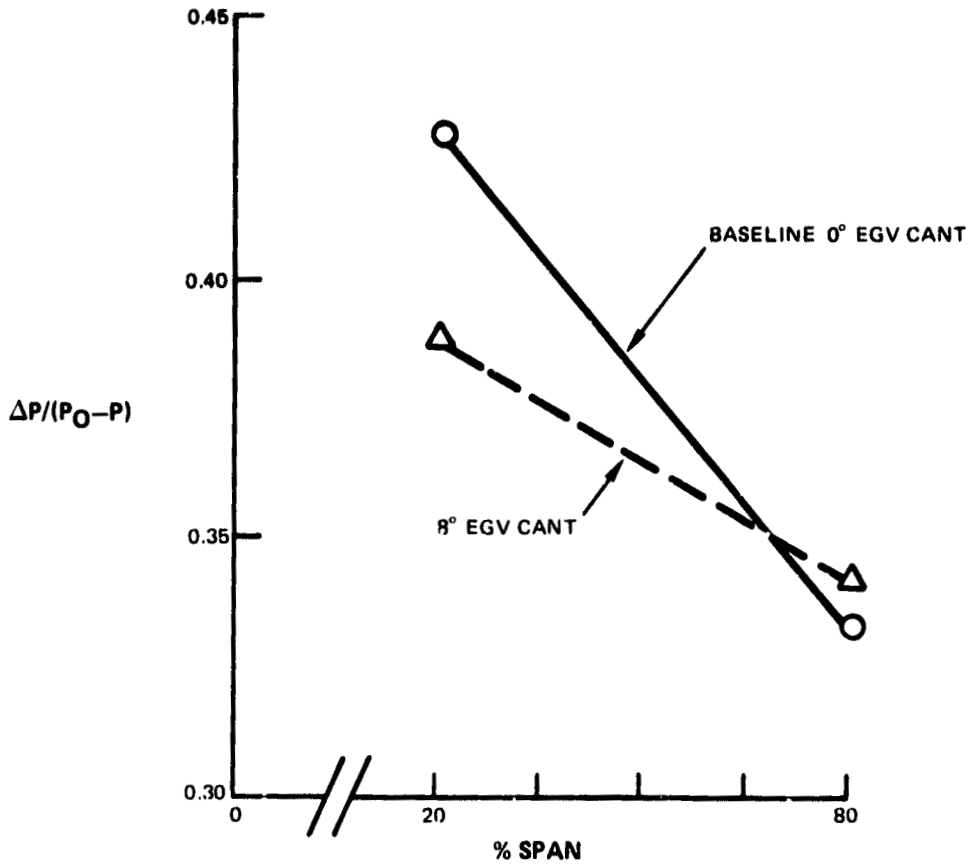

Figure 72 Analytical Predictions of Compressor EGV Canting. Data shows reduced spanwise pressure gradient and lower maximum wall loading with cant angle of eight degrees.

the overall impact on the compressor led to selection of a pre-turning angle of 5 degrees to maximize the combined prediffuser and compressor benefits.

Figure 73 indicates the study results for a range of prediffuser geometries assuming a constant prediffuser area ratio of 1.5 and a compressor exit guide vane outward turning of five degrees. The initial design, involving a nondimensional length of 3.0 with 19 degrees of total turning, was predicted to operate in the unstable region or as a separated prediffuser. In the recommended revised design, the nondimensional length was increased to 3.5 and turning was reduced to 14 degrees. Pressure loss was calculated to be below the goal level.

If needed, additional stability margin can be achieved by reducing the prediffuser turning using an alternate design with 8.5 degrees of turning. A slight increase in pressure loss is expected. Both the recommended and alternate designs will be evaluated in an experimental supporting technology program to substantiate the prediffuser/combustor front end design prior to final selection.

The predicted performance of the recommended prediffuser design is indicated in Figure 74. The average pressure recovery coefficient corresponds to a prediffuser efficiency of approximately 72 percent. The predicted skin friction coefficient for the outer wall also indicates separation-free operation of the prediffuser.

The final phase of the analytical preliminary design study involved evaluation of the sensitivity of the prediffuser operation to changes in inlet total pressure profile. An I.D. peaked profile was imposed on the recommended design to examine the most severe profile which might be experienced by the outer prediffuser wall. As seen in Figure 75, the recommended prediffuser design is predicted to operate separation-free, even with the severe I.D. peaked profile.

4.5.4.4 Combustor Front End Positioning and Sizing

The combustor hood is positioned relative to the prediffuser dump plane to minimize the overall pre-diffuser and shroud pressure losses. The hood is positioned to avoid interference with the structural struts.

The hood is sized consistently with current combustor designs having known adequate aerodynamic characteristics. The hood incorporates sufficient volume to establish plenum feed characteristics for the air ports in the bulkhead. Annular shroud areas between the diffuser case and the inner and outer combustor liners are sized to minimize pressure loss, accounting for blockage by fuel injectors and swirler ports. The ratio of the liner pressure drop to local dynamic head in the shroud flow is maintained at a value which ensures that aspiration of hot gases from the combustor liner will not occur.

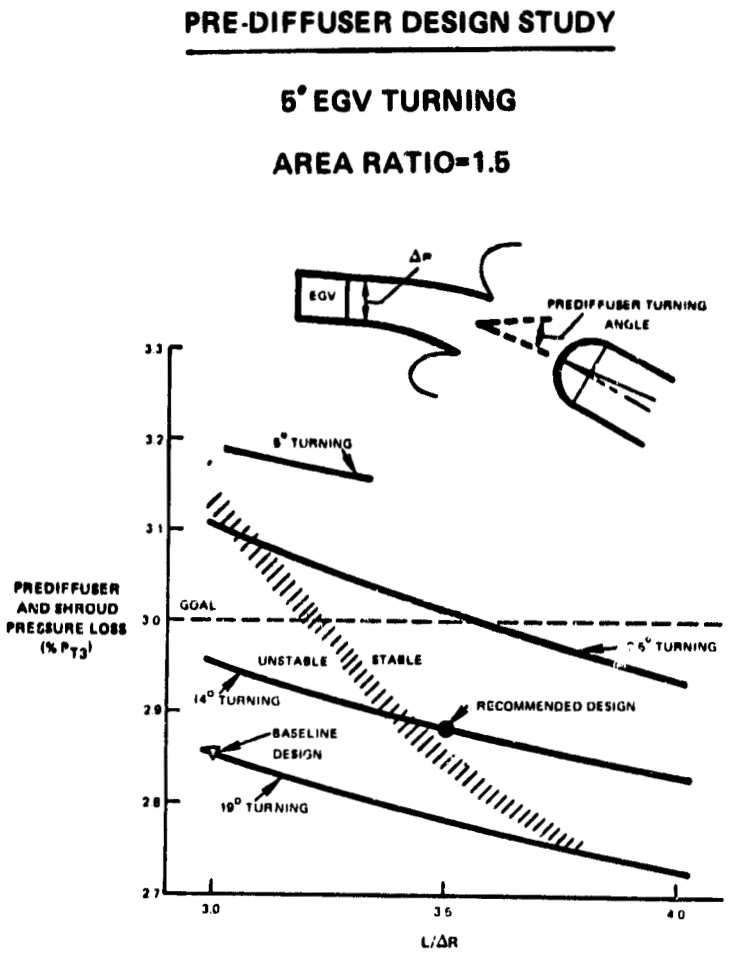

Figure 73 Diffuser Geometries. Data indicates predicted pressure losses and stability regions with various diffuser geometries and revised current geometry.

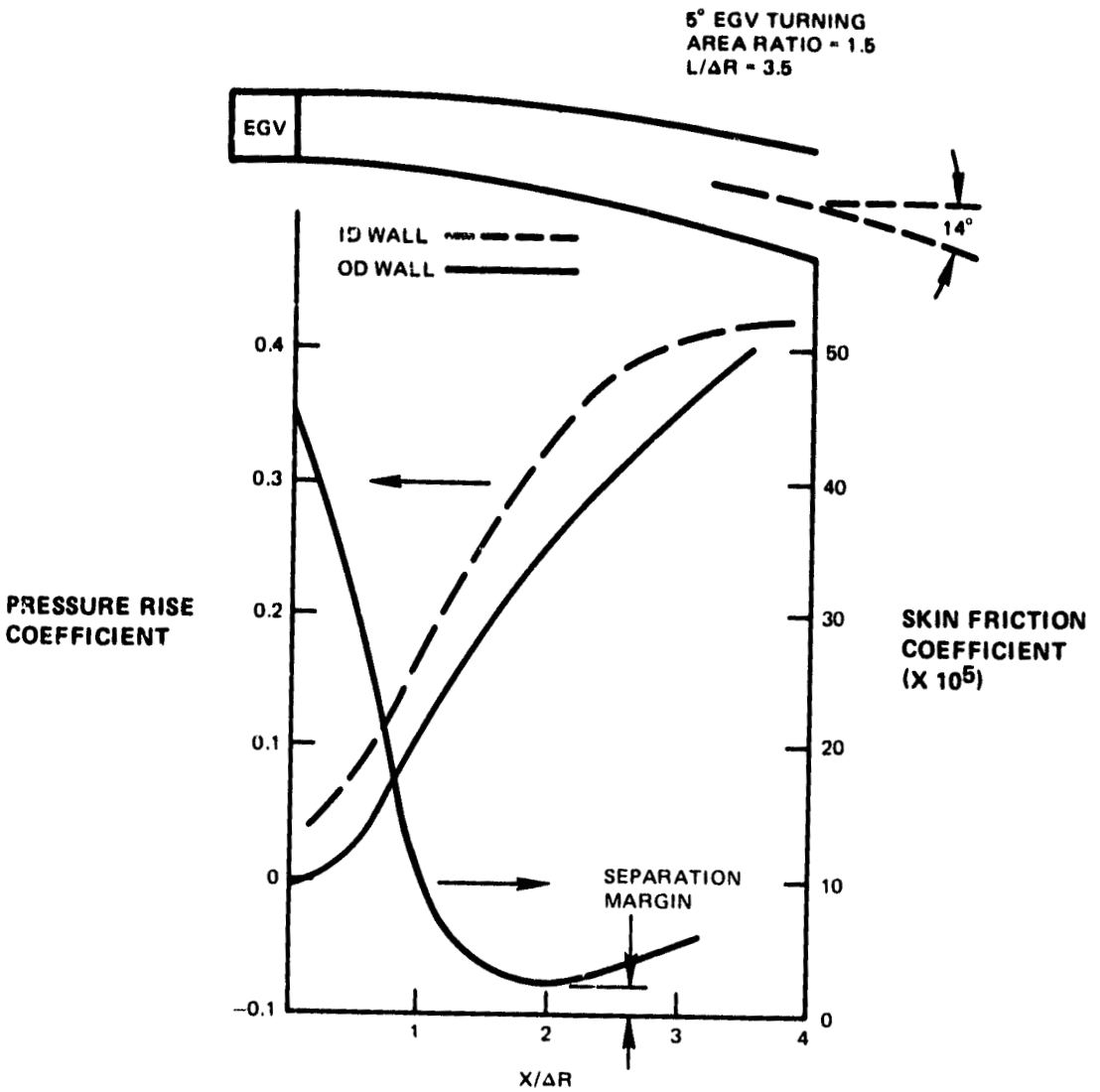

Figure 74 Predicted Performance of Revised Current Prediffuser. Data indicates separation-free operation.

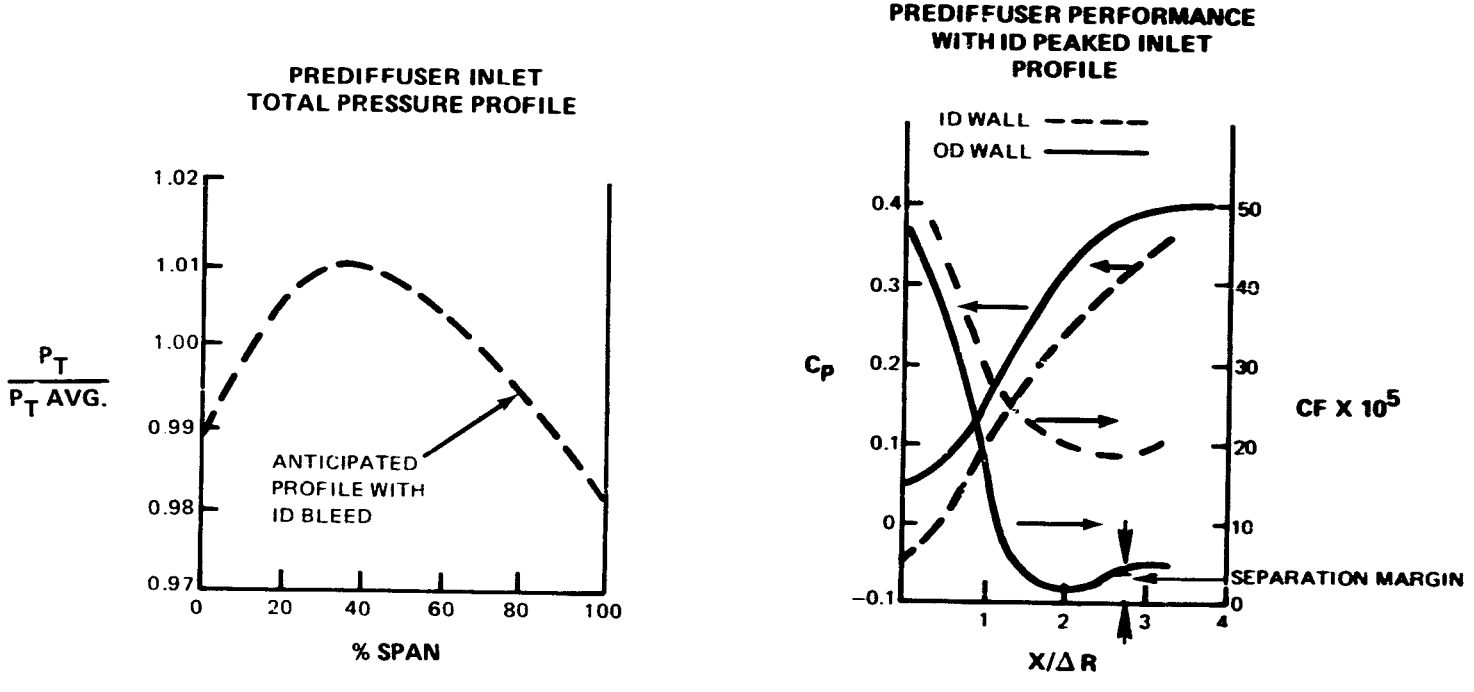

Figure 75 Predicted Performance of Revised Current Prediffuser Design. Data indicates separation-free operation with "worst" inlet profile.

The pilot zone dome height of the current design is 9.4 cm (3.7 in.) which maintains the same nozzle spacing to dome height ratio as the ECCP pilot zone. A larger recirculation zone is incorporated to improve relight capability at altitude and sea level and to minimize the tendency for fuel impingement on the liner walls and thus decrease low power emissions. Pilot zone volume was established to be sufficient to achieve the very high combustion efficiency required to meet emissions goals.

4.5.4.5 Combustor Liner Analysis

Initial liner design studies were conducted on a full hoop, louver type liner featuring extended lips of ODS material and an outer shell of Hastelloy X material, Figure 76. This analysis resulted in a predicted life of 3200 missions which was short of the 4900 mission goal.

In order to meet the program life goal, the scope of the Energy Efficient Engine liner design study was expanded to include convective cooling techniques with higher thermal effectiveness, and alternate construction techniques such as segmenting, to reduce high hoop stress. Materials considered for use with the advanced cooling designs were Hastelloy X, conventional turbine airfoil alloys offering good high temperature creep resistance, and oxide dispersion strengthened alloys.

The types of advanced cooling configurations considered are shown in Figure 77, Figure 78 and Figure 79.

The combustion gas boundary conditions imposed on the liner during the thermal analysis are shown in Figure 80. The axial variation of combustor flame temperature was based on a fuel distribution with 30 percent of fuel in the pilot zone and 70 percent in the main zone. The decrease in flame temperature in each zone reflects the mixing of liner cooling air and/or dilution air as the gases proceed downstream. Both convective and radiative heat fluxes to the walls were considered in the thermal analysis.

In evaluating the feasibility of the various cooling techniques, a limit was placed on liner cooling air of 35 percent of combustor airflow in order to ensure an adequate amount of air for dilution and emission control. At a cooling air level of 35 percent, both the louver and impingement-film cooled liners will operate with a maximum wall temperature (unstreaked) in excess of 1850°, the maximum operating temperature of ODS. All three convective cooling techniques are feasible with Hastelloy X, turbine alloys or ODS. See Figure 81.

The cooling and life prediction analyses resulted in a recommendation to select the segmented, counter-parallel FINWALL (CPFW) liner, of cast PWA 1455 material. Figure 82 illustrates the CPFW panel configuration in the Energy Efficient Engine combustor. The same construction technique could be used for counter-flow film cooling or impingement transpiration.

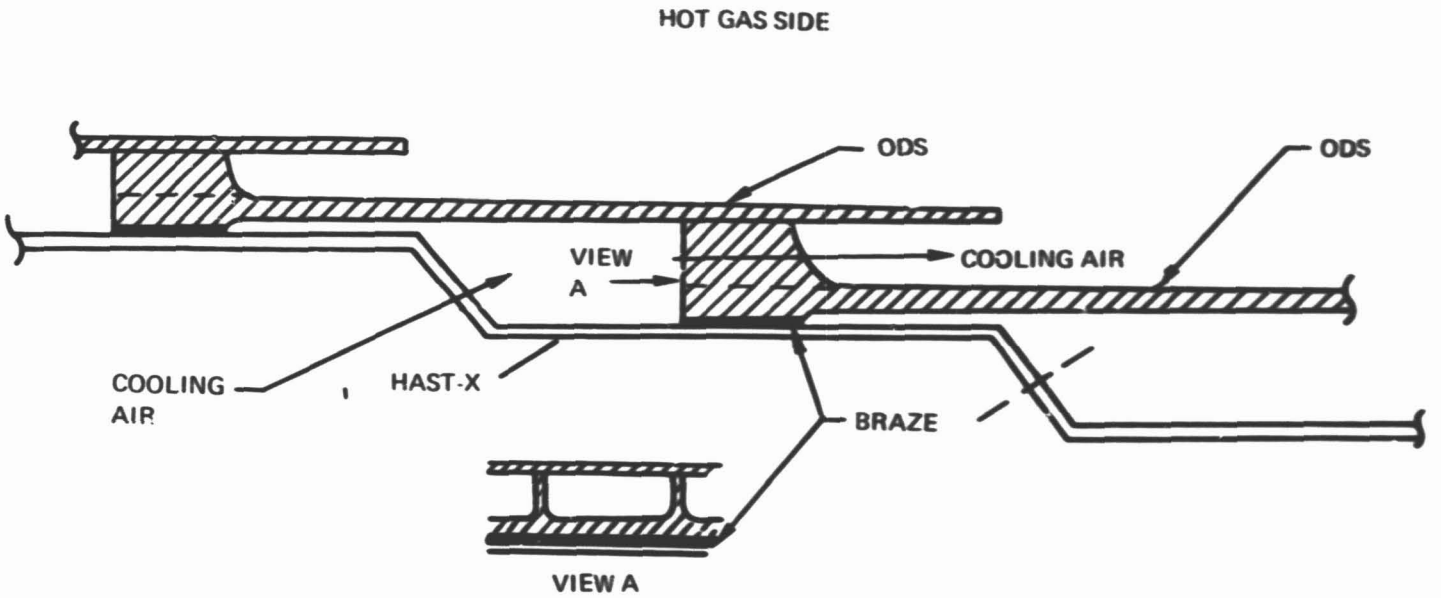

Figure 76 Initial Combustion Liner. Design included high temperature ODS material combined with a Hastelloy X outer shell.

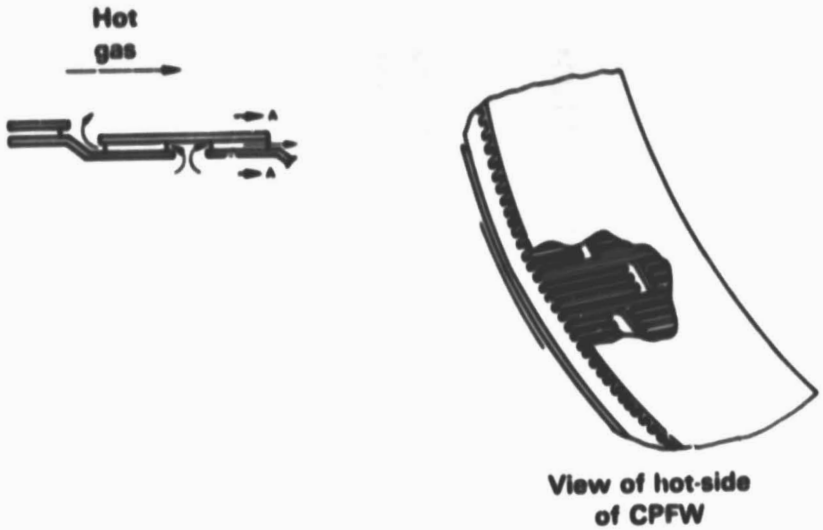

Figure 77 An Advanced Combustor Liner Cooling Configuration. Counter parallel Finwall (CPFW) Technique.

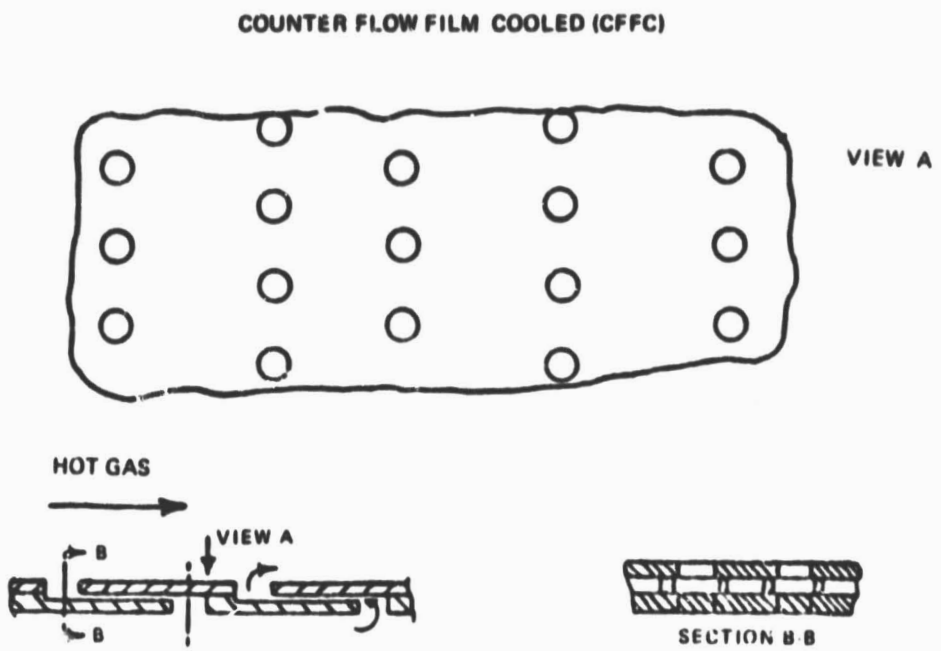

Figure 78 An Advanced Combustor Liner Cooling Configuration. Counter flow film cooled (CFFC) technique.

Figure 79 An Advanced Combustor Liner Cooling Configuration. Impingement film and transpiration technique.

J20945-5
792603

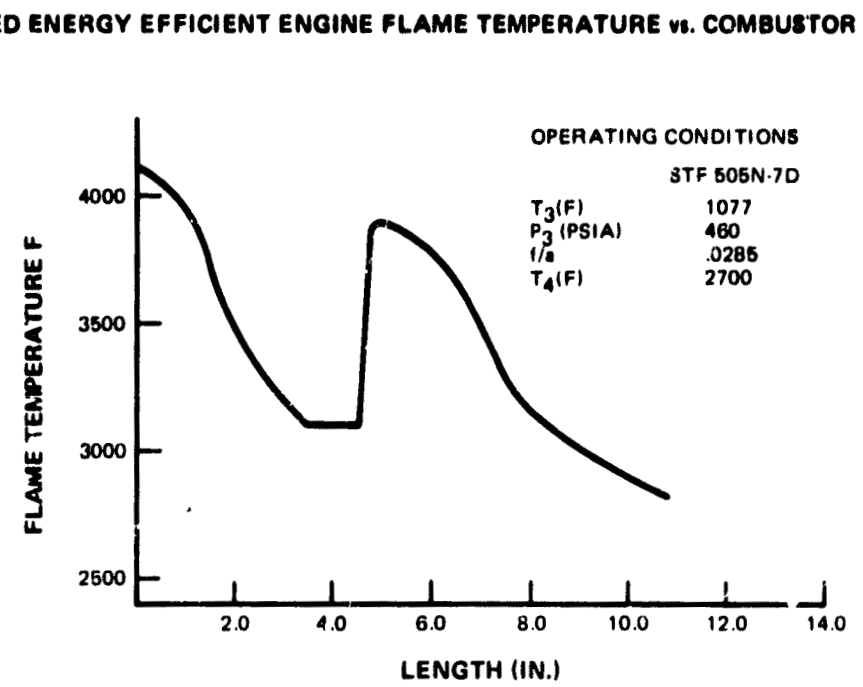

Figure 80 Combustor Liner. Thermal analysis imposed combustion gas boundary conditions.

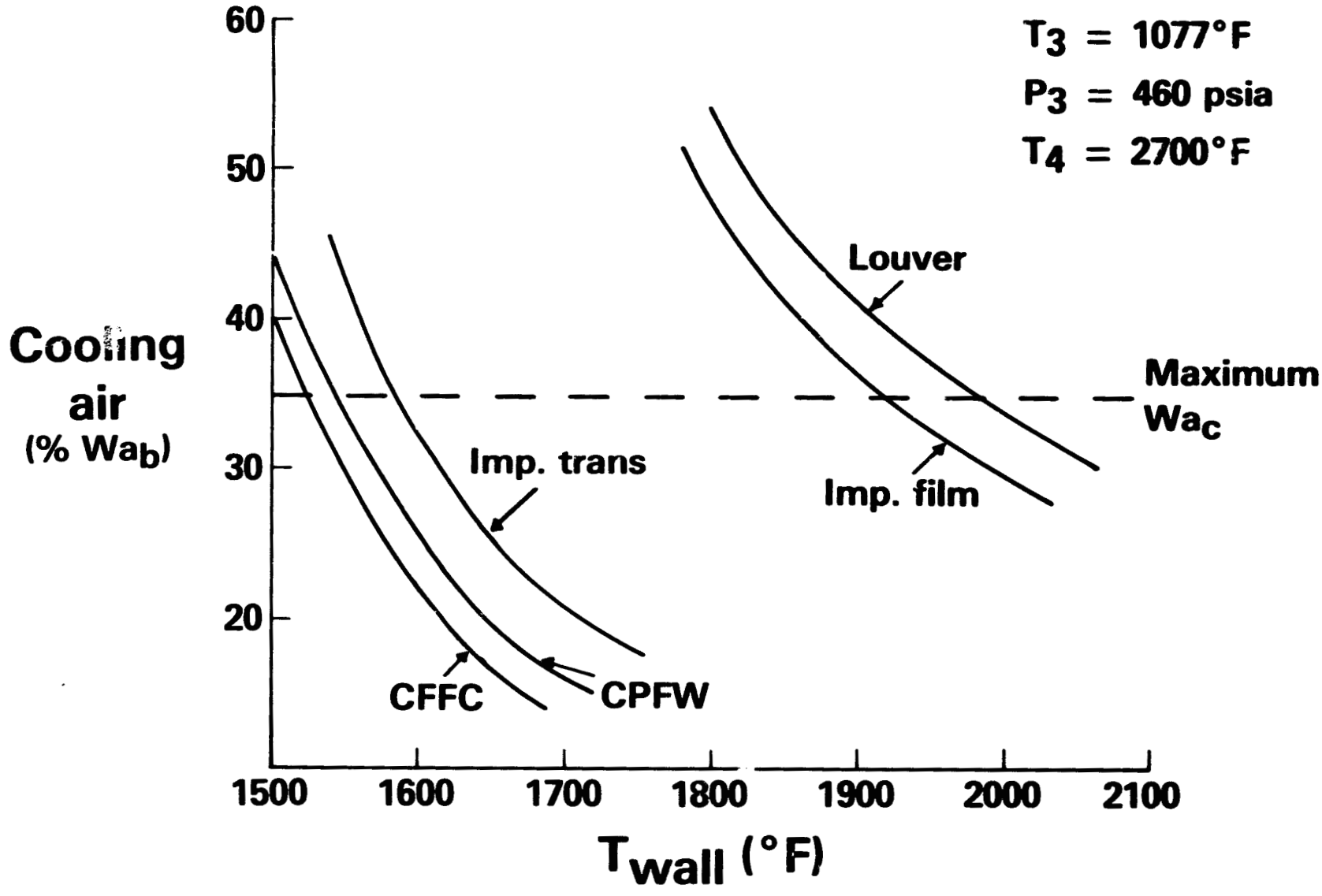

Figure 81 Combustor Liner Cooling. Analysis indicates feasibility of advanced cooling techniques.

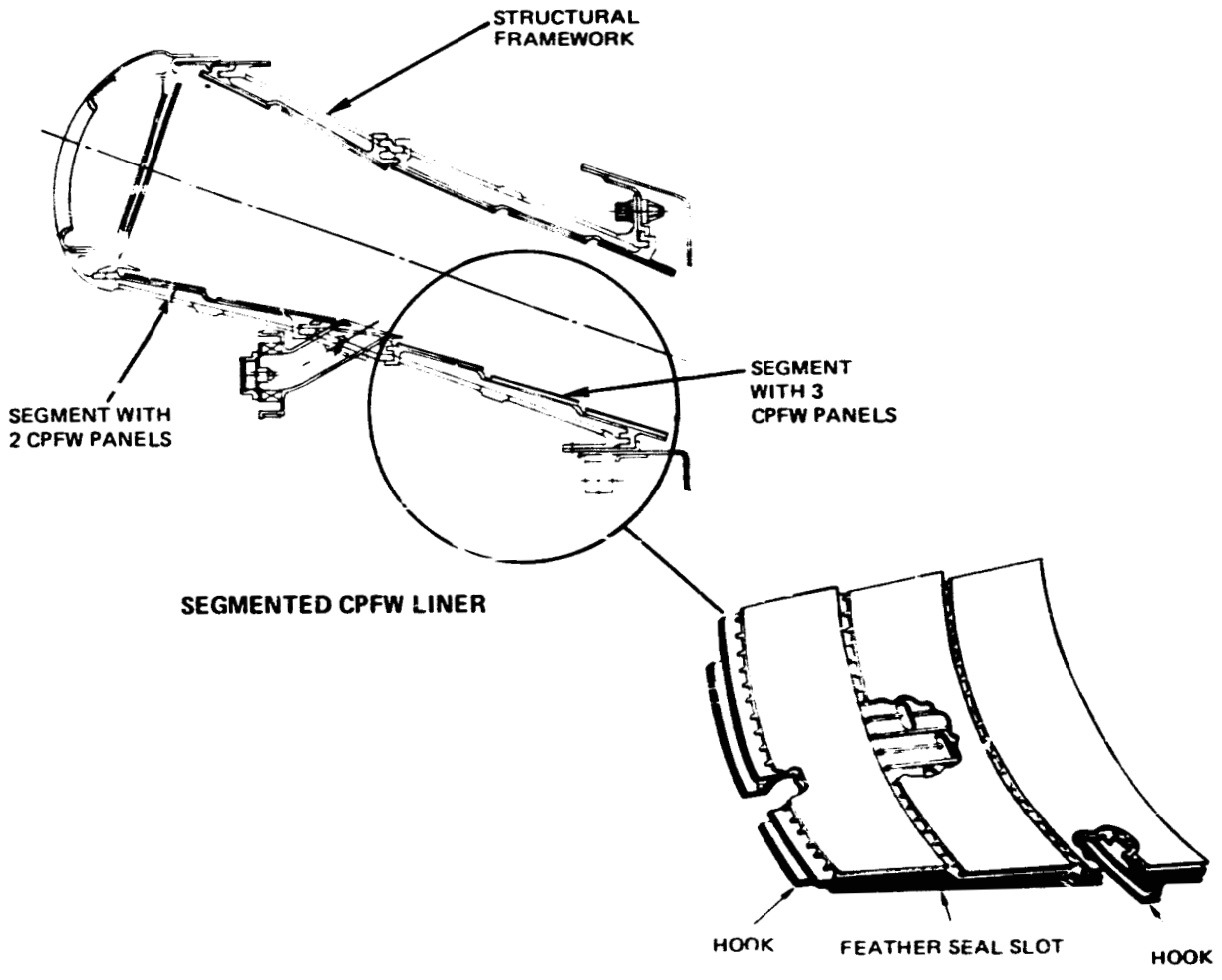

Figure 82 CPFW Panel Configuration in the Energy Efficient Engine Combustor. Segmented construction used to extend part life by stress reduction.

Segmented construction was utilized to improve life by breaking the hoop to reduce stresses. The inner and outer liners are formed by arranging 24 segments circumferentially in both the pilot and main zones to create the gas path. A total of 96 segments are required to assemble the complete combustor. Hooks on the back of each segment mate with circumferential rails on the structural framework to position the segments.

Table 32 is a summary of the liner study indicating that the Energy Efficient Engine combustor life goal can be achieved with segmented liners of turbine airfoil alloy (PWA 1455) or ODS alloy. The ODS impingement-transpiration cooled liner has high estimated leakage which may be reduced by detailed design efforts. Consideration of initial cost, maintenance cost, and direct operating cost reveals that neither candidate has a distinct advantage.

4.5.4.6 Case Analysis

4.5.4.6.1 Bleed Manifold Geometry Selection

Before embarking on a structural analysis of the diffuser case, two high pressure bleed manifolds (supply low power bleed requirements to aircraft) were analyzed. In both configurations customer bleed air is extracted downstream of the dump plane of the prediffuser section (Figure 83). In Configuration 1, bleed bosses must be welded close to the outer diffuser case ring, through which blow-off loads are transferred from the inner diffuser case to the external diffuser case. Configuration 2, which was selected as the more promising, avoids this problem by incorporating a toroidal manifold in which the customer bleed air is captured. The bleed bosses are machined into the manifold. The toroidal configuration also allows the placement of an ACC impingement tube as far back as the high-pressure compressor exit guide vane front attachment to maximize the stages affected by clearance control.

4.5.4.6.2 Case Stress Predictions

Thermal stresses and pressure loadings were calculated at the sea level, Mach 0.45 maximum pressure condition. Stresses and cyclic life initial estimates in critical case sections are summarized in Figure 84. Case thicknesses are set to limit the hoop stresses to 69 kN/cm^2 (100 ksi). Diffuser case inner and outer rings, which transfer the large blowoff load and the torque load from the inner to outer case, are estimated to be the life limiting regions in the case. Both rings are sized to provide a minimum of 20,000 missions life.

4.5.5 Design Summary

The combustor preliminary design summary is indicated in Table 33. All program goals are met except for NO_x emissions. NO_x reduction tech-

TABLE 32

ENERGY EFFICIENT ENGINE LINER STUDY SUMMARY

Configuration	Cooling Air (% Wa_b)	Leakage (% Wa_b)	T_{wall} (°F)	Life (cycles)	Weight (lb.)
CPFW Hoop (Hastelloy X)	32	0	1575	2500	125
CPFW Segments (PWA 1455)	32	3	1575	10,000	185
CPFW Segments (Hastelloy X)	32	3	1575	4000	-
CFFC Segments (PWA 1455)	34	3	1550	1000	-
Impingement-Transpiration Segments (PWA 1455)	33	3	1660	2600	185

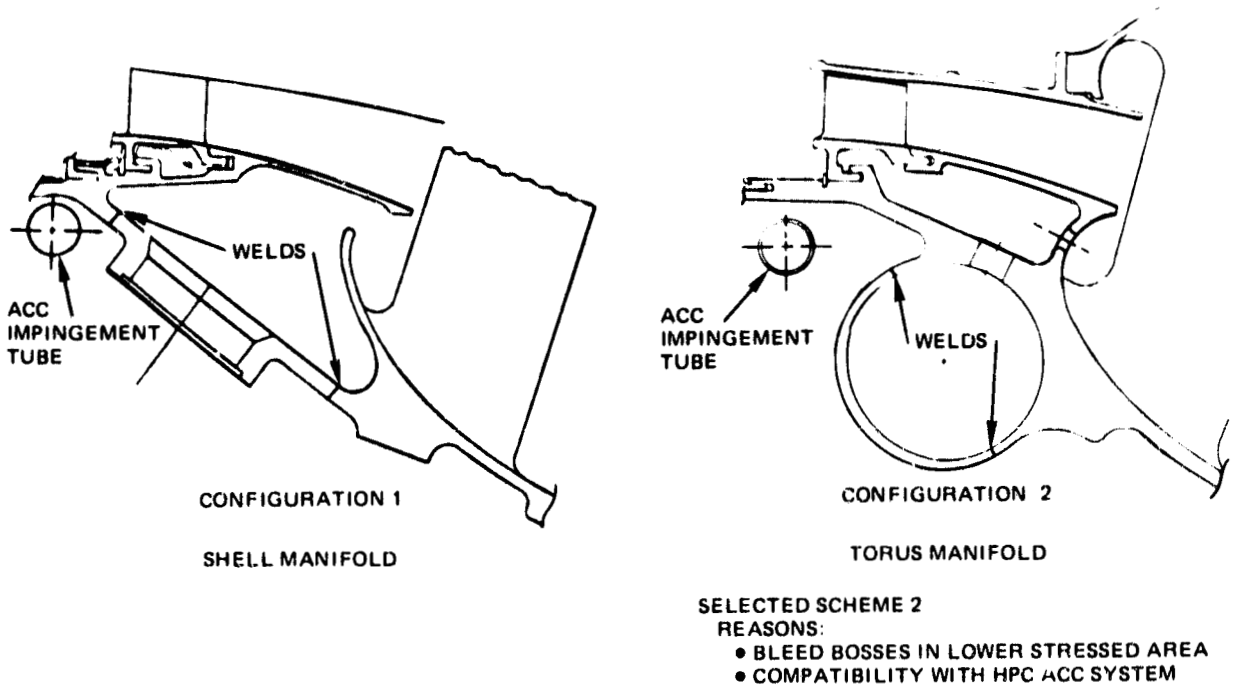

Figure 83 Diffuser Bleed Manifolds. Two configurations were investigated and torus design selected.

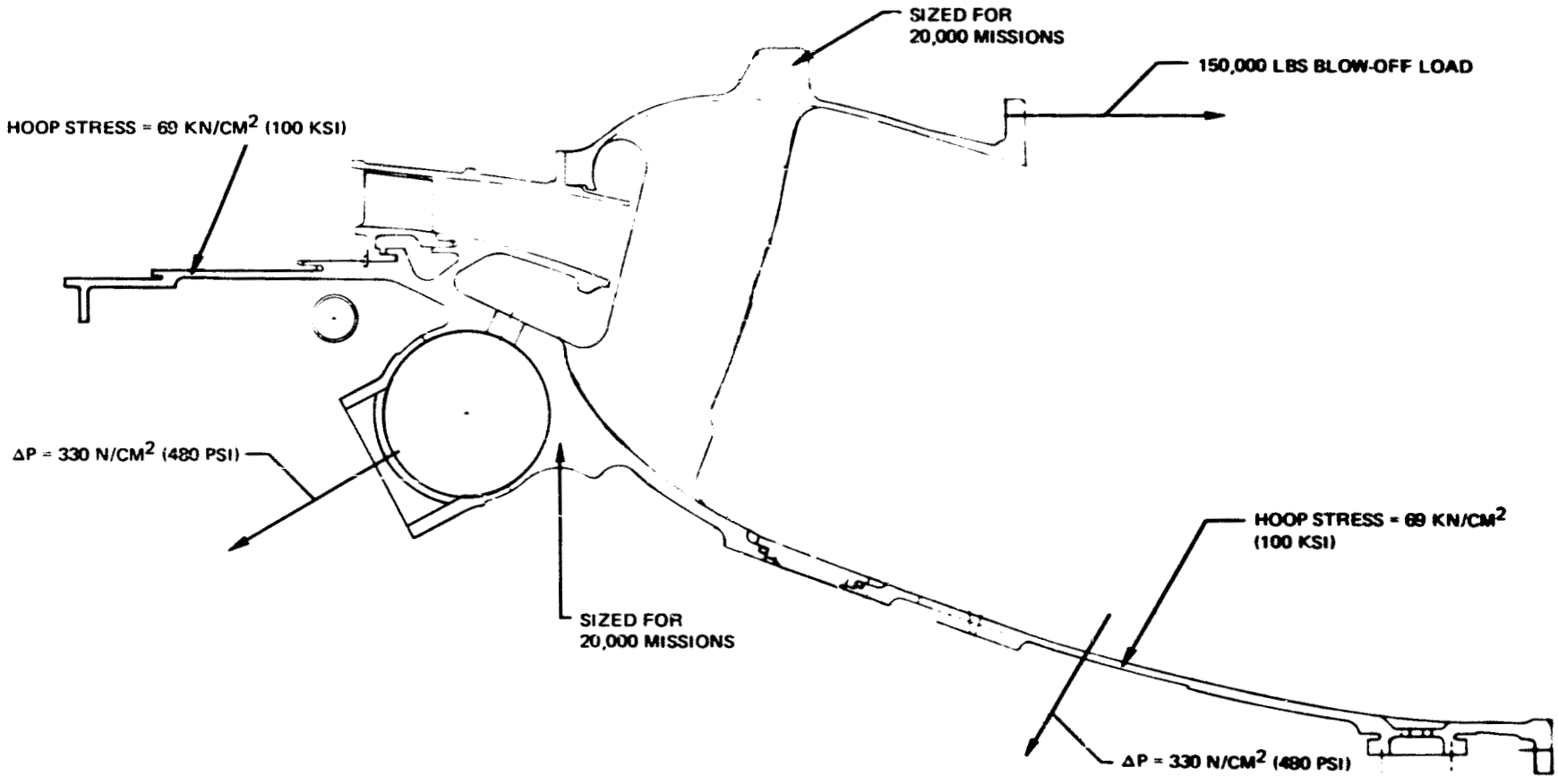

Figure 84 Combustor/Diffuser Case. Stress and cyclic lives of critical case sections are summarized.

TABLE 33

COMBUSTOR DESIGN STATUS

Overall Pressure Loss	5.5% P_{T3}
Maximum Temperature Pattern Factor	0.37 Max.
OD Skewed Radial Profile Exit Temperature	110°C (200°F) Peak
Emissions (W/Margins)	
HC	0.2
CO	1.7
NOx	4.6
Smoke Number (SAE)	20
Liner Low Cycle Fatigue Life (To Repair)	16,300 hr. 10,000 Missions

nology from this and other programs will be continually assessed for possible incorporation into the design to further reduce NO_x levels toward the goal levels.

4.6 HIGH-PRESSURE TURBINE

4.6.1 Design Requirements

The high-pressure turbine aerodynamic, structural, and mechanical design requirements were established by the engine cycle definitions at design and off-design flight conditions. Performance and durability considerations involved a number of key operating conditions.

General design requirements for the high-pressure turbine are summarized by Table 34.

Performance requirements were established at the 10,668m (35,000 ft) aerodynamic design point which is located between the two key high performance oriented operating conditions of maximum climb and maximum cruise. Goal high pressure turbine efficiency is also presented.

Commercial acceptability determined the high pressure turbine mechanical and structural design requirements. Design lives were established based on life analysis over the airplane mission engine duty cycle depicted by Figure 85.

4.6.2 Design Background

A series of high work single stage turbines were designed, fabricated, and tested at P&WA to calibrate the transonic turbine loss prediction systems and develop airfoil pressure distribution prediction capability. The data from the latest of this series, the High Work High Spool Engine (HHSE), with appropriate technology updates, is the basis for the high-pressure turbine design.

4.6.3 General Configuration Description

The high-pressure turbine is a highly loaded air cooled single-stage design. The major design features, depicted in Figure 86, are discussed in the following paragraphs.

4.6.3.1 Major Subassemblies

The disk is fabricated from MERL 80 material with advanced powder metallurgy techniques, to produce the required low cycle fatigue properties under the high blade pulls dictated by high rim speeds and blade root stress levels.

The disk rim region has four tooth blade attachment broaches with elliptical cooling air supply holes. Full-ring side plates, fabricated

TABLE 34

HIGH-PRESSURE TURBINE DESIGN REQUIREMENTS

Aerodynamic Design Parameters

Expansion Ratio	4.0
Enthalpy Change, (Δh), joules/g (BTU/lb)	449 (193)
Combustor Exit Temperature, ^{o}C (^{o}F)	1290 (2350)
Combustor Exit Airflow kg/sec (lb/sec)	30.7 (67.6)
Combustor Exit Pressure, kg/cm^2 (lb/in^2)	13.5 (192)

Mechanical Parameters

Number of Stages	1
Max.Disk Rim Speed, m/sec (ft/sec)	527 (1730)

Adiabatic Efficiency Goal

Design Point Efficiency	0.882

Life Requirements

	Hours	Cycles
Blades	10,000	2,200
Vanes	10,000	2,200
Disk	20,000	12,000

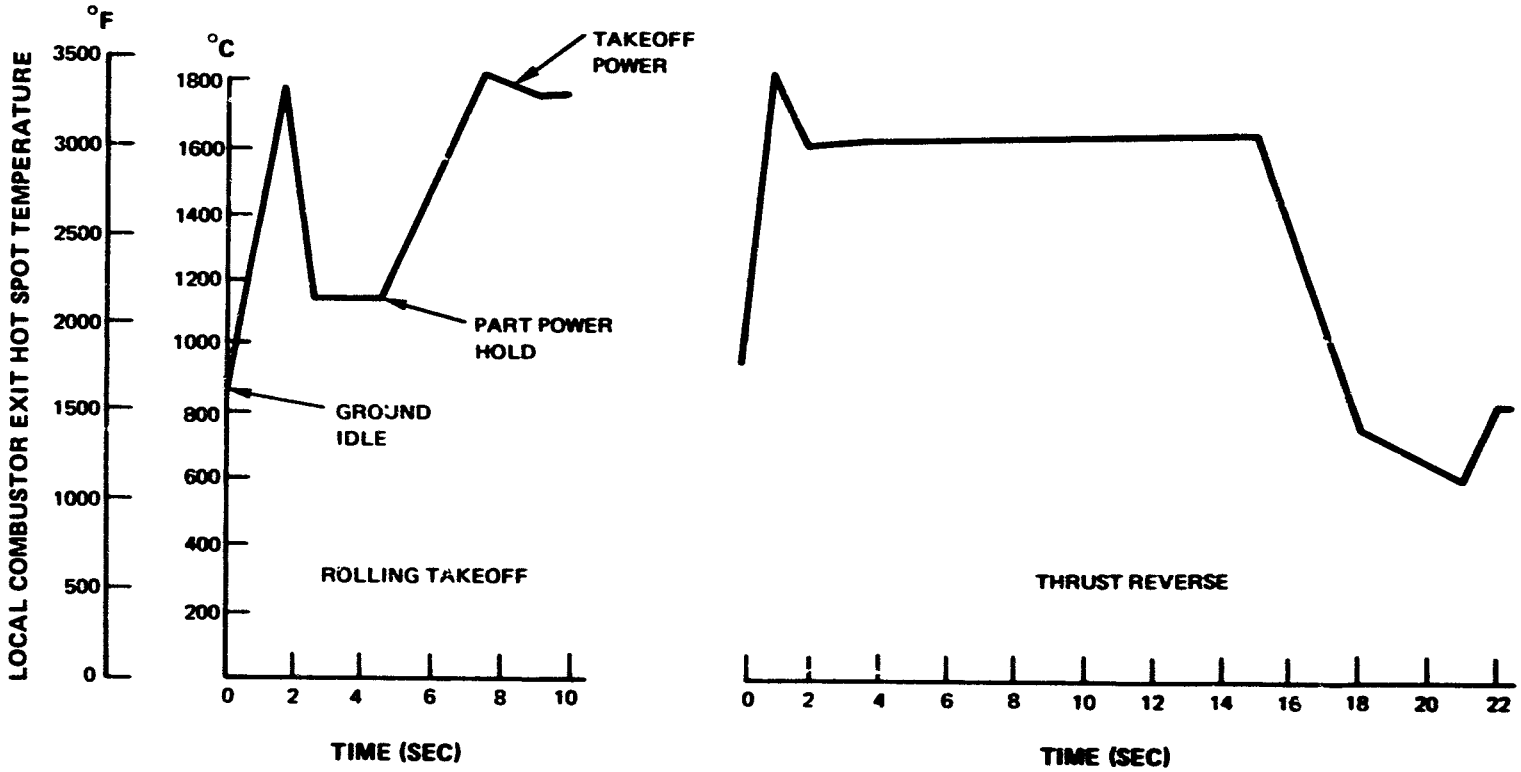

Figure 85 Combustor Exit Temperature. Variation throughout mission: used to predict life of high-pressure turbine parts.

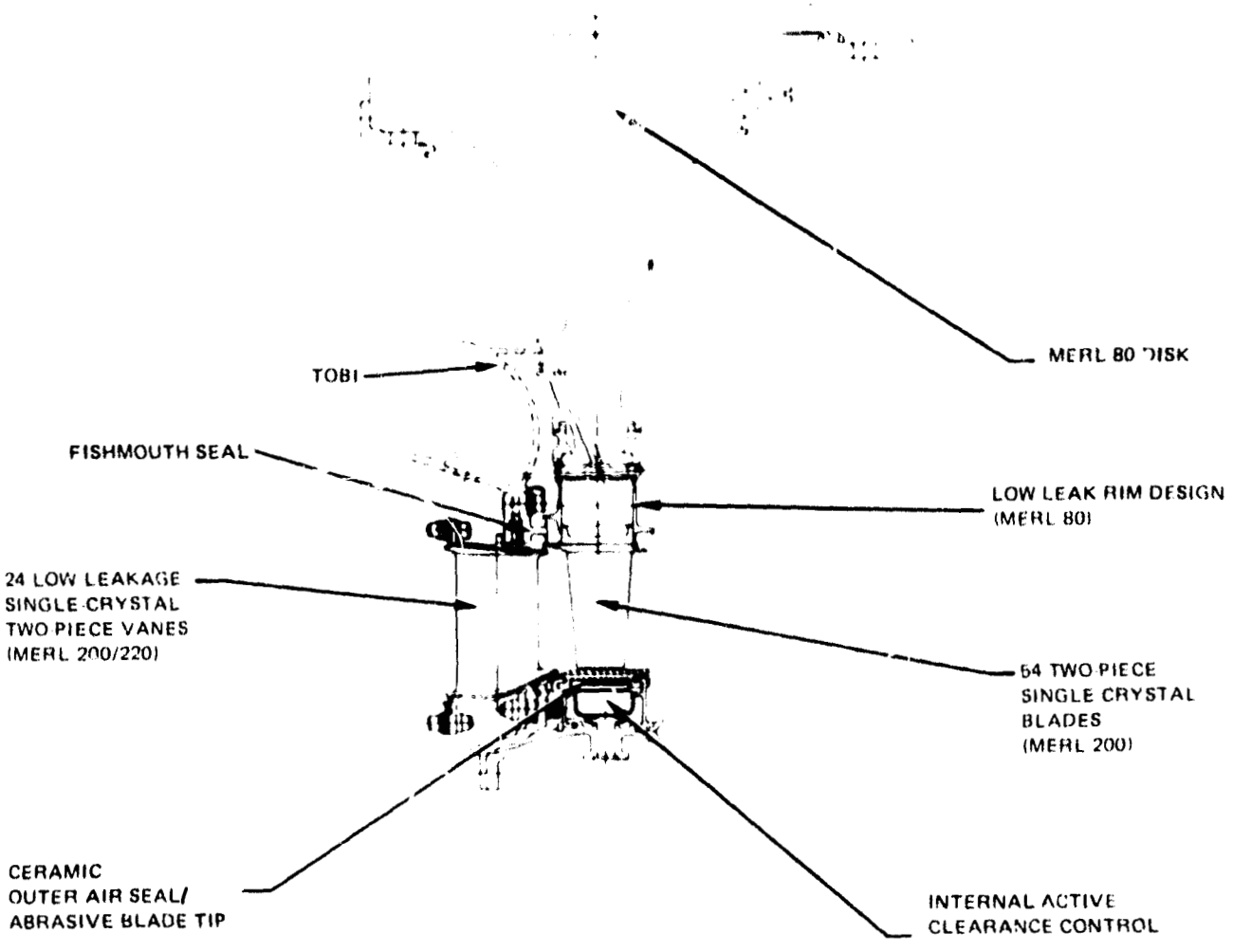

Figure 86 High-Pressure Turbine. Cross-section shows major design features.

from MERL 80, seal the disk attachment front and rear regions. Blade platform extensions form the rotational portion of the fishmouth seal on the disk front and the overlap rim seal at the disk rear.

The blades and vanes are of two-piece bonded construction. Both airfoil rows are fabricated from second generation single crystal alloys to allow the engine to operate at high combustor exit temperatures with a minimal cooling.

The case and outer airseal are shown in an expanded view in Figure 87. The outer airseal consists of 34 graded zirconium oxide ceramic segments and is cooled by impinging air on the O.D. surfaces. The clearance between the blade tips and the outer airseal is controlled by active clearance control (ACC). The internal active clearance control system utilizes a valving system to provide air from different compressor bleed stations to thermally control the position of the outer airseal. The ceramic outer airseal active clearance control, and abrasive blade tip treatment are all necessary to obtain the close operating clearances required in the engine.

4.6.3.2 Vane Cooling System

The vane cooling system is shown in Figure 88. The vane has three cavities with cross-flow impingement internal cooling augmented by film external cooling at the leading edge stagnation point, pressure surface, and suction surface fore section. Internal trailing edge region pedestals are supplied with coolant flow from the aft cavity; spent cooling air is exhausted from the trailing edge. The two forward cavities are fed coolant flow from both the inner and outer combustor liner. The rear cavity air is fed from the outer liner only. Coolant holes are sized consistent with previous successful designs to avert plugging of the holes during operation.

4.6.3.3 Blade Cooling System

An advanced multi-pass blade cooling system, allowed by the two-piece airfoil fabrication techniques, is utilized to increase cooling effectiveness by 10 percent relative to current technology. Increased cooling effectiveness, coupled with higher temperature capability of second generation single crystal materials, is used to meet life requirements with minimal coolant blade air. The advanced cooling system is shown in Figure 89.

Substantial blade spanwise twist and taper coupled with the narrow trailing edge wedge angle dictate that the airfoil be fabricated in two pieces. The leading edge region is cooled both by internal convection and by showerhead external film. The mid-section is cooled by three passes of coolant flow which is exhausted through high length-to-diameter ratio pedestals in the blade trailing edge region. Trip strips

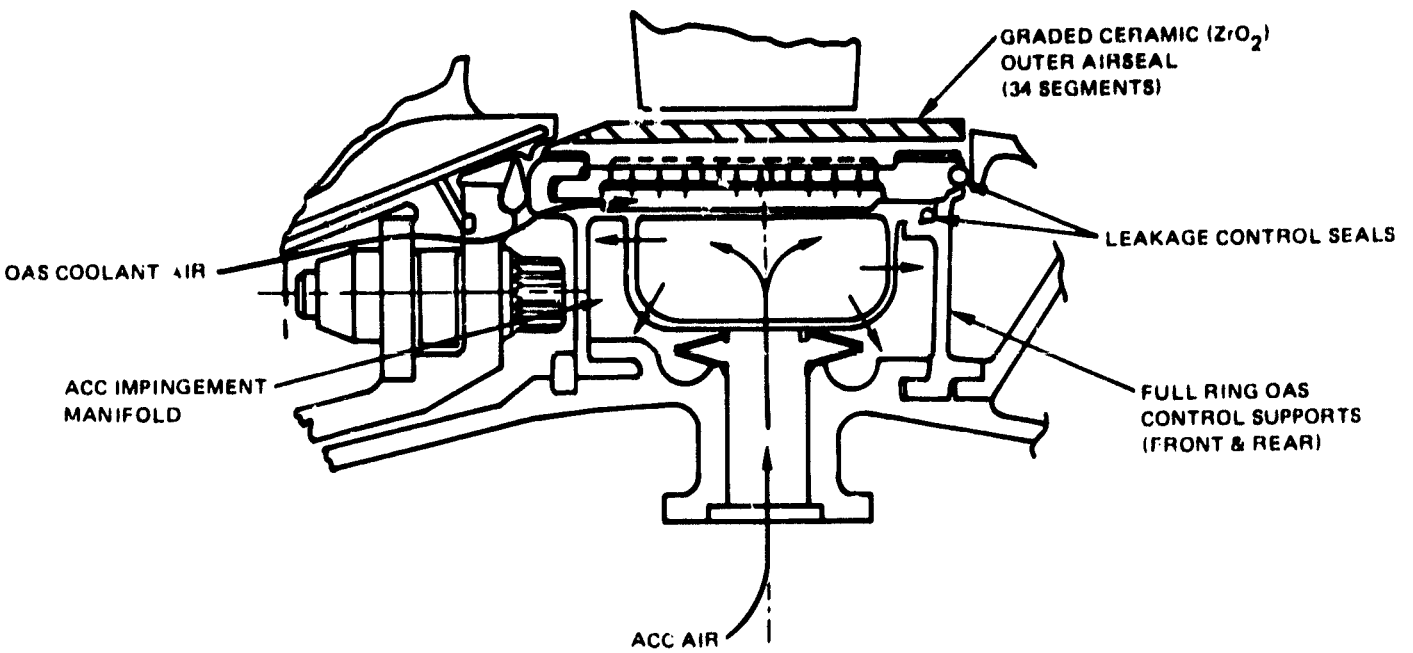

Figure 87 High-Pressure Turbine Case and Outer Airseal. Expanded view illustrates cooling air distribution.

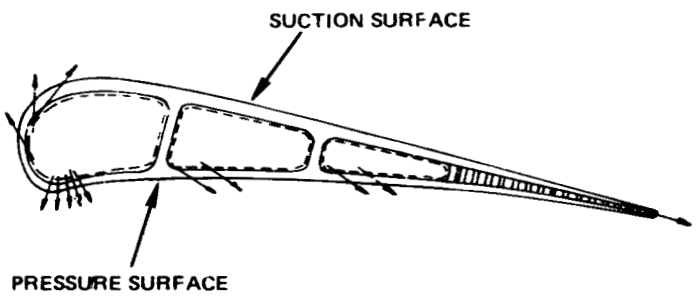

CROSS SECTIONAL VIEW

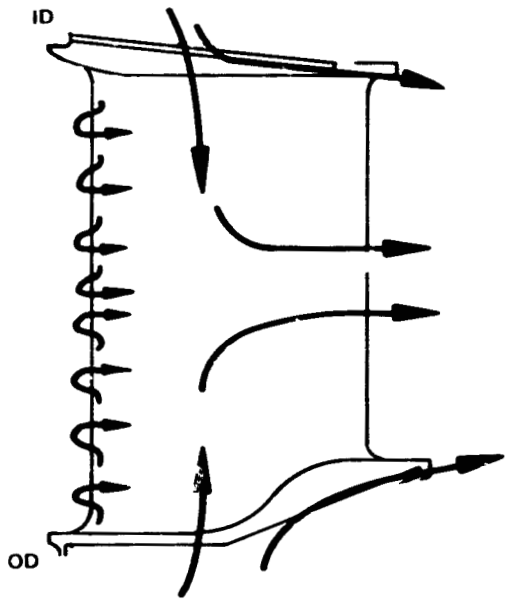

PROFILE VIEW

Figure 88 High-Pressure Turbine Vane. Configuration cross-section shows multiple cooling techniques applicable to the various airfoil sections.

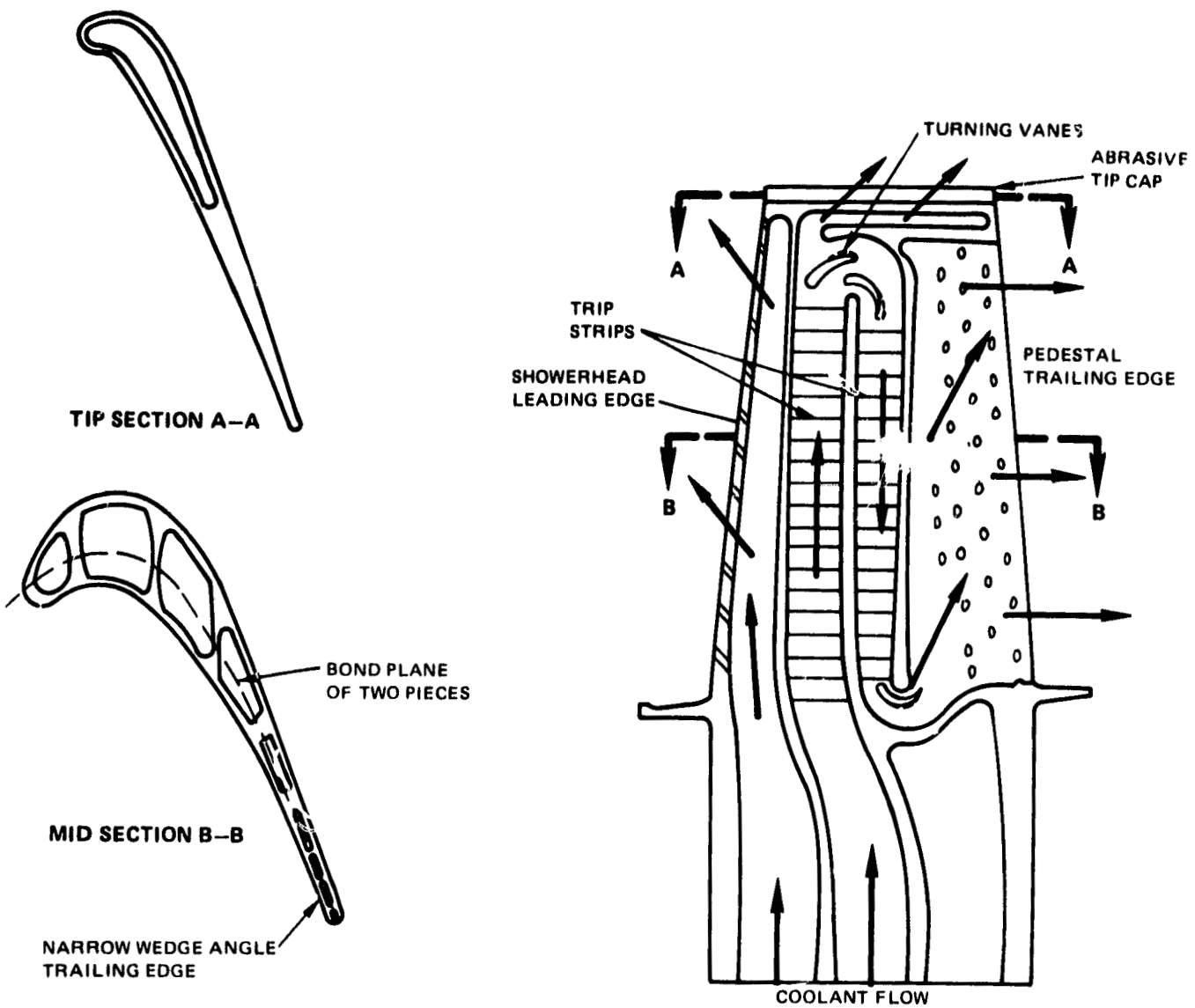

Figure 89 High-Pressure Turbine Blade. Advanced multi-pass cooling system used to increase cooling effectiveness.

on internal surfaces enhance heat convection to the air. Internal turning vanes are also included to avoid coolant flow separation from the airfoil ribs in the end sections. The blade tip region is cooled both by internal convection and by external film cooling.

4.6.3.4 Leakage Control

Secondary leakage is controlled by eliminating leakage paths or by more effectively sealing those that cannot be eliminated. The major leakage control features are called out in Figure 90. Feather seals and w-seals exemplify application of proven sealing concepts. Fishmouth seals are used to reduce the cavity purge flow required to avoid hot gas ingestion by 50 percent relative to conventional gas path seals. Full ring sideplates, vane twist restraint (Figure 91) and vane chordal surfaces (Figure 92) are used to eliminate several potential leakage paths.

4.6.3.5 Principal Aerodynamic Design Parameters

The major aerodynamic design parameters of the high-pressure turbine are shown in Table 35. The turbine is characterized by high wheel speeds and blade root stress levels coupled with advanced blade loadings (mean Zwiefel load coefficient, ϕ_z = 0.92). This combination of aerodynamic parameters minimizes the number of airfoils and is conducive to high efficiency.

4.6.3.6 Technology Development Requirements

Technology advancements in airfoil fabrication, blade cooling effectiveness, low leakage attachment configuration, and transonic aerodynamics - each have supporting technology development programs within the Energy Efficient Engine Program.

4.6.3.6.1 Airfoil Fabrication

Both vanes and blades are fabricated as two-piece single crystal airfoils. The basic technology required to cast the airfoil halves and then to transient-liquid-phase (TLP) bond the halves together has been the subject of extensive in-house development. Additional work in this fabrication program is required to apply the basic casting and bonding technology to the unique Energy Efficient Engine blade and vane shapes. The large size of the vanes and the severe twist and taper of the blades require special attention in both the casting and bonding techniques.

Bonding trials, to be investigated under this program, which are associated with highly cambered (125°) blades and the long internal ribs of the vanes. Casting and bonding trials of the preliminary design airfoils will be undertaken in the fabrication development program to ensure the successful fabrication of test hardware.

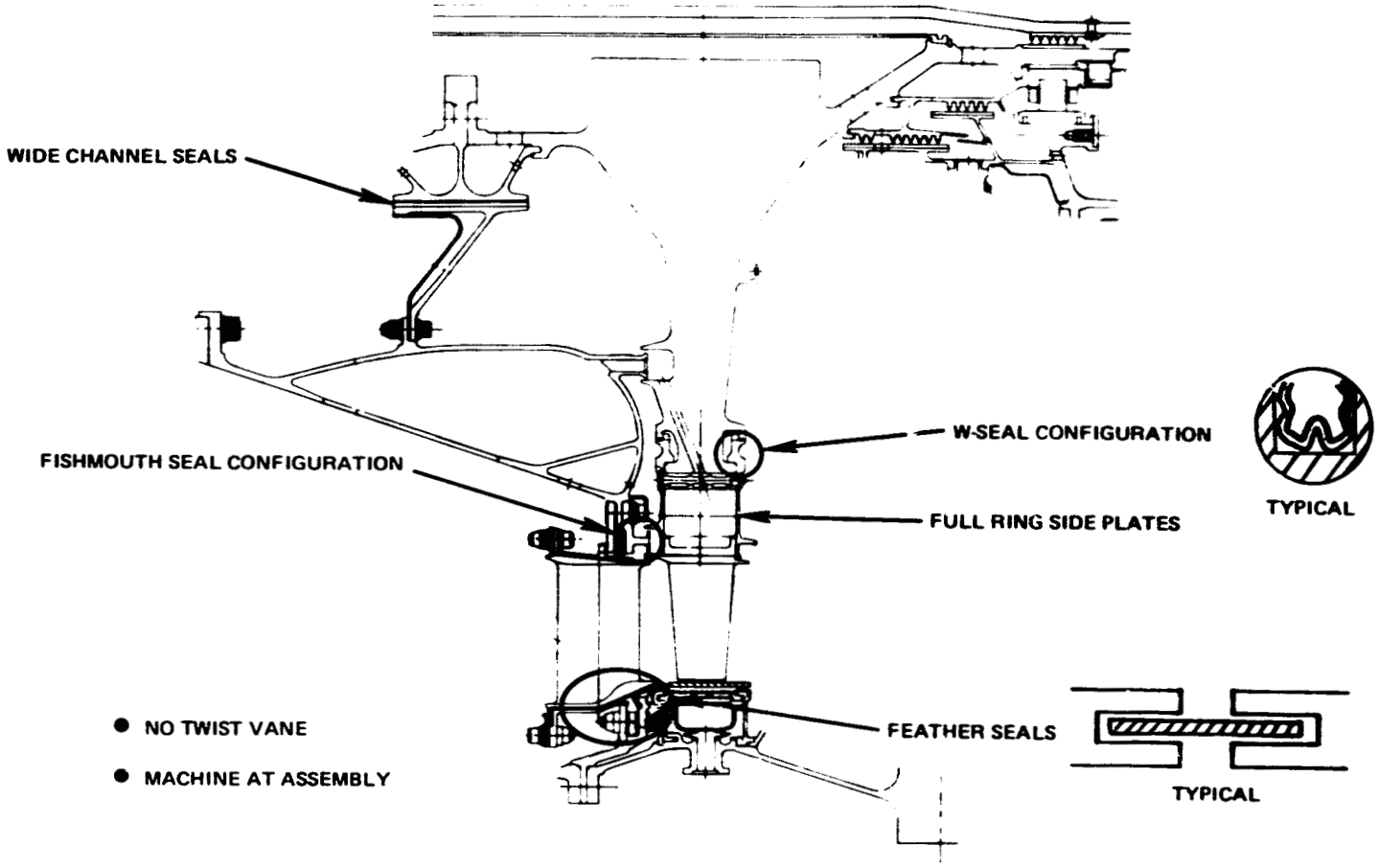

Figure 90 High-Pressure Turbine. Major leakage control features improve sealing.

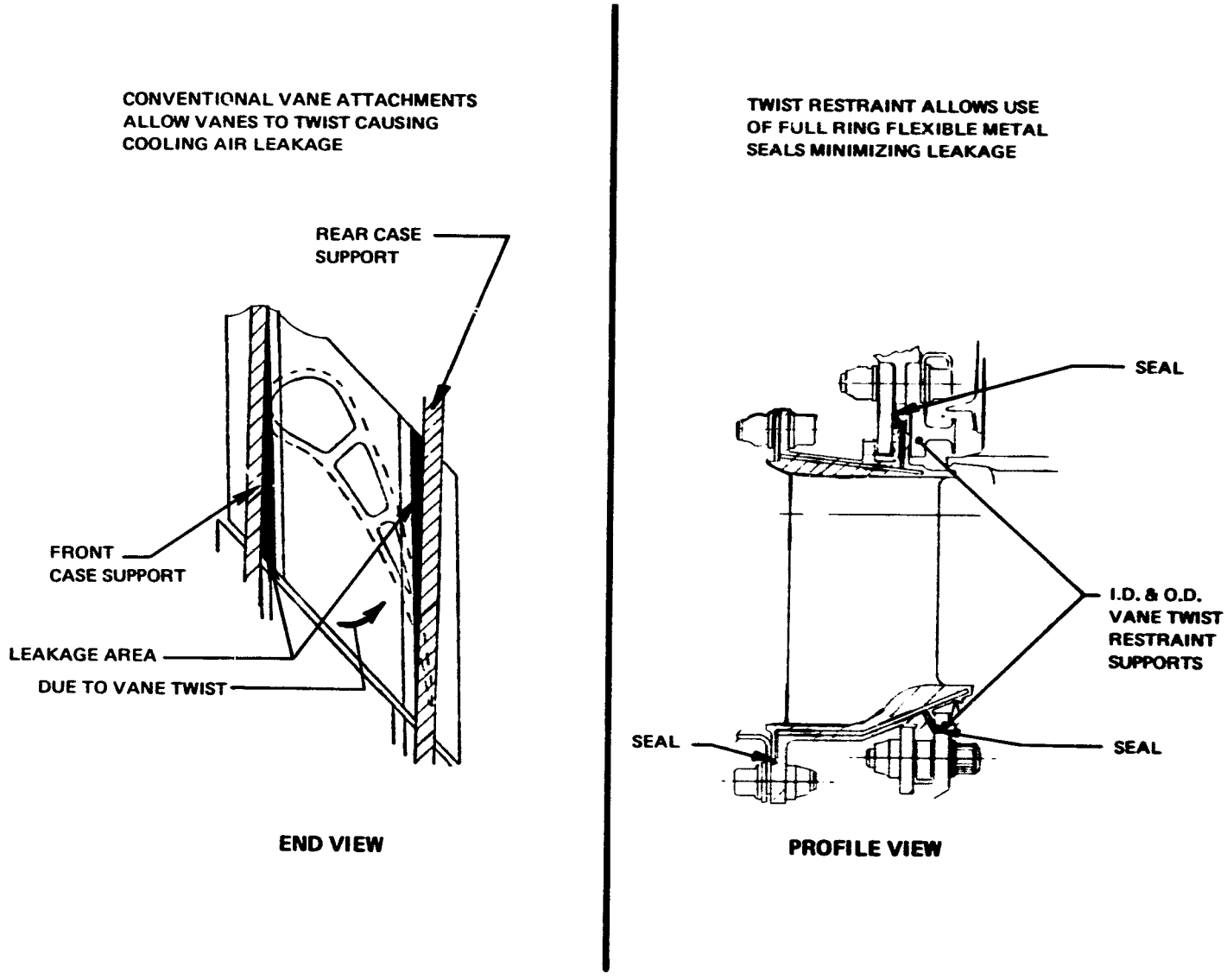

Figure 91 High-Pressure Turbine Vane. Twin-end restraints used to eliminate twist and resultant air leakage.

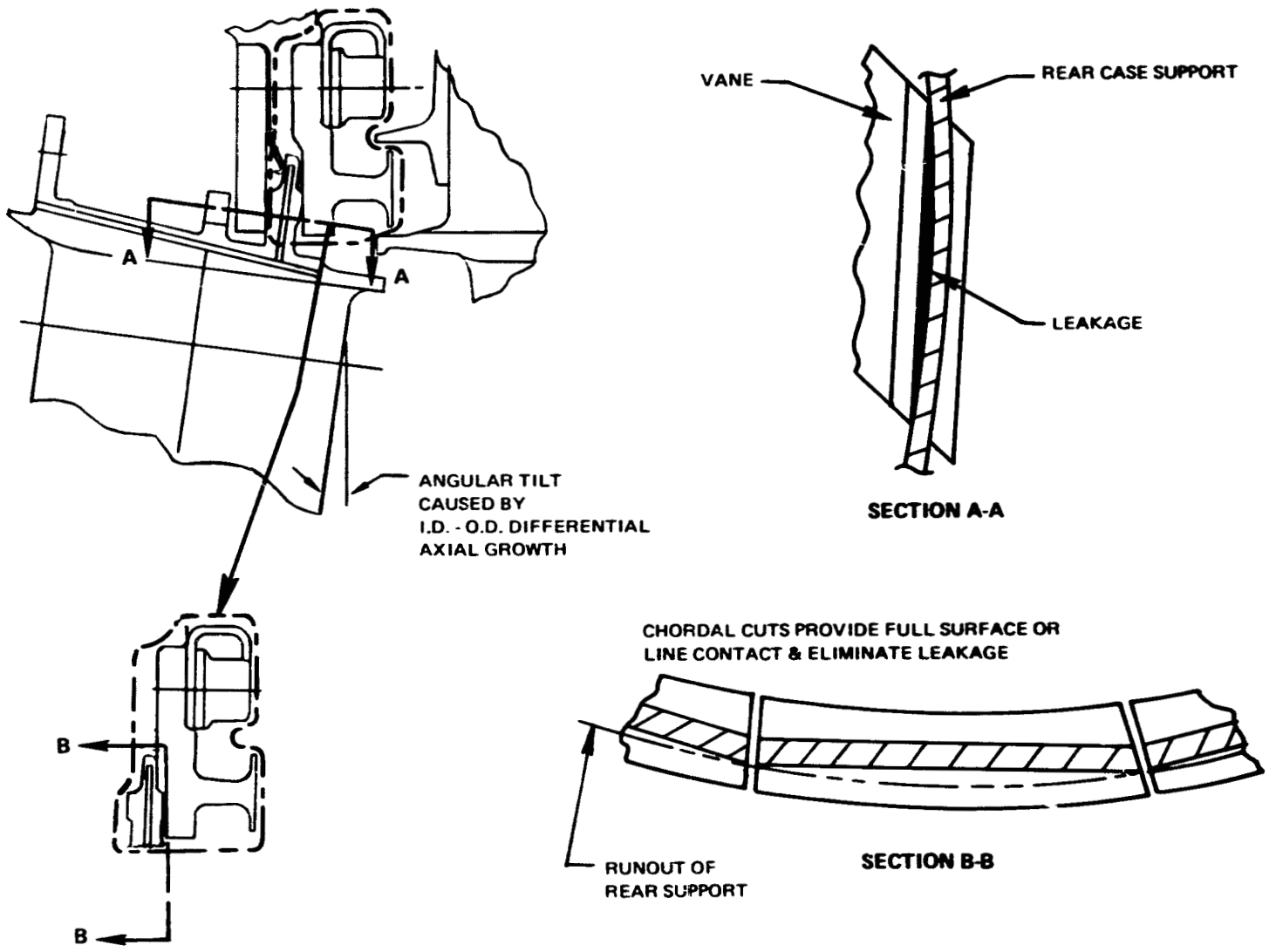

Figure 92 High-Pressure Turbine Vane. Chordal cuts used to eliminate air leakage when vanes tilt under load.

TABLE 35

HIGH-PRESSURE TURBINE AERODYNAMIC DESIGN PARAMETERS

No. of Stages	1
Expansion Ratio	4.0
Mean Velocity Ratio/NASA Load Coefficient	0.56/1.59
Average Blade Root Stress	
AN^2, - Maximum, $cm^2 rpm^2$ ($in^2 rpm^2$)	31.6×10^{10} (49×10^9)
Disk Rim Speed-Maximum, m/sec (fps)	527 (1730)
ΔH, joules/g (BTU/lb) - SLTO	484 (208)
Mean Blade Loading ($_2$)	0.92
Mean Blade Turning, deg.	118
Number of Blades	54
Number of Vanes	24

4.6.3.6.2 High Effectiveness Cooling

Blade cooling flow distribution will be verified in a cooling model supporting technology program. Initially a simplified large scale plexiglass model to simulate critical flow areas within the blade will be used to provide flow visualization. Information from these models will be used to place trip strips and turning vanes in the cooling flow passages during detail design. A scaled model of the blade (5X) will then be fabricated and tested to verify the design pressure drop of the coolant flow and to verify internal blade flow aerodynamics prior to component tests.

4.6.3.6.3 Leakage Control

Metal models of the blade and vane attachments will be used to quantify leakage rates of the preliminary design configuration. The attachment models will be reworked as necessary to further reduce the leakage. Plastic models of the attachment areas will be constructed to help visualize and eliminate leakage paths and to correct assembly problems which arise in complex attachment seal geometries during detail design.

4.6.3.6.4 Large Annulus Area, Transonic Aerodynamics

Aerodynamic supporting technology programs provide uncooled turbine testing and cooled plane cascade tests. Scaled uncooled turbine testing is used to establish the aerodynamic efficiency base of a large annulus area, low axial air velocity-to-wheel speed turbine and to select the final pressure reaction level of the turbine.

The effort consists of the design, fabrication, and testing of three scaled turbine builds to investigate various AN^2 levels, airfoil taper levels, pressure reaction levels and vane endwall design alternatives.

4.6.4 Supporting Analyses

The feasibility of the advanced mechanical and aerodynamic design concepts needed to meet the efficiency and life requirements was analytically verified.

4.6.4.1 Efficiency Prediction

Efficiency bookeeping for the high-pressure turbine is shown in Table 36. This predicted performance is consistent with a 43 percent reaction turbine with total cooling and leakage flow of 13.25 percent engine airflow and a blade tip clearance of 0.051 cm (0.020 in). The significant effect of aerodynamics improvements is based on analysis of the HHSE turbine test data which indicated that efficiency could be increased by lowering the vane exit Mach number and increasing the expansion across the blade for increased reaction. Therefore, the reac-

TABLE 36

HIGH-PRESSURE TURBINE EFFICIENCY PREDICTION
AERODYNAMIC DESIGN POINT

Base:	
Design System (uncooled), %	89.1
Technology Benefits:	
Improved Aerodynamics, %	+2.2
Cooling and Leakage, %	-3.1
Status, %	88.2

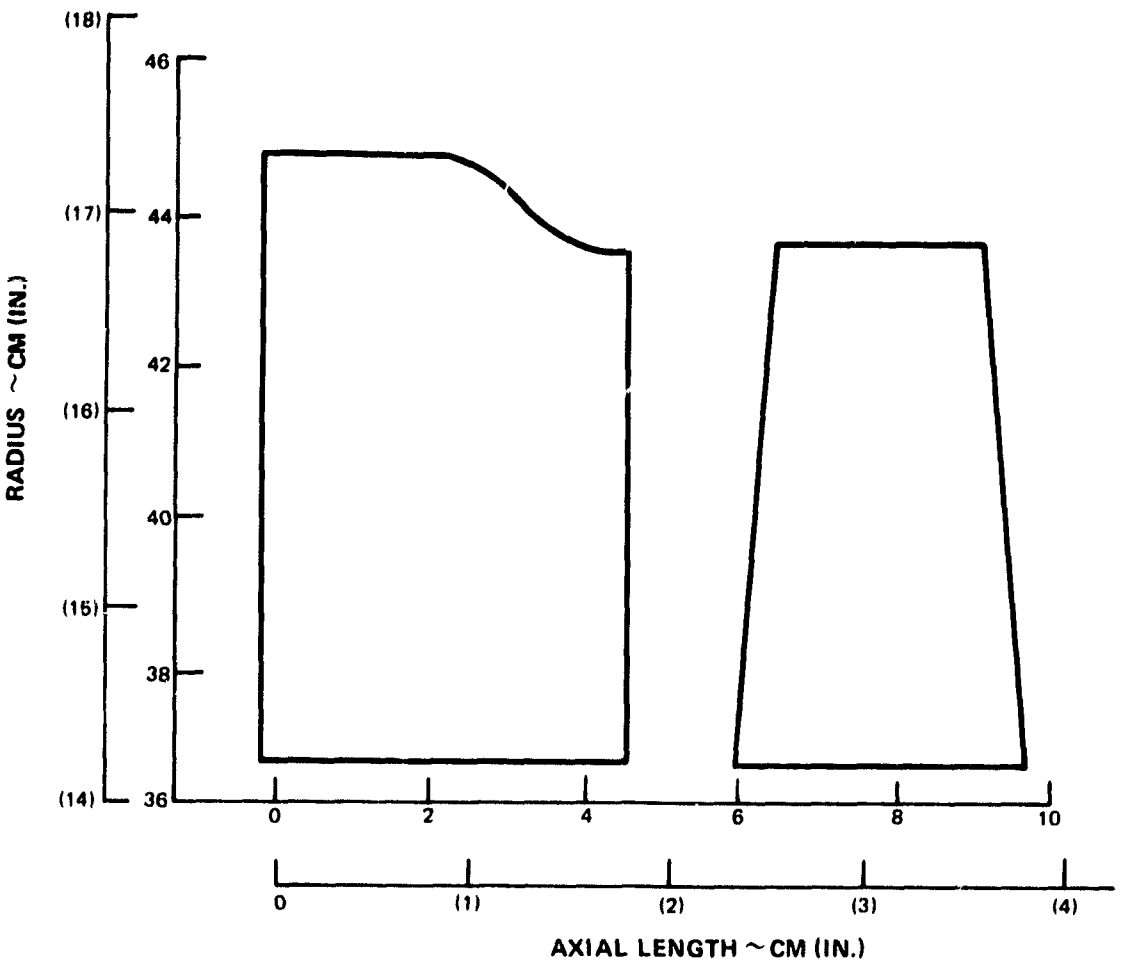

Figure 93 High-Pressure Turbine. Flowpath illustrates "S"-wall vane used to improve efficiency.

tion has been increased until a high spool thrust balance limit was reached at 43 percent reactions. The combination of higher blade root stress, increased rim speed, and higher reaction levels is calculated to increase the turbine efficiency by 2.2 percent.

4.6.4.2 Gaspath Aerodynamic Analyses

4.6.4.2.1 Flowpath Shape

The flowpath, shown in Figure 93, was drawn with an S-shaped wall vane configuration which has been shown to reduce vane secondary losses. The vane to blade row axial gapping was established from experience considering blade vibration stresses and efficiency effects.

4.6.4.2.2 Velocity Triangles

Blade inlet and exit velocity triangles, shown in Figure 94, were generated from the aerodynamic design requirements. These velocity triangles, with low inlet relative blade and transonic exit Mach numbers, are characteristic of high reaction, large annulus area turbines. Controlled vortexing, effective in high hub-tip radius ratio designs, is represented in the spanwise triangle differences.

4.6.4.3 Vane Analysis

The vanes are designed to turn axial inlet flow through 79.8 degrees. The high degree of gas turning over the long chord lengths of the vanes increases the difficulty of controlling secondary losses. Analysis has therefore been directed at minimizing aerodynamic losses and leakage paths.

4.6.4.3.1 Configuration Selection

Paired vanes, bonded together at both platforms, were examined in an effort to minimize vane platform leakage paths. However, the additional cooling air required to maintain commercial engine strain ranges in paired vanes more than offset the leakage flow reduction. Therefore, the 24 single-vane configuration was retained for the Energy Efficient Engine turbine.

Vanes with large blunt leading edges, followed by thin trailing edge wedge angles (4 degrees), and 8 to 12 degrees of transonic uncovered turning were chosen to facilitate vane cooling and to provide pressure distributions conducive to low aerodynamic losses. The vanes are essentially constant in cross-section and untwisted from hub to tip as dictated by the short airfoil spans.

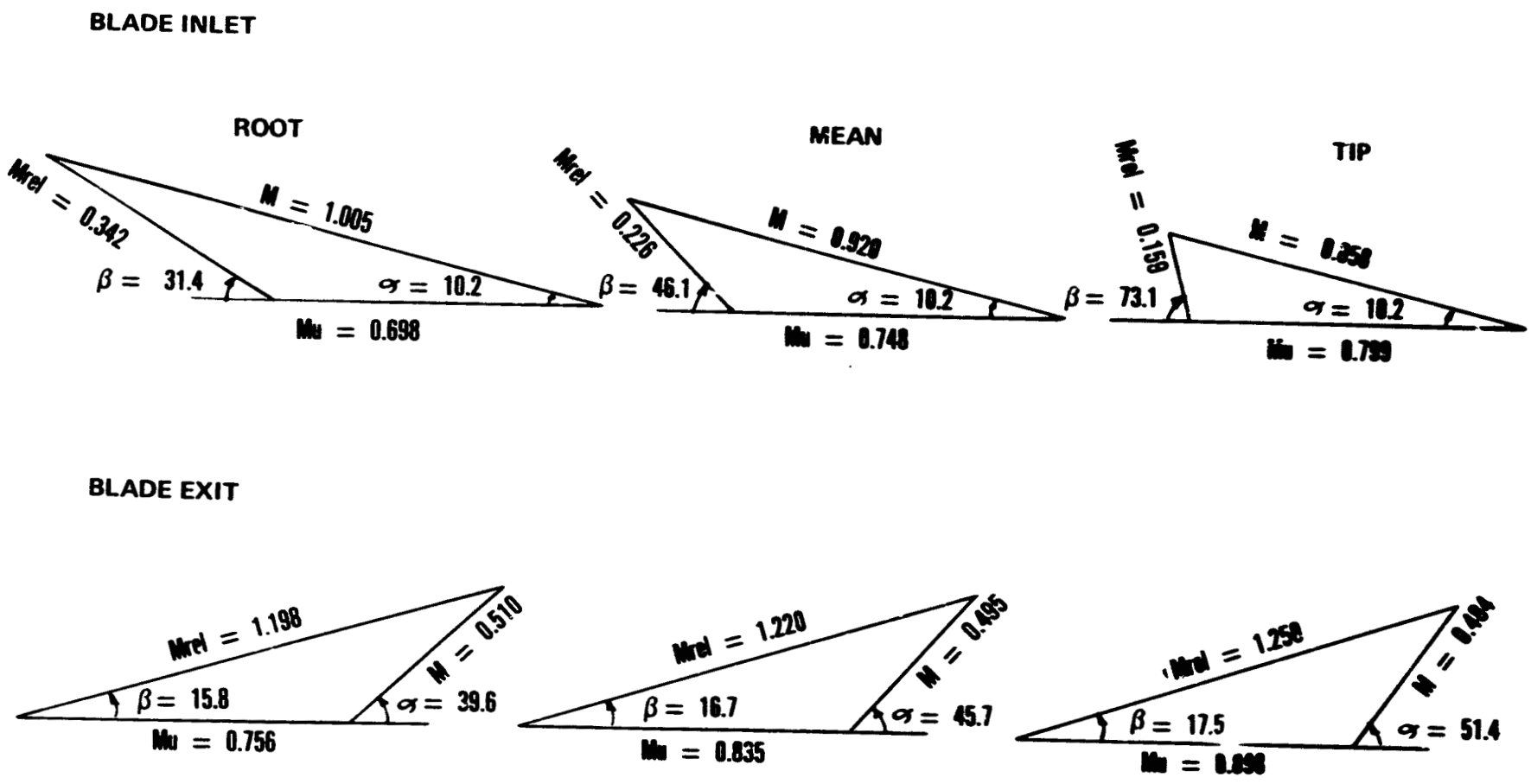

Figure 94 High-Pressure Turbine. Velocity triangles typify aerodynamics of high reaction, transonic turbines.

4.6.4.3.2 Twist Restraint

An existing NASTRAN model of a TF30 vane was used to investigate the feasibility of increasing the vane anti-twist restraint to minimize the leakage paths introduced as the vanes are subjected to high thermally induced twisting loads experienced in current vane designs. The results of this investigation are shown in Figure 95. The results showed that acceptable airfoil lives could be achieved with local increases in vane wall thickness. Based on these results, the vane attachments include the vane twist restraint features.

4.6.4.3.3 Durability and Cooling Analysis

The durability analysis of the vane consisted of both thermal and structural analysis. The thermal analysis considered internal and external heat loads. External heat transfer conditions were determined by a boundary layer analysis of the airfoil using modified hot gas temperatures to account for film cooling. The internal heat transfer characteristics were determined from in-house correlations which recognize both the cooling method and the cavity wall conditions. The cooling flows resulting from the thermal analysis for the first vane row at the heat transfer design point are shown in Figure 96.

The metal skin temperatures, Figure 97, are shown as a function of distance from the stagnation point for the 50 percent span vane section. Oxidation life of the vane based on these metal temperatures (See Table 37) exceeds the life required.

The structural analysis combines both the thermally and structurally induced stresses, then integrates the effects of the vane strains over the takeoff and reverse cycles to determine the vane creep and creep/-low cycle fatigue interaction lives. The most highly strained element is at the center of the vane forward. Vane strains over the cycles are shown in Figure 98. Vane creep and creep/low cycle fatigue lives resulting from the cycle analysis are shown in Table 37. The vanes meet or exceed the required lives in all failure modes.

4.6.4.4 Blade Analysis

To achieve the required velocity triangles, the blades have root turning of 132.8 degrees and tip turning of 89.6 degrees. Structural design requirements result in a Zwiefel load coefficient variation from 0.82 at the blade roots to 1.15 at the tips. These cumulative requirements result in a highly twisted and tapered blade geometry. Therefore, blade fabrication was of special concern in establishing design feasibility.

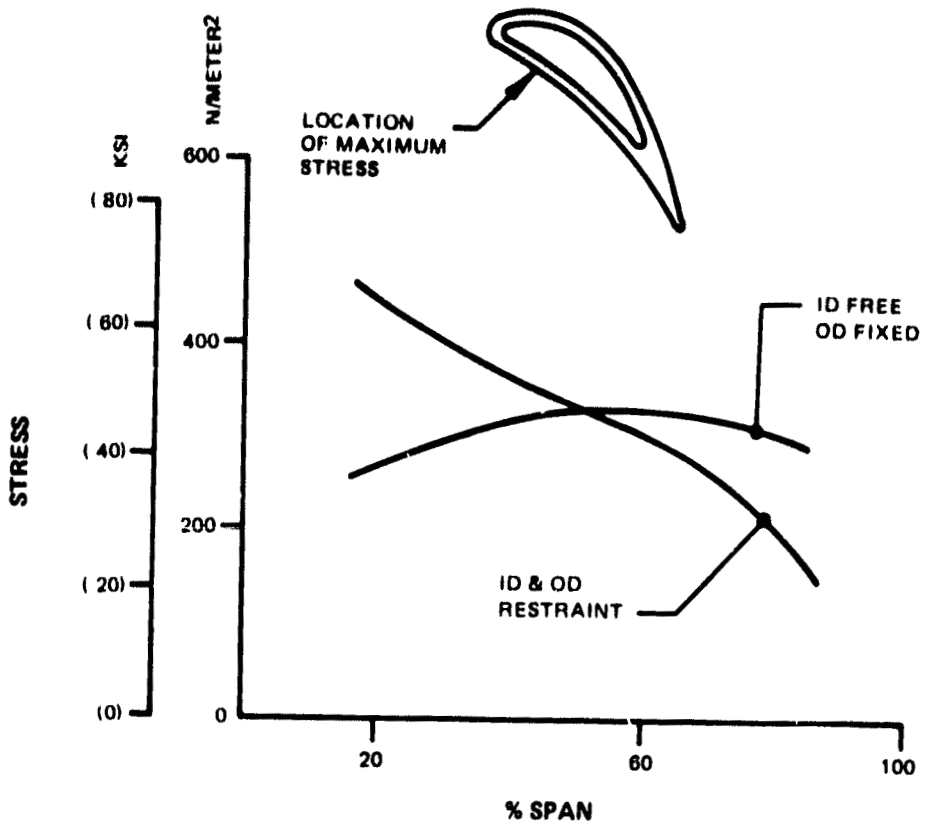

Figure 95 Twin-End High-Pressure Turbine. Vane restraint airfoil stress predictions used to predict acceptable life characteristics.

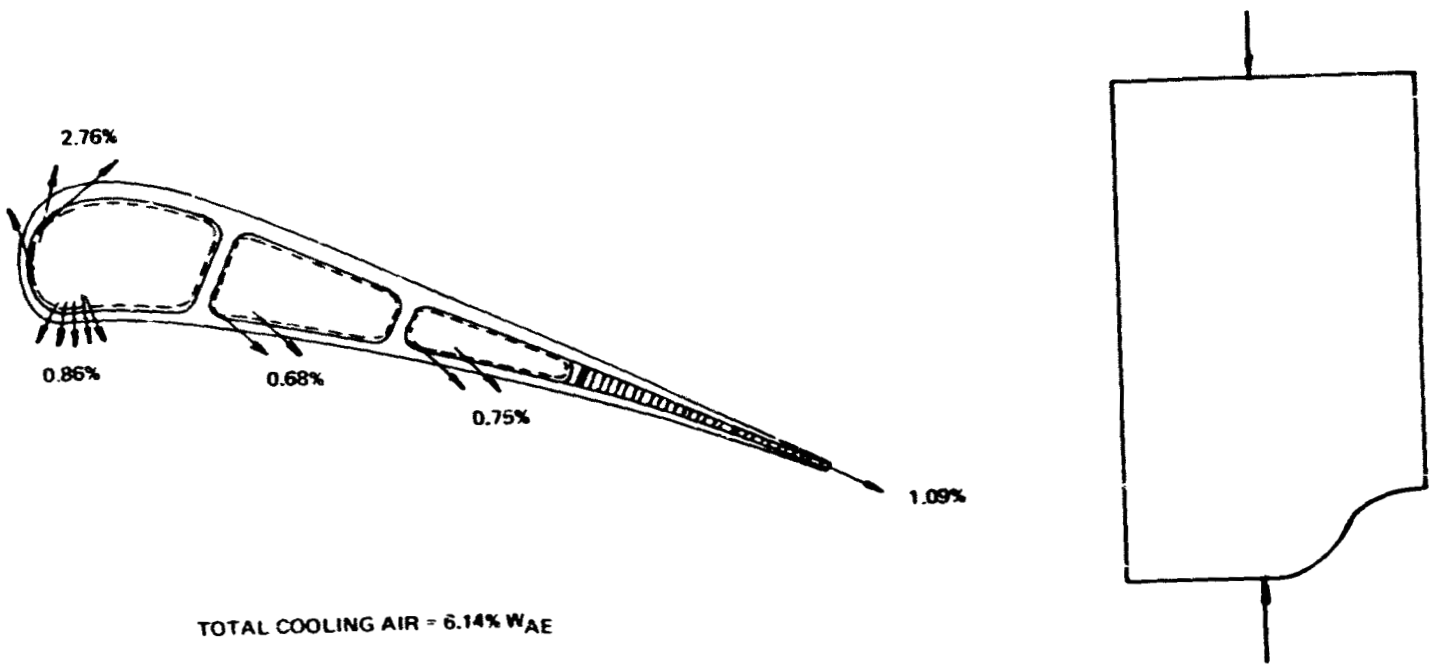

J20127-76
781511

Figure 96 High-Pressure Turbine Vane. Airfoil cooling flows show requirements based on thermal analysis.

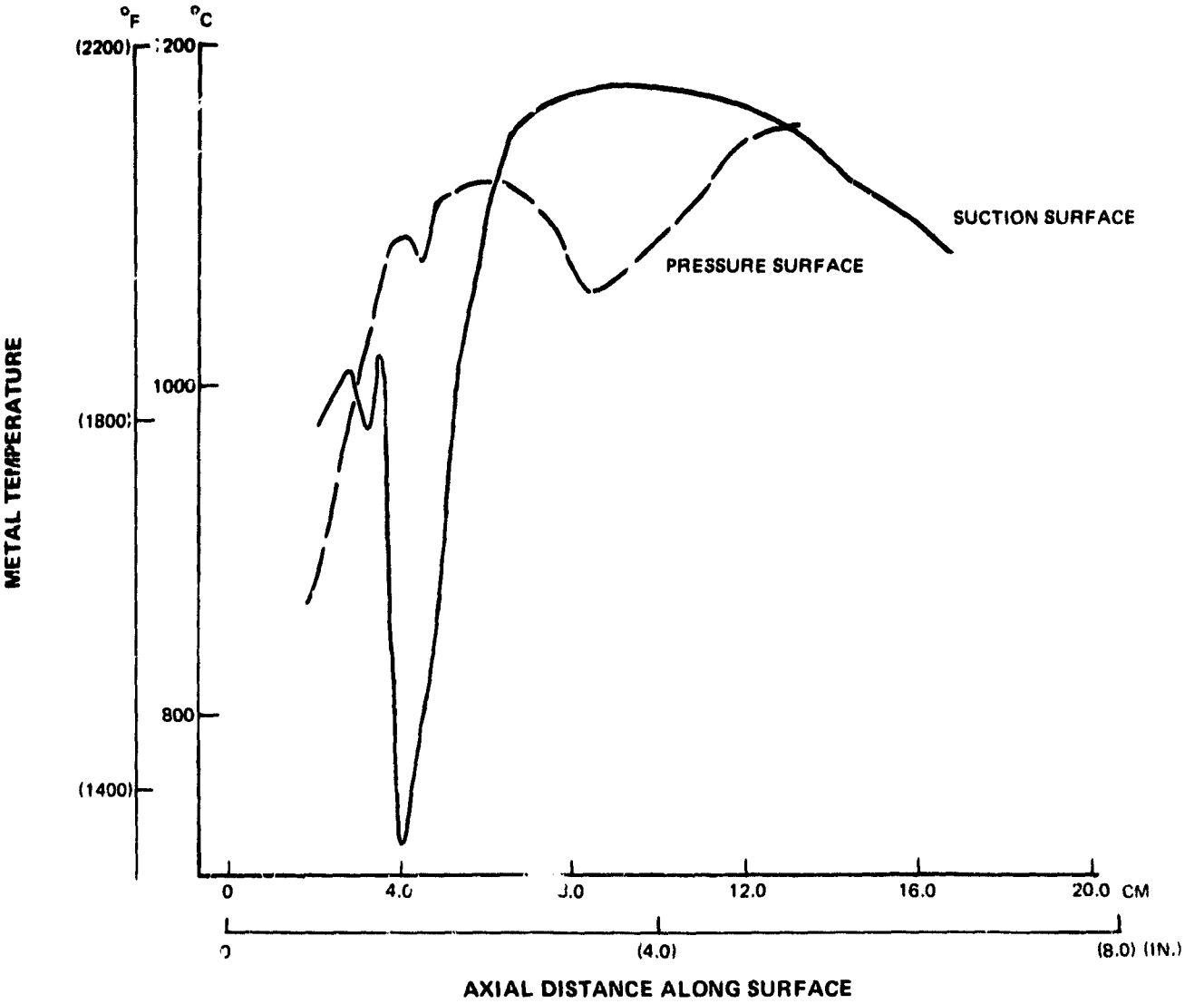

Figure 97 High-Pressure Turbine Vane. Predicted maximum metal temperatures used in oxidation life analysis.

TABLE 37

HIGH-PRESSURE TURBINE
VANE DURABILITY ANALYSIS

Failure Mode	Calculated Life
Oxidation	8000 Hrs (to first recoat)
Creep	10000 Hrs/2200 Missions
Creep/LCF Interaction	10000 Hrs/2200 Missions

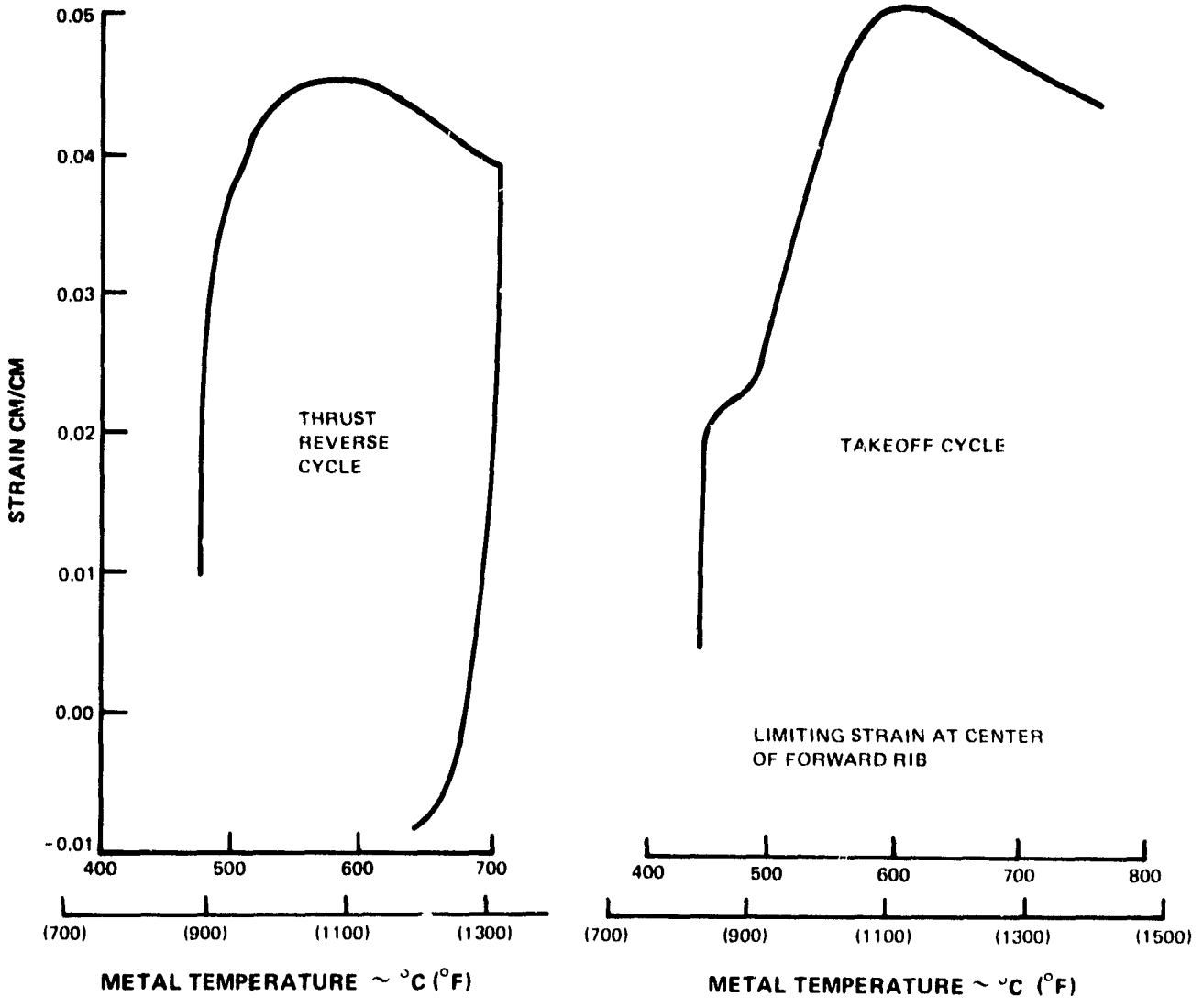

Figure 98 High-Pressure Turbine Vane. Estimated strain range over takeoff and reverse cycles used in creep low cycle fatigue analysis.

4.6.4.4.1 Fabrication Technique

A blade fabrication study was conducted to determine the casting feasibility, cooling effectiveness, and costs of one-piece, two-piece, and three-piece blades, shown in Figure 99. The conventional one-piece casting requires that the blade wall be thicker and the trailing edge wedge angle be increased to allow for possible casting ceramic core shift during manufacture. These changes reduce the cooling effectiveness and increase aerodynamic losses, causing an estimated turbine efficiency reduction of over one percent.

The three-piece blade eliminated the need for showerhead cooling and provided the most efficient blade coolant scheme which could result in a 0.2 percent higher efficiency than a two-piece blade. However, the high fabrication risk, coupled with increased cost and complexity, is unacceptable. Therefore, preliminary design is based on two-piece construction.

4.6.4.4.2 Cross-Sectional Shapes

The blade profiles have small (two degree) trailing edge wedge angles and four to eight degrees of transonic uncovered turning. The profiles are contoured to reduce shock losses, and to accelerate the flow through the blade gaging station. These airfoil shapes are important contributors to the high efficiency level of the high reaction turbine.

4.6.4.4.3 Durability and Cooling Analysis

Blade durability analysis was conducted similarly to that of the vane. The temperatures resulting from the thermal analysis for the limiting blade quarter root section are shown in Figure 100. Required blade internal configuration and cooling flow distribution is shown in Figure 101. The oxidation life of the blade based on this thermal analysis is shown in Table 38. The structural analysis shows the maximum strain level of 0.0035 cm/cm to be located at the blade trailing edge. Combining these results with an engine life cycle analysis indicates the blade to be creep/low cycle fatigue interaction limited with an operating life of 10,000 hours (Table 38). Based on the durability analysis, high-pressure turbine blades will meet life requirements.

4.6.4.4.4 Vibrational Analysis

A NASTRAN model of the blade was constructed to tune all high energy blade vibration modes out of the operating range. The model consists of plane stress plate elements for the airfoil skin and ribs (see Figure 102) with beam elements for the blade neck and spring rates to simulate the attachment region. This model also includes the single crystal material properties. Figure 103 shows the isodeflection contours of the first stiff vibrational mode of the airfoil and illustrates the tip trailing edge deflection that is typical of the other vibrational

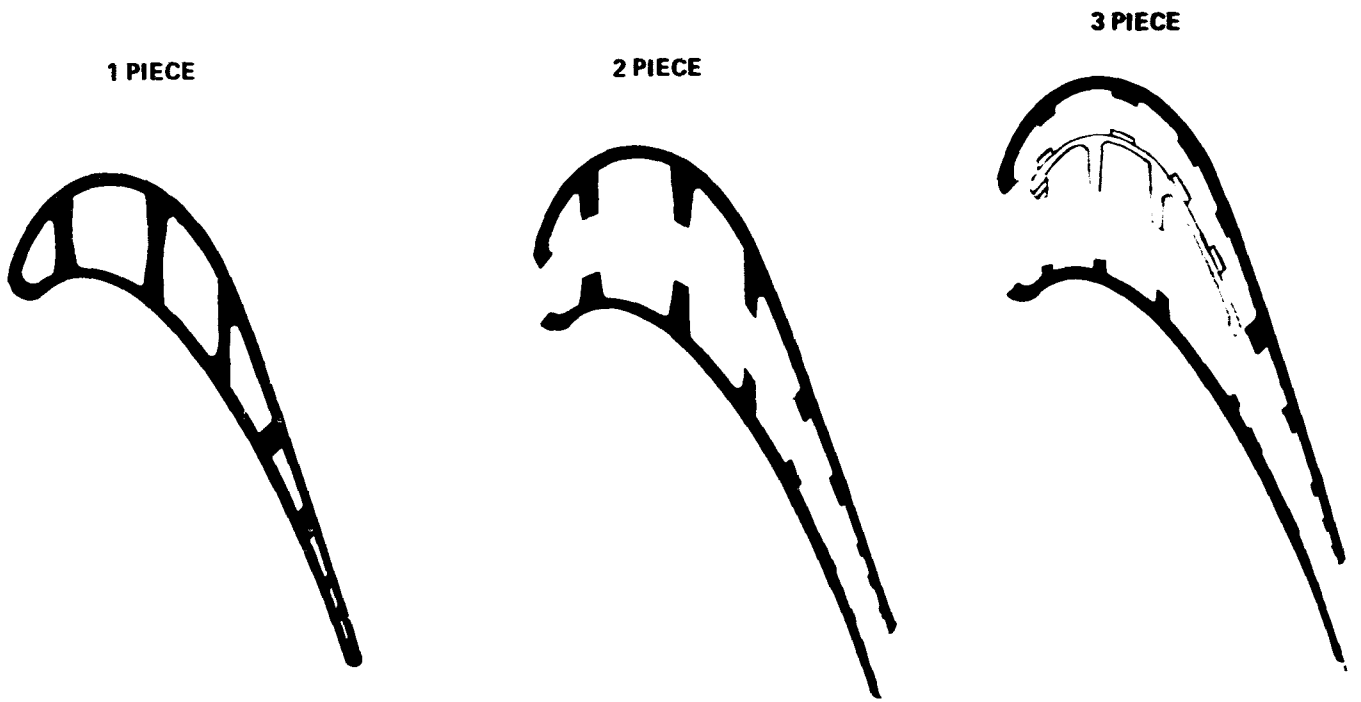

Figure 99 High-Pressure Turbine Blade Fabrication Techniques. Three concepts considered before selection of two-piece approach.

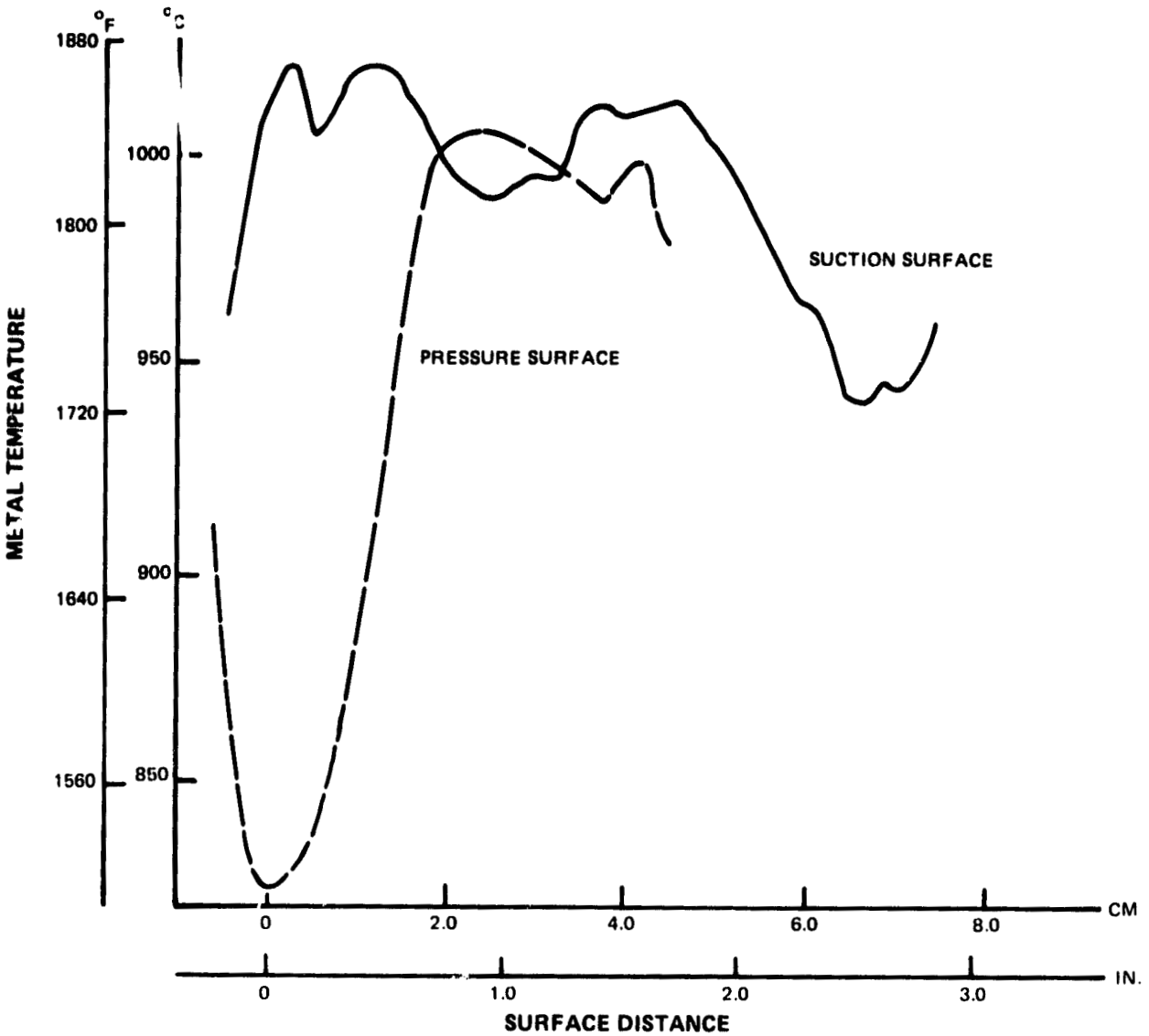

Figure 100 High-Pressure Turbine Blade. Predicted maximum metal temperatures used in oxidation life analysis.

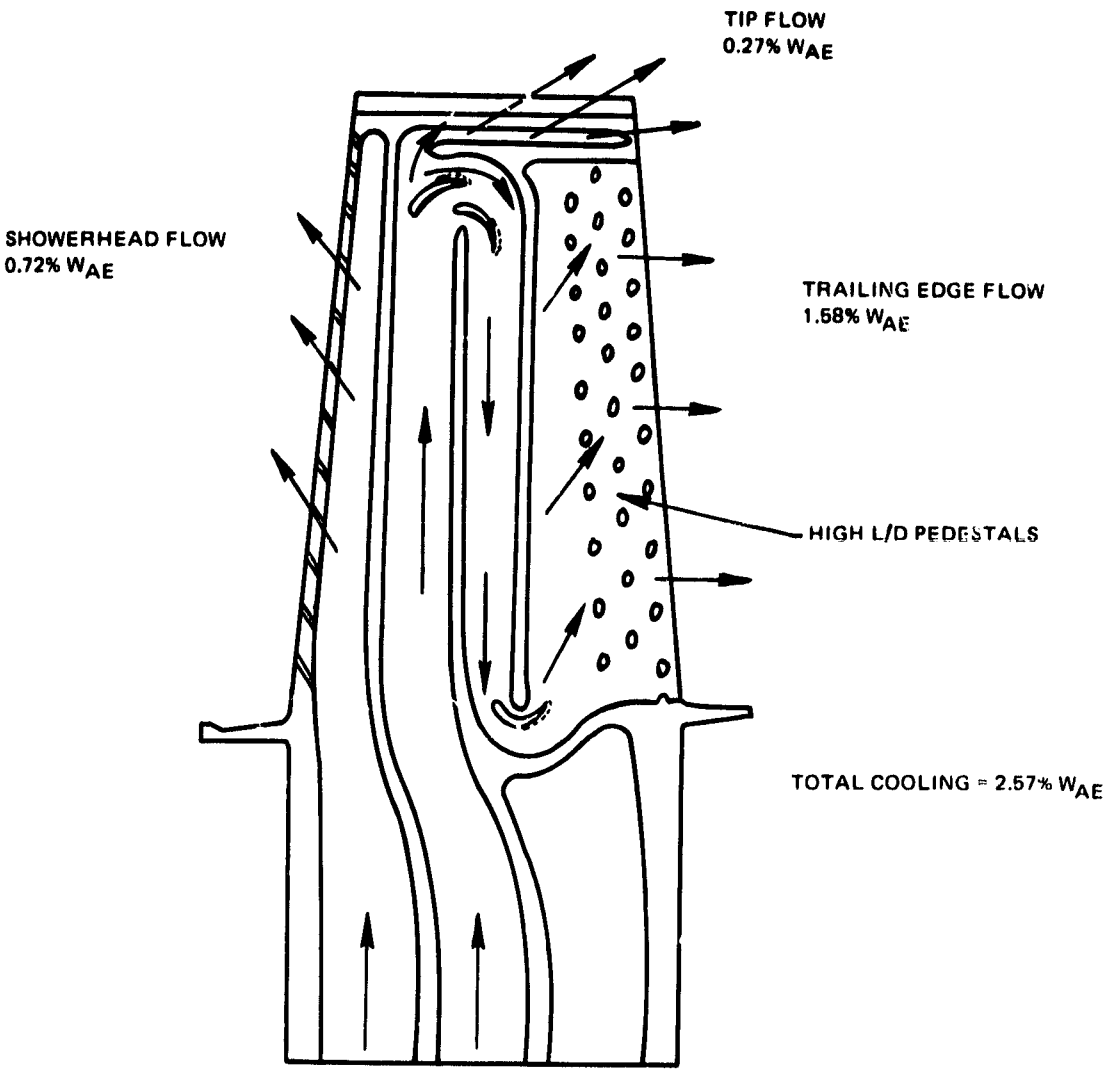

Figure 101 High-Pressure Turbine Blade. Cooling flows show requirements based on thermal analysis.

TABLE 38

HIGH-PRESSURE TURBINE
BLADE DURABILITY STUDY RESULTS.
DATA INDICATE ACCEPTABLE LIVES

Failure Mode	Calculated Life
Oxidation	10000 Hrs (to first recoat)
Creep/LCF Interation	10000 Hrs/2200 Missions

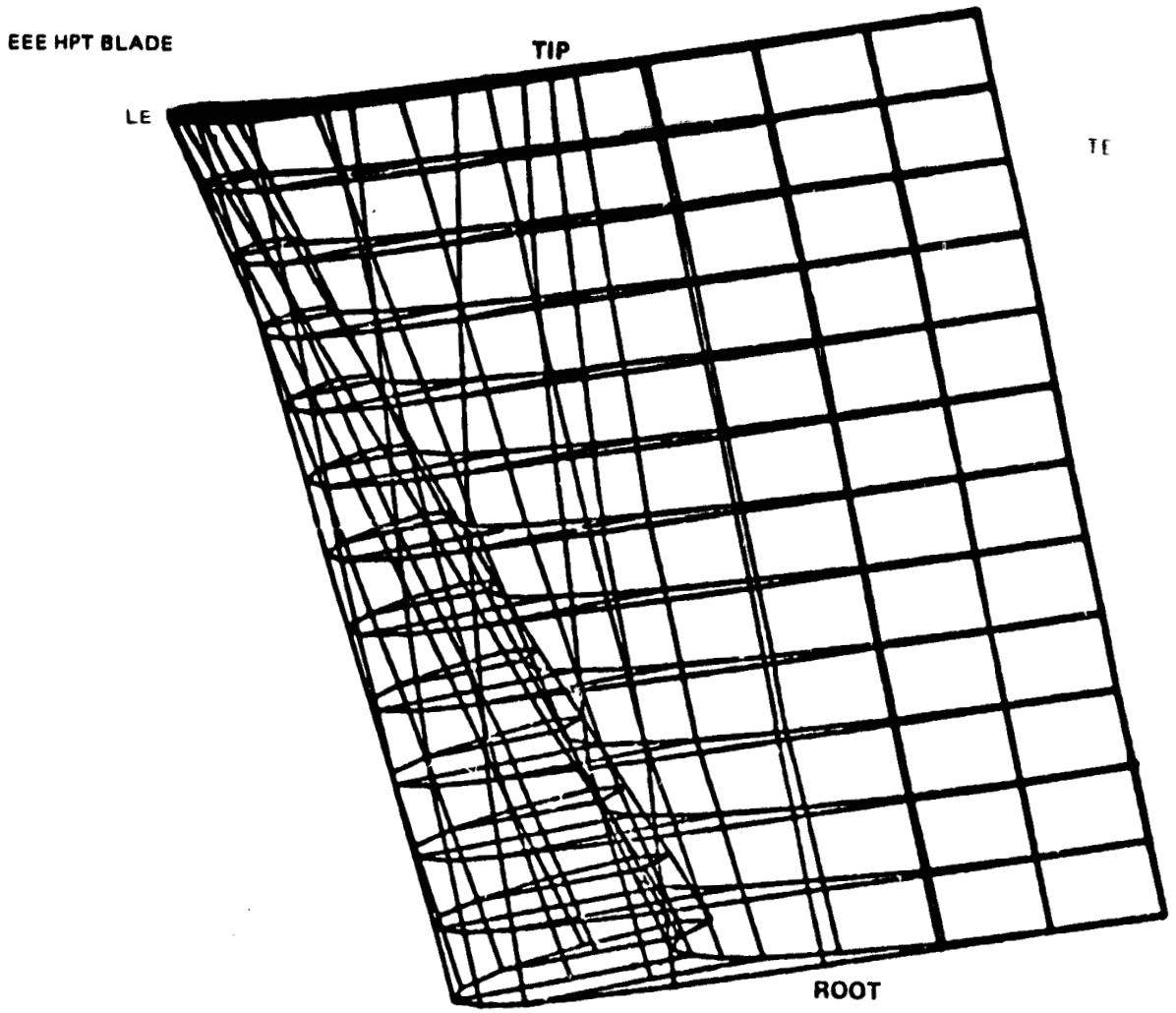

Figure 102 High-Pressure Turbine Blade. NASTRAN model used to investigate vibration.

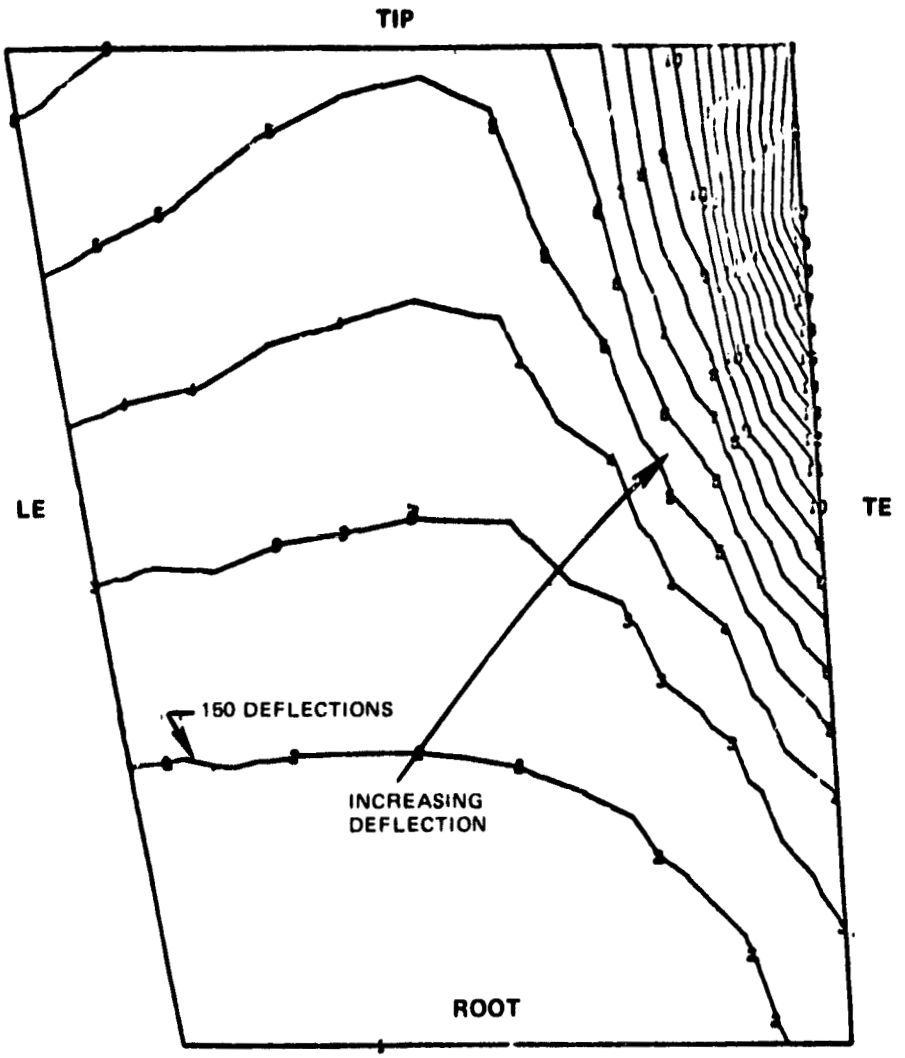

Figure 103 High-Pressure Turbine Blade. First stiff mode isodeflection contours illustrate tip trailing-edge deflection.

modes. A resonance diagram for the blade, constructed of a second generation single crystal material, (Figure 104) shows that high energy vibration modes are well outside the steady-state operating range from minimum cruise to maximum rpm.

4.6.4.5 Total Cooling and Leakage Flows

The preliminary design total estimated high-pressure turbine cooling and leakage flow is shown in Figure 105. Detailed design may decrease some of these flows; however, the preliminary design has demonstrated the feasibility of achieving commercial life in a highly efficient single-stage turbine design.

4.6.4.6 Blade-to-Disk Attachment Region Stress Prediction

The four-tooth blade attachment design used for stress analysis is shown in Figure 106. The stress summary resulting from the attachment structural analysis is presented in Table 39. In the disk attachment region, only the maximum concentrated fillet stress between the third and fourth disk teeth cause the disk attachment to fall short of required life. Better balancing of the blade load between the disk attachment teeth in the attachment region is expected to provide acceptable lives in all areas. The attachment region design will be further optimized during detailed design to arrive at a configuration which meets all of the design requirements.

4.6.4.7 Disk Analysis

4.6.4.7.1 Thermal Analysis

A transient thermal analysis of the disk over the entire engine flight cycle was conducted using the finite element model shown in Figure 107. The air temperatures around the disk are at sea level takeoff (standard +14°C). Steady state metal temperatures resulting from the analysis are also shown on the disk. This model is used to determine disk region stresses and to determine blade tip clearances throughout the engine flight cycle.

4.6.4.7.2 Disk Stresses and Low Cycle Fatigue Life

A structural summary of disk lives and stresses resulting from flight cycle analysis is shown in Table 40. The disk meets or exceeds all life requirements except in the midpoint region of the cooling holes. Local recontouring is expected to produce adequate life in this highly stressed region.

4.6.4.7.3 Sideplate Stresses and Life

A two dimensional finite element analysis of the full-ring sideplates, using a detailed breakup for the analysis, was used to predict stress

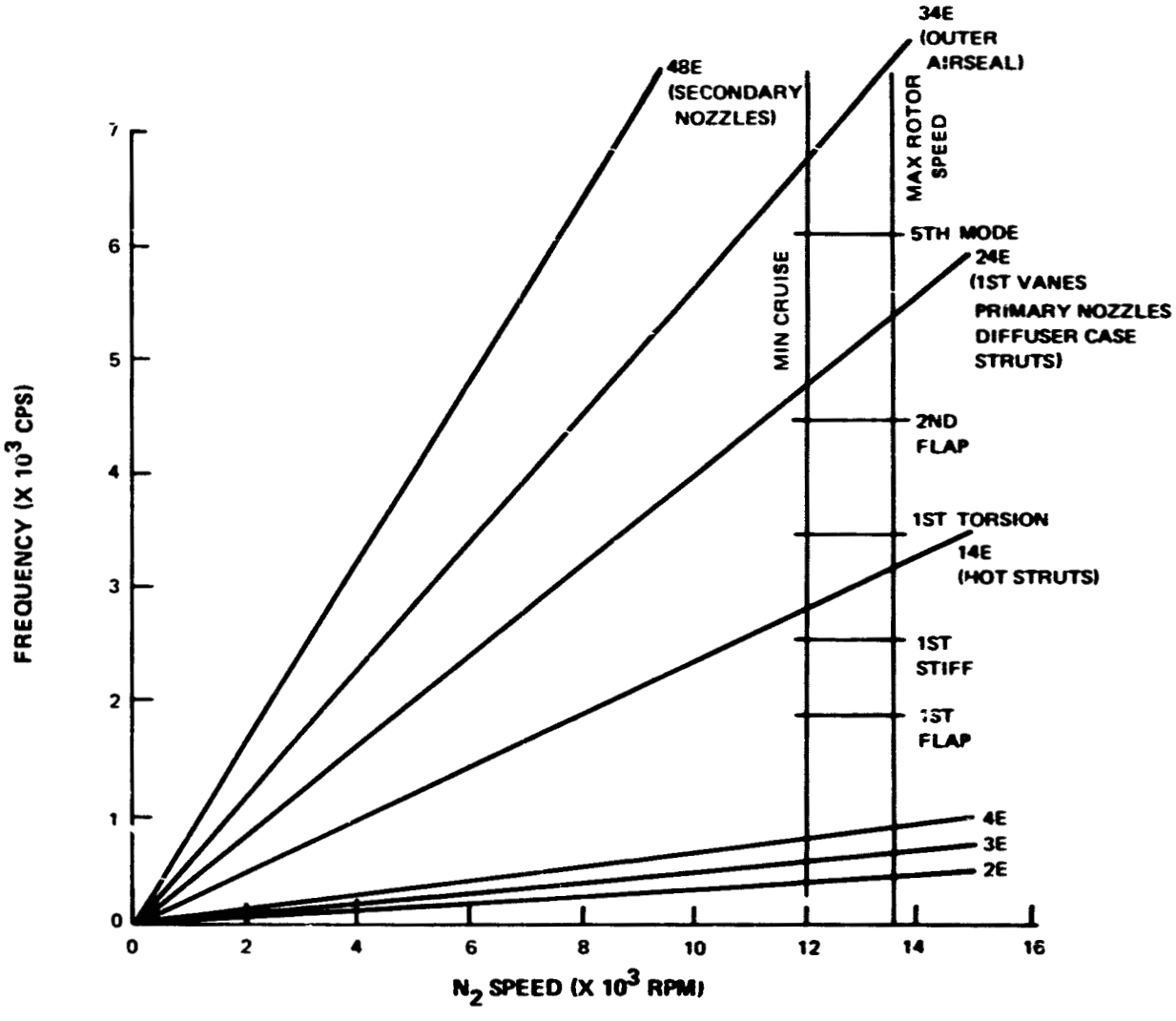

Figure 104 High-Pressure Turbine. Resonance diagram shows high energy modes well outside steady-state operating range from minimum cruise to maximum rpm.

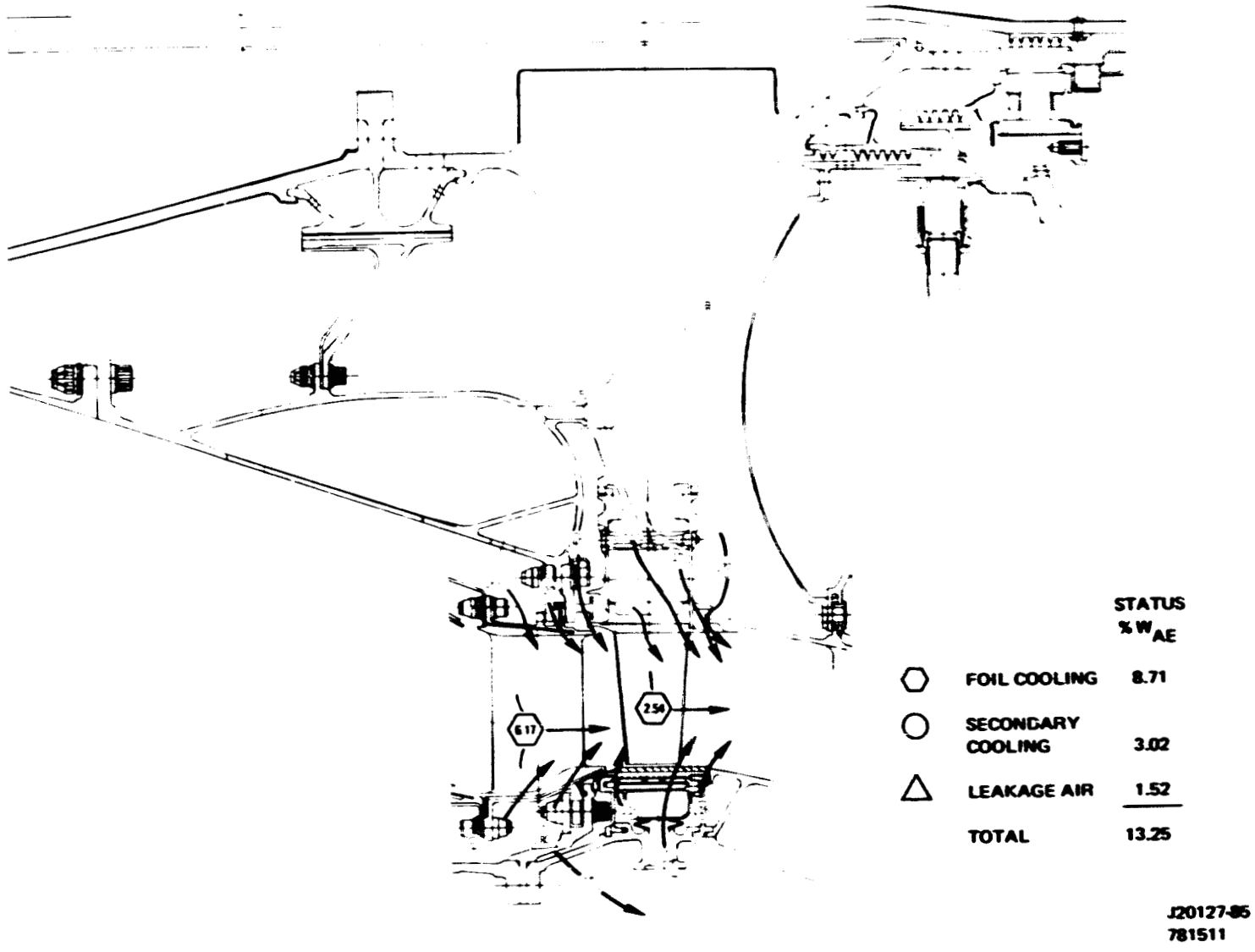

Figure 105 High-Pressure Turbine. Predicted cooling and leakage airflow shows total flow requirements.

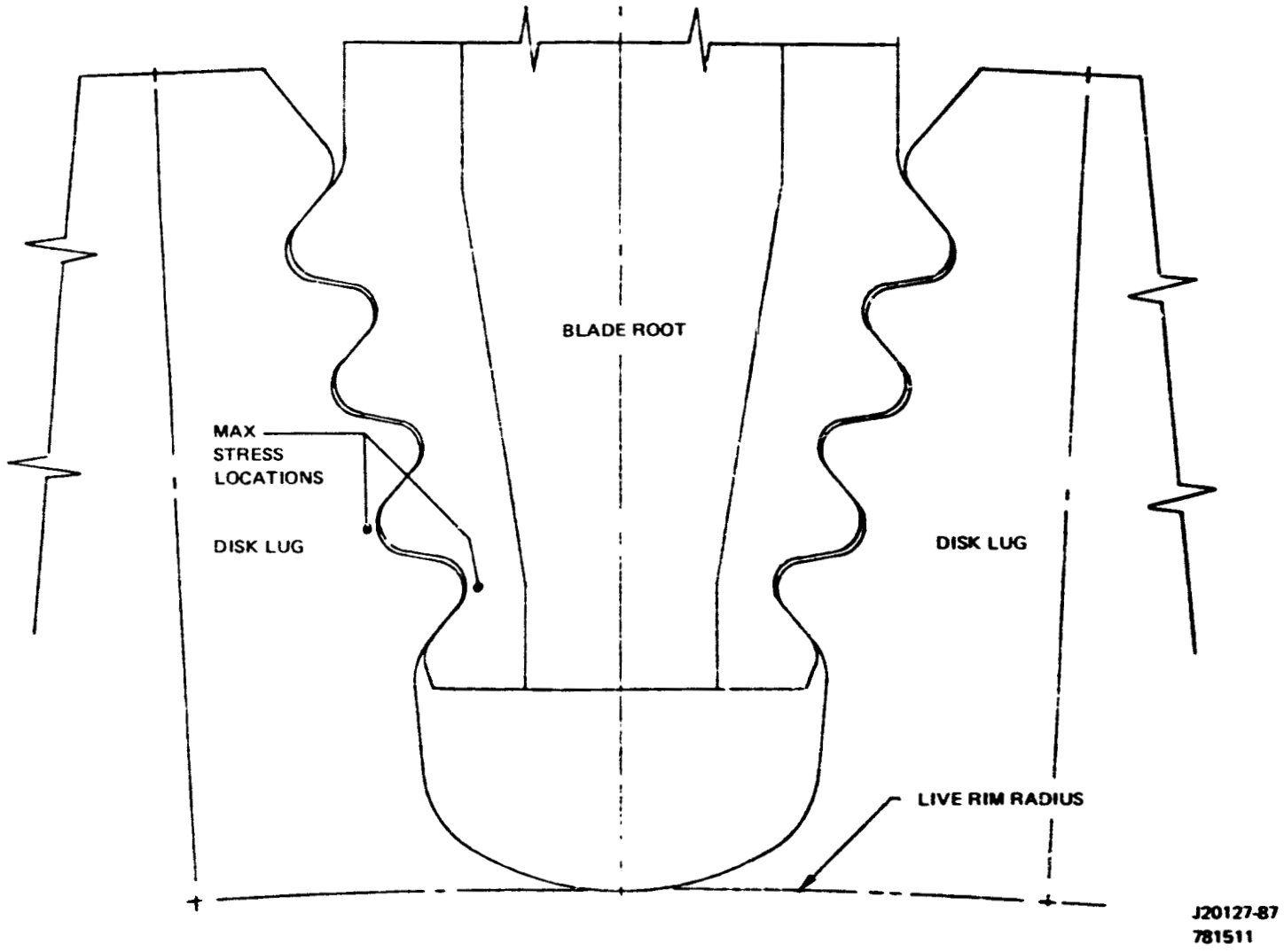

Figure 106 High-Pressure Turbine Blade. Four-tooth attachments used in stress analysis.

TABLE 39

HIGH-PRESSURE TURBINE DISK AND BLADE
ATTACHMENT REGION STRESS AND LCF LIFE PREDICTIONS SUMMARY

	Disk	Blade
Max Temperature, ^{o}C (^{o}F)	649 (1200)	649 (1200)
Max Bearing Stress, N/meter^2 (ksi)	1241 (180)	1241 (180)
Max Shear Stress, N/meter^2 (ksi)	296 (43)	283 (41)
Max P/A Stress, N/meter^2 (ksi)	531 (77)	386 (56)
Max Conc. Fillet Stress, N/meter^2 (ksi)	1519 (229)	1213 (176)
Low Cycle Fatigue Life - Missions	5000	6000
Failure Sequence (Vibration)	Airfoil/Blade Lug	Neck/Disk

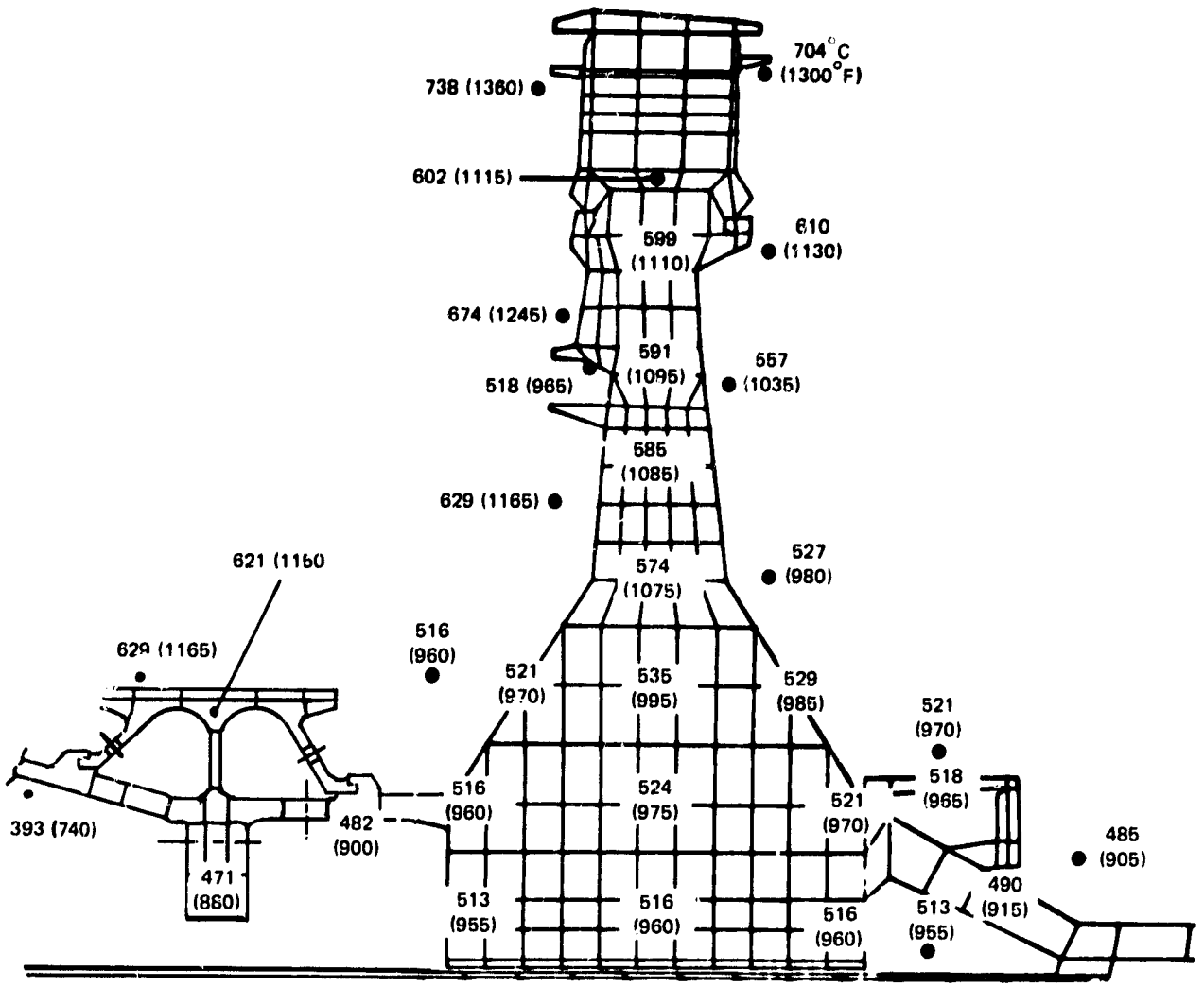

Figure 107 High-Pressure Turbine Disk. Finite element model used to predict acceptable life.

TABLE 40

HIGH-PRESSURE TURBINE DISK STRESS AND LIFE PREDICTIONS

	Calculated
Burst Margin	22%
Low Cycle Fatigue Lives (Missions)	
Bore	35,000
Rim Slot	65,000
Cooling Air Hole Entrance	10^5
Cooling Air Hole Exit	60,000
Cooling Air Hole Midpoint	6,000
Radial Stress in Web @ Burst Speed	1213 N/meter^2 (176 ksi)
Creep Analysis	Not Limiting

levels shown in Figure 108. The sideplate is predicted to meet the life requirement in all areas.

4.6.4.8 Case Analysis

The high-pressure turbine case is designed as a pressure vessel with failed blade containment capability.

4.6.4.8.1 Stress and Life Predictions

The O.D. case was analyzed to establish clearance and mechanical feasibility before starting the detailed design. The case proved to be feasible; however, local modifications may be necessary as the analysis is refined during the detailed design. Initial analysis was performed using a shell model of the case, ACC manifold, and OAS hooks with thermal loading and the imposed loading shown in Figure 109. The analysis showed all stress levels are within Pratt & Whitney Aircraft allowables. A refined stress analysis including stress concentration factors will be done during detailed design and the case configuration modified as necessary.

4.6.5 Design Summary

The results of the high-pressure turbine preliminary design are shown in Table 41. Required life has been achieved in all life limiting parts except in the disk attachment region. Based on previous experience, improvement of the attachment life to the requirement can be achieved with geometrical fine-tuning during detailed design.

4.7 TURBINE INTERMEDIATE CASE

4.7.1 Design Requirements

The turbine intermediate case provides (1) gaspath transition between the high-pressure turbine exit and the inlet of the low-pressure turbine, (2) a frame for the rear high and low rotor support, and (3) the rear engine mount. As such, the case affects the overall engine performance weight and cost. A basic aerodynamic requirement is to duct gasflow between the turbines, without separation, and with minimal loss. The case structural requirements relate to multiple interfaces with other engine assemblies. The varied design requirements are summarized in Table 42.

4.7.2 General Configuration Description

4.7.2.1 Overall Assembly

Figure 110 identifies the major design features of the turbine intermediate case assembly. The assembly consists of 14 structural struts, welded to an inner ring torque box, that traverse the gas path

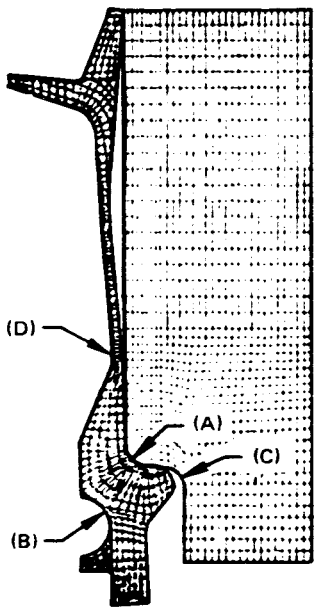

VIEW SHOWING
SIDEPLATE DEFLECTED
SHAPE FROM
2D ANALYSIS

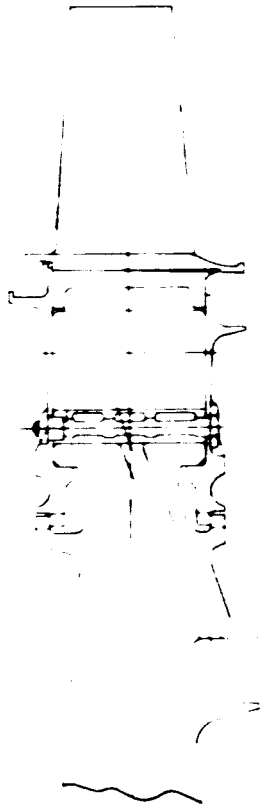

SNAP LOAD (LBS) N		1,993,336 (448122)
TOTAL RADIAL FORCE (LBS) N		14.479 X 10^6 (3.255 X 10^6)
SIDEPLATE FILLET (A)	STRESS*	953.4 N/METER^2 (138.3 KSI)
	LIFE	$>10^5$ MISSIONS
SIDEPLATE LUG (B)	STRESS*	965.2 N/METER^2 (140.0 KSI)
	LIFE	$>10^5$ MISSIONS
DISK FILLET (C)	STRESS*	1374.7 N/METER^2 (199.4 KSI)
	LIFE	25,000 MISSIONS
SIDEPLATE BOLT HOLE (D)	STRESS*	1287.1 N/METER^2 (186.7 KSI)
	LIFE	50,000 MISSIONS
BOLT LOAD NEWTONS (LBS)		
EXTERNAL CALCULATED LOAD		2891 (650)
PRELOAD		9119 (2050)

*CONCENTRATED STRESS

Figure 108 High-Pressure Turbine Disk. Sideplate stress and life prediction meet design requirements.

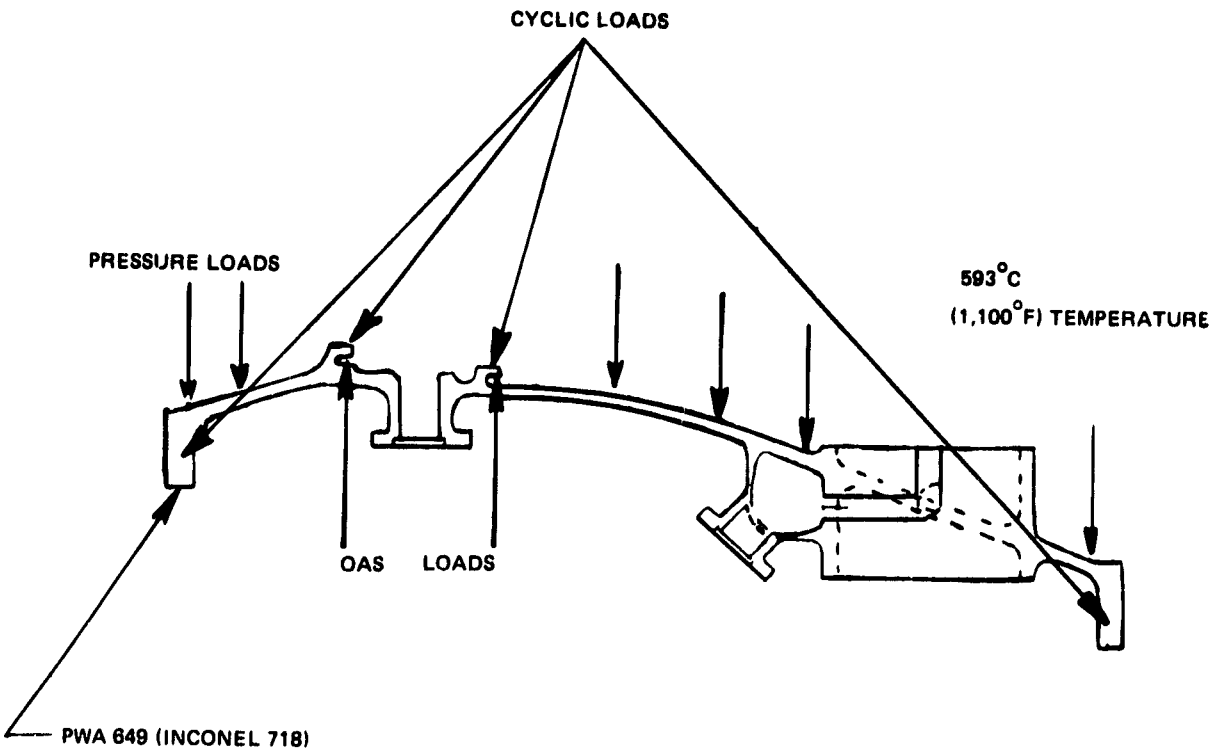

Figure 109 High-Pressure Turbine Case. Loads considered in stress predictions.

TABLE 41

HIGH-PRESSURE TURBINE PRELIMINARY DESIGN RESULTS
AERODYNAMIC DESIGN POINT

Expansion Ratio	4.03
Mean Velocity Ratio	0.56
Disk Rim Speed, m/sec (ft/sec)	527 (1730)
AN^2, cm^2 rpm^2 (in^2 rpm^2)	31.6×10^{10} (49×10^9)
Adiabatic Efficiency, %	88.2
Coolant/Leakage Flow, %	13.25
Life	
Blade, hr/missions	10,000/2200
Vane, hr/missions	10,000/2200
Disk, missions	5,000 (12,000 required)

TABLE 42
TURBINE INTERMEDIATE CASE DESIGN REQUIREMENTS

Aerodynamic

1. Provide transition duct to the low through-flow velocity, large diameter, low-pressure turbine.

2. Minimize low-pressure turbine inlet flow distortion.

3. Minimize transition duct pressure loss.

Structural/Mechanical

1. Achieve design lives of 15,000 hours for the strut vanes and 30,000 hours and 20,000 missions for all the remaining hardware

2. Provide the static support radial spring rates of 1.75×10^6 N/cm (1×10^6 lbs/in.) for the No. 4 bearing and 0.88×10^6 N/cm (0.5×10^6 lb/in.) for the No. 5 bearing required for acceptable high and low rotor dynamics characteristics.

3. Maintain structural integrity of the bearing support frame in the event of a turbine blade failure.

4. Minimize case ovalization caused by engine mount loads.

5. Provide oil service lines for the rear bearing compartment.

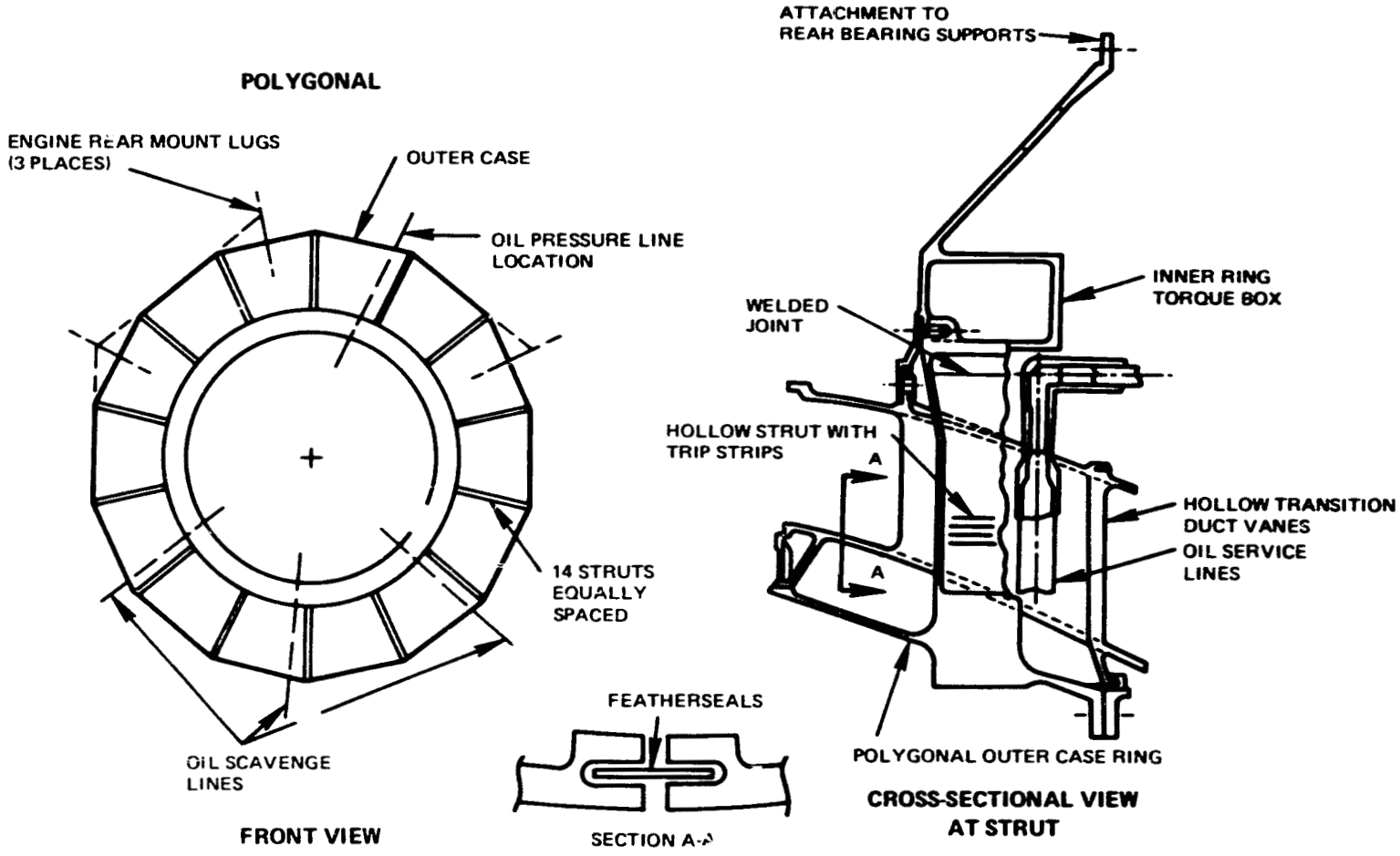

Figure 110 Turbine Intermediate Case. Drawing identifies major design features.

through hollow transition duct vanes and bolt to the outer case. This ring strut-ring structure, made from cast INCONEL 718 material, forms the rear bearing compartment support frame and rear engine mount frame. The number of struts was selected to preclude critical high-pressure turbine blade resonances within the operating range. The vanes reach a maximum thickness of 2.54 cm (1.0 in.) at approximately 40 percent of chord to clear the struts and oil service lines.

The vane row and gaspath walls are built-up from 14 circumferential segments. The gas path is sealed between segments with feather seals along both inner and outer walls. The segments are constructed of an advanced, cast, single crystal nickel base alloy (MERL 220) with a 97°C (175°F) higher temperature capability than present directionally solidified material to preclude the need for cooling at the highest operating temperatures encountered in the engine.

The torque box inner ring is needed to resist case tilting from the axially offset bearing loads. Several geometric shapes were studied and analyzed to determine deflection sensitivity to bearing loads. The box or rectangular shape was determined most effective in minimizing both radial deflections and case tilting. To ensure the axial stability needed under a vibratory situation or high shaft failure, the inner torque box is axially tied to the 14 fairing vanes (via a radially free joint for thermal freedom) which then transmit axial loads directly to the outer case.

The struts are sized to maximize radial and bending stiffness within the geometric limits of the hollow vanes through which they pass. The vane stagger angle (60 degrees from axial) initially resulted in excessive minimum axis bending of the vanes under axial or trunnion type loading. Adequate stiffness was regained by providing seven longer full-chord struts in locations not requiring service lines. The struts are cooled with 0.2 percent of 10th-stage compressor air to provide a suitable environment for the INCONEL 718 material. "Trip strips" are cast into the inner walls to increase cooling effectiveness.

The outer case features a polygonal design in the strut support region to minimize case ovalization from rear engine mount loads. The straight sections between struts tend to deflect in the tensile direction rather than bend out of plane as would a conventional curved section to reduce case circumferential deflections and ovalization under load.

4.7.2.2 Transition Duct Flowpath

The transition duct flowpath is shown in Figure 111. The overall length of the transition duct was set by airfoil axial gapping requirements imposed by vibratory considerations. The wall contours were established considering blockage effects and flow separation. The cross-sectional area distribution is compared with the actual flow area expected with the duct in Figure 112. Substantial flow blockage exists in the region

of the vane cascade which has been taken into account in designing for a steady pressure rise along the duct.

4.7.2.3 Technology Development Requirements

A transition duct test program will be used to verify the short, low loss, advanced technology preliminary design. The tests will investigate aerodynamic losses, local separation and exit flow distortion characteristics of the current duct design and, if required, of an alternate configuration.

The test rig will consist of a full annular duct with the 14 strut vanes, inlet vanes to create the high-pressure turbine exit flow swirl, and the low-pressure turbine inlet vanes.

Data will be taken at the aerodynamic design point condition and at off-design vane incidence angles. These data will include:

1. Total inlet pressure and air angle at the vane inlet and exit and at the low-pressure turbine inlet vane exit locations

2. O.D. and I.D. wall static pressures at various locations

3. Vane airfoil static pressure distribution

4. Boundary layer flow characteristics

5. Total pressure and air angle vs. circumferential location between vanes

4.7.3 Supporting Analyses

4.7.3.1 Flowpath Analysis

The flowpath shape was established using the Pratt & Whitney Aircraft two-dimensional streamline design system and a three-dimensional diffuser design system that includes the effects of swirl and endwall contour. Inlet and exit Mach numbers and swirl angles used in the analysis are shown in Figure 113. These analyses were used to support the following additional design tasks:

1. Vane airfoil contour definition

2. Pressure loss prediction

3. Endwall separation margin prediction

4. Flow distortion prediction

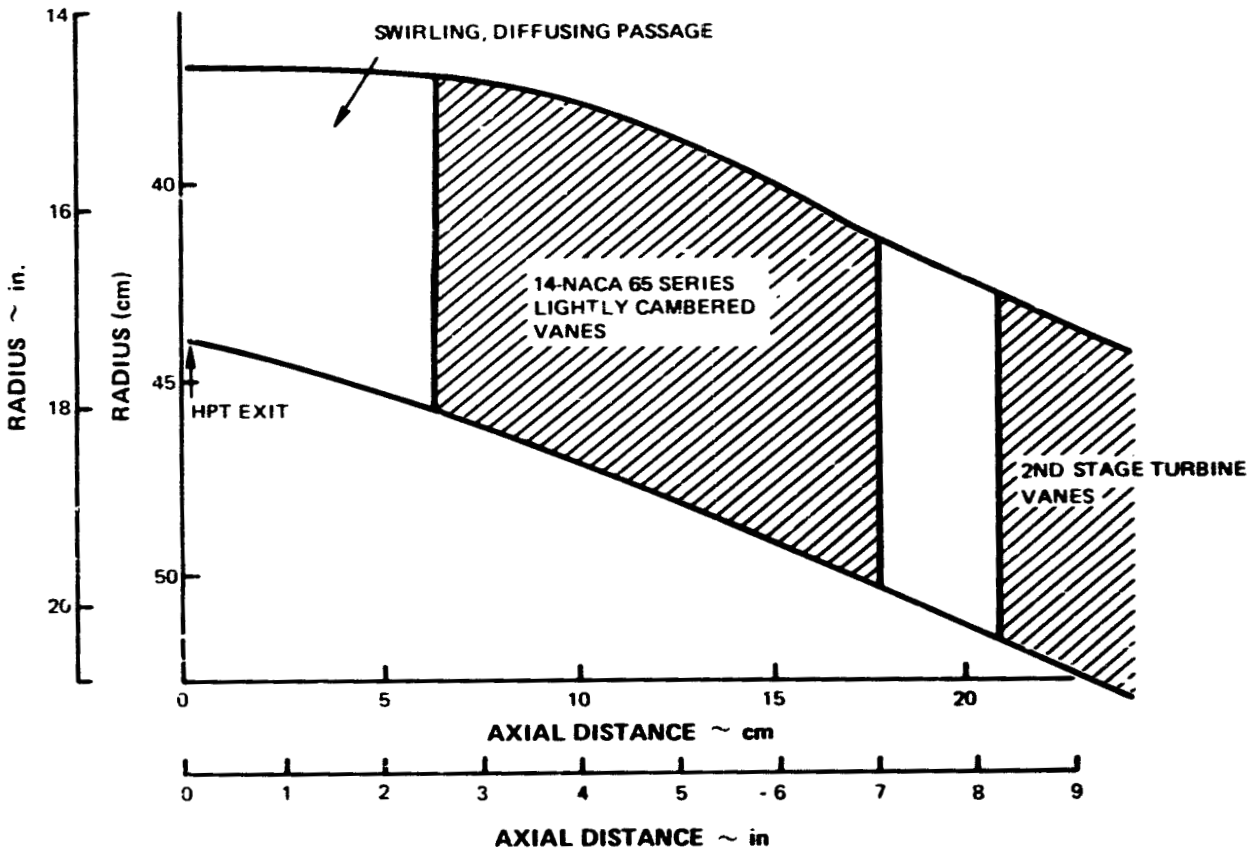

Figure 111 Turbine Intermediate Case. Drawing shows duct flowpath shape necessary to provide required diffusion between turbines.

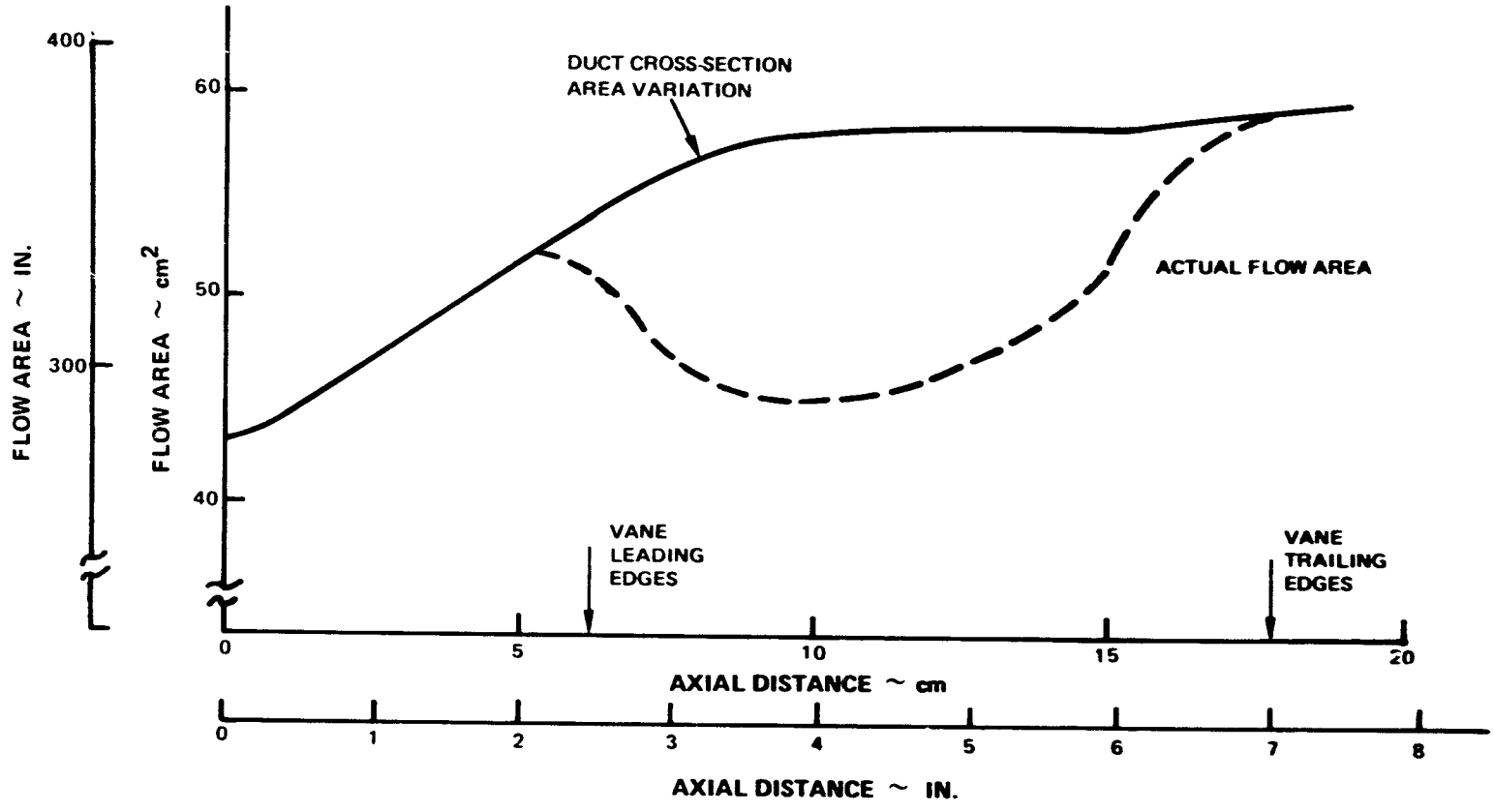

J20127-13
780611

Figure 112 Turbine Intermediate Case. Transition duct vane blockage shows level included in flowpath definition.

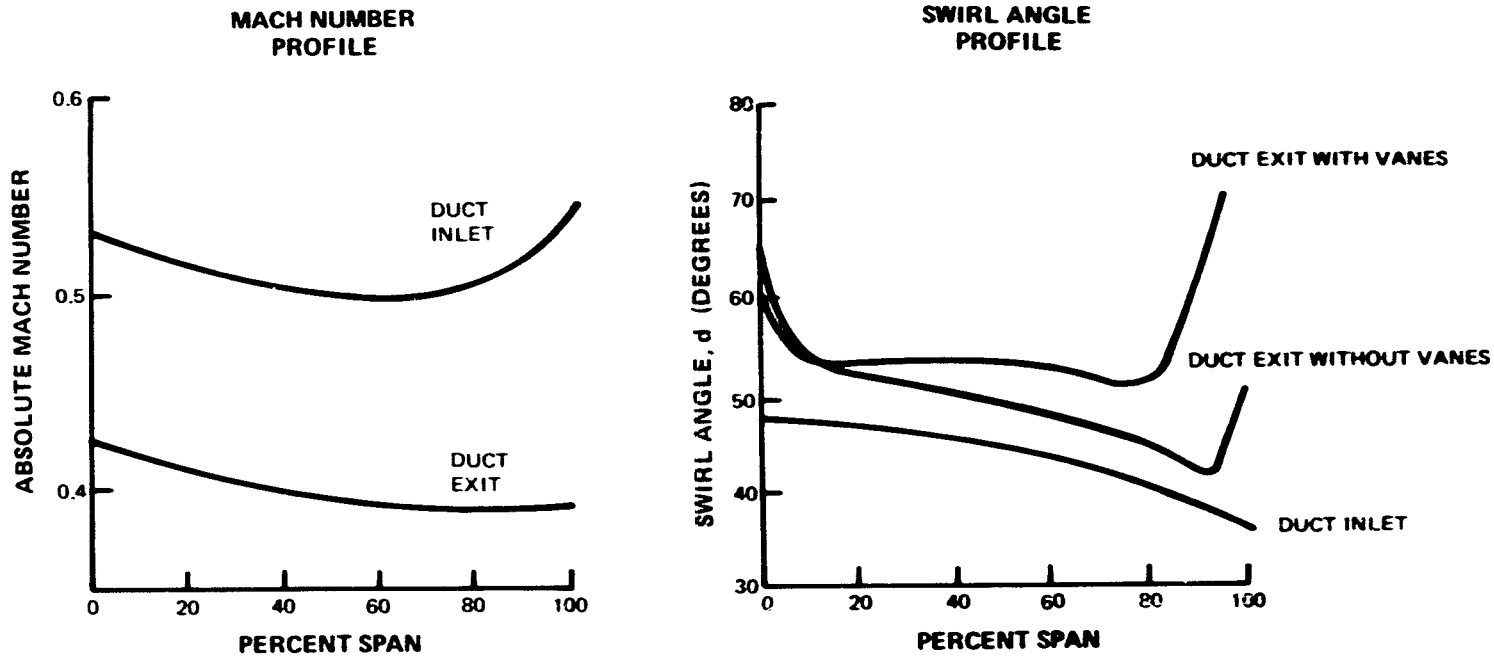

Figure 113 Turbine Intermediate Case. Transition duct inlet and exit Mach numbers and swirl angles indicate general diffusion and nearly constant swirl through duct.

The preliminary design of the turbine transition duct included a high turning versus low turning vane study. This study compared a design with low aspect ratio, lightly cambered vanes coupled with high aspect ratio low-pressure turbine inlet turning vanes to a design with only low aspect ratio, high turning vanes providing all the turning necessary between the high-pressure turbine exit and inlets to the low-pressure turbine blades.

The flowpaths of these two designs are compared in Figure 114. The results of this study showed that both vane designs were aerodynamically acceptable but that the high turning vane design required an additional 5.33 cm (2.1 in.) in engine length. The shorter, low turning vane design was selected based on the beneficial impact expected on engine weight.

4.7.3.2 Vane Airfoil Contour Definition

The high-pressure turbine/low-pressure turbine transition duct vanes are NASA 65 circular-arc airfoils with a maximum thickness of 2.54 cm (1.0 in.) established by the bearing support frame structural requirements. The vane airfoil aerodynamic design summary is shown in Table 43.

4.7.3.3 Pressure Loss Prediction

The total pressure loss through the turbine transition duct ($\Delta P_T/P_T$), as calculated with the Pratt & Whitney Aircraft two-dimensional streamline design system, is 1.5 percent.

4.7.3.4 Life Predictions

A vane thermal stress analysis was performed, and it was determined that the limiting life factor was surface oxidation. The vanes, of MERL 220/200 material with PWA 700 coating, are estimated to meet the 15,000 hour life goal with one "strip-and-recoat" repair.

Structural analysis of the ring-strut-ring case structure consisted of various shell stress and deflection analysis and a transient thermal analysis. The stresses induced by the thermal gradient between the cold bearing compartment and the hot outer case are maximum in the inner core where it joins the bearing support cylinder but the resulting low cycle fatigue (LCF) life meets the design life goals. The thermally induced strut loads vary from compression on acceleration to tension at steady state and are well within the allowable limits based on low cycle fatigue life and buckling criteria.

The turbine intermediate case structure was analyzed to insure that it could withstand the loads imposed by a high-pressure turbine or low-pressure turbine blade failure without buckling or bending. The limiting condition is a fourth-stage blade failure that results in

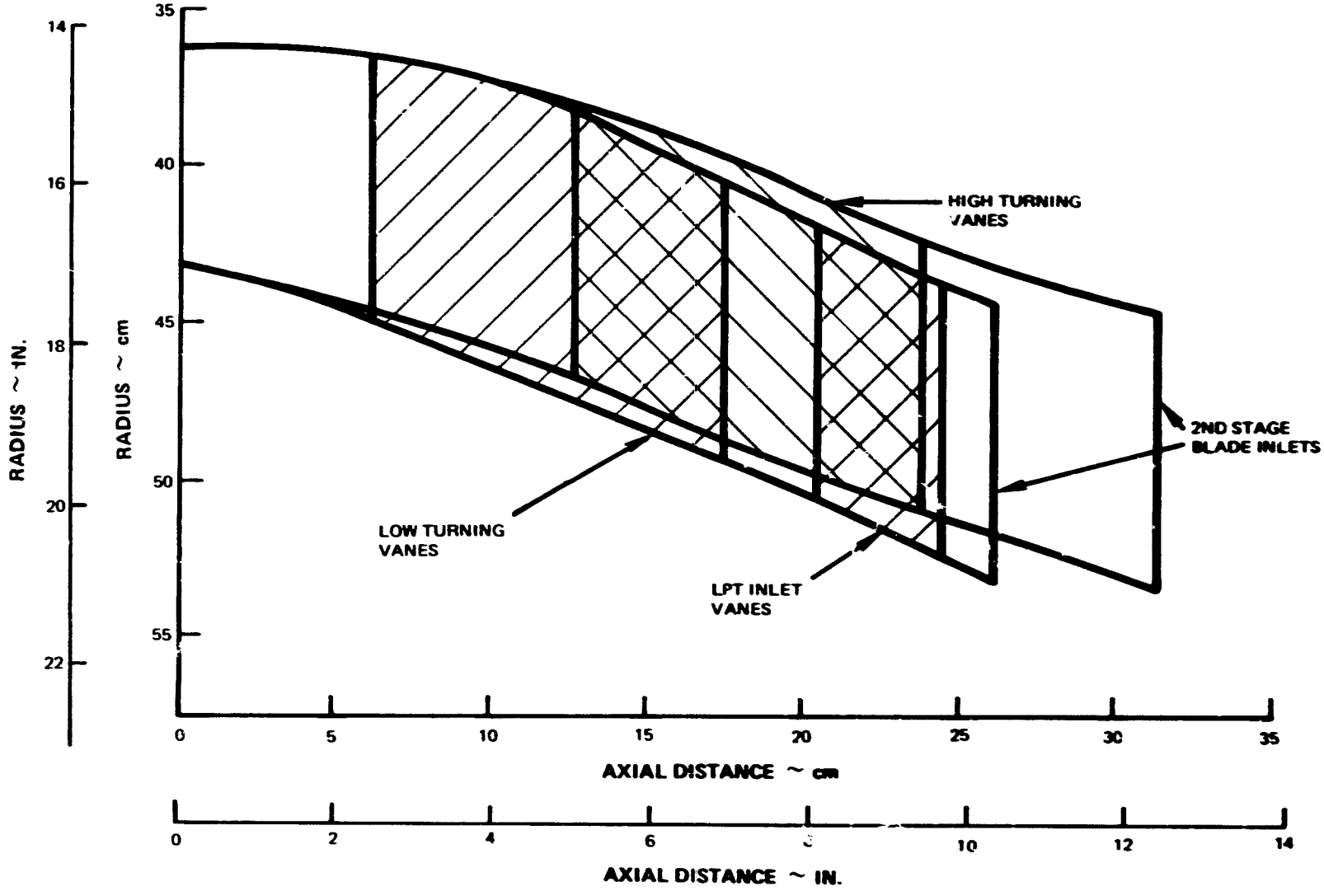

Figure 114 Turbine Intermediate Case. High and low turning vane designs were examined in selection of shorter low turning turbine intermediate case.

TABLE 43

TURBINE TRANSITION DUCT VANE AIRFOIL DESIGN DATA

	Root	Mean	Tip
Airfoil Type	65 C/A	65 C/A	65 C/A
Actual Chord Length	20.32 cm (8.0 in)	18.80 cm (7.4 in)	16.26 cm (6.4 in)
Max Thickness	2.54 cm (1.0 in)	2.54 cm (1.0 in)	2.54 cm (1.0 in)
Number of Airfoils	14	14	14
Inlet Gas Angle	144.5°	138.0°	132.1°
Exit Gas Angle	31.1°	31.2°	39.8°
Inlet Mach No.	0.451	0.446	0.466
Exit Mach No.	0.456	0.417	0.401

radial and trunnion loading of the turbine intermediate case structure equal to 97 percent capacity.

4.7.3.5 Endwall Separation Margin Prediction

Predicted wall friction coefficients for the I.D. and O.D. endwalls are presented in Figure 115 as determined by the three-dimensional flow analysis. The diffusing duct is predicted to be separation-free, as indicated by the low positive wall friction levels in the strut trailing edge region.

4.7.4 Design Summary

The analyses showed that the turbine intermediate case preliminary design configuration presently meets all design requirements. The results of the transition duct test program will verify the aerodynamic design or determine the recontouring necessary to assure low-loss, separation-free operation.

4.8 LOW-PRESSURE TURBINE

4.8.1 Design Requirements

General low-pressure turbine aerodynamic, structural, and mechanical design requirements were established by the engine cycle definitions at design and off-design flight conditions. More specific requirements resulted from an optimization study, which considered initial cost, maintenance cost, performance, weight, and technical risk. Performance and durability considerations involved a number of key operating conditions.

Table 44 summarizes the general design requirements for the low-pressure turbine. Performance requirements were established at the 10,668m (35,000 ft) aerodynamic design point located between the two key performance-oriented operating conditions of maximum climb and maximum cruise. The low-pressure turbine efficiency goal is also shown.

As in the other components, mechanical and structural design requirements were established based on commercial acceptability.

4.8.2 Design Background

The low-pressure turbine design concept and benefits were developed from experience on current production engines. The Energy Efficient Engine low-pressure turbine design efficiency was substantiated by combining efficiency experience engine with the technological improvements in the advanced turbine design.

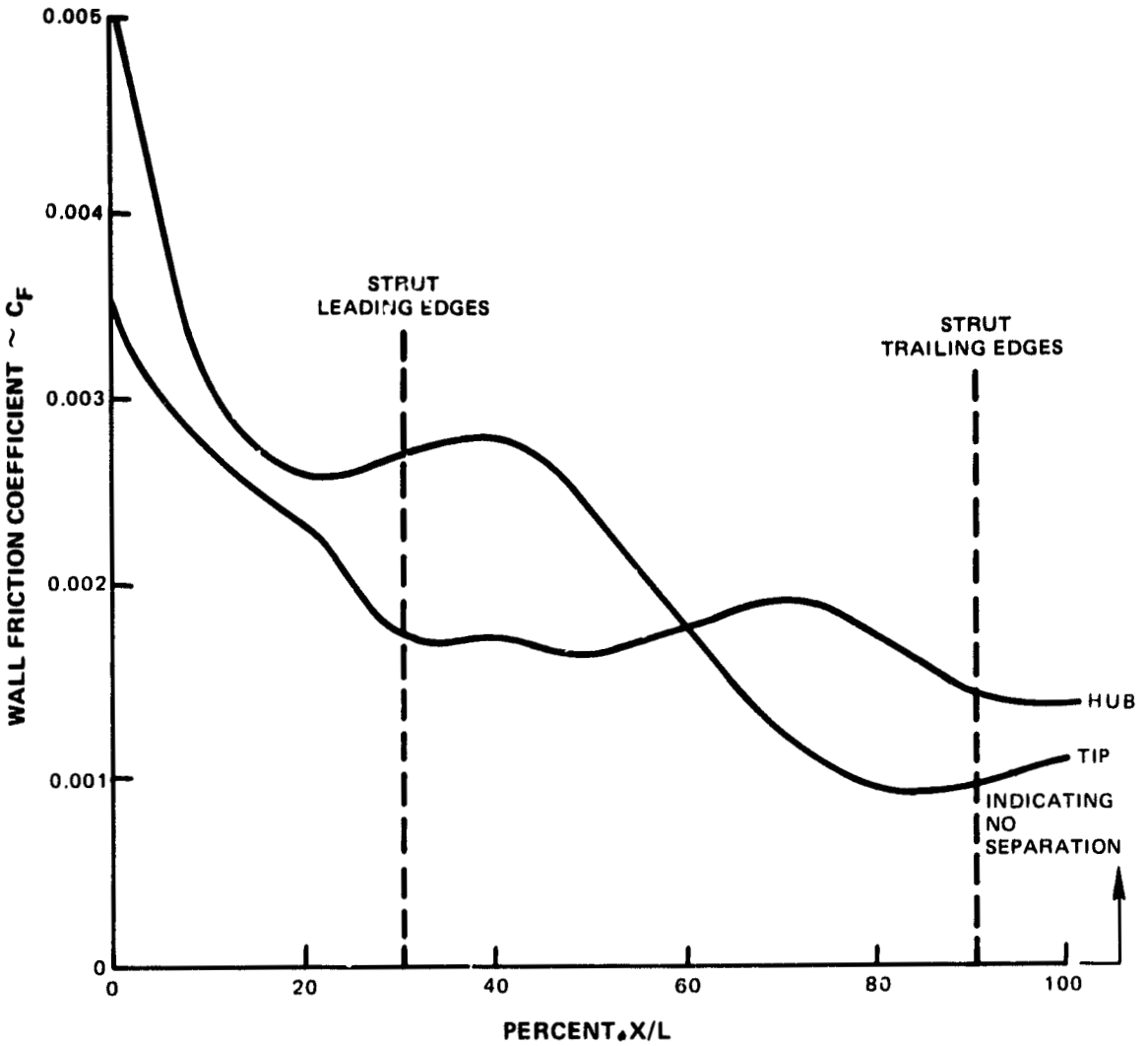

Figure 115 Turbine Transition Duct. Wall friction estimates indicate separation-free diffusion.

TABLE 44

LOW PRESSURE TURBINE DESIGN REQUIREMENTS
AERODYNAMIC DESIGN POINT

Aerodynamic Parameters	
Expansion Ratio	5.6
Enthalpy Change, (Δ h), joules/g (BTU/lb)	405 (174)
Inlet Temperature, ^{o}C (^{o}F)	837 (1540)
Inlet Airflow kg/sec (lb/sec)	35.7 (78.5)
Inlet Pressure, kg/cm^2 (lb/in^2)	3.3 (47)
Mechanical Parameters	
Number of Stages	4
Adiabatic Efficiency Goal	
Efficiency	0.915
Life Requirements	
Blade, hours	15,000
Vane, hours	15,000
Disk, hours/missions	30,000/20,000
Case, hours/missions	30,000/20,000

4.8.3 General Configuration Description

4.8.3.1 Major Subassemblies

The four-stage low-pressure turbine preliminary design, with the cross-section as shown in Figure 116, features tightened blade tip clearances, reduced leakage, and internal active clearance control.

The rotor assembly consists of four disks including two that have integrated hubs bolted-up to spacers that seal beneath the vane inner platform. Tip-shrouded blades are attached to the disks by two-tooth firtree-attachments. Vanes are supported by the case that is double-walled over the front two stages to accommodate the active clearance control. Inner and outer airseals of various types complete the assembly.

4.8.3.2 Advanced Aerodynamics

Extensive testing of various low-pressure turbine rigs at Pratt & Whitney Aircraft indicates that significant efficiency benefits are possible by using technical advancements in the area of aerodynamics. Analyses indicate that a 1.0 percentage point in efficiency is available by special contouring of the airfoils.

4.8.3.3 Leakage Control

Reduced leakage is intended to contribute significantly to the total low-pressure turbine performance benefits. The series of concepts to address leakage are listed in Table 45. Figure 117, which summarizes the various seal types, displays the slight advantage of wide channel seals over conventional two- and three-knife edge seals in the vane inner cavities.

4.8.3.4 Principal Aerodynamic Design Parameters

Table 46 lists the principal design parameters. The design parameters reflect a moderately loaded turbine of high expansion ratio required to drive the high bypass ratio fan.

4.8.3.5 Technology Development

A series of supporting technology programs are in progress to verify the advanced aerodynamic concepts. A boundary layer test program and the subsonic cascade program will directly impact the low-pressure turbine detail design. The boundary layer program will verify concepts used in designing the airfoils. Program results will be incorporated in low-pressure turbine detail design.

The low-pressure turbine subsonic cascade program is directed toward evaluating various airfoils to determine both the spanwise loss

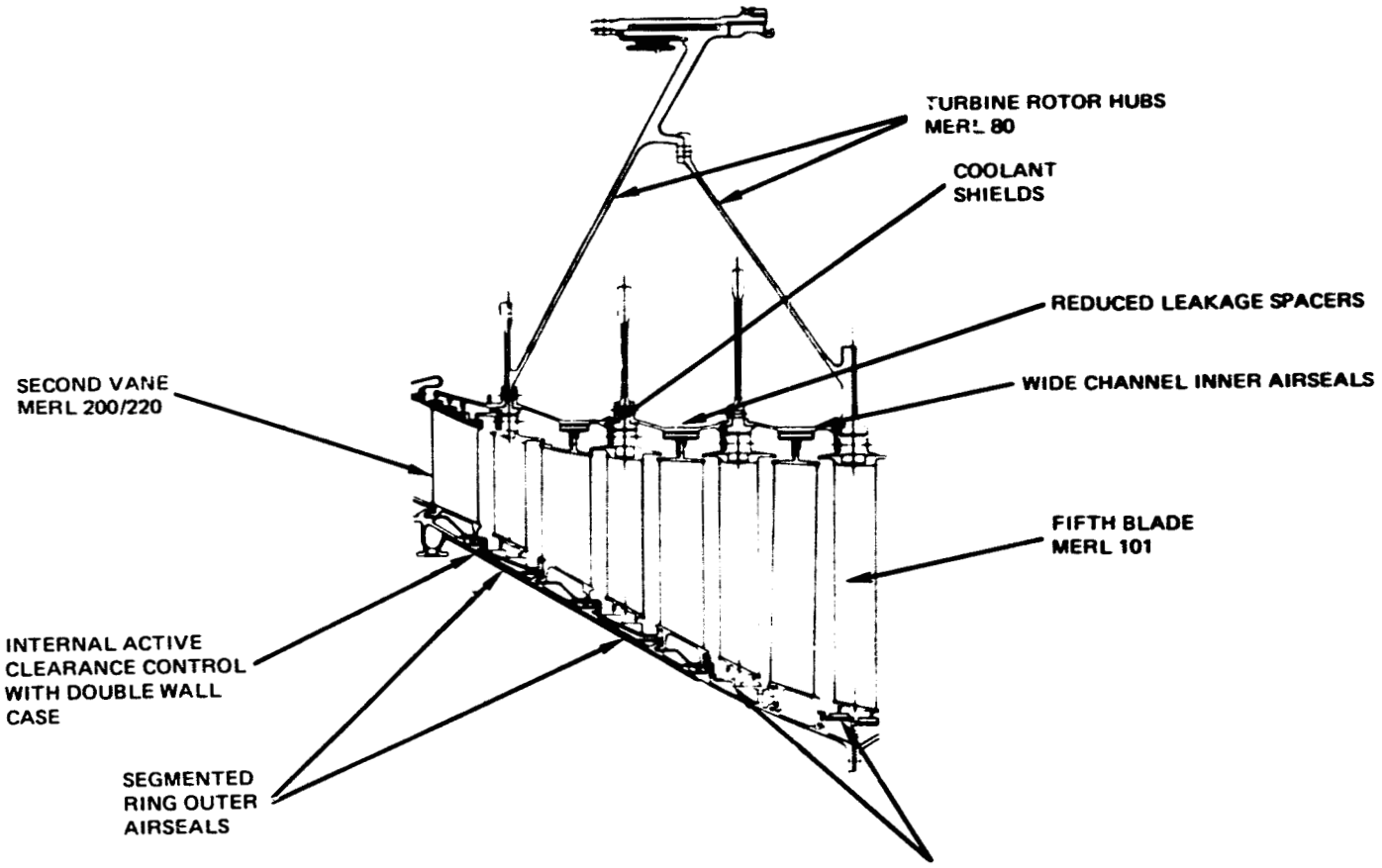

Figure 116 Low-Pressure Turbine. Cross-section shows major features.

TABLE 45

REDUCED LPT LEAKAGE CONCEPTS

1. Flow Guides
2. Wide Channel Seals
3. Coolant Shields
4. Reduced Cavity Size
5. Controlled Vortex Design
6. Active Clearance Control

TABLE 46

LOW PRESSURE TURBINE AERO DESIGN AERODYNAMIC DESIGN POINT

Number of Stages	4
Expansion Ratio	5.7
Mean Velocity Ratio/NASA Loading Parameter	0.47/2.26
Cx/U	0.73
Maximum Rim Speed, m/sec (ft/sec)	198 (650)
Inlet Speed Parameter, $N/\sqrt{T}$, rpm/$\sqrt{^{o}K}$ (rpm/$\sqrt{^{o}R}$)	110 (82.1)
Inlet Flow Parameter, $W\sqrt{T}/P$, $\sqrt{^{o}K}$ cm^2/sec ($\sqrt{^{o}R}$ in^2/sec)	36 (75.0
Blade Tip Clearance, cm (in)	0.05 (0.020)
Inlet Mach No. (Mean Absolute)	0.392
Exit Mach. No. (Mean Absolute)	0.404
Inlet Swirl Angle (Mean), degrees	-52.9
Exit Swirl Angle (Mean), degrees	+32.1
Number of Blades and Vanes	749
Efficiency	0.915

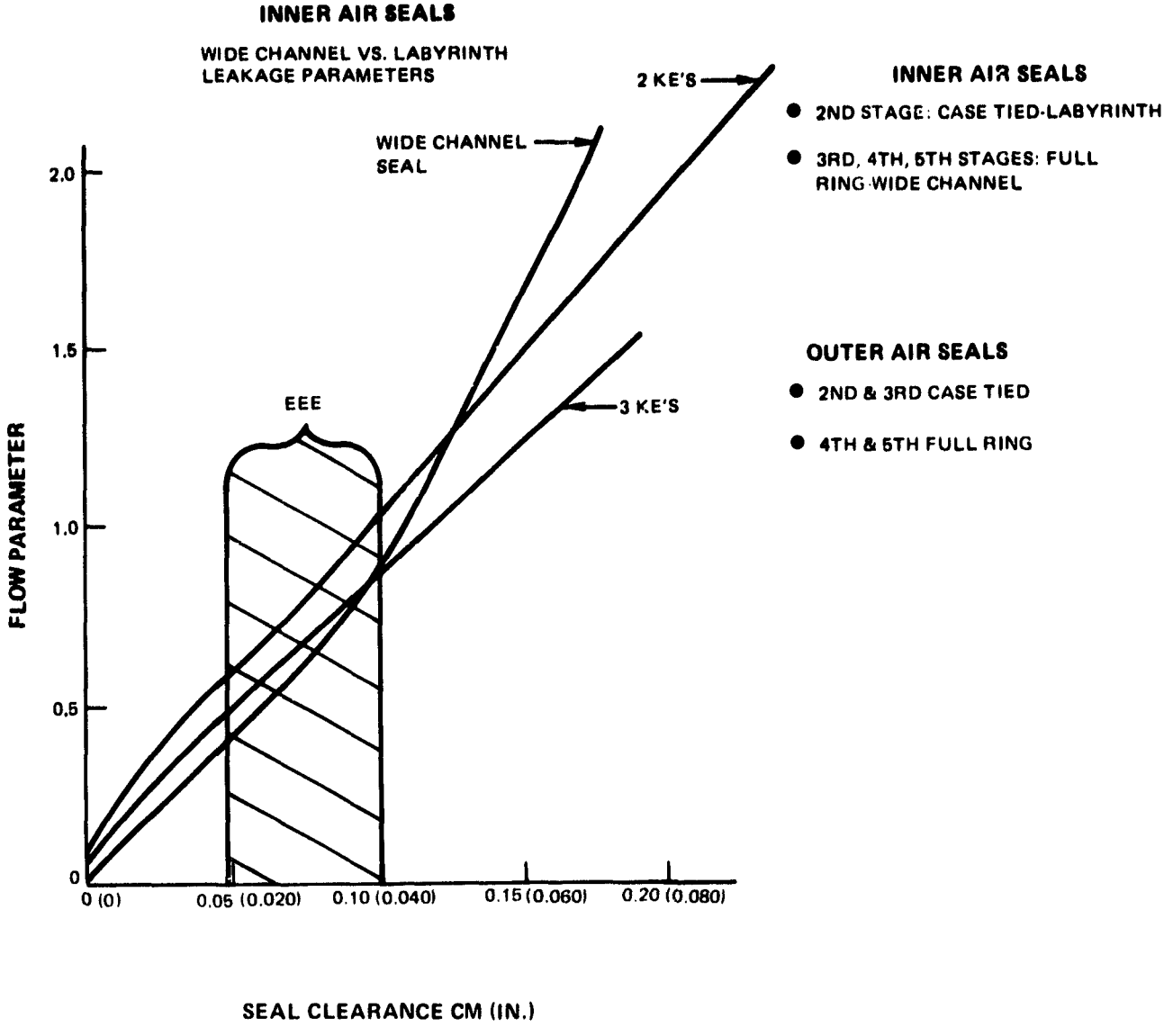

Figure 117 Low-Pressure Turbine Seal. Performance comparison shows type used at various low-pressure turbine locations and indicates reason for selecting wide channel inner airseals.

distribution and the losses over the operating range. Information from this program will be factored into the detail design.

4.8.4 Supporting Analyses

4.8.4.1 Efficiency Prediction

The low-pressure turbine is predicted to operate at the design point with an efficiency of 91.5 percent (Table 47). The efficiency prediction is based upon current production engine low-pressure turbine experience and includes the various technology benefits.

4.8.4.2 Low-Pressure Turbine Flowpath Selection

A five-stage turbine provided a 0.3 to 0.4 percent higher turbine efficiency potential, but was 22.7 to 45.4 kg (50 to 100 lb) heavier and cost $10,000 to $15,000 more than a four-stage turbine at the same velocity ratio. The additional stage was also estimated to increase maintenance costs by $1 per engine flight hour. These differences, when translated into fuel consumption and DOC, resulted in the trends shown in Figure 118. The 0.47 velocity ratio (2.26 work factor) turbine was selected as offering minimum DOC, providing near-minimum fuel burned, and representing a more significant step in technology than a higher velocity ratio, more lightly-loaded five-stage turbine.

4.8.4.3 Counter-Rotation Selection

The preliminary design has confirmed the selection of a counterrotating configuration as a feasible concept to increase efficiency. Only 13 degrees of turning by the second stage vanes were sufficient to provide the required blade inlet incidence. With corotation, approximately 100 degrees of turning would be necessary in the vane row. Differences in vane row losses were calculated to be equivalent to a low-pressure turbine efficiency difference of 0.5 percent. Study results are summarized in Figure 119.

4.8.4.4 Gas Path Aerodynamics

A complete cycle of aerodynamic analyses has been completed, resulting in flowpath definition, airfoil selection, and airfoil number (Figure 120). The velocity triangles are presented in Figures 121 through 124.

4.8.4.5 Rotor Construction Selection

Various construction schemes were analyzed during the preliminary design of the low pressure turbine, three of which are shown in Figure 125. A generalized shell analysis of the originally proposed construction was modeled to evaluate stresses and deflections. This analysis included transient thermal data, pressures and speeds. The single front hub of the design resulted in excessive centrifugal and

TABLE 47

LOW-PRESSURE TURBINE
DESIGN EFFICIENCY PREDICTION

Efficiency Base (JT9D-7A Low Pressure Turbine Tests)	89.0%
Improved Aerodynamics Benefits	1.0%
Reduced Work Factor	0.3%
Reduced Clearance and Leakage Benefit	1.2%
Status Efficiency	91.5 %

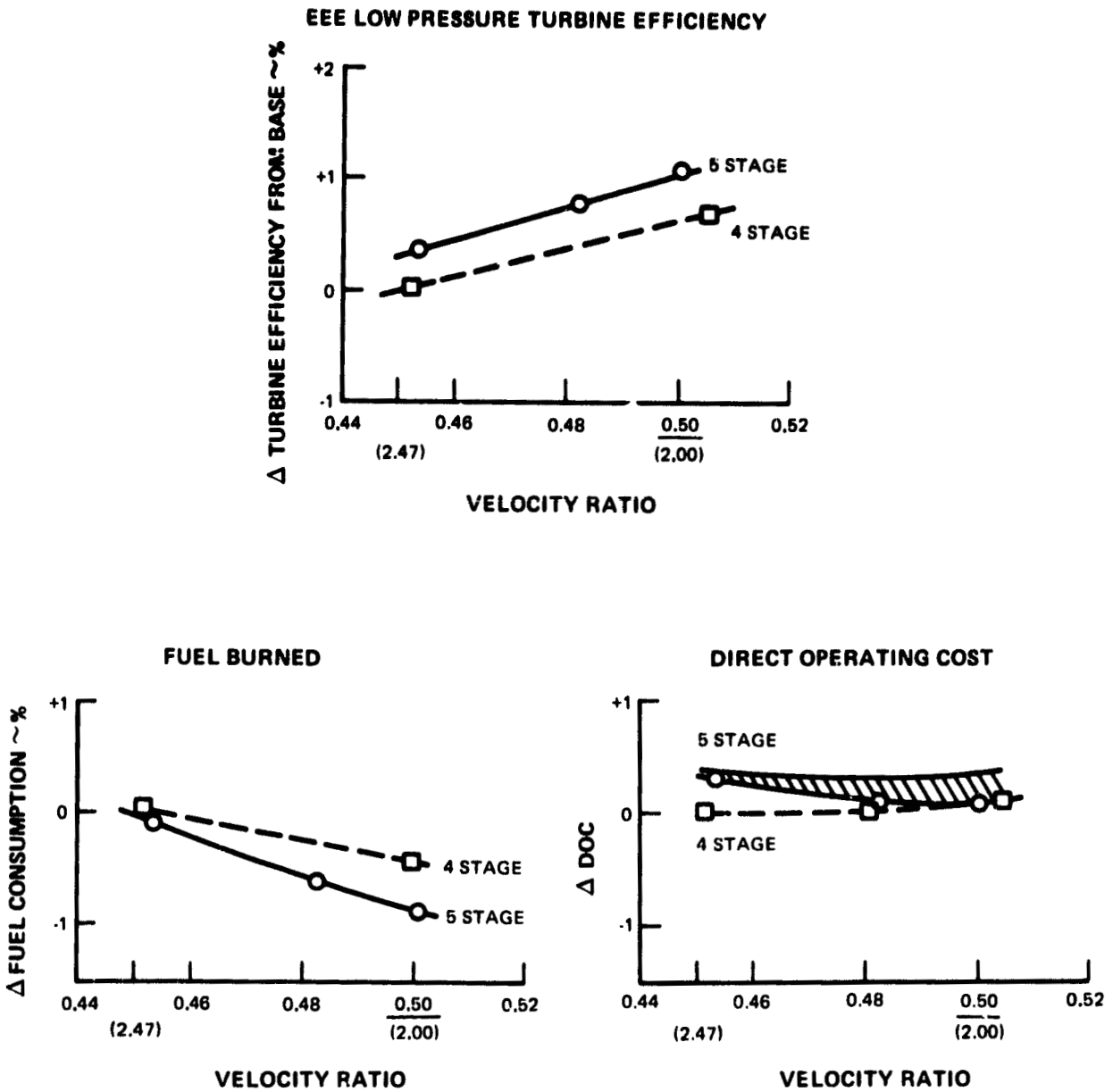

Figure 118 Low-Pressure Turbine. Results of four- and five-stage low-pressure turbine velocity ratio variation on efficiency, fuel burned, and DOC leading to selection of four-stage, 0.47 velocity ratio design.

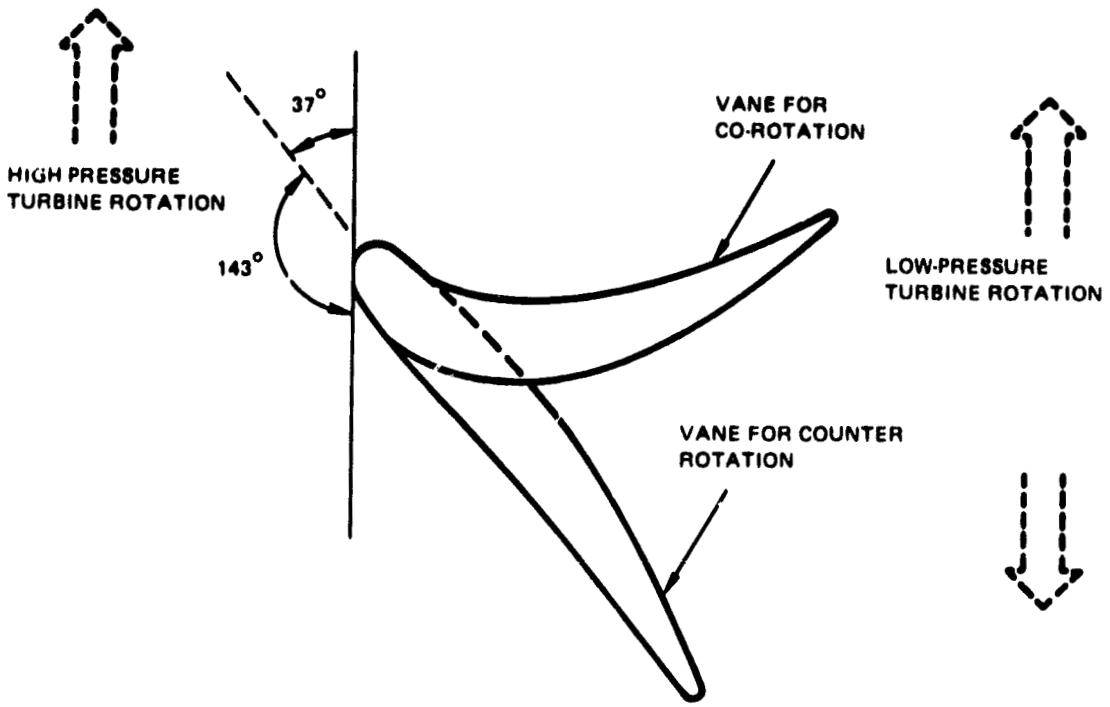

	COROTATION	COUNTERROTATION
VANE GAS INLET ANGLE	37.0°	143.0°
VANE GAS TURNING	100°	13°

COUNTERROTATION BENEFIT $\Delta\eta\% = 0.5$

Figure 119 Low-Pressure Turbine. Effects of direction of rotation on second vane contours and performance.

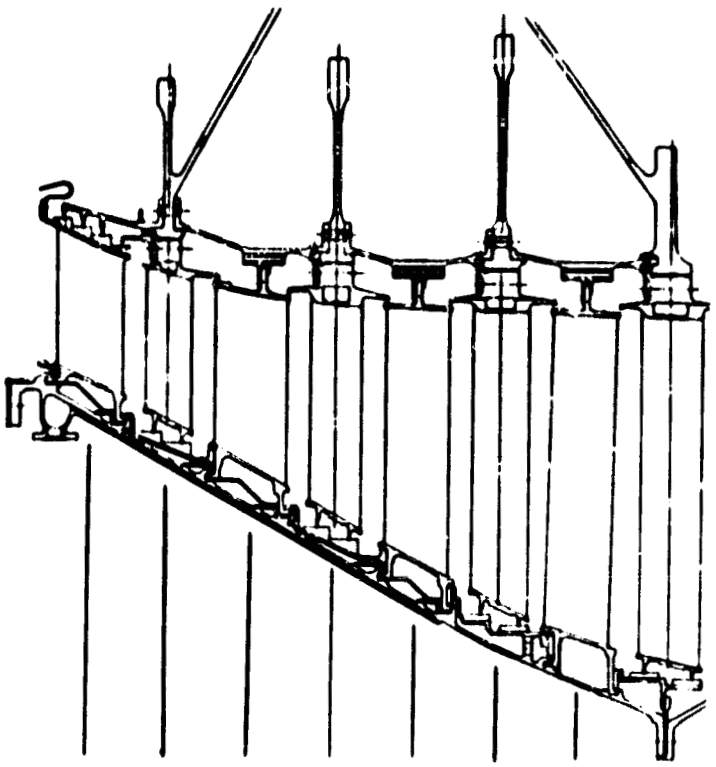

NUMBER OF AIRFOILS	64	116	84	104	87	94	102	108
MEAN VELOCITY RATIO/NASA LOAD FACTOR		0.45/2.47		0.47/2.26		0.48/2.17		0.50/2.00

Figure 120 Low-Pressure Turbine. Cross-section shows stage velocity ratios and airfoil count.

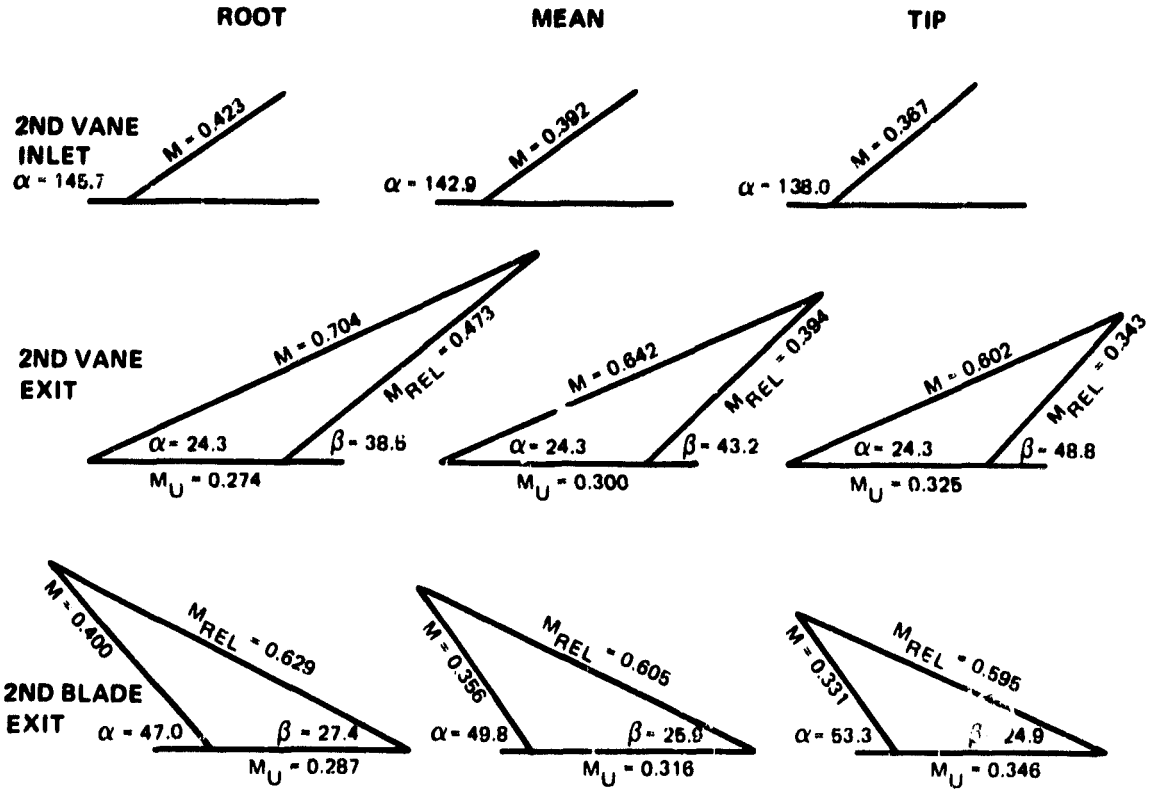

Figure 121 Second-Stage Low-Pressure Turbine. Velocity triangles show root, mean, and tip aerodynamics.

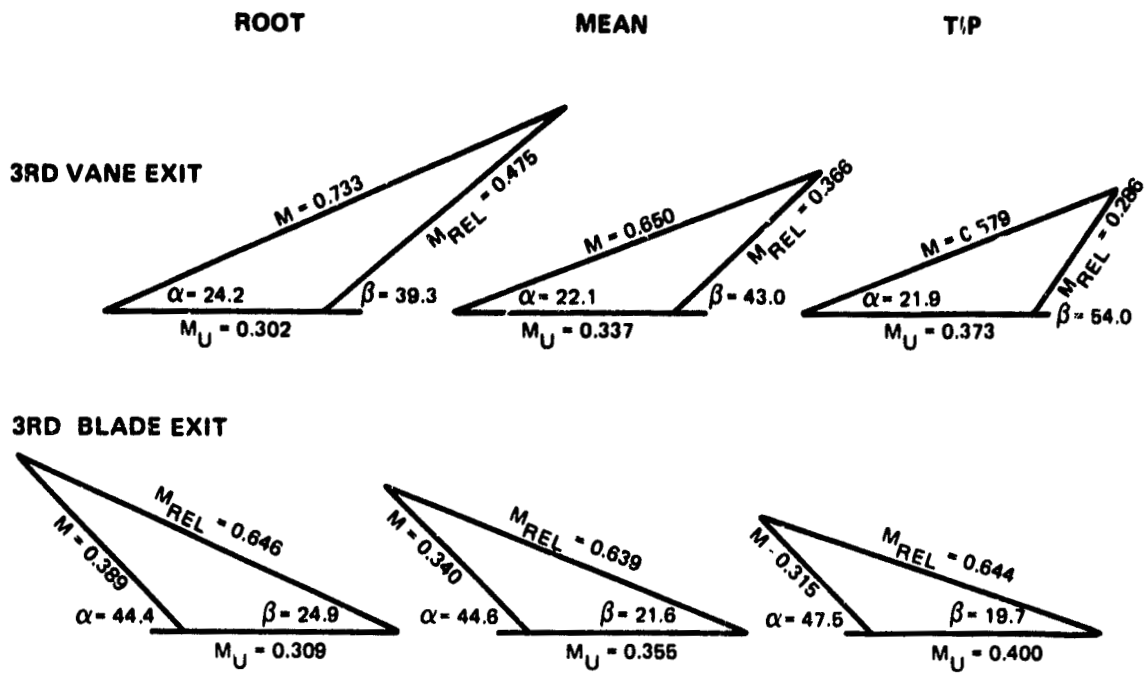

Figure 122 Third-Stage Turbine. Velocity triangles show root, mean, and tip aerodynamics.

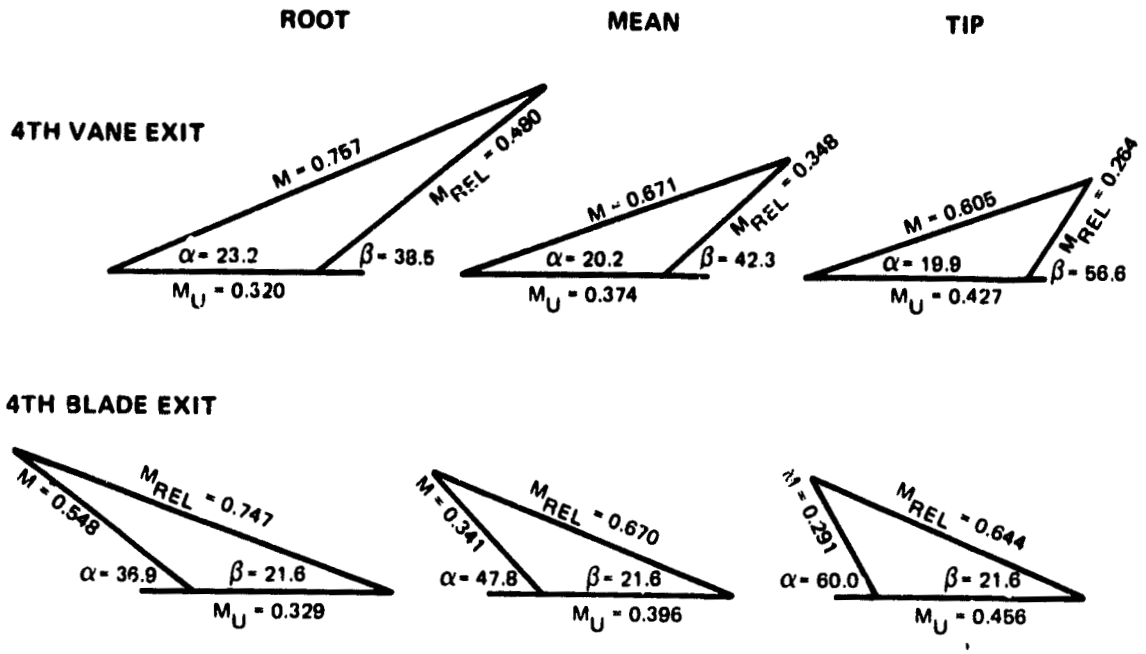

Figure 123 Fourth-Stage Turbine. Velocity triangles show root, mean, and tip aerodynamics.

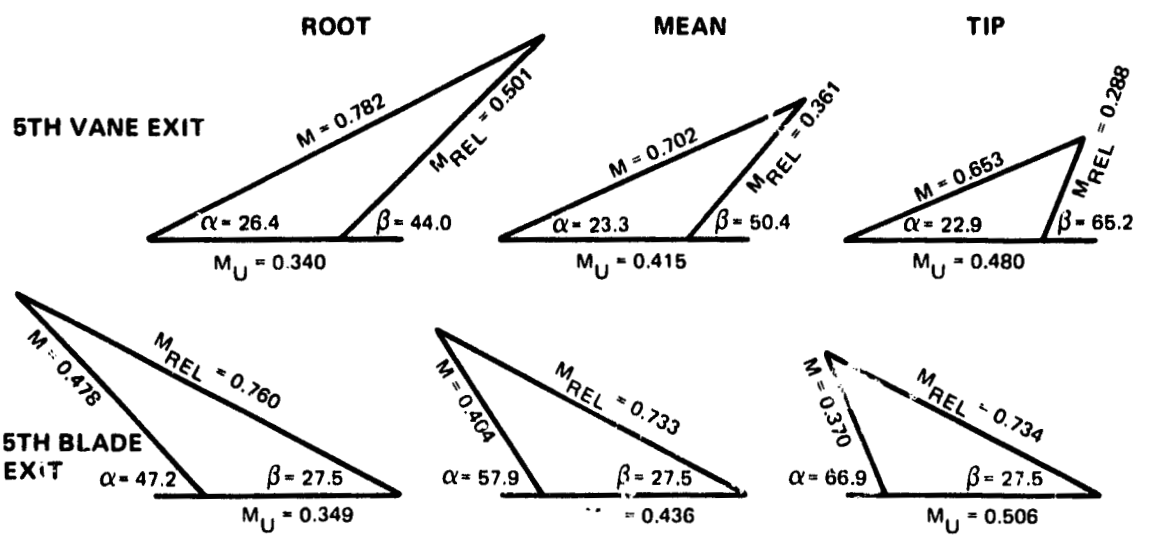

Figure 124 Fifth-Stage Turbine. Velocity triangles show root, mean, and tip aerodynamics.

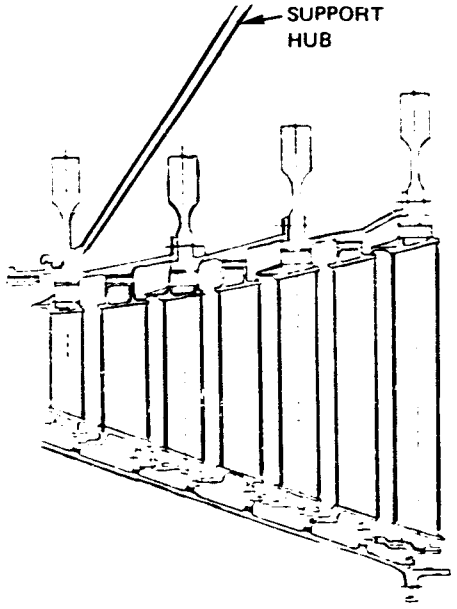

ORIGINALLY
PROPOSED
SCHEME NO. 1
(SINGLE SUPPORT HUB)

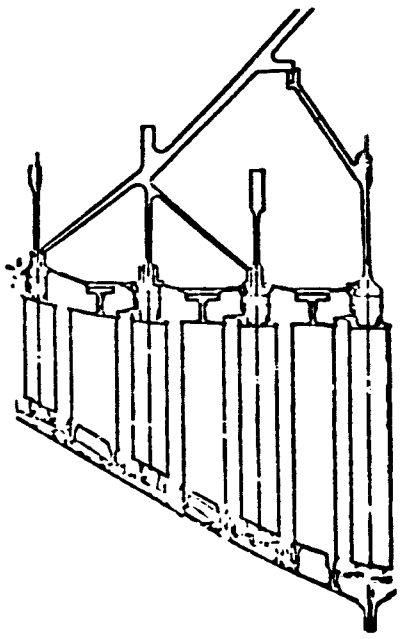

SCHEME NO. 2
(MULTIPLE SUPPORT
HUBS)

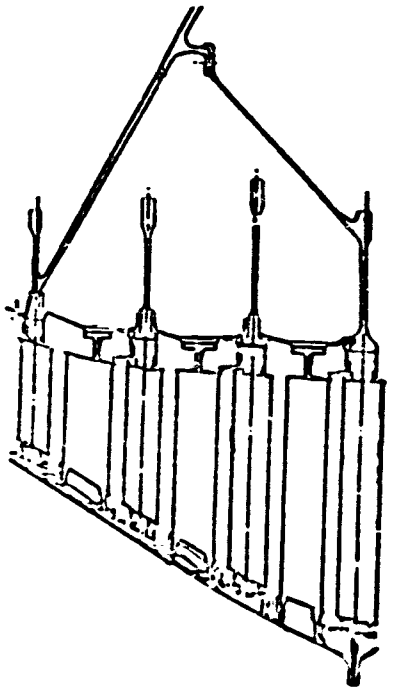

SELECTED SCHEME NO. 3
(TWO SUPPORT HUBS)

Figure 125 Low-Pressure Turbine. Candidates for rotor design including two-hub low-pressure turbine rotor selected.

pressure axial deflections at takeoff. Scheme No. 2 added the axial restraint required when analyzed in exactly the same manner but appeared to be unnecessarily complex. Rim cooling requirements and winged disk construction did not provide a simple rim cooling shield design so separate spacers with rim cooling shields were added. The hub design was simplified by revising the disk bores. Further thermal and structural analysis with the shell deck showed that Scheme No. 3 achieved the required axial deflections, had a more efficient cooling scheme, and was a simpler mechanical arrangement than Scheme No. 2. Scheme No. 3 was selected.

4.8.4.6 Rotor Life and Stress Analysis

A shell analysis on the rotor was used to determine the burst shape, general stress/deflection feasibility, and estimate the low cycle fatigue life of each component in the rotor. A mini-snap acceleration-deceleration cycle was analytically applied to the rotor which was modeled as a shell. This resulted in a stress excursion that was used to estimate the in-plane lives for the disk and hubs shown in Figure 126. All lives at the critical sections are predicted to exceed the requirements of the flight propulsion system and are considered to be feasible. Detail design of the low-pressure turbine rotor should result in burst limited shapes with predicted lives closer to the 20,000 - 30,000 mission requirement. When the design is optimized in detail design the rotor weight may be lower than the preliminary rotor as stresses are increased closer to their allowable limits.

4.8.4.7 Case Construction Selection

Three candidate case constructions evolved for the low-turbine case analysis shown in Figure 127. Blade tip clearance, thermal response, blade containment, structural support of vanes, turbine exhaust case, active clearance control, structural feasibility, and weight and cost all influenced the construction choice of the case. Two basic means of supporting the turbine vanes are by bolts or by case hooks. Weight trades showed the bolted design to be heavier than a hook design. In order to minimize leakage paths of cooling air, an inner wall was added to the design. By more efficient use of the cooling air, the case hook temperatures were lowered which allowed hook height to be reduced. This reduction allowed the outer case diameter to be reduced and thus a further weight savings was obtained with the double-walled construction.

The double-wall design also allowed high, heat transfer coefficients for the internal active clearance control design over the external design. Thus, reduced thermal growth and improved cruise clearances over external designs were obtained. The double-wall design also eliminated the tubes and bracketing hardware that was required with the external ACC design.

	ROTOR SECTION	CALCULATED LCF LIFE MISSIONS			
HUBS	A BOLT CIRCLE	$>10^5$			
	B COOLING HOLE	$>10^5$			
	C FILLET	$>10^5$			
DISKS		2ND STAGE	3RD STAGE	4TH STAGE	5TH STAGE
	D BORE	$>10^5$	$>10^5$	$>10^5$	$>10^5$
	E BOLT CIRCLE	$>10^5$	45,000	$>10^5$	—
	F RIM	$>10^5$	$>10^5$	$>10^5$	$>10^5$
BURST MARGIN		1.48	1.26	1.34	1.42

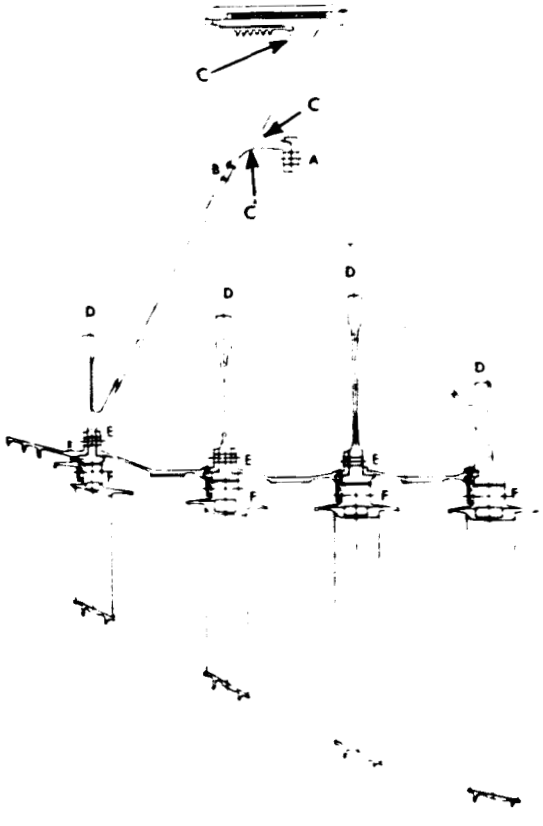

Figure 126 Low-Pressure Turbine. Rotor life predictions indicate adequate life.

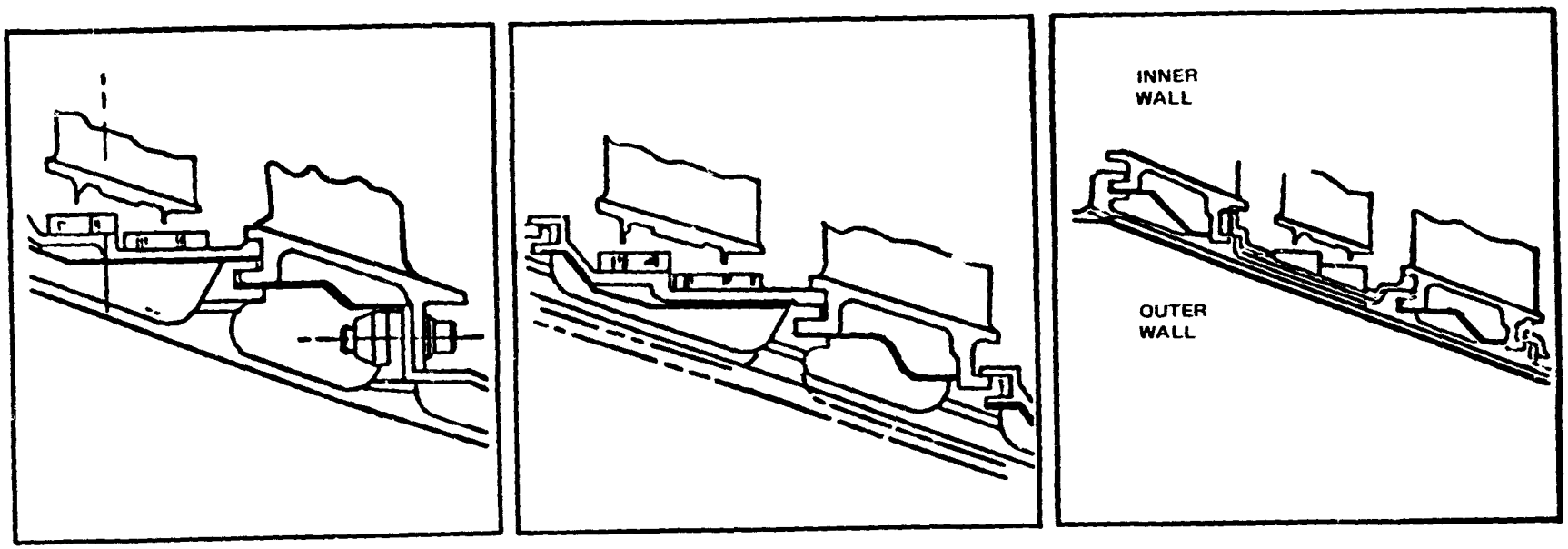

Figure 127 Low-Pressure Turbine Case. Configurations considered and double-wall case selected.

The double-walled design was chosen because it was lighter in weight, lower in cost and had a performance advantage over the bolted or hooked designs. It also offered the most flexibility to alter cooling air flow rates for changing structural and/or clearance requirements during development.

4.8.4.8 Case Stress Analysis

The double-walled design was modeled in a general shell analysis with pressures, temperatures and aerodynamic loads to obtain case stresses, deflections and transient radial growth at the blade tips. A mini-snap acceleration/deceleration transient cycle was applied to the case structure and the resultant stress and radial deflections used to calculate blade tip clearance. Case radial growth was plotted versus time against rotor radial growth. The results showed adequate closure between the case and blade tip to determine feasibility of attaining goal clearances.

The general shell deck was modeled using thicknesses that were machining-limited. A blade loss analysis was performed to see if the case would contain a blade in the event of a failure. Case analysis under each blade row showed that the thickness required to contain the blade was less than the machining limit of the material. Thus, the low pressure case construction didn't need to be thickened to satisfy containment requirements.

4.8.4.9 Blade and Vane Stress and Life

Vane and blade airfoil analyses were completed to determine the material, coating requirements and stresses in the low-pressure turbine airfoils. A preliminary life analysis was done on all four stages of uncooled clustered vanes cantilevered from the low turbine case. Gas bending moments at the vane tips were calculated and section properties for the second and fifth vane were used. Ratioed properties for the third and fourth vanes, which were based on the fifth-stage calculated values, were used in the analysis. The effects of clustering, outer fiber relaxation and JT9D metal temperature and coating experience are including in the life predictions. Figure 128 shows the LPT vane materials, failure mode and fatigue lives of all turbine airfoils. All airfoils are predicted to meet the life requirements of the flight propulsion system.

4.8.4.10 Stage Vibration

Preliminary calculations were made to determine the stage resonance and flutter characteristics of the low-pressure turbine rotors. Only the second and fifth stages of the turbine were analyzed because if these stages met the vibration criteria, all stages could be made to meet the criteria. The fifth stage resonance diagram for the coupled blade disk vibration is shown in Figure 129. The 3E first mode resonance has an

AIRFOIL TYPE	STAGE	MATERIAL/COATING	FAILURE MODE	LIFE (HRS)
VANE	2ND	MERL 220 (SINGLE CRYSTAL) / MERL 700 (NICRALY)	OXIDATION EROSION	>15,000*
	3RD	PWA 655 (INCONEL 713C) / PWA 73 (AL-SILICON)	CREEP	>15,000
	4TH	PWA 655 (INCONEL 713C) / NO COATING	CREEP	>15,000
	5TH	PWA 655 (INCONEL 713C) / NO COATING	CREEP	>15,000
BLADE	2ND	PWA 1422 (MAR-M 200 + Hf) / PWA 273 (DIFFUSED ALUMINIDE)	CREEP UNTWIST	>15,000
	3RD	PWA 655 (INCONEL 713C) / PWA 73 (AL-SILICON)	CREEP UNTWIST	>15,000
	4TH	PWA 655 (INCONEL 713C) / NO COATING	CREEP UNTWIST	>15,000
	5TH	MERL 101 (TI-AL) / NO COATING	CREEP UNTWIST	>15,000

*SCRAP LIFE (>9000 HRS.COATING LIFE)

Figure 128 Low-Pressure Turbine. Airfoil materials, predicted failure modes, and predicted lives that meet requirements.

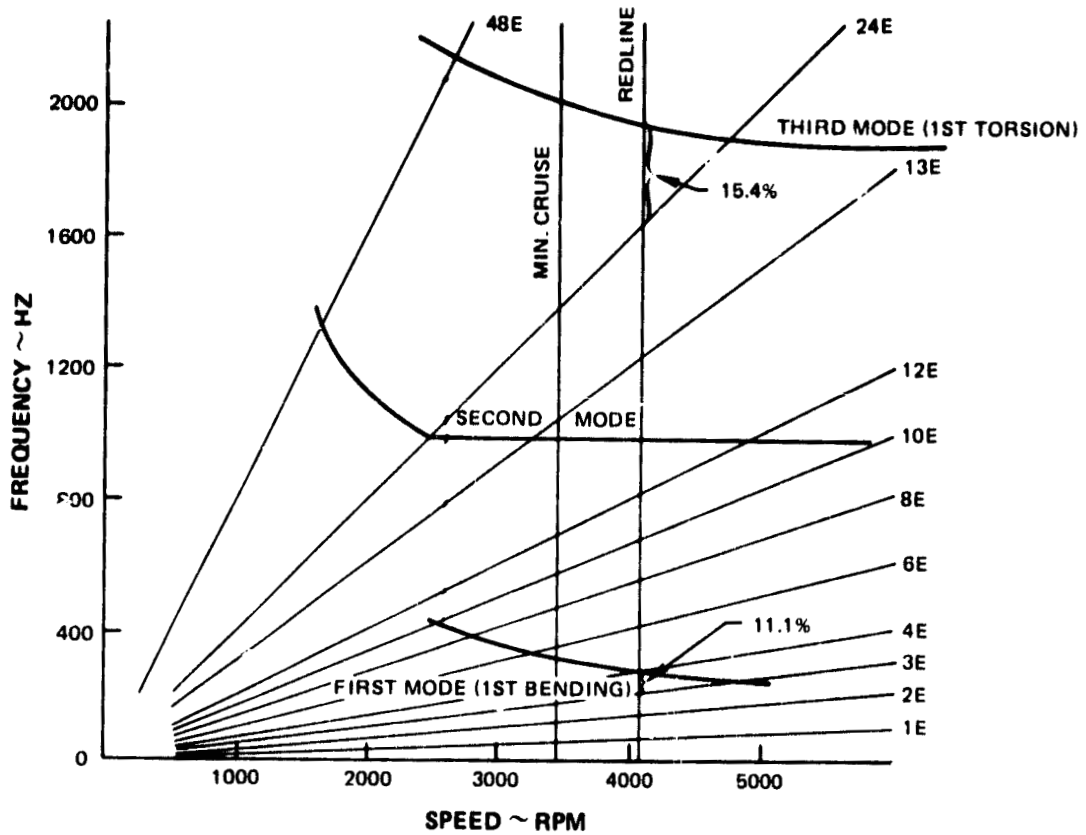

Figure 129 Fifth-Stage Turbine. Resonance diagram indicates adequate vibration margins.

11.1 percent frequency margin at redline. The 24E, exit guide vane order, third mode resonance has a 15.4 percent frequency margin at redline. A flutter analysis of this stage along with the second stage showed both to be stable in the operating range, as shown on Figure 130. This flutter analysis was based on the streamline generated for these two stages. The second stage exhibited no one-, two-, or three-excitation order resonances near the engine operating range. A rim thickness revision was necessary to drop 14E, the number of turbine intermediate case struts, first mode resonance, below the operating range. The change gives the required frequency margin at minimum cruise for the second stage.

The conclusion of this analysis is that low order resonances in the low pressure turbine can be tuned out of the engine operating range and all stages meet the criteria for stage vibration and flutter.

4.8.4.11 Attachment Stress Prediction

An attachment analysis for the blades and disks was performed to calculate critical stress levels. The preliminary design of the turbine blade attachment included the blade platform, selection of the broach shape and balancing of the blade root and airfoil loads at the attachment. The attachment design is limited by allowable stress levels or life requirements, section modulus (Z-ratio) and resonant frequency margin. Calculations of disk lug and blade attachment conventional stresses (bending, shear, bearing, and tensile) were performed on the rim widths and pitch that were established by the stage vibration analysis. A summary of this analysis is found on Figure 131. All disk and blade attachments have stresses that are well within Pratt & Whitney Aircraft experience.

4.8.5 Design Summary

The results of the low-pressure turbine preliminary design are shown in Table 48. All requirements set for the Energy Efficient Engine low-pressure turbine preliminary design were achieved. The aerodynamics and rotor tip clearances necessary for high efficiency were obtained while achieving the life requirements of a commercially acceptable low pressure turbine.

4.9 TURBINE EXHAUST CASE ASSEMBLY

4.9.1 Design Requirements

The turbine exhaust case supports the exhaust mixer and tailcone, and transfers loads from the nacelle to the engine. The case includes exit guide vanes to remove the low-pressure turbine discharge residual swirl and as such, has a very important effect on the overall engine performance, weight, and cost. The basic aerodynamic requirement of the turbine exhaust case is to redirect the exhaust gas from the turbine into the exhaust gas mixer, without separation and with minimum loss.

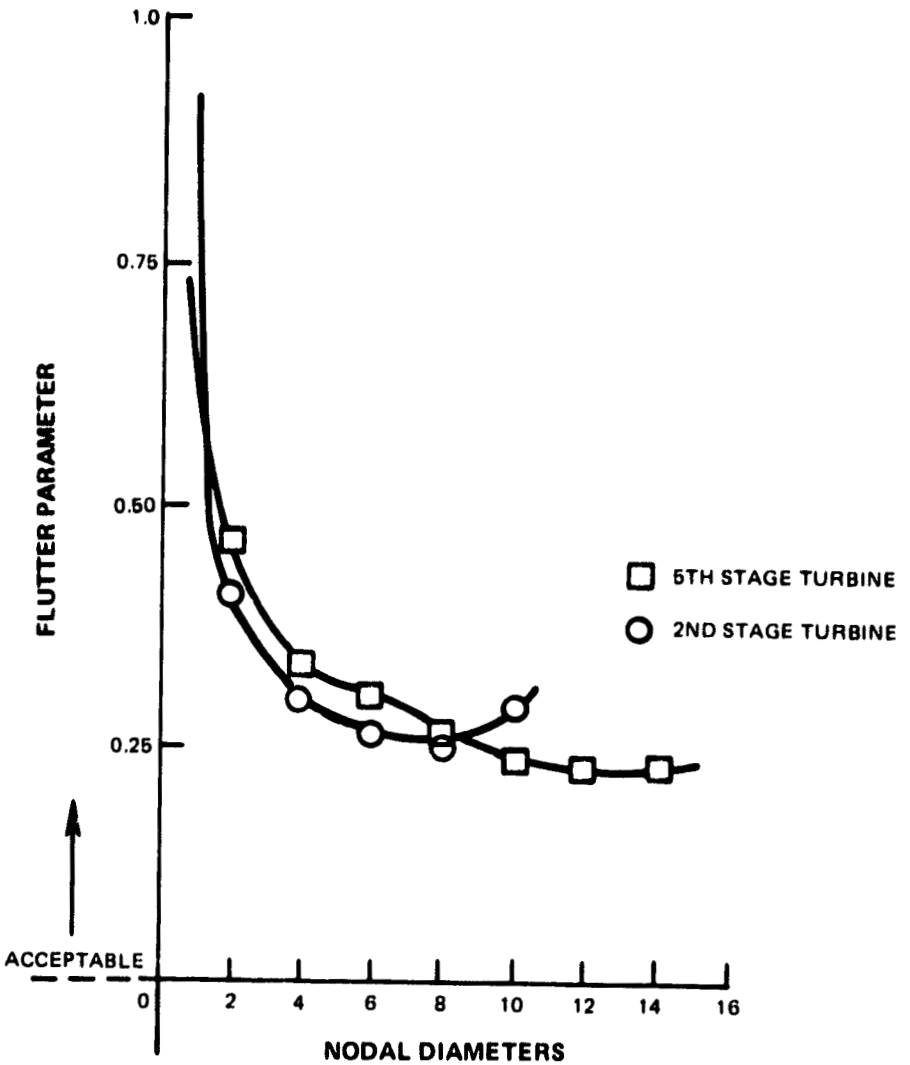

Figure 130 Second- and Fifth-Stage Turbine. Flutter analysis results indicate positive stability margins in both stages.

STRESS -N/M^2 (KSI)	2ND STAGE	3RD STAGE	4TH STAGE	5TH STAGE
BEARING	(56)	(70)	(43)	(40)
DISK SHEAR	(14)	(19)	(12)	(12)
BLADE SHEAR	(14)	(18)	(11)	(11)
DISK P/A	(15)	(17)	(14)	(15)
BLADE P/A	(11)	(13)	(10)	(11)

Figure 131 Low-Pressure Turbine. Blade attachment region stress results are well within P&WA experience.

The turbine exhaust case has many structural requirements because it interfaces with the nacelle and oth engine assemblies. Table 49 summarizes the case design requirements.

4.9.2 General Configuration Description

4.9.2.1 Mechanical Features

The turbine exhaust case (TEC) cross-section is shown in Figure 132. The TEC is a integral ring-strut-ring structure with the 24 airfoil shaped struts which serve as the low-pressure turbine exit guide vanes.

The inner ring supports the tailplug. The outer ring/case supports the mixer, carries the loads form cowl load transfer ring, and transfers the loads forward through the low-pressure turbine case and to the rear mounts.

The TEC is made of MERL 101, an advanced titanium-aluminum alloy, and is fabricated by butt welding sheet metal vanes between two fully machined inner and outer wrought rings, which have airfoil shaped standups matching the vane contours. The vane airfoils may be fabricated by conventional welding and subsequent closed die forming or more directly by a one-step superplastic forming/diffusion bonding advanced fabrication technique.

4.9.2.2 Aerodynamic Features

The aerodynamic design includes

1. NACA 65 series exit guide vane airfoils

2. Minimized endwall curvative and

3. Exit area based on mixer inlet requirements

The mean swirl angle of the low-pressure turbine exhaust flow is 31 degrees. The amount of swirl to be removed by the exit guide vanes remains to be established.Therefore, two exit guide vane designs with 0 and 10 degrees residual exit swirl have been designed and evaluated.

4.9.2.3 Technology Development Requirements

A turbine exit guide vane test program is planned to verify the preliminary design and to provide the exit guide vane part of the design data required to select a residual swirl into the mixer.The test rig will be a full annular cascade with the 24 exit guide vanes and inlet vanes to create the low-pressure turbine exit flow swirl. Tests will be conducted with both 0 and 10 degree exit swirl vanes.

TABLE 48

LOW-PRESSURE TURBINE PRELIMINARY DESIGN RESULTS
AERODYNAMIC DESIGN POINT

Expansion Ratio	5.60
Mean Velocity Ratio	0.47
Maximum Disk Rim Speed, m/sec (ft/sec)	198 (650)
Adiabatic Efficiency, %	91.5
Life	
Blades, hr.	15,000
Vanes, hr.	15,000
Disks, missions	20,000

TABLE 49

TURBINE EXHAUST CASE DESIGN REQUIREMENTS

Aerodynamic

1. Exit Mach No. of 0.33 to 0.35
2. Minimal duct pressure loss
3. Two designs with exit swirl angles of 0 and 10 degrees
4. Reynolds number than 2.5×10^5 at exit guide vane leading edges.

Structural/Mechanical

5. Meet required design life of 30,000 hours and 20,000 missions
6. Provide radial and trunnion springrates of the ring-strut-ring structure that tune tailplug pitch and bounce vibratory modes outside the excitation frequency.

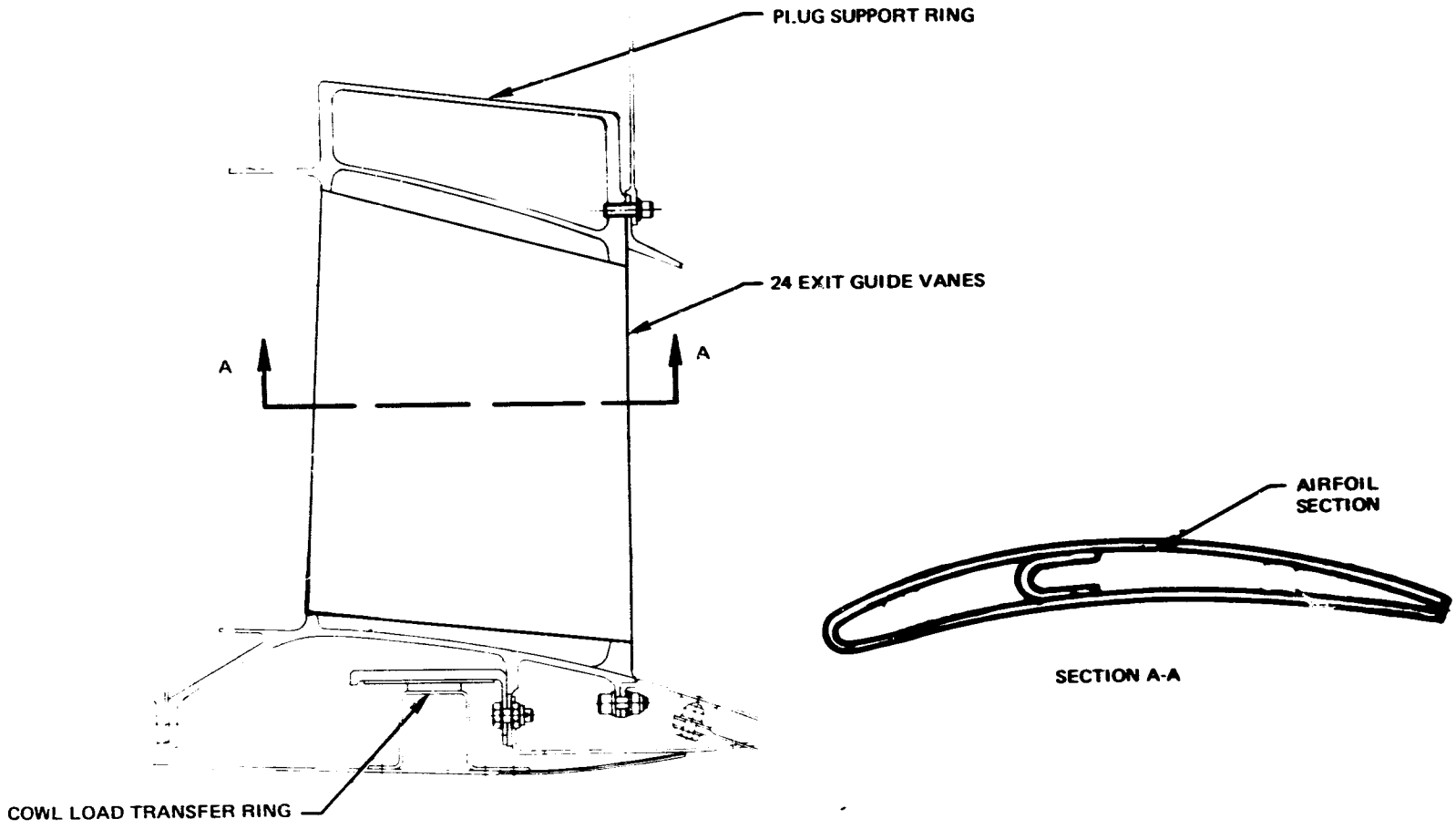

Figure 132 Turbine Exhaust Case. Cross-section shows exit strut and major features.

Data will be taken at the aerodynamic design point and off-design vane incidence angles. This data will include

1. Spanwise total inlet pressure and air angle at exit guide vane inlet and exit locations

2. Outside and inside diameter wall static pressure at various locations

3. Exit guide vane airfoil static pressure distribution

4. Spanwise total pressure and air angle vs. circumferential location between vanes

4.9.3 Supporting Analyses

4.9.3.1 Flowpath Shape

The flowpath, shown in Figure 133, was optimized with the Pratt & Whitney Aircraft two-dimensional streamline design system. The inlet and exit swirl angles, and Mach numbers are shown in Tables 50 and 51 for the 0 and 10 degree exit swirl configurations. The streamline analysis was also used to determine the exit guide vane airfoil shape and to predict pressure losses.

The exit guide vanes are NACA 65 series circular arc airfoils in the preliminary design. The detail airfoil design will be done using the turbine airfoil design system during the detail design to finalize the geometry.

4.9.3.2 Pressure Loss Prediction

The total pressure loss ($\Delta P_T/P_T$) was determined using compressor cascade curves that predict $\Delta P_T/P_T$ as a function of Mach Number, gap/chord ratio and turning. The predicted $\Delta P_T/P_T$ is 1.1% and 0.9% for the 0 and 10 degree exit swirl configuration, respectively.

4.9.3.3 Life Predictions

The structural feasibility of the preliminary design is based on operational experience with similar structures in more severe thermal environments which were fabricated from current, lower strength material.

A three-dimensional NASTRAN analysis of the ring-strut-ring structure was performed to determine trunnion and radial springrates. These springrates were used to determine the vibratory resonances of the tailplug. The turbine exhaust case structure was resized as needed to tune the tailplug pitch and bounce vibratory modes out of the operating speed ranges.

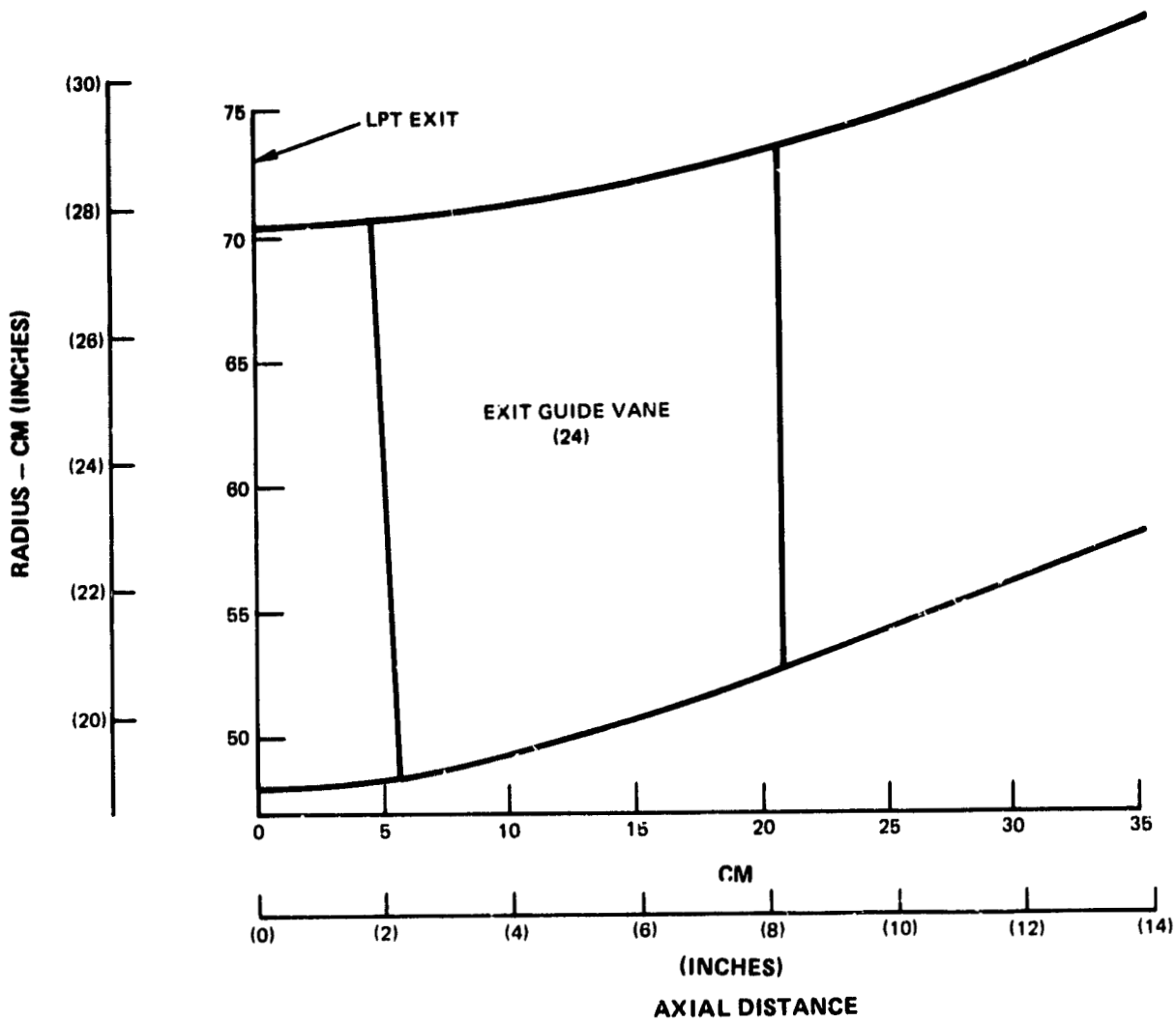

Figure 133 Turbine Exhaust Case. Flowpath geometry indicates shape required to provide minimum loss transition into exhaust mixer.

TABLE 50

LPT EXIT GUIDE VANE GEOMETRY AND AERODYNAMIC PARAMETERS (0 DEGREE EXIT SWIRL)

	Root	Mean	Tip
Airfoil Type*	65 C/A	65 C/A	65 C/A
Chord Length cm (in)	15.88 (6.25)	16.08 (6.33)	16.21 (6.38)
Number of Foils	24	24	24
Radius cm (in)	52.71 (20.75)	61.66 (24.275)	70.61 27.80
$_1$ Gas Degrees	49.25	58.72	69.15
$_2$ Gas Degrees	90.0	90.0	90.0
M_1	0.433	0.394	0.409
M_2	0.344	0.342	0.395

*NACA series airfoils for PDR feasibility; contoured airfoils will be examined during detail design.

TABLE 51

LPT EXIT GUIDE VANE GEOMETRY AND AERODYNAMIC PARAMETERS (10 DEGREE EXIT SWIRL)

	Root	Mean	Tip
Airfoil Type*	65 C/A	65 C/A	65 C/A
Chord Lenght cm (in)	16.51 (6.5)	16.51 (6.5)	16.51 (6.5)
Number of Foils	24	24	24
Radius cm (in)	52.71 (20.75)	61.66 (24.275)	70.61 27.80)
$_1$ Gas Degrees	48.8	58.7	69.5
$_2$ Gas Degrees	100.0	100.0	100.0
M_1	0.431	0.395	0.412
M_2	0.350	0.348	0.401

*NACA series airfoil for PDR feasibility detail; contoured airfoils will be examined during detail design.

The predicted tailplug resonant frequencies are given in Table 52.

4.9.4 Design Summary

The turbine exhaust case preliminary design configuration meets all of the design requirements. The results of the turbine exit guide vane test program will be used to verify the aerodynamic design and will be used, along with mixer tests, to select the final swirl angle.

4.10 MIXER/TAILPIPE

4.10.1 Design Requirements

Design requirements for the mixer and exhaust system were established by design and off-design engine cycle definitions. Table 53 summarizes the aerodynamic, mechanical, and structural design requirements. The mixer efficiency goal is also shown.

Performance requirements were established at the 10,668m (35,000 ft) aerodynamic design point, which is located between the two key performance oriented operating conditions of maximum climb and maximum cruise. Structural requirements were defined based on commercial engine acceptability.

4.10.2 Design Background

Pratt & Whitney Aircraft related exhaust mixer experience, based on a combination of scale model investigations and full scale engine tests, underlies the overall level of mixer efficiency projected for the Energy Efficient Engine.

High bypass ratio (approximately 5) exhaust mixer model tests provided the trend of mixer efficiency with mixing length ratio for early first generation mixer designs. The aggressiveness of the Energy Efficient Engine design is associated with its very short mixing length.

Recent mixer experience provides an example of how precision tailoring of basic design contours can improve mixer efficiency. With a mixer configuration typical of the JT8D-217 engine design, a large improvement of 15 percent in efficiency was achieved by scalloping the side panels of each convolution.

The use of sub-scale models has proven to be a convenient, economical way to estabish exhaust system characteristics. A comparison of model and full scale performance is illustrated in Figure 134. Agreement is well within acceptable limits at both takeoff and cruise conditions.

TABLE 52

SUMMARY OF TAILPLUG RESONANT FREQUENCY ESTIMATES

Vibratory Modes	Resonant Frequency
Pitch	4,800 rpm
Bounce	20,000 rpm

TABLE 53

MIXER/TAILPIPE DESIGN REQUIREMENTS
AERODYNAMIC DESIGN POINT

Aerodynamic Parameters	
Duct Stream Pressure Loss, %	0.18
Primary Stream Pressure Loss, %	0.24
Tailpipe Pressure Loss, %	0.34
Thrust Coefficient	0.996
Efficiency Goal	
Mixer Efficiency, %	85
Mechanical/Structural	
Mixer Length	50% of Current State-of-the-Art
Tailpipe Length	70% of Current State-of-the-Art
Number of Lobes	12
Life	30,000 Missions

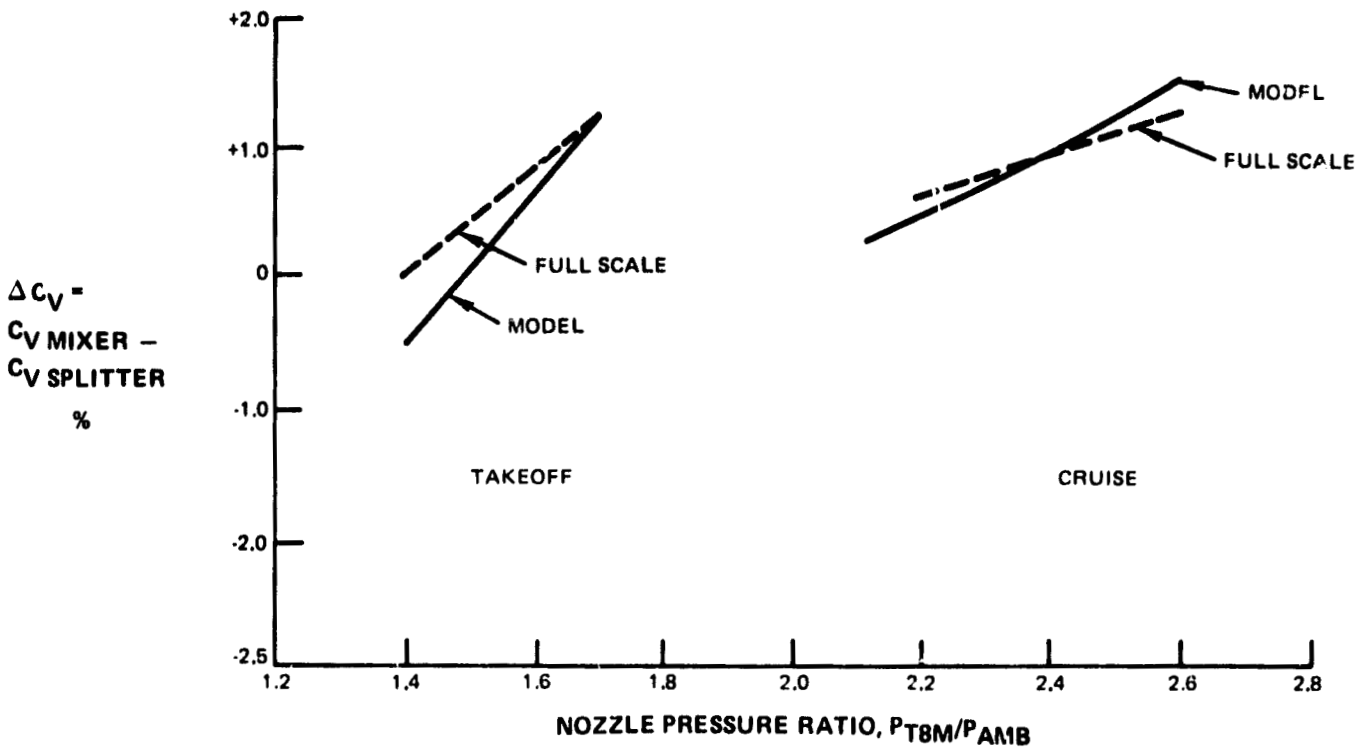

Figure 134 Thrust Coefficient. Comparison shows good agreement between model and full-scale JT8D-209 performance test results.

4.10.3 General Configuration Description

4.10.3.1 Major Subassemblies

The mixer/exhaust system consists of a convoluted 12-lobe scalloped mixer arranged around a central plug, housed within a converging tailpipe (Figure 135. The mixer and the rear half of the plug will be fabricated of titanium to minimize weight. The forward half of the plug is acoustically treated and of a high temperature nickel alloy (e.g. Inconel 625). The mixer is supported from the turbine exhaust case outer flange and by I.D. support struts attaching it to the central plug. These struts are capable of axial motion necessitated by the differential thermal growth between the plug and the mixer. The mixer is further stabilized by a titanium vibration damper on each outer lobe.

The mixer is symmetrical with equally spaced lobes. The lobes are tapered toward the exit plane to better control the area distribution in the primary flowpath.

The tailpipe is acoustically treated with aluminum perforated plate brazed to titanium honeycomb. The exhaust system also includes the aerodynamic fairing of the structural aircraft pylon, located upstream of the turbine exhaust case. The fairing is blended into the top lobe of the mixer, ending in a point slightly downstream as it intersects the tailpipe.

4.10.3.2 Vibration Damper

The vibration damper, illustrated in Figure 136, is designed to counteract the anticipated vibratory modes of the mixer. The damper is essentially a hood fitted to each lobe, attached to the mixer lobe at the downstream end, and wrapped around the scalloped outer edge. The damper extends upstream where it is held in an adjustable friction attachment. The temperatures anticipated in the mixer are also shown in Figure 136 for both takeoff and reverse conditions. In the reverse thrust mode, the fan stream is exhausted upstream of the mixer through the thrust reverser, but the primary flow is not diverted. Therefore, the mixer reaches the maximum operating temperature during the reverse thrust mode. The damper itself could be ventilated, if necessary, to prevent a heat build-up between the damper and mixer lobe. There are presently no thermal problems anticipated in the damper design.

4.10.3.3 Principal Aerodynamic Design Parameters

The principal aerodynamic parameters selected for the Energy Efficient Engine mixer are presented in Table 54. These parameters are compared relative to the technology level demonstrated in prior mixer programs that constitute the current state-of-the-art. The mixer length was aggressively set at one-half that of of previously tested high performance configurations. Analytical evaluations of the mixer design indi-

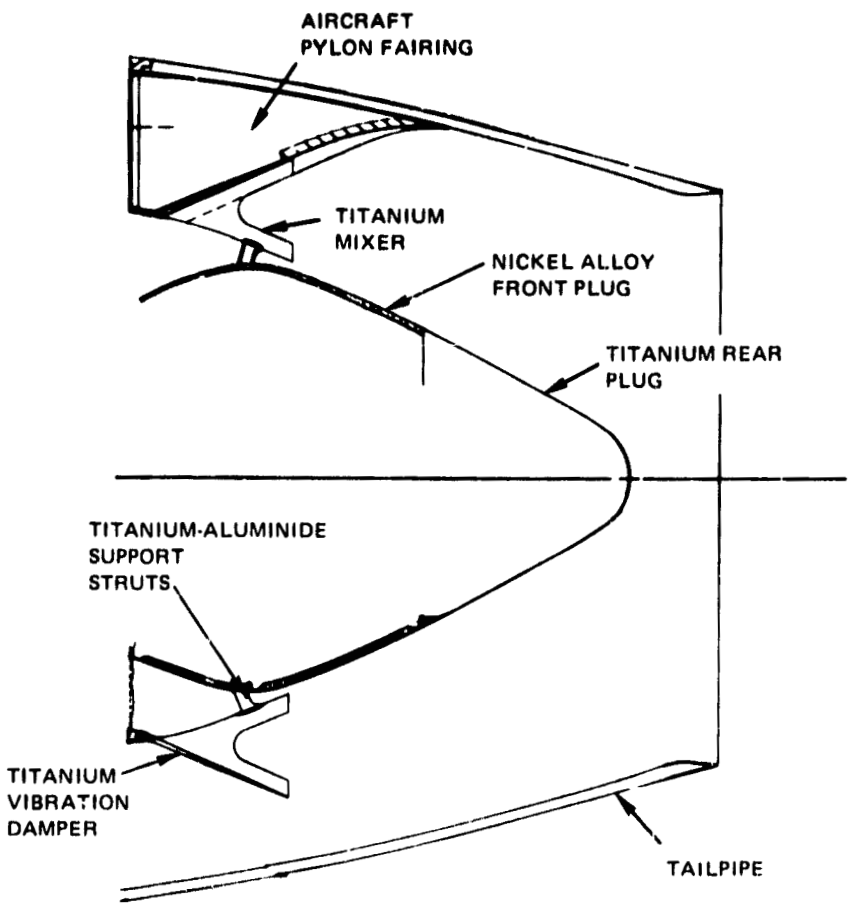

Figure 135 Mixer/Exhaust System. Cross-section shows major features.

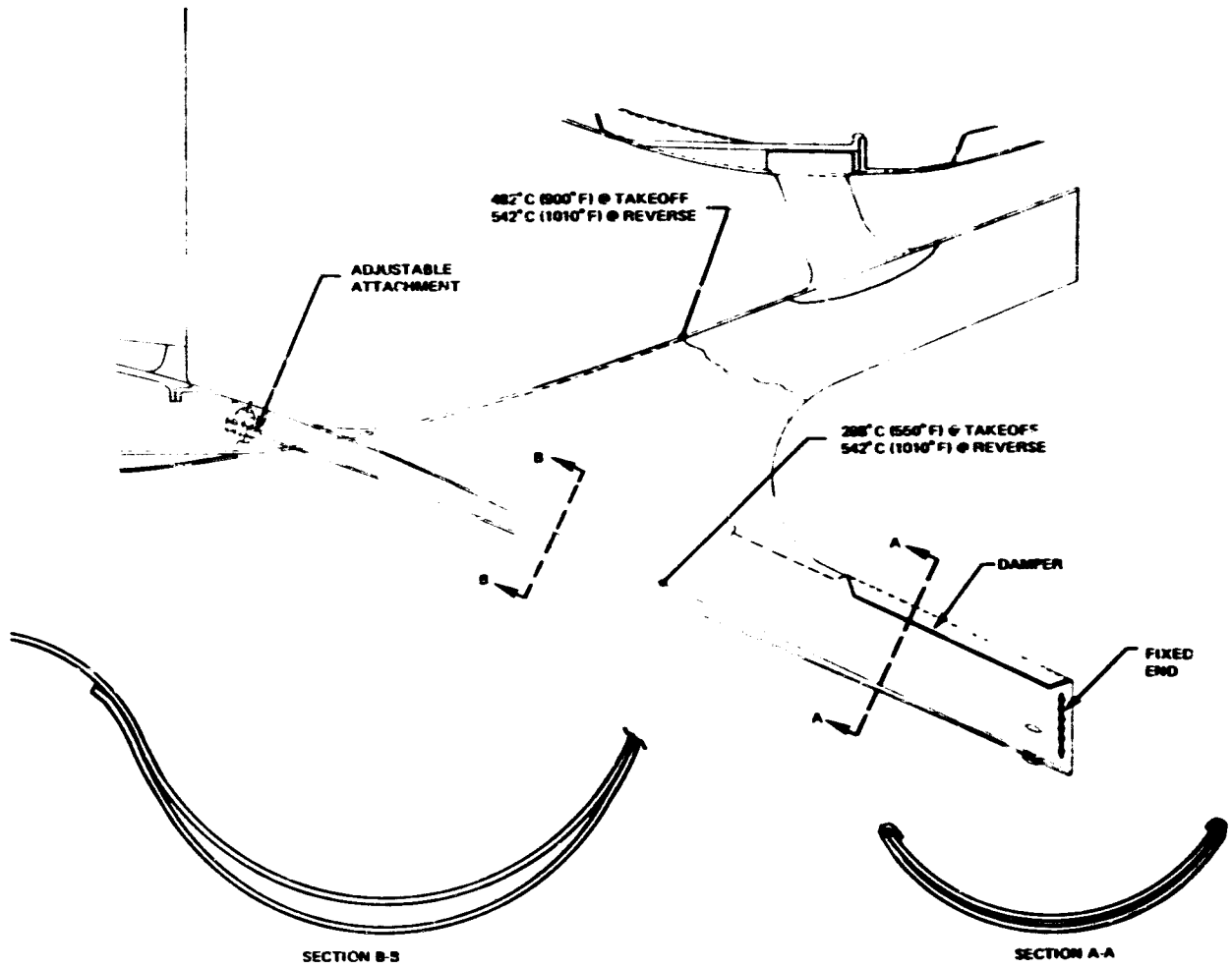

Figure 136 Mixer Outer Lobe Damper. Arrangement shows configuration selected to control vibrations.

TABLE 54

MIXER/EXHAUST SYSTEM AERODYNAMIC DESIGN SUMMARY
AERODYNAMIC DESIGN POINT

Mixer of Lobes	12
Relative Mixer Length	0.5 X Current State-of-the-Art
Relative Tailpipe Length	0.7 X Current State-of-the-Art
Mixing Efficiency	85%
Engine-to-Duct Stream Temperature Ratio	2.55
Engine-to-Duct Stream Pressure Ratio	0.91
Duct Stream Mach Number	0.55
Engine Stream Mach Number	0.42
Inlet Swirl Angle, degrees	0 to 10

cate no inherent flow separation problems, so the basic envelope of the mixer should be capable of high performance. The tailpipe length was also aggressively set at 70 percent of the current design levels. The effects of this length reduction may be offset by careful tailoring of the mixer exit geometry to further promote mixing between the two streams. The mixing efficiency projected for the Energy Efficient Engine is the same as demonstrated with existing designs; however, the reduced system length promotes an increasingly aggressive design.

4.10.3.4 Technology Development Requirements

A broad technology program has been initiated as part of the Energy Efficient Engine Component Development and Integration Program to achieve the performance goals selected for the Energy Efficient Engine mixer/exhaust system. The technology program will consist of a series of scale model tests aimed at quantifying the significance of the major mixer design parameters. These parameters are illustrated in Figure 137. The matrix of test configurations will be centered on the current flight propulsion system exhaust nozzle design. Variations in mixer length and contour will also be evaluated. The results of the scale model technology program will be incorporated into the design of the flight propulsion system, providing a continuous update of the actual design as information becomes available.

4.10.4 Supporting Analyses

4.10.4.1 Damper Concept Selection

During the design of the mixer, many concepts to stabilize the outer lobes of the mixer were considered. Several schemes are illustrated in Figure 138. Scheme A involves banding the whole mixer with a ring near the aft portion of the mixer. Plans for this arrangement were discarded because of potentially high pressure losses and thermal gradient problems. The outer ring containing the mixer lobes can be replaced by a series of radial struts as illustrated in Scheme B; however, the same problems exist. Another method of controlling the outer lobes of the mixer is shown in Scheme C. A series of diagonal struts could be incorporated, connecting the outer lobe to the inner lobe and to the short strut linked to the central plug. These design concepts would also engender significant performance losses. The damper design presented in Scheme D is the concept initially selected for the Energy Efficient Engine. This is a simple design, having a potentially low performance loss. In addition, it provides the capability of resolving identified critical frequency problems without completely revamping the concept.

4.10.4.2 Pressure Loading Analysis

The predicted static pressure loads acting on the mixer are illustrated in Figure 139. The maximum stress in the mixer is predicted at the

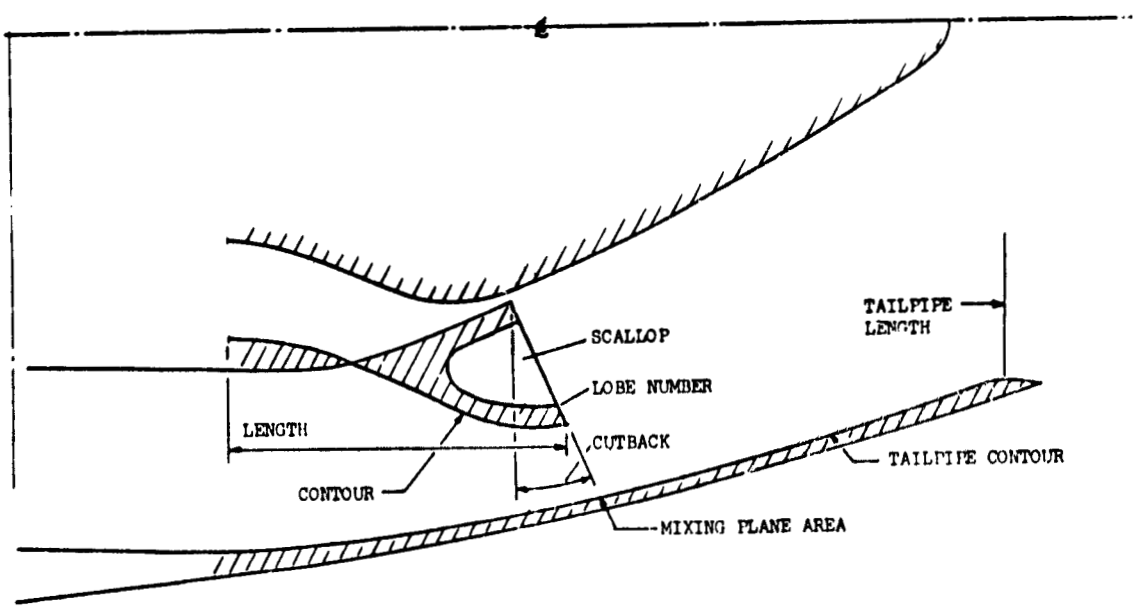

Figure 137 Mixer Technology Program. Mixer/exhaust system test variables are illustrated.

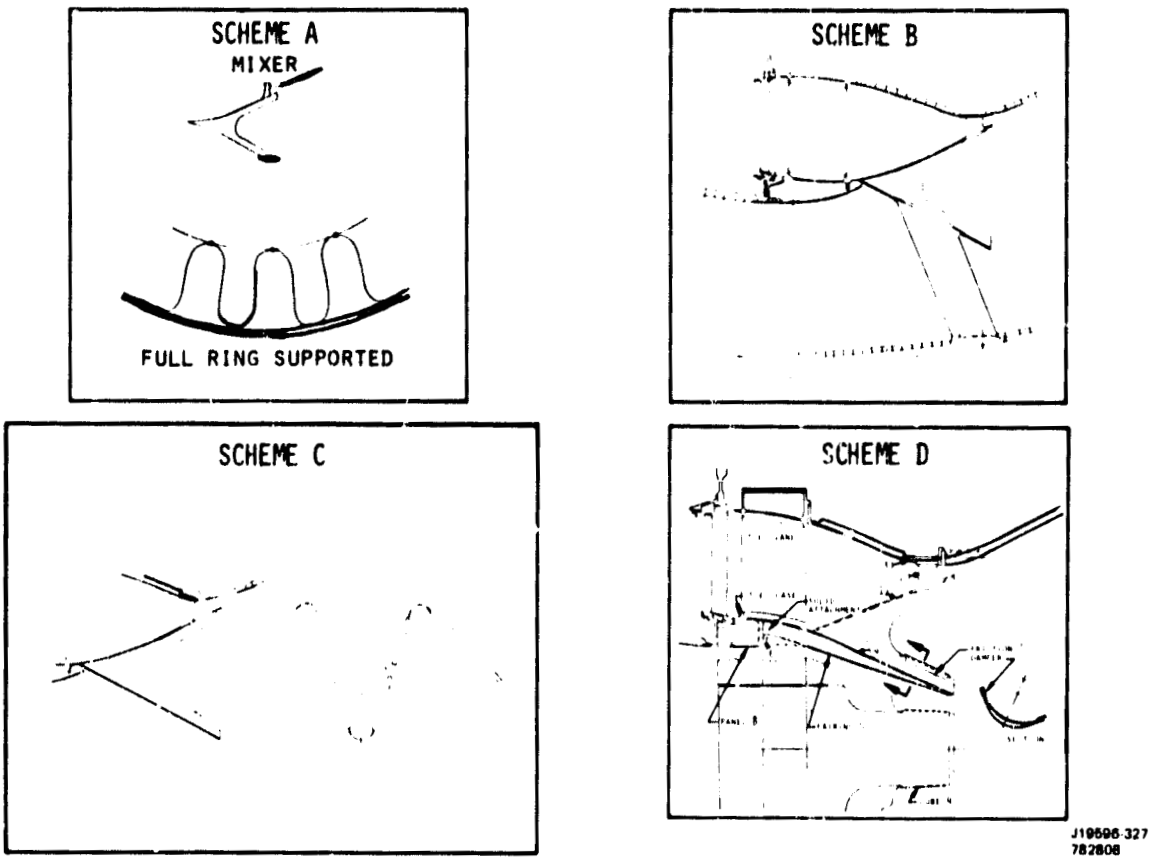

Figure 138 Mixer Outer Lobe Support. Drawings illustrate candidate configurations considered for damped design.

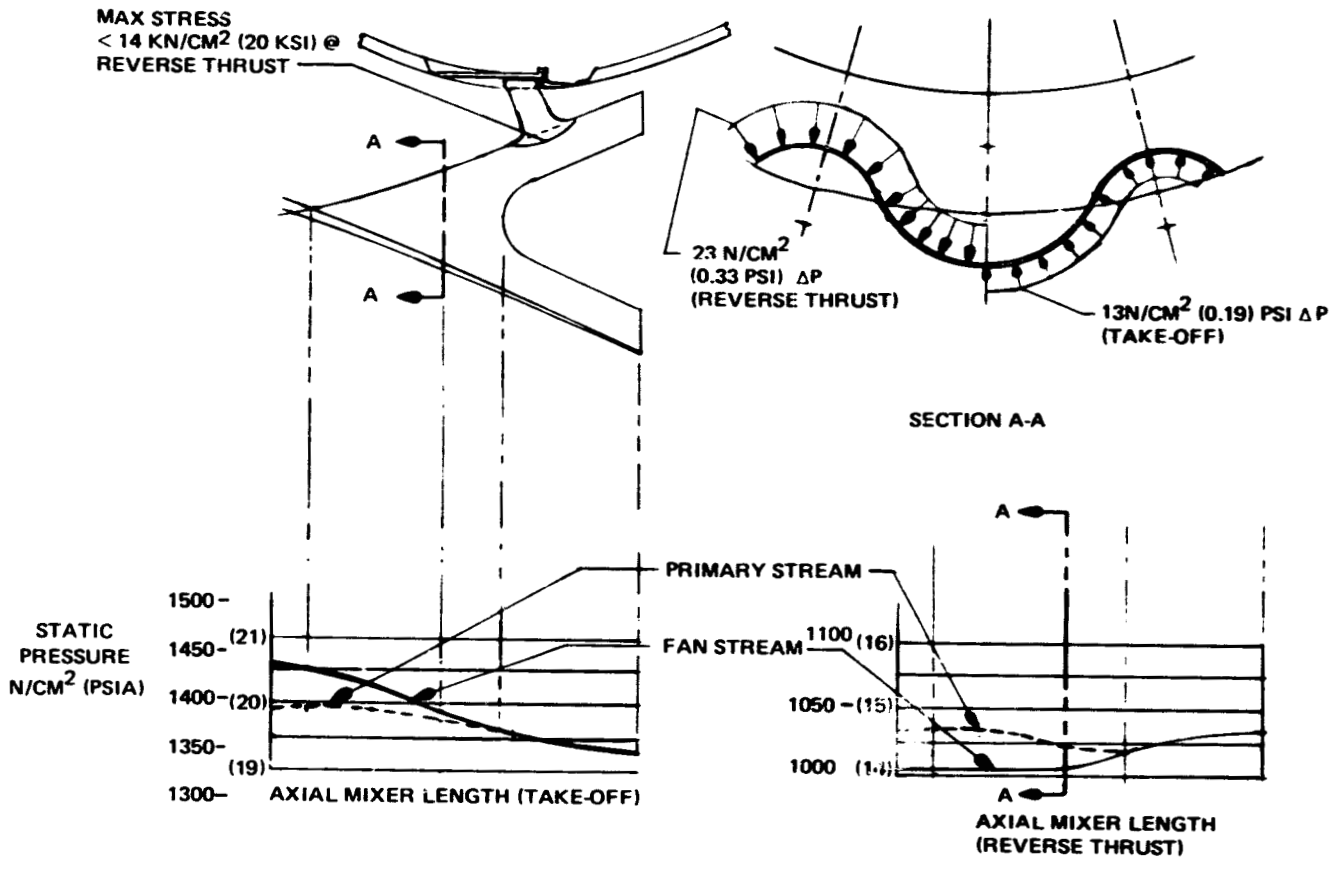

Figure 139 Mixer Static Pressure Load. Analysis shows maximum calculated stresses within material capabilities.

reversed thrust engine operating condition at the axial location where the differential pressure across the mixer is calculated to be 23 N/cm^2 (0.33 psi) (Section A-A, Figure 139). In this operating condition, the primary stream pressure is enough higher than the fan stream and the wall area is large enough that a net maximum outward load is produced on the mixer assembly. This outward load is reacted out primarily at the I.D. strut attached to the tailplug. The butt weld strut attachment to the mixer skin is calculated to be the maximum stress point. The calculated level is less than 14 kN/cm^2 (20 ksi), which is well within material limits.

4.10.4.3 Pressure Loss Analysis

The estimated pressure loss through the mixer on the fan stream side is 0.18%, and on the primary stream side is 0.24% at the cruise design point. The tailpipe pressure loss downstream of the mixer is estimated to be 0.34%. These estimates reflect skin friction losses of a high efficiency mixer/exhaust system without aerodynamic irregularities in the flowpath.

4.10.5 Design Summary

The results of the mixer preliminary design are summarized in Table 55. The preliminary design effort to date has met its basic requirements by defining a mixer configuration that will serve as an aerodynamic and mechanical baseline design. A 12-lobe convoluted mixer was selected to provide high performance, low weight, and favorable integration characteristics. This mixer will be fabricated primarily of titanium to minimize system weight. The design will be used as the starting point for the Energy Efficient Engine Supporting Technology Mixer Model Program and will be updated as the results of this program become available.

4.11 NACELLE SYSTEM

4.11.1 Design Requirements

Design requirements for the nacelle system were established on the basis of engine, installation, and overall performance considerations. Table 56 summarizes the aerodynamic, mechanical, and structural design requirements.

The Energy Efficient Engine nacelle must provide high performance, tolerate high angles-of-attack so as to minimize inlet distortion, and be fully-treated to reduce noise. The nacelle must also be installable in representative aircraft without sacrificing benefits in performance and weight. Composite materials must be used wherever possible to reduce overall installation weight.

TABLE 55

MIXER/TAILPIPE DESIGN SUMMARY
AERODYNAMIC DESIGN POINT

Efficiency, %	85
Duct Stream Pressure Loss, %	0.18
Primary Stream Pressure Loss, %	0.24
Tailpipe Pressure Loss, %	0.34
Thrust Coefficient	0.996
Mixer Length	50% Current State-of-the-Art
Tailpipe Length	70% Current State-of-the-Art
Number of Lobes	12
Life	Commercially Adequate With Efficient Vibration Damper

TABLE 56

NACELLE DESIGN REQUIREMENTS
AERODYNAMIC DESIGN POINT

Aerodynamic Parameters

Drag, % of Uninstalled Thrust	4.1
Inlet Recovery, P_{T2}/P_{T0}	0.997
Fan Stream Pressure Loss, %	1.1
Primary Stream Pressure Loss, %	0.6
Reverse Thrust (Landing), % of Forward Thrust	35

Mechanical/Structural

Direct thrust reversal to prevent reingestion
Maximize load sharing with engine cases
Provide easy access for engine core maintainability
Prevent fires
Provide airframe bleed and power requirements
Provide treatment for noise attenuation

Directive thrust reversal must be attained by properly selecting the cascade modules to direct the air as required. Thirty-five percent of the forward thrust should be reversed.

Door installation must provide for maintainability of the engine core by providing access to the gearbox, compressors, combustor, and turbines. Doors must also provide easy access to engine mounts to permit engine removal.

Airflow requirements are important to the nacelle design. Air is required to cool the electronic fuel control and to purge the core accessory compartment. Also, air of sufficient pressure and temperature is required to prevent ice formation on the inlet lip. In addition, air must be bled off the engine for cabin air conditioning. This air must first be cooled to 238°C (450°F) before entering the airframe.

Miscellaneous design requirements include incorporation of fire zones in the presence of flammable liquids. Each fire zone requires a supply of extinguishing fluid. Another design consideration is the gearbox, which must be provided to drive engine and aircraft accessories, such as the starter, generator, and oil and fuel pumps.

4.11.2 General Configuration Description

4.11.2.1 Aerodynamic Contours

The ground rules used in the aerodynamic design of the Energy Efficient Engine nacelle are illustrated in Figure 140. The internal length of the inlet was set by an acoustic treatment requirement calling for a treated length equal to one-half the fan diameter. The inlet hi-lite to throat area ratio was set at 1.25 and the hi-lite to maximum diameter ratio was set equal to 0.83. The maximum diameter of the nacelle was located at 0.4 of a maximum diameter downstream of the inlet leading edge. These criteria represent a consensus of aircraft manufacturers requirements established during integration coordination meetings.

The fan stream flow path, aft of the fan case, was designed around an essentially conical core cowl selected to simplify fabrication and to effectively carry loads around the engine. The fan duct is nearly a constant area passage blending into the mixer/exhaust system at the turbine exhaust case.

The mixer/exhaust system was sized to provide the necessary static pressure balance between the fan and primary streams at the exit plane of the mixer and to have a tailpipe length equal to one-half of the mixing plane diameter. The external boat-tail angle was set at 15 degrees, which results from the nozzle length, exit area, and mixing plane area relationships. The boat-tail angle is judged to be two or three degrees too high by some airframe companies based on their current design guidelines, but the limiting angle can only be selected

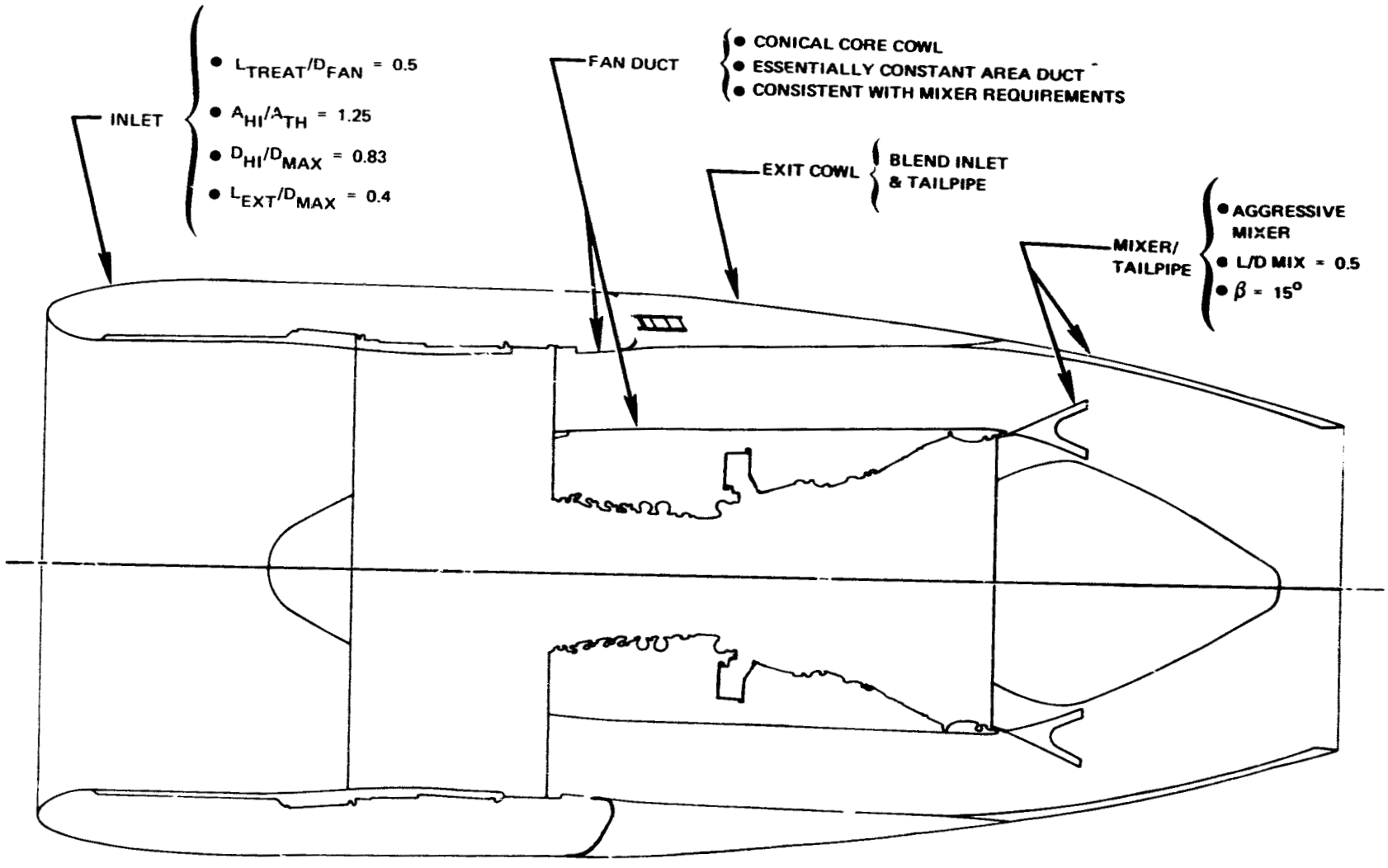

Figure 140 Nacelle System. Geometrical ground rules used in nacelle aerodynamic definition.

after completion of installed, under-the-wing tests of a mixed nacelle. Since no data along these lines is presently available, it was decided to retain the steeper boat-tail instead of lengthening the tailpipe to reduce the external angle at this time. The external lines of the nacelle were completed by blending the inlet and tailpipe, while allowing room for the thrust reverser in the mid-cowl section.

The aerodynamic requirements, therefore, result in a high performance nacelle which is consistent with acoustic requirements and compatible with advanced fabrication techniques.

4.11.2.2 Major Subassemblies

The nacelle cross-section is presented in Figure 141. The inlet duct is bolted to the fan case just forward of the fan blades. The section just forward of the fan blades in the inlet is composed of 5.1 cm (2.0 in.) deep honeycomb for noise treatment, and is surrounded by a wrapped layer of KEVLAR for containment. The length of containment forward of the fan blades is equal to the radius at the fan tip inlet times the tangent of 15 degrees The forward portion of the inside of the inlet is DYNA ROHR® for noise treatment. DYNA ROHR is composed of aluminum honeycomb with aluminum face sheets. The inside, or air stream side, is perforated and covered with a thin layer of BRUNSMET® a highly compacted fine steel mesh. DYNA ROHR is also used in the outer fan duct behind the fan exit case rearward to the tailcone. DYNA ROHR was chosen for its characteristics of:

1. low skin friction
2. good attenuation band width
3. future structural capability

The outer skin of the inlet, cowl doors, and D-shaped ducts is composed of aluminum honeycomb wrapped with a graphite/KEVLAR fabric for weight reduction. The cowl doors are located just behind the inlet and provide accessibility to the oil tank, electronic fuel control, and nitrogen tank. The cowl doors are hinged on both sides of the pylon and latched at the bottom.

Aft of the cowl doors are the D-shaped ducts, which house the thrust reverser and provide the load path between the front and rear mounts through the nacelle. The inner fan duct wall of the D-shaped ducts is titanium honeycomb bonded with aluminum braze material. The titanium is required to provide load carrying capability and to serve as a firewall around the gearbox compartment.

The tailcone is also made of aluminum brazed titanium honeycomb because of the high temperature exhaust gas that impinges on it. The tailcone is a full body of revolution and remains with the pylon when the engine is removed. The V-shaped groove at the aft end of the D-duct fits into a circumferential groove at the front of the tailcone. When the

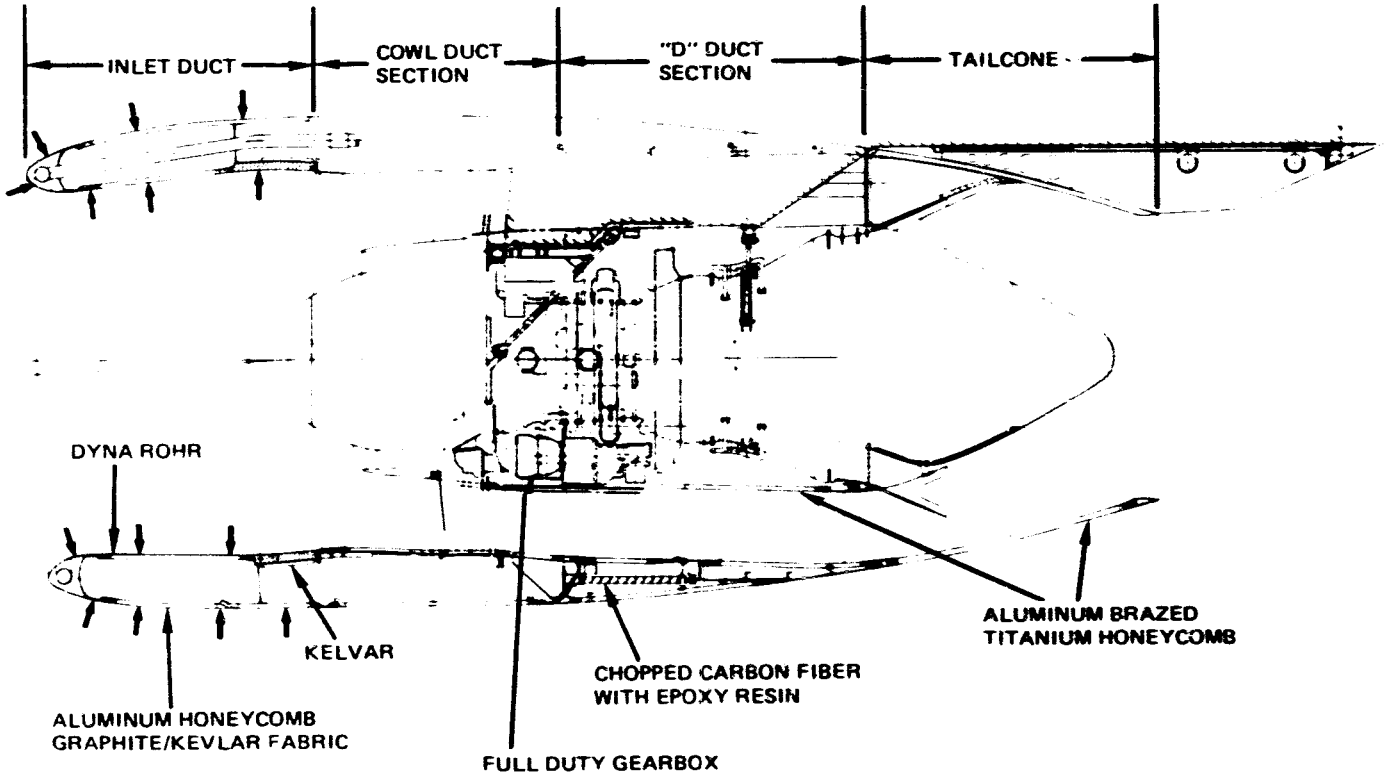

Figure 141 Nacelle System. Cross-section shows major features and materials.

D-shaped ducts are opened, the tailcone is supported by a T-shaped track bolted to the underside of the pylon. The tailcone is prevented from moving aft by a stop, bolted to the back of the track. With the stop removed, the tailcone can be slid aft, allowing the engine, mixer, and plug to be lowered vertically for quick engine change.

4.11.2.3 Mounting System

The mount system is designed to minimize engine case distortion and bending. This minimizes tip gap reductions in the fan, compressor, and turbines. The front mount transfers vertical, side, and thrust loads from the engine to the pylon, while the rear mount transfers vertical, side and torque loads. Figure 142 shows a schematic representation of the mount system.

The plane of the front mount is the aft face of the fan case. Vertical and side loads are taken through a spherical ball at one point on top just outboard of the high pressure compressor inlet. The outer face of the ball is free to slide back and forth during normal operation. The thrust load is transferred to the pylon through two drag links running from two brackets mounted on the engine horizontal centerline to a whiffle tree pinned to the aft end of the forging that contains the spherical ball. This eliminates both backbone bending in the core engine and fan case and rear mount vertical loads by a thrust moment induced by the thrust mount being attached to the engine above the horizontal centerline. If a thrust link should break, the thrust loads would be absorbed by the other thrust link and the spherical ball, as the engine slides forward against a stop. This would move the engine out of position on the pylon, giving visibility to the failure while preventing a more serious failure.

The rear mount plane is located at the turbine intermediate case. Vertical loads are taken by two rods running from the pylon to lugs located 25 degrees up from the horizontal centerline on the case to minimize case ovalization. Torque loads are resisted with a side drag link attached at the top of the case.

4.11.3 Supporting Analyses

4.11.3.1 Nacelle Performance

The performance characteristics of the nacelle are summarized in Table 57. The nacelle drag was estimated to be 4.1 percent of net thrust at cruise (Mn - 0.8/10,668 m or 35,000 ft). Total nacelle drag is assumed to be 1.15 times the nacelle skin friction. The inlet recovery was set at 0.9966, representative of high performance inlets. The total pressure loss in the fan stream, from the exit of the fan case to the tailpipe exit, is 1.12 percent. The total pressure loss in the primary stream, from the exit of the turbine exhaust case to the tailpipe exit is 0.58 percent. At design conditions, Mach numbers are 0.51 at the fan

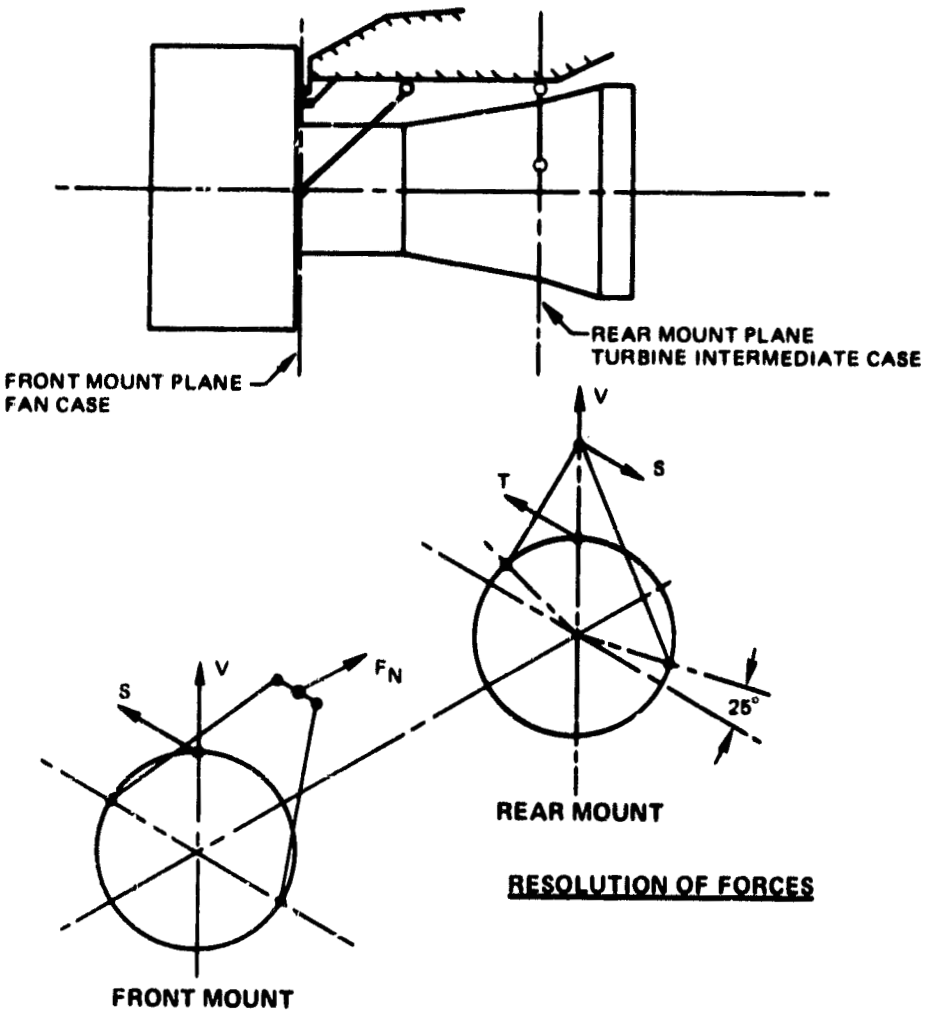

Figure 142 Nacelle Mounting. Schematic shows resolution of forces at front and rear mounts.

TABLE 57

NACELLE PERFORMANCE AT 10,668 m (35,000 ft),
M 0.8 MAXIMUM CRUISE

Nacelle Drag, D/T_n Uninst.	0.040
Inlet Recovery, P_{T2}/P_{TO}	0.9966
Fan Stream, $\Delta P_T / P_{TT}$	0.0112
Primary Stream, $\Delta P_T / P_T$	0.0058

case exit, 0.32 at the turbine exhaust case exit, 0.54 at the tailpipe entrance (mixer exit), and 1.0 at the exhaust nozzle throat. The nozzle exit plane gross thrust coefficient is presented in Figure 143. It corresponds to a convergent-divergent nozzle having an area ratio of 1.02, which was selected to enhance cruise performance at the higher pressure ratios.

4.11.3.2 Load Sharing Feature Definition

During maneuvers, and especially at takeoff, a large gust load is imposed on the inlet. This gust load produces a shear and bending moment on the nacelle that is transmitted through the engine to the mount system. This bending moment produces case distortions that reduce tip gaps and can cause seal rubs and a permanent loss in engine performance. Accordingly, the STF 505M-7 engine has an engine-nacelle load sharing system (Figure 144). This system is similar in concept to the the JT9D engine common nacelle, but with a higher percentage of load sharing.

The nacelle D-shaped ducts are held in V-shaped grooves at the aft end of the fan case and are clamped around a ring bolted to the engine turbine exhaust case. The inner and outer fan ducts thus form a beam with sufficient bending stiffness to isolate a large part of the cowl gust load from the engine. Analysis indicated that the two D-shaped ducts will carry about 80 percent of a vertical cowl moment and about 60 percent of a horizontal moment.

The hardware required for load sharing consists of V-shaped grooves at the interface of the fan case and D-shaped ducts (Figure 145). The D-shaped ducts are clamped in the V grooves with a strap and latch assembly. The ring that the D-shaped ducts rest on at the turbine exhaust case is halved and bolted together. The ring is bolted to a flange on the turbine exhaust case (TEC) using controlled torque bolts that fit in radially elongated holes as shown by Figure 146. The torque is low enough to permit differential radial growth between the engine and the nacelle, but high enough to resist the punching load caused by the cowl moment.

The D-shaped ducts must be latched tightly around the TEC. To accomplish this, a small tension latch is installed at the bottom of the ducts on the inside of the fan stream. The latch is accessible through a port in the outside of the D-shaped ducts.

Figure 146 shows the tension strap required to hold the duct tightly against the ring on the TEC. When the tension latch at the bottom is latched, the tension loads are transferred from the nacelle to the strap through adjustable pins on both sides of the D-shaped ducts. The pins fit into holes in the strap when the D-shaped ducts are closed. The pin adjustment must be made with the D-shaped ducts closed and latched. Access to the pins is achievable through access ports in the

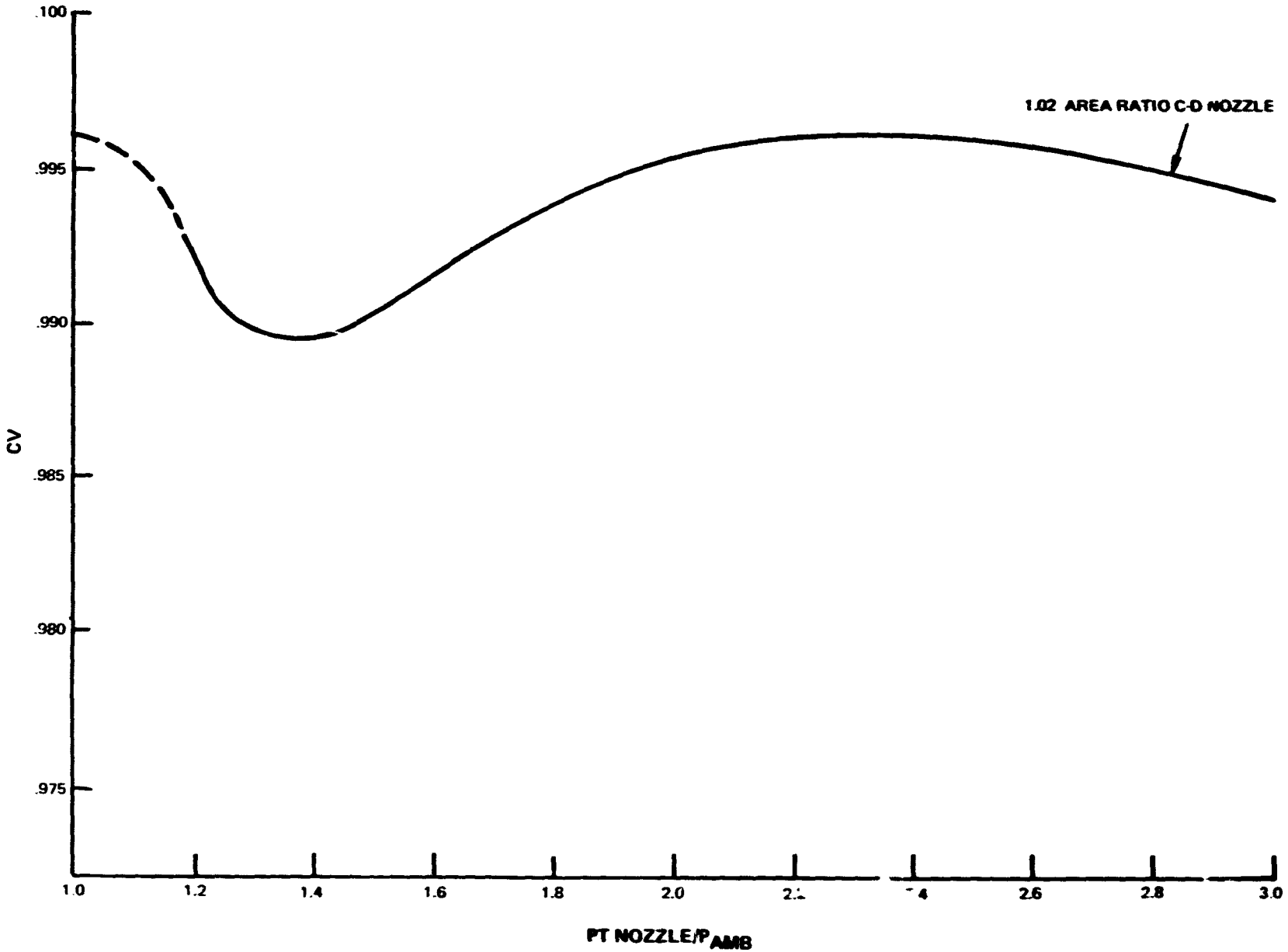

Figure 143 Nacelle System. Nozzle gross thrust velocity coefficient shows variation with nozzle expansion ratio.

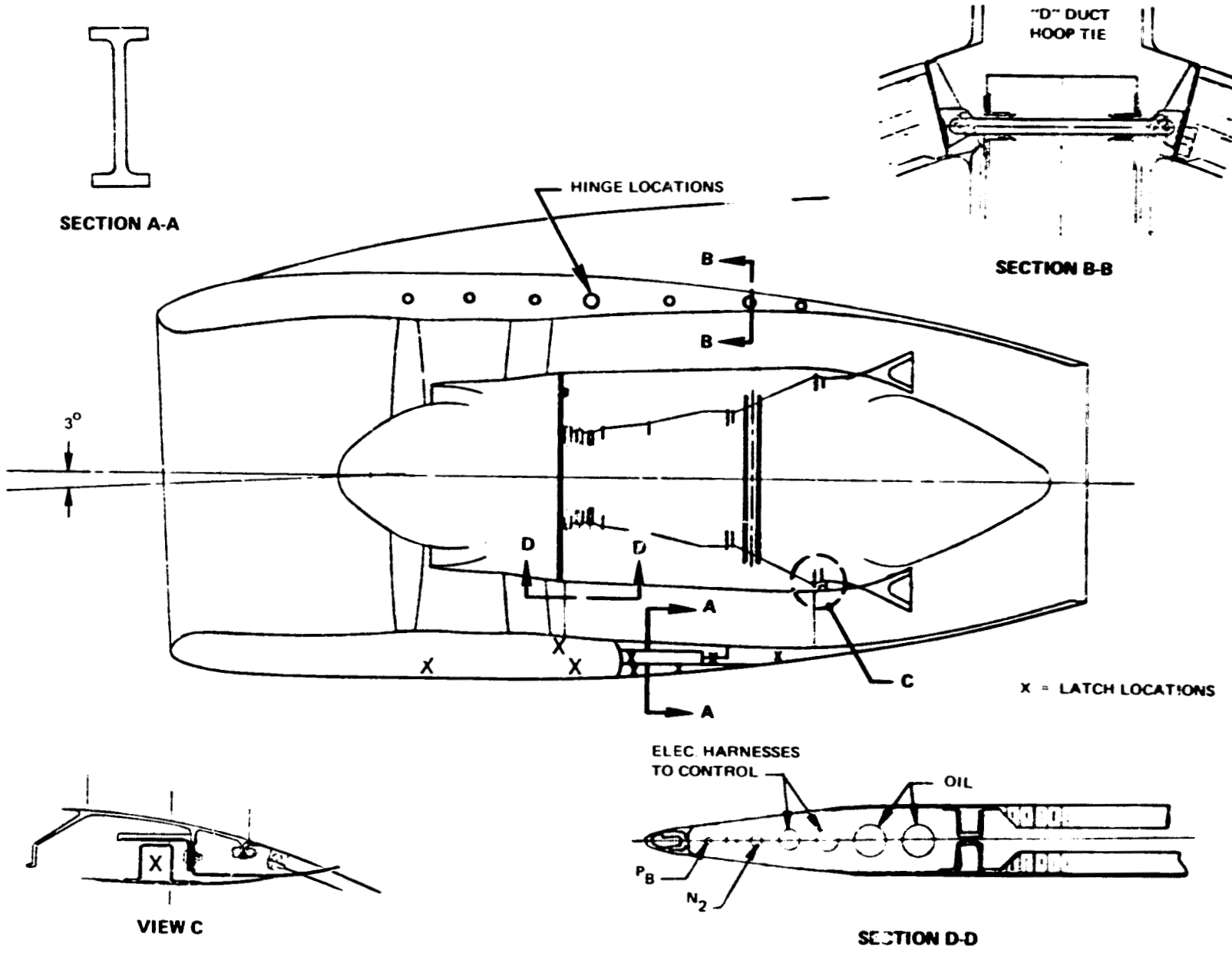

Figure 144 Nacelle System. Drawing shows engine-nacelle load sharing system.

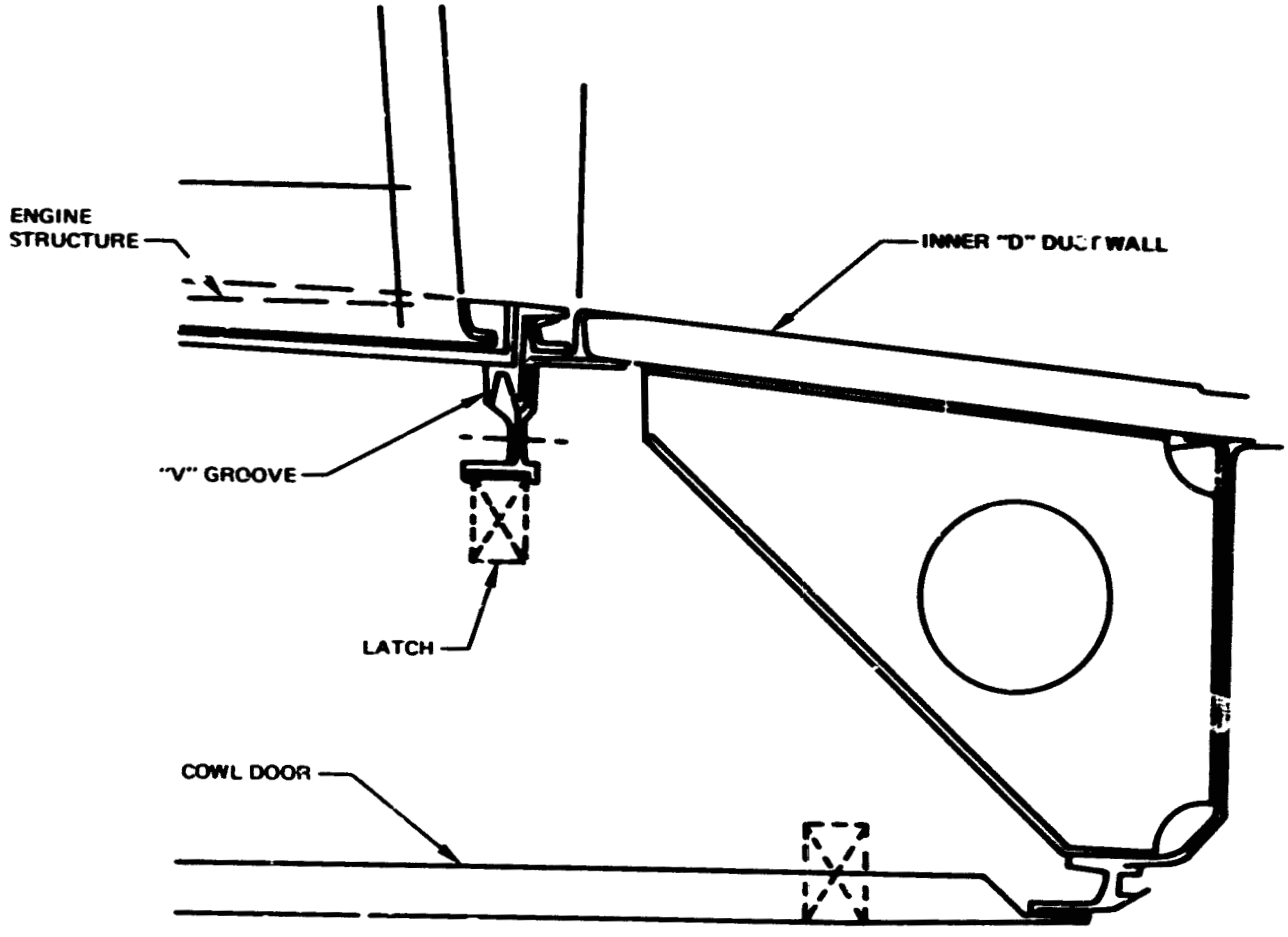

Figure 145 Nacelle Load Sharing. Inner cowl "V" groove transfers loads between engine and inner "D" duct wall.

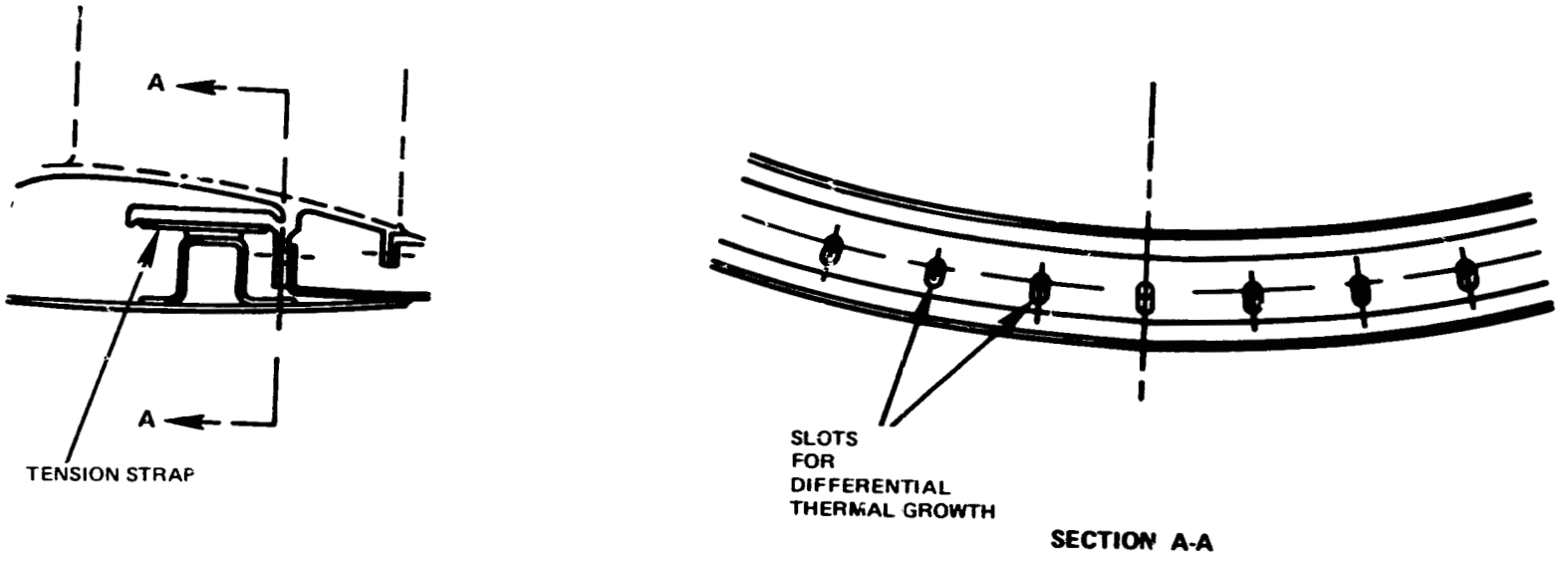

Figure 146 Nacelle Load Sharing. Transfers loads between "D" ducts and turbine exhaust case.

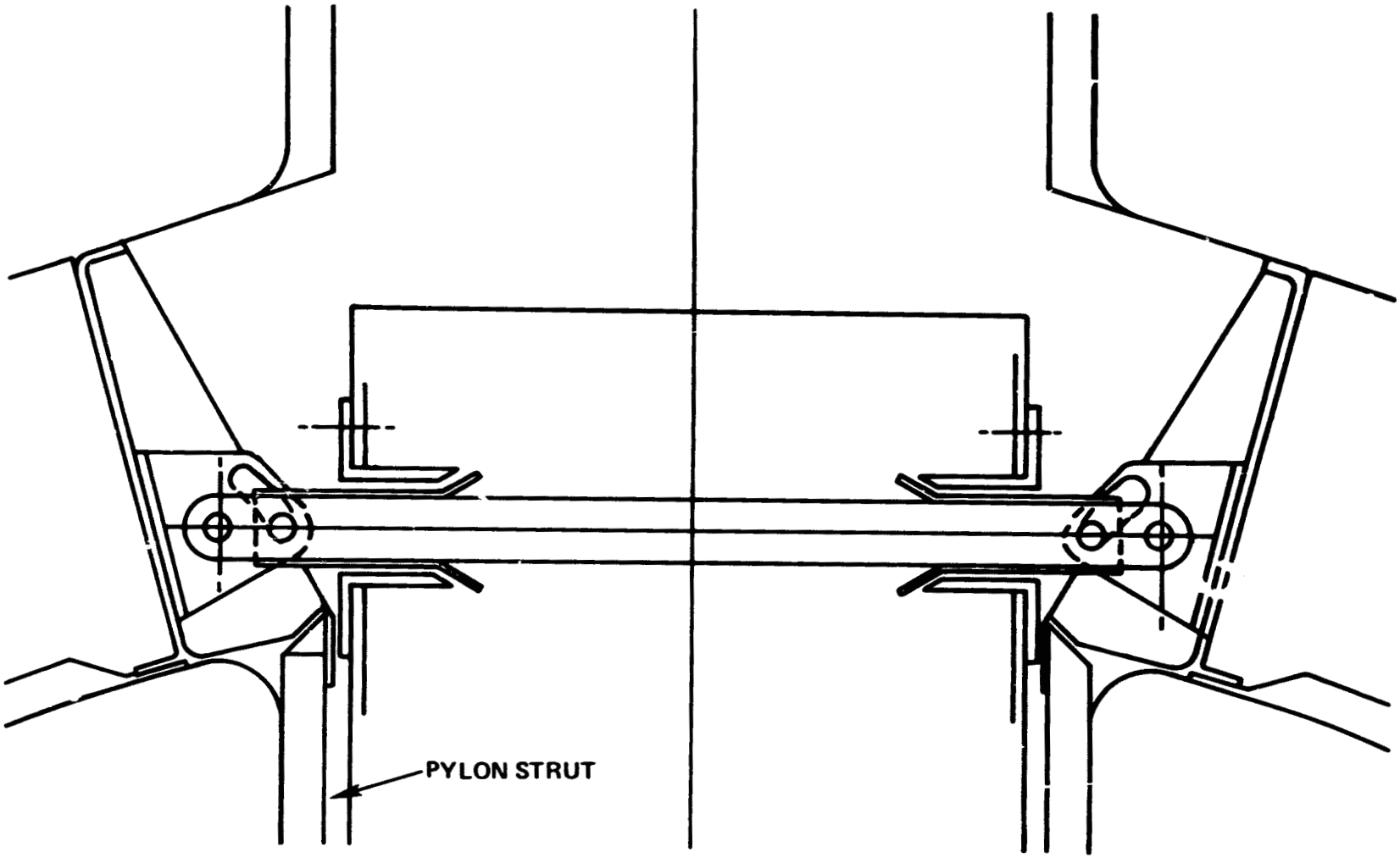

Figure 147 "D" Duct Cam-Actuation. Hinges transfer door weight to pylon as doors are opened.

outside of the D-shaped ducts. Field experience on the common nacelle system shows that pin adjustment is required only when an engine is changed.

The D-shaped ducts are hinged to floating tierods in the pylon and latched together at the bottom with tension latches. When the ducts are closed, they rest in V-shaped grooves at the back of the fan case and on a ring on the turbine exhaust case. The closed ducts form a beam-shaped structure that resists a large part of the cowl moment. This eliminates redundancy of the load path in the nacelle engine-pylon structure. It also negates any stresses caused by differential thermal growth between the hinges and the bottom of the engine. Figure 147 presents a sketch of one of two cam-actuated hinges that permit the hinges to float freely in the pylon when the D-shaped ducts are closed, but locks the ducts to the pylon when they are opened. When the D-shaped ducts are opened, a sleeve with a conical end is cammed outward until it seats on a female cone on the end of a tubular piece bolted to the pylon. The cam will be designed to activate the spool piece when the ducts are starting their outward swing. Bumpers are attached to the inside of the D-shaped ducts to prevent excessive deflection of the vertical panels at the top and bottom caused by pressure drop across the duct.

In order to transfer loads through the outer fan duct to the rear mount, I-beams have been provided between the cascade modules of the thrust reverser (Section A-A, Figure 144). Loads pass from the outer fan duct to the inner fan duct through the lower bifurcation shown in Section D-D of Figure 144. The lower bifurcation is formed by the two halves of the D-shaped ducts, the leading edge providing space for service lines to pass across the fan stream, and the rear compartment allowing gearbox compartment purge air to be dumped overboard.

4.11.3.3 Thrust Reverser Preliminary Design and Performance Prediction

The fan thrust reverser is located in the D-shaped ducts and swings open with the ducts for easy access to the core engine. Blocker doors, hinged to a synchronizing ring, are moved rearward by an air driven ball screw. As the blocker doors move aft, a drag link attached to the doors and the inner duct wall swings the doors into the fan stream, deflecting the fan exhaust radially outward through cascades. The cascades turn the air forward and upward as required by the particular aircraft installation for directed flow. The cascades are covered on the outside by a sleeve that translates aft during reverse. The translating sleeve is driven by a separate ball screw. This permits the motion of the blocker doors and translating sleeve to be programmed independently. The two ball screws are geared together and driven by a flexible cable from an air motor. If something in the system fails, the reverser is designed to remain in the position it occupied before failure. The air motor is actuated by eighth-stage compressor air. A cross-section of the thrust reverser configuration is presented in Figure 148.

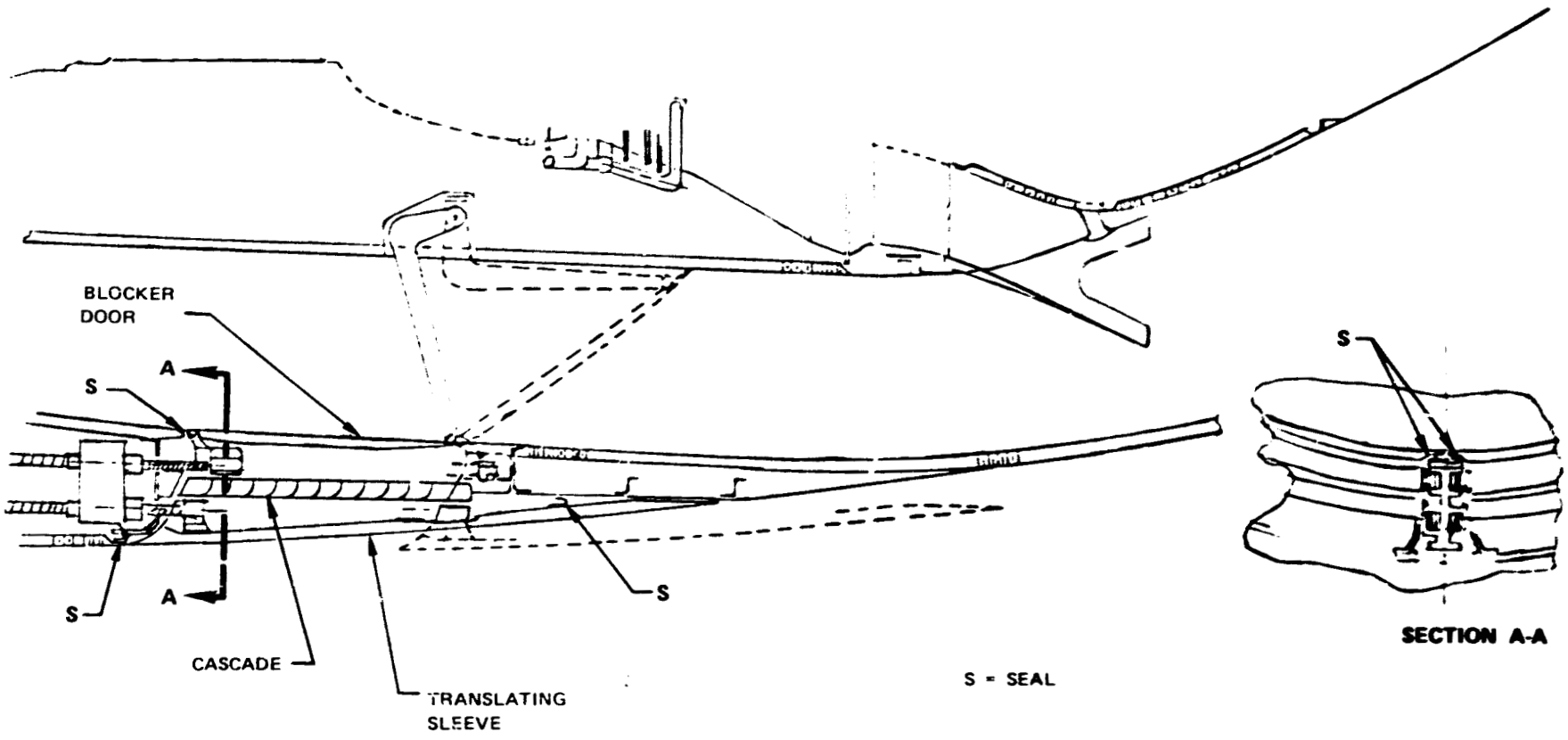

Figure 148 Fan Stream Thrust Reverser. Cross-section shows cascade and actuation mechanisms.

Structural continuity through the reverser section is provided by bi-panels at the top and bottom of the D-shaped ducts and by 10 I-beams located in between cascades. Integral with the I-beams are slots that enclose T-shaped tracks for the blocker door synchronizing ring and the translating sleeve.

The blocker door drag links are spring-loaded to keep the doors, when stowed, flush with the outer duct wall. The blocker doors are sealed with on-pressure flap seals so that the duct pressure vessel is created by the closed blocker doors and outer D-shaped duct walls. Flap seals are also used at the front and rear of the translating sleeve, and axially at the top and bottom of the reverser between the translating sleeve and D-shaped ducts. Flap seals are also used at the fore and aft V-shaped grooves. Bulb-type weather seals are used to seal cowl doors between the pylon and nacelle apron and between the tailcone and pylon.

The bottom 120 degrees of the thrust reverser is blocked off to prevent reverser air from blowing downward and from picking up runway debris. The cascades are sized for 50 percent reverser efficiency to provide 35 percent of the forward thrust in the reverse direction.

4.11.3.4 Air Management System Preliminary Design

Figure 149 is a schematic drawing showing the nacelle air management system. Customer bleeds are at the eighth- and fifteenth-stages of the compressor. Either eighth- or fifteenth-stage air is routed through the upper bifurcation to the pylon-mounted precooler. Fan air is bled off the walls of the upper bifurcation, used to cool the air and discharged through the side of the pylon. Inlet anti-icing air is bled from the eighth-stage and routed through the upper bifurcation through a valve to a spray ring in the inlet lip region.

Fan air for the high-pressure compressor active clearance control system (ACC) is bled off the inner D-shaped duct wall. The air goes through a two-way valve that directs it either to the high-pressure compressor ACC spray rings or dumps it upward into the inner compartment where it purges the compartment before exiting through the bottom bifurcation. Purge air will be metered to two to three air changes per minute. When the ACC system is flowing, ACC air is used as purge air with the number of air changes per minute estimated to be 15-20. The required exit area through the bottom bifurcation is estimated to be 155 cm^2 (24 $in.^2$) when the inner nacelle cavity is vented to ambient. The critical buckling pressure of the inner duct wall is estimated to be 9.7 N/cm^2 (14 psi) with a maximum pressure drop across the wall of 6.2 N/cm^2 (9 psi). This inner duct wall is a 2.54 cm (1 in.) thick honeycomb, 0.041 cm (0.016 in.) face sheet, aluminum brazed titanium honeycomb structure.

The compressor start valves are located at the 10th stage and the air is dumped into the fan stream through the valves. Hinged blow-out

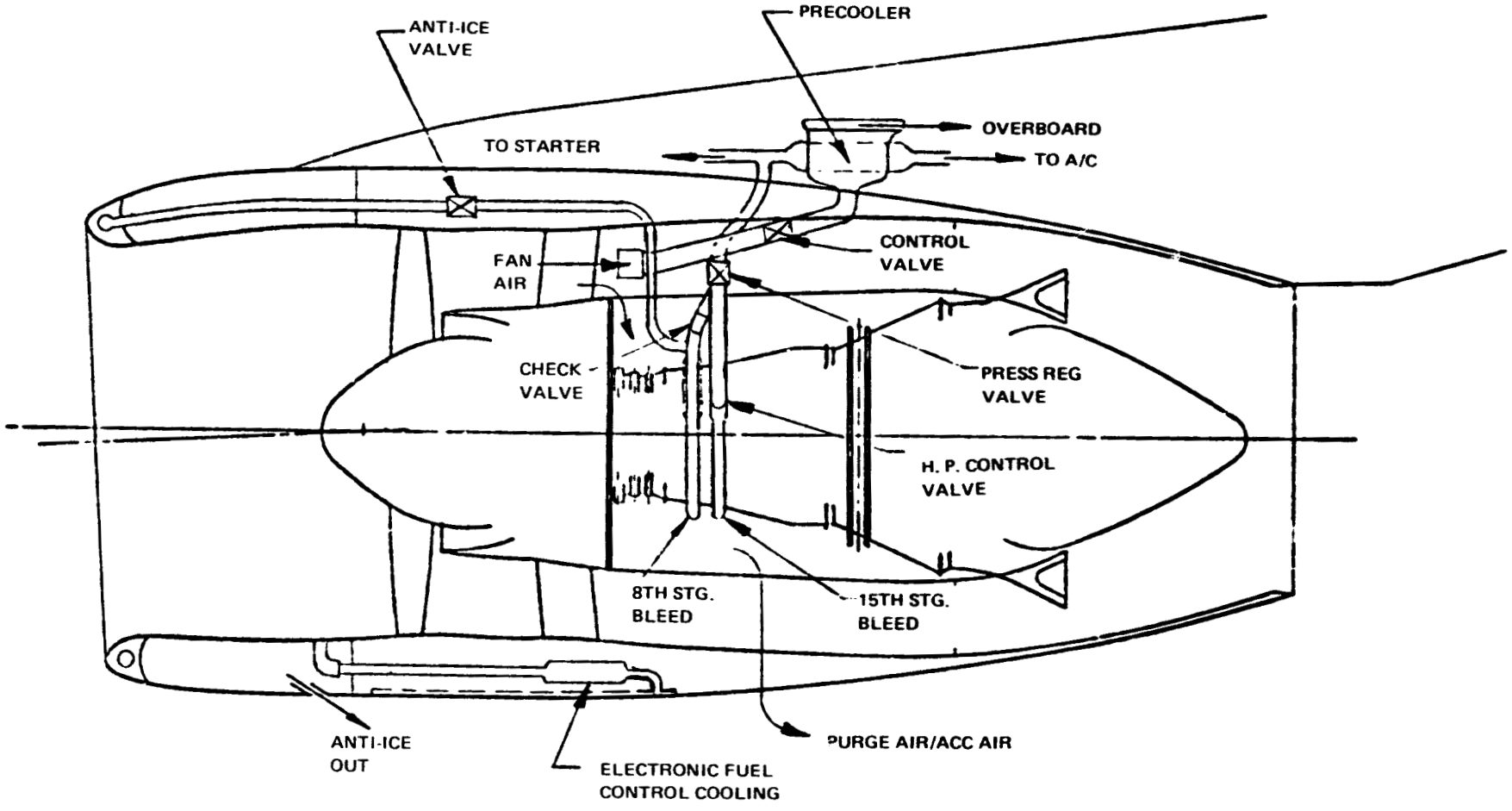

Figure 149 Nacelle Air Management System. Schematic shows system components.

panels are located on the inner D-shaped duct walls. If a high pressure air line should burst, the panels would blow open into the fan stream, relieving any pressure increase in the inner compartment.

The electronic fuel control located in the nacelle must be maintained below 93°C (200°F). At low flight speeds, air drawn off the outer wall of the nacelle is passed over the control box before being dumped into the inlet airstream ahead of the fan blade. Inlet ram air flows over the control in the reverse direction to perform cooling at higher flight speeds.

4.11.3.5 Fire Zone

Figure 150 shows the fire compartment and the means of venting. The high temperatures at the rear section of the high-pressure compressor case preclude the practical use of an axial firewall in the core compartment. As a result, all tubes carrying flammable fluids in this region are designed as double-walled and shrouded fixtures. The fire zone is provided with fire extinguishing fluid and temperature sensors for fire warning.

4.11.3.6 Accessory Arrangement

A number of possible accessory arrangements (see Figure 151) were studied to determine the implications on engine design and to select an arrangement for use in design analysis. All of the arrangements would appear feasible and would offer various trade-offs in terms of integration into the nacelle and in terms of accessibility provisions.

A full-duty core mounted accessory (shown in Figure 152) arrangement has been selected for use in the preliminary engine design since this arrangement is compatible with all of the studied installations, and has a minimal impact on engine, nacelle, or pylon design.

A listing of engine accessories is given in Table 58.

The tubes that connect accessories on the fan case to accessories on the core engine are routed through the bottom bifurcation, which is 7.6 cm (3.0 in.) max. thickness and is matched to the fan case strut in front of it to eliminate a two-per-revolution pulse in concert with the wider upper bifurcation.

The airframe accessories are listed in Table 59.

4.11.3.7 Materials Applications

The nacelle design includes extensive use of composite materials to reduce weight. Major unknowns associated with composites are long term durability and manufacturing costs. Although the cost of high strength fibers has decreased dramatically in the past ten years, and future

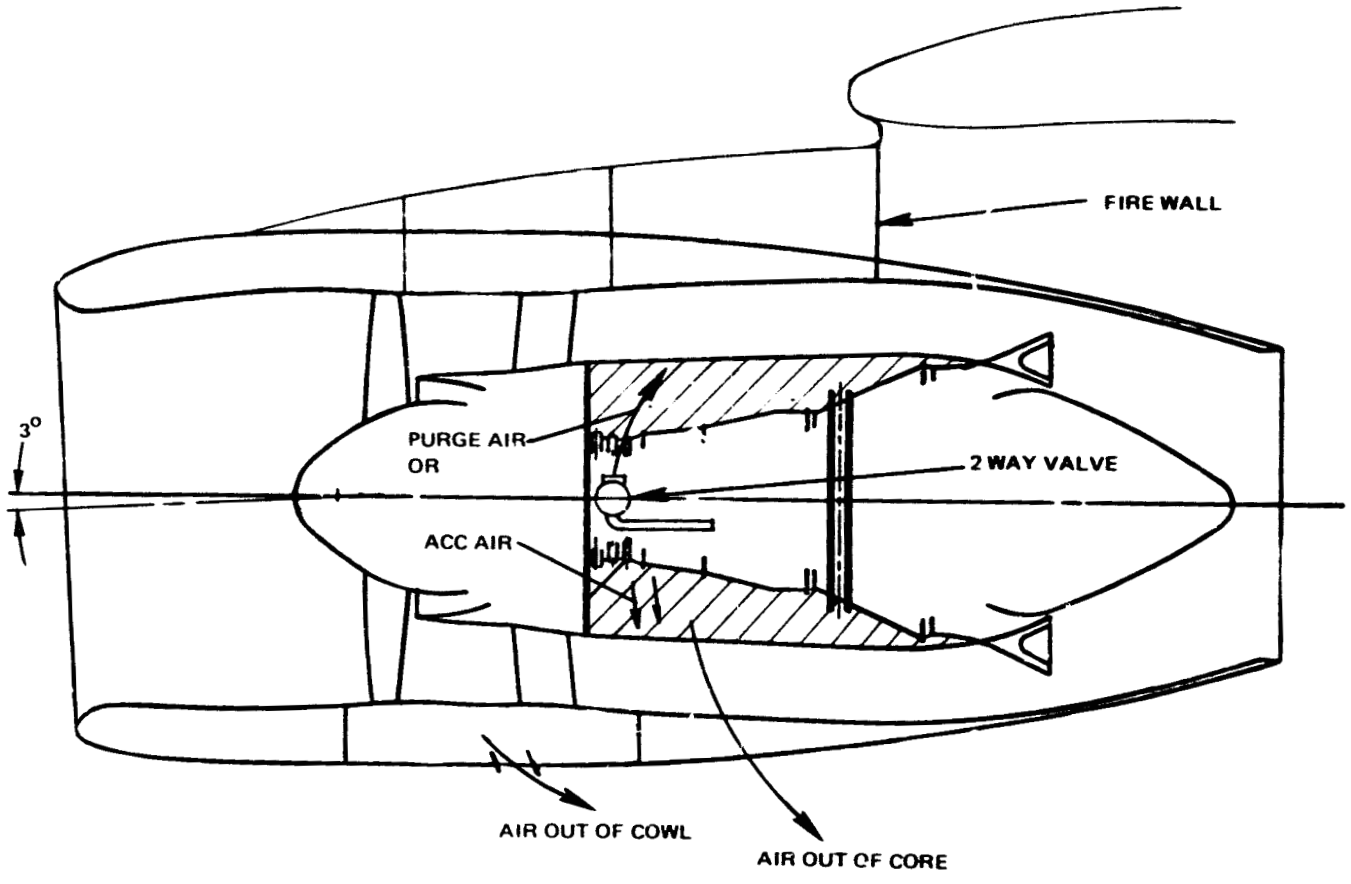

Figure 150 Fire Compartments and Nacelle Venting System. Schematic shows system components.

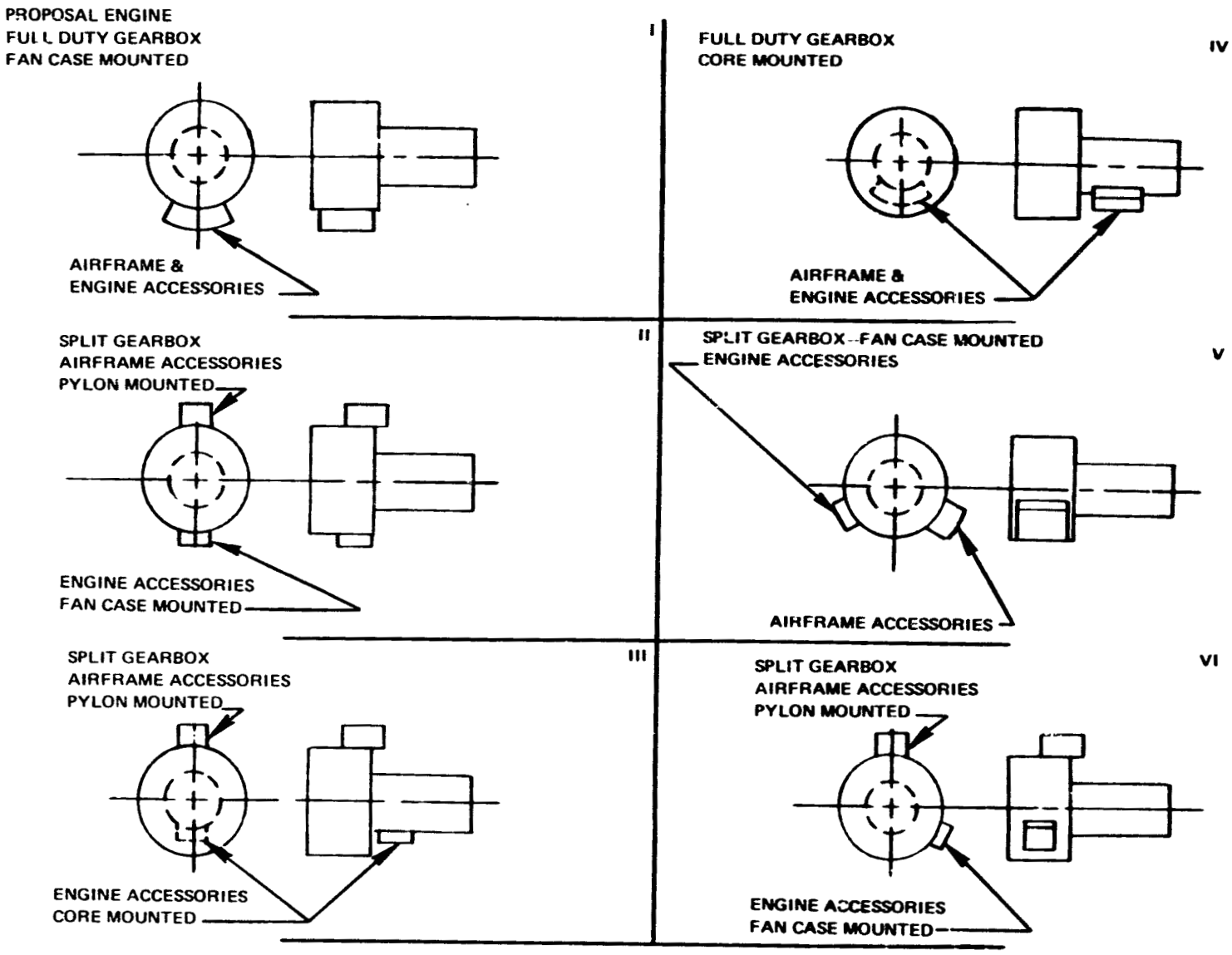

Figure 151 Accessory Arrangement. Design possibilities considered for future commercial transports.

Figure 152 Full-Duty Core Mounted Accessory Arrangement. Sketch shows location and arrangement of components.

TABLE 58

SUMMARY OF ENERGY EFFICIENT ENGINE ACCESSORIES

1. Two stage, dual drive fuel pump
2. Oil pump filter
3. 1 KVA alternator to power electronic fuel control
4. Main fuel flow metering package and fuel filter
5. Fan case mounted electronic fuel control
6. Fan case mounted oil tank
7. Fan case mounted nitrogen bottle (required to purge secondary fuel system, 11.4 kg (25 lb) weight full)
8. Air valves for start bleeds and active clearance control system

TABLE 59

SUMMARY OF AIRFRAME ACCESSORIES LOCATED ON ENGINE CORE

1. Two 144 l/min (38 gpm) hydraulic pumps
2. Starter
3. 90 KVA variable speed constant frequency generator
4. Pylon mounted precooler with 50 percent recirculation bleeding 8th- or 15th-stage compressor air

costs can be predicted to be even lower, manufacturing costs for a 1990 time frame are not known. For purposes of this study, it is assumed that composite structures will trade evenly with conventional structures in 1990. Materials used in the nacelle are summarized in Table 60.

4.11.4 Design Summary

The results of the nacelle preliminary design are summarized in Table 61. The preliminary design effort to date has met its aerodynamic, structural, and mechanical requirements. Good performance, low weight, and favorable integration characteristics are provided by the configuration. The design provides for a high percentage of load sharing with the engine cases, thus allowing better engine component tip clearance control. Maximum use of composite materials throughout minimizes the weight of the mixed flow, long duct nacelle. Unique design configurations allow maintainance access, reverse thrust targeting, noise attenuation, and fire prevention.

4.12 MATERIAL SELECTION

4.12.1 Engine Materials

The Energy Efficient Engine utilizes a combination of current commercial engine and advanced technology materials An engine cross-section foldout drawing, with material callouts is shown in Figure 153.

Material selections were made based on the maximum derived benefit in terms of engine direct operating cost (DOC). Trade factors were used to convert differences in engine cost, weight, and performance to equivalent differences in DOC (including interest costs). These trade factors dictated the use of lower cost current technology materials for most applications. Advanced technology materials were used to reduce weight, to improve performance, or to meet life requirements.

4.12.2 Advanced Material Applications

4.12.2.1 Alloys and Locations

The locations of the advanced material applications, shown in Figure 154, are listed in Table 62.

4.12.2.2 Alloy Description and Benefit

The Flight Propulsion System (FPS) preliminary design takes advantage of several advanced materials. These will be developed external to, and parallel with, the Energy Efficient Engine program. By the end of 1983, these materials will be at a development stage which will permit their

TABLE 60

SUMMARY OF MATERIALS USED IN NACELLE

1. Inlet lip and bulkhead - aluminum, used for lightweight construction and ease of manufacturing.

2. Outer inlet barrel and cowl doors - aluminum honeycomb with composite face sheet. NOMEX® honeycomb was considered but was rejected because of its low strength. The face sheets are a mixture of carbon and KEVLAR in an epoxy matrix. Carbon was chosen for its good conductivity, high tensile and compressive strength to weight ratios, its low future cost. The KEVLAR is added because of its good impact strength. The exact number and orientation of plies or fabric weave remain to be determined.

3. Inlet and outer D-duct walls - DYNA ROHR is bonded aluminum honeycomb with a porous steel mesh bonded to the air side. The porosity of the steel mesh, the size of the holes in the perforated sheet, and the depth of the honeycomb are varied to optimize the acoustic properties of the panels. It is anticipated that adhesive developments will result in acoustic panels with structural capability by the 1990's. The reasons for choosing DYNA ROHR are its good acoustic properties, low skin friction, and future structural capability.

4. Thrust reverser cascades - injection moldings of chopped carbon fibers in an epoxy matrix. This design, which is currently being service tested in a commercial fleet, has a claimed cost and weight saving of 40 percent over a metal design.

5. Inner duct wall and tailcone - Aluminum brazed titanium honeycomb. Titanium is needed for its high temperature capability up to 427°C (800°F) in tailcone. It is also used in the inner duct wall for the following reasons:

   a. high temperature capability eliminated need for heatshields

   b. capability to pass fire test

   c. high strength and stiffness are good for load sharing

   d. lighter weight when compared with an aluminum structure with equivalent strength, temperature capability, and fire resistance

   e. of concern are high cost and possible vulnerability to galvanic corrosion. Corrosion tests on closed cell panels have indicated no problem, but the open-cell configuration required for acoustic attenuation might be troublesome.

TABLE 61

NACELLE DESIGN SUMMARY

Drag, % of Uninstalled Thrust	4.1
Inlet Recovery, P_{T2}/P_{T0}	0.9966
Fan Stream Pressure Loss, %	1.12
Primary Stream Pressure Loss, %	0.58
Reverse Thrust, % of Forward Thrust	35 (Targeted)
Load Sharing	
Vertical Cowl Moment, %	79
Horizontal Cowl Moment, %	62

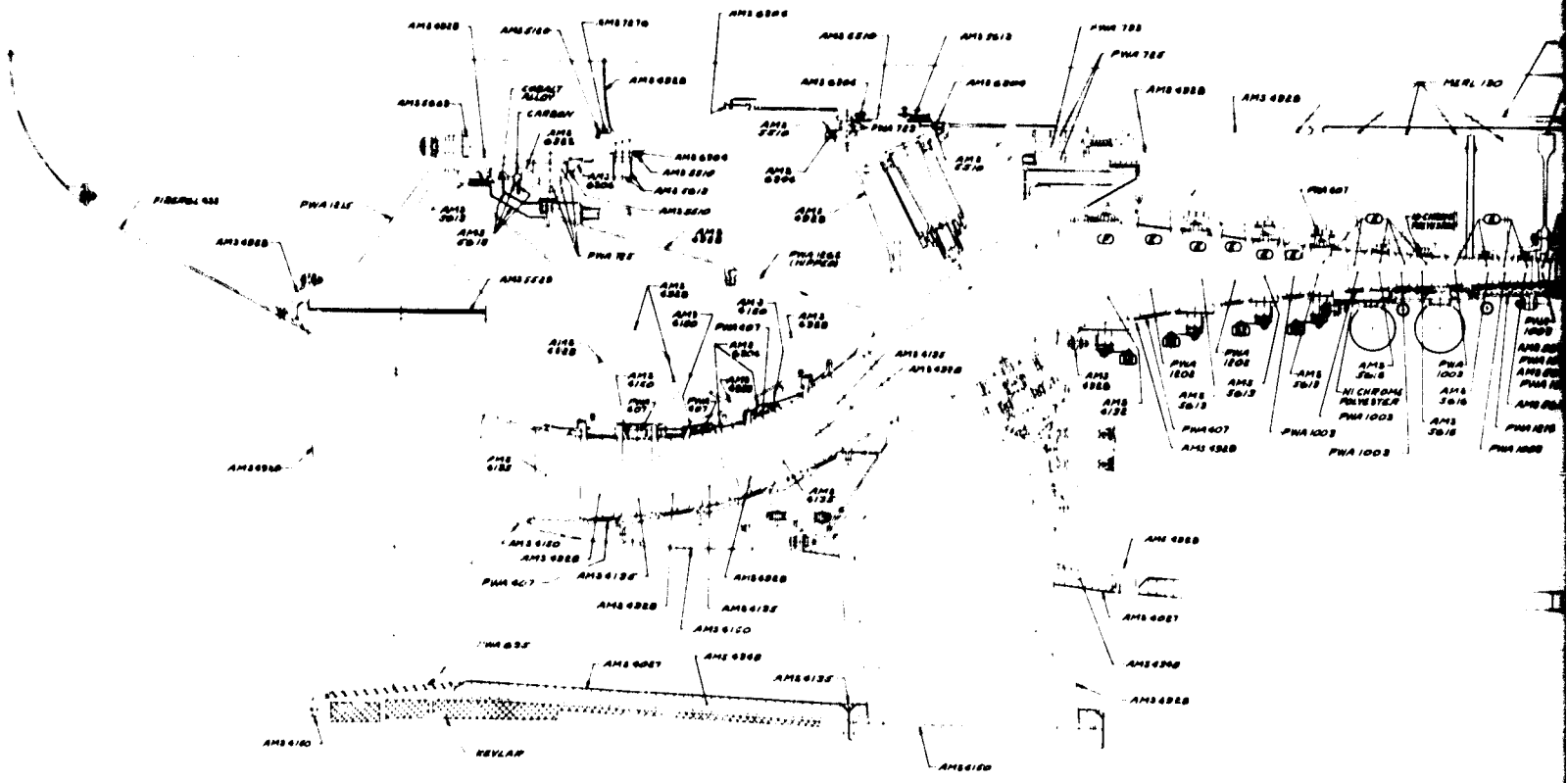
AMS 6928
AMS 6160
AMS 7870
AMS 6904
AMS 6910
AMS 7815
PWA 795
AMS 6908
AMS 6905
CARBON
AMS 6904
AMS 6910
AMS 7815
PWA 795
AMS 6908
AMS 6905
AMS 6910
AMS 6928
MERL 130
PWA 1615
AMS 6928
AMS 6910
AMS 7815
PWA 795
AMS 6910
AMS 6904
AMS 6910
AMS 6910
AMS 6910

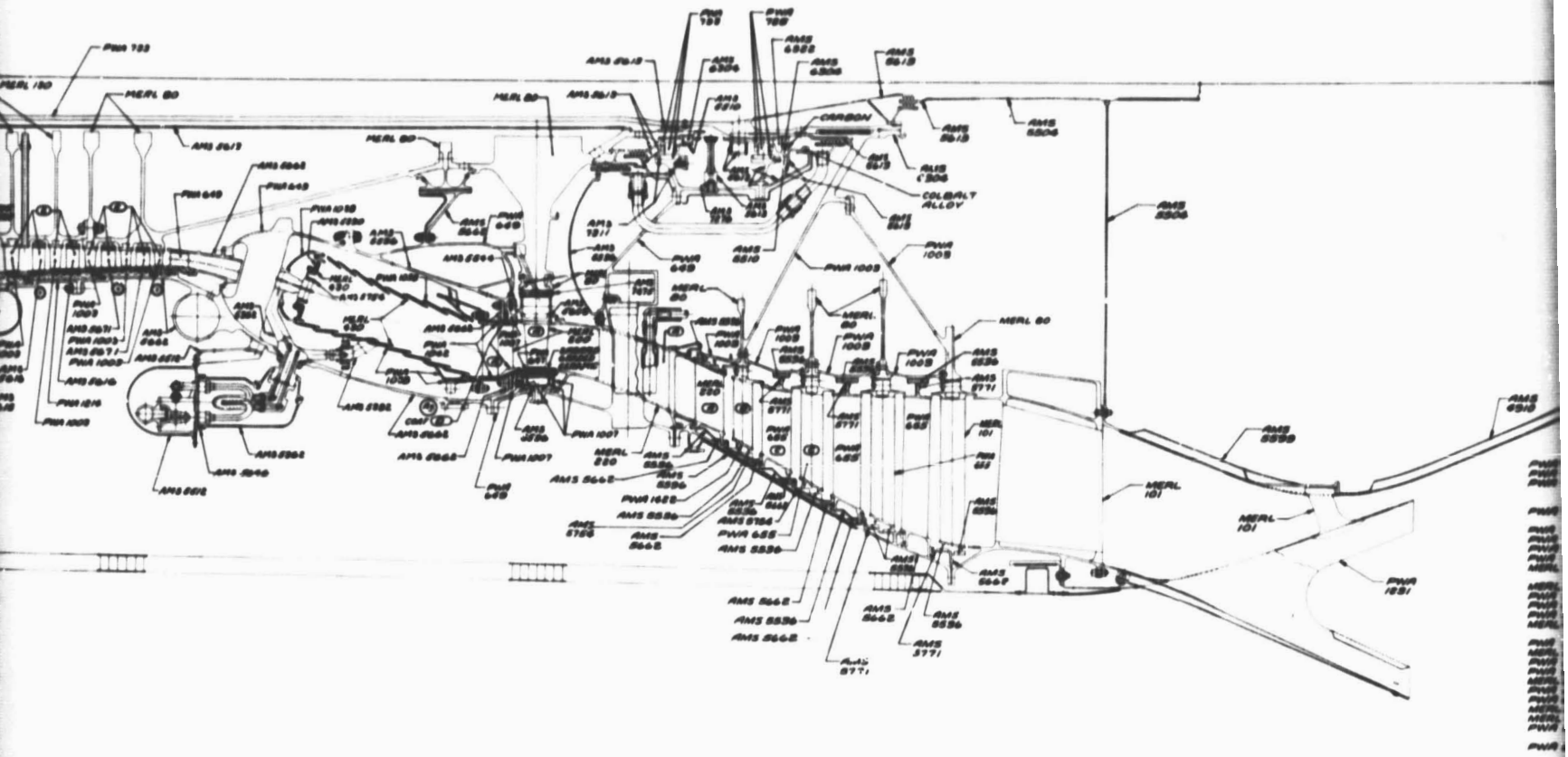

2 FOLDOUT FRAME

Figure 153 Energy Efficient Engine
Identification

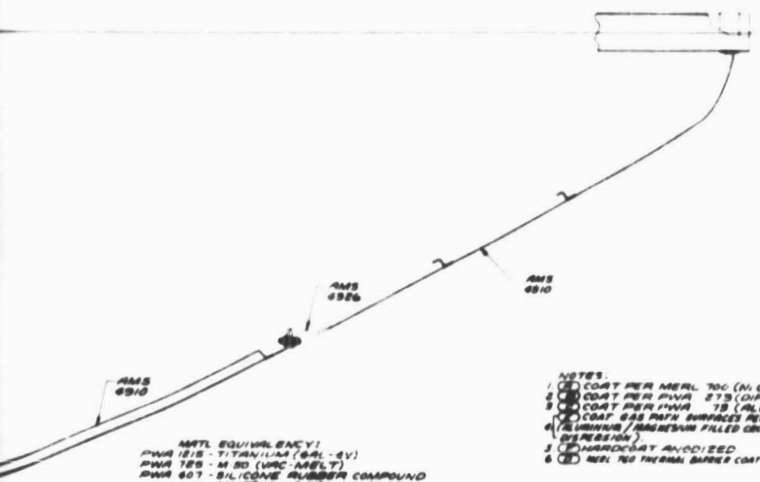

NOTES:
1. COAT PER MERL 76C (Ni-Cr-Al-Y)
2. COAT PER PWA 273 (DIFFUSED ALUMINIDE)
3. COAT PER PWA 73 (ALUMINUM SILICON)
4. COAT BASE PATH SURFACES PER PWA 646 (ALUMINUM / MAGNESIUM FILLED CHROMATE / PHOSPHATE DISPERSION)
5. HARDCOAT ANODIZED
6. REF. TBC THERMAL BARRIER COATING

MATL EQUIVALENCY:
PWA 1215 - TITANIUM (6AL-4V)
PWA 1216 - M-50 (VAC-MELT)
PWA 407 - SILICONE RUBBER COMPOUND CONTAINING HOLLOW GLASS MICRO SPHERES
PWA 655 - ORGANIC FIBER REINFORCED EPOXY RESIN COMPOSITE
PWA 725 - SAE 52100
PWA 795 - M-50 (DOUBLE VAC-MELTED)
PWA 1202 - TITANIUM (6AL-4MO-4V)
PWA 1005 - INCOLOY 901
MERL 150 - HIGH TENSILE STRENGTH TITANIUM ALLOY
MERL 80 - MODIFIED IN-100 ALLOY
PWA 1216 - TITANIUM (6AL-2SN-4ZR-2MO)
PWA 648 - INCONEL 718
PWA 1035 - HASTELLOY X
MERL 630 - OXIDE DISPERSOIDS (ODS) STRENGTHENED SHEET BURNER ALLOY
PWA 1042 - HAYNES 188
MERL 200 - SINGLE CRYSTAL NI ALLOY
PWA 1007 - WASPALOY
PWA 647 - MAR-M 509
MERL 150 - SINGLE CRYSTAL NI ALLOY
PWA 1422 - MAR-M 200 + HF
PWA 655 - INCONEL 718C
MERL 108 - TITANIUM ALUMI ALLOY
MERL 101 - TITANIUM ALUMINIDE ALLOY
PWA 1231 - TITANIUM ALLOY (6AL-2SN-4ZR-2MO) BETA ANNEALED, PRECIPITATION HEAT TREATED
PWA 1662 - CAST TITANIUM (6AL-4V)

3 FOLDOUT FRAMES

cient Engine Cross Section With Materials
ion

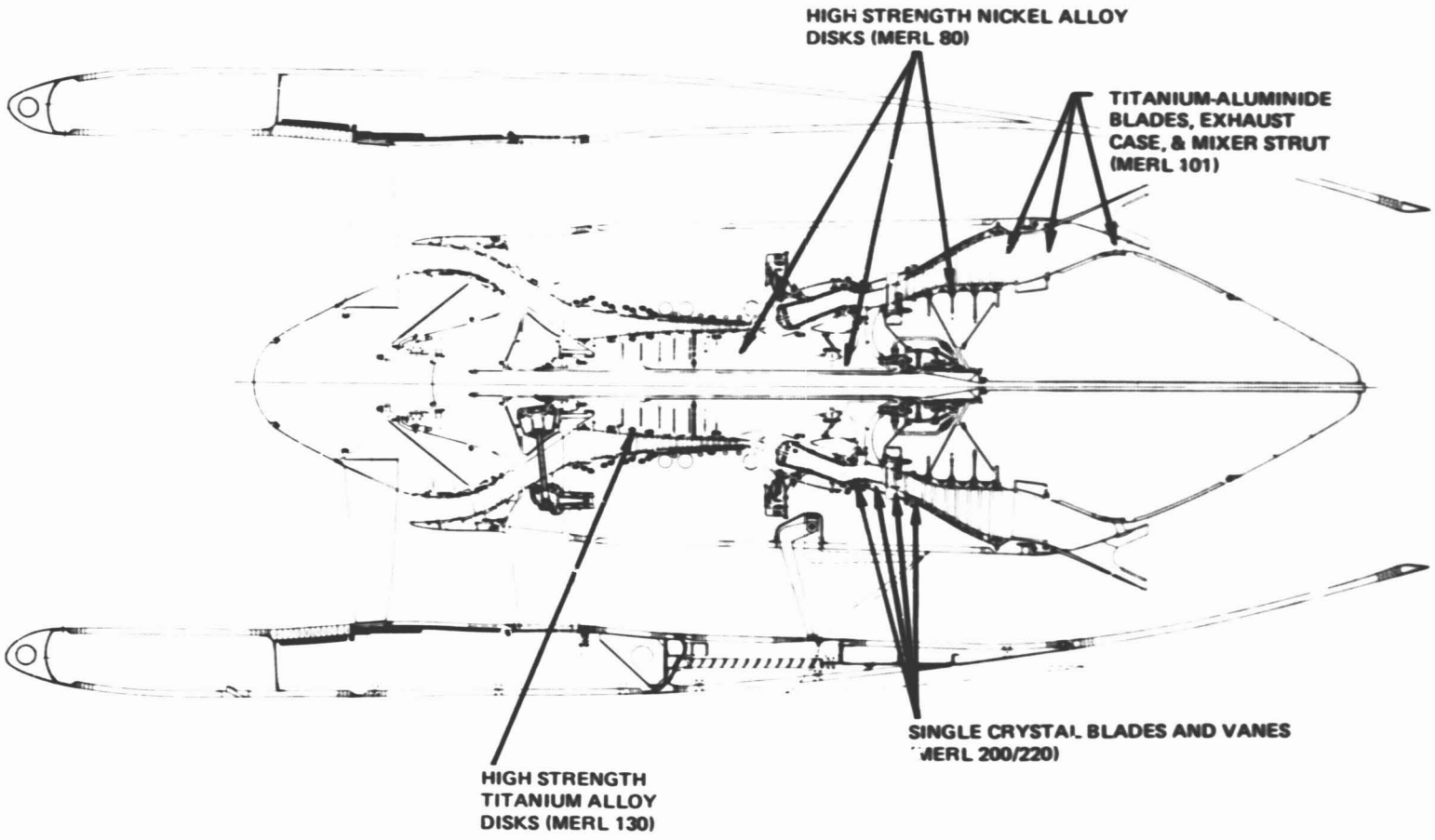

Figure 154 Propulsion System. Cross-section shows advanced material application for increased strength or reduced weight.

TABLE 62

SUMMARY OF ADVANCED MATERIALS APPLICATION

Material	Hardware Application
1. MERL 80 - High Strength Nickel Alloy	Rear-HPC, HPT and LPT Rotor Disks and Hubs
2. MERL 101 - Turbine Aluminide Alloy	5th-Stage LPT Blades, Turbine Exhaust Case
3. MERL 130 - High Strength Titanium Alloy	Mid-HPC Rotor Disks
4. MERL 200/220 - Single Crystal Cast Nickel Alloy	HPT Vanes and Blades, TIC Strut Vanes, 2nd Stage LPT Vanes

incorporation in a commercial engine development and certification program. Description and discussion of these materials are presented in the following paragraphs:

MERL 80

This heat treatable nickel-base alloy, with high strength-to-density ratio and high fatigue strength for applications to 760°C (1400°F) is formed by hot isostatic pressing (HIP) of powder metal. This alloy, similar to current PWA GATORIZED® IN-100, with improved smooth and notch low cycle fatigue properties, maintains GATORIZED tensile and stress rupture properties without subsequent forging. This allows low cost "near net shape" forming of parts by direct hot isostatic pressing.

Table 63 shows the comparison of Waspaloy and MERL 80 properties. Waspaloy is the high temperature disk material used in current Pratt & Whitney Aircraft commercial engines. MERL 80 is utilized in the FPS design for the high-pressure compressor rear rotor section, and the high- and low-pressure turbine disks. MERL 76, a high-temperature powder metal superalloy with a lower LCF capability relative to MERL 80, will be substituted in the experimental hardware.

The improved properties of MERL 80 permitted the high mechanical speed/large diameter high-pressure compressor without an excessive weight penalty. These properties also permitted the high AN^2 single-stage high-pressure turbine that meets design life goals, and the large diameter, low Cx/U low-pressure turbine without excessive weight penalties.

MERL 101

MERL 101 is a wrought titanium aluminum alloy (based on Ti_3-Al), with high creep strength-to-density ratio, for low stress application to 816°C (1500°F).

Table 64 presents a comparison of MERL 101 and cast INCONEL 713 nickel alloy. INCONEL 713 is a common low-pressure turbine blade material used in current commercial engines, specifically in the last stage blades of the low-pressure turbine. As a candidate for MATE 4, it would be available for use in 1982. Incone 713C (PWA 655) will be substituted in experimental hardware with a weight penalty.

MERL 101 is also specified in the FPS design for the turbine exhaust case struts and the mixer support struts. Inconel 625 will replace MERL 101 in the turbine exhaust case with a weight increase over the FPS design. Mechanically-attached Inconel 718 mixer support struts will be substituted with a small weight increase relative to the FPS.

The weight saving benefits of MERL 101 were 36.3 kg (80 lb) for the low-pressure turbine fifth-stage blade (vs. INCO 713) and 49.9 kg (110 lb) for the fabricated turbine exhaust case (vs. cast/sheet nickel alloy).

TABLE 63

COMPARISON OF WASPALOY AND MERL 80 PROPERTIES

	Waspaloy	MERL 80
538°C (1000°F) Ultimate Tensile Strength	Base	+15%
538°C (1000°F) Yield Strength	Base	+30%
Stress Benefit in Smooth Low Cycle Fatigue @ 538°C (1000°F) (Equal Lives)	Base	+50%
Stress Benefit in Notched Low Cycle Fatigue @ 538°C (1000°F) (Equal Lives)	Base	+40%
Density, kg/mm^3 ($lb/in.^3$)	9.25 (0.298)	7.89 (0.285)

TABLE 64

COMPARISON OF INCONEL 713 AND MERL 101 PROPERTIES

	INCONEL 713	MERL 101
816°C (1500°F) Yield Strength	Base	Base
816°C (1500°F) Ultimate Tensile Strength	Base	Base
816°C (1500°F) 300 Hour Stress Rupture Strength	Base	-50%
Elastic Modulus @ 816°C (1500°F) N/cm^2 ($lb/in.^2$)	16.2×10^6 (23.5×6)	10.3×10^6 (15×10^6)
Density, kg/cm^3 ($lb/in.^3$)	7.92×10^{-3} (0.286)	4.51×10^{-3} (0.163)

MERL 130

MERL 130 is a heat treatable wrought (beta processed) titanium base alloy, similar to 6Al-2Sn-4Zr-6Mo, with high tensile strength and high fatigue strength, for applications to 480°C (900°F).

Table 65 shows the comparison of MERL 130 properties to those of 6Al-2Sn-4Zr-2Mo titanium alloy, the common mid-HPC disk material used in current commercial engines. In the Energy Efficient Engine, MERL 130 is used in the high-pressure compressor mid-rotor section stages eight through 13. An electron beam (EB) welding program would ordinarily be conducted on this material as part of a normal engine development cycle, but because there is insufficient time to accomplish this, the experimental hardware will be fabricated from 6-2-4-2 Ti, for which EB weld data are on hand.

MERL 200/220

MERL 200/220 are specially cast heat treatable nickel-base superalloys having no grain boundaries (single crystal). These materials have improved stress rupture, creep, thermal fatigue, notch fatigue strength, and coated oxidation resistance over directionally solidified (DS) MAR-M-200, the high temperature/strength cast turbine blade and vane materials currently used in Pratt & Whitney Aircraft commercial engines. Table 66 presents a comparison of MERL 200/220 and D.S. MAR-M-200 properties.

MERL 200 is a second generation single crystal turbine blade and vane alloy. It is being developed under Pratt & Whitney Aircraft's IR&D program and will be available for use in 1983. Experimental hardware will be made from the first generation single crystal alloy PWA 1480. PWA 1480 blades and vanes will be designed with MERL 200 geometry and cooling levels, and will take a life debit for its 28°C (50°F) lower temperature capability. MERL 220 is a second generation single crystal turbine vane alloy with improved oxidation properties relative to MERL 200. It will be developed under Pratt & Whitney Aircraft's IR&D program and will be available for design use in 1983. The FPS design uses MERL 220 in the low pressure turbine transition duct fairing and second vane. The experimental hardware will use B-1900 (PWA 1455) turbine alloy in those areas and will accept a life penalty.

MERL 200/220 permitted the high AN^2 single-stage high-pressure turbine that meets design life requirements reduced the cooling air flow requirements of the high-pressure turbine blades and vanes, and allowed the turbine intermediate case (TIC) strut vanes and low-pressure turbine second-stage vanes to be uncooled.

TABLE 65

COMPARISON OF MERL 130 PROPERTIES TO 6Al-2Sn-4Zr-2Mo TITANIUM

	Ti-6Al-2Sn-4Zr-2Mo	MERL 130
480°C (900°F) Yield Strength	Base	+30%
480°C (900°F) Ultimate Tensile Strength	Base	+6%
480°C (900°F) 300 Hour 0.1% Creep Strength	Base	Base
Stress Benefit in Bore Low Cycle Fatigue @ 480°C (900°F) (Equal Lives)	Base	+20%

TABLE 66

COMPARISON OF MERL 200/220 PROPERTIES TO DIRECTIONALLY SOLIDIFIED MAR-M-200

	D.S. MAR-M-200	MERL 200	MERL 220
Temperature Benefit in Stress Rupture and Creep Strength (Equal Stresses and Lives)	Base	+ 56°C (+100°F)	+28°C (+50°F)
Temperature Benefit in Oxidation Resistance (Equal Lives)	Base	+ 56°C (+100°F)	+ 97°C (+175°F)
Strain Range Benefit in Thermal Fatigue (Equal Temperatures and Lives)	Base	+15%	+15%
Stress Benefits in Notched Low Cycle Fatigue @ 649°C (1200°F) (Equal Life)	Base	+15%	-
649°C (1200°F) Yield Strength	Base	+18%	+5%

4.13 CLEARANCE CONTROL

4.13.1 Objective, Goals and Major Considerations

The clearance control design objective is to minimize rotor-to-case radial clearances at all operating conditions, without incuring rubs during normal flight.

Component radial clearance design goals for takeoff and cruise conditions are summarized in Table 67.

The major considerations used in determining component radial clearance were:

1. Normal flight maneuvers and aerodynamic loads
2. Rotor and case thermal growth
3. Rotor centrifugal growth

4.13.2 Radial Gapping Procedure

The component radial clearances were predicted by estimating the rotor and case total growth rates (thermal, dynamic, and pressure) versus time to determine the minimum clearance time point (pinch point), and to establish the rotor-to-case cold clearance needed to preclude rubbing.

4.13.2.1 Rotor and Case Growth Response

A snap acceleration/deceleration engine cycle was used to predict the high-pressure turbine and low-pressure turbine component clearances, to establish feasibility of meeting goal clearances. Other phenomena, such as hot accelerations, were not included in the preliminary design effort. These will be considered in determining the final detail design clearances.

Turbine rotor and case growths were determined at transient and steady-state time points using a computerized shell analyses with input transient temperatures which were calculated using a computer model of the actual mechanical configuration and thermal environment. Typical rotor and case growth vs. time response curves are shown in Figure 155 and Figure 156.

The fan, low-pressure compressor, and high-pressure compressor growth responses were predicted from steady-state conditions only since these components are designed to ensure pinch points at steady-state takeoff.

TABLE 67

COMPONENT RADIAL CLEARANCE DESIGN GOALS - mm (in.)

	Takeoff	Cruise
Fan	-	2.18 (0.086)
LPC	-	0.56 (0.022)
HPC	0.48 (0.019)	0.33 (0.013)
HPT	0.74 (0.029)	0.51 (0.020)
LPT	1.52 (0.060)	0.51 (0.020)

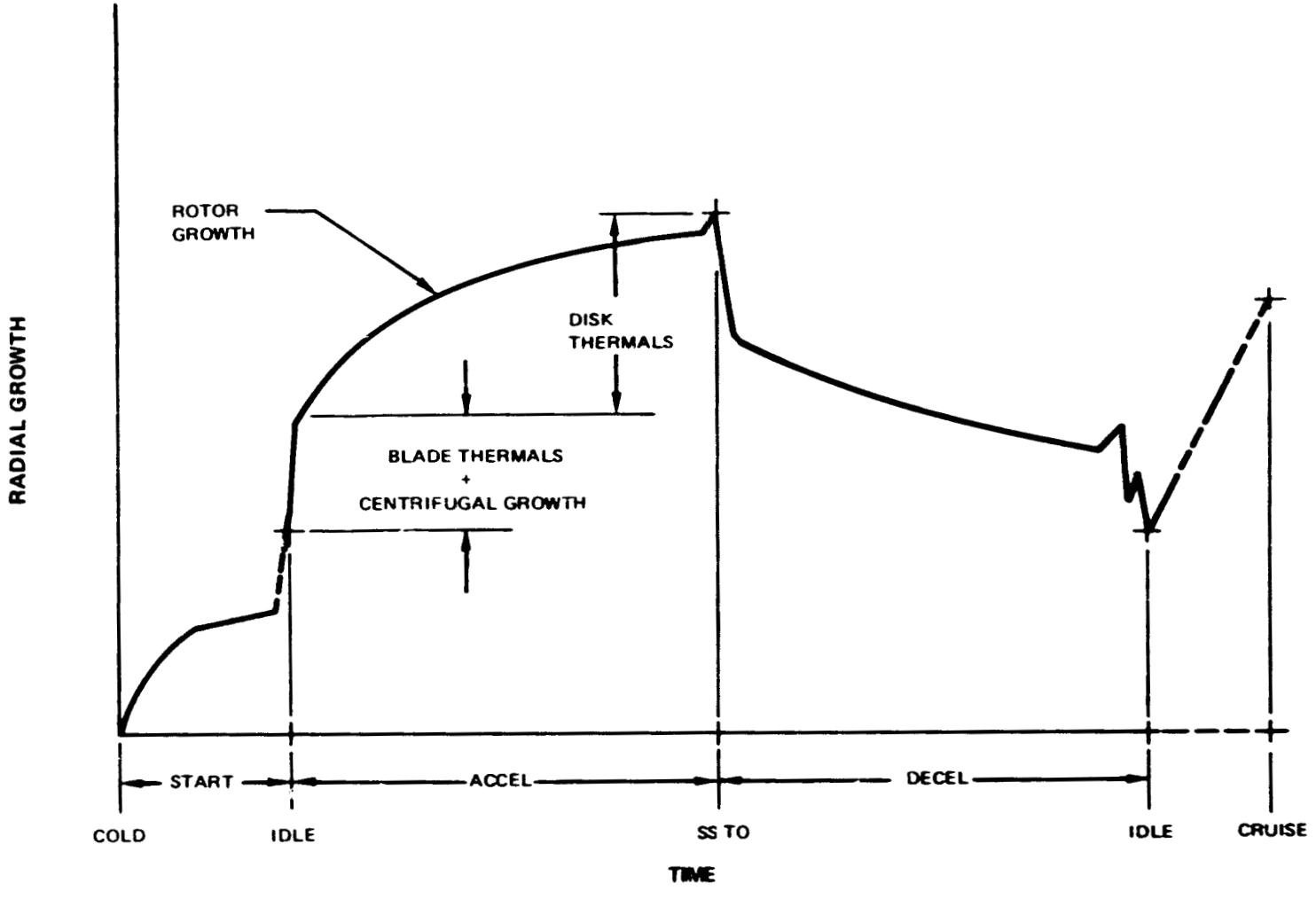

Figure 155 Transient Rotor Radial Growth. Pattern shows effects of thermal and centrifugal forces during mini-cycle.

J20127-169
782711

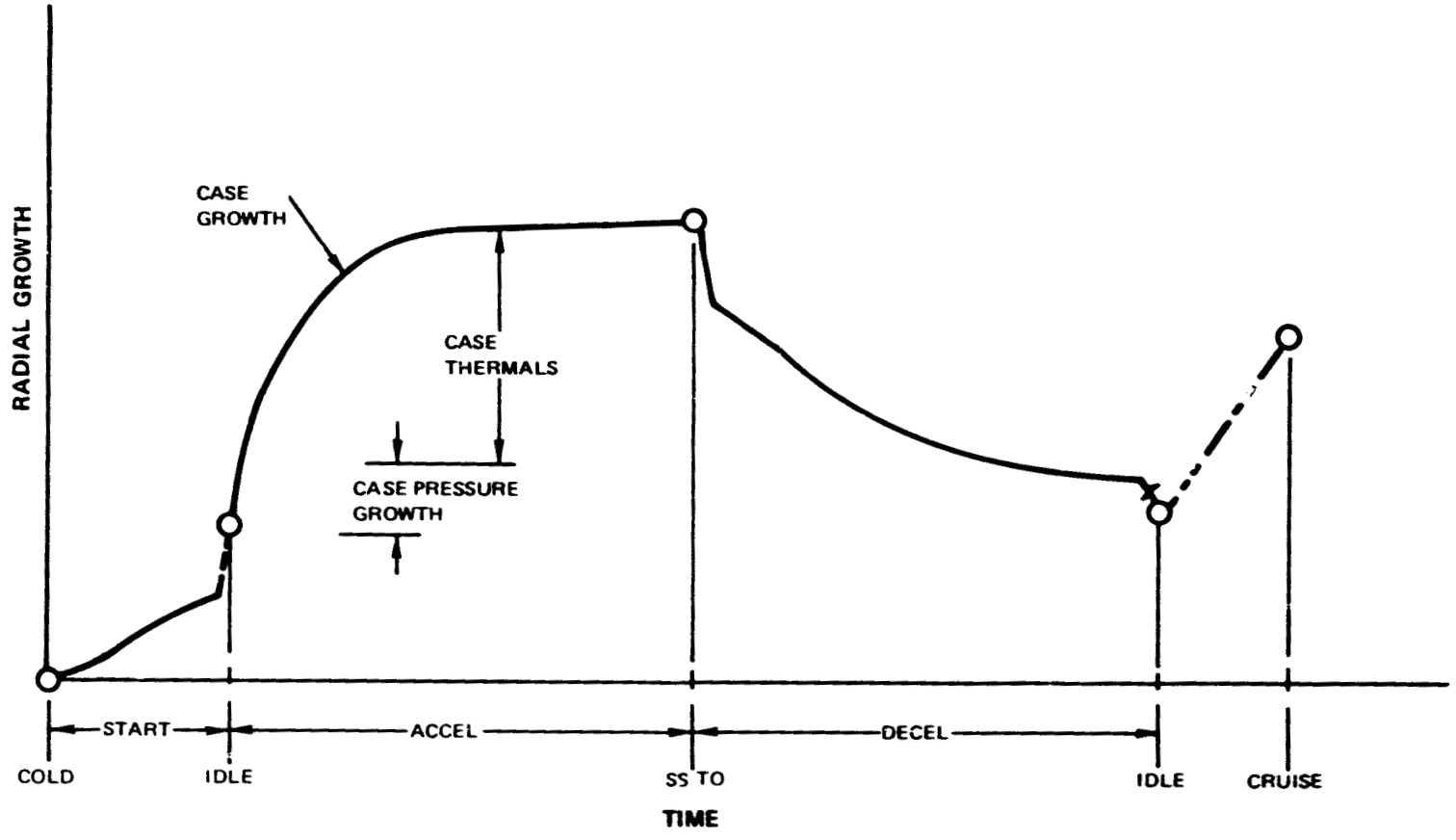

Figure 156 Transient Case Radial Growth. Pattern shows effects of pressure and thermals during mini-cycle.

4.13.2.2 Clearance Ingredients

The effects of the following items on the rotor-to-case clearances were considered in estimating the minimum allowable radial gap between rotors and cases:

1. Gravitational and gyroscopic mansuver deflections
2. Mount load ovalization
3. Cowl gust loads
4. Manufacturing tolerances and eccentricities
5. Bearing radial clearances
6. Normal rotor unbalance
7. Blade surge deflections
8. Unsymmetrical thermal and pressure distortion
9. Hot engine restart rotor whirl

The minimum required gaps were determined by combining the clearance effects of the listed items for each component (fan, low-pressure compressor, high-pressure compressor, high-pressure turbine and low-pressure turbine) at its critical operating condition.

Figure 157 shows a typical rotor response curve. In this example, the high-pressure turbine blade tip, with the required gap (actual high-pressure turbine value) is shown as the cross-hatched area above the rotor growth curve.

The rotor to case radial clearance at cold assembly and at other engine operating conditions can now be established by superimposing the case response curve above the rotor response curve. The position of the case response curve is established by minimizing the difference between the two curves (radial clearance), while providing the required gap at all operating conditions. The time point where the radial clearance equals the required gap is the pinch point. A typical final thermal response curve is shown in Figure 158 (high-pressure turbine blade tip) showing the radial clearances at cold assembly, idle, pinch point, SSTO and cruise.

4.13.3 Clearance Control Design Features

The clearance control design objective dictated many of the preliminary mechanical design features including:

1. Straddle mounted/stiff high spool

2. Three bearing low spool with optimal bearing locations

3. Structurally integrated nacelle/cowl with load sharing

4. Engine mount system designed to minimize case deflection

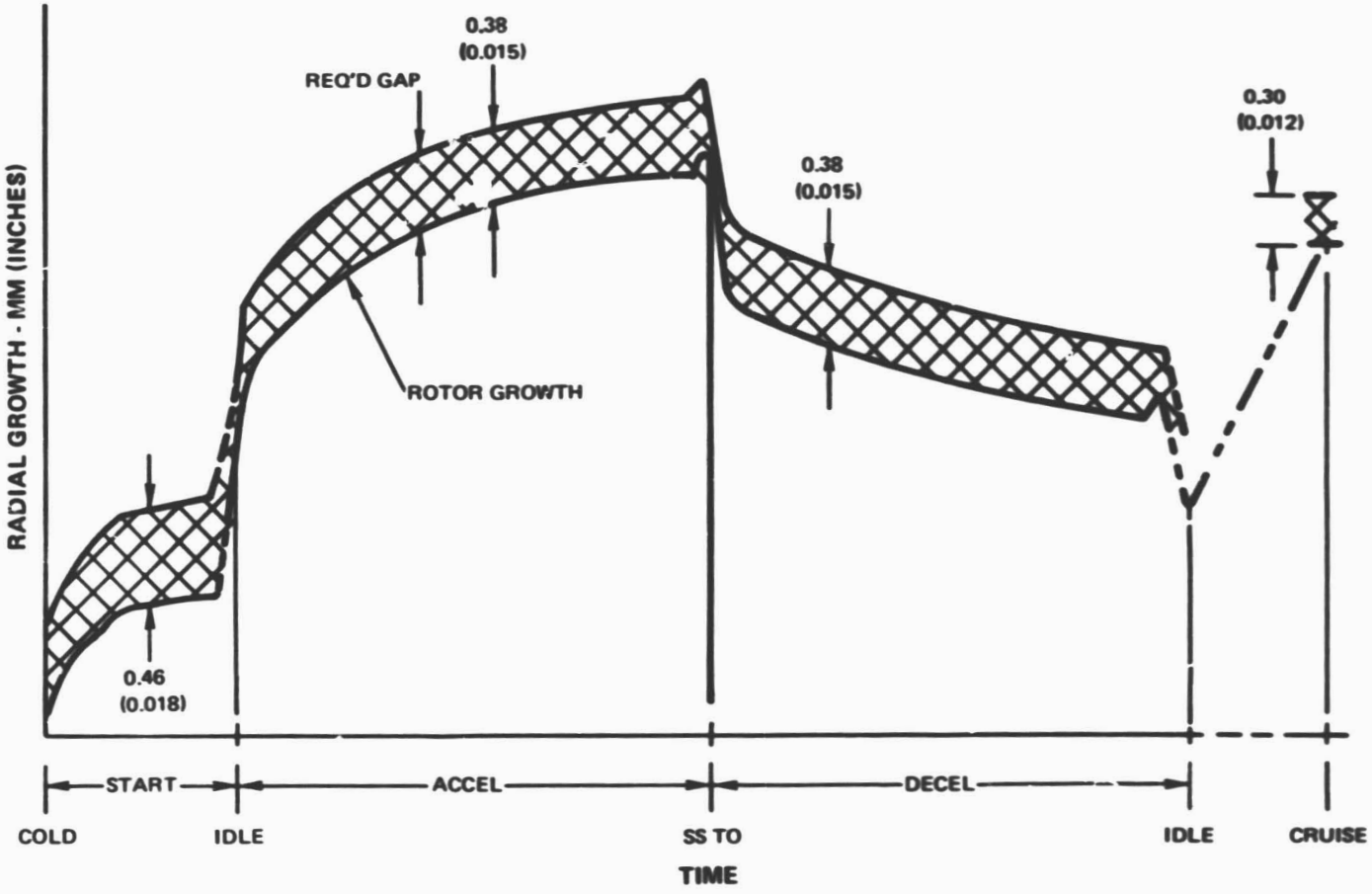

Figure 157 Typical Rotor Response. Curve shows gap needed to preclude rubs in normal service.

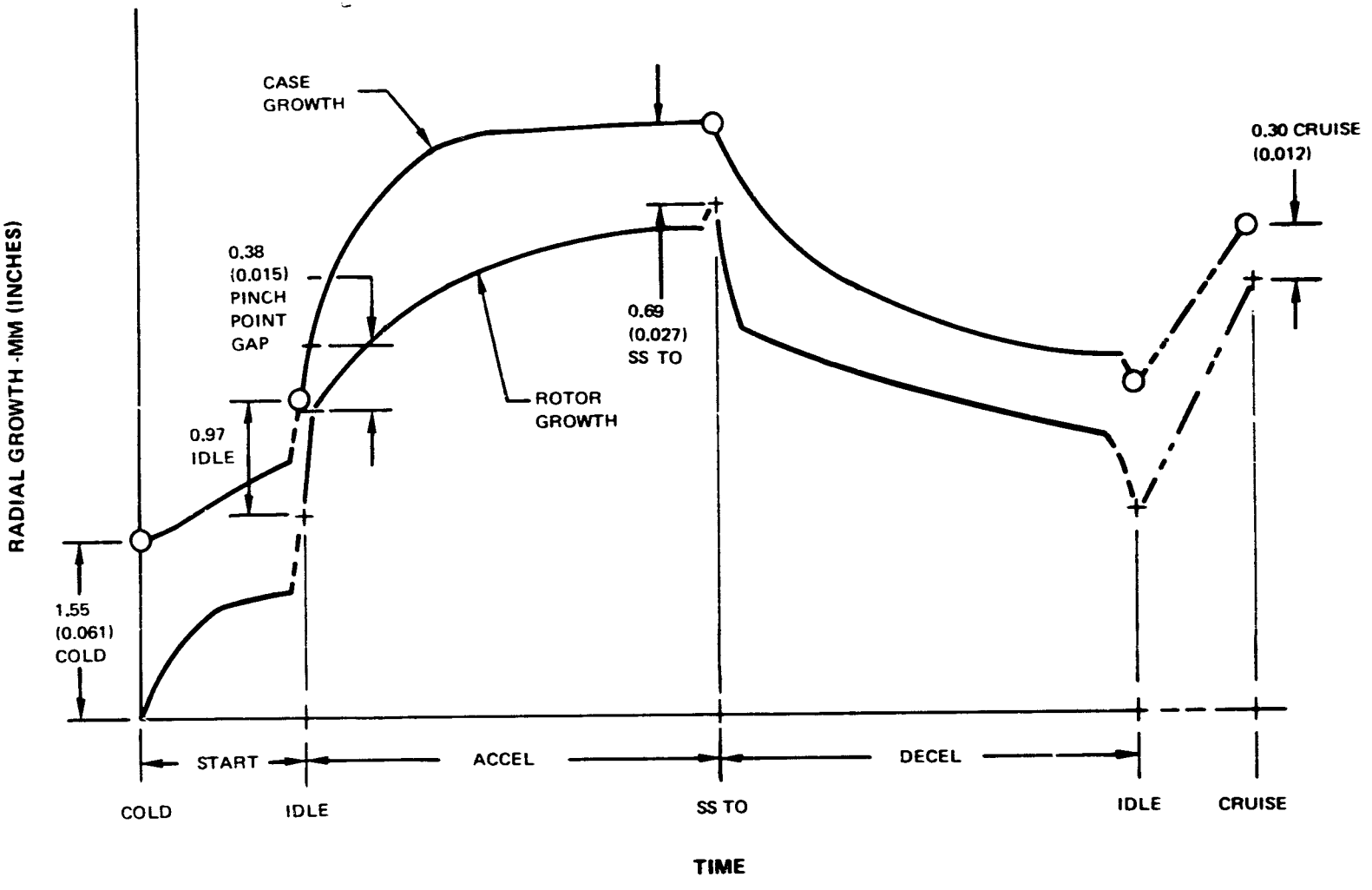

Figure 158 Typical Final Thermal Response. Curve shows case and rotor clearances to preclude rubs in normal service.

5. Active clearance control in the high-pressure compressor, high-pressure turbine, and low-pressure turbine

4.13.3.1 High Spool Rotor Support

The high spool rotor, shown in Figure 159, is straddle mounted between the two main shaft bearings that are located beneath the front high-pressure compressor stages and just aft of the high-pressure turbine rotor. The high-pressure compressor and high-pressure turbine components are coupled by a large diameter/stiff shaft. These design features reduce the high spool rotor-to-case deflections during flight maneuvers by eliminating overhung rotor stages that cause large rotor radial deflections, by locating the larger rotor masses near the support structure to force more similar rotor and static structure deflection characteristics, and by reducing the bending deflection of the high-pressure compressor/high-pressure turbine coupling shaft.

4.13.3.2 Low Spool Rotor Support

The low rotor, shown in Figure 160, is supported by three bearings: the first located just aft of the fan, the second located 40.6 cm (16.0 in.) aft of the first, and the third located beneath the front two low-pressure turbine stages.

The fan and low-pressure compressor are overhung from the two front bearings with wide axial spacing, or wheelbase to minimize the rotor deflections from gravitational or gyroscopic maneuver loads.

The rear bearing axial position was selected to provide the least rotor deflection in the low-pressure turbine at the small front stages, where clearances have a larger effect on efficiency than do the rear stages.

4.13.3.3 Structurally Integrated Nacelle

The structurally integrated nacelle, shown in Figure 161, minimizes clearance closures caused by aerodynamic cowl loads. The inlet cowl is supported by the engine outer fan case. Cowl loads are transferred to the aircraft pylon via the engine rear mount structure. Load sharing is accomplished by providing structural inner and outer fan ducts which share cowl loads with the core engine by providing alternate load paths to the engine rear mount, thereby reducing the core engine case backbone bending moments and deflections. Nacelle load sharing also reduces the fan case deflections caused by fan exhaust case trunnion loads by sharing the load through the outer fan duct and by providing fan exhaust case stiffening with the inner fan duct.

The amount of cowl load sharing provided by the structurally integrated nacelle is estimated at about 80 percent for vertical cowl loading and 60 percent for horizontal cowl loading. This difference in the percent

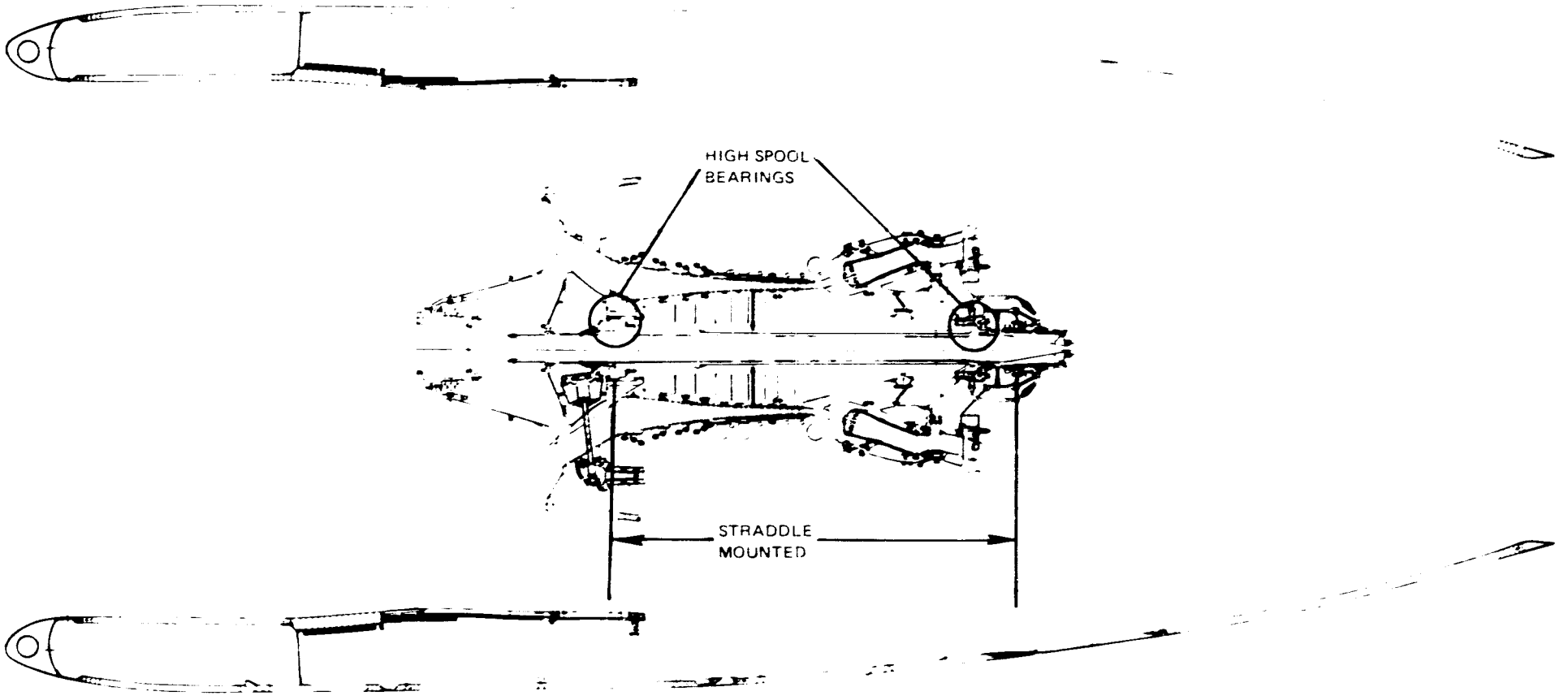

Figure 159 High-Spool Cross-Section. Stiff, short high spool is straddle-mounted for deflection restraint.

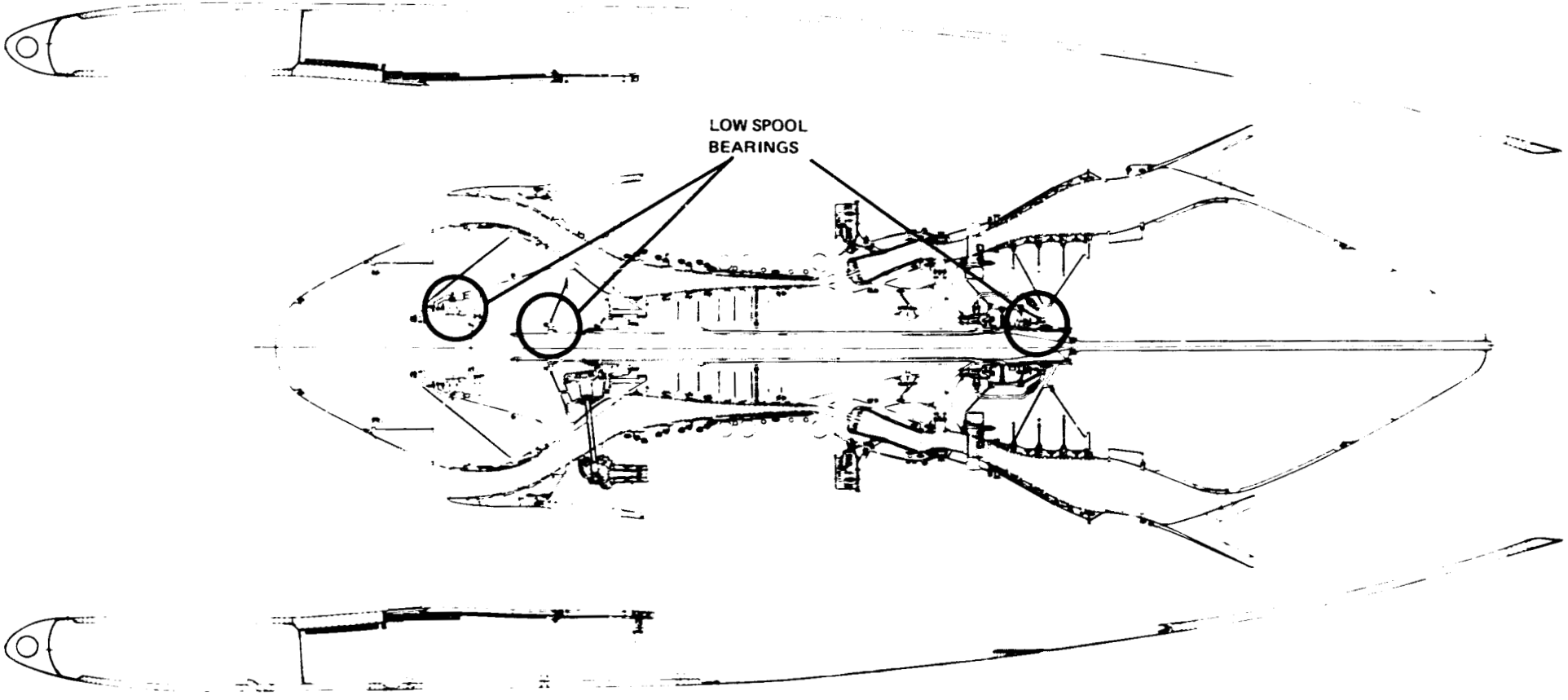

Figure 160 Low/High Spool Cross-Section. Optimally situated low spool support bearings for deflection restraint.

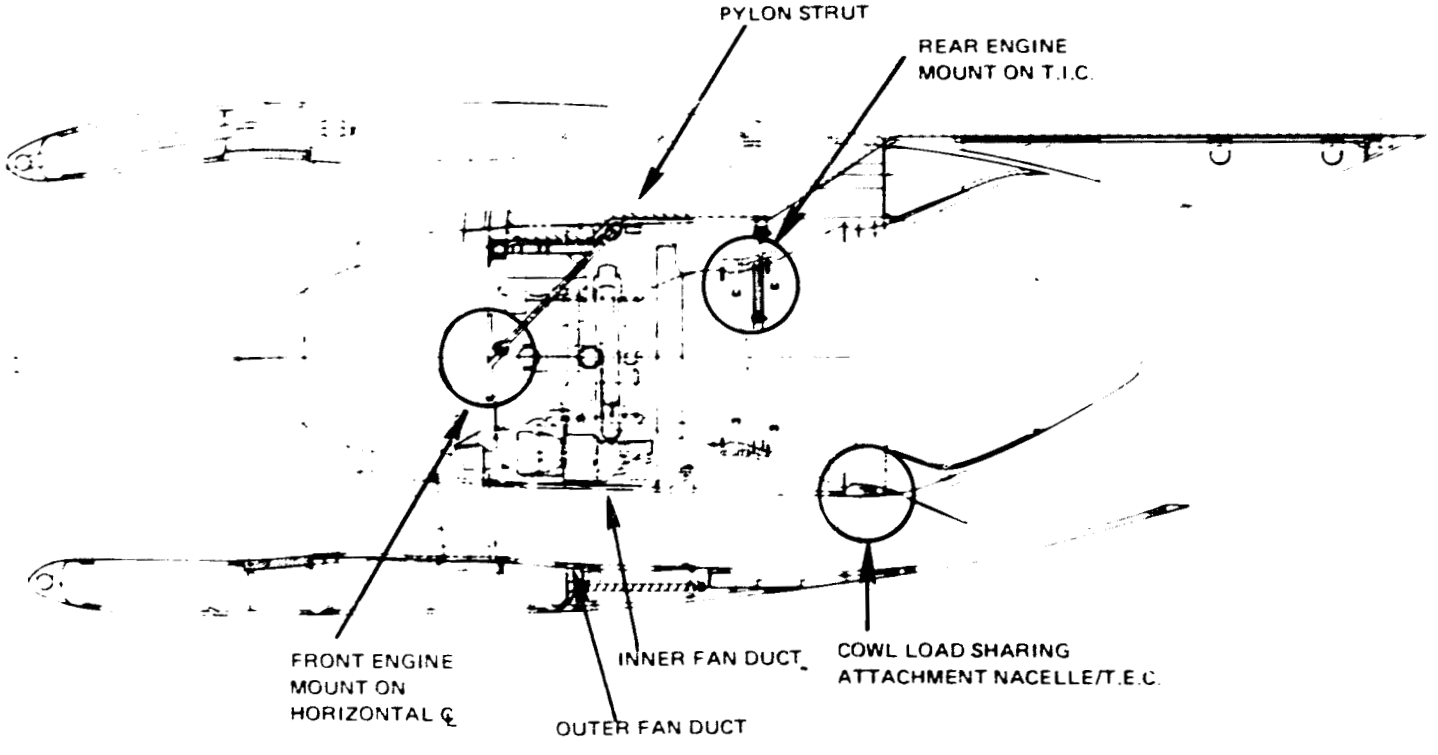

Figure 161 Structurally Integrated Nacelle. Cross-section shows cowl load sharing through structural ducts and unique thrust mount to reduce engine case loads and deflections.

of load sharing is a result of the upper pylon strut and lower D-shaped duct support flanges which produce greater axial stiffness in the vertical plane than in the horizontal plane.

4.13.3.4 Engine Mount System

The engine mounts are positioned to transmit loads to the pylon structure with a minimum of engine case inplane ovalization or "backbone" bending deflections. Dual front thrust mounts brackets are located on the horizontal centerline of the engine to be in line with the engine produced thrust and eliminate thrust induced "backbone" bending moments.

Two rear mount links, which carry vertical loads, are connected to the turbine intermediate support frame 25 degrees above the horizontal centerline and combined with the polygonal case design. This minimizes inplane ovalization deflection caused by the locally applied vertical mount loads.

4.13.3.5 Active Clearance Control (ACC)

An active clearance control (ACC) system, shown in Figure 162, is used to reduce cruise clearances in the rear of the high-pressure compressor, high-pressure turbine, and front two stages of the low-pressure turbine. The ACC system creates additional clearance closure at cruise by providing additional case cooling during higher altitude operation, thereby reducing case thermal growth.

The high-pressure compressor ACC system, shown in Figure 163, is an external system utilizing fan bleed air supplied externally through impingement tubes that cool the outer case during cruise operations.

The high-pressure and low-pressure turbine ACC systems, shown in Figure 164 and Figure 165, are internal systems utilizing 15th stage high-pressure compressor bleed during takeoff/climb and 10th-stage high-pressure compressor bleed as the cooling air source during cruise operations. The reduction in cooling air temperature associated with changing the cooling air source from the 15th-to 10th-stage provides the additional clearance closure at cruise by shrinking the case/airseal.

4.13.4 Rotor/Case Deflection Analysis

Rotor/case deflection analyses were used to assess the clearance closures caused by gravitational (G) and gyroscopic (gyro) flight maneuver loads, aerodynamic cowl loads, mount load case ovalization and bowed rotor whirl during a hot engine restart. These estimates, combined with other considerations such as tolerances and eccentricities, bearing radial clearances, and rotor whirl due to normal unbalance, were used to establish the minimum required gap (pinch point

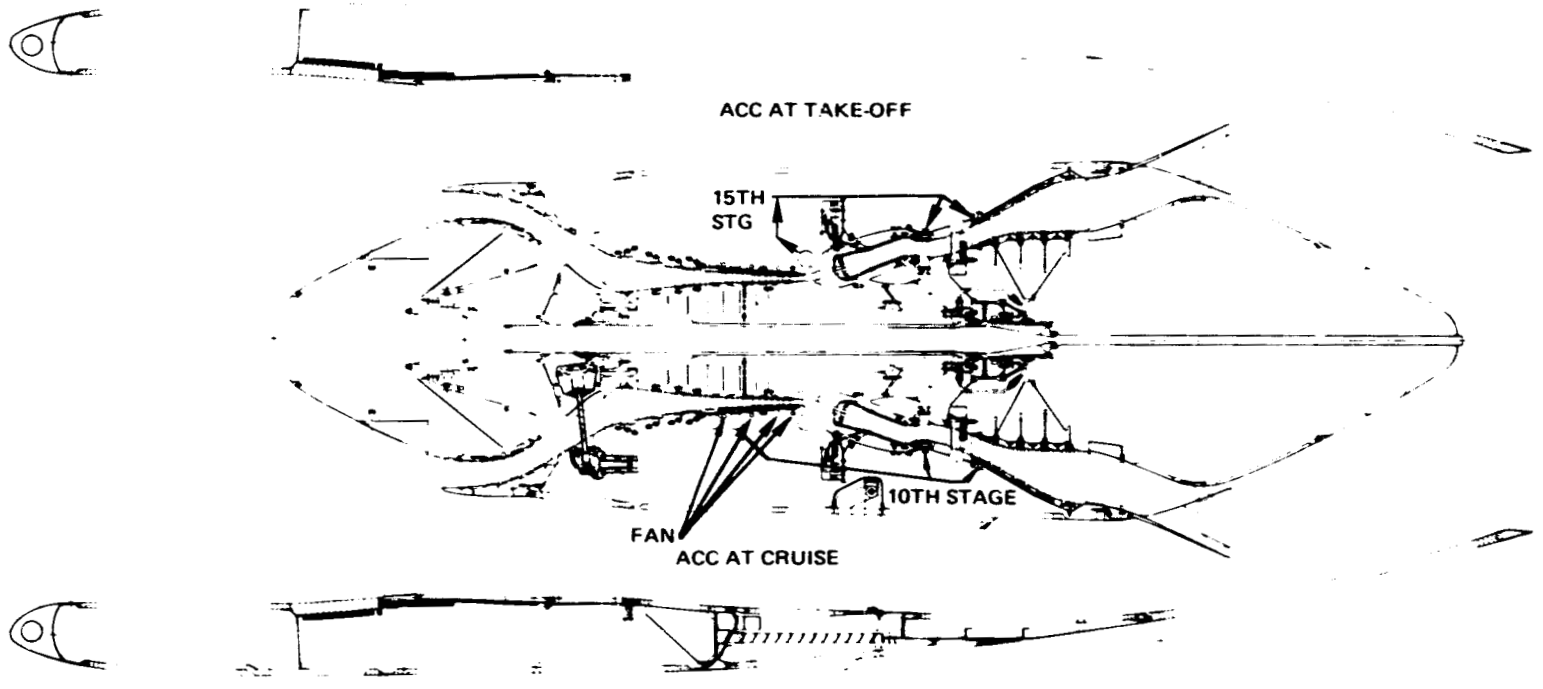

Figure 162 Active Clearance Control System. Cross-section shows multi-source case cooling approach to match individual component clearance requirements.

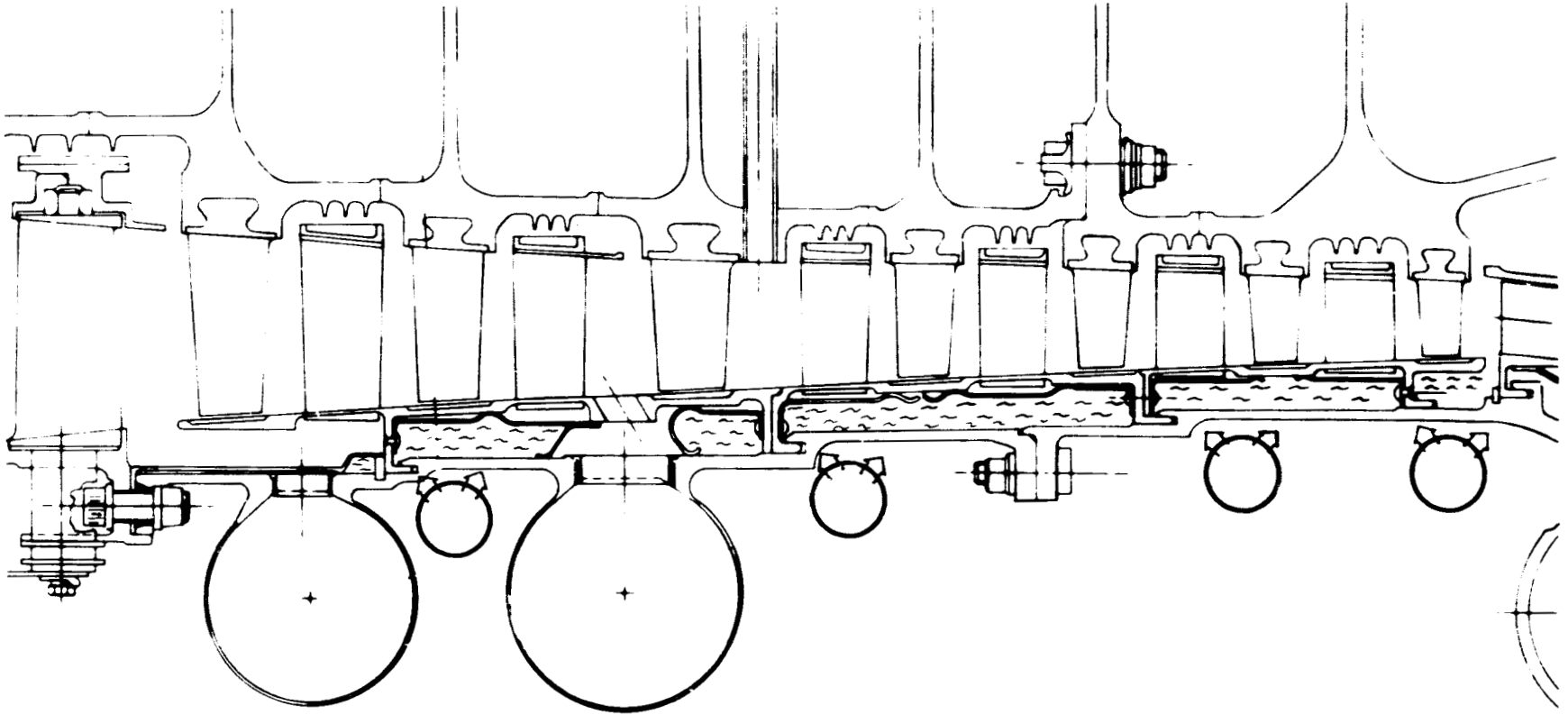

Figure 163 High-Pressure Compressor External Active Clearance Control. System utilizes fan air impingement tubes during cruise.

J20127-178
782711

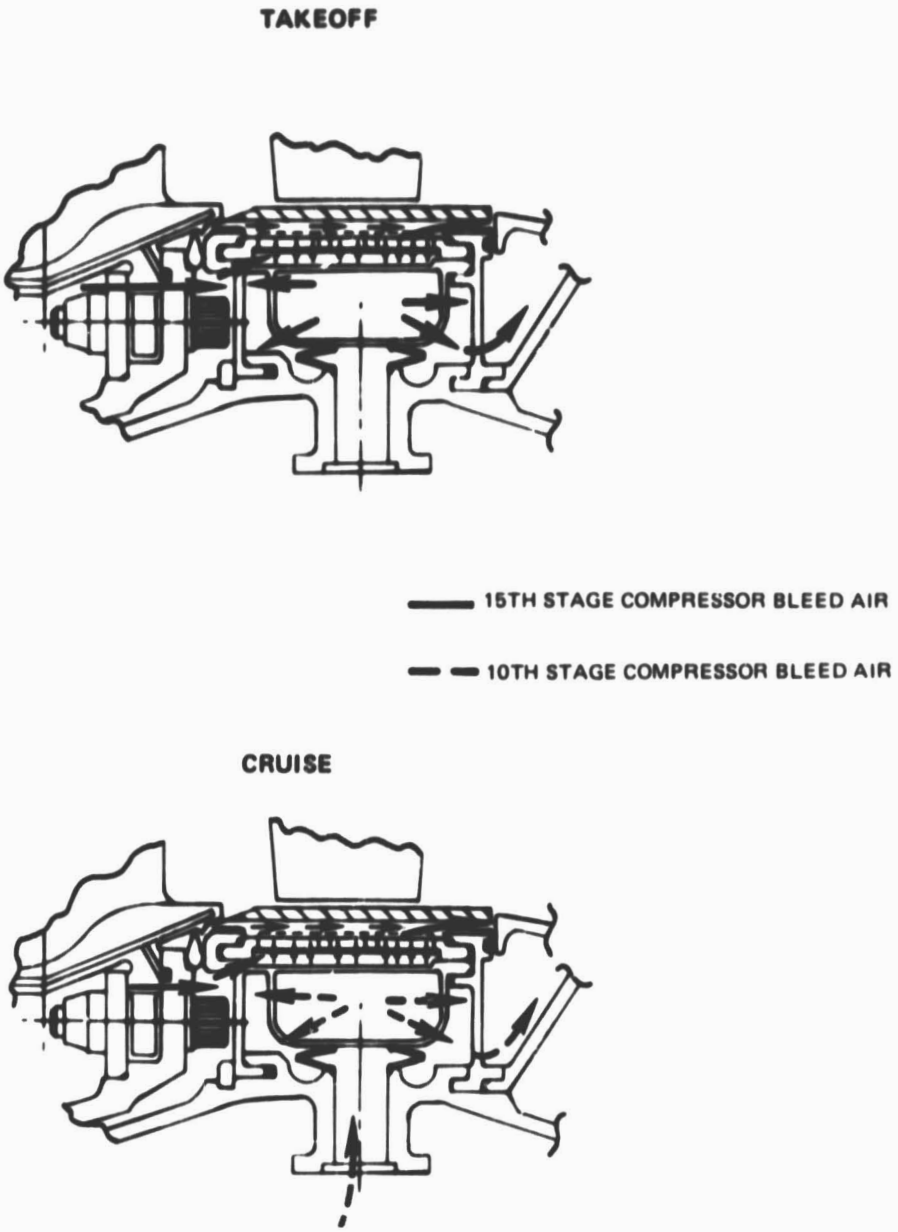

Figure 164 High-Pressure Turbine Internal Active Clearance Control. System uses two different air sources between takeoff and cruise for additional case shrinkage during cruise.

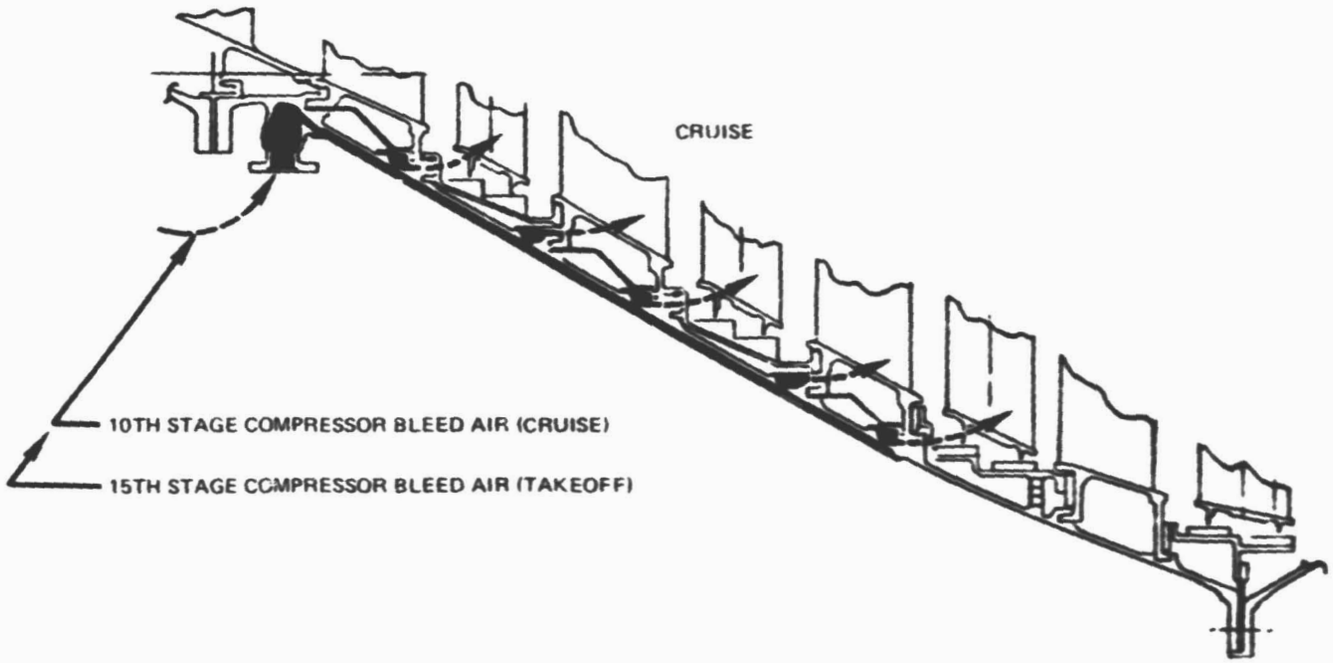

Figure 165 Low-Pressure Turbine Internal Active Clearance Control. System uses two different air sources between takeoff and cruise for additional case shrinkage during cruise.

clearance). Since these events do not occur at the same circumferential location or at the same time, the individual closure estimates were modified based on current commercial engine service experience to estimate the cumulative effect of the individual clearance closures at any given time.

4.13.4.1 Rotor-Frame Analysis Model

A computerized rotor-frame model was used to estimate the clearance closures caused by gravitational and gyroscopic flight maneuver loads and aerodynamic cowl loads. The computer model used in the low and high spool rotor dynamics analysis discussed in Section 4.15 is shown in Figure 166.

The model was used to analyze vertical and horizontal gravitational and pitch and yaw gyroscopic loadings during flight maneuvers and externally applied loads at the inlet case to simulate aerodynamic cowl loading.

4.13.4.2 "G" Load Maneuver Deflections

"G" loading levels expected in normal initial service were analyzed with the rotor-frame model. Deflection mode shapes, Figure 167, show the relative centerline deflections of the rotors and cases from which the rotor to case clearances closures were calculated. The resulting clearance closures, that occur in the fan through low-pressure turbine components, are shown in Table 68 at the takeoff/climb operating condition.

4.13.4.3 Gyroscopic Load Maneuver Deflections

The rotor-frame model was also used to analyze gyroscopic loading from normal flight maneuvers. The resulting predicted mode shape is shown in Figure 168. Estimated component clearance closures are shown in Table 69 for the take-off/climb operating condition.

4.13.4.4 Mount Load Case Ovalization

A NASTRAN analysis of the complete engine static structure was performed to estimate case ovalization caused by the locally applied engine mount loads. Internal axial loads were applied to the three-dimensional model shown in Figure 169 and reacted out at the front and rear engine mounts. The case ovalization deflections and resulting clearance closures only affected the high-pressure turbine and low-pressure turbine components, because of their close proximity to the rear mount. The gap required during takeoff/climb is shown in Table 70.

TABLE 68

GAP REQUIRED DURING ENGINE TAKEOFF/CLIMB
FOR NORMAL GRAVITATIONAL LOADS - mm (in)

		G's
Fan		0.36 (0.014)
LPC (Avg.)		0.20 (0.008)
HPC	9th Stage	0.061 (0.0024)
	15th Stage	0.056 (0.0027)
HPT		0.061 (0.0024)
LPT	2nd Stage	0.084 (0.0033)
	4th Stage	0.155 (0.0061)

TABLE 69

GAP REQUIRED DURING ENGINE TAKEOFF/CLIMB
FOR NORMAL GRAVITATIONAL AND GYROSCOPIC LOADS - mm (in.)

		G's	Gyro's
Fan		0.36 (0.014)	0.89 (0.035)
LPC (Avg.)		0.20 (0.008)	0.18 (0.007)
HPC	9th	0.061 (0.0024)	0.0028 (0.0011)
	15th	0.056 (0.0027)	0.0018 (0.0007)
HPT		0.061 (0.0024)	0.005 (0.0002)
LPT	2nd	0.084 (0.0033)	0.048 (0.0019)
	4th	0.155 (0.0061)	0.160 (0.0063)

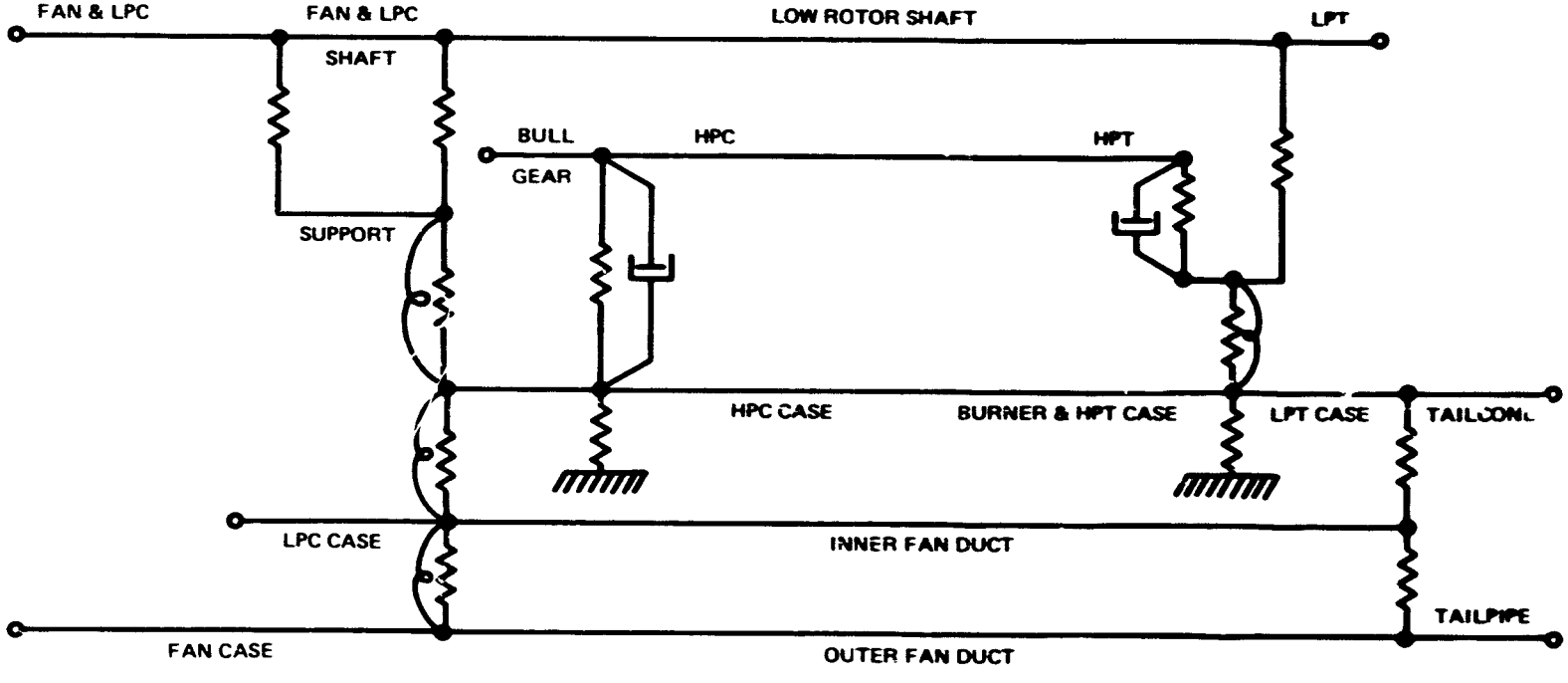

Figure 166 Computerized Rotor-Frame. Model used in estimating deflections under various loads.

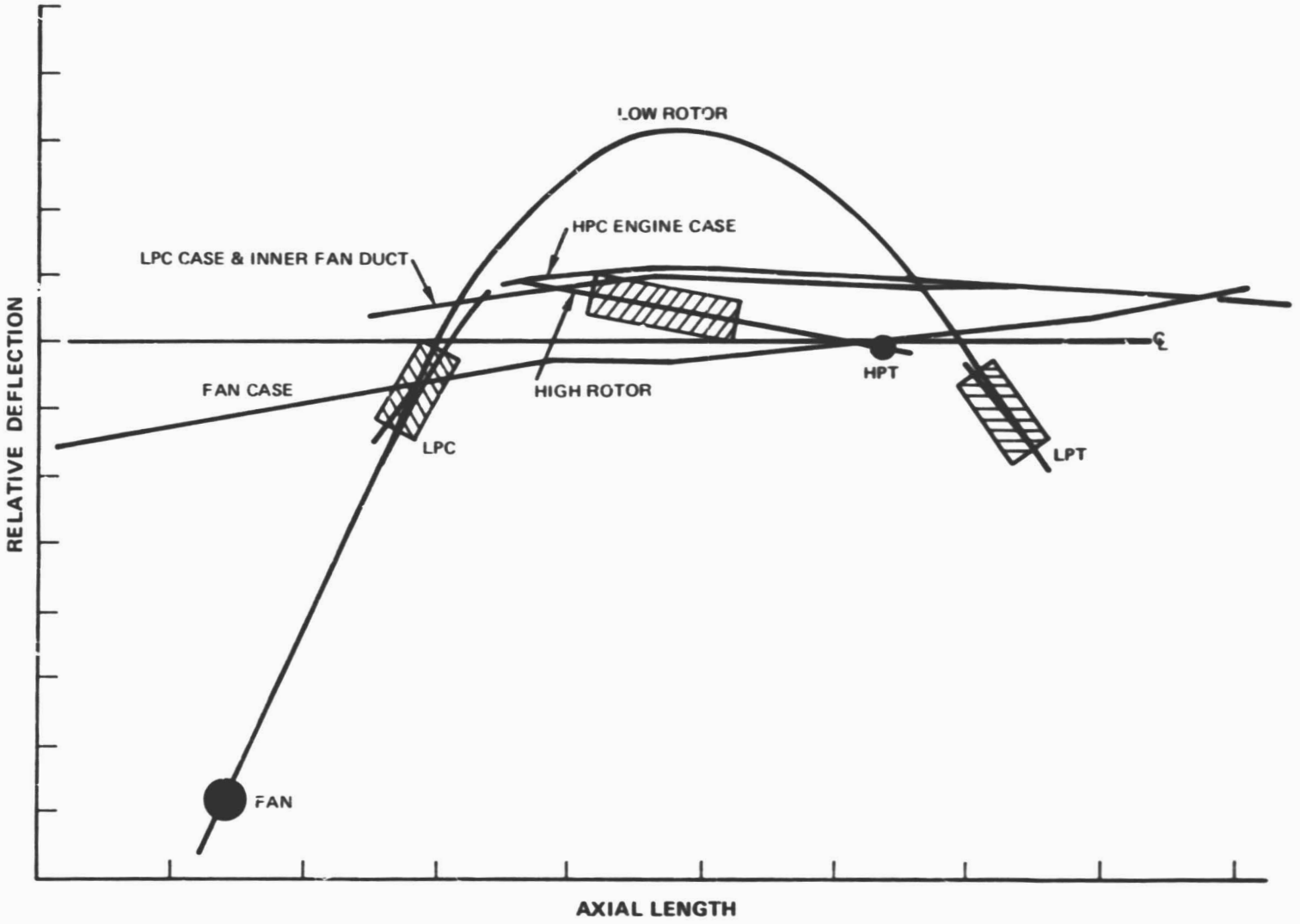

Figure 167 Deflected Mode Shapes. Rotor-case centerline deflections caused by "G" loads.

J20127-167
782711

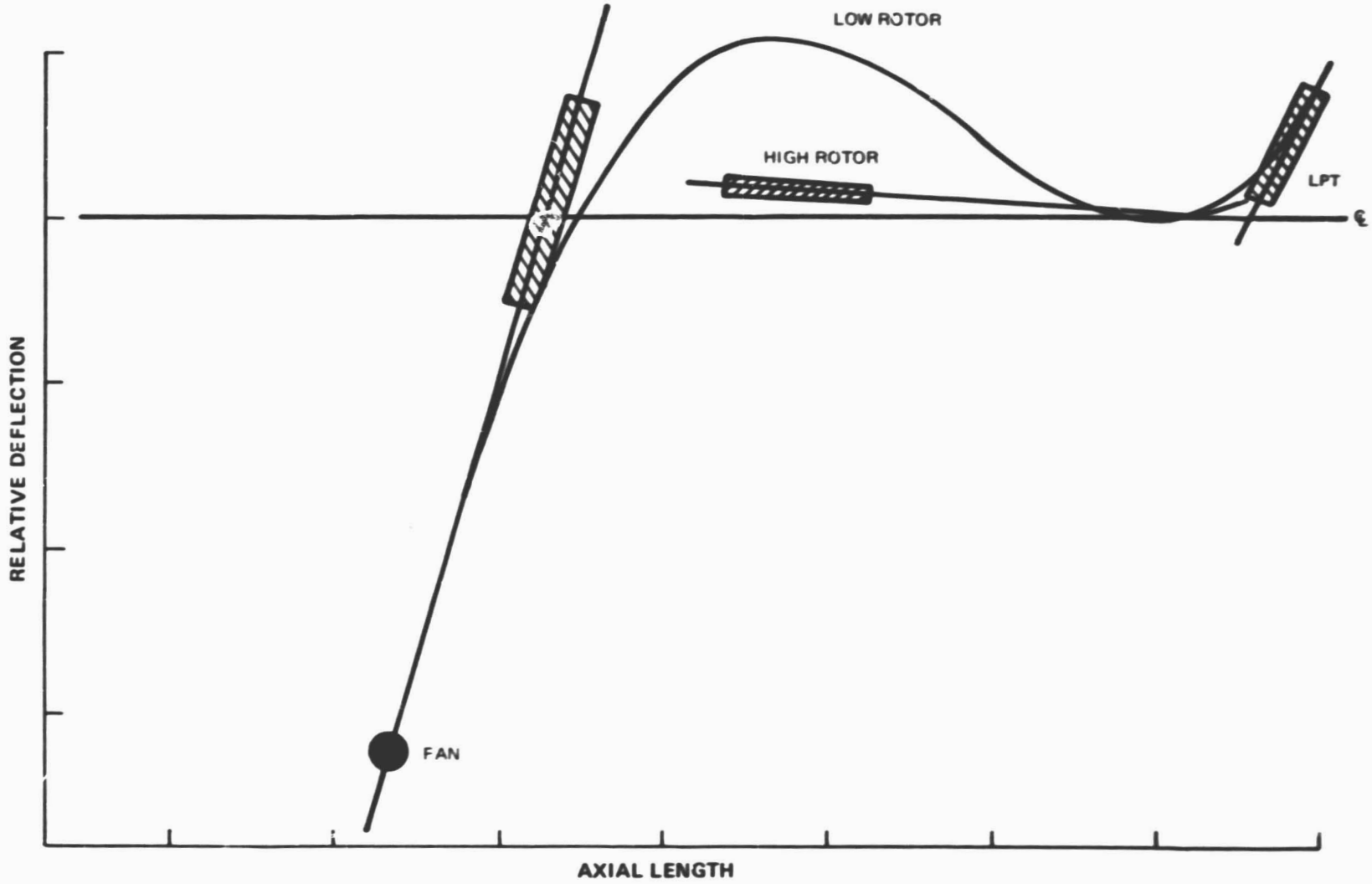

Figure 168 Deflected Mode Shapes. Rotor-case centerline deflections caused by gyroscopic loads.

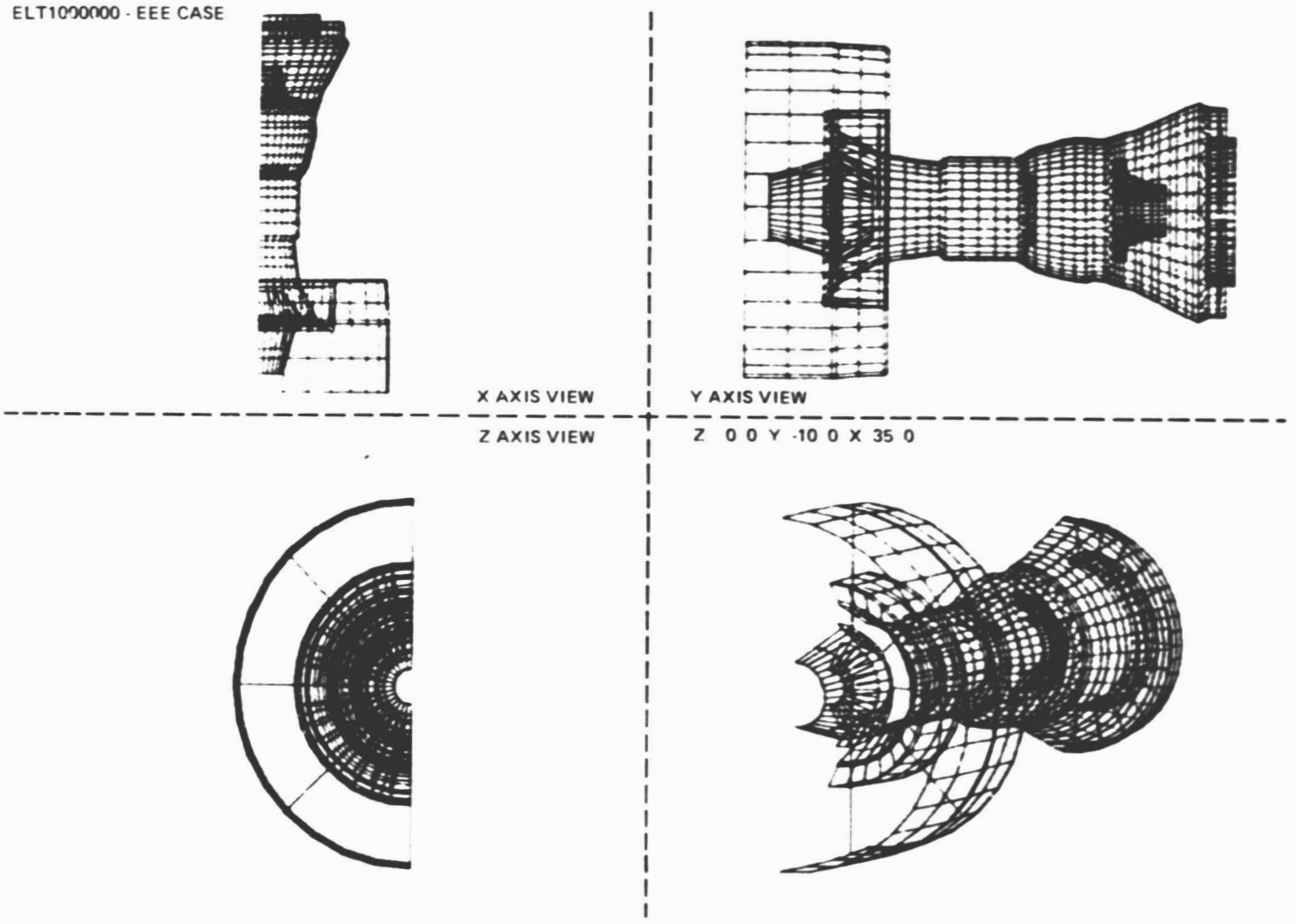

Figure 169 Three-Dimensional NASTRAN Analysis. Engine model used for analyzing case ovalization deflections.

TABLE 70

GAP REQUIRED DURING ENGINE TAKEOFF/CLIMB
FOR NORMAL GRAVITATIONAL AND GYROSCOPIC LOADS
AND MOUNT LOAD CASE OVALIZATION - mm (in.)

	G's	Gyro's	Mount Load Oval.
Fan	0.36 (0.014)	0.89 (0.035)	0.000
LPC (Avg.)	0.20 (0.008)	0.18 (0.007)	0.000
HPC 9th	0.061 (0.0024)	0.028 (0.0011)	0.000
15th	0.056 (0.0027)	0.018 (0.0007)	0.000
HPT	0.061 (0.0024)	0.005 (0.0002)	0.076 (0.003)
LPT 2nd	0.084 (0.0033)	0.048 (0.0019)	0.051 (0.002)
4th	0.155 (0.0061)	0.160 (0.0063)	0.025 (0.001)

4.13.4.5 Cowl Gust Load Induced Deflections

The rotor-frame model was used again to determine the clearance closures caused by aerodynamic (gust) cowl loads. The resulting component clearance closures are shown in Table 71 including the effects of cowl load sharing.

4.13.4.6 Other Clearance Considerations

Additional estimated clearance to allow for production tolerances and eccentricities, bearing radial clearances and rotor whirl caused by normal unbalance, are shown in Table 72. The magnitude of these other clearance considerations was minimized by incorporating all the advanced manufacturing and assembly techniques that were deemed feasible.

4.13.4.7 Total Gapping Required During Engine Takeoff/Climb and Cruise

The total gap required during takeoff/climb, to meet the clearance objective, was obtained by adding all the clearance closures together as shown in Table 73.

A similar deflection analysis was also performed at the cruise operating condition. Reduced flight maneuver, cowl and engine thrust loads were used that simulate normal cruise flight conditions. These required gaps at cruise are shown in Table 74.

4.13.4.8 Hot Engine Restart Thermal Bowed Rotor Deflections

The studies indicate that all of the initial rotor dynamics goals have been met. The high strain energy modes have been maintained above maximum rotor speed by stiff, lightweight high rotor construction. The high rotor bounce and pitch modes have been driven below idle by the incorporation of a soft effective front support mount. Minimum whirl during bowed rotor start conditions has been provided by a high efficiency viscous damper on the turbine intermediate case support structure.The predicted bowed rotor deflection versus rotor speed is shown in Figure 170 for the high-pressure compressor rear stage. These rotor deflections establish the required gap at cold assembly for the high spool components, shown in Table 75, to avoid hot engine restart rubs.

4.13.5 Component Response Characteristics and Clearance Results

Rotor tip and adjacent case seal growth response curves were generated, as outlined in Section 4.13.2.1, for all engine rotor stages. These response curves were combined with the required gaps at various operating conditions determined by the rotor/case deflection analysis, (Section 4.13.4), to establish preliminary blade tip clearances.

TABLE 71

GAP REQUIRED DURING ENGINE TAKEOFF/CLIMB
FOR NORMAL GRAVITIONAL AND GYROSCOPIC LOADS, MOUNT LOADS
AND COWL LOADS mm (in.)

	G's	Gyro's	Mount Load Oval.	Cowl Loads
Fan	0.36 (0.014)	0.89 (0.035)	0.000	0.38 (0.015)
LPC (Avg.)	0.20 (0.008)	0.18 (0.007)	0.000	0.051 (0.002)
HPC 9th	0.061 (0.0024)	0.028 (0.0011)	0.000	0.008 (0.0003)
15th	0.056 (0.0027)	0.018 (0.0007)	0.000	0.010 (0.0004)
HPT	0.061 (0.0024)	0.005 (0.0002)	0.076 (0.003)	0.003 (0.0001)
LPT 2nd	0.084 (0.0033)	0.048 (0.0019)	0.051 (0.002)	0.008 (0.0003)
4th	0.155 (0.0061)	0.160 (0.0063)	0.025 (0.001)	0.023 (0.0009)

TABLE 72

GAP REQUIRED FOR PRODUCTION TOLERANCE, ECCENTRICITIES,
BEARING CLEARANCES, AND NORMAL ROTOR WHIRL - mm (in.)

			HPC			LPT	
	Fan	LPC	9th	15th	HPT	2nd	4th
Rotor Tol.	0.05 (0.002)	0.05 (0.002)	0.025 (0.001)	0.025 (0.001)	0.025 (0.001)	0.025 (0.001)	0.025 (0.001)
Case Tol. & Eccen.	0.15 (0.006)	0.13 (0.005)	0.076 (0.003)	0.076 (0.003)	0.076 (0.003)	0.13 (0.005)	0.13 (0.005)
Bearing Clear.	0.05 (0.002)	0.05 (0.002)	0.025 (0.001)	0.05 (0.002)	0.10 (0.004)	0.10 (0.004)	0.10 (0.004)
Rotor Whirl	0.10 (0.004)	0.10 (0.004)	0.025 (0.001)	0.025 (0.001)	0.025 (0.001)	0.025 (0.001)	0.025 (0.001)
Total	0.36 (0.014)	0.33 (0.013)	0.15 (0.006)	0.18 (0.007)	0.23 (0.009)	0.28 (0.011)	0.28 (0.011)

TABLE 73

TOTAL GAP REQUIRED DURING ENGINE TAKEOFF/CLIMB - mm (in.)

	G's	Gyro's	Mount Load Oval.	Cowl Loads	Other	Total
Fan	0.36(0.014)	0.89(0.035)	0.000	0.38(0.015)	0.36(0.014)	1.98(0.078)
LPC(Avg.)	0.20(0.008)	0.18(0.007)	0.000	0.051(0.002)	0.33(0.013)	0.76(0.030)
HPC 9th	0.061(0.0024)	0.028(0.0011)	0.000	0.008(0.0003)	0.15(0.006)	0.25(0.010)
15th	0.056(0.0027)	0.018(0.0007)	0.000	0.010(0.0004)	0.18(0.007)	0.28(0.011)
HPT	0.061(0.0024)	0.005(0.0002)	0.076(0.003)	0.003(0.0001)	0.23(0.009)	0.38(0.015)
LPT 2nd	0.084(0.0033)	0.048(0.0019)	0.051(0.002)	0.008(0.0003)	0.28(0.011)	0.48(0.019)
4th	0.155(0.0061)	0.160(0.0063)	0.025(0.001)	0.023(0.0009)	0.28(0.011)	0.64(0.025)

TABLE 74

TOTAL GAP REQUIRED AT CRUISE - mm (in.)

	G's	Gyro's	Mount Load Oval.	Cowl Loads	Other	Total
Fan	0.295(0.0116)	0.445(0.0175)	0.000	0.071(0.0028)	0.36(0.014)	1.17(0.046)
LPC (Avg.)	0.130(0.0051)	0.081(0.0032)	0.000	0.076(0.003)	0.33(0.013)	0.61(0.024)
HPC 9th	0.048(0.0019)	0.015(0.0006)	0.000	0.000	0.15(0.006)	0.23(0.009)
15th	0.056(0.0022)	0.008(0.0003)	0.000	0.003(0.0001)	0.18(0.007)	0.28(0.011)
HPT	0.048(0.0019)	0.003(0.0001)	0.025(0.001)	0.000	0.23(0.009)	0.30(0.012)
LPT 2nd	0.066(0.0026)	0.023(0.0009)	0.025(0.001)	0.000	0.28(0.011)	0.41(0.016)
4th	0.124(0.0049)	0.081(0.0032)	0.025(0.001)	0.005(0.0002)	0.28(0.011)	0.51(0.020)

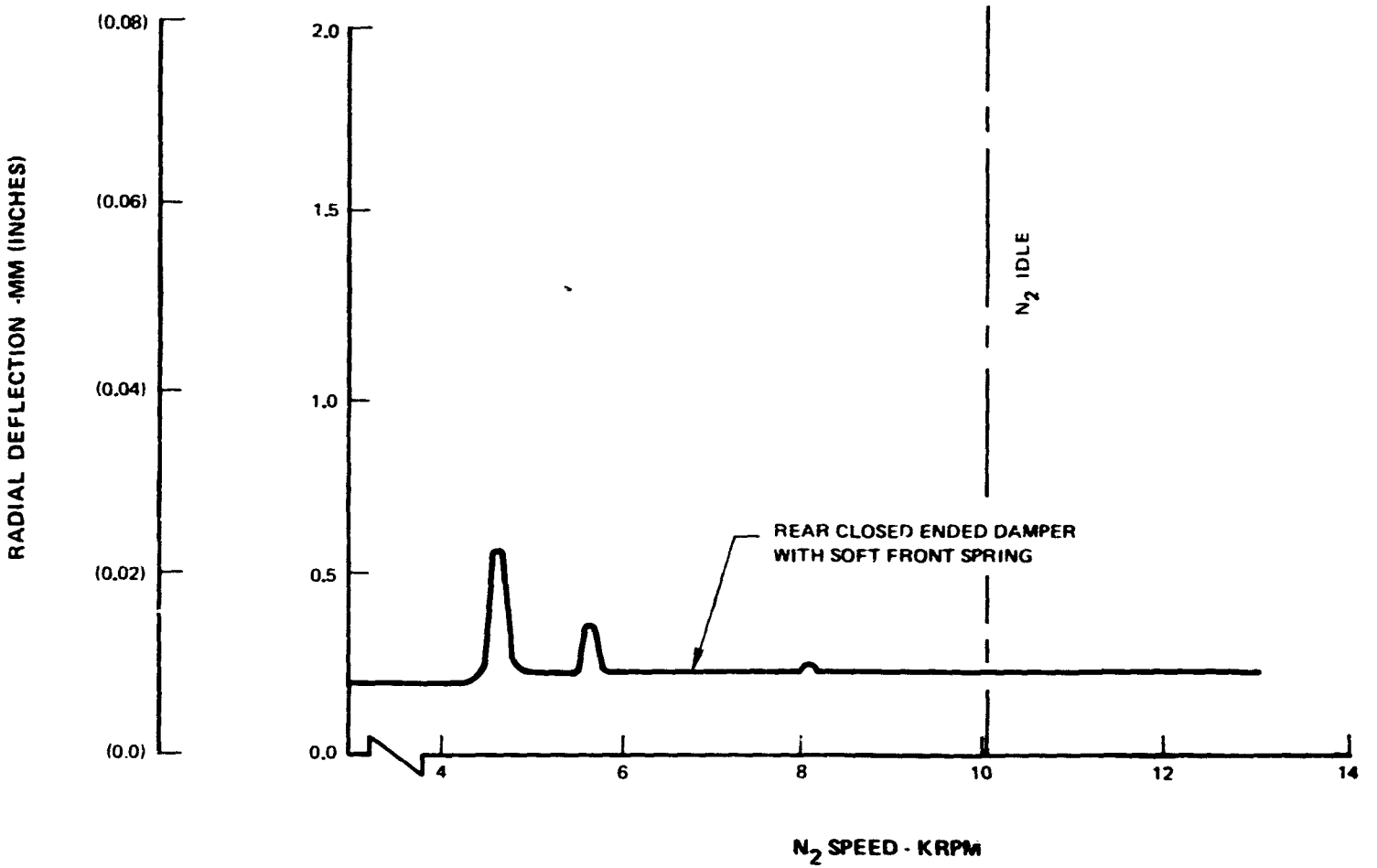

Figure 170 High-Pressure Compressor Rear Stage. Radial rotor deflection shows effect of acceleration with bowed rotor.

TABLE 75

GAP REQUIRED DURING ENGINE START - mm (in.)

Bowed Rotor Whirl	
HPC 9th	0.56(0.022)
15th	0.58(0.023)
HPT	0.46(0.018)

4.13.5.1 Fan/Low-Pressure Compressor

The rotor blade tips versus case seal growth response curves are shown in Figure 171 for the fan and low-pressure compressor. The pinch point occurs at steady-state takeoff where the required clearance is 1.98 mm (0.078 in.) and 0.76 mm (0.030 in.) respectively, for the fan and lowpressure compressor. The resulting cruise clearances are 2.44 mm (0.096 in.) for the fan and 0.56 mm (0.022 in.) for the low-pressure compressor.

4.13.5.2 High-Pressure Compressor

The response curves for the high-pressure compressor ninth and fifteenth-stages, are shown in Figure 172. The curves show that the pinch point occurs at steady state takeoff for the ninth stage and at cold assembly for the 15th stage.

4.13.5.3 High-Pressure Turbine

The response curve for the high-pressure turbine, with ACC, is shown in Figure 173. The curve illustrates that the pinch point occurs during engine acceleration from idle to takeoff where the required gap is 0.38 mm (0.015 in.). The resulting takeoff and cruise clearances are 0.69 mm (0.027 in.) and 0.30 mm (0.012 in), respectively.

4.13.5.4 Low-Pressure Turbine

The response curves for the low-pressure turbine second and fourth stages, with the effects of ACC, are shown in Figure 174. The curves show that the second-stage pinch point occurs during engine acceleration and the fourth-stage during deceleration, which reflect the seal response differences between a case-tied second-stage seal and free ring seal fourth-stage seal.

4.13.6 Summary of Results

The preliminary design component radial clearances are summarized at takeoff and cruise in Table 76. Results indicate feasibility of meeting the design goal clearances with the exception of the fourthstage low-pressure turbine. Modifications to the fourth- and fifthstage low-pressure turbine seals are planned for the detail design. This includes a case-tied fourth-stage design and a rearward extension of the active clearance control as required to meet their design goal clearance objectives.

Because component radial clearances will continue to change somewhat during the detailed design refinements, design goal clearances will continue to be reflected in component performance estimates until clearances become more final.

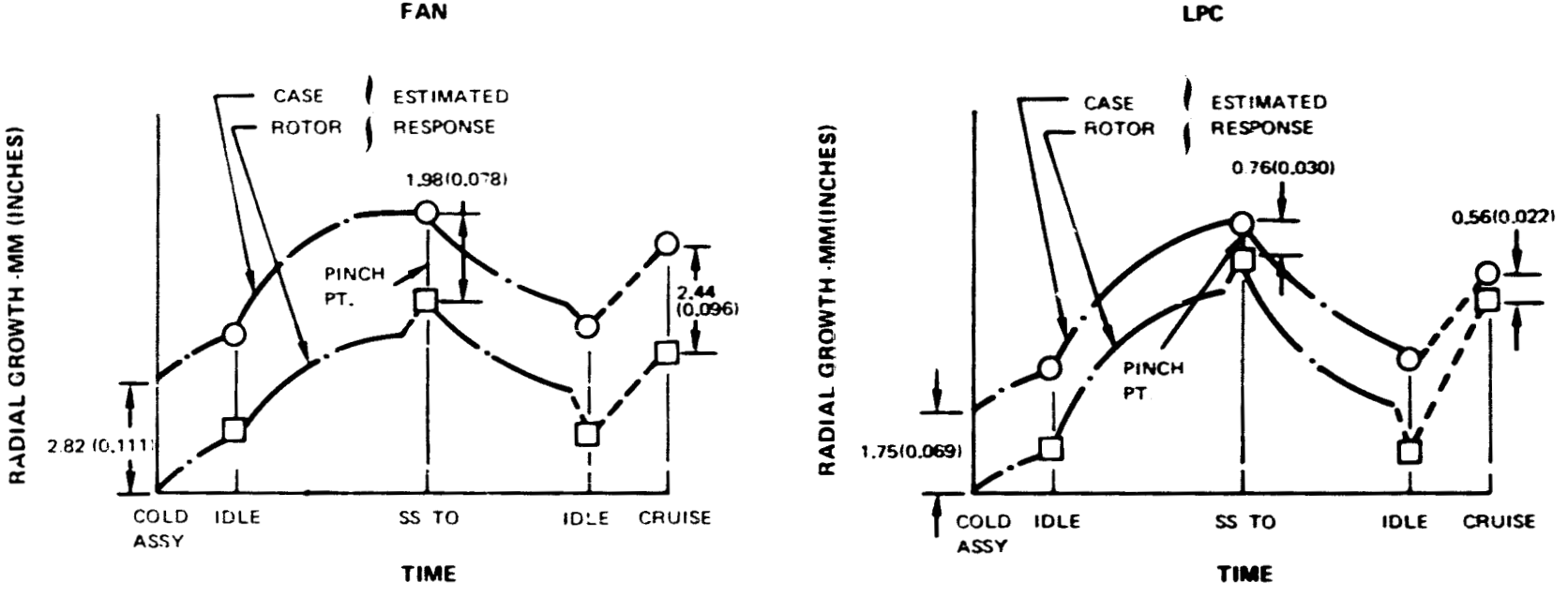

Figure 171 Fan and Low-Pressure Compressor. Radial growth shows pinch points at takeoff.

J20127-151
782711

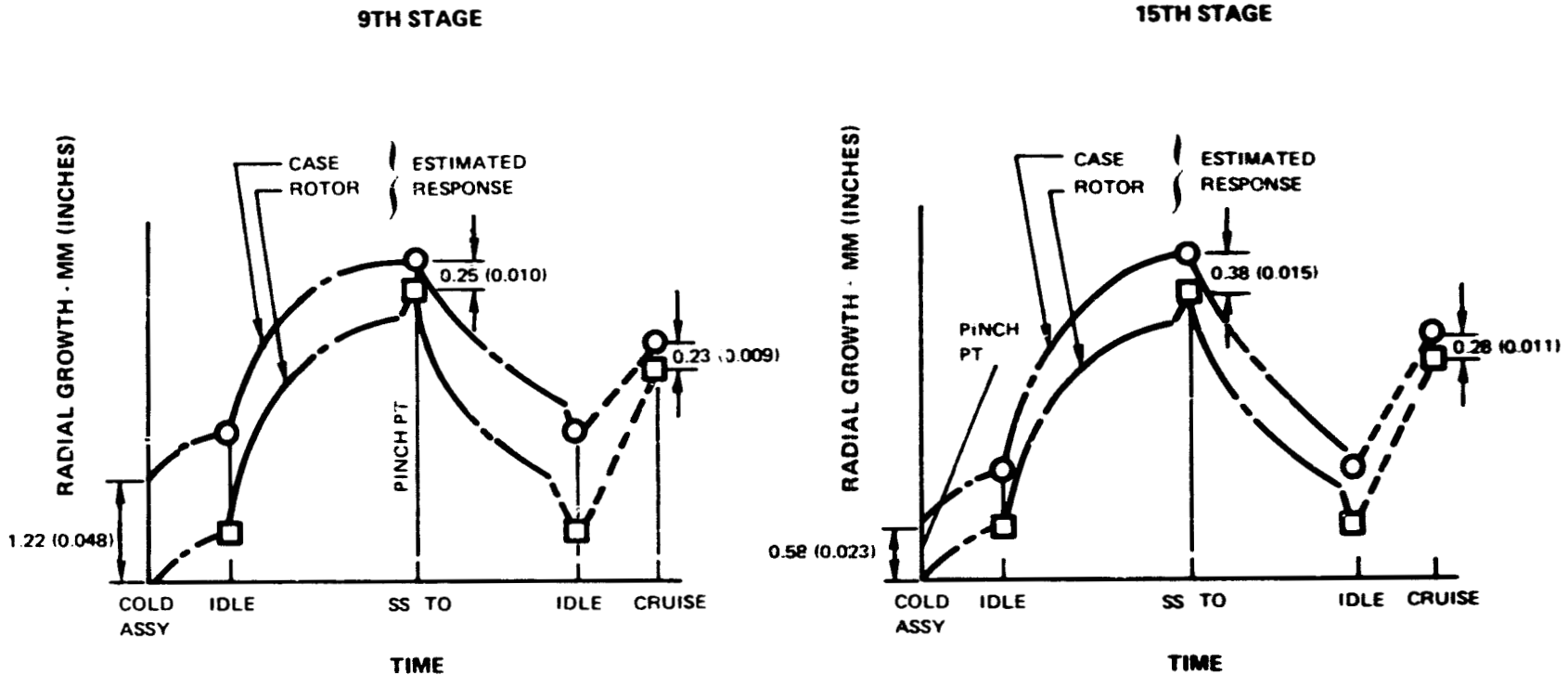

Figure 172 Ninth and Fifteenth High-Pressure Compressor Stage. Radial growth shows pinch point at takeoff and cold assembly.

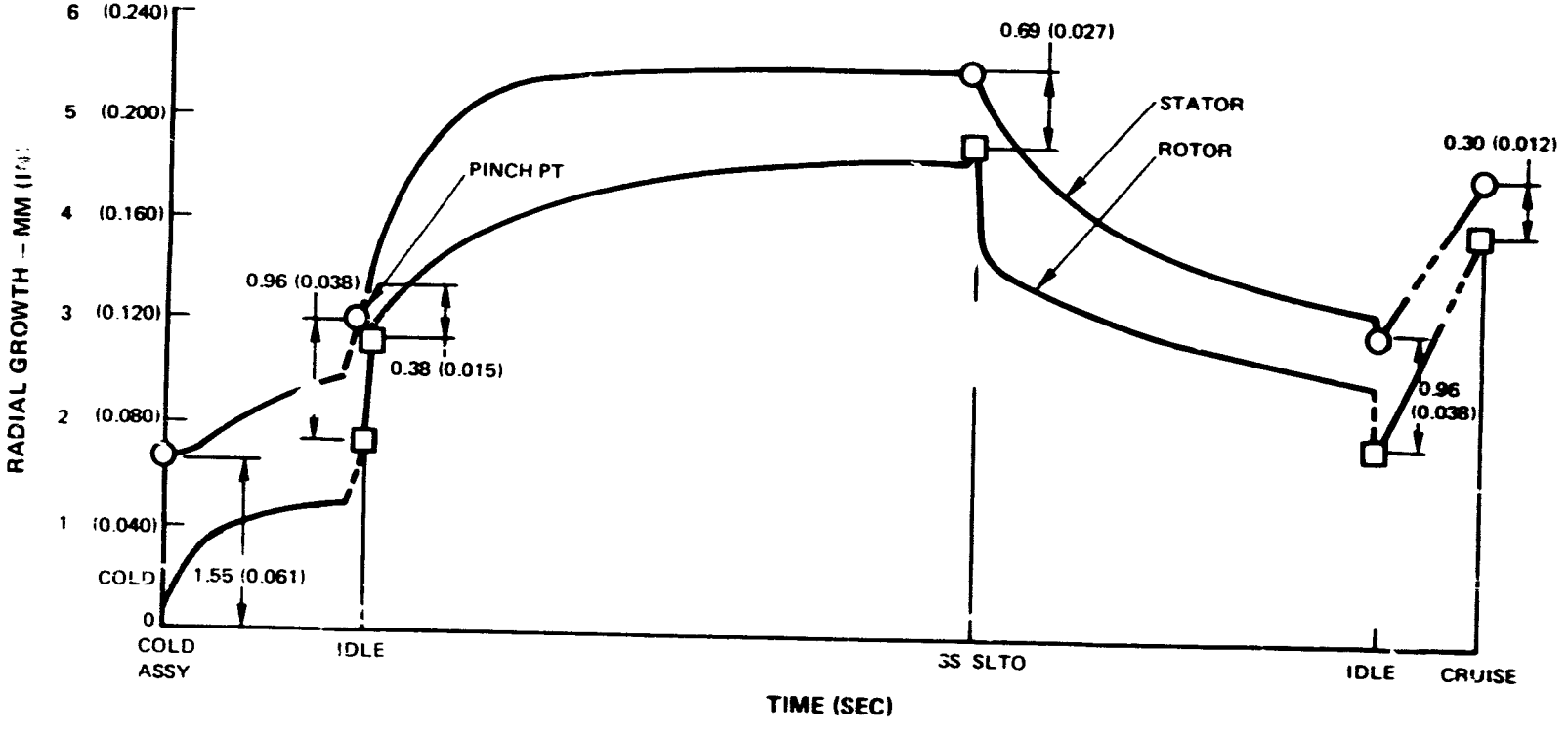

Figure 173 High-Pressure Turbine. Radial growth shows pinch point during engine acceleration.

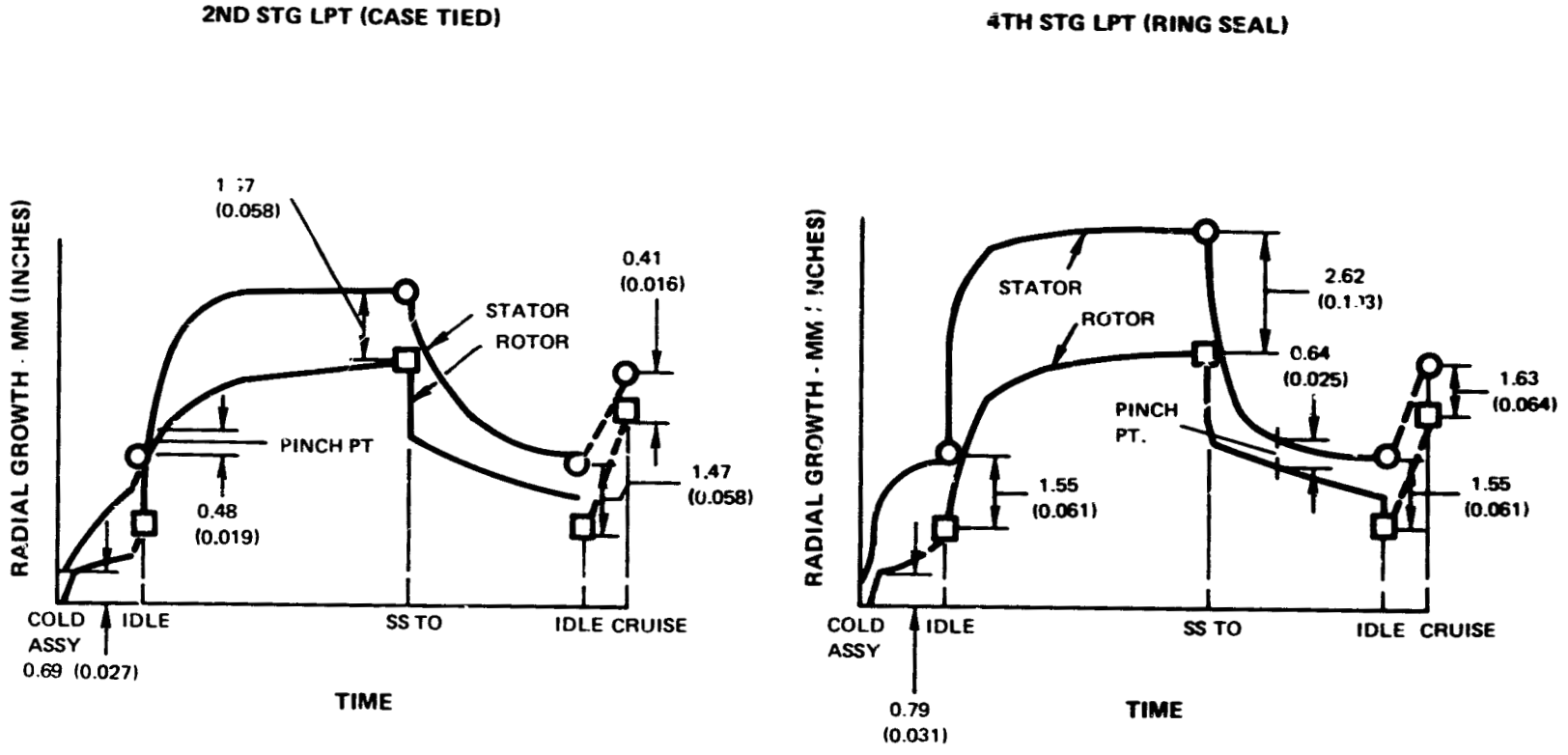

Figure 174 Low-Pressure Turbine. Radial growth shows 2nd- and 4th-stage pinch points during acceleration and during deceleration.

TABLE 76

SUMMARY OF REQUIRED COMPONENT RADIAL CLEARANCES (WITH ACC)
INDICATE GOALS ACHIEVED EXCEPT FOR FOURTH LPT STAGE

	Takeoff		Cruise	
	Minimum Required Clearance mm(in.)	Design Goal mm(in.)	Minimum Required Clearance mm(in.)	Design Goal mm(in.)
Fan	1.98(0.078)	-	2.44(0.096)	2.18(0.086)
LPC(Avg.)	0.76(0.030)	-	0.56(0.022)	0.56(0.022)
HPC 9th	0.25(0.010)	0.48(0.019)	0.23(0.009)	0.33(0.013)
15th	0.38(0.015)	0.48(0.019)	0.28(0.011)	0.33(0.013)
HPT	0.69(0.027)	0.74 (0.029)	0.30 (0.012)	0.51 (0.020)
LPT 2nd	1.47 (0.058)	1.52 (0.060)	0.41 (0.016)	0.51 (0.020)
4th	2.62 (0.103)	1.52 (0.060)	1.63 (0.064)	0.51 (0.020)

4.14 PERFORMANCE DETERIORATION

4.14.1 Suspected Mechanisms and Design Approaches

The general approach taken in the preliminary analyses of performance deterioration was to use JT9D operational experience as a base, to evaluate this experience in terms of flight propulsion system anti-deterioration design features, and to then estimate the resulting cruise TSFC deterioration. Substantial insight into deterioration continues to be obtained from the JT9D Engine Diagnostics Program, NAS3-20632. This on-going study effort has identified the five probable causes for JT9D-7A performance deterioration to be (1) increased tip clearance, (2) erosion, (3) turbine airfoil distortion, (4) seal and joint leakage, and (5) foreign object damage. Collectively, these causes are estimated to account for an average of 3.1 percent TSFC deterioration in 1000 flight cycles. When each of these causes was evaluated in terms of the flight propulsion system configuration, a corresponding 1.5 percent TSFC deterioration was predicted, thus meeting the program goal. The evaluation of these deterioration factors in the current preliminary design effort is discussed in the following sections.

4.14.1.1 Increased Tip Clearance

JT9D-7A operational experience analysis indicates that increased tip clearance is the most significant factor in performance deterioration. Throughout the engine, this form of deterioration is caused primarily by flight load induced rubs of airfoil tips against airseals. Seal and airfoil erosion are secondary contributors to in-service tip clearance increases in the high-pressure compressor. Similarly, turbine tip clearances are also increased because of airseal abrasion of blade tips and non-symmetric combustor exit temperature profiles.

4.14.1.1.1 Design Features and Analysis

Because of the importance of tip clearance retention, special features were incorporated into the flight propulsion system design to reduce the occurrence and consequence of rubs. These features fall into three categories: (1) abradable airseals, (2) stiff rotors and cases and cowl load sharing, and (3) improved thermal matching of rotors and cases.

Abradable airseals, in combination with abrasive blade tips, were incorporated in the compressors and turbines to minimize the loss of blade tip material. This approach is predicted to eliminate what has been a major cause of high-pressure turbine performance deterioration, the loss of blade material because of inadequate outer airseal abradability. Rubs would result in transfer of the blade material to the airseal, thus creating additional rubbing and blade wear.

Rotor and case configuration and design stiffnesses and the proper sharing of imposed loads between the nacelle duct walls (cowl) and engine cases were established by rotor-frame model analyses. Maneuver, thrust, and gust loads imposed on the flight propulsion system rotorframe model were determined from comprehensive JT9D-7A analytical models that were calibrated against service experience. In exercising the flight propulsion system model, the general philosophy was to design to avoid the early in-service rubs caused by "normal" flight loads and use the advanced design features to reduce the effects of "severe" flight loads. The deflections resulting from "normal" or once-per-flight loads are among those clearance determination factors discussed in Section 4.13. "Severe" flight load deflections are those that can be expected to occur sometime during the first 1000 cycles of service life and reflect such incidents as sudden shock, hard landings, diversionary maneuvers, clear air turbulence, and thunderstorms. The difference between the "normal" and "severe" load deflections is the radial tip clearance increase that defines the deterioration performance loss. These analyses indicated that thrust-caused deflections could be eliminated by mounting the engine on the horizontal centerline plane. In addition, cowl load sharing significantly decreases the deflections associated with gust loads.

A greater knowledge of the mechanisms of heat transfer and material properties allowed improved thermal matching of the flight propulsion system rotors and cases. Analyses tailored thermal responses by means of proper geometric shapes, property utilization, and secondary air system flow management. These responses were evaluated for all of the critical engine operating transients, thereby minimizing rubs throughout the entire mission.

4.14.1.1.2 Evaluation and Results

Final rotor-frame model analysis of the flight propulsion system configuration determined "normal" and "severe" load tip deflections for each component. These deflections were compared to determine radial clearance deteriorations. From them, efficiency effects were estimated and converted into TSFC, using performance influence coefficients for each component. These individual TSFC effects were then combined to arrive at an engine value.

A summary of predicted flight propulsion system tip clearance deterioration results is presented by Table 77. These results indicate that the engine is estimated to lose 0.78 percentage points TSFC because of tip rubs during 1000 cycles of in-service operation.

4.14.1.2 Erosion

Experience shows performance deterioration caused by erosion to be primarily a compression system problem. Sand and dirt particles entering the inlet wear and eventually blunt the airfoil leading edges.

TABLE 77

PERFORMANCE DETERIORATION ESTIMATES WITH SEVERE FLIGHT LOADS SHOWING CONTRIBUTION BY ALL COMPONENTS

	Normal Load[1] Deflections mm (in.)	Severe Load[2] Deflection mm (in.)	Radial Clearance Increase mm (in.)	ΔTSFC-%
Fan	1.65 (0.065)	2.64 (0.104)	0.99 (0.039)	+0.21 (0.008)
LPC	0.36 (0.014)	0.61 (0.024)	0.25 (0.010)	+0.08 (0.003)
HPC	0.10 (0.004)	0.15 (0.006)	0.05 (0.002)	+0.12 (0.005)
HPT	0.07 (0.003)	0.11 (0.004)	0.04 (0.002)	+0.11 (0.004)
LPT	0.29 (0.011)	0.47 (0.018)	0.18 (0.007)	+0.26 (0.010)
	Total ΔTSFC Due To Severe Flight Loads			+0.78

Notes:
(1) Deflections Due to "Once Per Flight" G, Gyro, and Gust loads
(2) Deflections Due to "Once Per Engine Life" G, Gyro, and Gust Loads

Tumbling from row-to-row causes the particles to break up, thus increasing the concentration. After long time operation, airfoil wear is such that some camber is lost in the low-pressure compressor, blade tips are worn in the high-pressure compressor, and airseals become grooved and pitted.

4.14.1.2.1 Design Features and Analysis

Compression system performance retention was addressed in the flight propulsion system preliminary design by incorporating three advanced concepts: (1) thick leading edge airfoils; (2) smooth, erosion resistant airfoils; and (3) erosion resistant, abradable airseals.

The aerodynamic design system was used to define thickened airfoil leading edges in the high-pressure compressor to increase their tolerance to erosion-causing particles. At the same time, the aft portions of the airfoils were carefully faired into the leading edges and contoured in such a manner to minimize losses and duplicate the performance characteristics of conventional leading edge airfoils.

Compression system design involved application of anti-fouling and erosion resistant coatings on the airfoils to increase durability and provide aerodynamic smoothness. Specific coating selections were made to reduce fan airfoil surface roughness caused by dirt accumulation and erosive pitting, low-pressure compressor airfoil surface and leading edge pitting, and high-pressure compressor gross surface and camber loss.

Airseal materials were selected for the design based not only on their abradable characteristics, but also on their capability to resist particulate erosion. Care was taken to ensure that the materials used merely scratch rather than chip under the impact of particles. Such materials were estimated to benefit performance by minimizing the increase in airfoil tip clearance and its circumferential extent.

4.14.1.2.2 Evaluation and Results

The compressor design system, in conjunction with the understanding of operational experience obtained from the JT9D work performed under Contract NAS3-20632, was used to evaluate flight propulsion system erosion deterioration in each component. Individual efficiency effects were converted into TSFC's, which were then combined into an engine value.

The resulting net erosion-caused TSFC deterioration in 1000 flight cycles was estimated to be 0.3 points. The evaluation showed that the higher cycle overall pressure ratio and the resulting smaller airfoils caused greater sensitivity to airfoil surface roughness and tip clearance, and increased the erosive particle concentration in the gaspath. Thick leading edges, erosion resistant coatings, and abradable

materials, therefore, were predicted to reduce TSFC deterioration improvement for the flight propulsion system despite these detrimental factors.

4.14.1.3 Turbine Airfoil Distortion

There are two types of high pressure turbine airfoil distortion that cause performance deterioration: (1) bow and (2) creep untwist. Second stage vanes, which are supported only at the outer diameter, untwist with time, opening triangular areas at the inner shrouds through which cooling air may leak into the gaspath and degrade turbine efficiency.

4.14.1.3.1 Design Features and Analysis

Because of its one stage high-pressure turbine configuration, the flight propulsion system has one less turbine blade row than the JT9D-7A, which was projected to make a net improvement in creep untwist deterioration. Vane attachment design improvements were incorporated to reduce vane bow and untwist. A beam program, based on the JT9D-7A operational data for bowing, was used for analysis, considering the differences in airfoil span, chord, metal temperature, and gas loads. Creep untwists were determined from geometrical and environmental data specifies using a methodology derived from a correlation of experience to rates of torsional and radial creeps.

4.14.1.3.2 Evaluation and Results

The evaluation of the flight propulsion system turbine airfoils for bow and untwist resulted in a net 0.3 points increase in TSFC for 1000 cycles of operation. A high-pressure turbine blade creep-oriented untwist problem was estimated to be the largest contributor to the estimated deterioration.

4.14.1.4 Seal and Joint Leakage

Experience has shown that case flange seals have a tendency to deteriorate early in service, and then stabilize. Little measurable performance impact from vane inter-platform leakage or leakage at vane attachments has been apparent.

4.14.1.4.1 Design Features and Analysis

Relative to the JT9D-7A, the one-stage high-pressure turbine of the flight propulsion system inherently has fewer joints and a shorter linear leakage path. In addition, careful attention was taken in configuring the designs of the flange and attachment seals.

4.14.1.4.2 Evaluation and Results

Linear leakage evaluation of the flight propulsion system indicated a minimal leakage deterioration associated with escape of cooling air

through gaps between adjacent vanes. The cause of this penalty was low static pressure at the vane platforms caused by increased vane Mach number for the one-stage turbine configuration. Converted to TSFC with influence coefficients, the net effect is an estimated 0.1 point deterioration.

4.14.1.5 Foreign Object Damage

Operational experience also shows the impact of foreign object damage on performance to be small. Damage sustained is also generally limited to repairable nicks and dents that occur on the leading edges of fan blades.

4.14.1.5.1 Design Features and Analysis

The general approach taken in the design of the flight propulsion system compression section to reduce foreign object damage was the incorporation of thicker leading edge airfoils, as discussed in Section 4.14.1.2.1.

4.14.1.5.2 Evaluation and Results

Evaluation of foreign object damage-caused performance deterioration indicated no improvement relative to the JT9D-7A, primarily because of higher wheel speed in the flight propulsion system. The analysis showed an estimated 0.1 points TSFC deterioration in 1000 cycles of service operation. Fan blade nicks are the primary cause.

4.14.2 Summary and Results

An evaluation of all significant mechanisms shows the flight propulsion system's 1000 cycle-operation total performance deterioration level to be 1.5 points TSFC. For the same point in operation with the JT9D-7A, the NAS3-20632 Diagnostic Program identified a 3.1 point deterioration in TSFC. As a result, indications at completion of preliminary design are that the flight propulsion system achieves its design goal of one-half the JT9D-7A deterioration rate. Table 78 summarizes these results, on a component basis, for both engines.

4.15 ROTOR VIBRATIONAL CONTROL

The rotor dynamics studies have verified the acceptability of the rotor construction and bearing arrangement. The critical speed results indicate acceptable sensitivity to imbalance. Damper requirements have been established to minimize rotor whirl under high rotor imbalance conditions.

TABLE 78

DETERIORATED PERFORMANCE PROJECTION
IN 1000 FLIGHT CYCLES

	Current Experience % Δ TSFC	EEE % Δ TSFC
Increased Tip Clearance	2.0	0.8
Erosion	0.4	0.3
Turbine Airfoil Distorion	0.7	0.3
Seal/Joint Leakage	0.0	0.1
Foreign Object Damage	0.1	0.1
Total % TSFC	+3.1	+1.5

4.15.1 Rotor Dynamics Goals

The rotor dynamics goals established for the study were:

1. To provide design features such as short, stiff, lightweight rotors to drive high strain energy modes above maximum rotor speed because of the great difficulty in providing sufficient damping to tolerate these modes with even normal rotor imbalance.

2. To tune the high rotor support springrates in order to provide a system whose bounce and pitch modes are below idle speed. This results in a high spool insensitive to imbalance during normal engine running.

3. To provide oil film dampers at selected locations to minimize whirl amplitudes due to engine start with a thermally bowed high rotor and thus allow tight clearances for improved component performance.

4.15.2 Anti-Vibration Design Features

The Energy Efficient Engine rotor support concept provides a very short straddle-mounted high rotor, which results from the single stage high-pressure turbine, the advanced 10-stage high-pressure compressor, and the short burner-diffuser section. Turbine intermediate case struts are located immediately behind the high-pressure turbine to tightly control the blade tip-to-case radial clearances. The low rotor has two bearings in the fan/LPC to provide moment restraint under gyroscopic loading, also allowing tight blade tip clearances. The low-pressure turbine rotor support bearing is located to minimize maneuver deflections of the more sensitive front stages.

4.15.3 Rotor-Frame Analytical Model

The entire engine rotor and case structure is modeled by a system of frames that simulate the two rotors, the inner engine case structure and the outer nacelle structure, and fan and low-pressure compressor case. These are inter-connected with a series of springs and dampers, accurately duplicating the stiffnesses of the bearings and bearing support structures. Damping coefficients are used to simulate the oil film dampers. The springs are either radial or torsional as required to properly define trunnion vibratory modes. Thus, the rotor-frame model is able to simulate the entire system under vibratory conditions. The engine-rotor frame model used to investigate vibration is shown in Figure 175.

4.15.4 Low Spool Rotor Vibration

The low rotor study results indicate two low amplitude modes between N_1 idle and N_1 max. rotor speed with the high response mode significantly beyond maximum rpm (Figure 176).

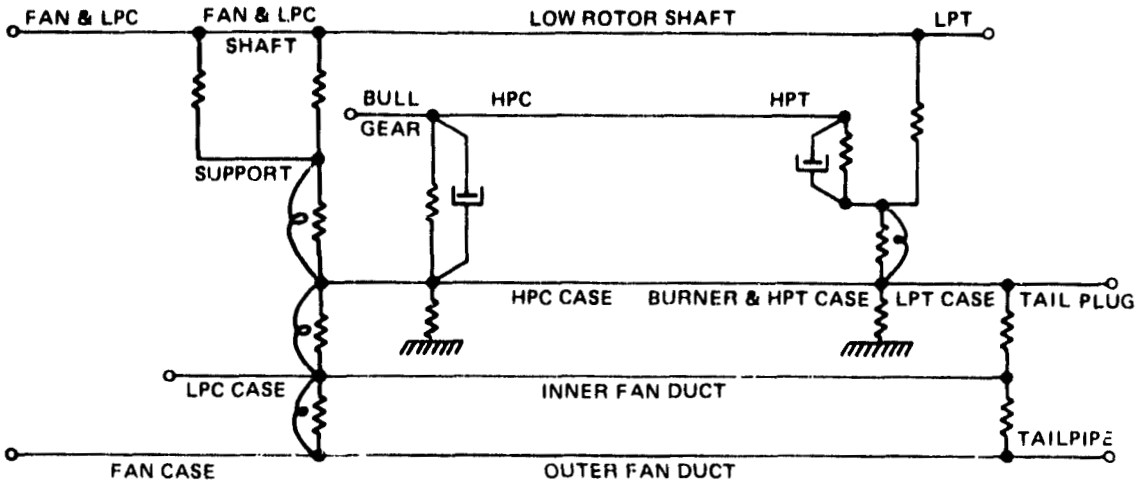

Figure 175 Rotor Dynamics. Computerized rotor-frame model used to study vibration.

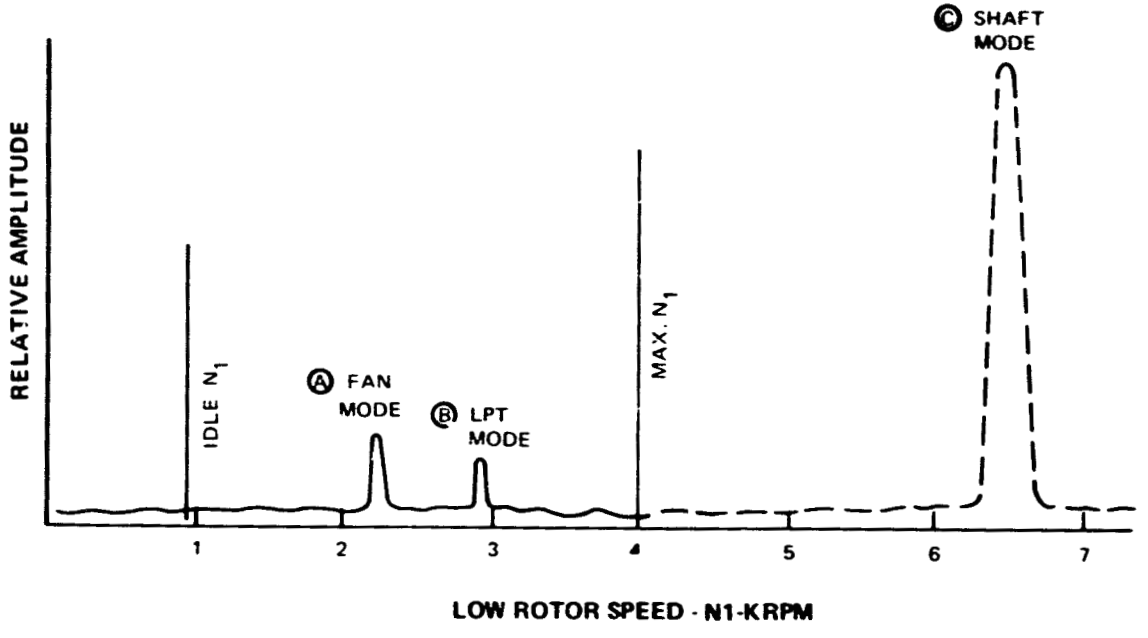

Figure 176 Low Rotor Imbalance Response. Amplitude predictions show only two low amplitude modes in operating range.

The mode shapes of Figure 177 show high [illegible] participation for the first low energy mode (A) with the fan rotor whirling in a pitch mode cantilevered off the No. 1 and No. 2 bearings. The second low amplitude mode (B) shows the low-pressure turbine pitching off the No. 5 bearing. The high energy mode shape (C), of academic interest only, shows significant shaft bending within the low rotor with little or no participation of the fan or low-pressure turbine. Percent strain energy represented by the first two modes, shown parenthetically on Figure 177, are sufficiently low to be of no concern.

4.15.5 High Spool Rotor Vibration

The high rotor modes, when originally calculated for the engine, revealed a moderately high energy mode within the engine running range. Further study indicated that if the high rotor front bearing effective spring stiffness could be reduced below 438,000 N/cm (250,000 lb/in), this mode could be driven below idle RPM. High rotor imbalance response, with both stiff and soft effective front spring mounts, is depicted in Figure 178. The resulting mode shapes for the soft spring mount show a high-pressure turbine bounce mode well below idle with the high-pressure turbine disk being the primary element of mass and the high rotor rear (No. 4) bearing being the prime stiffness element (see Figure 179). The high-pressure compressor pitch mode has been forced below idle by the presence of the soft effective front spring at the No. 3 bearing. This pitch mode exercises both the forward and rear bearing supports. Again, an academic mode is shown outside of the engine running range.

Techniques for achieving the forward soft front spring mount were then sought. Two soft spring options were considered (See Figure 180). The first is an open-ended oil film damper, eliminating the O-ring seals from the conventional close-ended damper. This provides significant reductions in spring-rates, coupled with a significant increase in oil flow. The second approach is a mechanical spring with a feature such as a wind-back shell structure to provide the required reduction in springrate. Studies were conducted on these concepts, with particular concern directed toward engine re-start with a thermally bowed high spool rotor.

The thermal bow condition (illustrated in Figure 181) results from the rapid shutdown of an engine which has been running at high power levels resulting in entrapment of large amounts of thermal energy within the engine. Within a short period of time, internal stagnant air is heated and rises to the top of the engine flowpath. This results in a rotor which is hot at the top and cooler at the bottom, causing an upward bow in the center of the rotor. A massive amount of imbalance is generated when the engine is restarted in the presence of the bowed rotor.

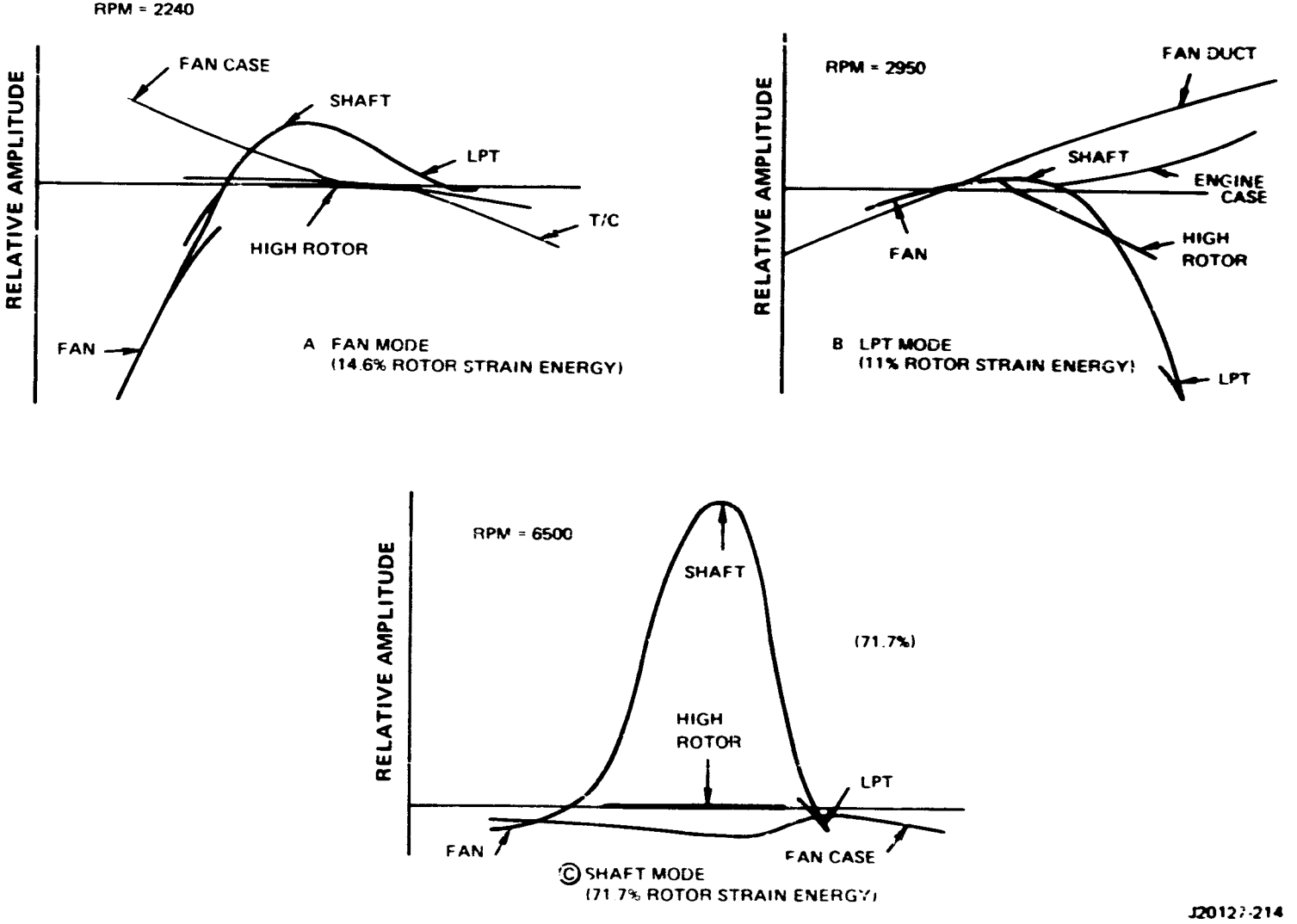

Figure 177 Low Rotor Critical Speeds and Mode Shapes. Predictions show strain energies in operating range to be

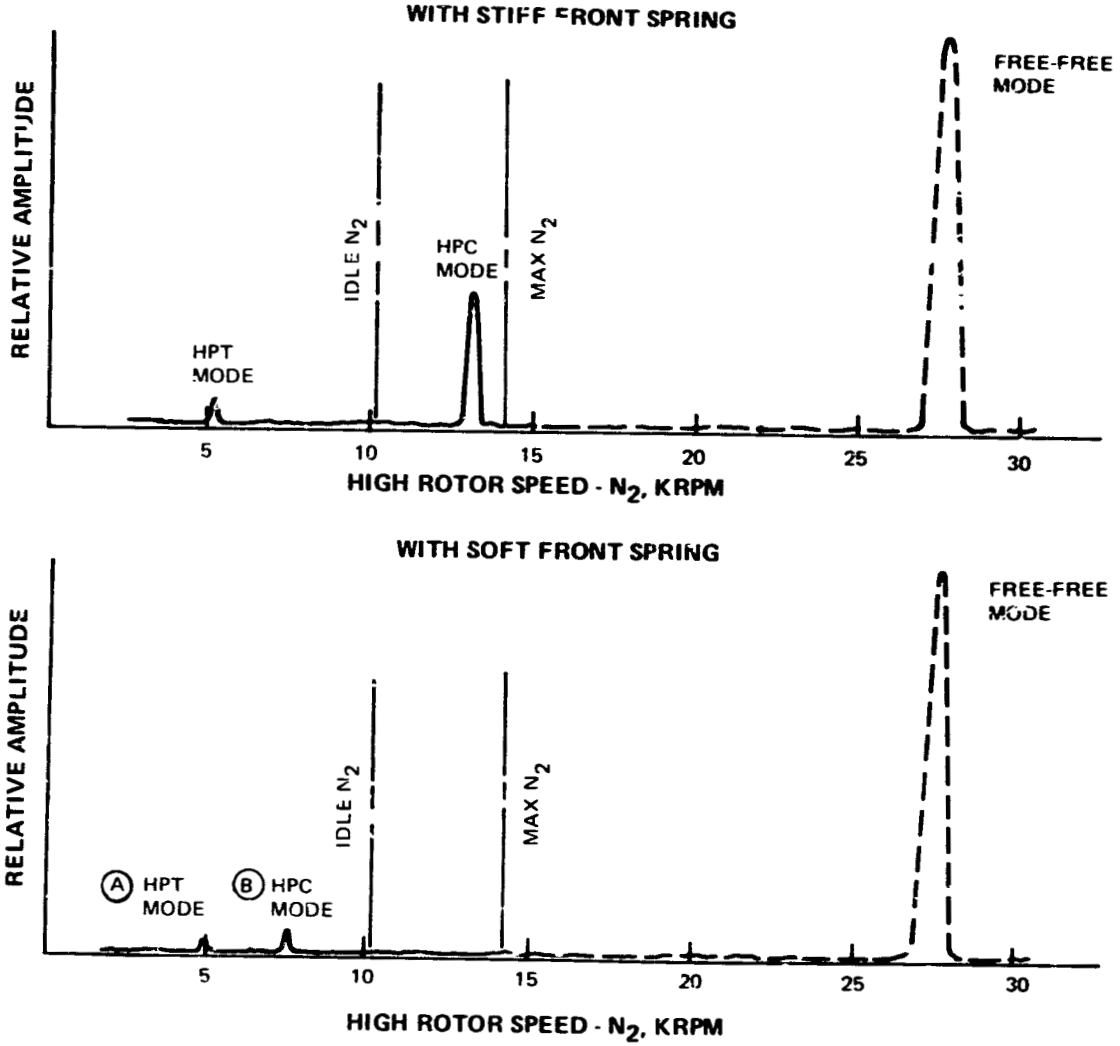

Figure 178 High-Spool Rotor Imbalance Response. Amplitude predictions show soft front spring is required to place HPC mode below idle.

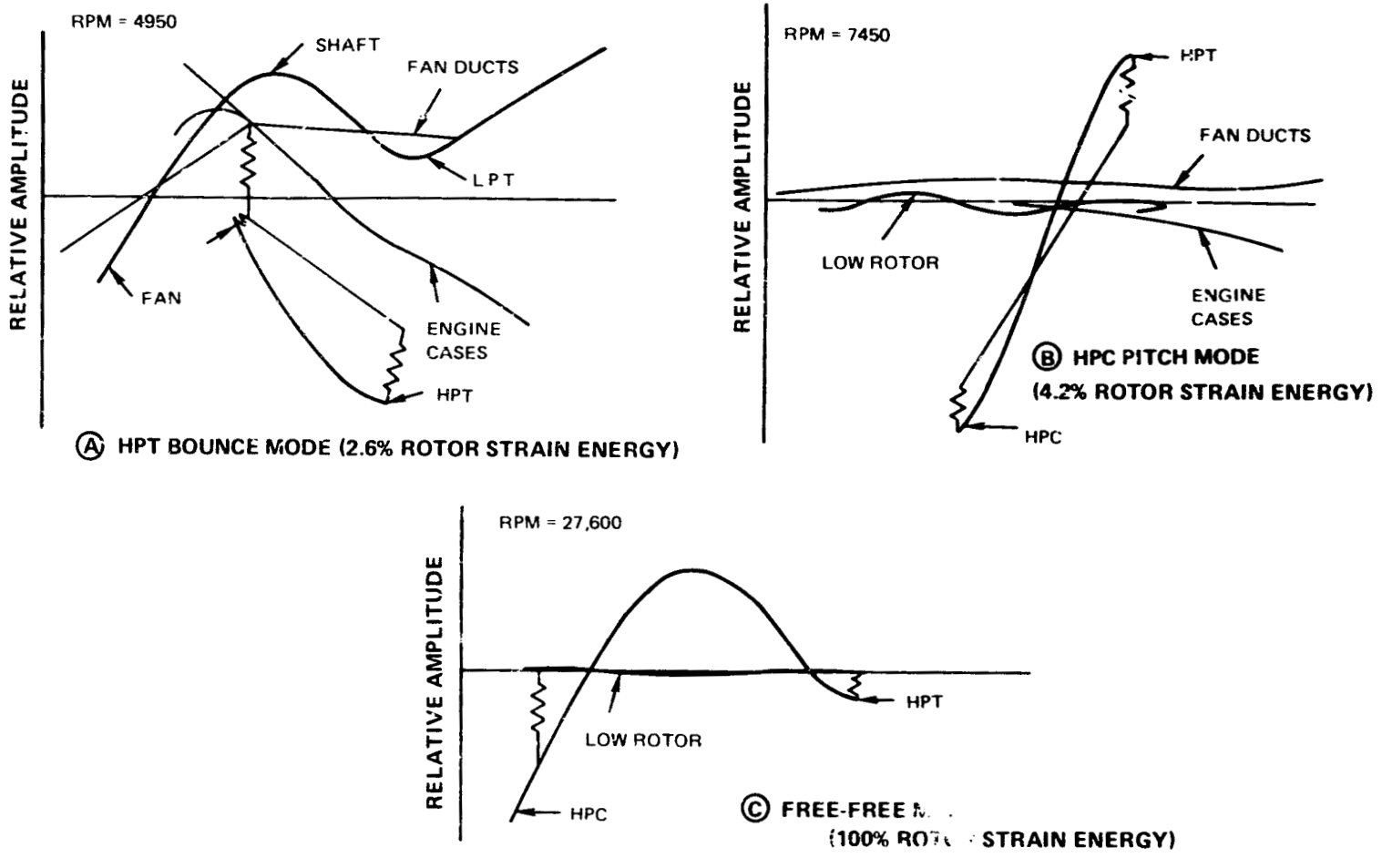

Figure 179 High-Spool Rotor Critical Speeds and Mode Shapes. Prediction shows soft front spring places HPC mode below idle

J20127-213
783011

- "OPEN ENDED" DAMPER

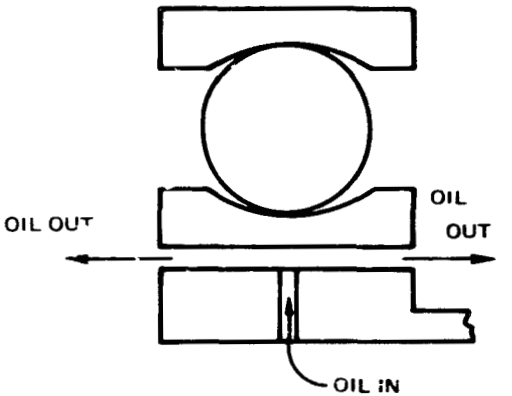

- MECHANICAL SPRING

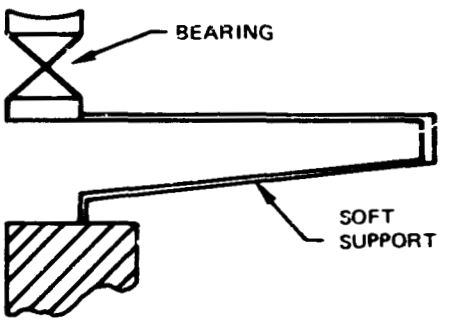

Figure 180 High Rotor Soft Front Spring Mount Configurations. Two options were considered in selecting mechanical spring.

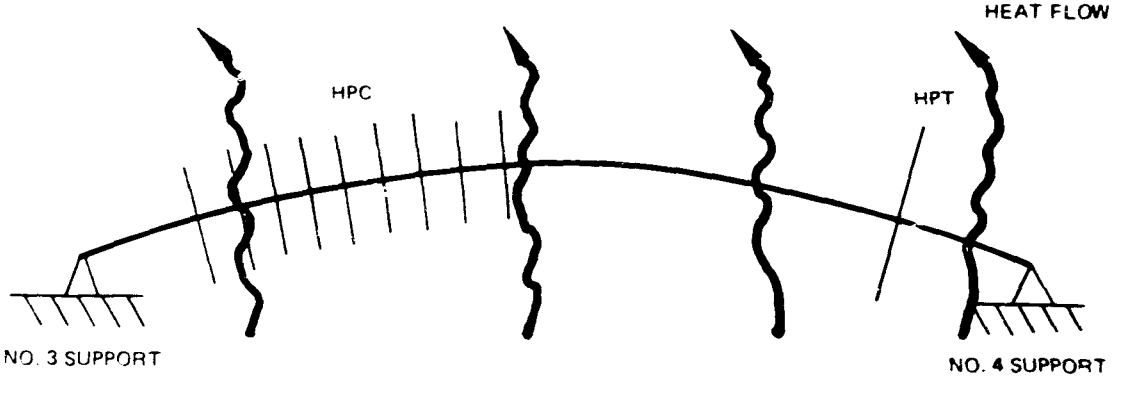

Figure 181 High Rotor Thermal Bow. Illustration shows how bow occurs after engine shut-down.

With an open-ended damper on the front of the high rotor the maximum deflection was calculated to occur at the rear of the high-pressure compressor with an unde ble whirl amplitude of approximately 0.178 cm (0.070 in.). Open-ended dampers, on both the front and rear bearing supports, reduces the whirl amplitude down to approximately 0.114 cm (0.045 in.) at the rear stages of the high-pressure compressor. Then, by replacing the front open-ended damper with a mechanical soft front spring, deflections were calculated to be approximately 0.076 cm (0.030 in.). The fourth and final configuration iteration resulted in a 0.056 cm (0.022 in.) deflection at the rear of the high-pressure compressor using a soft mechanical front spring and substituting a closed-ended damper at the rotor rear support.

This final configuration was studied in additional detail, with variations made in the damper clearance (oil film thickness). It was estimated that a 0.020 cm (0.008 in.) oil film thickness minimized high-pressure turbine whirl during the thermal bow condition. Larger oil film thicknesses increased high-pressure turbine whirl, but reduced whirl in the high-pressure compressor. Further detailed design studies, including transient thermal response of the high-pressure turbine and high-pressure compressor, will be used to establish the final overall damper configuration details.

4.15.6 Summary of Results

The vibration studies indicate that all of the initial rotor dynamics goals have been met. High strain energy modes have been maintained above maximum rotor speed by stiff, lightweight high rotor construction. The high rotor bounce and pitch modes have been driven below idle by incorporating a soft effective front support mount. Minimum whirl during bowed rotor start conditions has been provided by a high efficiency viscous damper on the turbine intermediate case support structure

4.16 MAINSHAFT BEARINGS AND SEALS

4.16.1 Design Description

The Energy Efficient Engine preliminary design has two bearing compartments, each with its own oil supply, scavenge, and breather provisions (see Figure 182). The forward compartment houses the low rotor thrust

bearing (No. 1), the low rotor front roller bearing (No. 2), and the high rotor thrust bearing (No. 3). The forward compartment is sealed from the compartment buffer environment by a dry face carbon seal (No. 1 Front Seal), and a six-lip knife-edge seal (No. 3 Rear Labyrinth), and is sealed from the buffer intershaft region air by a six-lip knife-edge seal (Front Intershaft Labyrinth). The rear compart-ment houses the high rotor roller bearing (No. 4) and the low rotor rear roller bearing (No. 5). The compartment is sealed from the inter-shaft buffer air by a six-lip knife-edge seal (Rear Intershaft Labyrinth) and is sealed from the compartment-enclosing buffer air by a five-lip knife-edge seal (No. 4 Front Labyrinth) and a dry face carbon seal (No. 5 Rear Seal).

4.16.2 Main Bearings Design and Analysis

The procedure for sizing all the bearings began with the optimization of the high rotor bearings. The choice of the DN* level of the No. 3 and No. 4 bearings required a detailed study. From that study and from criteria unique to each bearing, the Energy Efficient Engine preliminary design mainshaft bearing system was evolved.

4.16.2.1 Bearing DN Selection

The selection of the optimum DN level for both the high and low rotor bearings required the consideration of many design factors that are not uniquely pertinent to the design of rolling contact bearings. These evaluation factors are discussed below.

1. Low Rotor Critical Speed: Critical speed is a function of rotor speed, shaft mean diameter, and the span of the shaft-supporting bearings. The Energy Efficient Engine low rotor bearing span was determined from a rotor support study conducted early in the program. The rotor speeds were determined from cycle studies. The low rotor shaft outer diameter was limited by the high rotor shaft inner diameter with allowance for intershaft coolant/buffer flow.

2. Low Rotor Spline Stress: The higher the DN level (larger diameter high rotor shaft), the larger the low shaft diameter and the number of spline teeth. Keeping spline teeth contact area large and bearing stress low, prevents tooth galling.

3. Engine Thrust Growth: In the event thrust growth is required by adding a supercharging stage to the front of the low-pressure compressor, the front bearing would be moved forward, increasing

*DN is an indicator of bearing surface speed. DN is the product of bearing bore diameter (millimeters) and maximum rotor speed (rpm).

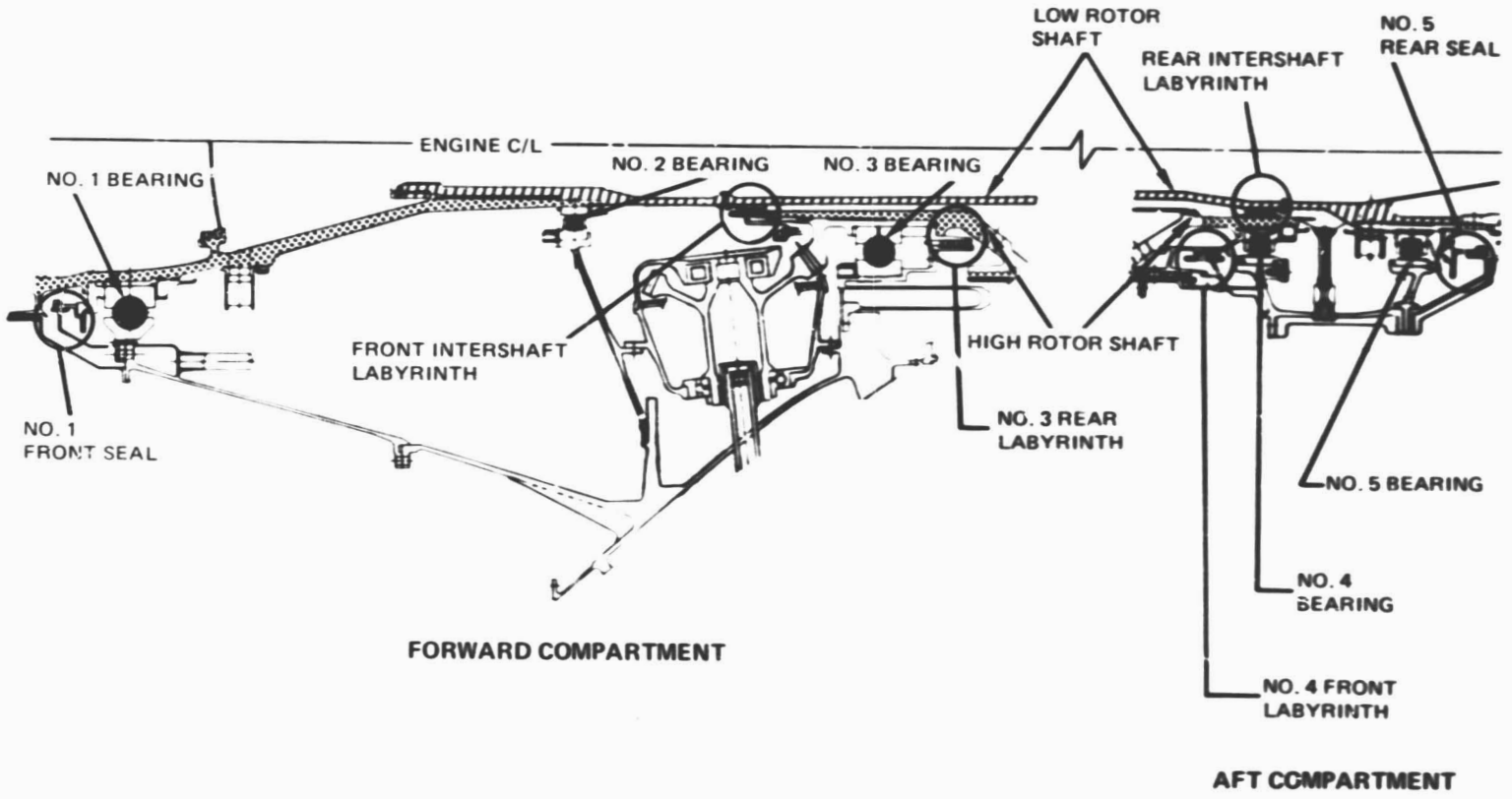

Figure 182 Mainshaft Bearings and Seals. Cross-section shows two-compartment design.

the low rotor unsupported span. Sufficient low shaft critical speed margin must be provided to allow for resultant shaft length extension.

4. High Rotor Bearing Life: Adequate fatigue life for the ball bearing and adequate fatigue and wear lives for the roller bearing must be provided.

5. High Rotor Heat Rejection: Heat rejection due to bearing surface speeds must be minimized to control lubricant temperature.

6. Engine Weight/Cost: The impact of weight and cost on high rotor bearing DN is related to bearing size and to the need for altering associated hardware.

7. Low Pressure Turbine Tip Clearance: Higher DN levels allow the use of a larger diameter low shaft, decreasing rotor deflection under load. Reduced low rotor tip clearance and improved performance would result.

The DN study, conducted over a range from 2.0 to 2.5 million DN, led to the choice of 2.3 million DN for the Energy Efficient Engine. Consideration for low rotor critical speed margin (including 20 percent thrust growth) and low rotor spline stress dictated a minimum of 2.3 million DN. No additional engine benefit was estimated above 2.3 million DN. The impact of weight, cost, and low turbine tip clearance was small over the study range. Analysis indicates adequate high rotor bearing lives and heat rejection at 2.3 million DN.

4.16.2.2 Ball Bearing Design Parameters (See Table 79)

Ball bearing construction details are similar for the two thrust bearing locations in the Energy Efficient Engine. Durability concerns are critical at both locations, with bearing fabrication precision somewhat more critical at the No. 3 location due to the 2.3 million DN maximum speed. Critical design features at both locations are rolling-element size and quantity, race curvature, lubrication and cooling, and ring mounting. These features are discussed below:

Rolling-Element Size and Quantity

1. No. 1 Location: The ball complement was selected when thrust loads were known (major changes to low rotor thrust balance are not readily obtained). The choice of 23 balls of 2.86 cm (1.125 inch) diameter provides adequate rolling contact fatigue life without excessive weight and heat generation. It also recognizes cage strength requirements and bearing bore diameter constraints imposed

TABLE 79

BALL BEARING DESIGN PARAMETERS

Bearing Location	Bore mm	O.D. mm	DN M rpm-mm	Ball Diameter cm	Ball Quan.	Race Cur.(2) %D Ball	Thrust Load kg	Fatigue(3) Life hr	Heat Gen. kg-cal/min
No. 1	270	380	0.95	2.858	28(1)	52/51.5	6.58K	10K	75.6
No. 3	170	260	2.30	2.858	19	52/51.25	3.17K	10K	277.2

NOTES

(1) Ball complement meets criterion for blade loss impact loading
(2) Race Radius of curvature/ball diameter
(3) Design Life: 10K hours
Materials: M50 balls and rings, AMS 6415 (with Ag coating) cage

by shaft strength and assembly considerations. The ball complement also meets design criterion for load capacity required to support blade loss impact loading without fracture.

2. No. 3 Location: The ball complement was selected for maximum thrust load range consistent with bearing bore diameter (DN level) and duty cycle fatigue life requirements. The choice of nineteen, 2.86 cm (1.125 inch) diameter balls allows a 31,136 N (7000 lb) thrust load at SLTO conditions and 3,114 N (700 lb) at flight idle. The thrust load range provides 10,000 hour life without overly compromising skid prevention considerations. The ball complement also recognizes cage strength constraints.

Race Curvature

Ball contact stress can be reduced and bearing life increased by reducing radius of curvature of the race. This is done at the expense of increased heat generation and operating temperature with reduced tolerance to deviation from the specified internal clearance and contact angle. The radius of curvature of both inner and outer races is typically 52 percent of ball diameter.

In high DN bearings, reduced outer race curvature compensates for increased outer race contact load due to ball centrifugal force. Outer race curvature is reduced at both No. 1 and No. 3 locations (51.5 percent and 51.25 percent, respectively) with a larger reduction at No. 3 due to the higher DN level.

High DN level increases ball spin on the inner race, making heat generation more sensitive to reduced inner race curvature. Inner race curvatures are set at 52 percent at both the No. 1 and No. 3 locations in the engine.

Ring Mounting

Thrust bearing inner rings are mounted on shaft hubs with radial interference fits; suitable shaft stack clamping loads are applied with spanner nuts. The No. 1 bearing outer ring is bolted directly to the compartment housing to assure non-rotation under high fan unbalance and structural integrity under fan blade loss. The No. 3 bearing outer ring is "slip fitted" into its housing and secured with a spanner nut to take the relatively low normal and blade loss radial loads.

4.16.2.3 Roller Bearing Design Parameters (See Table 80)

Roller bearing construction details are substantially different for each location. Functional and durability design concerns are much more critical at the high spool (No. 4) location than the other locations. The principal features which vary with location are cage and roller guidance, lubrication and cooling, preloading, rolling element size and quantity, and ring mounting and damping.

TABLE 80

ROLLER BEARING DESIGN PARAMETERS

Bearing Location	Bore mm	O.D. mm	DN M rpm-mm	Roller Diameter mm	Roller Length mm	Roller Quan.	Radial Load kg	Fatigue[3] Life hr	Heat Gen. kg-cal/min
No. 2	135	195	0.4	15	15	24	1.32K	100K	20.2
No. 4[1]	170	260	2.3	18.5[2]	16[2]	28	0.82K	10K	100.8
No. 5	170	240	0.6	18.5	18.5	28	1.18K	100K	25.2

NOTES:

(1) No. 4 bearing preloaded and oil-damped
(2) L/D 1.0 produces reduced tendency for roller skew (wobble) at high speeds
(3) Design life: 10K hours
Materials: M50 rollers and rings, AMS 6415 (with Ag coating) cage

1. Cage and roller guidance: Cage and roller drag forces and related heat generation and roller skidding tend to be minimized when the roller end guide flanges which limit roller skew are integral with the inner ring, and when the O.D. surfaces of these flanges mate with the I.D. surface of the roller separator (cage) to control cage centrality. This arrangement has been applied to the critical No. 4 location and selectively to the low spool locations. Shaft assembly and lubrication considerations at the No. 2 location favor outer ring cage and roller guidance, and the low DN level of that location allows free selection of either arrangement.

2. Preloading: Roller bearings are preloaded with a combination of ring flexibility, internal radial clearance, and multiple lobed race surface out-of-roundness which produces two or three roller load zones independently of external loading. Preloading generates radial load to prevent excessive roller skidding at high speed and low external load; and with three load zones, it centers the rotor and provides a predictable, nearly linear radial spring-rate. The high spool (No. 4) roller bearing is preloaded; the low spool bearings are not. Low rotor bearing skidding and stiffness characteristics are manageable without preload.

3. Roller size and quantity: The roller complement for the No. 4 location is selected to obtain maximum theoretical rolling contact fatigue life and favorable roller guidance wear life. Roller diameter is increased until fatigue life ceases to increase because of increasing outer race contact stress from centrifugal roller loading. Roller diameter, pitch diameter, and cage strength considerations establish roller quantity. Roller length in the No. 4 location departs from the conventional one to one relationship with roller diameter in order to reduce the tendency toward dynamic disturbances which produce roller skew or wobble at high operating speeds. Reducing roller length to 86.5 percent of roller diameter reduces radial load capacity somewhat, but promotes improved roller end face and guide flange wear life statistics.

   The No. 4 and No. 5 bearings share similar envelope dimensions; for convenience the No. 4 roller complement was selected for the No. 5 location.

   The No. 2 bearing is lightly loaded. Roller size and quantity are selected according to bearing pitch diameter and cage strength considerations. Smaller rollers could be used without compromising rolling contact life, but the reduced cage cross section would compromise cage strength and resistance to secordary damage if rolling contact fatigue were to occur.

4. Ring mounting and damping: All inner rings are assembled tight on the shafts and are designed to remain tight at all operating conditions. Ring slippage is further prevented by substantial axial clamping force applied through a "spanner" nut. The No. 4 bearing

outer ring also serves as the inner member of a journal type "squeeze film" damper that uses lubrication oil as the damping fluid. Ring rotation must be prevented by providing lugs that engage the axial retainer plate at one end of the ring.

The No. 2 and No. 5 bearing outer rings are mounted by means of conventional spanner nuts, with the outer rings slip-fitted into the housings.

4.16.3 Buffer/Breather Air Management

The second of two major studies (bearing DN selection was the first) in the area of Mainshaft Bearings and Seals involved selection of compartment buffer and breather schemes. The study featured, but was not limited to, the separate effects of buffer source, mainshaft seal type, intersump breather tube, and breather vent system on weight, cost, performance, oil consumption, and economic factors.

4.16.3.1 Design Concept Evolution (See Figure 183)

The originally proposed buffer system featured a pressurization scheme that used air bleed from the 11th stage mid-compressor location, much like other Pratt & Whitney Aircraft Group engines. The carbon seals at each compartment boundary were adequately pressurized, but the 386°C (725°F) temperature of the leakage air added unwanted heat to the compartments and forced temperature to be a critical consideration in the design of the low shaft.

The breather system in the proposal engine carried the spent buffer air and oil mixture directly to the gearbox and then overboard via the deoiler. Despite the plan to mount the rotary deoiler external to the gearbox, the path of the air-oil mixture through the gearbox presented a fire hazard.

Because of these concerns and others having to do with heat rejection and with oil weepage at idle and windmilling, a study of various systems was done highlighting (1) optimum bleed location, (2) breather vent system, and (3) seal type.

The system chosen for the Energy Efficient Engine bleeds the buffer air from the high-pressure compressor inlet I.D. where the temperature is only 121°C (250°F). The lower temperature air invites the use of labyrinth seals at two compartment boundaries (more breather flow but less expensive air) and simpler labyrinth seals at the intershaft positions. The No. 1 front and No. 5 rear dry face carbon seals have been retained to control the breather flow and oil consumption. The chosen scheme further carries the spent buffer air through low aftmounted deoilers and then from the low shaft to the engine exhaust. The cooler compartment environment reduces engine heat

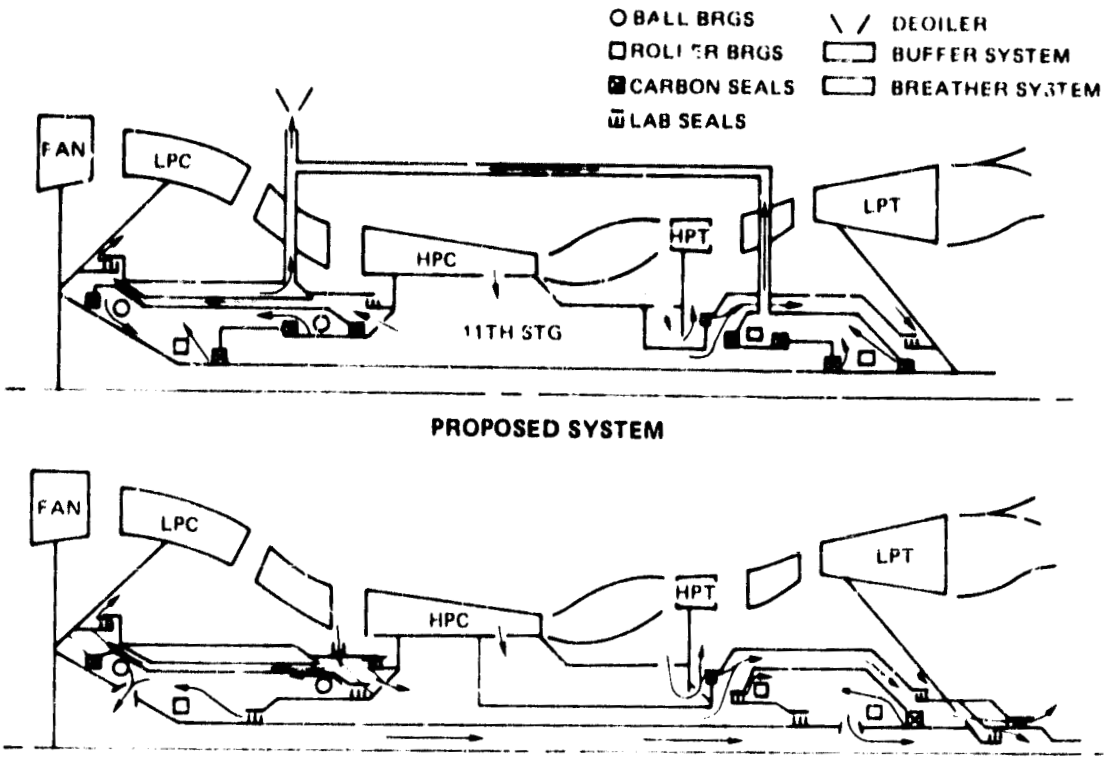

Figure 183 Bearing Compartment Buffer/Breather System. Schematic shows original and current configurations.

rejection, and the breather vent to sub-ambient pressure ensures at least improved, if not total, resistance to oil weepage during idle and windmilling operation.

4.16.3.2 Benefits of Selected System

The center vent breather system combined with the cold buffer system saves weight and cost. A lighter low shaft evolved from the study; the buffer temperature of 386°C (725°F) was a critical design consideration in the proposal engine. The cold buffer scheme reduced the need for a large number of carbon seals, thereby lowering the compartment heat generation and eliminating the need for an air-oil cooler. Along with the removal of the gearbox deoiler, the above changes to the system provided a savings of 57.6 kg (127 lb) and $8800.

The center vent breather/cold buffer system increased oil system reliability and safety. The lower buffer temperature reduces the danger of bearing compartment fires; the elimination of breather air from the gearbox removes a potential fire hazard from that area. Oil weepage at idle and windmilling is reduced by increasing the carbon and labyrinth seal pressure drop in two ways. The buffer air source pressure at the high-pressure compressor inlet at idle and during windmilling is higher than at the 11th stage I.D. and the breather discharges to the sub-ambient level of the exhaust cone. Fire propagation from the turbine exhaust to the bearing compartments, a possible consideration in selecting the center vent breather approach, is not cause for concern. With normal breather flow rates, the air-oil mixture is too lean to support combustion; with above normal breather flow rates, the flow velocity is above the flame propagation rate.

Not to be overlooked in assessing the many benefits of the cold buffer system is the maintainability and reliability improvement of labyrinth seals.

4.16.3.3 Labyrinth Seal Design Parameters (See Table 81)

The labyrinth seal configurations chosen for the intershaft and compartment boundary locations are of the 6 knife-edge and 5 knife-edge straight through type with abradable rub surfaces. To minimize seal leakage and oil consumption, the smallest seal clearances possible at each location were selected. With one exception, the operating radial clearances are 0.2 mm (0.008 in.). Because of the rotor deflection at the front intershaft seal location during engine bowed rotor starts (abnormal whirl),the smallest operating radial clearance possible is 0.45 mm (0.018 in.).

4.16.3.4 Carbon Seal Design Parameters (See Table 82)

The dry face carbon seals, retained in the design for reasons of breather flow and oil consumption, are of low surface speed, well

C-5

TABLE 81

LABYRINTH SEAL DESIGN PARAMETERS

Seal Location	No. Elements	Rub Surface	Radial Clearance mm (in.)	Seal Leakage m^3/min (ft^3)/min
Front Intershaft	6	Abradable	0.46 (0.018)	3.82 (135)
No. 3 Rear	5	Abradable	0.2 (0.008)	1.70 (60.0)
No. 4 Front	5	Abradable	0.2 (0.008)	1.70 (60.0)
Rear Intershaft	6	Abradable	0.2 (0.008)	1.56 (55.1)

TABLE 82

CARBON SEAL DESIGN PARAMETERS

Seal Location Type	Seal Dia. cm	Surf. Speed m/sec	Dam Width cm	Seal Leakage m^3/min (ft^3/min)	Wear Life hrs	Gen. Heat kg-cal/min
No. 1 Front Dry Face	31.8	61.3	0.381	0.17(6.0)	20K	20.2
No. 5 Rear Dry Face	21.8	42.1	0.381	0.11(3.9)	20K	15.2

within design practice. Tne face width and seal unbalanced load were defined to minimize heat generation and guarantee 20,000 hour wear life (domestic mission).

The total carbon seal leakage of 0.28 m^3/min (10 ft^3/min) and the total labyrinth seal leakage of 8.78 m^3/min (310 ft^3/min) combine as a breather flow of 9.06 m^3/min (320 ft^3/min) which denotes an oil consumption rate of 0.303 liters/hr (0.08 gallons/hr).

4.16.4 Lubrication System

The Energy Efficient Engine lubrication system could be briefly described as . system featuring a regulated oil supply system, a conventional scavenge system, and low shaft-mounted rotary deoilers. Ignored in such a description, however, would be the numerous means employed to minimize the oil flow and optimize the oil distribution for minimum bearing and seal heat generation. As a result, the need for an air-oil heat exchanger has been eliminated without compromise to mainshaft bearing and seal durability.

4.16.4.1 System Schematic

The lubrication system is shown schematically in Figure 184. The regulated oil supply system provides a constant oil flow to each compartment regardless of high rotor speed by use of a pressure regulating valve across the pressure pump/main oil filter combination. Three scavenge pumps are provided in the gearbox, one for each bearing compartment and one to drain the gearbox sump. Low shaft-mounted paddle-wheel or rotary deoilers are placed in each compartment to separate the oil mist from the breather air with low pressure loss.

4.16.4.2 Front Compartment Heat Generation/Oil Flow Rates

Approximately 55 percent of sea level takeoff heat generation and 53 percent of total regulated oil supply flow exist in the front compartment. Only 15 percent heat generation and 18 percent total oil flow is chargeable to the low rotor, however.

4.16.4.2.1 No. 1 Bearing/No. 1 Front Carbon Seal (Figure 185)

The heat generation of the No. 1 bearing is relatively low, making operating temperature less sensitive to oil flow rate and supply location. All oil is supplied through the inner ring split, with internal splash cage land lubrication. Operating temperature levels and thermal gradients are well within safe limits with 5.44 kg/min (12 lb/min) oil supply flow rate.

Lubrication of the rotating seal plate is by 1.18 kg/min (2.6 lb/min) oil flow, introduced through oil passages evenly spaced around the

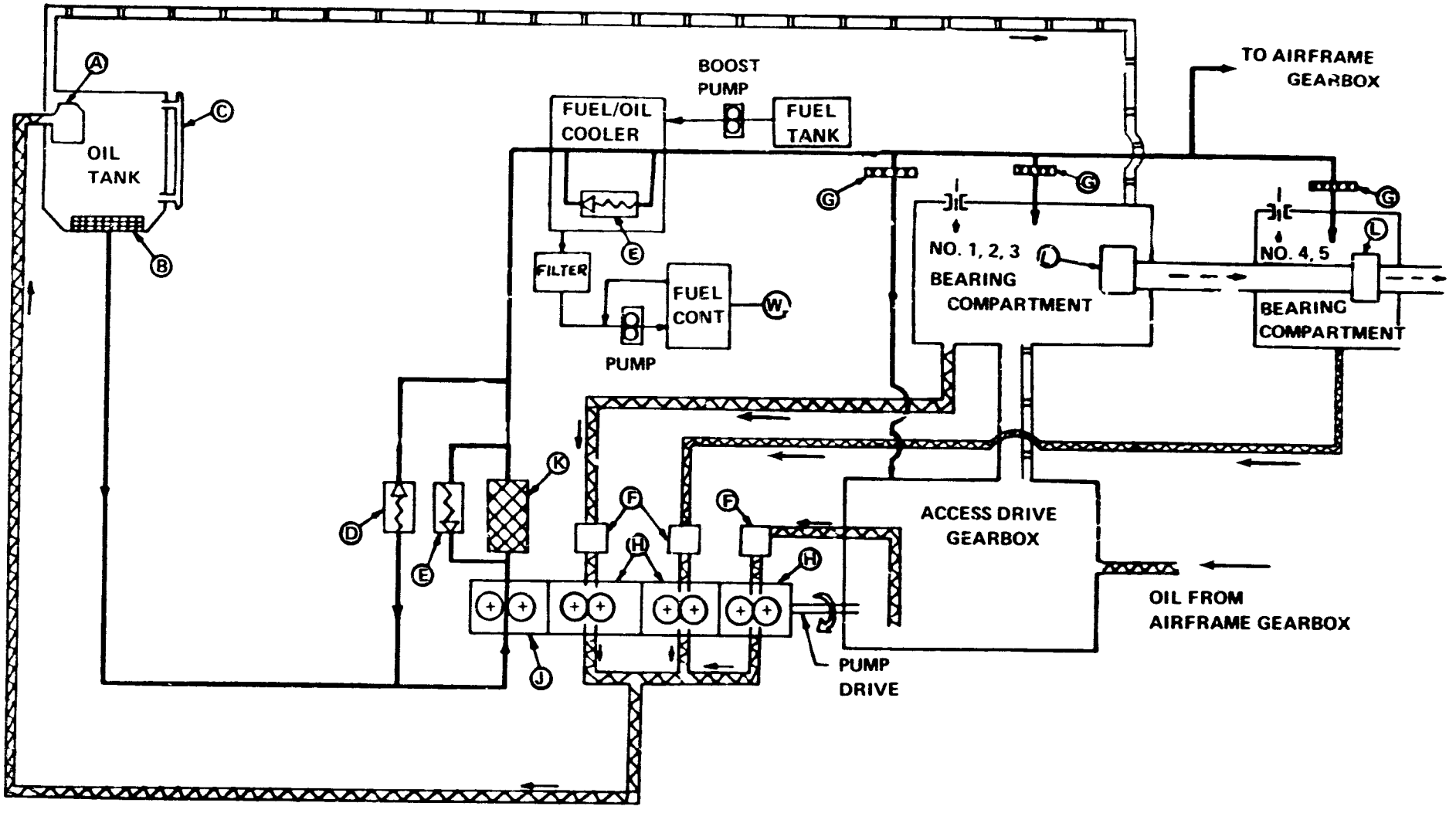

Figure 184 Lubrication System. Schematic shows subsystem components.

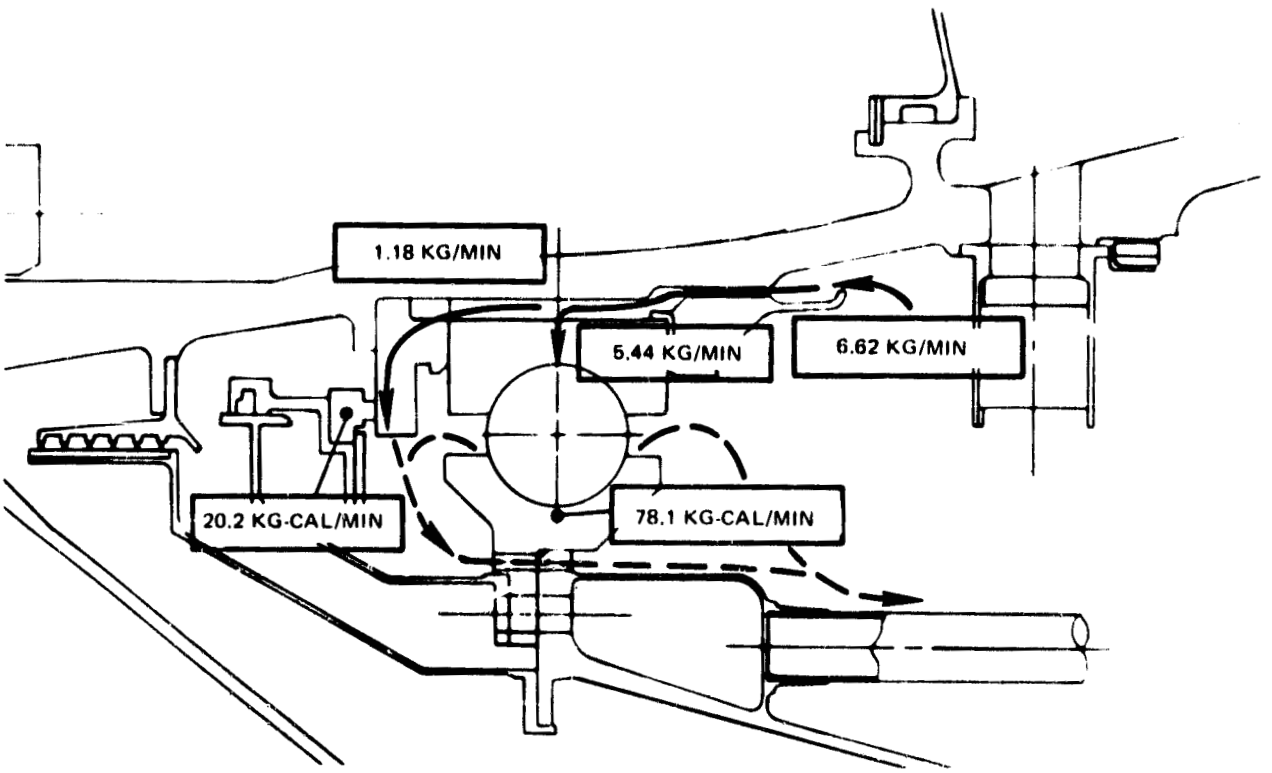

Figure 185 No. 1 Bearing. Cross-section shows heat generation and oil flow distribution for the No. 1 bearing.

circumference. The holes are skewed with the engine centerline to improve cooling effectiveness. The combined SLTO heat generation of the No. 1 elements is 98.3 kg-cal/min (390 Btu/min).

4.16.4.2.2 No. 2 and No. 3 Bearings (Figure 186)

No. 3 bearing heat generation and operating temperatures are highly sensitive to oil flow rate and supply location. Oil supply is divided between the inner ring split and the cage guide surfaces on the inner ring. The outer ring is predicted to operate at about 36°C (65°F) above inner ring temperature. This temperature gradient could be reduced somewhat with increased oil flow but only at the expense of greatly increased heat generation. The 11.34 kg/min (25 lb/min) oil flow selected provides a reasonable compromise between operating temperature and heat generation.

Splash lubrication is substituted for the more costly direct lubrication of the No. 2 bearing guide surfaces. A fixed oil jet directed at the inner ring should provide adequate cooling and lubrication for the bearing.

The towershaft bearings and the teeth of the main gear are lubricated with 2.72 kg/min (6 lb/min) oil flow.

The combined SLTO heat generation of the No. 2 and No. 3 bearings and the towershaft/gear elements is 335.1 kg-cal/min (1330 Btu/min).

4.16.4.3 Rear Compartment Heat Generation/Oil Flow Rates

Figure 187 depicts the complex lubrication features of the rear compartment. It is significant to note that, unlike the front compartment with its cool environment, the rear compartment suffers significant heat pick-up from its environment.

4.16.4.3.1 No. 4 and No. 5 Bearings/No. 5 Rear Carbon Seal

At the No. 4 location, oil is supplied directly to the inner edges of the roller guide surfaces and also to the center of each cage guide surface. These surfaces and the mating roller and cage surfaces are prone to wear at high speed. Inner ring cooling, also critical at high speed, is provided by directing oil through closely spaced axial grooves in the bore of the inner ring. The oil flow for protecting these areas is 6.35 kg/min (14 lb/min).

To provide commonality, the same slot configuration is used in the No. 5 bearing even though the required oil flow is less. The damping and preloading features of the No. 4 bearing, however, prevent complete commonality. The No. 5 rear carbon seal plate has the skewed coolant holes, distributing 0.9 kg/min (2 lb/min) oil flow to the rubbing face area.

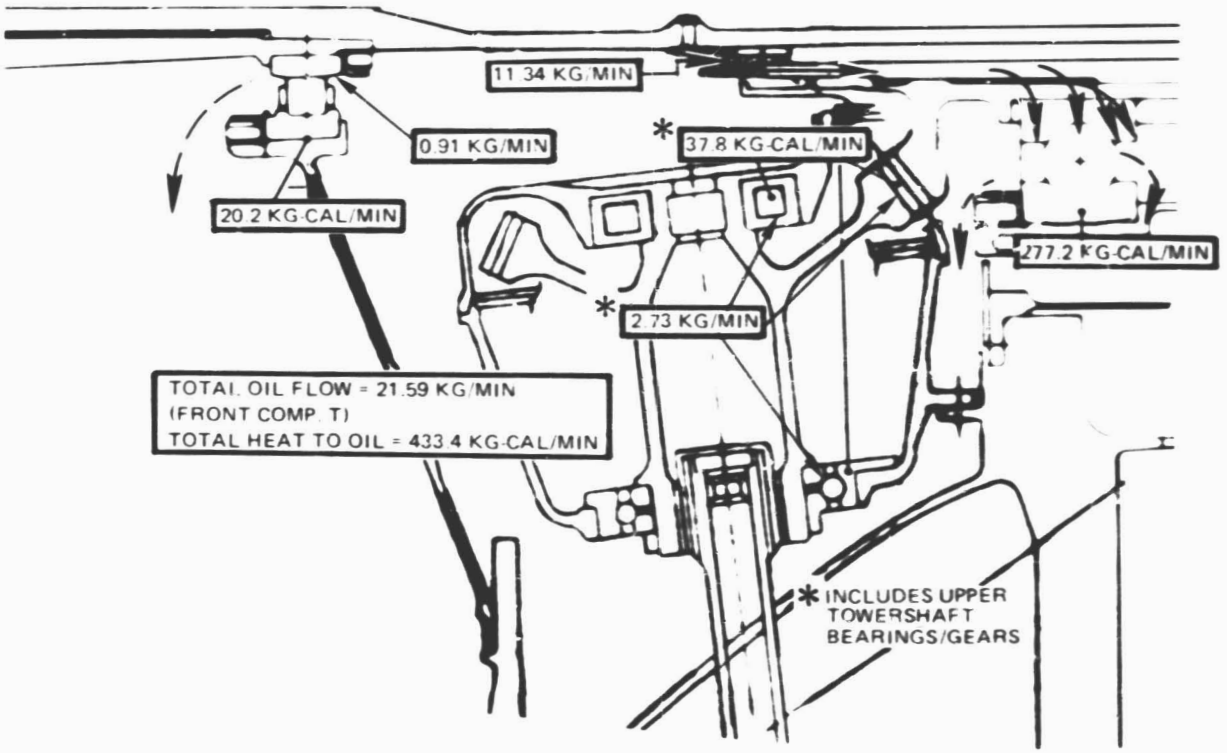

Figure 186 No. 2 and No. 3 Bearing Area. Cross-section shows heat generation and oil flow distribution for the No. 2 and No. 3 bearings.

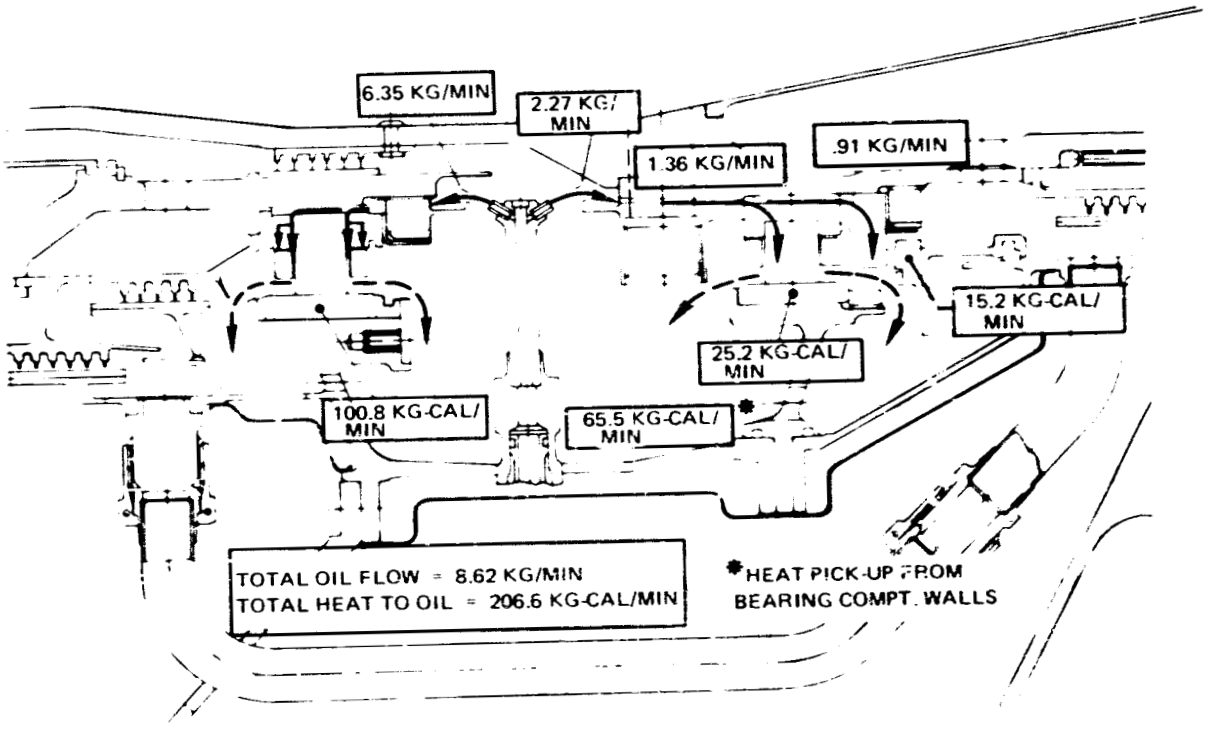

Figure 187 Rear Bearing Compartment. Cross-section shows heat generation and oil flow distribution for the No. 4 and No. 5 bearings.

Including the 65.5 kg-cal/min (260 Btu/min) heat pick-up from the compartment walls, the total compartment SLTO heat generation is 206.6 kg-cal/min (820 Btu/min).

4.16.4.4 Fuel Heat Sink Analysis

An analysis was conducted to determine the necessity of an air-oil cooler in the lubrication system. This analysis estimated the quantity of heat rejected to the oil by the bearings, carbon seals, gears, labyrinth seals, and compartment walls. It was then determined whether all of the heat rejected to the oil could be absorbed by the fuel without exceeding reasonable fuel temperatures at the fuel control.

Figure 188 summarizes the results of the fuel heat sink study. Fuel system component temperature rise is calculated for each of five representative flight conditions and the ultimate fuel temperature at the fuel control is determined. The stabilized flight condition that determines the need for air-oil cooling is not SLTO where the greatest heat generation exists, but the 15,240 meter (50,000 ft) maximum cruise, Mn 0.8 standard day, where heat generation is lower but fuel flow even lower with respect to SLTO. The fuel temperature at the latter flight condition (107°C or 225°F) would not dictate supplementary cooling.

The fuel temperatures at the two idle conditions are of some concern, especially at 10,668 m (35,000 ft), idle Mn 0.8 standard day. Limiting fuel temperature to approximately 150°C (300°F) is desirable at this and all transient conditions. A means to overcome this transient problem lies in the selection of the type of oil system. If a nonregulated oil system is assumed, a benefit is derived from reduced oil flow at idle (when the rotor speeds are low) in that less heat is picked up in the compartments and transmitted to the fuel. It is believed that when this alternative approach is studied during the detailed design phase, no compromise to compartment integrity will be found and that the fuel temperatures at the fuel control will be reduced to approximately 135°C (275°F).

4.17 SECONDARY FLOW SYSTEM

4.17.1 Design Functions

The secondary flow system is (1) the source of component coolant, (2) the source of bearing compartment buffers/breathers, (3) the means for rotor thrust balance control, (4) the source of aircraft/engine service bleeds, and (5) the source of active clearance control coolant.

4.17.2 Main Design Features

The secondary flow system flow system is built around the six distinct design features shown on Figure 189. Each feature exercises partial control over the major coolant sources by setting the operating pressures, the flow rate, and/or the temperature.

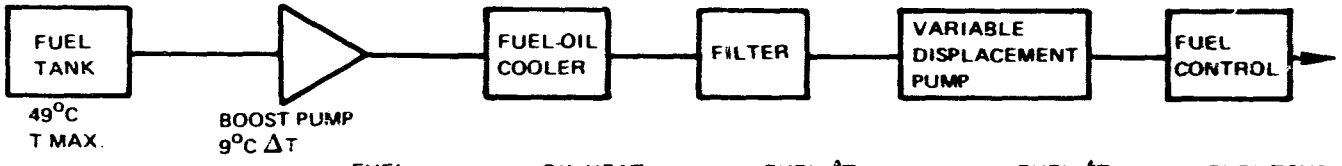

FLIGHT CONDITION	FUEL FLOW KG/MIN	OIL HEAT REJECTION KG-CAL/MIN	FUEL ΔT (FLO COOLER) °C	FUEL ΔT (PUMP) °C	FUEL TEMP TO ENGINE °C
SEA LEVEL TAKE-OFF MN 0.45, +61°F (MAX. N2)	91.6	781.2	17	14	89
10,667 METERS, MAX. CRUISE MN 0.8 STD. DAY (ADP)	44.0	367.9	17	17	92
15,239 METERS, MAX CRUISE MN 0.8 STD. DAY	21.0	315.0	30	19	107
SEA LEVEL, IDLE STATIC, STD. DAY	7.5	241.9	64	28	150
10,667 METERS, IDLE MN 0.80 STD. DAY	5.4	224.3	83	28	168

FUEL TYPE: JP-5
OIL TYPE: PWA 521 II (MIL 23699)

Figure 188 Fuel Heat Sink Analysis. Study shows estimated fuel temperature rise from tank to engine (engine delivery fuel temperature below 150°C limit at all operating points except transient idle conditions)

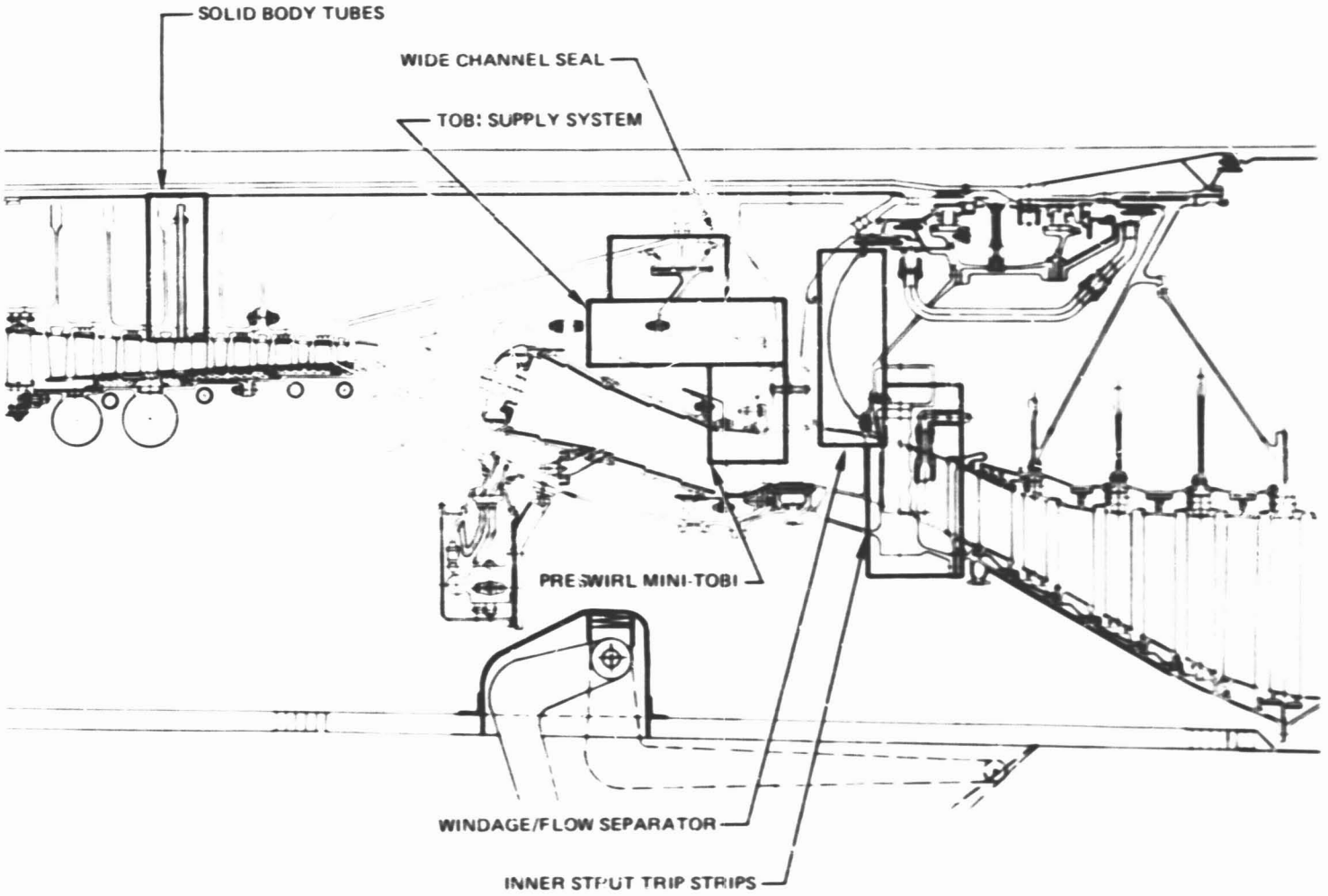

Figure 189 Secondary Flow System. Cross section shows six principal system design features.

4.17.2.1 Solid Body Tubes

Low rotor disk coolant air is bled from behind the 11th-stage rotor I.D., directed through solid body tubes attached to the drum, and allowed to flow aft to the low-pressure turbine in the space between the compressor drum and bore tube. The solid body tubes confine the bleed flow to solid body rotation, preventing significant pressure loss caused by what would otherwise be free vortex behavior. Without the tubes, the bleed would have to be moved to the 13th stage, thereby increasing both performance penalty and the coolant air temperature.

4.17.2.2 Wide Channel Seal

A wide-channel seal is used between the high-pressure compressor and high-pressure turbine to balance opposing rotor axial loads within thrust bearing load constraints. This seal throttles the pressure level of the high-pressure compressor secondary air flow discharge to that of the high-pressure turbine inlet, with minimal leakage involved. A wide channel seal configuration was incorporated at this location based on analysis that estimated leakage to be reduced by approximately 50 percent relative to a more conventional multi-knife edge labyrinth seal.

The current wide-channel seal design, as shown in Figure 190, consists of a smooth-surface rotor which is immediately adjacent to a mating stator having a surface consisting of honeycomb. MERL 80 is used as the basic seal material because of the high temperatures and stresses created in the event of a rub.

A clearance goal (Aerodynamic Design Point) of 0.20 mm (0.008 in.) was established at the outset of the preliminary design effort. Rotorframe analysis of the current configuration indicates the clearance to be 0.38 mm (0.015 in.). During detail design, the wide-channel seal configuration will be adjusted to obtain a better thermal match between the rotor and stator, and thus minimize the clearance further.

Preliminary analysis of wide channel seal behavior during an assumed severe rub caused some concern regarding the current configuration. The major concerns were in regard to the ability of the seal surface to smoothly abrade rather than chunk, and whether the heat generated can be transferred in such a manner as to avoid overheating and severe distortions or breakage. To overcome these concerns, material will be added during the detail design effort to thicken the seal, especially in the rotor portion. In addition, testing of the thickened configuration under severe rub conditions is required so that the structural risk can be better quantified and assessed.

4.17.2.3 TOBI Supply System

Tangential on-board injection (TOBI) nozzles are used to preswirl high-pressure turbine blade coolant air up to wheel speed at the disk drilled coolant hole entry. The system is unique in that the coolant

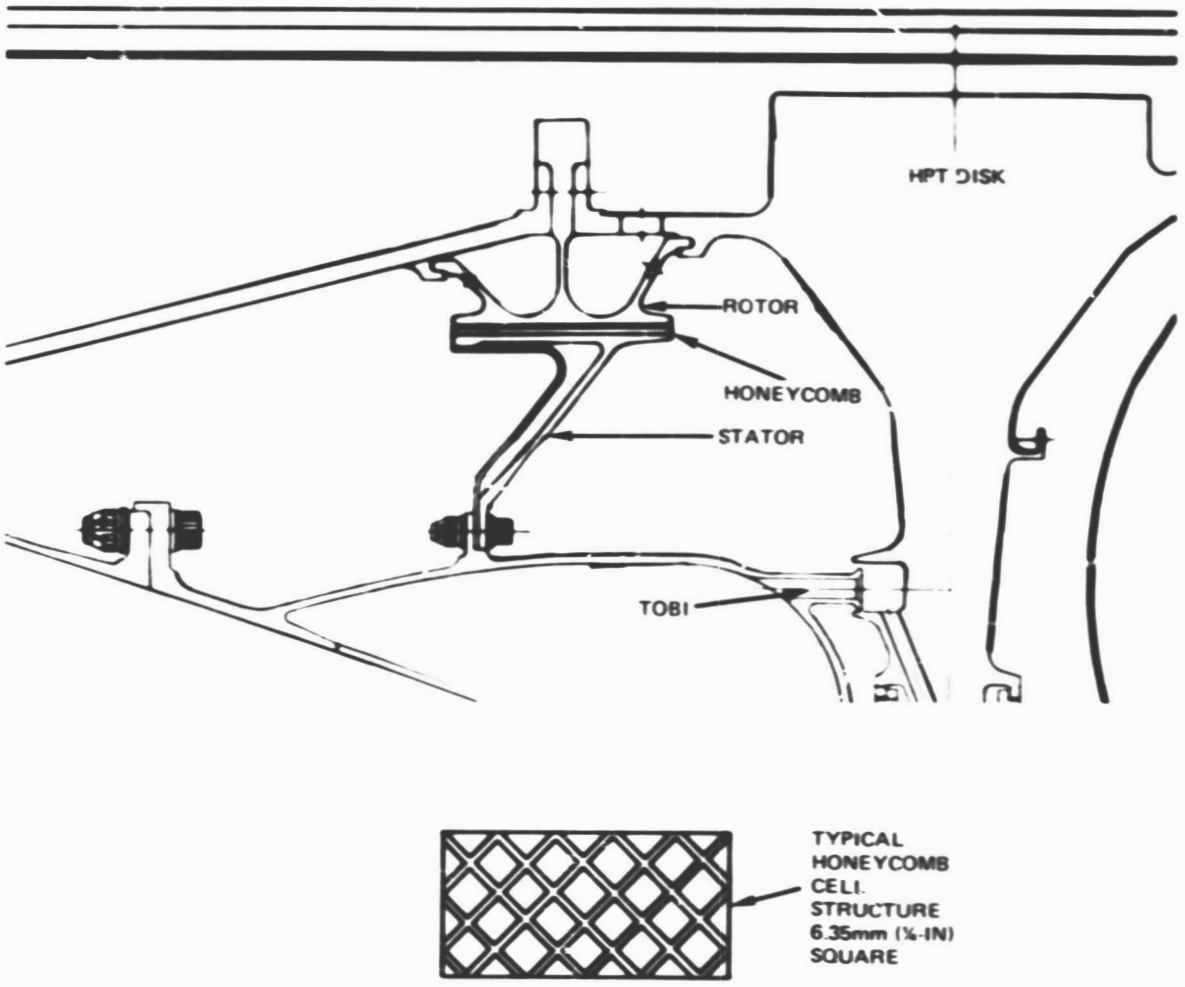

Figure 190 Wide Channel Seal. Schematic drawing shows design features.

flow is bled directly from the compressor discharge I.D., ahead of the exit guide vane row to cool the rear compressor shaft before being preswirled in the nozzles shown in Figure 191. The use of all the blade coolant to absorb the windage heat generated by the high-speed large-diameter shaft, minimizes the coolant temperature rise. Nozzle pressure is balanced with the vane exit pressure to minimize leakage into the main gas path.

4.17.2.4 Preswirl Mini TOBI

Air for cooling and purging the high-pressure turbine disk front rim cavity is also introduced through preswirler nozzles located in the TOBI case to reduce the windage heat generation and flow rate necessary for adequate cooling.

4.17.2.5 Windage Flow Separator

The flow separator was included in the design to prevent air used to cool the bore at the high-pressure turbine disk from mixing with the low pressure turbine disk coolant air, isolating the high-pressure turbine disk thermal environment to effectively control the disk axial temperature gradients, and to control windage losses from the rear side of the high-pressure turbine disk. An estimated reduction of 42°C (75°F) in low-pressure turbine disk environment temperature is the most obvious benefit; rear bearing compartment and low-pressure turbine rotor environments are also enhanced.

4.17.2.6 Mid-Turbine Trip Strips

The coolant channels within the mid-turbine struts incorporate turbulence inciters (trip strips) to increase the convective heat transfer coefficients. Without the trip strips, cooling of the struts would require approximately twice the compressor airbleed to provide comparable metal temperatures.

4.17.3 Secondary Flow Rate, Pressure, and Temperature Predictions

Figure 192 is the detailed secondary flow map for the flight propulsion system showing the temperatures, pressures, and coolant flow levels as controlled by the design features described in Section 4.17.2. The secondary flow system was fully modeled to understand its operation at numerous flight conditions including both coolant flow and leakages. Also shown are the buffer and breather flow systems, as described in Section 4.16 in more detail.

4.17.4 Component Cooling System

All component cooling (Figure 193) is accomplished with air bled from three compressor sources: (1) 10th-stage O.D., (2) 11th-stage I.D., and (3) compressor discharge. The coolant flow is conditioned (pressure,

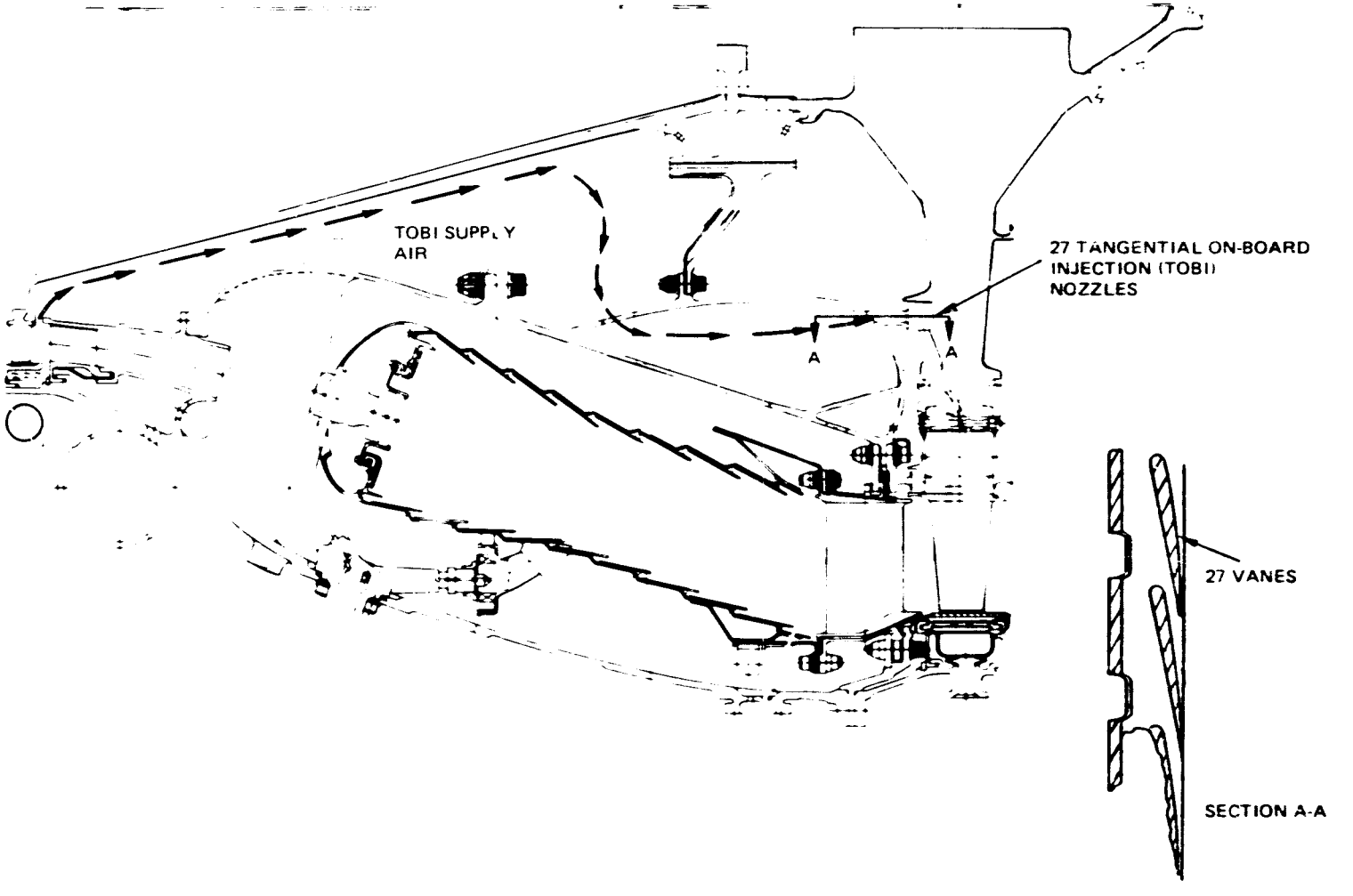

Figure 191 Pressure Balanced Choked TOBI System. Cross-section shows air routing.

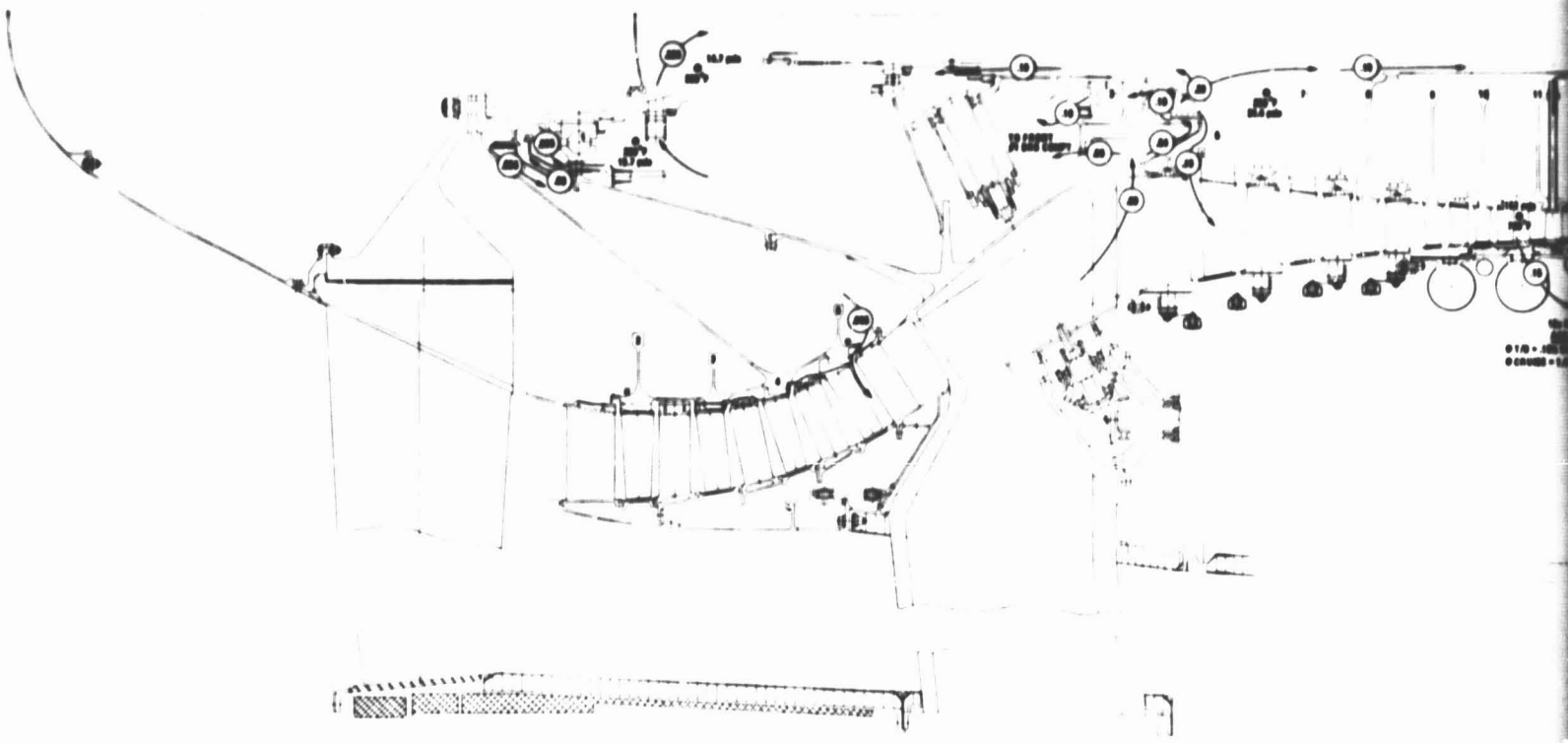

ORIGINAL PAGE IS
OF POOR QUALITY

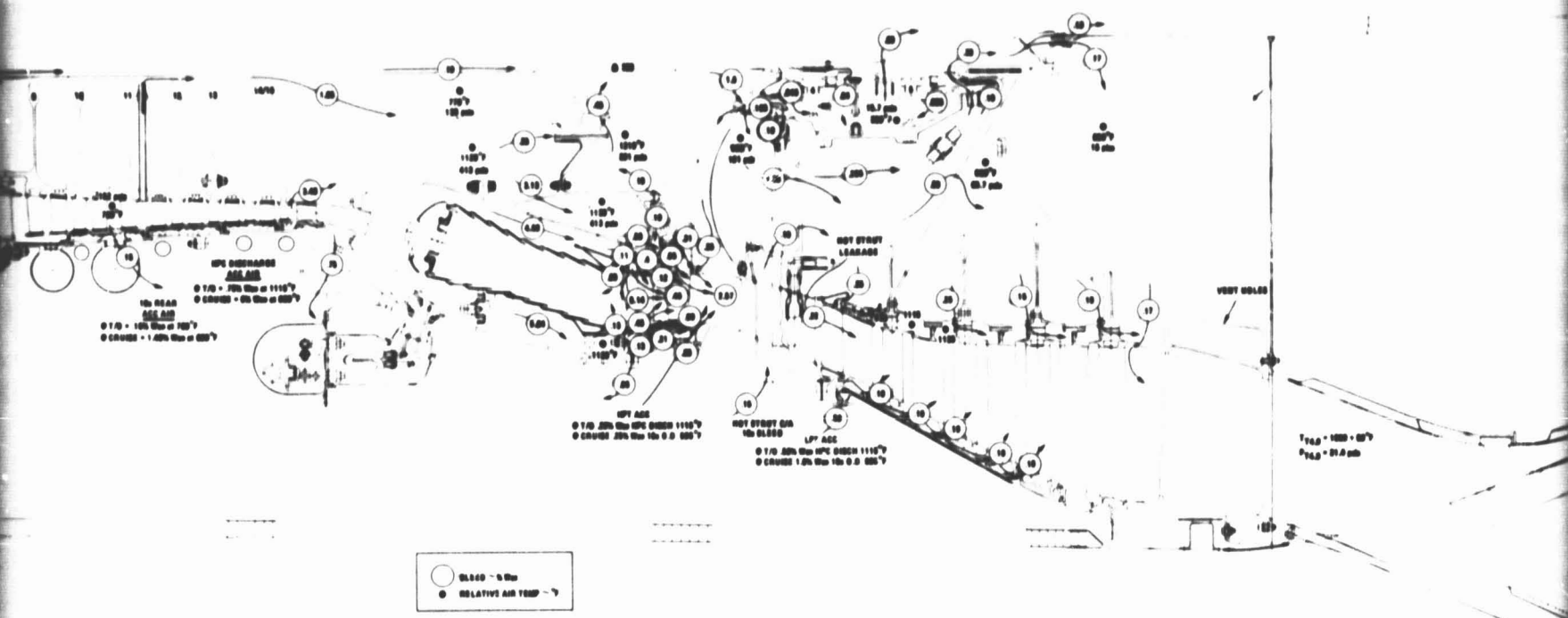

2 FOLDOUT FRAME

Figure 192 Engi
pre

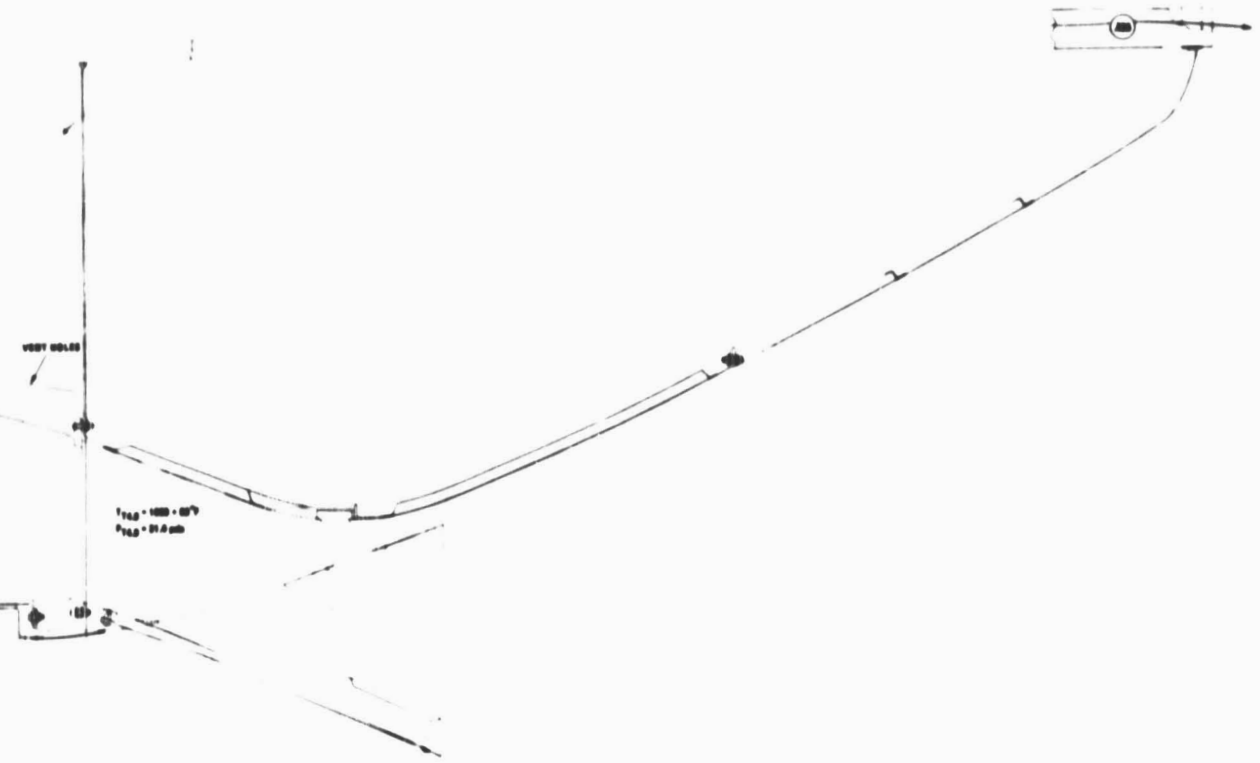

Figure 192 Engine Secondary Flow Map. Drawing shows flow rates, pressures, and temperatures at various locations.

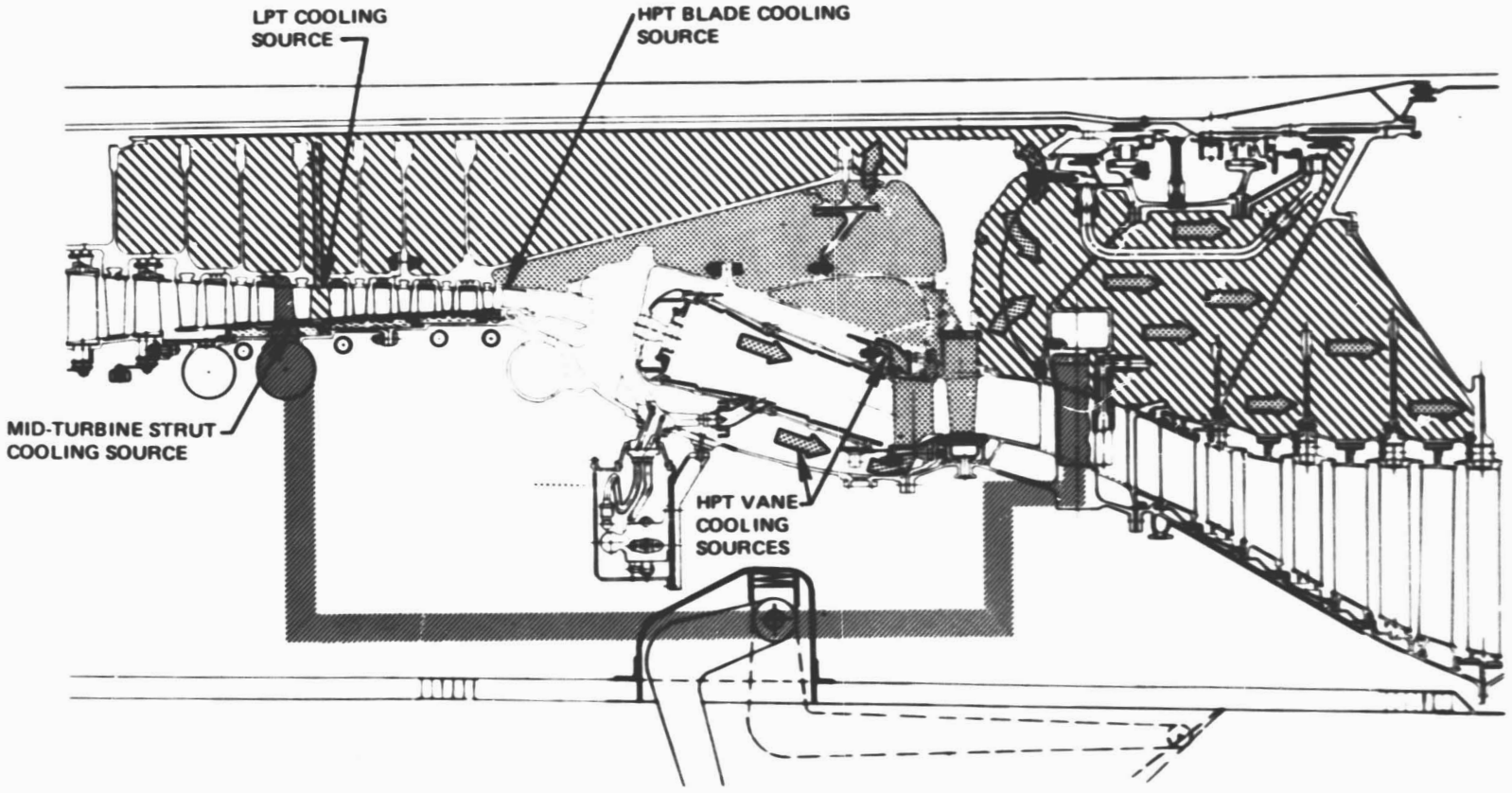

Figure 193 Component Cooling Air Systems. Drawing shows sources and distribution paths.

temperature or flow regulated) by one or more of the design features depending upon its intended use (i.e., low-pressure turbine, high-pressure turbine, or mid-turbine strut cooling).

4.17.4.1 Low-Pressure Turbine Cooling

Flow bled from the 11th compressor stage I.D. travels inboard through the solid body tubes, filling the entire cavity bounded by the low spool shaft, a compressor disk rear surface, and the high-pressure compressor rear hub/high turbine shaft. The flow is introduced into the low-pressure turbine region through holes in the high-pressure turbine shaft, mixed with compressor discharge bleed air, and directed into the low-pressure turbine disk region. The coolant envelopes the web and bore regions of the disks, is guided through spacer-end rim shields to the disk attachments, and finally leaked back into the main gas path. The distribution of coolant is dictated entirely by attachment cooling requirements of the first three low-pressure turbine stages and by disk surface and hub cooling requirements in the last turbine stage.

4.17.4.2 High-Pressure Turbine Cooling

The means for supplying cooling to the high-pressure turbine blades and the disk front rim cavity is described in Section 4.17.2.3.

Cooling air is introduced into the I.D. and O.D. of vanes directly from the combustor liner regions. The coolant flow is metered within the vanes.

Disk surface cooling is provided by wide channel seal leakage air and by a small amount of TOBI leakage on the front side and the mixture of low-pressure and high-pressure coolant air on the rear side.

4.17.4.3 Mid-Turbine Strut Cooling

Flow bled from the 10th compressor stage O.D. is delivered to the mid-turbine struts by external tubes. The coolant passes over trip strips in the regenerative cooling passages, cooling the struts. Spent cooling air is then discharged into the low-pressure turbine disk coolant cavity.

4.17.5 Active Clearance Control and Bleed Air Systems

The secondary flow system supplies the active clearance control flows and the engine and aircraft bleeds (See Figure 194). Air is bled from the compressor discharge manifold at SLTO and delivered to the high-pressure turbine outer airseal and to the low-pressure turbine case cooling annulus. At cruise power, the flows to these same areas are provided from the 10th-stage O.D. manifold, but the percent cruise coolant flow directed through the low-pressure turbine case annulus is twice that used at takeoff.

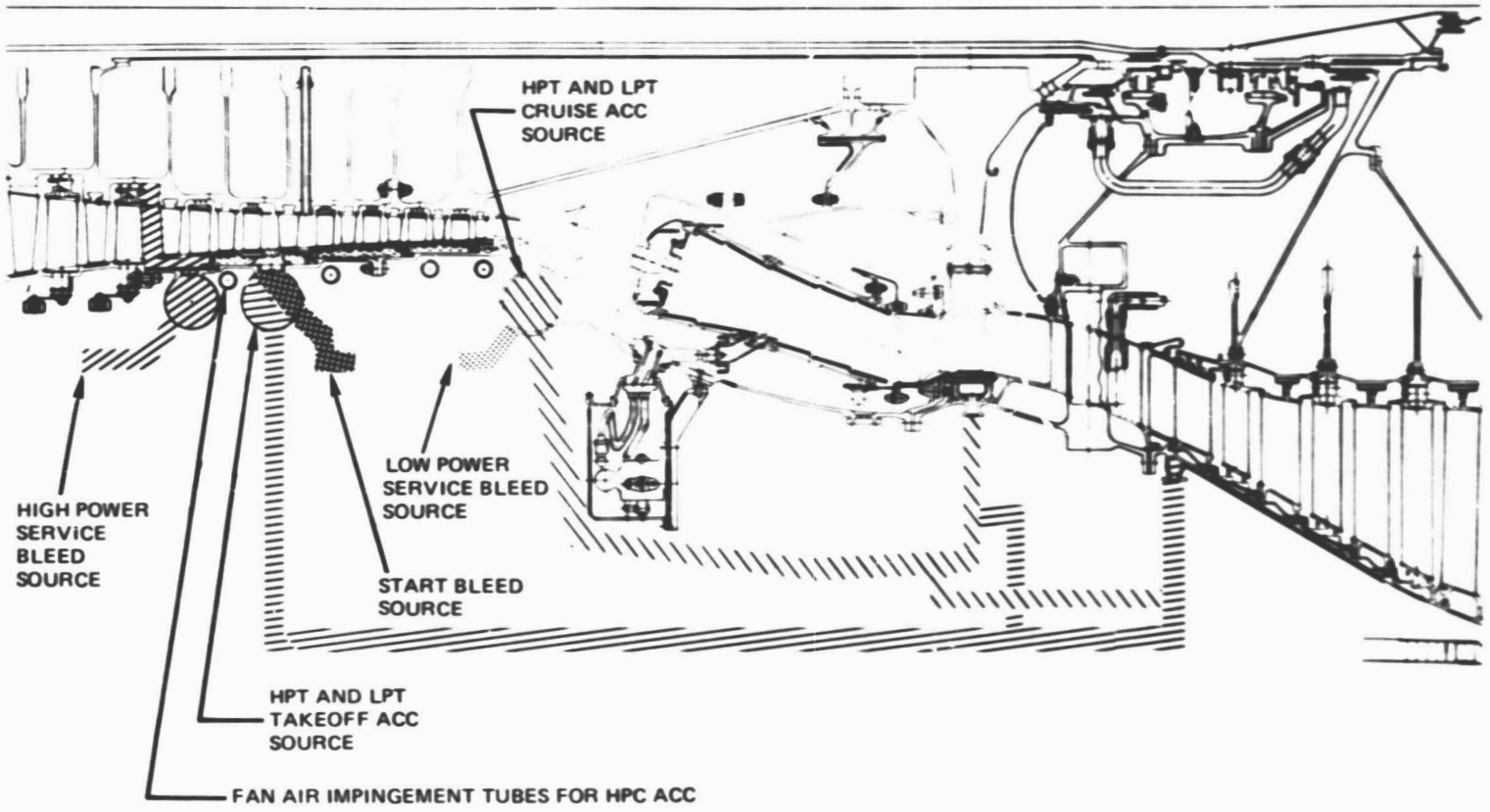

Figure 194 Schematics of Active Clearance Control and Bleed Air Secondary Flow Systems. Schematic illustrates sources and external routing.

The amount and location of the engine and aircraft bleeds are determined, recognizing performance and stability criteria and maintaining consistency with past commercial engine/aircraft requirements.

4.17.6 Rotor Thrust Balance Control

The estimated high rotor thrust load represents the vector summation of six large loads. The calculated 31,100 N (7,000 lb) net load at SLTO is only five percent of the 498,000 N (112,000 lb) front turbine load (See Figure 195) and would appear to be subject to substantial error potential. The loads are a function of the local gas path pressure that is measurable and correctable. The chosen secondary flow system uses this relationship to protect against thrust load sensitivity.

If pressure measurements during the experimental program indicate that target thrust loads were not attained, thrust adjustment is made possible by altering the radius of the compressor discharge seal (R_A on Figure 195). A 17,770 N (4,000 lb) adjustment is possible with each 1.27 cm (0.5 in.) radial movement.

The low rotor thrust load, like that of the high rotor, is also the result of six individual loads, some of which are large (see Figure 196). Sensitivity to load variations is small in the low rotor system since the net load is at least 15 percent of the largest individual load.

A thrust adjustment scheme for the low rotor is currently excluded from the design since sufficient bearing fatigue life is predicted.

4.18 ELECTRONIC CONTROL

4.18.1 Requirements

The objective of the control definition task was to define a preliminary flight engine control system concept based on full authority digital electronic control technology to provide control of functions defined for the engine. The required control functions are:

1. Manage fuel for a two-stage combustor. The metered fuel flow range is from 112.5 kg/hr to 6525 kg/hr (250 lb/hr to 14500 lb/hr). Fuel flow is split between a pilot and a main fuel manifold. Fuel flow is 100 percent pilot flow in the start and idle region with a shift to 30 percent pilot and 70 percent main flow above idle. The fuel metering system must be capable of handling low lubricity and broad specification fuel up to 1035 N/cm^2 (1500 psi) pressure. The control will allow the engine to perform to its potential while preventing compressor stall, preventing excessive temperature levels during transients, and maintaining stable engine operation between idle and maximum power. The control will provide engine rating for all flight conditions. The control will prevent catastrophic engine failure in the event of a control failure.

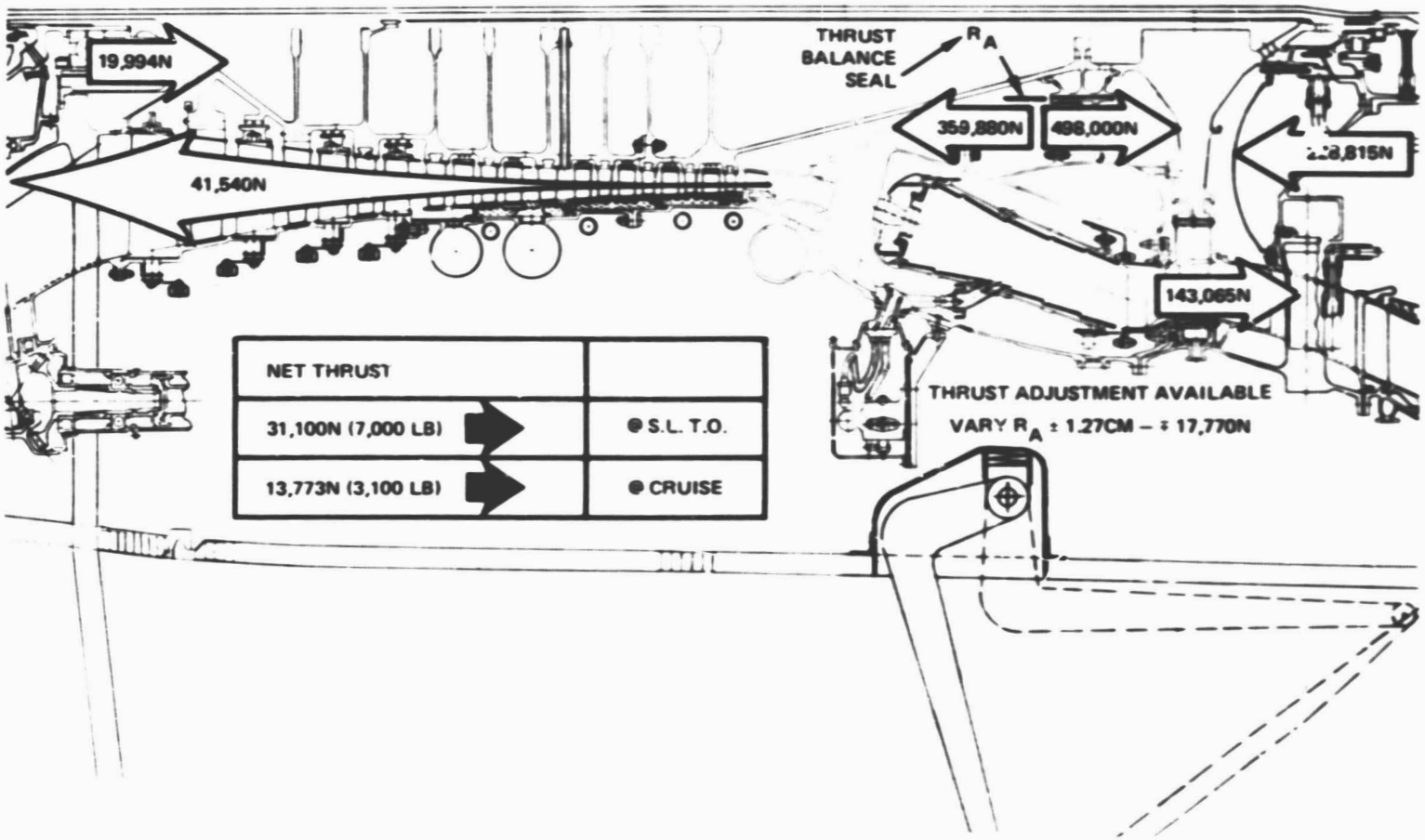

Figure 195 Estimated High Rotor Axial Loads and Net Thrust at Takeoff. Illustration shows thrust adjustment possible with wide channel radius change.

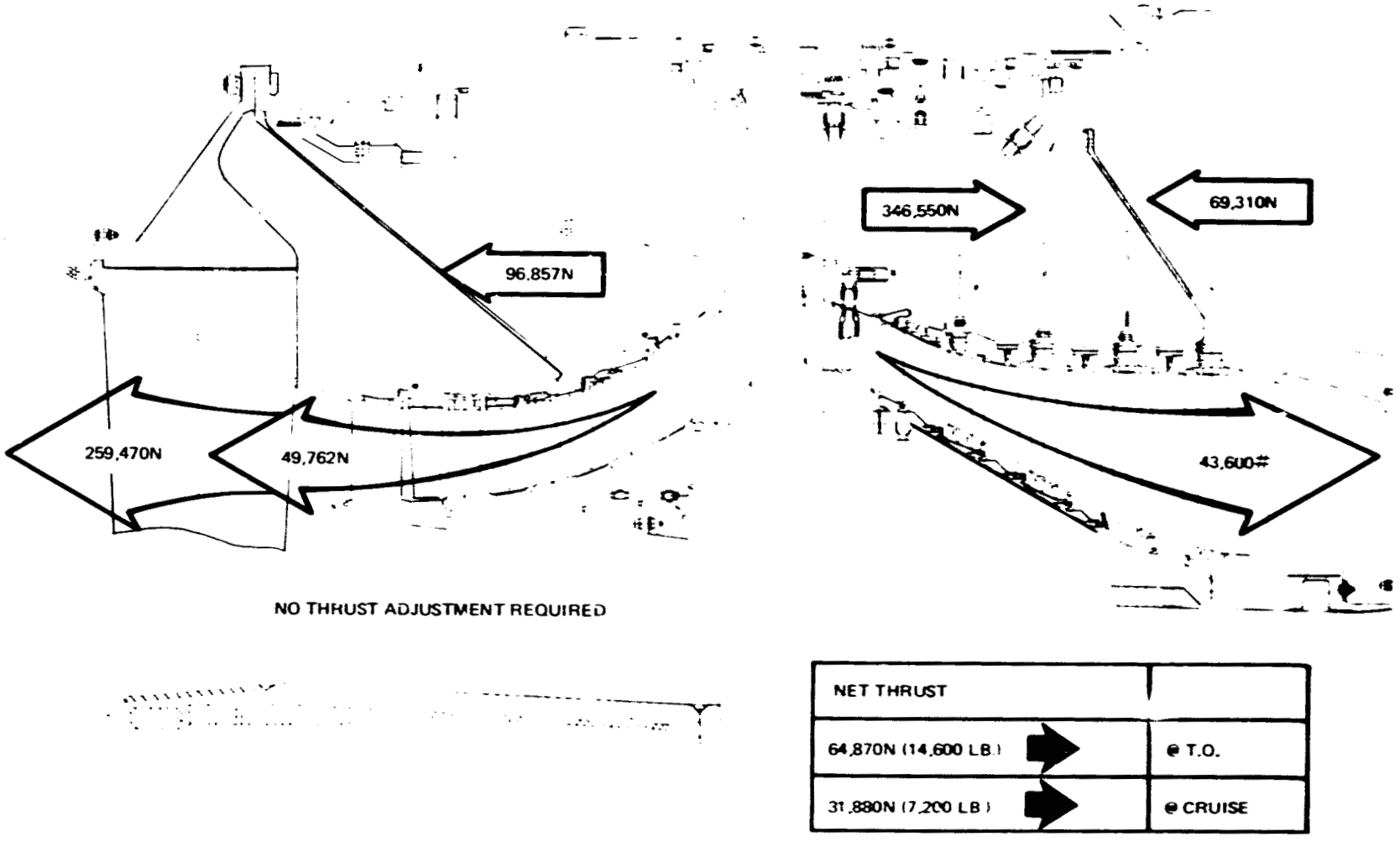

Figure 196 Estimated Low Rotor Axial Loads and Net Thrust at Takeoff. Data indicates acceptable bearing loads without thrust adjustment device.

2. Control variable high-pressure compressor inlet guide vane and the first three stages of stator vanes.

3. Control two position start bleeds and intercompressor surge bleeds.

4. Control two separate air valves for active clearance control.

Sensed parameters and ranges are shown by Figure 197.

4.18.2 Preliminary Definition Selection and Description

The selected control system is shown in simplified block diagram form by Figure 198.

The primary control mode is isochronous governing on low rotor speed (NL) with governing on high rotor speed at idle. Low rotor governing was chosen because of its good correlation with thrust and its relative insensitivity to bleed and stator vane setting variations. Controlling on high rotor speed at idle prevents speed variations associated with horsepower extraction.

The control logic will be implemented with a single-channel full authority digital control with selective redundancy of critical components to provide the optimal balance between mean time between failure (MTBF), cost, weight, and maintainability. The electronic box will be vibration isolation mounted on the fan case and air cooled. The box is projected to weigh approximately 6.08 kg (13.5 lb) and occupy approximately 4100 cc (250 in^3).

The control system will be powered by a dedicated shunt regulated permanent magnet alternator. The memory, Central Processor Unit (CPU), and Input/Output will be Large Scale Integrated and Very Large Scale Integrated chips of N-Mos design for low power and high reliability.The control outputs will be digital switching in nature. Modulated outputs will be saturated high frequency drivers, pulse width modulated through Gallium Arsenide switches into dual solenoids or a torque motor. The CPU will contain its own Random Access Memory and Read Only Memory as well as Digital/Analog and Analog/Digital conversion if analog signals are needed. The interface chips will communicate with the CPU via a common bi-directional bus. The control will use a minimum of custom chips because of cost and reliability. Discrete outputs to solenoids will be low level electrical signals that activate remote Gallium Arsenide switches mounted on the solenoids to reduce heat dissipation in the control box. Inputs will be digital wherever possible to reduce interface hardware.

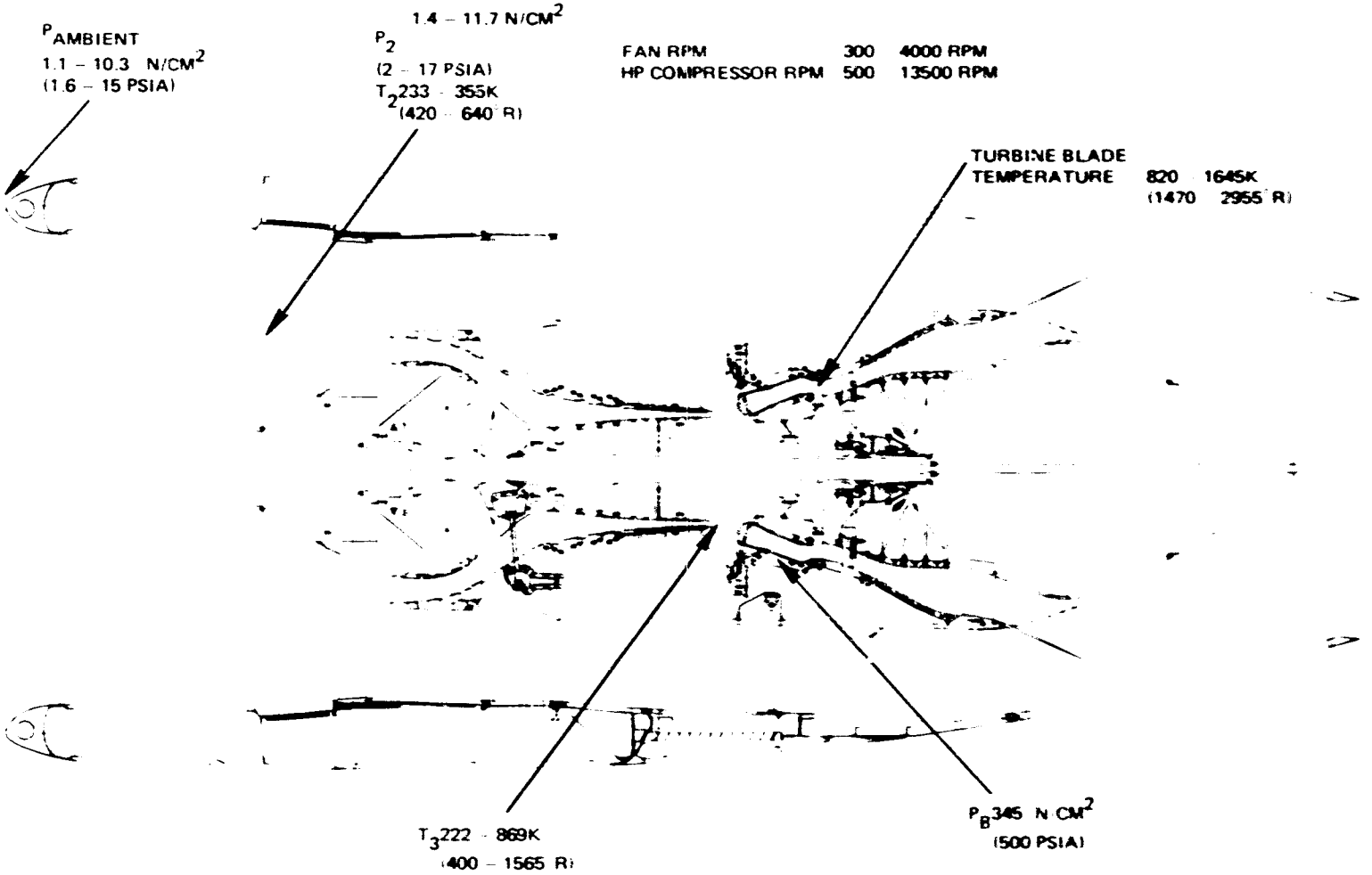

Figure 197 Electronic Control. Engine cross-section shows ranges of parameters sensed by control.

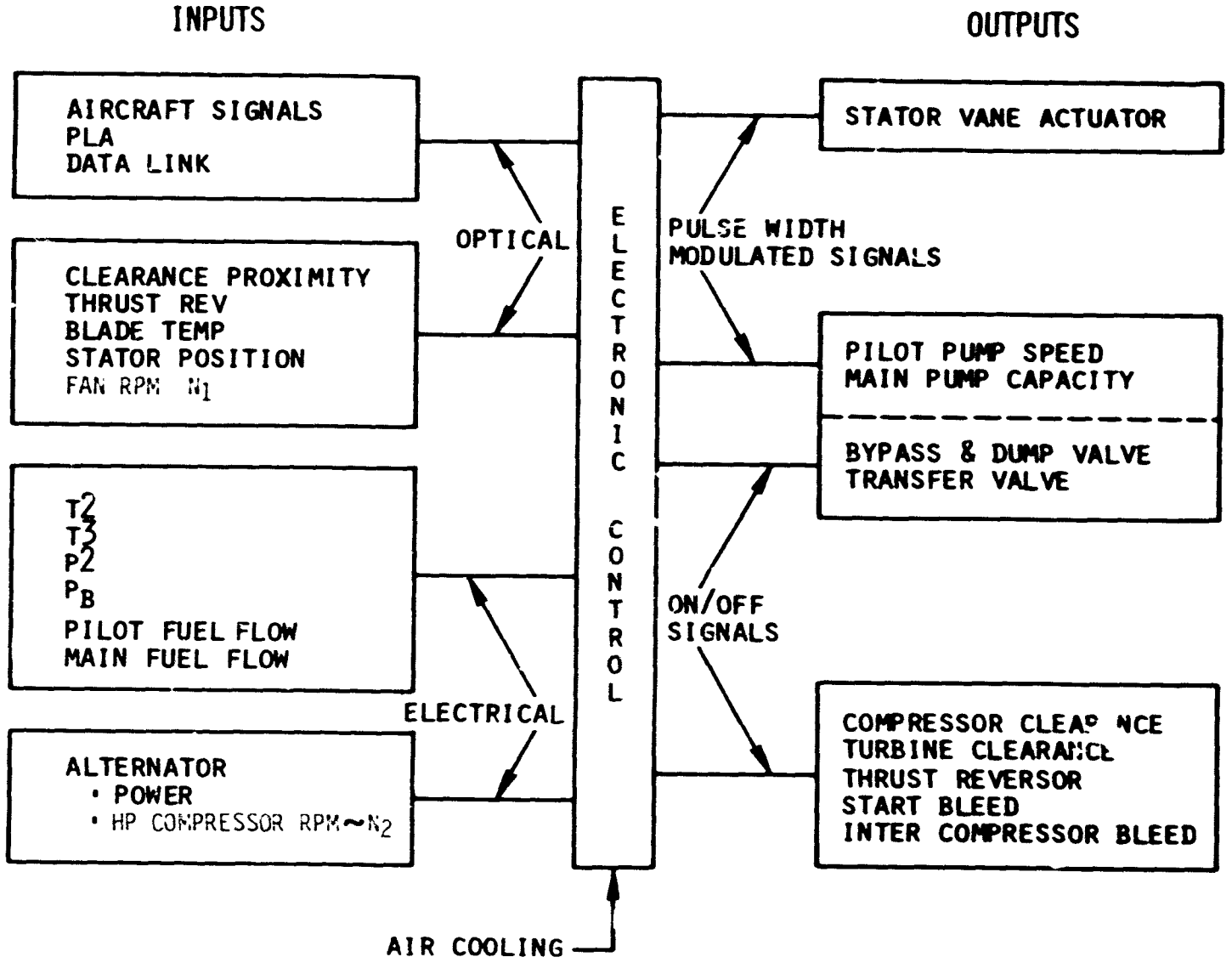

Figure 198 Control Preliminary Definition. Block diagram illustrates inputs and outputs.

The most significant technology areas embodied in the selected system are:

1. Fiber optic data transmission
2. Optic proximity sensing of turbine blade clearance
3. Optical pyrometer sensing of turbine blade metal temperature
4. Optic sensing of low rotor speed
5. Optic position feedback for actuators
6. Shedding vortex fuel flow measurement
7. Pulse width modulated digital outputs
8. High temperature Gallium Arsenide switches
9. Fuel flow management scheme

Fuel flow management and stator vane actuation, both of which illustrate technology innovations, are discussed below.

4.18.3 Fuel Flow Management

The fuel flow management system selected to provide the unique requirements of the two-stage combustor is shown schematically by Figure 199. The system provides fuel flow management and hydraulic pressure for stator vane and bleed actuators with minimum fuel temperature rise and at minimum system cost and weight. The control is required to separately meter fuel flow to the pilot and main zone fuel nozzles. Because of a high turndown ratio and use of fuels with low coking temperature, a substantial change from current pumping/metering systems is dictated. The selected pumping/metering scheme uses a small gear pump that is driven by an F100 pump clutch derivative that varies pump speed to meter fuel flow to the pilot zone. The use of controlled pump speed reduces weight by eliminating the need for a metering valve and bypass valve. Fuel from the pilot pump is used for actuator pressurization (SVA, pump actuator, and bleed actuator) or burned; no fuel flow is bypassed to pump inlet. This single pass-through method of pumping results in the lowest possible temperature rise. Pilot fuel flow is measured by a "Shedding Vortex" flow meter which is used to correct pilot pump speed. A bypass and dump valve in the pilot line recirculates pilot pump flow to pump interstage before pressurization to prevent dead ending the positive displacement pump. When in the bypass mode, the bypass and dump valve drains the pilot nozzles and manifold to the ecology tank.

An inlet throttled centrifugal pump supplies fuel to the main nozzle manifold. The main zone fuel pump is located in the same housing as the pilot pump and boost pump; however, it is driven off a separate gearbox drive. The pump inlet area is modulated by the control to provide a desired flow as measured by a "Shedding Vortex" flow meter. Low temperature rise is possible because no flow is recirculated and pump discharge pressure is no higher than necessary. The pump is run dry during start and low power when fuel flow to the main nozzle is not required. A check valve in the pump discharge prevents main manifold

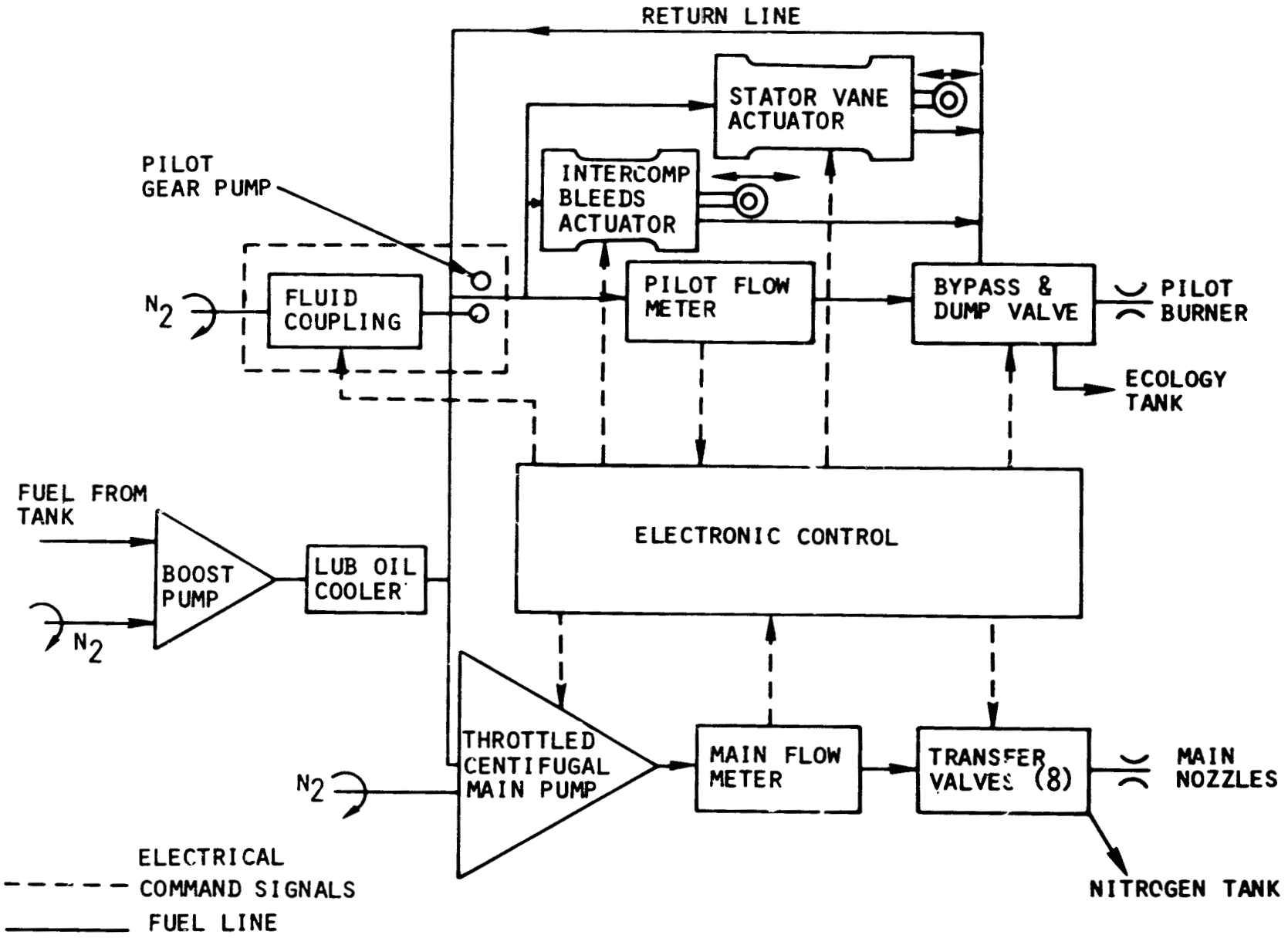

Figure 199 Fuel Flow Management System. Schematic shows sub-system relationships.

fuel from draining back into the pump when the pump is being run dry. Eight secondary transfer valves mounted on the bulkhead seal off the combustor end of the main manifold during dry pump operation to prevent main manifold fuel from draining into the combustor. When main zone operation is needed (above idle), the secondary transfer valves are opened to allow fuel flow to the main nozzles; the main pump area is simultaneously opened to provide main zone fuel flow and pressure. Acceleration time is minimized by having the fuel bottled up in the manifold and thus eliminates manifold fill time. During main zone shutdown, the transfer valve purges the main zone nozzles with a short blast of nitrogen to prevent coking.

4.18.4 Stator Vane Actuation

Figure 200 illustrates the control loop for variable stator vane actuation. Control of actuator position is by a pulse width modulated Digital Output Interface (DOI) signal from the control to high temperature Gallium Arsenide switches mounted on solenoids on the actuator. Vane position is sensed by an optical encoder and fed back to the control through a fiber optic cable. The control provides the light source for the optical encoder and converts the light encoded signal to electrical signals for use in the digital computer.

4.18.5 Technology Development Requirements

As a result of this study, technology was selected on the basis of fulfilling the control requirements of an advanced commercial engine such as the Energy Efficient Engine, while minimizing control system cost and weight, and improving reliability. Several of the recommended technologies will require R&D type programs in order to advance the "state-of-the-art" to the point of readiness for commercial engine application in the late 1980's, early 1990's time frame. These are listed below in two categories - technologies required for the selected system and desirable technologies to enhance the capabilities of the control system in the areas of clearance control and hot section overtemperature protection:

1. Required Technologies

    a. Shedding vortex flow meter - solid state electronic flow meter with variable frequency output

    b. Optic parameter sensing and transmission

    c. High temperature power switch - Gallium Arsenide technology

    d. Digital Output Interface Actuators - pulse width modulated digital output compatible with analog power devices such as hydraulic pistons

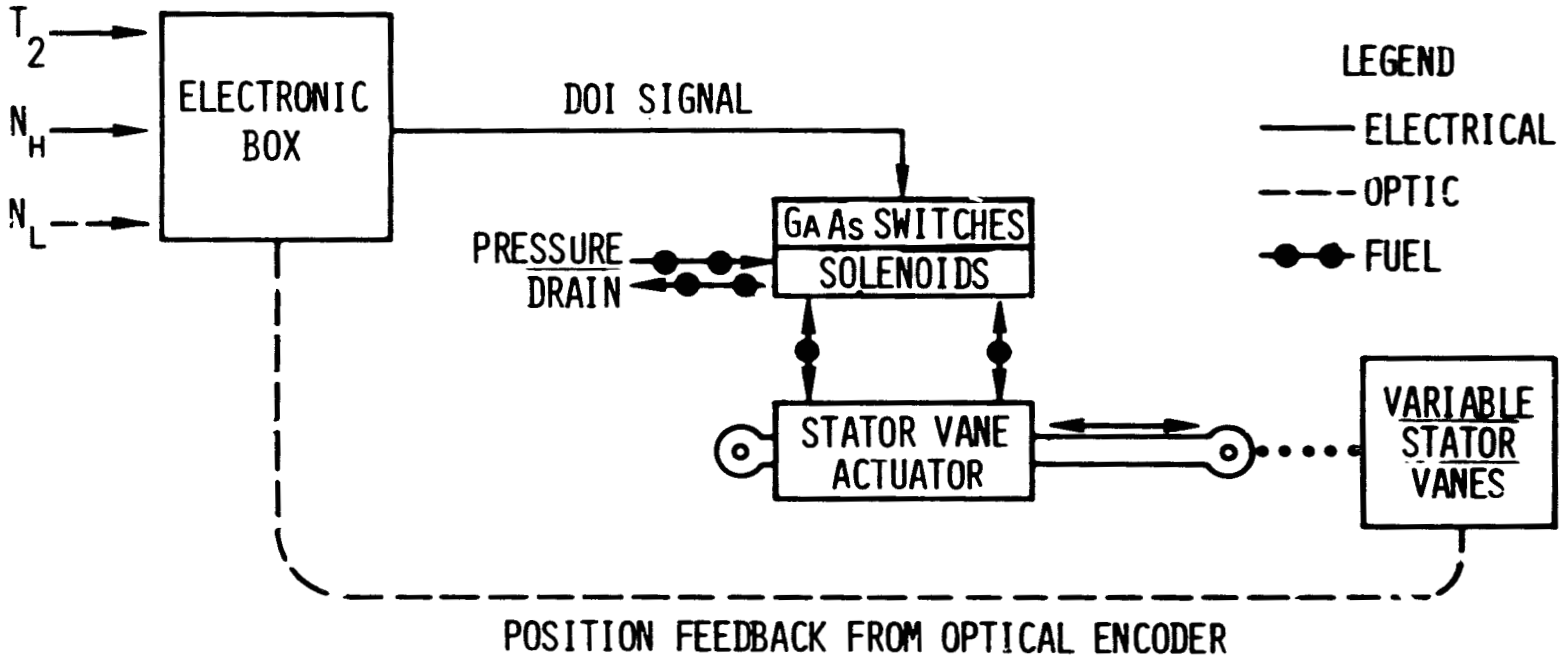

Figure 200 Variable Stator Vane Actuation Control Loop. Schematic shows subsystem relationships.

e. Variable speed pump drive

f. Air cooling of the electronic box

2. Desirable Technologies

a. Optic proximity sensor for turbine blade clearance measurement

b. Optical pyrometer for turbine blade metal temperature measurement

4.18.6 System Benefits

The benefits which accrue from the control systems defined for the flight propulsion system can be generally characterized as quantifiable (cost and weight reductions) and intangible (reduced pilot workload).

The common elements of the selected system were compared with a current JT9D system to quantify cost and weight savings. The resulting savings are shown in Table 83.

Those benefits which, although real, are not readily quantifiable are discussed in the following paragraphs.

1. The selected fuel pumping system precisely matches the engine fuel requirements under all operating conditions and therefore minimizes fuel temperature rise. Maximum heat sink availability for oil cooling and easing broad specification fuel handling problems is thus provided.

2. The system provides pilot workload relief through automatic rating control. Fixed throttle settings at takeoff, climb and cruise, full throttle capability without overboost, and linear throttle response are some of the advantages to the pilot.

3. Reduced maintenance cost is effected by the elimination of control trim requirements and by the self test capabilities of the electronic control.

TABLE 83

COST/WEIGHT SAVINGS OF ELECTRONIC CONTROL
RELATIVE TO JT9D HYDRO-MECHANICAL SYSTEM

Cost	$28, 000
Weight	96 lbs.

Accuracy of schedules and flexibility of the control with respect to schedule changes will provide long term operating cost benefits.

Those benefits which, although real, are not readily quantifiable are discussed in the following paragraphs.

1. The selected fuel pumping system precisely matches the engine fuel requirements under all operating conditions and therefore minimizes fuel temperature rise. Maximum heat sink availability for oil cooling and easing broad specification fuel handling problems is thus provided.

2. The system provides pilot workload relief through automatic rating control. Fixed throttle settings at takeoff, climb and cruise, full throttle capability without overboost, and linear throttle response are some of the advantages to the pilot.

3. Reduced maintenance cost is effected by the elimination of control trim requirements and by the self test capabilities of the electronic control.

4. Accuracy of schedules and flexibility of the control with respect to schedule changes will provide long term operating cost benefits.

5.0 ENGINE AND AIRCRAFT SYSTEM ANALYSIS

Engine and aircraft evaluations were conducted under the Propulsion System/Aircraft Integration Evaluation (PS/AIE). Complete results are documented in Reference 7. This section is a synopsis of the major results obtained from the initial evaluations conducted during the flight propulsion system preliminary design.

Pratt & Whitney Aircraft was aided in these evaluations by three airplane manufacturers: Boeing Commercial Airplane Company, Douglas Aircraft Company, and Lockheed-California Company. Using JT9D-7A and Energy Efficient Engine performance results and characteristics furnished by Pratt & Whitney Aircraft, the airplane companies sized and evaluated the performance of their advanced airplanes with both engines. From these analyses, they furnished Pratt & Whitney Aircraft with airplane weights and dimensions, aerodynamics, fuel burned on design and typical missions, engine size, and flight conditions and airframe noise at FAR 36 noise measuring points. They also provided design and typical mission sensitivities to TSFC, propulsion system weight, and nacelle drag.

5.1 ENGINE CYCLE AND PERFORMANCE

Selection of the Energy Efficient Engine cycle was based on the extensive cycle/configuration studies previously conducted during the Energy Efficient Engine Preliminary Design and Integration Studies and reported in Reference 1.

Engine cycle parameters, component performance levels, and overall engine performance levels are shown in Table 84 for representative mission points. Except for the two noise points, engine parameters are generally shown with regard to an ideal inlet, isolated nacelle drag, and non-use of customer air bleed or power extraction. The two noise points (for approach and takeoff) are fully installed with a flight inlet, isolated nacelle drag, and customer bleed and power extraction as used for predicting engine noise. The aerodynamic design point is used for component design and represents a typical cruise altitude and Mach number at a power setting between maximum cruise and maximum climb power. All cycle parameters are based on this condition.

Table 85 summarizes the cycles and performance of the Energy Efficient Engine and the JT9D-7A reference engine at the NASA specified cruise condition. The cycle differences, plus component performance improvements and the mixed exhaust flow of the Energy Efficient Engine result in an estimated reduction in installed cruise TSFC of 14.9 percent relative to the JT9D-7A engine at the maximum cruise condition of 10,668 m (35,000 ft) and Mach 0.8.

A statistical approach was taken in estimating the probability of meeting the 12 percent TSFC reduction design goal based on the perform-

TABLE 84

ENGINE CYCLE AND PERFORMANCE AT REPRESENTATIVE MISSION POINTS

	Aero. Design Point	Sea Level Static Takeoff	Takeoff Noise Point	Mid-Altitude Climb	End Climb	Maximum Cruise	85% Maximum Cruise	Approach Noise Point
Altitude ~ m ~(ft)	10,668 (35,000)	0 (0)	366	6,705 (22,000)	10,668 (35,000)	10,668 (35,000)	10,668 (35,000)	120 (394)
Mach No.	0.8	0	0.245	0.7	0.8	0.8	0.8	0.208
Ambient Temp	Std. Day	Std.+14°C (+25°F)	Std.+10°C (+18°F)	Std.+10°C (+18°F)	Std.	Std.	Std.	Std.+10°C (+18°F)
Inlet Ram Recovery	1.00	1.00	0.997	1.00	1.00	1.00	1.00	0.9965
Power Extraction ~ kW ~(hp)	0. 0.	0. 0.	112.6 (151)	0. 0.	0. 0.	0. 0.	0. 0.	112.6 (151)
Customer Bleed kg/sec (lb/sec)	0. 0.	0. 0.	1.193 (2.63)	0. 0.	0. 0.	0. 0.	0. 0.	1.202 (2.65)
Thrust (Excl. drag) ~ N ~(lb)	47,372 (10,650)	182,880 (41,115)	132,712 (29,836)	70,216 (15,786)	50,672 (11,392)	45,419 (10,211)	38,604 (8,679)	37,773 (8,492)
Nacelle Drag ~ N (lb)	1,825 (410)	0 (0)	739 (166)	2,440 (548)	1,825 (410)	1,825 (410)	1,825 (410)	565 (127)
Fuel Flow kg/hr (lb/hr)	2,658 (5,860)	6,133 (13,521)	5,859 (12,916)	4,104 (9,047)	2,855 (6,295)	2,549 (5,620)	2,179 (4,803)	1,795 (3,959)
FAN								
$w\sqrt{\theta}$ kg/sec (lb.sec)	707(1560)	619(1364)	614(1353)	675(1486)	722(1591)	699(1541)	668(1473)	387(854)
Bypass Ratio	6.51	7.02	7.10	6.88	6.37	6.59	6.94	9.39
RPM	3660	3626	3565	3710	3741	3614	3444	2219
Pressure Ratio								
Duct Section	1.74	1.57	1.54	1.65	1.79	1.71	1.61	1.16
I.D. Section	1.56	1.44	1.43	1.51	1.59	1.55	1.49	1.15
Efficiency								
Duct Section	0.873	0.882	0.880	0.875	0.871	0.873	0.869	0.870
I.D. Section	0.902	0.914	0.915	0.910	0.900	0.904	0.911	0.913
LP COMPRESSOR								
Pressure Ratio	1.77	1.64	1.61	1.72	1.80	1.75	1.68	1.24
Efficiency	0.899	0.907	0.907	0.907	0.896	0.900	0.900	0.827

TABLE 84 (Cont'd)

ENGINE CYCLE AND PERFORMANCE AT REPRESENTATIVE MISSION POINTS

	Aero. Design Point	Sea Level Static Takeoff	Takeoff Noise Point	Mid-Altitude Climb	End Climb	Maximum Cruise	85% Maximum Cruise	Approach Noise Point
HP COMPRESSOR								
$w\sqrt{\theta}$ Inlet ~ kg/sec ~(lb/sec)	40.0(88.1)	37.2(82.0)	37.2(82.0)	38.0(84.0)	40.3(88.9)	39.7(87.5)	38.7(85.3)	27.5(60.7)
RPM	12,362	13,006	12,905	12,801	12,473	12,291	12,048	11,251
Pressure Ratio	14.0	12.8	12.6	13.3	14.2	13.9	13.3	8.3
Efficiency	0.882	0.889	0.888	0.884	0.880	0.883	0.887	0.864
COMBUSTOR								
Efficiency	0.9995	0.9995	0.9995	0.9995	0.9995	0.9995	0.9995	0.9995
HP TURBINE								
$W\sqrt{T}/P$ inlet ~ $\frac{kg\sqrt{^\circ K}\ m^2}{sec\ kN}$	0.94	0.94	0.94	0.94	0.94	0.94	0.94	0.945
~ $\left(\frac{lb\sqrt{^\circ R}\ in^2}{sec\ lb}\right)$	(19.1)	(19.1)	(19.1)	(19.1)	(19.1)	(19.1)	(19.1)	(19.2)
Rotor Inlet Temp $^\circ C$ ($^\circ F$)	1225(2238)	1369(2495)	1348(2457)	1341(2446)	1257(2295)	1206(2203)	886(2081)	917(1683)
Pressure Ratio	4.03	4.03	4.03	4.03	4.02	4.03	4.05	3.95
Efficiency	0.882	0.873	0.873	0.873	0.882	0.882	0.882	0.876
Total Cooling Air (% Core Flow)	15.95	15.45	15.45	15.45	15.95	15.95	15.95	15.45
LP TURBINE								
$W\sqrt{T}/P$ inlet ~ $\frac{kg\sqrt{^\circ K}\ m^2}{sec\ kN}$	3.7	3.7	3.77	3.7	3.7	3.7	3.8	3.7
~ $\left(\frac{lb\sqrt{^\circ R}\ in^2}{sec\ lb}\right)$	(76.3)	(76.4)	(76.5)	(76.4)	(76.1)	(76.3)	(76.6)	(76.1)
Pressure Ratio	5.60	4.92	4.86	5.37	5.70	5.55	5.33	2.65
Efficiency	0.915	0.902	0.900	0.903	0.916	0.914	0.910	0.845
MIXER								
Efficiency	0.85	0.85	0.85	0.85	0.85	0.85	0.85	0.85

TABLE B4 (Cont'd)

ENGINE CYCLE AND PERFORMANCE AT REPRESENTATIVE MISSION POINTS

	Aero. Design Point	Sea Level Static Takeoff	Takeoff Noise Point	Mid-Altitude Climb	End Climb	Maximum Cruise	85% Maximum Cruise	Approach Noise Point
PRESSURE LOSSES								
Combustor	0.055	0.055	0.055	0.055	0.055	0.055	0.0556	0.061
Turbine Transition Duct	0.015	0.015	0.015	0.015	0.015	0.015	0.015	0.015
Turbine Exhaust Case	0.009	0.007	0.007	0.008	0.009	0.009	0.008	0.0016
Core Mixer	0.0024	0.0019	0.0018	0.0022	0.0025	0.0024	0.0022	0.0005
Fan Duct	0.006	0.0054	0.0056	0.006	0.006	0.006	0.006	0.0034
Duct Mixer	0.0018	0.0017	0.0017	0.0018	0.0018	0.0018	0.0018	0.0012
Tailpipe	0.0034	0.0029	0.0030	0.0032	0.0034	0.0034	0.0032	0.0015
NOZZLE								
Gross Thrust Coefficient	0.9958	0.9900	0.9906	0.9960	0.9955	0.9960	0.9960	0.9935

TABLE 85

ENERGY EFFICIENT ENGINE AND JT9D-7A
CRUISE CYCLE AND PERFORMANCE COMPARISON
(NASA Specified Condition of 10,668 m (35,000 ft),
Mach 0.8 at Maximum Cruise Power on Standard Day)

Cruise Cycle Parameters	Energy Efficient Engine	JT9D-7A in B747-200 Nacelle
Fan Corrected Airflow $w\sqrt{\theta}/\delta$ kg/sec ~(lb/sec)	699 (1541)	774 (1711)
Fan Bypass Ratio	6.59	5.09
Fan Pressure Ratio	1.71	1.58
Overall Pressure Ratio	37.4	25.4
Turbine Rotor Inlet Temp °C (°F)	1206(2203)	1088(1990)
Cruise Performance Parameters		
Installed Thrust N(lb)	43,300(9726)	44,300(9957)
Installed TSFC kg/hr/N (lb/hr/lb)	0.059 (0.576)	0.069 (0.677)

(1) Performance includes flight inlet and isolated nacelle drag. Customer bleed and power extraction effects are excluded.

ance estimates. Individual component performance level probabilities were statistically combined using TSFC influence coefficients to produce a curve of overall TSFC probability. Results of this analysis indicated a greater than 99 percent probability of meeting the TSFC reduction design goal.

5.2 EXHAUST EMISSIONS

Flight propulsion system exhaust emissions were calculated by Pratt & Whitney Aircraft. Estimates of gaseous emissions and smoke levels for the engine are presented in Table 86. These estimates are based on two-stage ECCP Vorbix combustor engine data for carbon monoxide (CO) and total unburned hydrocarbon (THC) emissions and single-stage carburetor tube combustor rig data for oxides of nitrogen (NO_x) and smoke emissions.

The emissions are reported as an EPAP (Environmental Protection Agency Parameter), which represents a weighted average of emissions indices (EI) during a typical landing and takeoff (LTO) cycle within the airport environment. It is composed of different engine power settings for a length of time typical of a particular class of aircraft. The power settings and time blocks corresponding to the Energy Efficient Engine class engines (Class T2) is shown in Table 87. The equation for the EPA parameter can be expressed as:

$$EPAP = \frac{\sum_{i}^{cycle} (EI)_i \, (W_f)_i \, (TIM)_i}{\sum_{i}^{cycle} (TIM)_i \, (F_N)_i}$$

where

	EI	=	lbm of pollution/1000 lbm of fuel
	W_f	=	lbm/hour of fuel flow
	TIM	=	time in mode, mins.
	F_N	=	net thrust (lbf)
	subscript i	=	engine operating mode

TABLE 86

ESTIMATED EMISSIONS AND SMOKE CHARACTERISTICS

	EPAP*
CO	1.7
THC	.19
NO_x	4.6
Smoke No.	20 (max)

*lbm-pollutant/1000 lb_f thrust. hr/cycle

TABLE 87

LANDING AND TAKEOFF CYCLE
Standard Day

Operating Mode	% Takeoff Thrust	Time in Mode (min)
Taxi/Idle (out)	Assigned (mfg)*	19
Takeoff	100	0.7
Climb out	85	2.2
Approach	30	4.0
Taxi/Idle (in)	Assigned (mfg)*	7

*Uninstalled idle thrust of 7% is being employed for Energy Efficient Engine

The CO EPAP was calculated from the ECCP data on a combustor inlet temperature (T_{t3}) basis. This involved correcting the engine data for Energy Efficient Engine pressure levels and evaluating the EI's at the appropriate Energy Efficient Engine combustor inlet temperatures. The THC EI's were observed to be approximately 1/10 of the CO values. The pressure correction for these constituents is linear, i.e.,

$$CO_{EEE} = CO_{ref} \frac{P_{t3\ ref}}{P_{t3\ EEE}} \; ; \; THC = 0.1\ CO$$

The NO_x EPAP was calculated from rig data on a fuel-air ratio (f/a) basis. The data were corrected for pressure and temperature and correlated against measured fuel/air ratio. The NO_x EI's corresponding to Energy Efficient Engine fuel/air ratios were then employed to calculate the EPAP. The pressure/temperature correction utilized for the calculations was:

$$NO_{x\ EEE} = NO_{x\ ref} \left(\frac{P_{t3\ EEE}}{P_{t3\ ref}} \right)^{1/2} \exp \left(\frac{T_{t3\ EEE} - T_{t3\ ref}}{288} \right)$$

$$\exp 18.8\ (H_{ref} - H_{EEE}) \frac{V_{ref}}{V_{EEE}}$$

where P_{t3} - combustor inlet pressure (pounds/square inch)

T_{t3} - combustor inlet temperature (degrees K)

H - humidity (lbm H_2O/lbm air)

V - combustor reference velocity (feet/second)

The humidity and reference velocity terms drop out of the equation since the rig and Energy Efficient Engine combustor reference velocities are approximately equal and all data are corrected to the standard 60 percent relative humidity.

The maximum smoke level anticipated during the LTO cycle was estimated from the rig data at a value of $(f/a)_4\ P_{t3}$ product corresponding to takeoff conditions. Use of these correlation parameters enables estimation of smoke levels for high-pressure ratio engines operating at comparable f/a ratios to current test combustors.

The levels of gaseous emissions, as shown in Table 86, include allowances for engine-to-engine variations and development margins. The breakdown of these margins are shown in Table 88.

The allowance for engine-to-engine variation, which represents a two sigma level, was determined by statistical analysis of JT9D engine pilot lot data consisting of 19 engines.

5.3 PROPULSION SYSTEM WEIGHT

Table 89 presents the weight by engine section at the end of the preliminary design phase. Included in the total bare engine weight is the fuel control system, ignition system, a full duty core mounted gearbox, oil tank, fuel-oil cooler, airframe bleed provisions, acoustic treatment in the fan case, and the nose spinner. The nacelle weights shown in Table 89 include nacelle structure, acoustic treatment, fan thrust reversers, and reverser actuation mechanism.

The bare engine weight was estimated by a component weight estimating technique used extensively at Pratt & Whitney Aircraft. This technique is an analytical procedure utilizing computer programs for accuracy. The weight of each engine component was estimated during various stages of design definition evolution.

Nacelle weight was estimated by scaling similar components of existing nacelles to Energy Efficient Engine size, then adjusting these scaled weights to account for the use of advanced materials. Aggressive use of composites and titanium in the nacelle permits weight reductions of 18 percent in the inlet, 27 percent in the fan cowl, and 10 percent in the fan reverser and core cowl compared to conventionally constructed metal components.

The bare engine weight estimate is 2.5 percent more than that of the JT9D-7A engine scaled to produce the same 10,688 m (35,000 ft), 0.8 Mach number installed maximum cruise thrust. This weight increase is due primarily to the lower aspect ratio shroudless fan, and the addition of an exhaust mixer.

Total nacelle weight is 18.5 percent higher than the JT9D-7A/-200 nacelle scaled to the same 10,668 m (35,000 ft), 0.8 Mach number installed maximum cruise thrust size. This increase is caused by the full length, mixed flow design of the Energy Efficient Engine nacelle. This design differs from that of the B747-200 nacelle, which incorporates a short duct, separate flow design. Adding nacelle to bare engine weight produces a total propulsion system weight six percent higher than that of the scaled JT9D-7A/-200 engine.

5.4 PROPULSION SYSTEM PRICING AND MAINTENANCE

Breakdowns of Energy Efficient Engine price and total maintenance cost estimates are listed in Table 90 for the major engine sections.

TABLE 88

SUMMARY OF MARGINS

Emissions	Engine-to-Engine Variation percent	Development Margin percent	Total percent
CO	14	20	34
THC	27	20	47
NO_x	12	10	22

TABLE 89

STF505M-7 FLIGHT PROPULSION SYSTEM WEIGHT STATEMENT

Engine Section	Weight kg (lb)
Compression System	1842 (4060)
Diffuser/Combustor	322 (710)
Turbines	1333 (2940)
Mixer/Tailplug	116 (255)
Controls/Accessories	333 (735)
Total Bare Engine	3946 (8700)
Nacelle	1286 (2835)
Inlet	277 (610)
Fan Cowl	88 (195)
Fan Reverser/Core Cowl	796 (1755)
Tailpipe	125 (275)
Total Propulsion System	5232 (11535)

TABLE 90

ENERGY EFFICIENT ENGINE PRICE AND MAINTENANCE COST
COMPONENT BREAKDOWN

	Price (percent)	Maintenance Cost (percent)
Compression Section	40.5	27.0
Diffuser/Combustor	10.0	10.0
Turbines	34.0	47.0
Mixer/Plug	3.0	0.5
Controls and Accessories	10.0	5.5
Assembly, Test, Line Maintenance	2.5	10.0
Total	100.0	100.0

When these modular cost differences are added to assembly, disassembly, test costs during shop visits and line maintenance costs, the Energy Efficient Engine is currently estimated to have 0.8 percent higher bare engine price and 2.9 percent lower maintenance cost relative to the JT9D-7A engine, scaled to the same installed maximum cruise thrust at 10,668 m (35,000 ft), Mach 0.8.

The engine and spare parts prices of the Energy Efficient Engine were established from production cost estimates. A Bill-of-Materials was generated from design layouts comprising major parts that represent over 90 percent of the total engine cost.

The engine production cost was reviewed with current engines to ensure that the estimate was reasonable. Direct operating cost and maintenance cost incorporate selling price rather than production cost levels. Therefore, budgetary and planning prices were generated by the Pratt & Whitney Aircraft Financial Department from the production cost estimates. The pricing method used for the Energy Efficient Engine was consistent with that used for the JT9D-7A.

Nacelle price estimates were included in the airframe price formula used in the economic calculation. The price of the Energy Efficient Engine nacelle is approximately 19 percent greater than that of the scaled B747-200 nacelle.

As in the case of nacelle weight, this difference is due to the -200 nacelle being a short duct, separate flow configuration, while the Energy Efficient Engine nacelle is a long duct, mixed flow design.

The maintenance cost estimate includes maintenance material, labor, and outside repair costs. Outside repair cost is part repair not normally performed in an airline repair shop. Individual estimates were made for both international and shorter range domestic missions.

Maintenance material cost estimates are obtained utilizing a computer simulation programmed to model the operation and maintenance of a fleet of engines over a 15 year period. Mature scrap lives, module mean time between repair (MTBR) and parts prices provide the major input from which a 15 year cumulative average MMC estimate is derived. The maintenance material costs of disks, prorated over 15 years, and of miscellaneous parts (those parts not modeled individually) are combined with airfoil, seal, sideplate, and case costs to obtain the total estimate. Mature parts scrap and repair lives are derived from the analysis of spare parts sales records, data obtained from various JT9D engine operators and other sources within Pratt & Whitney Aircraft.

Maintenance labor cost analysis covers maintenance performed on the flight line, in the operator's shop, and on parts shipped to a repair vendor. Manhours per repair (MH/REPAIR) and mean-time-between-repair (MTBR) are estimated for each of the modules of the engine. The labor,

in terms of manhours per engine flight hour, is calculated by dividing the manhours per shop repair for each module by its MTBR. The hourly labor for the complete engine is obtained by summing the shop labor for the individual modules with a separately estimated value for flight line maintenance.

A preliminary analysis of nacelle maintenance cost performed in support of the accessory location study indicated that an Energy Efficient Engine type nacelle design could have an advantage over a -200 type installation in engine removal labor costs. This advantage would be partially offset by the lower MTBR of the Energy Efficient Engine relative to the JT9D-7A. For the purposes of airplane economics comparisons, the Energy Efficient Engine and JT9D-7A/-200 nacelle maintenance costs were assumed to be equal.

Since the pricing formulas used in these calculations are subject to change, absolute prices and maintenance costs have not been included in this report. Future changes will not affect the economic comparisons between the Energy Efficient Engine and JT9D engine, since the pricing method used for both engines was completely consistent.

5.5 STUDY AIRCRAFT AND ENGINE INSTALLATIONS

At the start of the evaluation, each of the airplane manufacturer subcontractors - Boeing, Douglas, and Lockheed - as well as Pratt & Whitney Aircraft, defined aircraft suitable for introduction into commercial service in the early 1990's. These aircraft reflected the market conditions and technology levels each company felt would prevail in that time period. The definitions included design and typical mission ranges, number of passengers, design Mach number, configuration, and types and levels of advanced technologies assumed. Tables 91 and 92 present summaries of the domestic and intercontinental airplane configurations of each airplane manufacturer subcontractor. Drawings of these airplanes are shown in Figures 201 through 205. Airplane configurations defined by Pratt & Whitney Aircraft for inhouse evaluations are included for comparison. Engine installation ground rules for engine placement, thrust reverse, and bleed and power extraction needs were established for the evaluation.

Boeing, Douglas, and Lockheed each developed installation ground rules for mounting a mixed-flow long duct engine from under-the-wing pylons. These ground rules represent the best compromise among a number of conflicting considerations such as interference aerodynamics, wing flutter, jet wake impingement, pylon weight, and ground clearance. Since Lockheed and Douglas each considered trijets, they also evaluated tail engine installations. These installations followed L1011 and DC10 practice, respectively.

Reverse thrust level and directivity requirements are dependent on the airplane configuration. Reverse thrust directivity is necessary to

TABLE 91

DOMESTIC AIRPLANE DEFINITIONS

	Boeing	Douglas	Lockheed	P&WA
Type	Twinjet	Trijet	Trijet	Trijet
In Service Date	1990's	1990's	1990's	1990's
Design Range km (NM)	3700 (2000)	5550 (3000)	5560 (3000)	5560 (3000)
Passengers	196	458	500	440
Cruise Speed Mach	0.8	0.8	0.8	0.8
Field Length m (ft)	1830 (6000)	2440 (8000)	2130 (7000)	2440 (8000)
Initial Cruise Altitude m (ft)	10670 (35000)	10060 (33000)	10670 (35000)	10670 (35000)
Wing Loading kg/m^2 (lb/ft^2)	439.4 (90.0)	522.4 (107.0)	560.5 (114.8)	569.4 (116.6)
Wing Aspect Ratio	10.24	9.83	10	12
Typical Range km (NM)	1850 (1000)	1850 (1000)	2590 (1400)	1300 (700)
Typical Load Factor %	55	60	55	55

TABLE 92

INTERCONTINENTAL AIRPLANE DEFINITIONS

	Douglas	Lockheed	P&WA
Type	Trijet	Quadjet	Quadjet
In Service Date	1990's	1990's	1990's
Design Range km (NM)	10190 (5500)	12040 (6500)	10190 (5500)
Passengers	438	500	510
Cruise Speed Mach	0.8	0.8	0.8
Field Length m (ft)	3350 (11000)	3050 (10000)	3350 (11000)
Initial Cruise Altitude m (ft)	9450 (31000)	10360 (34000)	10060 (33000)
Wing Loading kg/m^2 (lb/ft^2)	670.9 (137.4)	644.6 (132.0)	673.8 (138.0)
Wing Aspect Ratio	9.83	10	12
Typical Range km (NM)	2780 (1500)	5560 (3000)	3700 (2000)
Typical Load Factor %	60	55	55

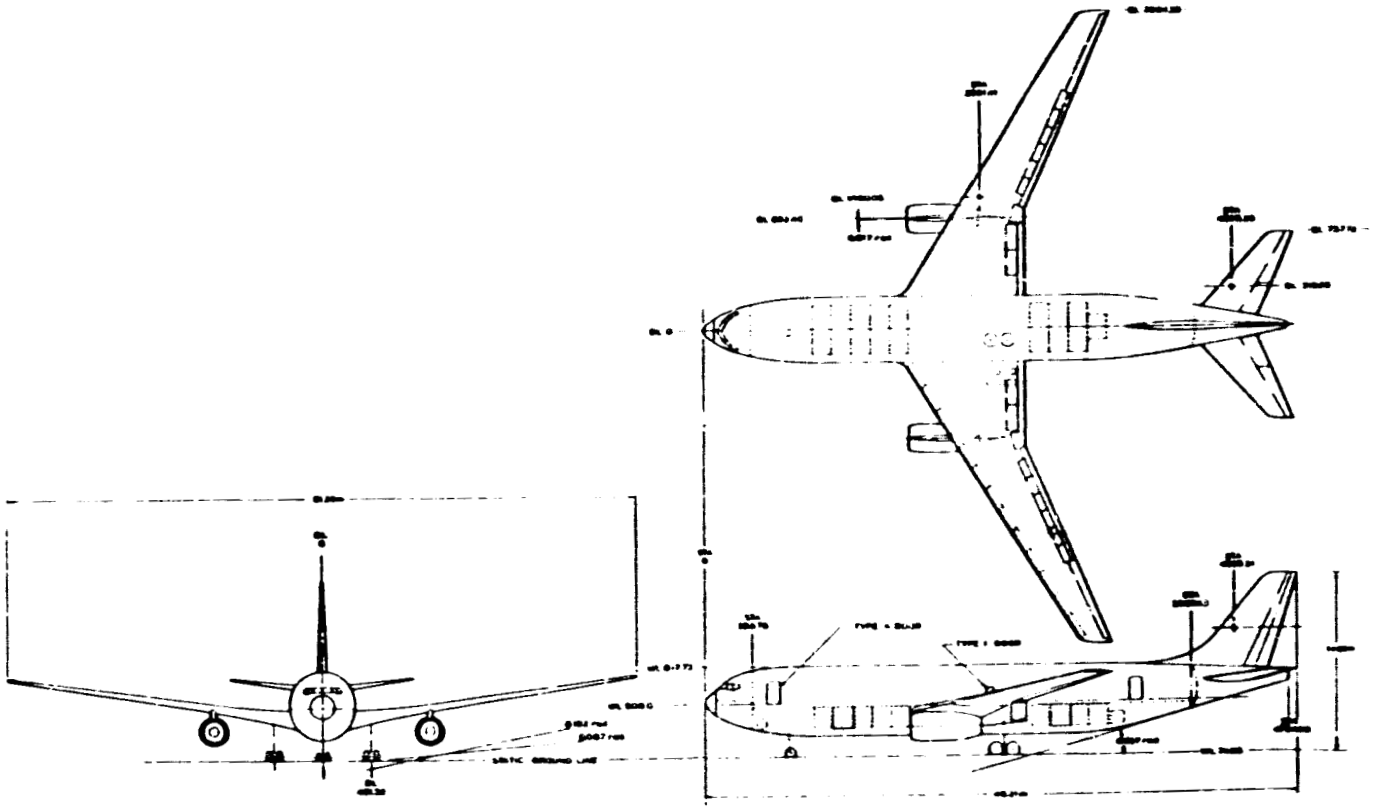

Figure 201 Boeing Airplane. Boeing chose to concentrate on one airplane, a domestic twinjet with wing mounted engines.

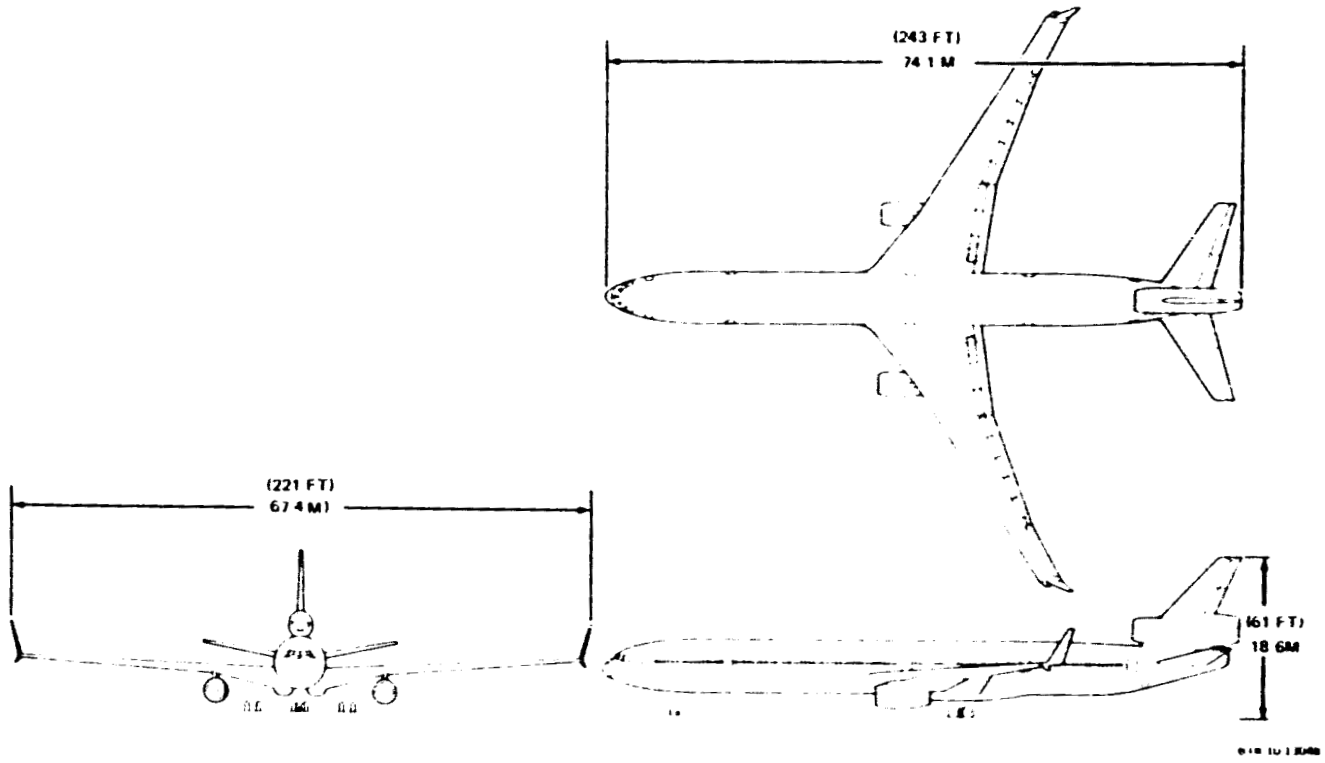

Figure 202 Douglas Domestic Airplane. Both Douglas airplanes, the intercontinental as well as the domestic, are based on a DC10 trijet derivitive with a stretched fuselage and an all new wing.

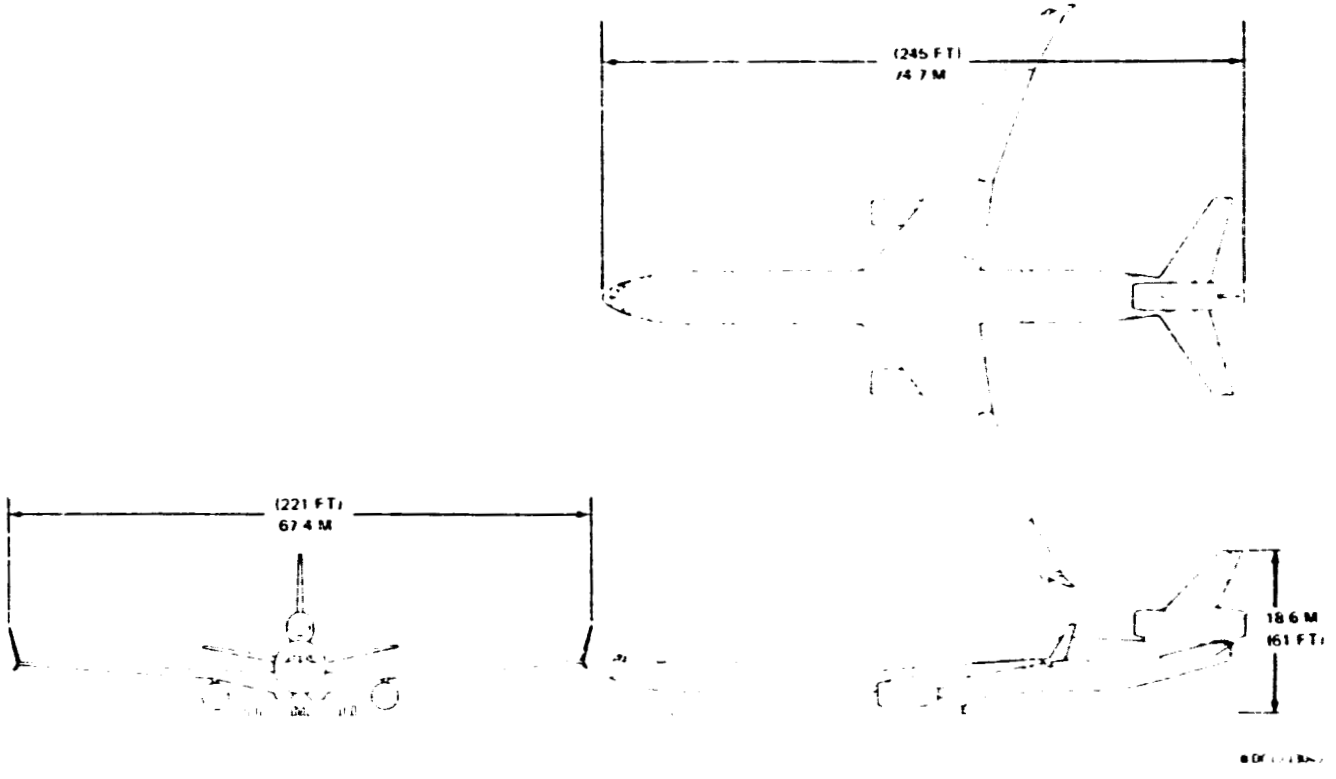

Figure 203 Douglas Intercontinental Airplane. Although the domestic and intercontinental airplanes have different thrust requirements, they are externally similar, having the same wing, fuselage, and empennage.

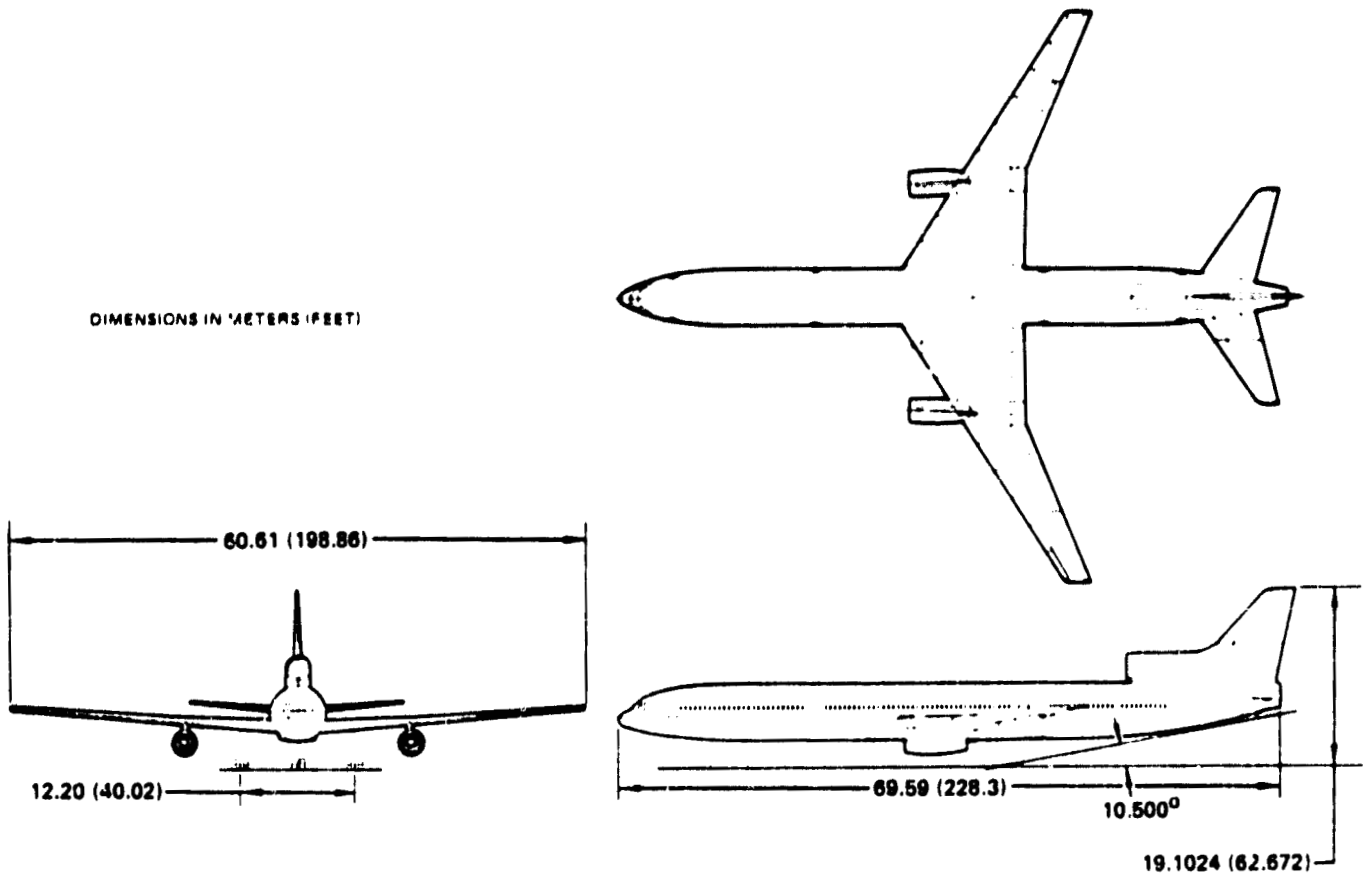

Figure 204 Lockheed Domestic Airplane. Lockheed chose a three-engine configuration similar to the L1011 for its domestic airplane.

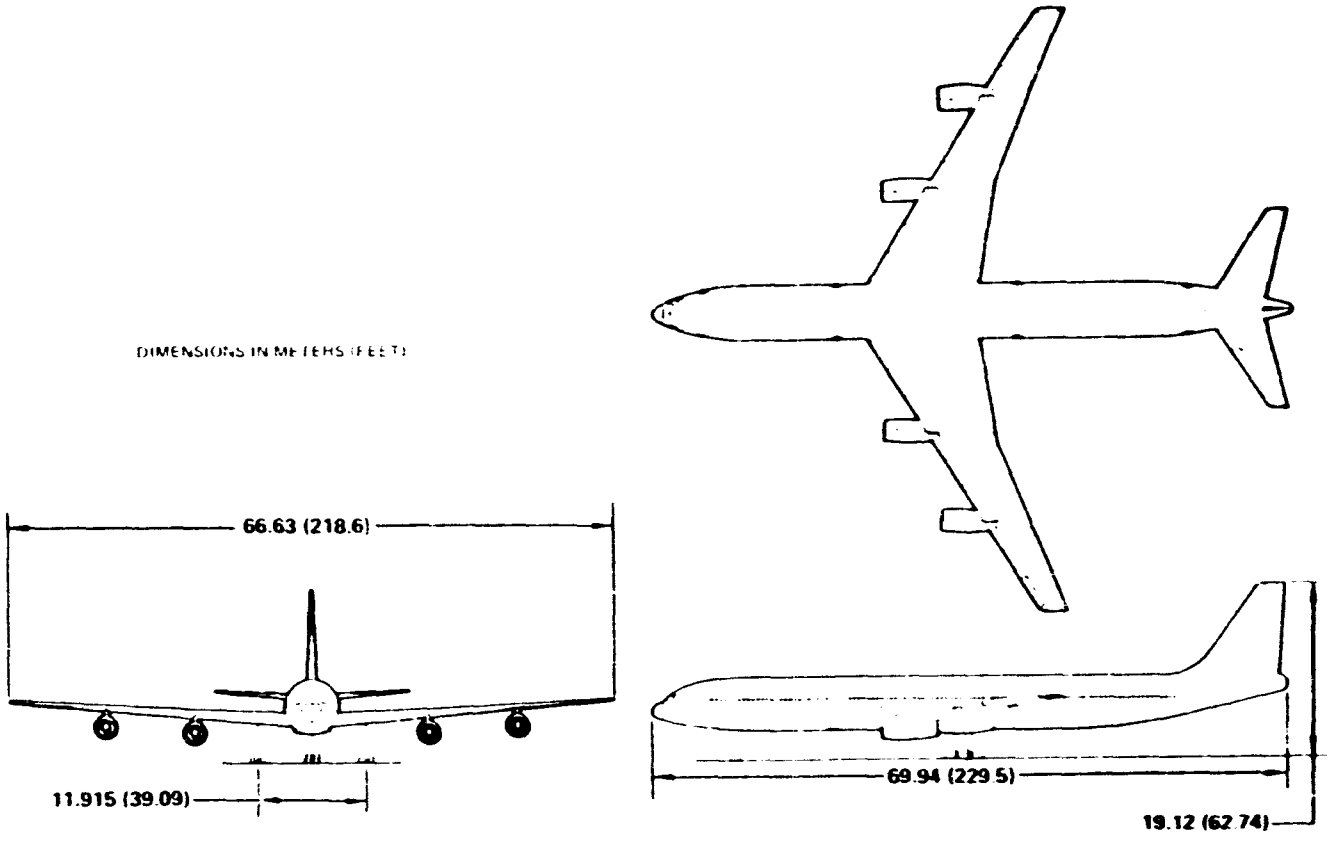

Figure 205 Lockheed Intercontinential Airplane. Lockheed chose a four engine wing-mounted configuration for its intercontinental airplane.

prevent reingestion of engine exhaust, to avoid interference with control surfaces, and to prevent impingement of exhaust on the airplane. The Energy Efficient Engine nacelle was designed with 12 replaceable fan duct reverser cascade sections to permit tailoring of the reverse flow directivity to match the individual requirements of each installation.

The reverse thrust capability of the Energy Efficient Engine exceeds 35 percent at speeds lower than 50 knots, without requiring low rotor overspeed or violating low-pressure compressor surge margin requirements. An allowance for 10 percent duct flow leakage past the blocker doors was included in these calculations.

Bleed and horsepower extraction requirements were established by each of the airplane manufacturers and by Pratt & Whitney Aircraft. For the purposes of this evaluation, Lockheed chose to use the bleed and horsepower schedules provided by Pratt & Whitney Aircraft with the engine data, while Boeing and Douglas modified engine performance to reflect individually selected extraction schedules.

5.6 AIRCRAFT FUEL CONSUMPTION

Using Pratt & Whitney Aircraft supplied Energy Efficient Engine and JT9D-7A engine isolated nacelle performance data, the airplane manufacturers evaluated the mission performance of both engines.

Once the airplane has been sized to perform the design mission, it can then be "flown" on a typical mission. The typical mission represents the average stage lengths and load factors during actual operation. Thus, typical mission performance more closely simulates airline operation than does design mission performance.

Mission fuel burned advantage of the Energy Efficient Engine compared to the JT9D reference engine is shown in Figure 206 for design missions and in Figure 207 for typical missions. As could be expected, the results correlate well with design fuel fraction. The Energy Efficient Engine has a greater performance advantage over the JT9D engine during climb and descent than it does at cruise. This is illustrated in the fuel burned comparison by mission segment for the Pratt & Whitney Aircraft airplane, shown on Table 93. Overall, fuel burned reductions vary from 13.1 percent for the Boeing domestic twinjet on a typical mission, to 18 percent for Lockheed and Pratt & Whitney Aircraft intercontinental jets and Douglas domestic airplanes on design missions. Average fuel burned reductions are 16.3 percent on typical missions and 16.9 percent on design missions.

5.7 OPERATING ECONOMICS

By using the NASA specified economic model, airplane performance evaluation results received from the airplane companies were combined

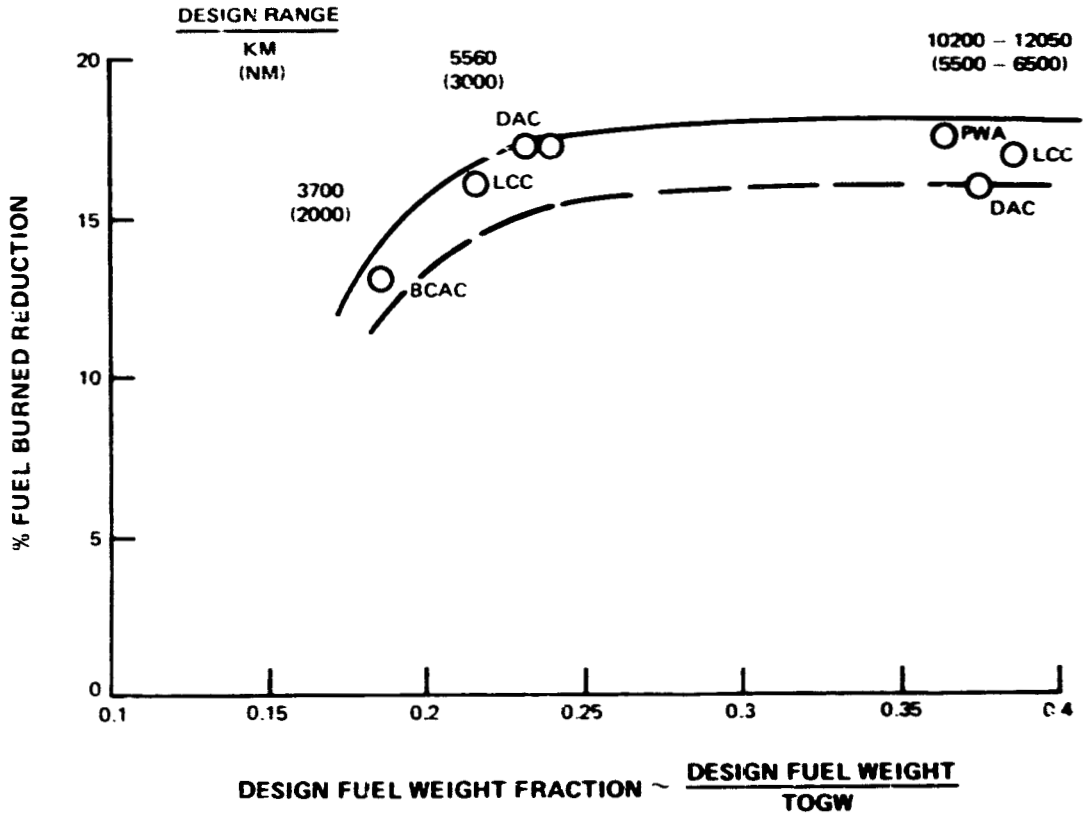

Figure 206 Energy Efficient Engine Fuel Savings on Typical Missions - STF505M-7 Relative to JT9D-7A

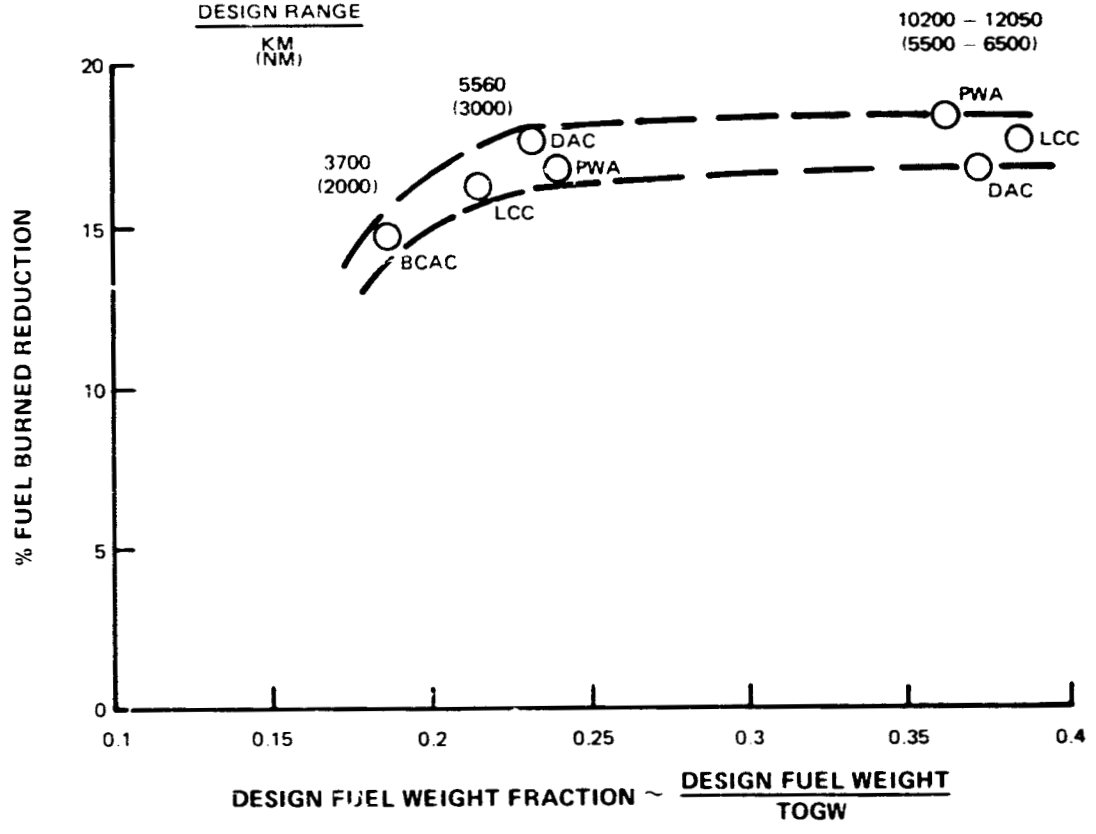

Figure 207 Energy Efficient Engine Fuel Savings on Design Range Missions - STF505M-7 Relative to JT9D-7A

TABLE 93

ENERGY EFFICIENT ENGINE FUEL BURNED ADVANTAGE BY MISSION SEGMENT
ILLUSTRATING INCREASED REDUCTION POTENTIAL AT CLIMB
AND DESCENT RELATIVE TO CRUISE

2000 NM Mission - Pratt & Whitney Aircraft
Intercontinental Airplane

	JT9D-7			STF505M-7			
	Distance km	Fuel kg	Fuel/km kg/km	Distance km	Fuel kg	Fuel/km kg/km	Fuel/km Reduction With STF 505M-7 Percent
Taxi + Takeoff	-	1954	-	-	1280		
Climb	282	6512	23.09	317	5638	17.79	23.0
Cruise	3213	30597	9.52	3197	25308	7.92	16.8
Descent	209	751	3.59	190	431	2.27	36.8
Total Mission	3704	39814	10.75	3704	32656	8.82	18.0
Reserves	-	13590	-	-	11159	-	

700 NM Mission - Pratt & Whitney Aircraft
Domestic Airplane

	JT9D-7A			STF505M-7			
Taxi + Takeoff	-	1225	-	-	817	-	
Climb	295	4967	16.84	351	4578	13.04	22.6
Cruise	796	5938	7.46	757	4745	6.27	16.0
Descent	205	550	2.68	188	308	1.64	38.8
Total Mission	1296	12679	9.78	1296	10448	8.06	17.6
Reserves	-	10685	-	-	9001	-	

with engine price and maintenance costs calculated by Pratt & Whitney Aircraft to produce airline operating economics comparisons of the Energy Efficient Engine to the JT9D reference engine.

The basic form of the economic model evolved from the 1967 Air Transport Association of America (ATA) operating cost method. The formulas have been modified to reflect changes in airplane technology and airline operating environments occurring since 1967, based on 1977 Boeing updates of the ATA operating costs methods. Detailed information on assumptions and in the economic model is presented in Reference 7.

The components of direct operating cost (DOC) include costs of the crew, fuel, airframe and engine maintenance, depreciation, and insurance. Flight crew costs, which include both wages and fringe benefits, are based on three-person crews. Fuel cost reflects fuel burned on the mission and fuel price. Fuel prices of 10.5¢/liter (40¢/gal)-domestic and 11.9¢/liter (45¢/gal)-intercontinental are used to represent 1985 prices expressed in 1977 dollars. Maintenance costs include materials, labor, and burden. Engine maintenance costs were first calculated for the base size (scale factor of 1.0) JT9D engine and the Energy Efficient Engine. Costs were scaled to the engine size required to fly the design missions and were then adjusted to the proper flight length. Depreciation is the total investment in the airplane (airframe and engines plus spares) minus residual value (10 percent in this case) divided by depreciation period (15 years) and hours flown per year. The insurance rate used is 0.5 percent per year of fly-away price, which is price of the airplane without spares.

DOC "pie" charts are shown in Figure 208 (a through g), for the seven study aircraft on typical missions which are more representative of actual airline operation. The primary reason for the DOC advantage of the Energy Efficient Engine over the JT9D engine is reduced fuel consumption. In general, the longer range airplanes with higher fuel fractions tend to show more DOC advantage for the Energy Efficient Engine. Company to company variations at similar fuel fractions reflect differences in design philosophies and modeling techniques. For example, the rate at which airplane structure weight changes with TOGW variation will differ between airplane models. Even with these differences; however, the DOC reduction potential of the Energy Efficient Engine versus fuel fraction falls within ±1 percent. Comparison of the DOC pie charts clearly shows why the Boeing airplane should show less DOC advantage for Energy Efficient Engines. The fuel cost portion of DOC for this airplane is significantly lower than the others, and, therefore, has less effect on overall DOC. In smaller, shorter range airplanes (Boeing twin-jet carries 196 passengers 2000 Naut. Mi. vs. 400-500 passengers and 3000 to 6500 Naut. Mi. in the other airplanes), DOC tends to become dominated by crew costs, and depreciation. The sum of crew costs and depreciation of the Boeing airplane is 60 percent greater than fuel cost. In the longest range Lockheed intercontinental airplane, the sum is equal to fuel cost.

3700 km (2000 N.Mi.) Boeing 196 Passenger Domestic Twinjet on
1850 km (1000 N.Mi.) typical mission

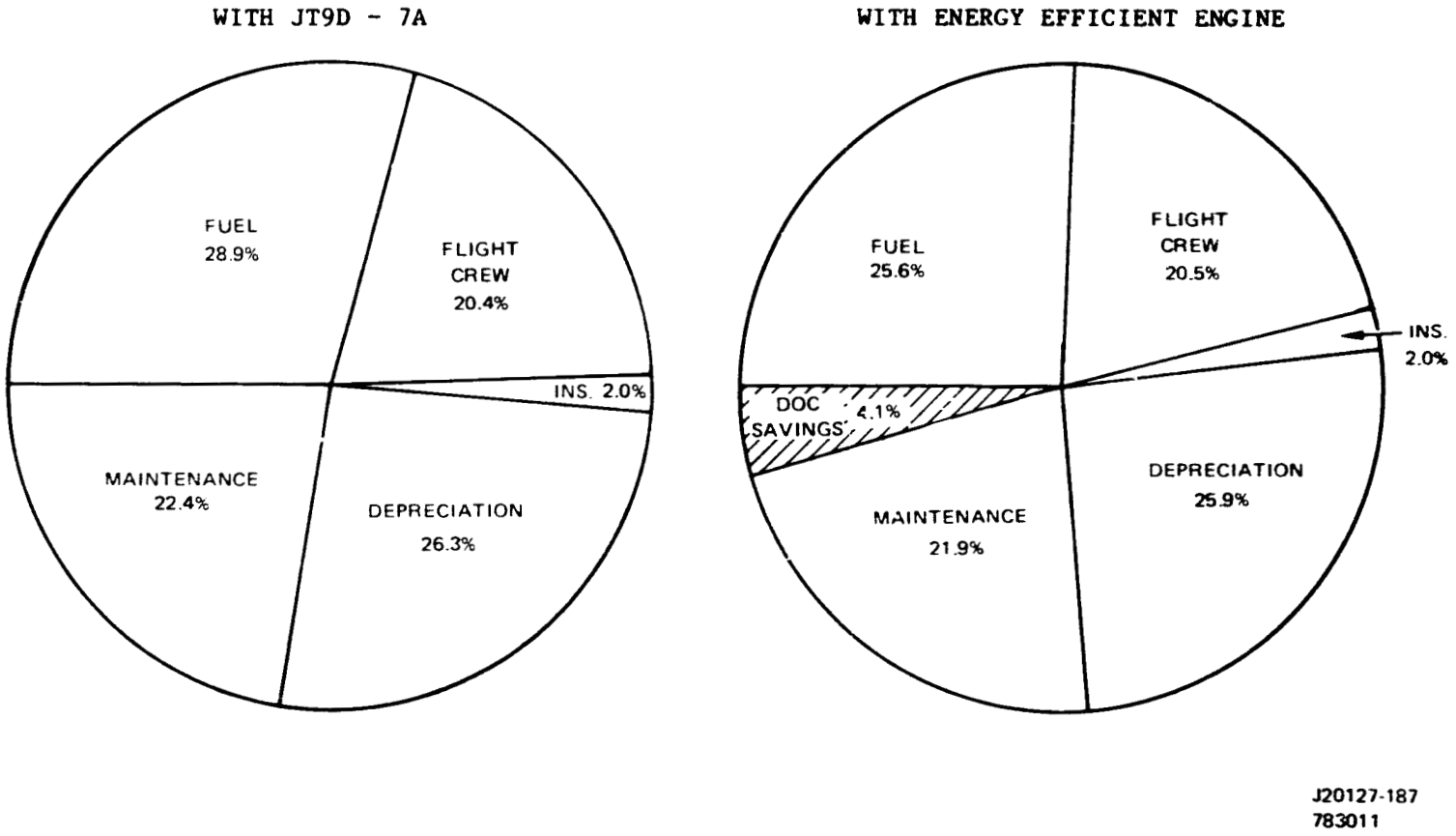

Figure 208 A Direct Operating Cost Pie Charts Ranked By Design Fuel Fraction Illustrating Energy Efficient Engine DOC Reduction Relative to JT9D-7A

5560 km (3000 N.Mi.) Lockheed 500 Passenger Domestic Trijet on
2590 km (1400 N.Mi.) Typical Mission

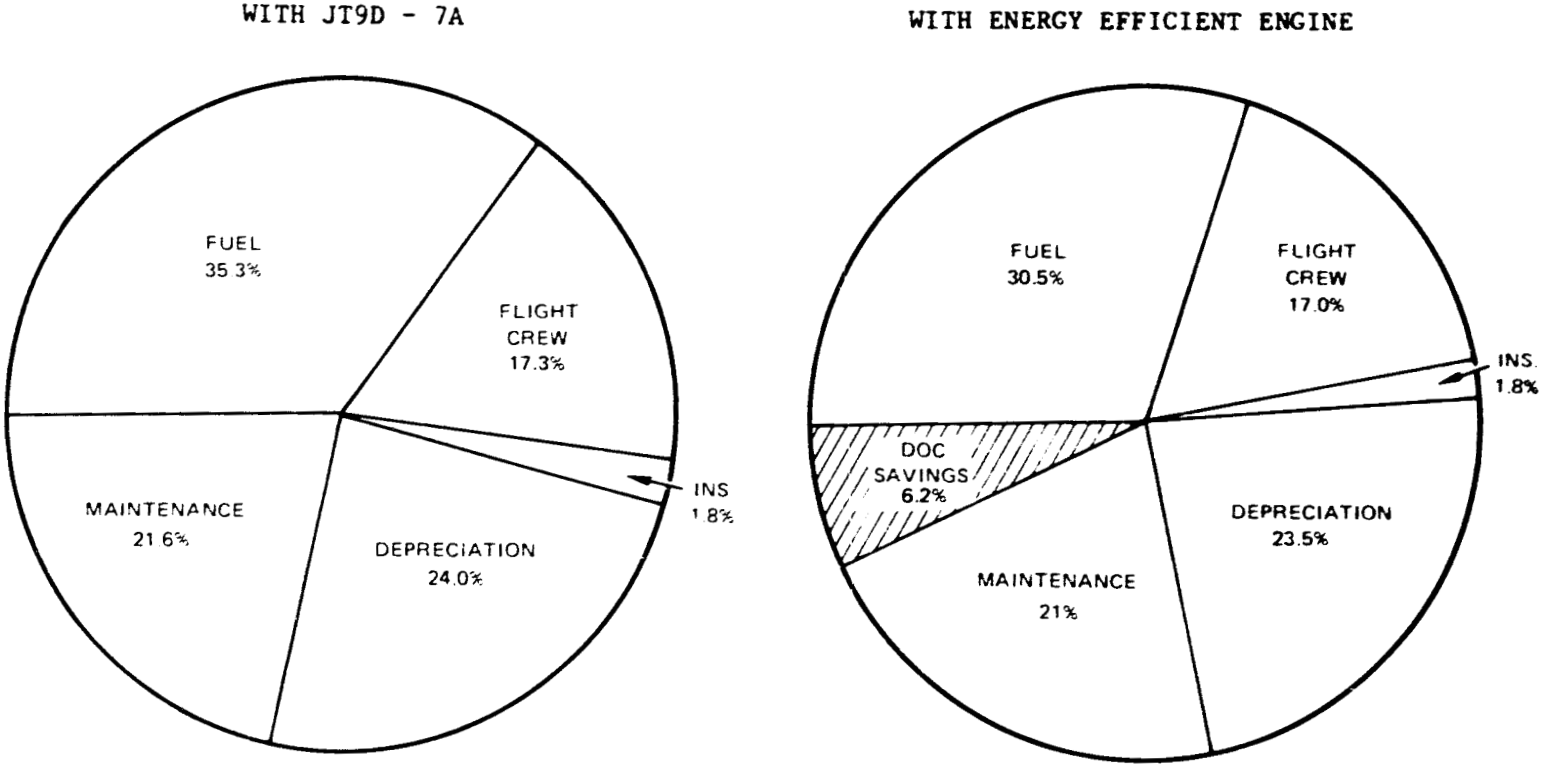

Figure 208 B Direct Operating Cost Pie Charts Ranked By Design Fuel Fraction Illustrating Energy Efficient Engine DOC Reduction Relative to JT9D-7A

J20127-191
783011

5560 km (3000 N Mi.) Douglas 458 Passenger Domestic Trijet on
1850 km (1000 N.Mi.) Typical Mission

WITH JT9D - 7A

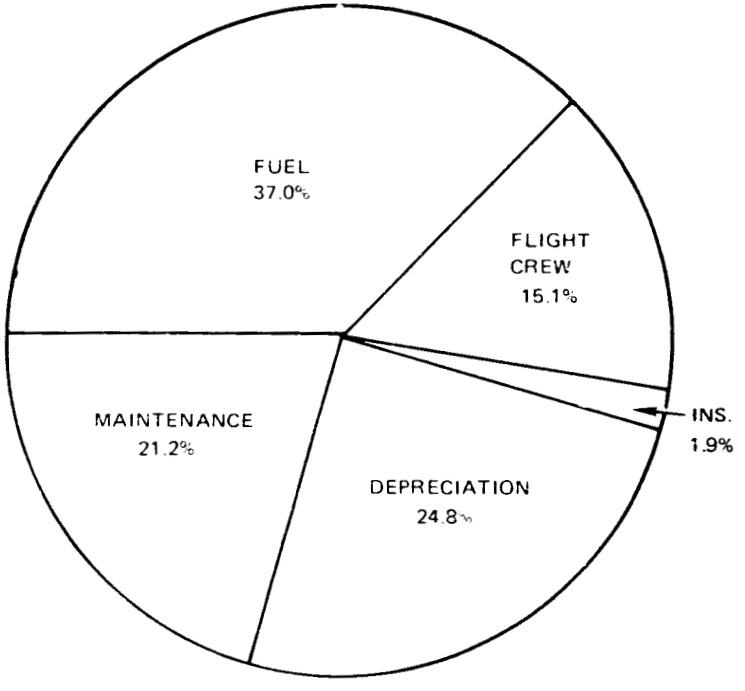

WITH ENERGY EFFICIENT ENGINE

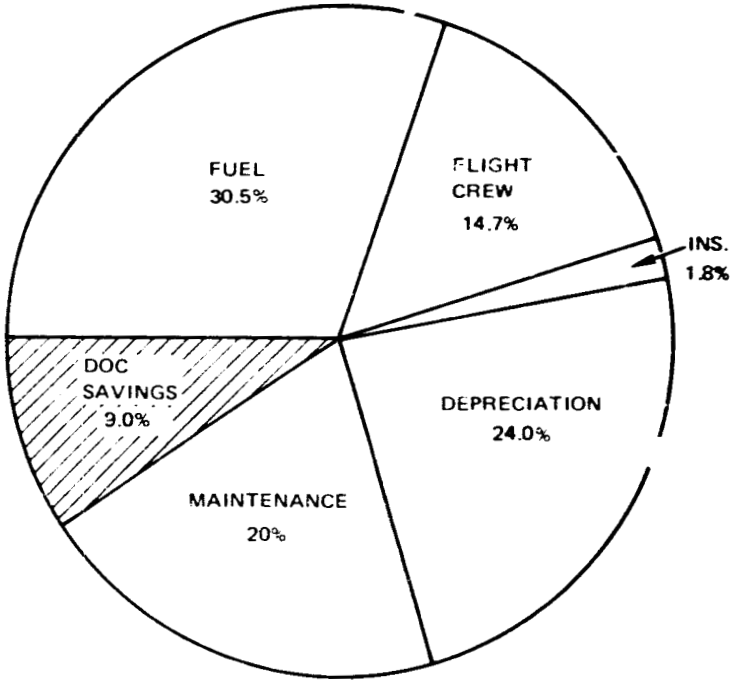

J20127-188
783011

Figure 208 C Direct Operating Cost Pie Charts Ranked By Design Fuel Fraction Illustrating Energy Efficient Engine DOC Reduction Relative to JT9D-7A

5560 km (3000 N.Mi.) P&WA 440 Passenger Domestic Trijet on
1300 km (700 N.Mi.) Typical Mission

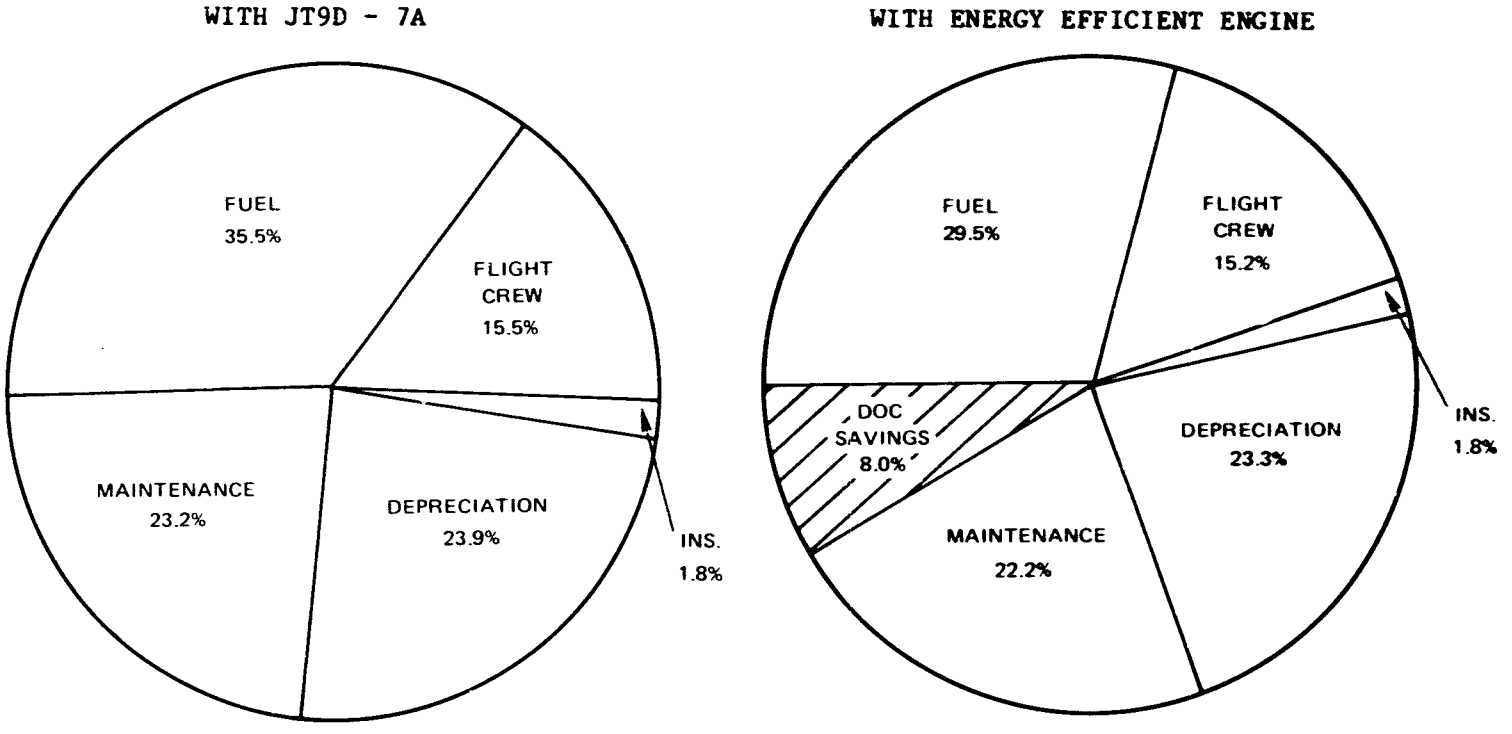

J20127-192
783C11

Figure 208 D Direct Operating Cost Pie Charts Ranked By Design Fuel Fraction Illustrating Energy Efficient Engine DOC Reduction Relative to JT9D-7A

10,190 km (5500 N.Mi.) P&WA 510 Passenger International Quadjet on 3750 km (2000 N.Mi.) Typical Mission

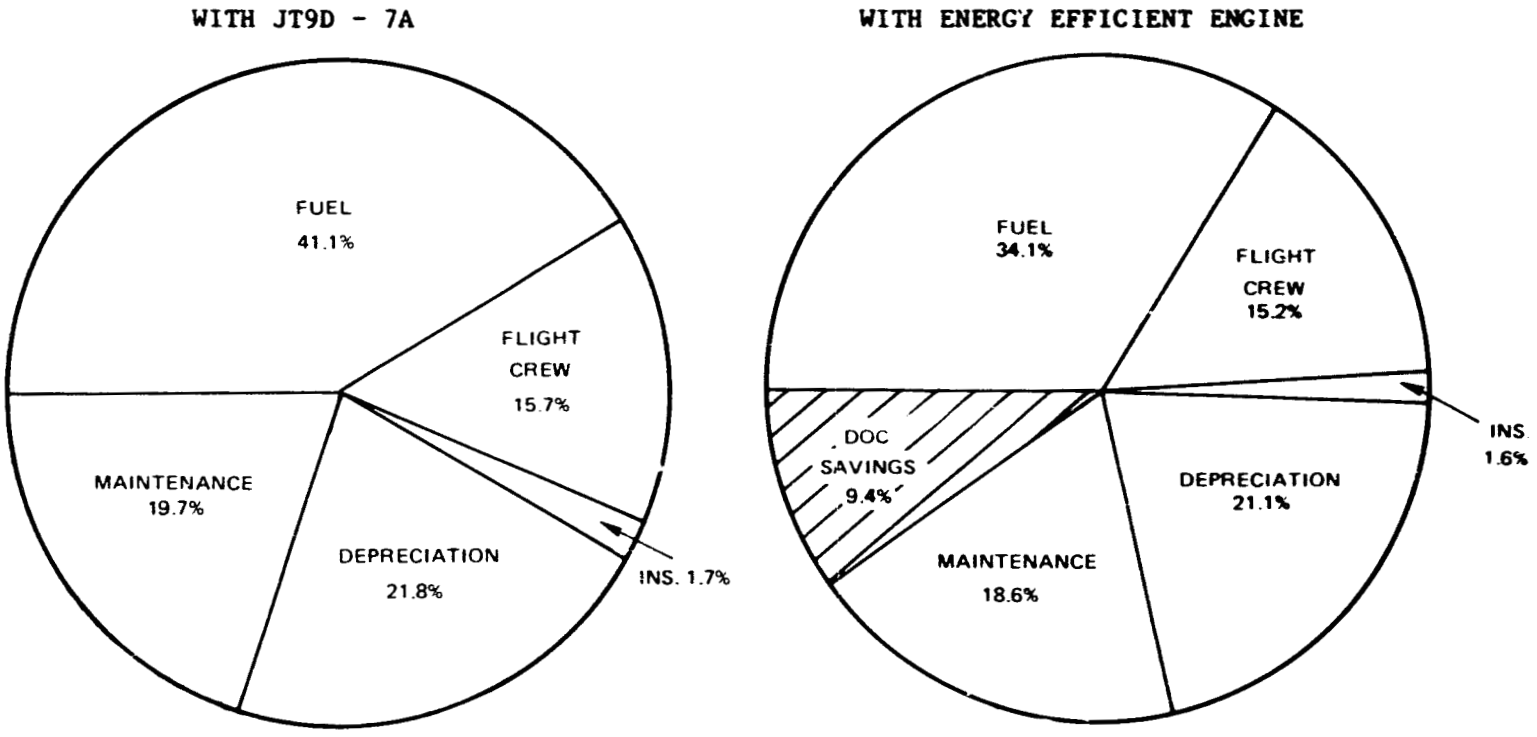

Figure 208 E Direct Operating Cost Pie Charts Ranked By Design Fuel Fraction Illustrating Energy Efficient Engine DOC Reduction Relative to JT9D-7A

J20127-193
783011

10,190 km (5500 N.Mi.) Douglas 438 Passenger International Trijet on 2780 km (1500 N.Mi.) Typical Mission

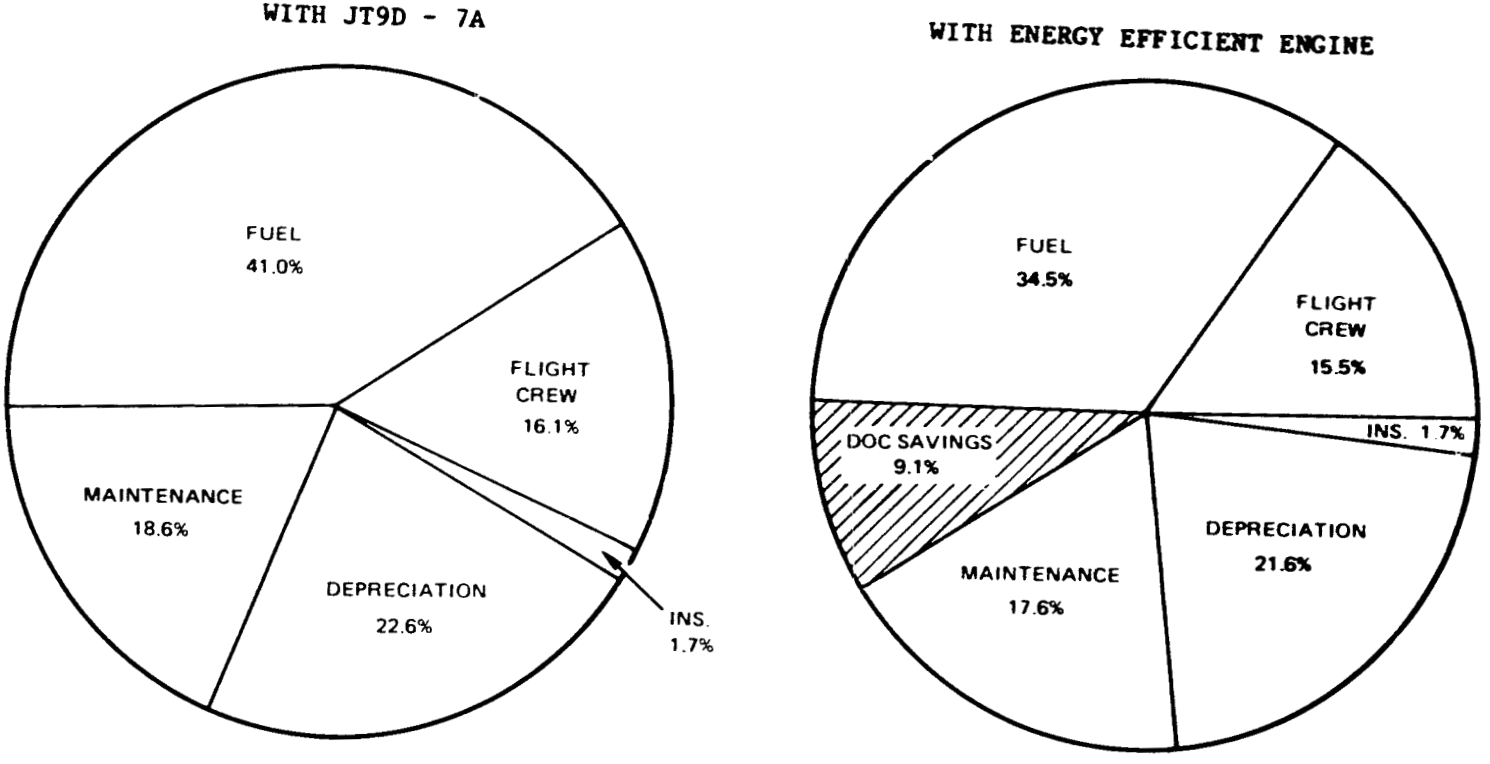

Figure 208 F Direct Operating Cost Pie Charts Ranked By Design Fuel Fraction Illustrating Energy Efficient Engine DOC Reduction Relative to JT9D-7A

J20127-189
783011

12,040 km (6500 N.Mi.) Lockheed 550 Passenger International Quadjet on 5560 km (3000 N.Mi.) Typical Mission

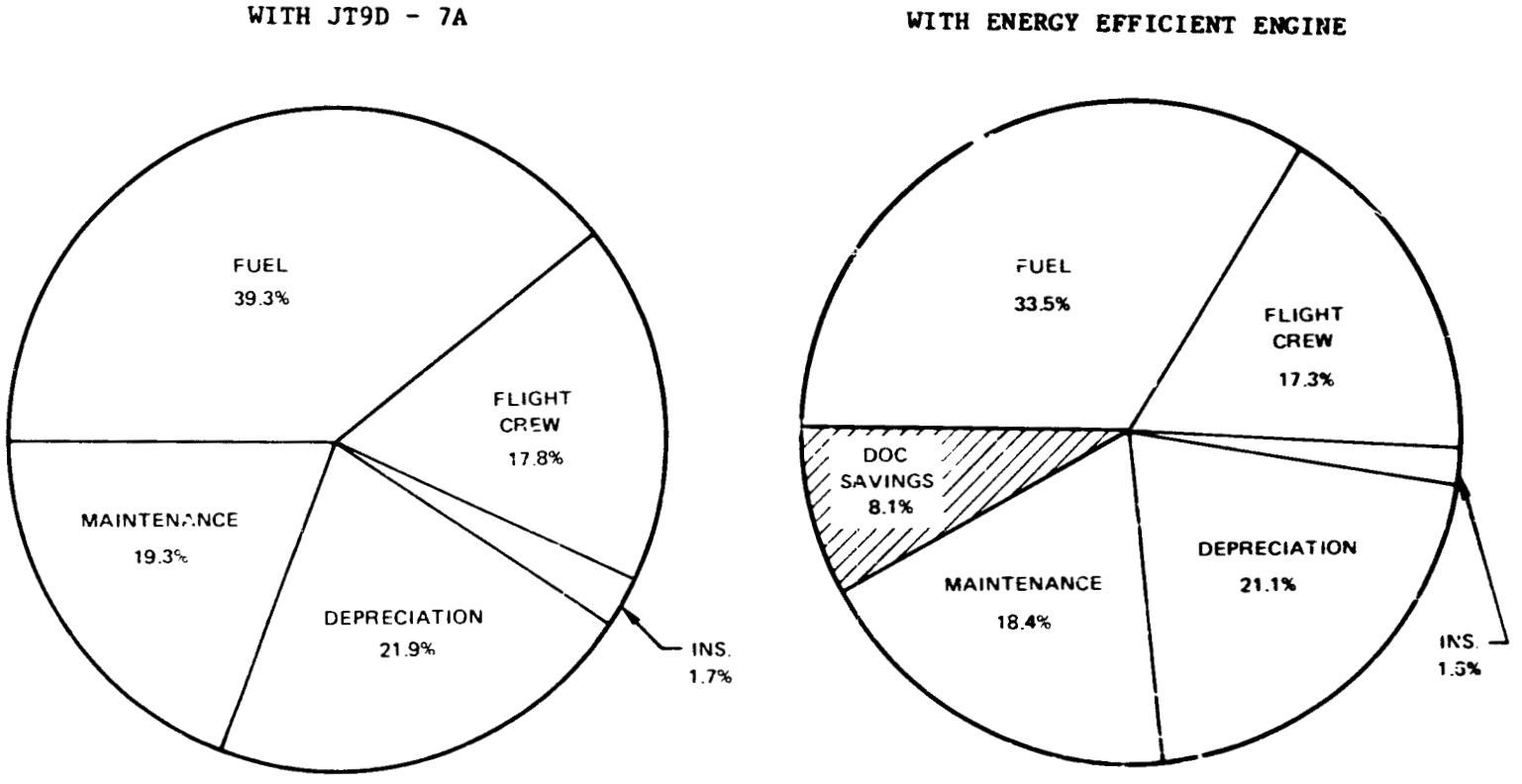

Figure 208 G Direct Operating Cost Pie Charts Ranked By Design Fuel Fraction Illustrating Energy Efficient Engine DOC Reduction Relative to JT9D-7A

J20127-190
78301.

Based on these results, a statistical probability analysis indicated that all of the airplanes, except the Boeing twinjet, have a greater than 99 percent probability of meeting the five percent minimum DOC reduction design goal. The average overall probability of achieving a five percent DOC is estimated at 86 percent.

Return on investment (ROI) was also evaluated for Energy Efficient Engine and JT9D reference engine powered airplanes. A traditional discounted cash flow technique, where the annual ROI is determined by zero present value of future cash flow benefits, was used. Cash flow is defined as after-tax profits plus depreciation, where depreciation is a non-cash expense.

Cash flow = (Revenue - DOC - IOC - Taxes) + Depreciation

A tax rate of 50% was assumed. Details of the indirect operating cost calculation procedure and the revenue assumptions may be found in Reference 1.

The return on investment advantages of Energy Efficient Engine powered study aircraft over JT9D reference engine powered study aircraft are shown in Table 94. These results are for typical missions and are the difference in absolute ROI between the two engines in each airplane.

5.8 NOISE

Noise levels were predicted for all study airplanes using acoustic prediction procedures developed by Pratt & Whitney Aircraft to estimate the noise characteristics of each source. Predicted noise levels are within FAR Part 36-1978 noise limits by adequate margins, providing high probability of compliance with the FAR Part 36-1978 requirements.

The considered noise sources included the fan, core (combustor), turbine, jet exhaust, and airframe. Current Pratt & Whitney Aircraft procedures were used to predict the characteristics of each source as a function of acoustic design and performance parameters.

An overview of the acoustic design is shown in Figure 209. Engine acoustic features include widely spaced fan blades and exit stators (4 times blade chord length gaps at the outer radii), a long duct mixed flow nacelle, and a scalloped exhaust mixer.

Extensive use has been made of acoustic treatment in the inlet and fan discharge duct to suppress fan blade passing tones and buzzsaw noise and turbine generated tones. Treatment requirements were determined from hardwall (untreated) noise estimates for both takeoff and approach conditions to define the dominant noise sources and their spectral characteristics. This information established the treatment tuning requirements to obtain the attenuation needed to meet noise goals.

TABLE 94

RETURN ON INVESTMENT ADVANTAGE OF EEE OVER JT9D REFERENCE ENGINE

	Domestic (percent)	Intercontinental (percent)
Boeing	+0.32	-
Douglas	+2.27	+2.68
Lockheed	+1.19	+2.20
P&WA	+1.75	+2.38

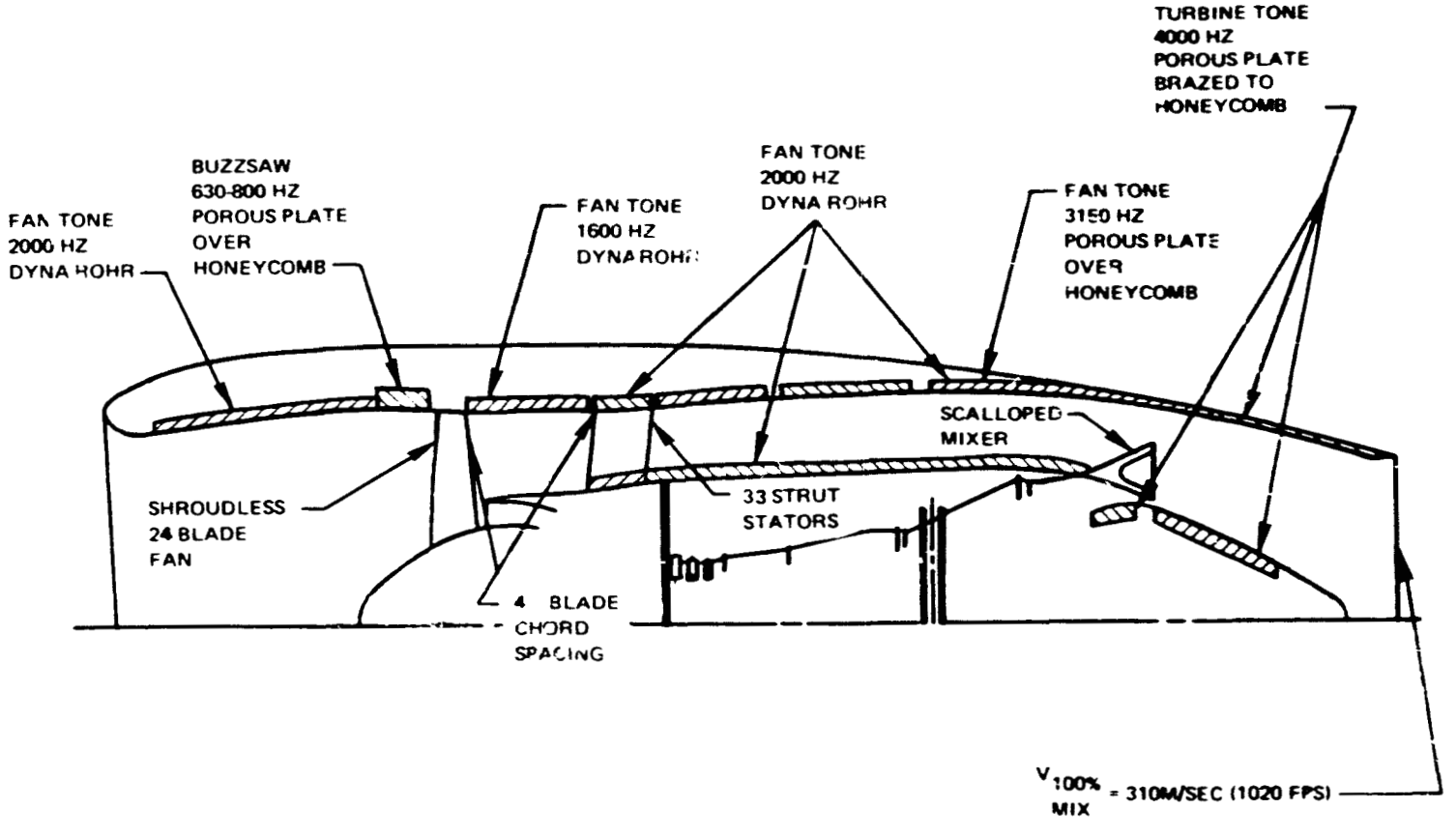

Figure 209 Acoustic Configuration Schematic with Frequency-Tuned Acoustic Treatment

J20127-219
783011

Airplane noise levels predicted in this study were performed on an individual component -- fan, core, turbine, jet, airframe -- basis. For most components the predictions were derived from a component data base established from engine noise measurements. Correlating parameters -- developed from analytical procedures to condense data from several tests and configurations -- were used to scale predicted noise levels from each component data base.

Fan noise, dominant during both takeoff and approach, is the most important noise source. Since the JT9D-7A and the Energy Efficient Engine fan sections have similar acoustic designs, the JT9D data base was used for the fan noise predictions. The similarities included single-stage configuration, no inlet vanes, similar tip-speeds/ pressure-ratio relationships, and substantial fan-to-exit vane spacing.

One significant difference between the acoustic designs of the JT9D and Energy Efficient Engines fan section is that while the JT9D contains a large enough number of fan exit vanes to acoustically "cut-off" the fundamental blade passing tone generated by the fan-stator interactions, the Energy Efficient Engine does not. Structural and performance consideration for Energy Efficient Engine preclude the use of acoustically optimum numbers of vanes; therefore, the interaction that generates blade passing tone is "cut-on". Procedures do not exist to define the impact on noise of these differences. It has been assumed that any adverse effect would be offset by the increased rotor-stator spacing of the Energy Efficient Engine, which is nearly double that of the JT9D.

Core noise predictions rely on a data base gathered from a variety of Pratt & Whitney Aircraft engines and combustors. An analytically developed correlating parameter includes terms for fuel/air ratio, inlet temperature, flow parameter, and number of fuel nozzles.

Turbine noise levels were predicted using test results obtained from a variety of low and high bypass ratio engines. The correlating parameter includes terms for loading, tip speed, flow parameter, blade-to-vane row spacing, and size.

Recently revised SAE procedures (SAE ARP 876, March 1978) were used for jet noise predictions. These procedures correlated noise level with the logarithm of the jet velocity. Mixing of 85 percent was assumed for the force mixed, common flow nozzle. This is consistent with the percent mixing assumed for performance calculations.

Airframe noise levels for Pratt & Whitney Aircraft study airplanes were estimated by relating airframe noise data with airplane takeoff gross weight obtained from various published data. Airframe noise estimates for airplane manufacturer study airplanes were provided by each manufacturer. These airframe noise levels were in general agreement with those predicted by the procedures used by Pratt & Whitney Aircraft.

Noise levels were predicted for each engine component and for the airframe at 10 degree increments (5 degree increments at critical angles). Tone corrected perceived noise levels (PNLT) were calculated at each angle. These calculations were performed by using the one-third octave band levels for each noise source and for the combined sources (total noise). From the relationship between the total noise PNLT versus time, effective perceived noise levels were then calculated for comparison with noise certification requirements.

As expected, the fan was the dominant noise source at all conditions. At certain conditions, the jet and airframe also contributed significantly to the total noise. Figure 210 shows the relative impact of each noise component for the three noise certification conditions. At approach, the fan noise propagation forward of the inlet is the dominant noise source; however, at the other two conditions, the aft propagating fan noise dominates. Airframe noise is the second highest noise source at approach. At takeoff and sideline conditions, the jet is the second highest noise contributor.

5.8.1 Predicted Noise Levels Versus Objectives (FAR Part 36-1978)

Based on predicted noise levels, all study airplanes could comply with the noise certification requirements of FAR Part 36-1978. Figure 211 shows the noise levels for the study airplanes and the FAR requirements for the three certification conditions. It can be noted that the requirements for each condition are a function of airplane takeoff gross weight. In addition, for the takeoff condition, the requirement is a function of the number of engines. Noise levels for all study airplanes are well below the limits -- with one exception, the Boeing twinjet at takeoff, which exceeds the limit by one-half an EPNdB. This small excess does not prevent the airplane from meeting certification requirements as the regulations permit trading of a surplus at one condition for an excess of up to 2 EPNdB at another condition.

It should also be noted that no attempt was made to refine for minimum noise the nacelle configuration of the Boeing twinjet, or any of the other study airplanes defined by the airframe manufacturers. The nacelle configuration optimized for the Pratt & Whitney Aircraft defined airplanes was used throughout this effort.

At approach, the two Douglas trijets had significantly more margin below the limit than the other study airplanes. The lower estimated noise levels resulted primarily from the lower values of thrust required for the Douglas airplanes because of higher lift designs and lower flap setting requirements.

Optimization for minimum noise of the performance of all study airplanes and of the nacelle configurations of the airframe manufacturer designed airplanes would decrease the nominal noise levels.

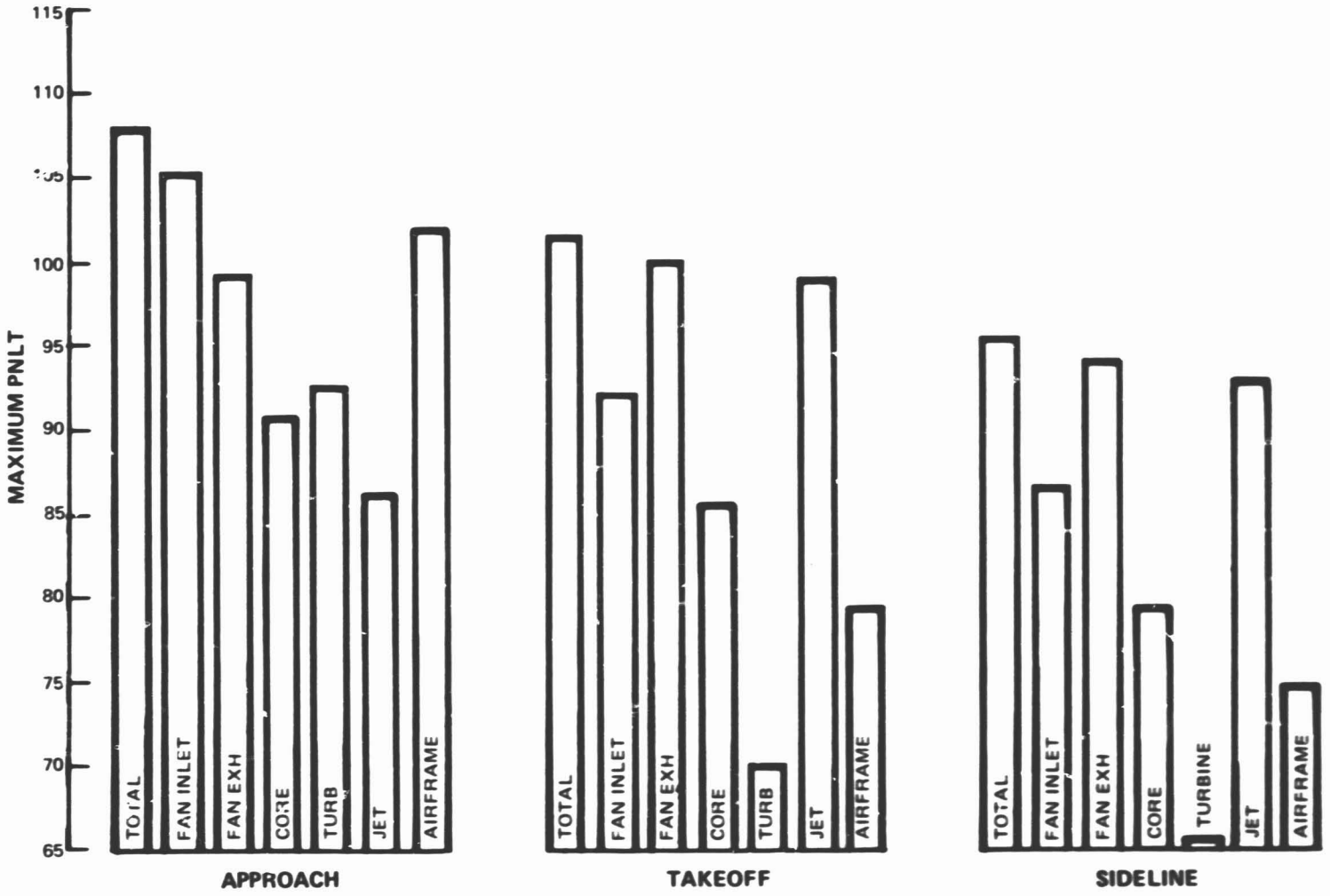

Figure 210 Component Attenuated Noise Predictions for P&WA Trijet, Illustrating Importance of Fan, Jet and Airframe Noise

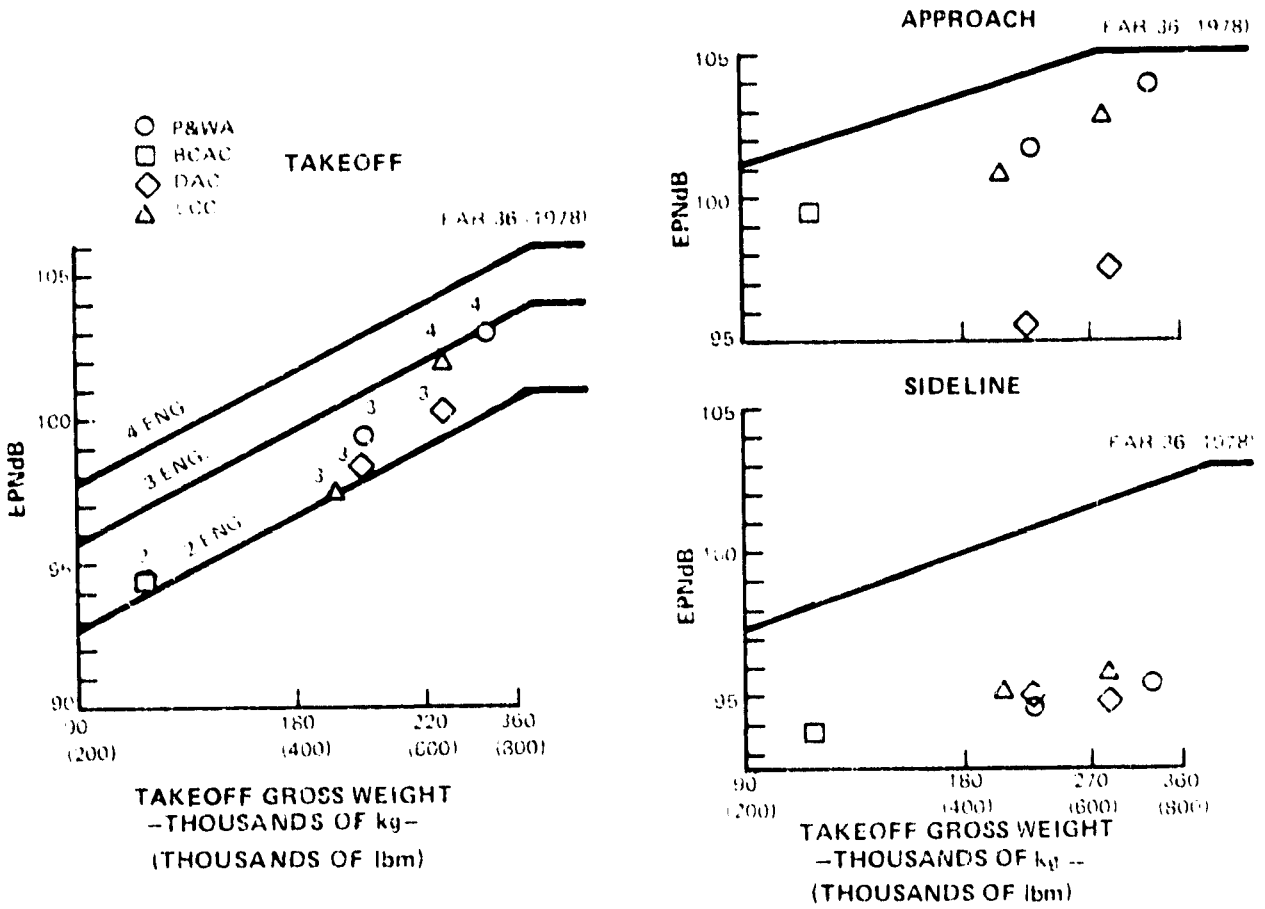

Figure 211 Predicted Noise Levels Versus FAR Part 36-1978

5.8.2 Probabilities of Success

The probability of complying with the noise certification requirements of FAR Part 36-1978 was estimated using statistical procedures and considering the predicted noise regulation margins and noise prediction uncertainty. The standard deviations for the noise predictions were estimated to be ±3 EPNdB for approach and ±2.7 EPNdB for sideline and takeoff conditions. The estimated probabilities are summarized in Table 95.

5.9 THRUST GROWTH

A growth path for the Energy Efficient Engine has been defined in two thrust steps:

A. An initial growth step of about 15 percent thrust increase with no major changes in nacelle geometry. This is accomplished through a combination of core supercharging to produce a 45:1 overall pressure ratio, a four percent higher fan pressure ratio, a small, 2.8 cm (1.1 in), increase in fan diameter, and 37°C (67°F) higher turbine rotor inlet temperature.

B. A second growth step of about 25 percent thrust increase which requires a new nacelle. The engine changes include a 45:1 increased overall pressure ratio, 27.2 cm (10.7 in) increased fan diameter, and 95°C (172°F) higher turbine rotor inlet temperature.

Both growth steps are accomplished at constant technology; i.e., no improvements in materials, coatings, or aerodynamic technology are assumed.

Engine design changes required to achieve the growth steps are as follows: For Step (A), the single-stage fan is replaced with a single-stage design of higher pressure ratio, increased tip speed and slightly greater specific flow and diameter than the base. The low-pressure compressor has an added supercharging stage. The high-pressure compressor is aerodynamically unchanged, but operates at higher rpm's and gaspath temperatures as a result of increased inlet temperature; its pressure ratio and corrected airflow are unchanged from the base. The combustor operates at increased exit temperature; first vane cooling flow is increased accordingly. High-pressure turbine airfoil cooling flows are increased to maintain life at the elevated rotor inlet temperature, and the high-pressure turbine is rebladed (same annulus) because of cooling air and expansion ratio changes. The low-pressure turbine has a cooled first vane row added for hot section life; no aerodynamic changes are required. The forced mixer/plug are revised to furnish the mixing plane area adjustments which the cycle revisions require; no significant changes in total mixing plane area or

TABLE 95

AIRCRAFT NOISE COMPLIANCE PROBABILITIES

Aircraft Configuration	Probability of Complying With FAR Part 36-1978 Requirements
Lockheed Domestic Trijet	0.92
Lockheed International Quadjet	0.86
Douglas Domestic Trijet	0.95
Douglas International Trijet	0.93
Boeing Domestic Twinjet	0.63
P&WA Domestic Trijet	0.84
P&WA International Quadjet	0.79

jet nozzle are required. The inlet throat geometry and the external forward nacelle lines remain unchanged with the possible exception of an added spool section to extend the length.

Growth Step B requires more extensive changes to the engine, some of which are illustrated on Figure 212. The base engine fan is replaced with a scaled-up fan having the same aerodynamic parameters. The low-pressure compressor has an added supercharging stage. As in Step A the high-pressure compressor is unchanged aerodynamically but operates at elevated pressures, temperatures and rotor speed; pressure ratio and corrected flow are unchanged from the base. Burner exit temperature is increased and first turbine vane cooling flow is further increased from Step A. High-pressure turbine cooling flows are increased to maintain life, and the high-pressure turbine is rebladed (same annulus) as for Step A. Since the low rotor speed is decreased as a result of increased fan diameter at the same corrected tip speed, more extensive low-pressure turbine changes are required than for Step A. The low-pressure turbine has increased elevation, requiring a new transition section between the turbines, and has an added (fifth) stage. Both the first vane and first blade of the low-pressure turbine are cooled. Because of the increased airflow and cycle changes, mixing plane geometry differs from the base engine, requiring mixer/plug revisions. The entire nacelle for this growth engine is new.

Changes in engine cycle, performance, and airflow/diameter are summarized in Table 96 for the two growth steps. Thrust growth will be accompanied by a slight improvement in installed TSFC -- flight inlet, nacelle drag, no bleed or power extraction -- for Step (A) and a significant improvement for Step (B). The improved TSFC will be a result of increased overall compression ratio and rotor inlet temperature, which partially offsets the fuel consumption penalty of increased FPR. In addition, the nacelle drag/thrust of step (A) is lower than the base because the thrust is greater without an increase in diameter. For Step (B), the decrease in TSFC is a direct result of the thermal efficiency improvement associated with the OPR/RIT increases, since fan pressure ratio is constant (propulsive efficiency is nearly constant). Drag/thrust for Step (B) is nearly the same as for the base engine.

Thrust growth can be achieved with small impact on noise. The effects on engine noise of the two approaches for growth are summarized in Figure 213. The increases in fan pressure ratio (Option A) and fan size (Option B) result in small increases in fan noise (less than one dB). Jet velocity increases associated with Option A results in approximately a two dB increase in jet noise. By increasing bypass ratio (Option B) the jet velocities are reduced to produce additional thrust growth potential with small (less than one dB) jet noise increase. If a constant thrust loading is assumed (takeoff gross weight increases at the same rate as engine thrust), the original noise rule margins would be retained with the possible exception of very heavy airplanes at the approach condition as the approach noise limit remains constant with takeoff gross weight increases above 280,000 kg (617,300 lb).

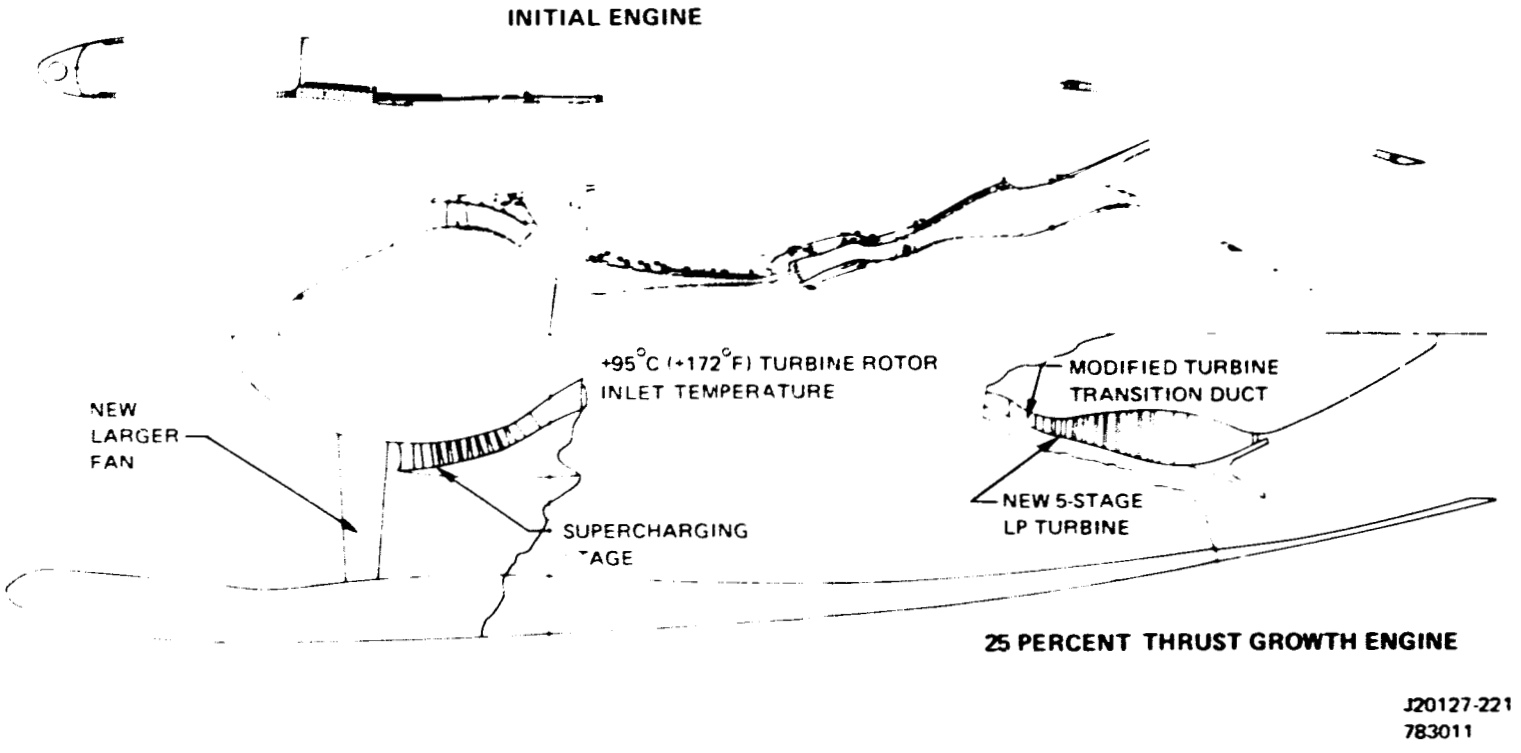

Figure 212 Design Revisions Assumed for Twenty-Five Percent Thrust Growth

TABLE 96

GROWTH CYCLE PERFORMANCE AT AERODYNAMIC DESIGN POINT
RELATIVE TO BASE ENERGY EFFICIENT ENGINE

	Step A 15% Thrust Increase	Step B 25% Thrust Increase
Change in Corrected Airflow - kg/sec (lbm/sec)	+36 (+78)	+186 (+410)
Change in Fan Pressure Ratio	+0.07	0
Change in Bypass Ratio	-0.59	+0.82
Change in Overall Pressure Ratio	+6.4	+6.4
Change in Rotor Inlet Temperature - ^{o}C (^{o}F)	+37 (+67)	+95 (+172)
Change in Turbine Cooling Air - (% Core Flow)	+3.3	+5.7
Change in Fan Diameter - cm (in)	+3 (+1.1)	+27 (+10.7)
Change in TSFC - (percent)	-0.2	-1.1

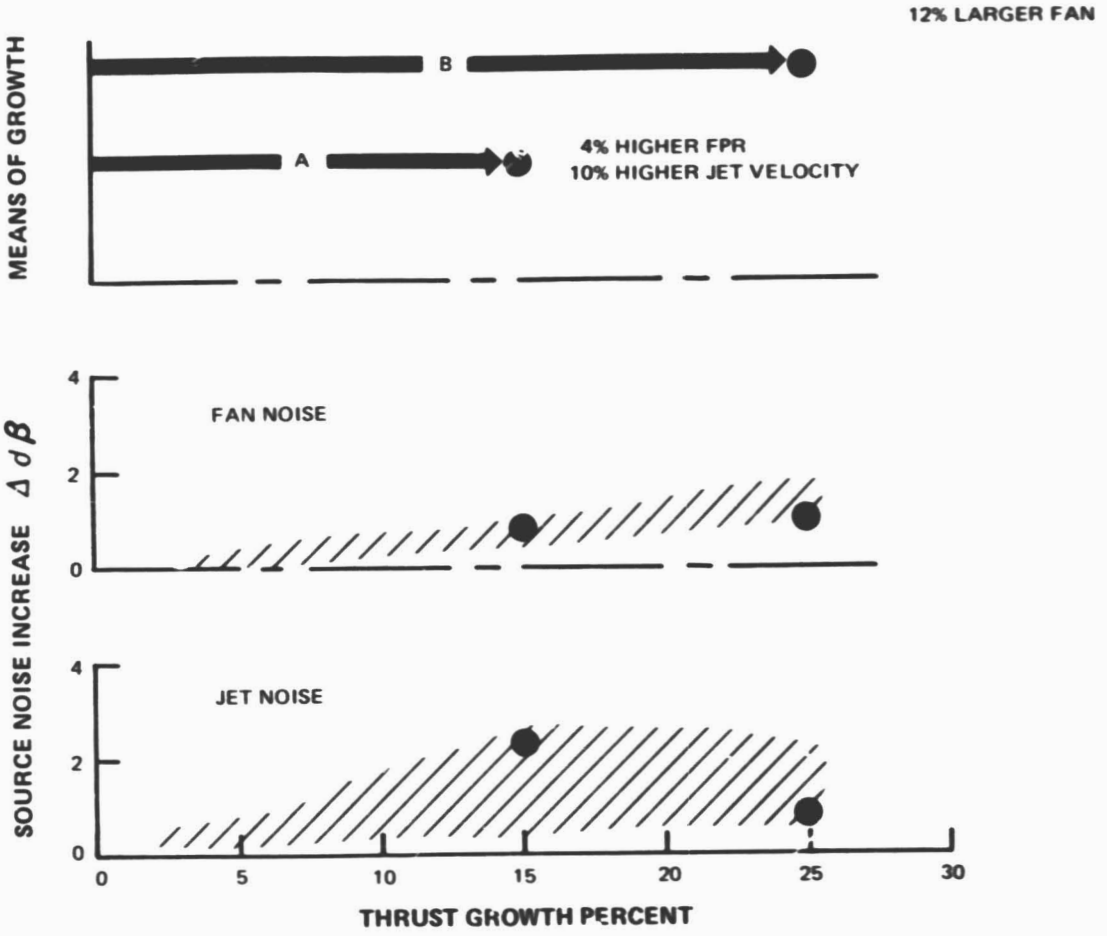

Figure 213 Fan and Jet Noise Constituents Increase By Up to 2 EPNdB with Selected Growth Paths

6.0 CONCLUSIONS

1. The feasibility of the Energy Efficient Engine design was verified.

   Preliminary analysis and design efforts on the Flight Propulsion System and its components were completed and were shown to satisfy the design requirements.

2. A 14.9 percent TSFC reduction, relative to that of the JT9D-7A engine, surpasses the NASA minimum design goal of 12 percent for newly-installed engines. Performance deterioration can also be reduced by 50 percent with successful use of fuel conservative design technology.

   Tighter running clearances were achieved by structural integration, nacelle load sharing, improved thermal matching, and active clearance control.

   Design contoured airfoils were used throughout the engine to increase component efficiency.

   Improved seals and higher effectiveness cooling techniques were used to reduce parasitic losses.

   Higher cycle pressure ratio and exhaust mixing were included to improve cycle efficiency.

3. An average DOC reduction of 8.2 percent, relative to the JT9D-7A, surpasses the NASA goal of at least five percent.

   Over two thirds of the DOC reduction was attributable to reduced fuel costs associated with the fuel savings as calculated on seven representative future study aircraft.

   Advanced materials allowed full utilization of single-stage high-pressure turbine technology and overall airfoil count reduction of 35 percent relative to the JT9D-7A which essentially accounted for the remainder of the DOC reduction.

4. Predicted noise levels for the study airplanes meet FAR Part 36-1978 certification requirements, generally by a sufficient margin to provide a high probability of compliance.

   Acoustic treatment was used peripherally throughout the nacelle, and fan blades were widely spaced from the exit guide vanes to control the fan dominant noise source.

5. Low power gaseous emissions of CO and THC and smoke levels meet the NASA goals of the EPA proposed 1981 regulations. NO_x predictions exceed the upper limits defined in the NASA goals.

Two-stage combustion with carburetor tube main zone fuel injectors was used to minimize gaseous emissions and smoke. The combustor incorporates the best known emissions reduction technology identified by Pratt & Whitney Aircraft in-house and NASA funded programs.

7.0 LIST OF ABBREVIATIONS AND SYMBOLS

a	-	air
A	-	cross-sectional area, ft^2, $in.^2$, cm^2, m^2
ACC	-	Active Clearance Control
ADP	-	aerodynamic design point
AMAC	-	advanced multistage axial compressor
AMB	-	ambient
BTU	-	British thermal unit
C		Celsius (centigrade)
C/A	-	circular arc (airfoil)
CFFC	-	counter flow film cooled
C/L	-	center line
CLB	-	maximum climb
cm	-	centimeter
CO	-	carbon monoxide
CPFW	-	counter parallel FINWALL techniques
cps	-	cycles per second
CPU	-	central processor unit
CR	-	maximum cruise
CTOL	-	Conventional Takeoff and Landing Aircraft
Cx/u	-	Axial velocity-to-wheel speed ratio
D	-	diameter, ft, in., cm, m
DB	-	diffusion bonding
db	-	decibel
diam	-	diameter
DCA	-	double circular arc
DN	-	bearing bore diameter x maximum rotor speed
DOC	-	direct operating cost
DOI	-	digital output interface
EB	-	electron beam
ECCP	-	Experimental Clean Combustor Program
EGV	-	Exit Guide Vane
EI	-	Emission Index
EPA	-	Environmental Protection Agency
EPAP	-	EPA Parameter
EPN	-	Effective Perceived Noise
f	-	fuel
F	-	Fahrenheit
FAA	-	Federal Aviation Administration
FAR	-	Federal Aviation Regulation
FEGV	-	fan exit guide vane
F_N	-	net thrust
FPS	-	Flight Propulsion System
ft	-	foot
ft/sec	-	feet per second

7.0 LIST OF ABBREVIATIONS AND SYMBOLS (Cont'd)

G	-	gravitational
gal	-	gallon
g.p.m.	-	gallons per minute
gyro	-	gyroscopic
h_s, h_t	-	enthalpy static and total Btu/lb, Btu/kg
HC	-	hydrocarbon
HHSE	-	High Work High Spool Engine
HPC	-	high pressure compressor
HPT	-	high-pressure turbine
Hz	-	hertz (cycle per second)
IC/LS	-	integrated core/low spool
I.D.	-	inner diameter
IGV	-	inlet guide vane
in.	-	inch
IR&D	-	Independent Research & Development
K	-	Kelvin
kg	-	kilogram
km	-	kilometer
ksi	-	1000 pounds per square inch ($N/meter^2$)
l	-	liter
lb	-	pound
lbm	-	pound mass
lb/sec	-	pounds per second
LCF	-	low cycle fatigue
LPC	-	low-pressure compressor
LPT	-	low-pressure turbine
M	-	Mach number
m	-	meter
mm	-	millimeter
MATE	-	Materials for Advanced Turbine Engine
MCA	-	multiple circular arc
MERL	-	Materials Engineering and Research Laboratory
Naut. Mi.	-	nautical mile
N	-	newton
N	-	rotational speed
NO_x	-	nitrogen oxides
OAS	-	outer airseal
O.D.	-	outside diameter
O.D.S. (ODS)	-	oxide dispersion strengthened
OPR	-	overall pressure ratio

7.0 LIST OF ABBREVIATIONS AND SYMBOLS (Cont'd)

P	-	absolute pressure, lb/ft^2, Kg/m^2
P_3	-	pressure, station 3
psi	-	pounds/square inch
psia	-	pressure, static (N/Cm^2)
P_{t3}	-	pressure, atmosphere
QEC	-	quick engine change
ROI	-	return on investment
RPM	-	revolutions per minute
RTCS	-	real time control system
S	-	stator
SAE	-	Society of Automotive Engineers
sec	-	second
sfc	-	specific fuel consumption
SLS	-	sea level static
SLTO	-	sea level takeoff
SMD	-	Sauter mean diameter (droplet size)
SOAPP	-	State-of-the-Art Performance Program
SPF	-	superplastic forming
sta.	-	station
T	-	temperature
TEC	-	turbine exhaust case
THC	-	total unburned hydrocarbons
Ti	-	titanium
TIM	-	time in mode
TLP	-	transient liquid phase
T/O	-	takeoff
TOBI	-	tangential on-board injection
TSFC	-	thrust specific fuel consumption
T_{t3}	-	total temperature, station 3
T_3	-	static temperature, station 3
T_4	-	total temperature, station 4
u	-	rotor velocity, ft/sec, m/sec
V	-	velocity, ft/sec, m/sec
Vo mix	-	vortex burn and mixing
V_I	-	pilot zone volume
WAB	-	burner airflow
WAC	-	compressor airflow
WAE	-	engine core (stream) airflow
Wf	-	lbm/hour fuel flow
Wp	-	pilot zone airflow
Zp	-	cascade loss

7.0 LIST OF ABBREVIATIONS AND SYMBOLS (Cont'd)

α - angle of attack, degrees
β - blade air angle
Δ - finite change
θ - mean turning angle
η - efficiency, percent
μ - absolute viscosity
ρ - density, GR/cm^3
σ - surface tension, dynes/cm

8.0 REFERENCES

1. Gray, D. E., et al: "Energy Efficient Engine Preliminary Design and Integration Studies, NASA CR-135396, Nov. 1978.

2. Anon.: EPA 40 CFR, Part 87, Subpart H of the Federal Register, Volume 38, No. 136, July 17, 1973.

3. Roberts, W. B.: "A Design Point Correlation for Losses Due to Part-Span Dampers on Transonic Rotors," American Society of Mechanical Engineers, Paper No. 78-GT-153, 1978.

4. Aerodynamic Design of Axial Flow Compressors, NASA SP-36, U. S. Government Printing Office, Washington, D.C. 1965, pps. 227-252.

5. Spadaccini, L. J.: "Autoignition Characteristics of Hydrocarbon Fuels at Elevated Temperatures and Pressures," The American Society of Mechanical Engineers, Paper No. 76-GT-3, 1976.

6. Marek, C. J., Papathakos, L. C., and Verbulecz, P. W.: "Preliminary Studies of Autoignition and Flashback in a Premixing-Prevaporizing Flame Tube Using Jet-A Fuel at Lean Equivalence Ratios," NASA Lewis Research Center, NASA TM-X-3526, May 1977.

7. Owens, R. E.: "Energy Efficient Engine Propulsion System - Aircraft Integration Evaluation," NASA CR-159488, March 1979.

9.0 MAILING LIST

NASA Headquarters
600 Independence Ave., S.W.
Washington, DC 20546
Attn: RTP-6/ R. A. Rudey

NASA Headquarters
600 Independence Ave., S.W.
Washington, DC 20546
Attn: RTM-6/ L. Harris

NASA-Lewis Research Center
21000 Brookpark Road
Cleveland, OH 44135 MS 301-4
Attn: N.T. Saunders,(20 copies)

NASA-Lewis Research Center
21000 Brookpark Road
Cleveland, OH 44135 MS 301-4
Attn: J. W. Schaefer

NASA-Lewis Research Center
21000 Brookpark Road
Cleveland, OH 44135
Attn: J.A. Ziemianski, MS 301-4

NASA-Lewis Research Center
21000 Brookpark Road
Cleveland, OH 44135
Attn: J.F. Dugan, Jr., MS 301-2

NASA-Lewis Research Center
21000 Brookpark Road
Cleveland, OH 44135 (MS 60-3)
Attn: Library (2 Copies)

NASA-Lewis Research Center
21000 Brookpark Road
Cleveland, OH 44135 (MS 5-5)
Attn: Rept. Control Office

NASA-Lewis Research Center
21000 Brookpark Road
Cleveland, OH 44135
Attn: M.A. Beheim, MS 86-1

NASA-Lewis Research Center
21000 Brookpark Road
Cleveland, OH 44135
Attn: R.W. Schroeder, MS 500-207

NASA-Lewis Research Center
21000 Brookpark Road
Cleveland, OH 44135
Attn: R.W. Hall, MS 49-1

NASA-Lewis Research Center
21000 Brookpark Road
Cleveland, OH 44135
Attn: W.C. Strack, MS 500-307

NASA-Lewis Research Center
21000 Brookpark Road
Cleveland, OH 44135
Attn: R.E. Jones, MS 60-6

NASA-Lewis Research Center
21000 Brookpark Road
Cleveland, OH 44135
Attn: L.P. Ludwig, MS 23-2

NASA-Lewis Research Center
21000 Brookpark Road
Cleveland, OH 44135
Attn: J.F. Groeneweg, MS 500-206

NASA-Lewis Research Center
21000 Brookpark Road
Cleveland, OH 44135
Attn: W.M. Braithwaite, MS 60-6

NASA-Lewis Research Center
21000 Brookpark Road
Cleveland, OH 44135
Attn: R.H. Johns, MS 49-3

NASA-Lewis Research Center
21000 Brookpark Road
Cleveland, OH 44135
Attn: L.J. Kaszubinski, MS 21-4

NASA-Lewis Research Center
21000 Brookpark Road
Cleveland, OH 44135
Attn: R.W. Niedzwiecki, MS 60-6

NASA-Lewis Research Center
21000 Brookpark Road
Cleveland, OH 44135
Attn: AFSC Liaison Off., MS 501-3

NASA Ames Research Center
Moffett Field, CA 94035
Attn: 202-7/L.J. Williams

NASA Langley Research Center
Langley Field, VA 23365
Attn: R. Leonard

NASA Headquarters
600 Independence Ave., S.W.
Washington, DC 20546
Attn: RJP-2/ R. S. Colladay

NASA-Lewis Research Center
2000 Brookpark Road
Cleveland, OH 44135
Attn: D.L. Nored, MS 301-2

NASA Headquarters
600 Independence Ave., S.W.
Washington DC 20546
Attn: Library

NASA-Lewis Research
21000 Brookpark Road
Cleveland, OH 44135
Attn: L.E. Macioce, MS 301-4

NASA-Lewis Research Center
21000 Brookpark Road
Cleveland, OH 44135
Attn: E.W. Conrad, MS 301-2

NASA-Lewis Research Center
21000 Brookpark Road
Cleveland, OH 44135 (MS 3-19)
Attn: TECH.UTILIZATION OFF.

NASA-Lewis Research Center
21000 Brookpark Road
Cleveland, OH 44135
ATTN: W.L. Stewart (MS 3-5)

NASA-Lewis Research Center
21000 Brookpark Road
Cleveland, OH 44135
Attn:M.J. Hartmann MS 5-3

NASA-Lewis Research Center
21000 Brookpark Road
Cleveland, OH 44135
Attn: R.A. Rudey, MS 60-4

NASA-Lewis Research Center
21000 Brookpark Road
Cleveland, OH 44135
Attn: R.J. Weber,MS 500-307

NASA-Lewis Research Center
21000 Brookpark Road
Cleveland, OH 44135
Attn: T.P.Moffitt, MS 77-2

NASA-Lewis Research Center
21000 Brookpark Road
Cleveland, OH 44135
Attn: D.C. Mikkelson, MS 86-1

NASA-Lewis Research Center
21000 Brookpark Road
Cleveland, OH 44135
Attn: K.E. Skeels, MS 500-313

NASA Ames Research Center
Moffett Field, CA 94035
ATTN: Library

NASA-Lewis Research Center
21000 Brookpark Road
Cleveland, OH 44135
Attn: R.L. Davies, MS 105-1

NASA-Lewis Research Center
21000 Brookpark Road
Cleveland, OH 44135
Attn: J.R. Mihaloew, MS 100-1

NASA-Lewis Research Center
21000 Brookpark Road
Cleveland, OH 44135
Attn: C.L. Ball, MS 5-9

NASA-Lewis Research Center
21000 Brookpark Road
Cleveland, OH 44135
Attn: Army R&T Prop. Lab, MS 77-5

NASA Ames Research Center
Moffett Field, CA 94035
Attn: 202-7/M.H. Waters

NASA Langley Research Center
Langley Field, VA 23365
Attn: D. Maiden

NASA Dryden Flight Research Ctr.
P. O. Box 273
Edwards, CA 93523
Attn: J.A. Albers

Department of Defense
Washington, D.C. 20301
Attn: R. Standahan
3D1089 Pentagon

Wright-Patterson Air Force Base
Dayton, OH 45433
Attn: H.J.P. VonOhain
AFAPL/CCN

Wright-Patterson Air Force Base
Dayton, OH 45433
Attn: E.E. Bailey (NASA Liaison)
AFAPL/DO

Wright-Patterson Air Force Base
Dayton, OH 45433
Attn: R.P. Carmichael
ASD/XRHI

Eustis Directorate
U.S. Army Mobility R&D Laboratory
Fort Eustis, VA 23604
Attn: J. Lane, SAVDL-EU-Tapp

Dept. of Transportation NASA/DOT
Joint Office of Noise Abatement
Washington, DC 20590
Atn: C. Foster

Federal Aviation Administration
Noise Abatement Division
Washington, DC 20590
Attn: J. Woodhall

Naval Air Propulsion Test Center
Trenton, NJ 08628
Attn: J.J. Curry

U.S. Naval Air Test Center
Code SY-53
Patuxent River, MS 20670
Attn: E.A. Lynch

Environmental Protection Agency
2565 Plymouth Road
Ann Arbor, MI 48105
Attn: R. Munt

Curtiss Wright Corp.
Woodridge, NJ 07075
Attn: S. Moskowitz

Cummins Engine Co. Tech. Center
500 S. Poplar
Columbus, IN 47201
Attn: J.R. Drake

AVCO/Lycoming
550 S. Main Street
Stratford, CT 06497
Attn: H. Moellmann

The Garrett Corporation
AiResearch Manufacturing Co.
Torrance, CA 90509
Attn: F.E. Faulkner

Teledyne CAE, Turbine Engines
1330 Laskey Road
Toledo, OH 43612
Attn: W.Q. Wagner

General Electric Co./AEG
Neumann Way
Evandale, OH 45215
Attn: M. Hemsworth (3)

General Electric Co./AFG
1000 Western Ave.
Lynn, MA 01910
Attn: R.E. Neitzel

Wright-Patterson Air Force Base
Dayton, OH 45433
Attn: E.C. Simpson
AFAPL/TB

Wright-Patterson Air Force Base
Dayton, OH 45433
Attn: H.I. Bush
AFAPL/TB

Wright-Patterson Air Force Base
Dayton, OH 45433
Attn: R. Ellis
ASD/YZN

Wright-Patterson Air Force Base
Dayton, OH 45433
Attn: Col. C.E. Painter
ASD/EN

Navy Department
Naval Air Systems Command
Washington, DC 20361
Attn: W.Koven, AIR-03E

Navy Department
Naval Air Systems Command
Washington, DC 20361
Attn: J. L. Byers, AIR-53602

Naval Air Propulsion Test Center
Trenton, NJ 08628
Attn: A.A. Martino

Environmental Protection Agency
1835 K Street, NW
Washington, DC 20460
Attn: J. Schettino

Curtiss Wright Corporation
Woodridge, NJ 07075
Attn: S. Lombardo

USAVRAD Command
P.O. Box 209
St. Louis, MO 63166
Attn: Robert M. Titus (Astio)

Detroit Diesel Allison Div. GMC
P. O. Box 894
Indianapolis, IN 46206
Attn: W.L. McIntire

Detroit Diesel Allison Div. GMC
333 West First Street
Dayton, OH 45402
Attn: F. Walters

Williams Research Co.
2280 W. Maple Road
Walled Lake, MI 48088
Attn: L. Cruzen

The Garrett Corporation
AiResearch Manufacturing Co.
402 S. 36 Street
Phoenix, AZ 85304

Attn: F.B. Wallace

Pratt & Whitney Aircraft Group
Government Products Division
P. O. Box 2691
West Palm Beach, FL 33402
Attn: B.A. Jones

Boeing Commercial Airplane Co.
P. O. Box 3707
Seatle, WA 98124
Attn: D.C. Nordstrom

Douglas Aircraft Co.
McDonnell Douglas Corp.
3655 Lakewood Boulevard
Long Beach, CA 90846

Attn: R.T. Kawai, Code 36-46

Douglas Aircraft Co.
McDonnell Douglas Corp.
3655 Lakewood Boulevard
Long Beach, CA 90846

Attn: M. Klotzsche

AIRFRAME MANUFACTURERS

Boeing Com ' Airplane Co.
P. O. Box 37
Seattle, WA 9 4
Attn: P.E. Johnson MS 23-50

Lockheed California Co.
Burbank, CA 91502
Attn: R. Tullis, Dept. 75-21

Lockheed California Co.
Burbank, CA 91502
Attn: J. I. Benson

Boeing Aerospace Co.
P. O. Box 3999
Seattle, WA 98124
Attn: H. Higgins

Gates Learjet Corp.
P. O. Box 7707
Wichita, KS 67277
Attn: E. Schiller

Lockheed Georgia Co.
Marietta, GA 30060
Attn: H. S. Sweet

Gruman Aerospace Corp.
South Oyster Bay Road
Bethpage, NY 11714
Attn: C. Hoeltzer

AIRLINES

American Airlines
Maint. & Engr. Center
Tulsa, OK 74151
Attn: W. R. Neeley

Pan American World Airways, Inc.
JFK International Airport
Jamica, NY 11430
Attn: J. G. Borger

Pan American World Airways, Inc.
JFK International Airport
Jamica, NY 11430
Attn: A. MacLarty

United Airlines
San Francisco Int. Airport
Maint. Operations Cntr.
San Francisco, CA 94128

Attn: J. J. Overton

AiResearch Man. Co.
111 South 34th Street
PO Box 5217
Pnoenix, Arizona 85010
Attention C.E. Corrigan
(93-120/503-4F)

The Boeing Co., Wichita Div.
Wichita, KS 67210
Attn: D. Tarkelson

General Dynamics Covair
P. O. Box 80847
San Diego, CA 92138
Attn: S. CAmpbell, MZ 631-00

McDonnell Aircraft Co.
McDonnel Douglas Corp.
P. O. Box 516
St. Louis, MO 63166

Attn: F. C. Claser Dept. 243

Eastern Airlines
International Airport
Miami, FL 33148
Attn: A. E. Fishbein

FluiDyne Engineering Corp.
5900 Olson Memorial Highway
Minneapolis, MN 55422
Attn: J. S. Holdhusen

Lockheed California Co.
Burbank, CA 91502
Attn: J. F. Stroud, Dept. 75-42

Boeing Aerospace Co.
P. O. Box 3999
Seattle, WA 98124
Attn: D. S. Miller MS 40-26

Lockheed Georgia Co.
Marietta, GA 30060
Wichita, KS 67277
Attn: E. Schiller

Rockwell International
International Airport
Los Angeles Division
Los Angelos, CA 90009

Attn: A. W. Martin

TransWorld Airlines
605 Third Avenue
New York, NY 10016
Attn: A. E. Carrol

Hamilton Standard
Bradley Field
Windsor Locks, CT 06096
Attn: A. T. Reiff, MS 1-2-2

Solar Division
International Harvester
2200 Pacific Highway
San Diego, CA 92112

Delta Airlines, Inc.
Hartsfield-Atlanta Int. Airport
Atlanta, GA 30320
Attn: C. C. Davis

Hamilton Standard
Bradley Field
Windsor Locks, CT 06096
Attn: P. J. Dumais, MS 1A-3-1

Rohr Corporation
P. O. Box 878 - Foot & H Street
Chula Vista, CA 92012
Attn: Library

Westinghouse Electric Corp.
P. O. Box 5837
Beulah Road
Pittsburgh, PA 15236

Attn: Library

University of Tennessee
Space Institute
Tullahoma, TN 37388
Attn: Fr. V. Smith

Gas Dynamics Laboratories
Aerospace Engineering Building
University of Michigan
Ann Arbor, MI 48109

Attn: Dr. C. W. Kaufmann

TRW Equipment Corp.
TRW Inc.
23555 Euclid Ave.
Cleveland, OH 44117

Attn: I. Toth

Aerospace Corporation
R&D Center
Los Angelos, CA 90045
Attn: Library

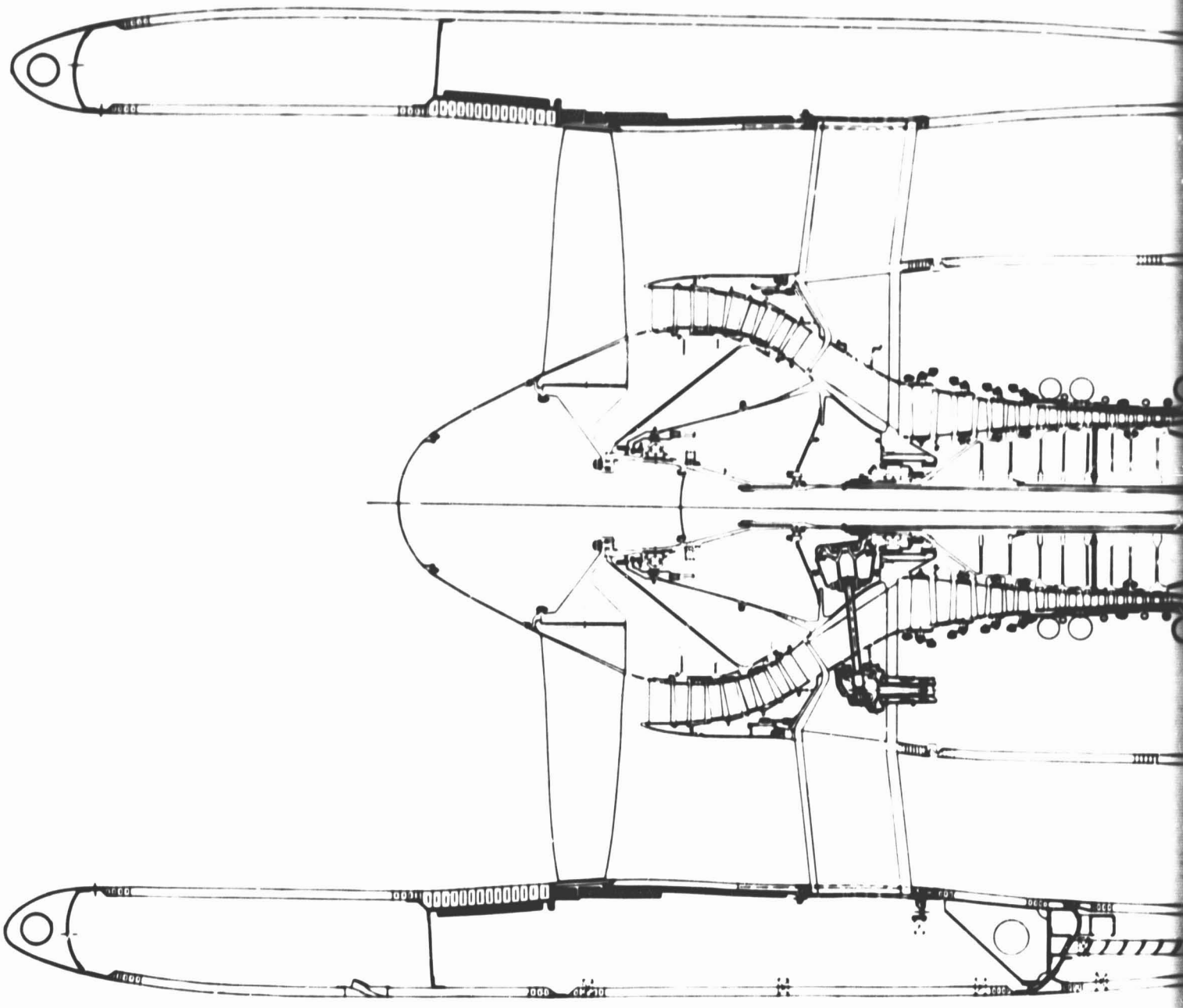

FOLDOUT FRAME

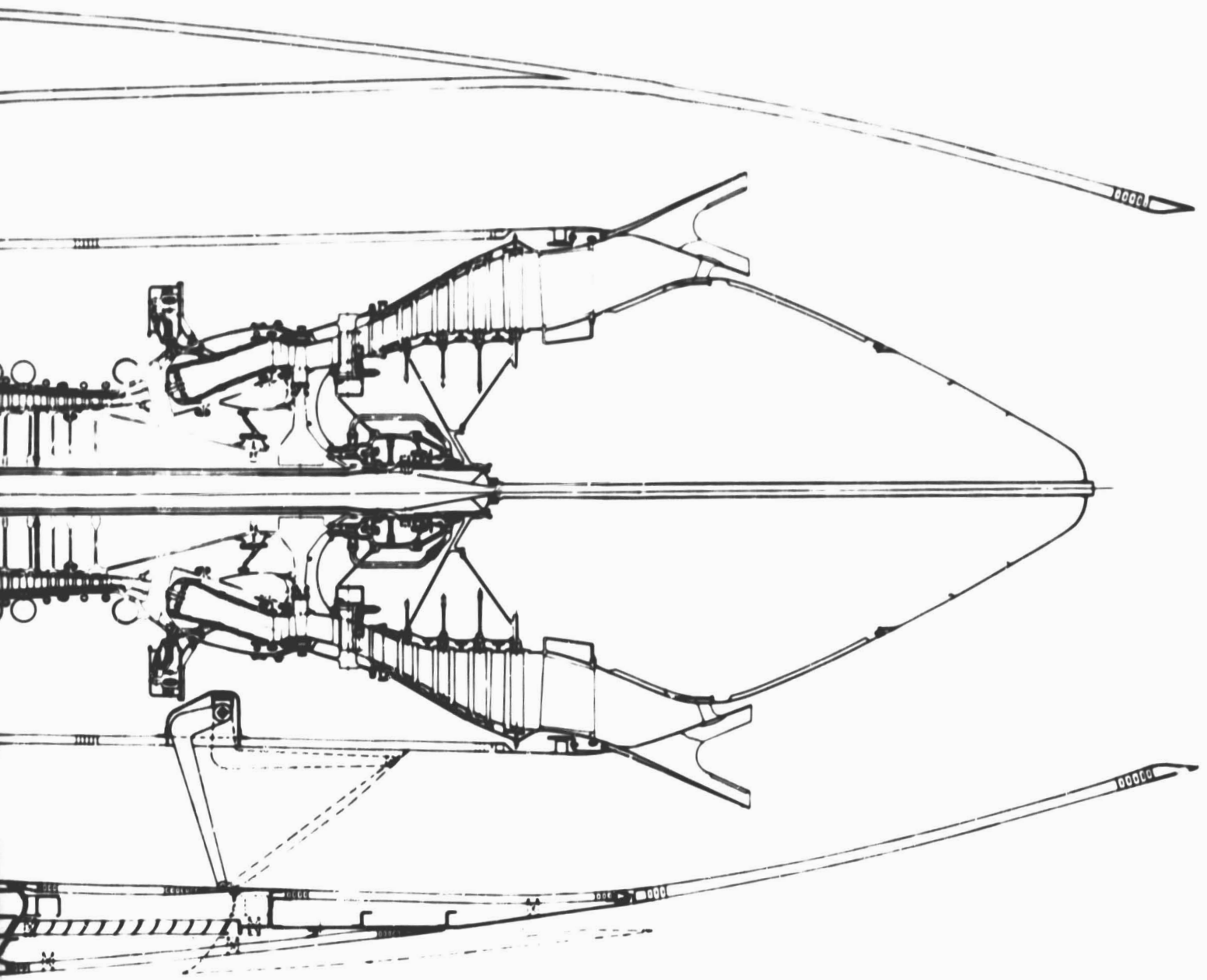

WITHOUT FRAME

Pratt & Whitney Aircraft Energy Efficient Engine
(STF 505M-7) Cross Section